

Fluid Mechanics and Its Applications

Erik Dick

Fundamentals of Turbomachines



Springer

Fluid Mechanics and Its Applications

Volume 109

Series Editor

André Thess, German Aerospace Center, Institute of Engineering Thermodynamics, Stuttgart, Germany

Founding Editor

René Moreau, Ecole Nationale Supérieure d'Hydraulique de Grenoble, Saint Martin d'Hères Cedex, France

The purpose of this series is to focus on subjects in which fluid mechanics plays a fundamental role. As well as the more traditional applications of aeronautics, hydraulics, heat and mass transfer etc., books will be published dealing with topics which are currently in a state of rapid development, such as turbulence, suspensions and multiphase fluids, super and hypersonic flows and numerical modelling techniques. It is a widely held view that it is the interdisciplinary subjects that will receive intense scientific attention, bringing them to the forefront of technological advancement. Fluids have the ability to transport matter and its properties as well as transmit force, therefore fluid mechanics is a subject that is particularly open to cross fertilisation with other sciences and disciplines of engineering. The subject of fluid mechanics will be highly relevant in such domains as chemical, metallurgical, biological and ecological engineering. This series is particularly open to such new multidisciplinary domains. The median level of presentation is the first year graduate student. Some texts are monographs defining the current state of a field; others are accessible to final year undergraduates; but essentially the emphasis is on readability and clarity.

Springer and Professor Thess welcome book ideas from authors. Potential authors who wish to submit a book proposal should contact Nathalie Jacobs, Publishing Editor, Springer (Dordrecht), e-mail: Nathalie.Jacobs@springer.com.

Indexed by SCOPUS and Springerlink

More information about this series at <http://www.springer.com/series/5980>

Erik Dick

Fundamentals of Turbomachines



Springer

Erik Dick
Department of Flow, Heat and Combustion
Mechanics
Ghent University
Gent
Belgium

ISSN 0926-5112 ISSN 2215-0056 (electronic)
Fluid Mechanics and Its Applications
ISBN 978-94-017-9626-2 ISBN 978-94-017-9627-9 (eBook)
DOI 10.1007/978-94-017-9627-9

Library of Congress Control Number: 2014954750

Springer Dordrecht Heidelberg New York London
© Springer Science+Business Media Dordrecht 2015

This work is subject to copyright. All rights are reserved by the Publisher, whether the whole or part of the material is concerned, specifically the rights of translation, reprinting, reuse of illustrations, recitation, broadcasting, reproduction on microfilms or in any other physical way, and transmission or information storage and retrieval, electronic adaptation, computer software, or by similar or dissimilar methodology now known or hereafter developed.

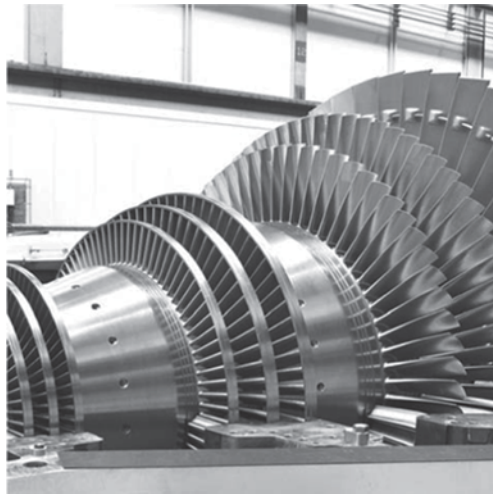
The use of general descriptive names, registered names, trademarks, service marks, etc. in this publication does not imply, even in the absence of a specific statement, that such names are exempt from the relevant protective laws and regulations and therefore free for general use.

The publisher, the authors and the editors are safe to assume that the advice and information in this book are believed to be true and accurate at the date of publication. Neither the publisher nor the authors or the editors give a warranty, express or implied, with respect to the material contained herein or for any errors or omissions that may have been made.

Printed on acid-free paper

Springer is part of Springer Science+Business Media (www.springer.com)

Preface



This book is the English language version of a course on turbomachines, taught in Dutch by the author at Ghent University from 1992 to 2013. It was composed at the occasion of the change to English as teaching language in master programmes in engineering, starting with the academic year 2013–2014. Meanwhile, the text was adapted to include some modern evolutions in the field of turbomachinery, however avoiding advanced topics, since the objective of the book is to teach fundamentals of turbomachines.

In the first chapter, the basic equations of fluid mechanics and thermodynamics are derived from first principles, formulated for application to turbomachines. With this chapter, the necessary prior knowledge for the study of turbomachines is refreshed. The prior knowledge needed is basic fluid mechanics and basic technical thermodynamics. For fluid mechanics, this comprises topics such as mechanical properties of fluids, fluid statics, equations of flow in integral and differential form, dimensional analysis and internal laminar and turbulent flow of constant density

fluids. For technical thermodynamics, the supposed prior knowledge encompasses thermal properties of fluids, first law and second law of thermodynamics, basic heat engine cycles, gas mixtures, combustion and detailed analysis of steam cycles.

The course on turbomachines is taught at Ghent University in two parts. Chapters 1–10 form a first part, taught to all master students in electromechanical engineering. This part requires basic knowledge of flow past profiles, boundary layer flow and high speed flow of compressible fluids, which are topics often covered in an advanced fluid mechanics course. The necessary fundamentals of these topics are explained in the beginning of Chap. 2 and in Chap. 4. The second part is Chaps. 11–15, taught to students with specialisation in mechanical energy engineering. This part requires somewhat more advanced knowledge of fluid mechanics. Relevant topics are transition, turbulence and heat transfer in boundary layer flows and shock and expansion phenomena in high speed flows of compressible fluids. However, care has been taken not to rely too much on prior knowledge of these topics.

The objective of the book is, as already said, study of the fundamentals of turbomachines. The approach is analysis of all kinds of turbomachines with the same theoretical framework. Basic equations are formulated for a general equation of state of a fluid. Specification of constant density or ideal gas is only done when analysing particular machines. The building up of theory is mixed in the sense that first derivations are general, but that elaboration of the theoretical concepts is done on a particular machine, however taking into account the possibility for reuse on other machines or generalisation from constant density formulation to variable density formulation. The analysis starts with radial and axial fans, because these machines are the simplest ones. The next machines are steam turbines. The order of treating the different types of turbomachines is governed by the possibility of gradually building up the theoretical concepts. For each of the machine types, a balance is sought between fundamental understanding and acquiring knowledge of practical aspects. The main concern is always fundamental understanding and bringing the reader to independent reasoning. The point of view taken by the author is that readers should be able to understand what they see when a turbomachine is opened. They should also be able to make a reasoned choice of a turbomachine for a specific application and understand its operation. Design is not a primary objective. Design requires a more specialised study, although basic design of the simplest turbomachines such as a centrifugal fan, an axial steam turbine or a centrifugal pump is possible with the topics covered in the book.

Ghent, September 2014

Erik Dick

Acknowledgements

The following companies kindly provided figures.

For fans: ebm-papst; Fläkt Woods; TLT-Turbo.

For pumps: ANDRITZ; Flygt (a Xylem company); Grundfos; Johnson Pump (SPX Flow Technology); Klaus Union; Sulzer; Sundyne; Wilo.

For steam turbines: Alstom; MAN Diesel & Turbo; Siemens Energy.

For hydraulic turbines: ANDRITZ HYDRO.

For wind turbines: ENERCON; Vestas.

For power gas turbines: Mitsubishi-Hitachi Power Systems; Siemens Energy.

For aero gas turbines: GE Aviation; Rolls-Royce.

For radial compressors, radial turbines and turbochargers: ABB Turbo Systems; Dresser-Rand; KBB Kompressorenbau Bannewitz; MAN Diesel & Turbo.

The following publishers gave permission to reprint figures.

ASME; SAGE Publications; Springer Verlag; Vogel Buchverlag.

Author Biography



Erik Dick was born on December 10, 1950 in Torhout, Belgium. He obtained a M.Sc. in electromechanical engineering from Ghent University in 1973 and a Ph.D. in computational fluid dynamics in 1980. From 1973 he worked as researcher and became full professor of mechanical engineering at Ghent University in 1995, where he teaches turbomachines and computational fluid dynamics. His area of research is computational methods and turbulence and transition models for flow problems in mechanical engineering. He is author or co-author of about 125 papers in international scientific journals and about 250 papers at international conferences. He is the recipient of the 1990 Iwan Akerman award for fluid machinery of the Belgian National Science Foundation.

List of Symbols

a		acceleration	m/s ²
	or	axial interference factor	–
A		through-flow section area	m ²
b		rotor width in axial direction	m
	or	tangential interference factor	–
	or	bypass ratio	–
c		chord	m
	or	velocity of sound	m/s
c_a		axial chord	m
C_D		drag coefficient	–
c_f		friction coefficient	–
Cf		centrifugal force by rotor rotation	N/kg
C_{Fu}		tangential force coefficient	–
C_L		lift coefficient	
C_M		Pfleiderer moment coefficient (3.30)	–
Co		Coriolis force by rotor rotation	N/kg
c_p		differential specific heat at constant pressure	J/kgK
C_p		pressure coefficient	–
	or	integral specific heat at constant pressure	J/kgK
C_P		power coefficient	–
C_T		thrust coefficient	–
Cu		centrifugal force by curvature	N/kg
d		diameter	m
D		drag per unit of span	N/m
DF		diffusion factor	–
D_{loc}		local diffusion factor	–
D_s		specific diameter (7.7)	–
e		internal energy per unit of mass	J/kg
E_k		kinetic energy per unit of mass	J/kg

E_m		mechanical energy per unit of mass	J/kg
E_p		pressure energy per unit of mass	J/kg
f		force per unit of mass	N/kg
	or	friction factor (2.30)	—
	or	fuel-air ratio	—
f_R		curvature factor (3.26)	—
g		gravitational force per unit of mass	N/kg
h		enthalpy	J/kg
	or	blade height or scroll height	m
H_m		manometric head	m
I		rothalpy	J/kg
k		equivalent sand-grain roughness	m
L		lift per unit of span	N/m
\dot{m}		mass flow rate	kg/s
M		rotor moment	Nm
M_d		disc or wheel friction moment	Nm
M_{shaft}		shaft moment	Nm
M_{st}		static moment of meridional section	m ³
$NPSH$		net positive suction head (8.5)	—
n		polytropic exponent	
\vec{n}		unit normal	—
p		pressure	Pa
P		power	W
Pf		Pfleiderer factor (3.23)	m ³
q		heat transferred per unit of mass	J/kg
	or	dynamic pressure	Pa
q_{irr}		heat by dissipation inside flow path	J/kg
q_{irr}^0		heat by dissipation outside flow path	J/kg
\underline{Q}		volume flow rate	m ³ /s
	or	heat transferred per unit of time	J/s=W
r		radius	m
	or	pressure ratio	—
R		kinematic degree of reaction	—
	or	radius of curvature	m
	or	gas constant	J/kgK
Re		Reynolds number	—
R_p		pressure degree of reaction (3.1)	—
R_s		isentropic degree of reaction (6.16)	—
s		entropy	J/kgK
	or	spacing of blades	m

S		surface area	m^2
t		time	s
	or	thickness of blades	m
T		temperature	K or $^{\circ}\text{C}$
	or	thrust force	N
u		blade speed (radius x rotational speed)	m/s
U		gravitational potential energy	m/s
v_0		inflow velocity	m/s
v_e		energy reference velocity	m/s
w		flow velocity in relative frame	m/s
W		work per unit of time	J/s=W
x		coordinate along streamline	m
	or	coordinate in axial direction	m
y		coordinate perpendicular to streamline	m
	or	coordinate in circumferential direction	m
z		coordinate in vertical direction	m
	or	coordinate in radial direction	m
Z		number of blades	—
α		angle of absolute velocity w.r.t. meridional plane	$^{\circ}$
β		angle of relative velocity w.r.t. meridional plane	$^{\circ}$
Γ		circulation along a contour	m^2/s
δ		boundary layer thickness	m
ΔW		rotor work per unit of mass	J/kg
ε		Pfleiderer work reduction factor (3.23)	—
η_i		internal efficiency	—
η_m		mechanical efficiency	—
η_p		polytropic efficiency	—
	or	propulsive efficiency (12.7)	
η_s		isentropic efficiency	—
η_{sre}		isentropic re-expansion efficiency (11.7)	—
η_t		thermal efficiency (12.9)	—
η_{td}		thermodynamic efficiency (12.9)	—
η_{tt}		total-to-total isentropic efficiency	—
η_v		volumetric efficiency	
η_{∞}		infinitesimal efficiency	—
θ		angular coordinate	rad
	or	flow turning angle	rad
κ		heat transfer coefficient (11.18)	J/kJK
λ		speed ratio (u/v_0)	—

	or	coefficient in Pfleiderer factor Pf	—
μ		dynamic viscosity	Pas
ν		kinematic viscosity	Pas
ξ		pressure loss coefficient	—
ρ		density	kg/m ³
σ		solidity c/s	—
	or	Stodola slip factor (3.20)	—
	or	cavitation number(8.1)	—
σ_a		axial solidity c_a/s	—
σ_M		moment solidity (3.31)	—
τ		shear stress	N/m ²
	or	obstruction factor (Fig. 3.16)	—
ϕ		flow coefficient v_a/u or v_{2r}/u_2	—
Φ		flow factor (7.4)	—
ψ		work coefficient $\Delta W/u_2^2$	—
Ψ		head factor (7.5)	—
ψ_0		rotor total pressure coefficient	—
ψ_r		rotor static pressure coefficient	—
ω		rotor of relative velocity	m ² /s
	or	enthalpy loss coefficient	—
Ω		rotational speed	rad/s
Ω_s		specific speed (7.6)	—
Ω_{ss}		suction specific speed (8.14)	—

Subscripts

0		inlet of machine or installation	
	or	total state	
1		just upstream of rotor	
1b		just downstream of rotor inlet	
2		just downstream of rotor	
2b		just upstream of rotor outlet	
3		outlet of machine or installation	
∞		far away from object	
	or	with infinite number of blades	

	or	on infinitesimal flow path	
a		in axial direction	
c		compressor	
	or	critical or choking value	
d		discharge/delivery side	
def		deflection	
dyn		dynamic value	(12.6–12.7)
gas		gas value	(12.6–12.7)
id		ideal	
irr		due to irreversibility	
m		in meridional direction	
	or	mechanical or manometric or mean	
mean		mean value	
o		optimum	
p		pressure side	
prop		propulsive value	(12.6–12.7)
r		in radial direction or in relative frame	
	or	rotor or reversible	
s		suction side or stator	
	or	isentropic	
ss		isentropic for stator	
sr		isentropic for rotor	
sre		isentropic re-expansion value	
t		theoretical value	
	or	turbine	
T		tip value	
tt		total-to-total isentropic	
u		in circumferential direction	

Superscripts

*		design value
	or	choking value
—		average
→		vector quantity
b		blade value

Contents

1	Working Principles	1
1.1	Definition of a Turbomachine	1
1.2	Examples of Axial Turbomachines	2
1.2.1	Axial Hydraulic Turbine	2
1.2.2	Axial Pump	4
1.3	Mean Line Analysis	5
1.4	Basic Laws for Stationary Duct Parts	7
1.4.1	Conservation of Mass	7
1.4.2	Conservation of Momentum	7
1.4.3	Conservation of Energy	9
1.4.4	Forms of Energy: Mechanical Energy and Head	10
1.4.5	Energy Dissipation: Head Loss	12
1.5	Basic Laws for Rotating Duct Parts	14
1.5.1	Work and Energy Equations in a Rotating Frame with Constant Angular Velocity	14
1.5.2	Moment of Momentum in the Absolute Frame: Rotor Work	16
1.5.3	Moment of Momentum in the Relative Frame: Forces Intervening in the Rotor Work	21
1.5.4	Energy Component Changes Caused By the Rotor Work	23
1.5.5	Rotor Work in the Mean Line Representation of the Flow	24
1.6	Energy Analysis of Turbomachines	25
1.6.1	Mechanical Efficiency and Internal Efficiency	25
1.6.2	Energy Analysis of an Axial Hydraulic Turbine	26
1.6.3	Energy Analysis of an Axial Pump	30
1.7	Examples of Radial Turbomachines	33
1.8	Performance Characteristics	36
1.9	Exercises	40
	References	46
2	Basic Components	47
2.1	Aerofoils	47
2.1.1	Force Generation	47
2.1.2	Performance Parameters	49

2.1.3	Pressure Distribution	51
2.1.4	Boundary Layer Separation	52
2.1.5	Loss Mechanism Associated to Friction: Energy Dissipation	55
2.1.6	Profile Shapes	58
2.1.7	Blade Rows with Low Solidity	59
2.2	Linear Cascades	60
2.2.1	Relation with the Real Machine	60
2.2.2	Cascade Geometry	61
2.2.3	Flow in Lossless Cascades: Force Components	62
2.2.4	Significance of Circulation	65
2.2.5	Flow in Lossless Cascades: Work	67
2.2.6	Flow in Cascades with Loss: Force Components	68
2.2.7	Flow in Cascades with Loss: Energy Dissipation and Work by Drag Force	70
2.2.8	The Zweifel Tangential Force Coefficient	72
2.2.9	The Lieblein Diffusion Factor	74
2.2.10	Performance Parameters of Axial Cascades	75
2.3	Channels	75
2.3.1	Straight Channels	75
2.3.2	Bends	77
2.4	Diffusers	79
2.4.1	Dump Diffusers	79
2.4.2	Inlet Flow Distortion	79
2.4.3	Flow Separation	81
2.4.4	Flow Improvement	81
2.4.5	Representation of Diffuser Performance	82
2.4.6	Equivalent Opening Angle	84
2.4.7	Diffusion in a Bend	85
2.5	Exercises	87
	References	95
3	Fans	97
3.1	Fan Applications and Fan Types	97
3.1.1	Fan Applications	97
3.1.2	Large Radial Fans	98
3.1.3	Small Radial Fans	99
3.1.4	Large Axial Fans	99
3.1.5	Small Axial Fans	100
3.1.6	Cross-Flow Fans	100
3.2	Idealised Mean Line Analysis of a Radial Fan	101
3.2.1	Idealised Flow Concept: Infinite Number of Blades	101
3.2.2	Degree of Reaction	102
3.2.3	Relation Between Rotor Blade Shape and Perfor- mance Parameters	103
3.2.4	Performance Characteristics with Idealised Flow	105

3.3	Radial Fan Analysis for Lossless Two-Dimensional Flow with Finite Number of Rotor Blades	106
3.3.1	Relative Vortex in Blade Channels	106
3.3.2	Velocity Difference over a Rotating Blade	107
3.3.3	Slip: Reduction of Rotor Work	112
3.3.4	Number of Blades and Solidity: Pfleiderer Moment Coefficient	115
3.3.5	Number of Blades: Examples	118
3.4	Internal Losses with Radial Fans	120
3.4.1	Turning Loss at Rotor Entrance	120
3.4.2	Incidence Loss at Rotor Entrance	120
3.4.3	Displacement by Blade Thickness	122
3.4.4	Rotor Friction Loss and Rotor Diffusion Loss	123
3.4.5	Dump Diffusion Loss at Volute Entrance	123
3.4.6	Incidence Loss at Volute Entrance	125
3.4.7	Friction Loss Within the Volute	126
3.4.8	Diffusion at the Rotor Inlet	126
3.4.9	Flow separation at Rotor Inlet and Rotor Outlet	127
3.4.10	Applicability of the Loss Models	129
3.4.11	Optimisation of the Rotor Inlet of a Centrifugal Fan	129
3.4.12	Characteristics Taking Losses into Account	131
3.5	Overall Performance Evaluation	134
3.5.1	Mechanical Loss	134
3.5.2	Leakage Loss	135
3.5.3	Overall Efficiency with Power Receiving Machines	135
3.5.4	Overall Efficiency with Power Delivering Machines	136
3.6	Rotor Shape Choices with Radial Fans	136
3.7	Axial and Mixed-Flow Fans	140
3.7.1	Degree of Reaction with Axial Fans	140
3.7.2	Free Vortex and Non-Free Vortex Types	141
3.7.3	Axial Fan Characteristics; Adjustable Rotor Blades	143
3.7.4	Mixed-Flow Fans	144
3.8	Exercises	146
3.8.1	Centrifugal Pump (Idealised Flow)	146
3.8.2	Rotor of a Centrifugal Fan (Finite Number of Blades and Internal Losses)	146
3.8.3	Number of Blades of a Rotor of a Centrifugal Fan	147
3.8.4	Volute of a Centrifugal Fan	147
3.8.5	Leakage Flow Rate with Centrifugal Fan	147
3.8.6	Centrifugal Pump (Finite Number of Blades and Internal Losses)	148
3.8.7	Axial Fan (Idealised Flow): Analysis on Average Diameter	148
3.8.8	Axial Fan (Idealised Flow): Free Vortex and Non-Free Vortex	149

3.8.9	Inlet Guide Vane with a Centrifugal Fan	149
3.8.10	Change of Rotational Speed with Centrifugal and Axial Fans	149
3.8.11	Two-Stage Axial Fan	150
3.8.12	Axial Turbine	151
	References	151
4	Compressible Fluids	153
4.1	Basic Laws	153
4.2	Compressibility and Velocity of Sound	156
4.3	Compressibility Effect on the Velocity-Pressure Relation	158
4.4	Shape of a Nozzle	160
4.5	Nozzle with Initial Velocity	162
4.6	Nozzle with Losses: Infinitesimal Efficiency	163
4.7	Isentropic and Polytropic Efficiencies	167
4.8	Exercises	171
	References	174
5	Performance Measurement	175
5.1	Pressure Measurement	175
5.1.1	The Metal Manometer	175
5.1.2	The Pressure Transducer	175
5.1.3	The Digital Manometer	176
5.1.4	Calibration of Pressure Meters	177
5.2	Temperature Measurement	177
5.2.1	The Glass Thermometer	177
5.2.2	The Temperature Transducer	177
5.2.3	The Digital Thermometer	178
5.3	Flow Rate Measurement	178
5.3.1	Reservoir	178
5.3.2	Flow Over a Weir	178
5.3.3	Pressure Drop Devices	179
5.3.4	Industrial Mass Flow Rate Meters	180
5.3.5	Positioning of Flow Rate Meters in Ducts	180
5.4	Torque Measurement	181
5.4.1	Swinging Suspended Motor or Brake	181
5.4.2	Calibrated Motor	181
5.4.3	The Torque Transducer	181
5.5	Rotational Speed Measurement	182
5.5.1	Pulse Counters	182
5.5.2	The Speed Transducer	182
5.5.3	Electric Tachometer	182
5.6	Laboratory Test of a Pelton Turbine	182
5.6.1	Test Rig	182
5.6.2	Measurements	183

5.6.3	Measurement Procedure	183
5.6.4	Calculations	184
5.6.5	Measurement Example	184
5.7	Laboratory Test of a Centrifugal Fan	184
5.7.1	Test Rig	184
5.7.2	Measurements	187
5.7.3	Measurement Procedure	187
5.7.4	Calculations	188
5.7.5	Measurement Example	188
5.8	Laboratory Test of a Centrifugal Pump	189
5.8.1	Test Rig	189
5.8.2	Measurements	190
5.8.3	Measurement Procedure	190
5.8.4	Calculations	191
5.8.5	Measurement Example	192
6	Steam Turbines	193
6.1	Applications of Steam Turbines	193
6.2	Working Principles of Steam Turbines	195
6.3	The Steam Cycle	199
6.4	The Single Impulse Stage or Laval Stage	200
6.4.1	Velocity Triangles	200
6.4.2	Work and Energy Relations	201
6.4.3	Stage Efficiency Definitions	204
6.4.4	Blade Profile Shape	205
6.4.5	Loss Representation	208
6.4.6	Optimisation of Total-to-Static Efficiency	209
6.5	The Pressure-Compounded Impulse Turbine or Rateau Turbine	212
6.5.1	Principle	212
6.5.2	Efficiency	213
6.6	The Velocity-Compounded Impulse Turbine or Curtis Turbine	214
6.7	The Reaction Turbine	217
6.7.1	Degree of Reaction	217
6.7.2	Efficiency	218
6.7.3	Axial Inlet and Outlet	222
6.8	Steam Turbine Construction Forms	224
6.8.1	Large Steam Turbines for Power Stations	224
6.8.2	Industrial Steam Turbines	229
6.9	Blade Shaping	231
6.9.1	HP and IP Blades	231
6.9.2	LP Blades	233
6.10	Exercises	236
	References	246

7	Dynamic Similitude	247
7.1	Principles of Dynamic Similitude	247
7.1.1	Definition of Dynamic Similitude	247
7.1.2	Dimensionless Parameter Groups	248
7.1.3	Similitude Conditions	248
7.1.4	Purpose of Similitude Analysis	250
7.1.5	Dimensional Analysis	251
7.1.6	Independent and Dependent Parameter Groups	252
7.1.7	Dimensionless Parameter Groups in Turbomachines with a Constant Density Fluid	252
7.1.8	Strong and Weak Similitude Conditions	254
7.2	Characteristic Numbers of Turbomachines	254
7.2.1	Definition of a Characteristic Number	254
7.2.2	Specific Speed and Specific Diameter	255
7.2.3	Relation Between Characteristic Numbers and Machine Shape	257
7.2.4	Design Diagrams	259
7.2.5	Shape of Characteristic Curves	261
7.2.6	Power Specific Speed	262
7.3	Application Example of Similitude: Variable Rotational Speed with a Pump	263
7.4	Imperfect Similitude	266
7.4.1	Effect of Reynolds Number with the Same Fluid	266
7.4.2	Effect of Relative Roughness	267
7.4.3	Effect of Viscosity	268
7.4.4	Rotor Diameter Reduction: Impeller Trimming	270
7.4.5	Reduced Scale Models	271
7.5	Series and Parallel Connection	272
7.5.1	Parallel Connection of Fans	272
7.5.2	Parallel Connection of Pumps	273
7.5.3	Series Connection of Fans	274
7.6	Turbomachine Design Example: Centrifugal Fan	276
7.7	Exercises	279
	References	282
8	Pumps	283
8.1	Cavitation	283
8.1.1	Cavitation Phenomenon and Cavitation Consequences	283
8.1.2	Types of Cavitation	284
8.1.3	Cavitation Assessment: Cavitation Number and Required Net Positive Suction Height	286
8.1.4	Optimisation of the Inlet of a Centrifugal Pump Rotor	289
8.1.5	Net Positive Suction Head of the Installation	291
8.1.6	Increasing the Acceptable Suction Height	292

8.2	Priming of Pumps: Self-Priming Types	293
8.2.1	Side Channel Pump	293
8.2.2	Peripheral Pump (regenerative pump)	295
8.2.3	Self-Priming Centrifugal Pump	296
8.2.4	Jet Pump	297
8.3	Unstable Operation	297
8.4	Component Shaping	299
8.4.1	Simply and Doubly Curved Blades in Radial Rotors	299
8.4.2	Mixed-Flow and Axial Pumps	300
8.4.3	Pump Inlet	300
8.4.4	Pump Outlet	301
8.4.5	Vaneless Diffuser Rings	301
8.4.6	Vaned Diffuser Rings	302
8.4.7	Volute	303
8.4.8	Return Channels	305
8.5	Internal Parallel and Series Connection Of Rotors	305
8.5.1	Reason for Internal Parallel or Series Connection	305
8.5.2	Internal Parallel Connection of Rotors	306
8.5.3	Internal Series Connection of Rotors: Multistage Pumps	306
8.6	Constructional Aspects	307
8.6.1	Rotor	307
8.6.2	Stator	307
8.6.3	Shaft Sealing	307
8.6.4	Bearings	309
8.6.5	Axial Force Balancing with Single-Stage Pumps	309
8.6.6	Axial Force Balancing with Multistage Pumps	310
8.6.7	Wear Rings	311
8.7	Special Pumps	311
8.7.1	Borehole Pumps	312
8.7.2	High-Pressure Pumps	312
8.7.3	Sealless Pumps: Circulation Pumps, Chemical Pumps	312
8.7.4	Slurry Pumps	313
8.7.5	Pumping of Solid Materials	314
8.7.6	Vertical Submerged Pumps	314
8.7.7	Partial Emission Pumps	315
8.7.8	Pumps for Viscous Fluids	315
8.8	Exercises	316
8.8.1	Looking up Pump Characteristics	316
8.8.2	Verification of an NPSH-Value	316
	References	317
9	Hydraulic Turbines	319
9.1	Hydraulic Energy	319
9.2	Hydraulic Turbine Types	320
9.2.1	Large Turbines (> 10 MW)	320
9.2.2	Small Turbines (< 10 MW)	322

9.3	Pelton Turbines: Impulse Turbines	324
9.3.1	Performance Characteristics	324
9.3.2	Specific Speed	326
9.3.3	Determination of the Main Dimensions	328
9.3.4	Flow Rate Control and Over-Speed Protection	328
9.4	Francis and Kaplan Turbines: Reaction Turbines	329
9.4.1	Shape of the Velocity Triangles: Kinematic Parameters	329
9.4.2	Optimisation of the Velocity Triangles	330
9.4.3	Degree of Reaction and Speed Ratio	331
9.4.4	Velocity Triangles with Varying Degree of Reaction	332
9.4.5	Specific Speed and Meridional Shape of Francis Turbines ..	333
9.4.6	Flow Rate Control with Reaction Turbines	335
9.4.7	Examples (Figs. 9.16, 9.17)	337
9.5	Bulb and Tube Turbines	338
9.6	Reversible Pump-Turbines	340
9.7	Exercises	342
	References	345
10	Wind Turbines	347
10.1	Wind Energy	347
10.2	Types of Wind Energy Conversion Systems	348
10.2.1	Drag Machines	348
10.2.2	High-Speed Horizontal-Axis Turbines	349
10.2.3	Technical Aspects of Horizontal-Axis Wind Turbines for Electricity Generation	351
10.2.4	Low-Speed Horizontal-Axis Wind Turbines	355
10.2.5	Vertical-Axis Wind Turbines	356
10.3	Wind Turbine Performance Analysis	358
10.3.1	Momentum Analysis (Single Streamtube Analysis)	358
10.3.2	Multiple Streamtube Analysis	361
10.3.3	Blade Element Analysis	363
10.4	Adaptation to a Wind Regime	365
	References	368
11	Power Gas Turbines	369
11.1	General Concept and Components	369
11.1.1	Definition of a Gas Turbine	369
11.1.2	Comparison with Other Thermal Engines	371
11.1.3	Example of a Power Gas Turbine	372
11.1.4	Compressor Part	374
11.1.5	Turbine Part	377
11.1.6	Combustion Chamber	381
11.2	Thermodynamic Modelling	384
11.2.1	Isentropic Efficiency with Adiabatic Compression or Expansion	384
11.2.2	Reheat Effect	387

11.2.3	Infinitesimal Efficiency; Polytropic Efficiency	389
11.2.4	Thermodynamic Properties of Air and Combustion Gas ...	392
11.2.5	Heat Capacity Representation	396
11.2.6	Cooled Expansion	396
11.2.7	Compression with Extraction	401
11.3	Performance of Simple-Cycle Power Gas Turbines	402
11.3.1	Idealised Simple Cycle	402
11.3.2	Simple Cycle with Component Efficiencies and Different Heat Capacities of Air and Combustion Gas	403
11.3.3	Simple Cycle with Component Efficiencies, Cooling and Variable Gas Properties	405
11.4	Performance of Power Gas Turbines with Enhanced Cycles	409
11.4.1	Compression with Intercooling	409
11.4.2	Expansion with Reheat	411
11.4.3	Recuperator	412
11.4.4	Combined Gas and Steam Cycles	413
11.4.5	Steam Injection	416
	References	417
12	Thrust Gas Turbines	419
12.1	Thrust Generation	419
12.1.1	Screw or Propeller	419
12.1.2	Reactor or Jet Engine	423
12.1.3	Rocket	426
12.2	Overview of Aircraft Gas Turbine Engines	427
12.2.1	Turbojet	427
12.2.2	Turboprop and Turbo-Shaft	427
12.2.3	Bypass Turbojet	428
12.2.4	Turbofan	428
12.2.5	Prop-fan and Unducted Fan	429
12.2.6	Geared Turbofan	432
12.3	Performance Parameters of Aircraft Propulsion Systems	432
12.3.1	Specific Thrust	432
12.3.2	Dynamic Power	433
12.3.3	Gas Power and Dynamic Efficiency	433
12.3.4	Thermal Power, Thermodynamic Efficiency and Thermal Efficiency	433
12.3.5	Propulsive Power and Propulsive Efficiency	434
12.3.6	Overall Efficiency	434
12.3.7	Rocket	435
12.3.8	Generalisation for Double-Flow Engines	435
12.3.9	Specific Fuel Consumption	437
12.4	Performance of the Gas Generator and the Single-Jet Engine	438
12.4.1	Analysis with Loss-Free Components	439
12.4.2	Analysis with Component Losses	441

12.5	Performance of Double-Flow Engines	444
12.5.1	Unmixed Flows (Double-Jet Engine: Turbofan, Turboprop)	444
12.5.2	Mixed Flows (Bypass Engine)	448
12.5.3	Intercooling and Recuperation	450
12.6	Technological Aspects of the Turbofan Engine	451
12.6.1	Discs and Shafts	451
12.6.2	Vanes and Blades	451
12.6.3	Combustion Chamber	452
12.6.4	Mixer and Thrust Reverser	454
12.7	Exercises	454
12.7.1	Single-Flow Jet Engine	454
12.7.2	Single-Flow Jet Engine with Post-Combustion	455
12.7.3	Turbofan with Separate Flows	456
12.7.4	Turbofan with Mixed Flows	456
12.7.5	Optimisation of Turbine Inlet Temperature with a Turbofan Engine	456
12.7.6	Helicopter Rotor	456
12.7.7	Ramjet	457
	References	457
13	Axial Compressors	459
13.1	Mean Line Analysis	459
13.1.1	Velocity Triangles	460
13.1.2	Fundamental Equations	461
13.1.3	Loss Representation	462
13.1.4	Loss Coefficients	465
13.1.5	Force Components	465
13.1.6	Diffusion Factor and Loss Correlations	466
13.1.7	Kinematic Parameters	470
13.1.8	Secondary Flow: Principle	471
13.1.9	Radial Variation of Flow: Principle	473
13.1.10	Optimisation of a Stage	474
13.1.11	Blade Shape	476
13.1.12	Attainable Pressure Ratio	478
13.2	Secondary Flow	478
13.2.1	Definition of Secondary Flow	478
13.2.2	Passage Vortex and Trailing Vortices	479
13.2.3	Corner Vortices	480
13.2.4	Horseshoe Vortex	480
13.2.5	Leakage Vortex and Scraping Vortex	480
13.2.6	Loss Assessment	481
13.3	Radial Flow Variation	481
13.3.1	S_1 - S_2 Decomposition	481
13.3.2	Radial Equilibrium	482
13.3.3	Free Vortex Blades	483

13.3.4	Forcing of the Vortex Distribution	485
13.3.5	Effect of End Wall Boundary Layers	487
13.3.6	Three-dimensional Blade Design	488
13.4	Compressor Blade Profiles	491
13.4.1	Subsonic and Supercritical Cascades	491
13.4.2	Transonic Cascades	494
13.4.3	Supersonic Cascades and Transonic Cascades with High Inlet Mach Number	496
13.5	Performance Characteristics and Operating Range	497
13.5.1	General Shape of a Characteristic Curve	497
13.5.2	Rotating Stall	498
13.5.3	Choking	499
13.5.4	Surge	501
13.5.5	Operating Range	502
13.6	Exercises	505
	References	506
14	Radial Compressors	509
14.1	Construction Forms and Applications	509
14.1.1	Rotor Types	509
14.1.2	General Shape of a Radial Compressor	511
14.1.3	Comparison Between Radial and Axial Compressors	512
14.1.4	Examples of Radial Compressors	513
14.2	Kinematic Parameters	516
14.3	Pressure Ratio	519
14.4	Rotor Shape	521
14.4.1	Number of Blades	521
14.4.2	Inducer	523
14.5	Diffusers	525
14.5.1	Flow Non-homogeneity at Rotor Outlet	525
14.5.2	Mixing Zone	526
14.5.3	Vaneless Diffusers	527
14.5.4	Vaned Diffusers	527
14.6	Performance Characteristics	528
14.6.1	Flow Instability	528
14.6.2	Choking	528
14.6.3	Operating Characteristics and Operating Range	529
14.7	Exercises	531
14.7.1	Velocity Variation at Constant Radius in a Rotor	531
14.7.2	Variable Geometry	533
	References	533
15	Axial and Radial Turbines for Gases	535
15.1	Axial Turbines	535
15.1.1	Kinematic Parameters	535
15.1.2	Radial Variation of Flow Parameters	541

15.1.3	Blade Profiles	542
15.1.4	Three-dimensional Blade Design	545
15.1.5	Vane and Blade Clocking	546
15.1.6	Operating Characteristic of Axial Turbines	546
15.2	Radial Turbines	549
15.2.1	Shape and Functioning	549
15.2.2	Kinematic Parameters	551
15.2.3	Operating Characteristic of Radial Turbines	553
15.2.4	Radial Turbine Applications	554
15.3	Dimensional Analysis with Compressible Fluids	554
15.3.1	Independent and Dependent Π -groups	554
15.3.2	Dimensionless Compressor and Turbine Characteristics ...	556
15.3.3	Corrected Quantities	556
15.4	Exercises	557
	References	558
Index	561

Chapter 1

Working Principles

Abstract In this chapter, we study the working principles of turbomachines with a number of characteristic examples. Further, we derive the basic laws for energy exchange between a shaft and a fluid and the laws describing energy changes on the fluid side. We also analyse the role of the energy exchanging forces and introduce definitions of efficiency.

1.1 Definition of a Turbomachine

A turbomachine is a machine that exchanges energy between the continuous flow of a fluid and a continuously rotating blade system, with the energy exchange based on flow-generated forces. Energy may be transferred from the flow to the rotating machine components or vice versa. In the first case, energy extracted from the flow is used to drive a rotating component, generally called a *rotor* (bladed drum, bladed wheel or collection of bladed wheels), driving on its turn a useful external load. The machine may then be called shaft power delivering, or for short, *power delivering*, but typically it is termed a *turbine*, irrespective of the fluid.

Possible fluids are:

- water: *water turbine* or hydraulic turbine
- steam (vapour): *steam turbine*
- air in natural wind: *wind turbine*
- gas produced by combustion of a fuel in pressurised air: *gas turbine*
- other fluid, as refrigerant in a cooling cycle: *expansion turbine*.

When energy is supplied to the fluid by the rotor, the machine has to be driven by an external motor. It may be called shaft power receiving, or shortly, *power receiving*. Specific names are used, depending on the fluid and the energy component that is mainly increased. Energy exchanged between a rotor and a fluid is mechanical energy in a technical sense (this will be explained in Sect. 1.4.4). Mechanical energy essentially can only take two forms within the machine itself: velocity-associated energy (kinetic energy) and pressure-associated energy (pressure potential energy in case of a constant density fluid).

Examples of power receiving machines are:

- *incompressible fluid* (water, oil), dominantly a pressure increase: *pump*
- *compressible fluid* (air, gas, vapour)
 - high pressure increase: *compressor*
 - low pressure increase (especially with air): *fan* (puts air into motion).

1.2 Examples of Axial Turbomachines

We consider two examples with water: a hydraulic turbine and a pump.

1.2.1 Axial Hydraulic Turbine

Figure 1.1 sketches a longitudinal section of a small hydraulic turbine. In the flow sense, the machine consists of three components: a stator part, encompassing an *inlet* and a *guide ring*, a rotor (runner) and a stationary diverging pipe. Both the guide ring and the runner are bladed. Figure 1.2 shows a cylindrical section through the guide ring and the rotor, indicating the velocities in the absolute (v) and the relative frame (w). Subscript 1 indicates the rotor inlet, subscript 2 the rotor outlet. The absolute frame is attached to the stationary casing of the machine. The relative frame rotates together with the rotor. The velocity u stands for the relative frame velocity (rotational speed Ω)

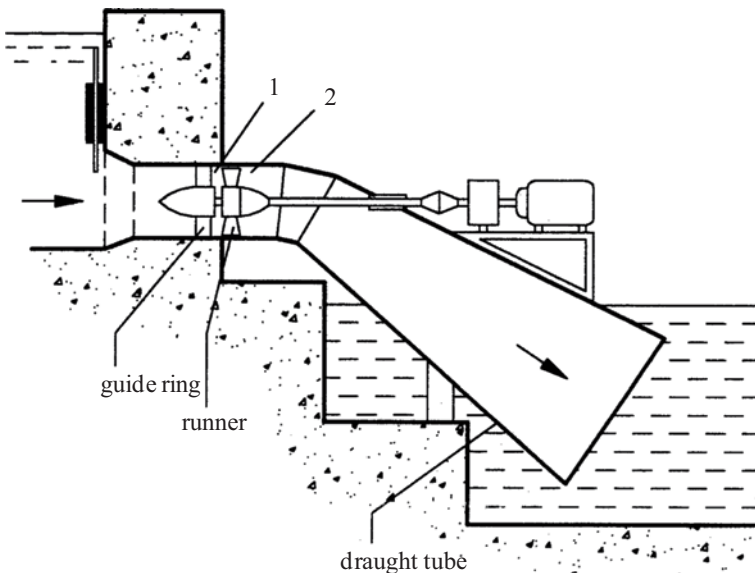


Fig. 1.1 Longitudinal section of an axial hydraulic turbine

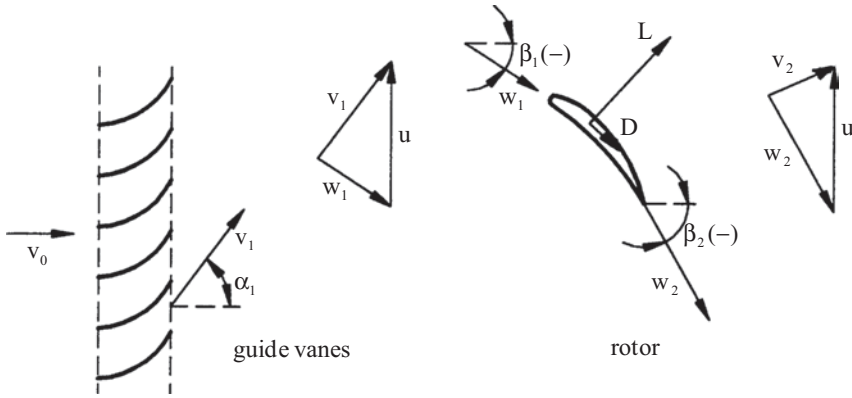


Fig. 1.2 Cylindrical section of guide vane ring and runner blade of an axial hydraulic turbine

multiplied with radius r), called *blade speed*. The absolute flow velocity vector (\vec{v}) is the vector sum of the blade speed (\vec{u}) and the relative flow velocity vector (\vec{w}).

The components have the following functions.

- Inlet and guide ring:
 - guiding fluid to the rotor and distributing it over the rotor
 - generating kinetic energy: $v_1^2 / 2$.

The kinetic energy originates from a pressure drop, where pressure upstream of the machine is built up from gravitational potential energy (see the further Eq. 1.5). Acceleration of the flow with hydraulic turbines such as in Fig. 1.1 is never strong. Guiding the fluid is the main function. We here apply the terms *guide ring* and *guide vanes*. Stationary objects guiding the flow are typically called *vanes*, while the term *blade* is mostly used for a rotary object, but the term blade is also used for either. In other machines, flow acceleration may be the most important, as with steam turbines. The stator is then said to be composed from nozzles and the term *nozzle ring* is used.

- *Rotor (or runner)*: energy extraction from the flow.

In the relative frame: $w_2^2 / 2 > w_1^2 / 2$. Kinetic energy is generated, corresponding to pressure drop (see the further Eq. 1.13). In the absolute frame, kinetic energy decreases: $v_2^2 / 2 < v_1^2 / 2$. Both the decrease of pressure and kinetic energy correspond to energy transfer from the flow to the rotor. The energy transfer principle can already be understood. By the profile shape of the blades, resembling an aircraft wing profile, turning of the relative velocity at the rotor inlet (w_1) towards a more tangential direction at the rotor outlet (w_2), generates a *lift force* (L). This lift is approximately perpendicular to the average relative velocity and has the sense indicated in the figure. The tangential component of the lift is in the sense of the blade speed u . This implies that the running blade is driven by the flow, which corresponds to work done by the flow on the rotor. We also note that the drag force D has a tangential component opposing the motion.

- The outlet stator component has various functions and may get various names depending on the function to be emphasised:
 - collecting water beyond the rotor: collector
 - converting a part of the kinetic energy at the rotor outlet to pressure potential energy: pressure at rotor outlet decreases, increasing the pressure difference over the rotor: diffuser
 - exploiting the downward height, in other words guiding the water to the downward level. This generates a pressure decrease at the rotor outlet from the gravitational potential energy: draught tube.

The latter function is often the most important one. For example: $v_2 = 5 \text{ m/s}$ (typical): $v_2^2 / 2 = 12.5 \text{ J/kg}$; 2.5 m height difference between rotor outlet and tail water: gravitational potential energy $gz \approx 25 \text{ J/kg}$. Extraction of the energy associated to the downward height is efficient. Kinetic energy recovery is a process involved with high losses. So, mostly the term *draught tube* is used.

The turbine discussed here is called *axial*, since streamlines, in principle, lie on cylinders with an axis coinciding with the centre of the machine shaft (real machines are mostly slightly conic). The velocity vectors mainly have axial and tangential components (radial components are very small). There are also machines with flow occurring approximately in planes perpendicular to the shaft; in other words, the velocity vectors mainly have radial and tangential components (the axial components are very small). These machines are called *radial*. Their working principle is more complex. These machines are discussed later in this chapter. Also intermediate forms exist, called diagonal machines or *mixed-flow* machines. There are still other types such as tangential (peripheral) and diametrical (cross-flow) machines. For the present, the fundamental discussion is limited to axial machines, as the study of their working principle is the simplest.

1.2.2 Axial Pump

Figure 1.3 shows an axial pump for use as a submerged pump in a vertical pipe or a pit. The working principle is similar to that of an axial turbine, but with an inverse sense of the energy exchange. Figure 1.3 shows also a cylindrical section, drawn with horizontal flow direction.

The following parts can be distinguished.

- Inlet: guiding the fluid towards the rotor and accelerating the fluid, as with a turbine. There are no guide vanes. In principle, the flow direction stays axial, but the fluid swirls somewhat due to the rotation of the rotor. In some pumps, pre-swirl is prevented by guide vanes in the axial direction.
- Rotor (or *impeller*): transferring energy to the fluid. The turning of the relative velocity at the rotor inlet w_1 onto a more axial direction at outlet w_2 generates a lift force in the indicated sense. The lift has a tangential component in the sense opposite to the blade speed u . Work to be supplied to the rotor by a driving motor corresponds with this. Energy is transferred from the rotor to the fluid. The

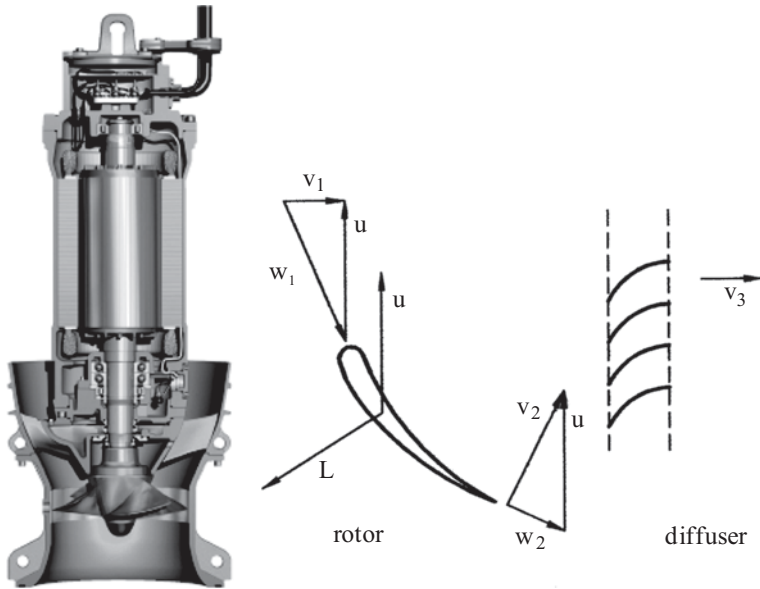


Fig. 1.3 Axial pump (courtesy Flygt, a Xylem company); cylindrical section of a rotor blade and the diffuser ring

energy transfer is partly noticeable by the kinetic energy increase in the absolute frame ($v_2^2 / 2 > v_1^2 / 2$) and partly by the kinetic energy decrease in the relative frame ($w_2^2 / 2 < w_1^2 / 2$) with a corresponding pressure increase.

- **Diffuser:** a stationary ring of vanes downstream of the rotor turns the entering velocity v_2 into the axial direction (tangential component of the velocity becomes zero) while the axial velocity component is reduced by increased through-flow area. Kinetic energy in the flow decreases ($v_3^2 / 2 < v_2^2 / 2$), causing pressure increase. The stator part downstream of the rotor converts kinetic energy into pressure. Therefore, this component is termed a *diffuser*.

The rotating component of a pump is sometimes called the *impeller*. The meaning of the term is to impart motion to the fluid. As such, this is a general term well describing the role of the rotor in a power receiving machine, but it is typically only used with radial pumps and radial compressors. The term *runner*, mentioned in the previous section is, as such, also a general term completely equivalent to the term rotor, but it is typically only used with hydraulic turbines.

1.3 Mean Line Analysis

The fundamental analysis of a turbomachine applies the *average flow concept*. For a machine with periodicity in the circumferential direction (axial, radial, mixed-flow), the flow is calculated by averaging quantities in the circumferential direction

(also called tangential direction) for a given axial and radial position. The real flow is always unsteady due to the presence of the running rotor. The average flow is steady at a constant speed of rotation, due to the circumferential periodicity of rotor and stator blade systems. It is further assumed that the average flow is described by steady flow equations. Strictly, this cannot be correct, as products of flow quantities occur in the flow equations. The average value of a product does not equal the product of the average values. Deviation terms are generated, which in fluid mechanics are called Reynolds terms. The terms arrived at here are similar to the terms generated by averaging a turbulent flow in time. The Reynolds terms are ignored (or replaced by a model) in a fundamental analysis. The approximation is good, as long as circumferential flow variations are not very significant. As a rule, this is the case with a machine operating not extremely far away from design conditions. When the flow periodicity is seriously broken, the approximation is less good. In principle, some prudence is called for when applying relations from a circumferentially averaged flow representation. But, generally, this flow model produces quite accurate relations. The following example may illustrate this.

$$u = u_0 + u_a \sin \omega t \rightarrow \bar{u} = u_0,$$

$$u^2 = u_0^2 + 2 u_0 u_a \sin \omega t + u_a^2 \sin^2 \omega t \rightarrow \overline{u^2} = u_0^2 + \frac{1}{2} u_a^2,$$

$$\frac{\sqrt{\overline{u^2}}}{\bar{u}} = \sqrt{1 + \frac{1}{2} \left(\frac{u_a}{u_0}\right)^2} \rightarrow \frac{u_a}{u_0} = 0.2: \quad \sqrt{\overline{u^2}} \approx 1.01 \bar{u}.$$

Further approximations are introduced in analyses meant for fundamental understanding. With an axial machine, it is assumed that the streamlines of the average flow lie on cylinders, in other words, that there is no radial velocity component. It is further assumed that there is no variation of flow quantities in the radial direction. Due to these simplifications, the flow becomes one-dimensional in the sense that only axial variation of flow quantities is considered. The flow stays multidimensional in the sense that velocity has two components, an axial and a tangential one. The flow analysis thus achieved is mostly termed *mean line analysis*. It means that relations on a mean streamline in the circumferentially averaged flow are considered to be representative for the whole machine. Similar approaches are introduced with other machine types to come to a one-dimensional flow representation. For a machine with circumferential periodicity, the streamlines of the average flow lie on surfaces of revolution. With a mean line analysis, the flow is described on a *mean circumferential streamsurface*, assuming that there is no variation of flow quantities in the circumferential direction and in the direction perpendicular to this surface. A mean line analysis is not very accurate and is mainly meant, as already said, for fundamental understanding. Hereafter, we derive the basic laws for one-dimensional flows.

1.4 Basic Laws for Stationary Duct Parts

We first derive some basic laws for an elementary duct part, stationary in an absolute frame. The geometry is less complex than within a turbomachine. Gradually, we will extend to basic laws that can be applied to turbomachines. Figure 1.4 shows an elementary part of a duct. The axis of the duct part is denoted by x . The inlet section A_1 and the outlet section A_2 are perpendicular to this axis. With a one-dimensional representation, the flow is uniform in sections perpendicular to the axis and flow quantities only vary in the x -direction. Density is denoted by ρ and pressure by p .

1.4.1 Conservation of Mass

With a steady flow, the mass entering the duct part during a time interval dt , also leaves it:

$$\rho_2 A_2 v_2 dt = \rho_1 A_1 v_1 dt,$$

$$\text{or} \quad \dot{m} = \rho v A = \text{constant (mass flow rate)}. \quad (1.1)$$

1.4.2 Conservation of Momentum

According to Newton's second law, the change of momentum per time unit of a system with a constant mass equals the sum of the applied forces. We consider the system with constant mass in the duct part at the time t . At time $t + dt$, the system has moved as shown in Fig. 1.4. The momentum change during the time interval dt is

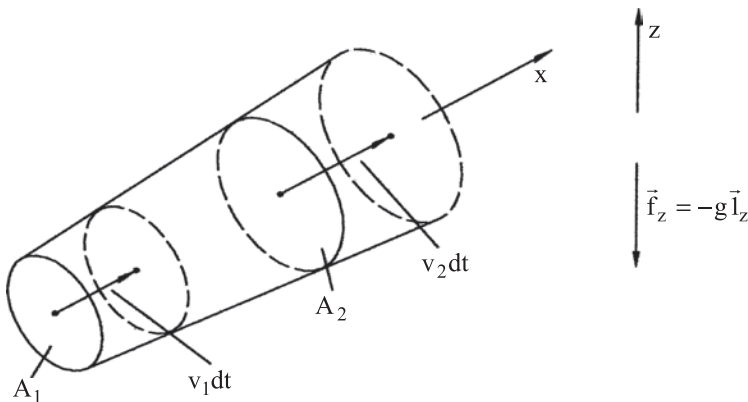


Fig. 1.4 Elementary duct part for mass and momentum balances

$$\rho_2 v_2 A_2 dt \vec{v}_2 - \rho_1 v_1 A_1 dt \vec{v}_1,$$

and equals the sum of the forces multiplied by dt .

So:
$$\rho_2 v_2 A_2 \vec{v}_2 - \rho_1 v_1 A_1 \vec{v}_1 = \sum \vec{F},$$

or through (1.1)
$$\dot{m}(\vec{v}_2 - \vec{v}_1) = \sum \vec{F}. \quad (1.2)$$

The relations (1.1) and (1.2) apply to any part of the duct. The flow even need not be confined by walls and may be part of a streamtube. Relations (1.1) and (1.2) in their general form already provide solutions for many simple flow problems.

We further consider the case of a duct part (stationary material walls), in which, provisionally, only pressure force and gravity force are considered as internal forces. Gravity per mass unit (N/kg) is denoted by $\vec{f}_z = -g\vec{I}_z$, with the z -axis vertically directed upward and g being the gravity acceleration.

For an elementary part with length dx , the momentum law projected into the x -direction is

$$\dot{m}(v + dv - v) = pA - (p + dp)(A + dA) + (p + 1/2 dp)dA - \rho A dx g \vec{I}_z \cdot \vec{I}_x.$$

With $dx \vec{I}_x \cdot \vec{I}_z = dz$ and $gdz = dU$ (gravitational potential energy) it follows

$$\rho v A dv = -A dp - \rho A dU. \quad (1.3)$$

After multiplication by the velocity and division by the mass flow rate it follows

$$d(1/2 v^2) + \frac{1}{\rho} dp + dU = 0. \quad (1.4)$$

Equation (1.4) is a *work equation*, called *Bernoulli's equation*. With a constant density fluid ($\rho = \text{constant}$), the equation may be integrated over a streamline to

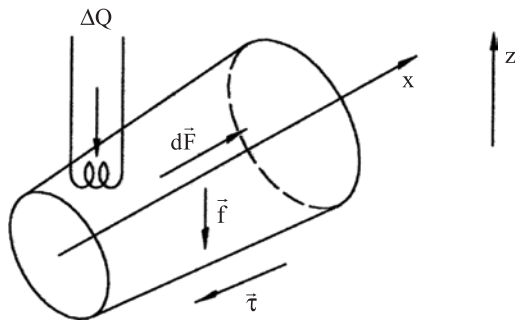
$$1/2 v^2 + \frac{p}{\rho} + U = \text{constant}.$$

We further take friction forces and active forces into account. The friction force exerted on the flow per surface unit (= shear stress) in the direction of the velocity, but with opposite sense, is denoted by τ . With an *active force* is meant a force that exchanges energy between the surroundings and the flow. The force component in the flow direction, calculated positively in the flow sense, is indicated by dF in Fig. 1.5.

The momentum equation (1.3) has to be completed now with the right-hand side

$$-\tau O dx + dF,$$

Fig. 1.5 Elementary duct part with active force, friction and heat exchange



with O being the circumference. This gives, after multiplication by velocity and division by mass flow rate:

$$\frac{-\tau O dx v}{\rho A v} + \frac{dF v}{\rho A v}.$$

The first term may be considered as the work per time unit done on the moving fluid by the friction force per unit of mass flow rate, or the work per unit of mass. The second term is, similarly, the active force work per unit of mass. We denote the additional terms by

$$-dq_{irr} + dW \text{ (J / kg)}.$$

In the notation we already take into account that the work of the friction force on the moving fluid, with friction on a stationary material wall, is equal to the friction-generated heat; this is the energy dissipation (see Sect. 1.4.5 and see Chap. 2, Sect. 2.1.5). The work of the active force is positive when work is done on the fluid ($\overline{dF \cdot \vec{v}} > 0$).

Bernoulli's equation (work equation) becomes

$$d \frac{1}{2} v^2 + \frac{1}{\rho} dp + dU + dq_{irr} = dW. \quad (1.5)$$

1.4.3 Conservation of Energy

The first law of thermodynamics states that, with a fixed mass system, energy increase equals the sum of work supplied and heat supplied. We denote the heat supplied to the elementary duct part per time unit by Q (J/s = W). We denote work supplied per time unit by the active force by W :

$$W = dFv = dW\dot{m}.$$

The energy law states:

$$\dot{m}(E + dE - E) = pAv - (p + dp)(A + dA)(v + dv) - \rho A dx \mathbf{g} \cdot \vec{l}_z \cdot \vec{l}_x v + W + Q.$$

We note that no work is done by the pressure force and the friction force on the duct wall, as this wall stands still. The symbol E represents mechanical energy in the fundamental sense, i.e. the sum of internal and kinetic energy ($E = e + \frac{1}{2} v^2$).

It follows that $\dot{m} dE = \dot{m} \frac{p}{\rho} - \dot{m} \frac{p + dp}{\rho + d\rho} - \dot{m} dU + W + Q$.

After division by mass flow rate, it follows:

$$d(e + \frac{1}{2} v^2 + \frac{p}{\rho} + U) = dW + dq. \quad (1.6)$$

Heat supplied to the fluid per mass unit is denoted by dq . We further apply the term *enthalpy* $h = e + p/\rho$, so that

$$d(h + \frac{1}{2} v^2 + U) = dW + dq. \quad (1.7)$$

1.4.4 Forms of Energy: Mechanical Energy and Head

The energy content of a mechanical system is, in technical sense, the maximum amount of work and heat that can be produced by it. According to the energy balance (1.7), the energy components of a steady flow are enthalpy, kinetic energy and gravitational potential energy. In fundamental sense, there is only one energy form in a mechanical system: kinetic energy. With a macroscopic description of a flow, we use macroscopic velocity as the mass weighted average velocity of the microscopic fluid particles (atoms or molecules), averaged for a small volume. The kinetic energy of the particles is divided into the macroscopic kinetic energy ($v^2/2$) and the kinetic energy of the motion around the macroscopic average. The latter term is denominated internal energy (e). The term potential energy indicates recoverable work done against a conservative force (in the present case: gravity). A force is *conservative* if the force per mass unit can be noted as the gradient of a scalar that is only space-dependent. For gravity it is

$$\vec{g} = -g\vec{l}_z = -\nabla(gz).$$

The *displacement work* of this force, for an elementary displacement $dx\vec{l}_x$ is

$$-g\vec{l}_z \cdot dx\vec{l}_x = -gdz = -dU.$$

So, the displacement work done against gravity is the total differential of the term U . Work supplied for a displacement between two points is thus independent of the path followed. This implies that no work is required for a displacement with coinciding initial and final points. Consequently, work stored in the fluid, done against a conservative force, is entirely recoverable and may thus be considered as energy.

Pressure-related work does not have the same character. The resulting force of the pressure exerted onto a fluid particle, with volume V and surface S , is

$$-\int_S p \vec{l}_n dS,$$

with dS representing an elementary surface part and \vec{l}_n the corresponding external normal. According to the gradient integral theorem, the resulting pressure force is

$$-\int_V \nabla p dV.$$

The pressure force per volume unit is $-\nabla p$. The pressure force per mass unit is

$$-\frac{1}{\rho} \nabla p.$$

The *displacement work* of the pressure force is

$$-\frac{1}{\rho} \nabla p \cdot dx \vec{l}_x = -\frac{1}{\rho} dp,$$

where dp is the pressure change over the infinitesimal path. Differentials are applied in this sense in equations (1.5), (1.6) and (1.7). The displacement work of the pressure force constitutes a total differential if density is only a function of pressure: $\rho = \rho(p)$. In principle, no fluid meets this requirement, as density is always also a function of temperature. With a liquid, density only weakly depends on pressure and temperature. In practise, a constant density is mostly assumed. The fluid is then said to be *incompressible*. Strictly, the term means that density is pressure-independent. Commonly, *constant density* is meant. With constant density, $(1/\rho)dp$ constitutes a total differential. The term p/ρ is then, for a steady flow, potential energy, called *pressure potential energy*. For variable density, the term p/ρ cannot be defined as potential energy. However, due to the form of the energy balance (1.6), there is the wish to consider it as energy as it may be the source of work or heat. Strictly, the term $d(p/\rho)$ constitutes the sign-changed total work of the pressure. Principally, the term $-d(p/\rho)$ should be kept in the right-hand part of (1.6). In the same way, the term $-(1/\rho)dp$ should be kept in the right-hand part of (1.5). We write the terms in the left-hand part, however, as we wish to formulate statements about the work and the heat exchanged between the surroundings and the flow. The term $-d(p/\rho)$ is termed *pressure work* or *flow work*. The term p/ρ is added to the internal energy and the sum is termed *enthalpy* (see thermodynamics).

Pressure work consists of two parts:

$$-d\left(\frac{p}{\rho}\right) = -\frac{1}{\rho}dp - pd\left(\frac{1}{\rho}\right).$$

The first part is the *displacement work*. The second part is the *volume change work*. More in general, the second part is the *deformation work*, the sum of volume change work and form change work. The form change work of pressure is zero, however (pressure force perpendicular to the surface). The difference between work associated to the gravity force and the pressure force is that the work term of the former is identical in the work balance (1.5) and the energy balance (1.6). This expresses the complete recoverability of work done against the gravity force.

In technical sense, the *mechanical energy* of a system is defined as the maximum amount of work that can be produced by it. For constant density, mechanical energy of a flow can easily be identified from the work balance (1.5). The maximum work can be produced by a flow without shear forces and is the sum of the kinetic energy ($\frac{1}{2}v^2$), the pressure potential energy (p/ρ) and the gravitational potential energy (U), where the potential energies have to be calculated with respect to reference conditions of pressure and position. Mostly, the reference conditions are not relevant, because only changes of potential energies intervene. So, for constant density, mechanical energy of a flow is defined by

$$E_m = \frac{1}{2}v^2 + p/\rho + U. \quad (1.8)$$

In hydraulics, the term *head* is used for mechanical energy (J/kg) divided by the gravity acceleration ($9.81m^2/s^2$), expressed as a height (m). The term is also used for the rise of this quantity by a pump and the drop of it by a hydraulic turbine. With machines exchanging energy, it is more convenient to use changes of energy. Thus, it has become a modern practice in machine analyses to use the term head for a change of mechanical energy. From now on, we will mostly use the term head in this sense for all types of turbomachines.

For a fluid with variable density, the definition of mechanical energy of a flow remains the maximum amount of work that can be produced by the fluid and its value is still derived from the work balance (1.5). In Chaps. 1–3 we will only use fluids with constant density and the expression (1.8) thus applies. We will treat the extension to compressible fluids later in Chaps. 6 and 11.

1.4.5 Energy Dissipation: Head Loss

The term $-dq_{irr}$ in the work equation (1.5), when put at the right-hand side, has been described as work of the friction force on the moving fluid. According to the terminology of the previous section, this is *displacement work*. Note that, until now, we have applied the basic laws to an elementary duct part that is stationary to the coordinate system in which we determine the flow quantities. The forces

on the duct wall stand still. No work is associated with them for a control volume positioned with its envelope upon the duct wall. So we considered, when drawing up the energy balance, the pressure force work and the friction force work on the envelope as being zero. Neither is there any work of the friction force onto the inlet and outlet sections (velocity perpendicular to these sections). The total work of the friction force is thus zero. The total work consists of displacement work and deformation work. The latter is the sum of volume change work and form change work. The volume change work of the friction force is zero, however (principally: friction force tangential to the surface). With a stationary duct part, the displacement work of the friction force on the moving fluid equals the form change work in value. The latter is the source of friction heat (see fluid mechanics and see Sect. 2.1.5).

Energy dissipation is reduction of the work capacity of the sum of the energies in a system. For a steady flow, the sum of the energies is the sum of enthalpy, kinetic energy and gravitational potential energy (Eq. 1.7). The work capacity is expressed by the mechanical energy, i.e. the part of the energy that can be used for work generation. The mechanism that reduces the mechanical energy is the deformation work associated to friction forces, either friction internally in the fluid or friction between the fluid and walls. The deformation work converts mechanical energy into heat. Technically, it is mostly said that there is *head loss*. The dissipation mechanism with the friction force will be further analysed in Chap. 2, Sect. 2.1.5. The effect of dissipation may be grasped already now by taking the difference between the *energy equation* (1.7) and the *work equation* (1.5):

$$dh - \frac{1}{\rho} dp - dq_{irr} = dq \text{ or } Tds = dh - \frac{1}{\rho} dp = dq_{irr} + dq. \quad (1.9)$$

We thus obtain the expression of the second law of thermodynamics on the production of entropy (s) for an infinitesimal duct part. Eq. (1.9) already gives confidence that the term dq_{irr} represents energy dissipation. The equation may also be written as

$$de = dq_{irr} + dq - p d\left(\frac{1}{\rho}\right).$$

This expression shows that friction causes heating of the fluid. The third term is *heating by compression* (volume change work of pressure). This term is zero for a constant density fluid.

When applying the energy theorem, we put the envelope of the control volume onto the duct wall. Since the choice of a control volume is arbitrary, we may also opt to position its envelope just inside the fluid. Then, the envelope has velocity v and $-dq_{irr}$ represents the total work of the friction force on the control volume. The new choice does not change the formulation of the momentum equation, but changes the formulation of the energy equation. Within the one-dimensional flow representation, velocity is uniform over a cross-section. This implies that we should consider the entire flow retardation due to wall friction as concentrated between the envelope of the control volume and the duct wall. Within this zone, dissipation by friction

force occurs. Thus, denoting the heat transferred through the duct wall towards the fluid by dq , the heat transferred through the envelope of the control volume equals $dq_{irr} + dq$. The energy law thus has $dW - dq_{irr} + dq_{irr} + dq$ as its right-hand part, with the second term representing the friction force work and the third term representing the heat generated by dissipation. The resulting energy equation is the same as the one with the first choice of the control volume.

The reasoning becomes more complex for a streamtube part within the fluid, without a control volume envelope coinciding with a material wall. The product of the friction force and the flow velocity then no longer corresponds to the work dissipated into heat. In other words, this work may contain an active part. In Chap. 2, we will demonstrate that the work equation in form (1.5) and the energy equation in form (1.7) stay valid for an arbitrary infinitesimal part of a streamline within a steady flow. But, the general validity of the energy equation (1.7) is obvious on the basis of the first law of thermodynamics, if one accepts that a part of the work dW may be due to friction forces. However, quantifying that work and the heat dq transferred to the fluid originating from the dissipation on the nearby streamlines might be difficult. The general validity of the work equation (1.5) is, in the same way, obvious on the basis of the second law of thermodynamics, but again a problem might arise in quantifying the active and the dissipative parts of the work. This is further discussed in Chap. 2.

1.5 Basic Laws for Rotating Duct Parts

1.5.1 *Work and Energy Equations in a Rotating Frame with Constant Angular Velocity*

In a relative frame rotating at a constant angular velocity ($\vec{\Omega}$) with respect to an absolute frame, the basic laws of mechanics and thermodynamics still hold, provided that two fictitious forces are introduced: centrifugal force and Coriolis force. These follow from the relation between absolute and relative velocities according to (Fig. 1.6):

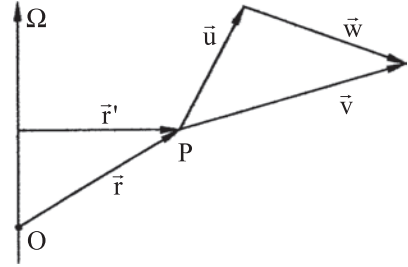
$$\vec{v} = \vec{\Omega} \times \vec{r} + \vec{w}. \quad (1.10)$$

Here, $\vec{\Omega}$ is the rotational speed vector, \vec{r} the coordinate vector of the considered point P with respect to an origin on the rotation axis, and \vec{w} the relative velocity.

The relation between an absolute displacement $d\vec{r}$ and a relative displacement $\delta\vec{r}$ is

$$d\vec{r} = \vec{\Omega} \times \vec{r} dt + \delta\vec{r} \quad \text{or} \quad \frac{d\vec{r}}{dt} = \vec{\Omega} \times \vec{r} + \frac{\delta\vec{r}}{dt}. \quad (1.11)$$

Fig. 1.6 Relative and absolute velocities for constant speed of rotation



Formula (1.11) also defines the relation between time differentiation in the relative frame and time differentiation in the absolute frame for any vector quantity as this may be considered being proportional to the difference of two coordinate vectors.

The differentiation rule applied to the velocity relation (1.10) results in:

$$\vec{a} = \frac{d\vec{v}}{dt} = \vec{\Omega} \times (\vec{\Omega} \times \vec{r}) + \vec{\Omega} \times \vec{w} + \vec{\Omega} \times \frac{\delta \vec{r}}{dt} + \frac{\delta \vec{w}}{dt} = \vec{\Omega} \times (\vec{\Omega} \times \vec{r}) + 2 \vec{\Omega} \times \vec{w} + \vec{a}_{rel},$$

where \vec{a} and \vec{a}_{rel} respectively represent the absolute and the relative accelerations.

The basic laws may thus be applied in the relative frame, on condition of the introduction of the (so-called) fictitious forces (per mass unit):

$$\text{Centrifugal force: } \vec{Cf} = -\vec{\Omega} \times (\vec{\Omega} \times \vec{r}) = -\vec{\Omega} \times (\vec{\Omega} \times \vec{r}') = \Omega^2 \vec{r}',$$

$$\text{Coriolis force: } \vec{Co} = -2\vec{\Omega} \times \vec{w},$$

where \vec{r}' represents the radial distance vector of point P with respect to the axis of rotation. From now on, this radial vector will be denoted by \vec{r} , as in a cylindrical coordinate system.

An additional term comes in the right-hand part of the momentum equation:

$$\rho A dx \Omega^2 \vec{r} \cdot \vec{I}_x = \rho A \Omega^2 r dr = \rho A \Omega^2 d \frac{r^2}{2} = \rho A d \frac{u^2}{2}.$$

Here, we applied $dx \vec{I}_x \cdot \vec{I}_r = dr$ and $u = \Omega r$ represents the *blade speed*. The Coriolis force does not contribute to the work on the streamline.

From multiplication by the velocity and division by the mass flow rate it follows that the additional term in the right-hand part of the work equation makes $d u^2/2$, with as a consequence

$$d \frac{1}{2} w^2 + \frac{1}{\rho} dp + dU + dq_{irr} = dW + d \frac{1}{2} u^2. \quad (1.12)$$

In other words, there is a centrifugal force contribution to the work on the streamline. The same contribution has to be added in the energy equation.

The work dW is zero on a rotor, since forces affecting the rotor perform no work within the frame that is turning with the rotor. Variation of gravitational potential energy within the rotor is negligible, with as a consequence:

$$\text{Work : } d \frac{1}{2} w^2 + \frac{1}{\rho} dp + dq_{irr} = d \frac{1}{2} u^2, \quad (1.13)$$

$$\text{Energy : } dh + d \frac{1}{2} w^2 = d \frac{1}{2} u^2 + dq. \quad (1.14)$$

From now on, we will use the term *stagnation enthalpy* or *total enthalpy*. This is the enthalpy adopted by a fluid particle, if flow locally would be brought to a halt adiabatically. With the subscript 0 denoting the stagnation, the total enthalpy in the absolute frame and the total enthalpy in the relative frame are

$$h_0 = h + \frac{1}{2} v^2, \quad h_{0r} = h + \frac{1}{2} w^2.$$

Similarly, we will use the term *total pressure* or *stagnation pressure* as the pressure obtained if the flow locally would be brought to zero velocity in absence of heat exchange (adiabatic) and without losses (reversible). If necessary to make the difference with total quantities, the basic quantities will be called the static ones; so: *static pressure* and *static enthalpy*.

The energy equation in the relative frame is sometimes expressed using a quantity $I = h_{0r} - \frac{1}{2} u^2$, called *rothalpy* (*rotating total enthalpy*). The centrifugal force is $\overline{Cf} = \Omega^2 \vec{r} = \nabla(\frac{1}{2} \Omega^2 r^2) = -\nabla(-\frac{1}{2} u^2)$. Thus, the term $-\frac{1}{2} u^2$ is the associated potential energy. The energy equation then becomes $dI = dq$. For an axial machine, $u = \text{constant}$, and the energy equation simplifies to $dh_{0r} = dq$. We will not often use the term rothalpy. This means that the work term associated to the centrifugal force will mostly be written explicitly as in (1.13) and (1.14).

1.5.2 Moment of Momentum in the Absolute Frame: Rotor Work

Figure 1.7 sketches the meridional section of a streamtube enclosing the entire blade height of a pump rotor. The *meridional section* of a rotating object is a section containing the axis of rotation. This term is borrowed from geography. v_m denotes the *meridional component* of the absolute velocity. The velocity component in the circumferential (or tangential) direction is denoted by v_u . According to the mean line flow representation, there is no velocity component perpendicular to the average circumferential streamsurface. The meridional velocity may be decomposed in an axial component v_a and a radial component v_r .

Figure 1.7 shows two possible rotor forms. The left-hand rotor has a *shroud*. This type is called *closed* or *shrouded*. The blades of the right-hand rotor fit directly in the casing with a clearance. This type is termed *open* or *unshrouded*. The part of the rotor that fits on the shaft is called the *hub*. The inner part of the rotor that carries

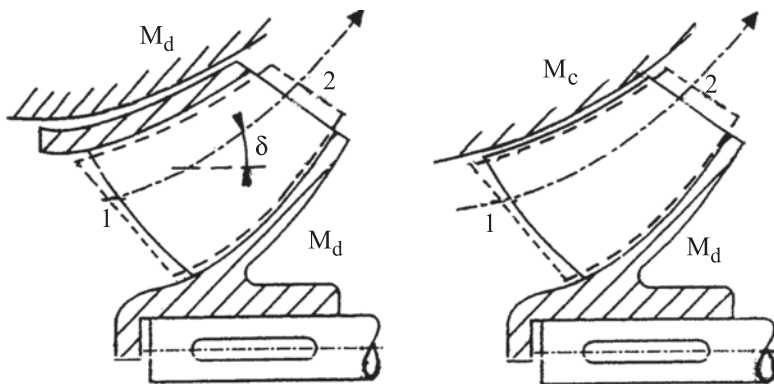


Fig. 1.7 Meridional streamtube section: closed and open rotors with mixed-flow pumps

the blades is mostly called the *rotor disc* (in general, the disc is curved), but the term *hub* is often used for the complete inner part. The flow is guided by the blade surfaces. With a closed rotor, the flow is guided by the shroud and the hub as well. The shroud and hub then constitute the *end walls*. With a closed rotor, all guiding surfaces are in the relative frame. With an open type, the end wall at the hub side is in the relative frame and the end wall at the casing side is in the absolute frame. We first analyse the closed form.

Closed Rotor (Shrouded) At the shroud and hub outsides, the surrounding fluid exerts friction forces. The moment of those friction forces around the shaft is usually termed *disc friction moment* M_d (here: disc and shroud together; we may call it *wheel friction moment*). By M_d we denote the moment exerted on the material rotor parts by the surrounding fluid. This moment is always braking; the sense of this moment is opposite to the rotation sense. Forces exerted on the blade surfaces and the end walls (pressure forces and friction forces) constitute a moment around the shaft. The moment of these forces, calculated as exerted on the flow, is denoted with M . We consider the moments M and M_d as positive in the running sense of the rotor. M_d is directed against the running sense and is negative. The flow moment M is positive with a driven machine (receiving shaft power) and negative with a driving machine (delivering shaft power). The sum of the reaction moment ($-M$) and the disc friction moment (M_d) must be kept in balance by a moment exerted on the shaft (M_{shaft}). We also consider this shaft moment as positive in the running sense. So M_{shaft} is positive with a driven machine and negative with a driving one.

The moment balance of the material rotor parts requires

$$M_{shaft} - M + M_d = 0.$$

With a driven machine we note

$$M_{shaft} = M - M_d. \quad (1.15)$$

The moment M_{shaft} exerted on the shaft by the external motor is then positive. M and $-M_d$ are both positive. The moment M_{shaft} is divided into two parts: the M part reaches the flow and the $-M_d$ part is absorbed by disc friction.

With a driving machine we note

$$-M = -M_{shaft} - M_d. \quad (1.16)$$

The flow moment M is negative, i.e. the flow exerts a positive moment $-M$ on the rotor. The shaft moment is negative as well, i.e. the machine exerts a positive moment $-M_{shaft}$ on the coupled load. The moment $-M$ is divided into two parts: the $-M_{shaft}$ part reaches the shaft. The $-M_d$ part is absorbed by disc friction.

We consider a control volume as sketched in Fig. 1.7. As usual, we indicate the rotor inlet with subscript 1 and the outlet with subscript 2. By taking the moment around the rotation axis of Newton's momentum law, we obtain that the change per time unit of the moment of momentum in the flow equals the moment of the forces exerted on the control volume:

$$\dot{m}(r_2 v_{2u} - r_1 v_{1u}) = M. \quad (1.17)$$

The moment M encompasses both contributions of pressure forces and of shear forces on material surfaces. When drawing up of the former expression, it is assumed that shear stresses on the inlet and outlet faces of the control volume do not form a moment around the rotation axis. This assumption follows from the circumferentially averaged flow representation, where shear stresses have no tangential component. This assumption is also very good with a real flow.

Multiplication of (1.17) by the speed of rotation Ω results in

$$\dot{m}(u_2 v_{2u} - u_1 v_{1u}) = P.$$

P is the power transferred from the rotor to the flow through the flow moment M .

Division by the mass flow rate generates the equation:

$$u_2 v_{2u} - u_1 v_{1u} = \Delta W, \quad (1.18)$$

with ΔW the work done on the flow by the flow moment M .

Multiplication of equation (1.15) by Ω results in

$$P_{shaft} = P - P_d.$$

With a power receiving machine, P_{shaft} is the power supplied to the shaft by the driving motor. The term $-P_d$ represents the power associated to the dissipation by disc friction. After division by the mass flow rate we note

$$\Delta W_{shaft} = \Delta W + q_{irr}^o. \quad (1.19)$$

The term q_{irr}^o represents the part of the shaft work that is dissipated by disc friction forces. In (1.19) this term is represented with a positive sign, as it always is arithmetically positive in this equation.

Analogously, Eq. (1.16) for a power delivering machine results in

$$-\Delta W = -\Delta W_{shaft} + q_{irr}^o, \quad (1.20)$$

where $-\Delta W$ is the work done by the flow on the rotor and $-\Delta W_{shaft}$ is its fraction supplied to the shaft. The term q_{irr}^o is the part of $-\Delta W$, dissipated by disc friction.

With the driven machine (1.19), ΔW is the work done by the rotor on the flow. With a driving machine (1.20), $-\Delta W$ is the work done by the flow on the rotor. For both, we use the term *rotor work*. With a driving machine, we note $-\Delta W$ as

$$-\Delta W = u_1 v_{1u} - u_2 v_{2u}. \quad (1.21)$$

The work ΔW done on the flow with the driven machine is partly dissipated in the flow by friction forces, as indicated by Bernoulli's Eq. (1.5). Analogously, internal dissipation occurs as well with a driving machine. The effects of *dissipation during energy exchange* (q_{irr}^o) and of *internal dissipation* (q_{irr}) will be studied below.

Open Rotor (Unshrouded) The foregoing derivations do not, in principle, change with an open rotor. The difference is that the friction force on the casing directly contributes to the moment exerted on the flow. We again term M the resulting moment exerted on the flow by the forces on the blade surfaces and the end surfaces, including the casing. Equation (1.17) is then still valid. Equation (1.18) may be formally derived from it, but the meaning of ΔW as rotor work is then not immediately obvious.

The flow moment may be divided into two parts:

$$M = M_b + M_c.$$

M_b is the part originating from the blade surfaces and the hub, in other words, the material rotor surfaces and M_c is the contribution by the casing. Both moments are considered as being exerted on the flow. With a driven machine, M_b is positive and M_c negative. With a driving machine, M_b and M_c are both negative. M_c is, like M_d , always negative. The moment balance on the material rotor parts is

$$M_{shaft} - M_b + M_d = 0,$$

where M_d represents the disc friction moment of the hub.

$$\text{It follows that } M_{shaft} = M_b - M_d = M - M_c - M_d. \quad (1.22)$$

After multiplication by Ω it follows that

$$P_{shaft} = M\Omega - M_c\Omega - M_d\Omega. \quad (1.23)$$

The term $-M_c\Omega$ is always positive and thus has the same nature as the term $-M_d\Omega$. After division by the mass flow rate we obtain

$$\Delta W_{shaft} = \Delta W + q_{irr}^o,$$

where $M\Omega = \dot{m}\Delta W$ and $-M_c\Omega - M_d\Omega = \dot{m}q_{irr}^o$.

The result for ΔW_{shaft} is then the same as (1.19).

Interpretation of the moment balance (1.22) is quite simple. For a driven machine, it means that the shaft moment M_{shaft} is divided into two parts: the M_b part reaches the blades (the rotating machine parts) and the $-M_d$ part is absorbed by disc friction. Further, the blade moment M_b is divided into two parts: the M part reaches the flows and the $-M_c$ part is absorbed by friction on the casing.

To interpret the power balance (1.23), we note that the moment M_c equals the integral of the scalar product of the friction force $\vec{\tau}dS$ exerted on the flow and a unit vector along the blade speed \vec{u} , multiplied by the radius. The term $M_c\Omega$ then follows from the scalar product of the friction force $\vec{\tau}dS$ and the blade speed \vec{u} . With the relation between the absolute and the relative velocities, $\vec{v} = \vec{u} + \vec{w}$, it follows

$$M_c\Omega = \int \vec{\tau} \cdot \vec{u} dS = \int \vec{\tau} \cdot \vec{v} dS - \int \vec{\tau} \cdot \vec{w} dS,$$

or

$$-M_c\Omega = \int -\vec{\tau} \cdot \vec{v} dS - \int -\vec{\tau} \cdot \vec{w} dS.$$

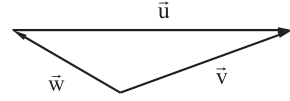
The term with the integrand $-\vec{\tau} \cdot \vec{v}$ represents the dissipation by the friction force on the casing. The term with the integrand $-\vec{\tau} \cdot \vec{w}$ is physically fictive, but may be considered as the dissipation that would be generated if the friction force were acting in the relative frame. The difference between both terms may thus be considered as the disc friction dissipation associated to the friction force acting on a fictitious shroud of the rotor. The term with the integrand $-\vec{\tau} \cdot \vec{w}$ then has to be considered as internal dissipation within the flow.

The interpretation of the power balance (1.23) for a driven machine is that the shaft power is split into three parts: the part $M\Omega$ reaches the flow, the part $-M_c\Omega$ is dissipated at the casing and the part $-M_d\Omega$ is dissipated at the rotor disc.

We note, both for an open and a closed rotor, as equation for the rotor work:

$$\Delta W = u_2 v_{2u} - u_1 v_{1u}. \quad (1.24)$$

This equation is termed *Euler's turbomachine equation* or *Euler's work equation*. It is considered to be the most important basic equation in turbomachinery theory. The equation has been derived here for work done by a rotor on the flow (driven machine). It is, of course, also valid for work done in the opposite sense (driving machine). Henceforth, we will refer to Euler's work equation (1.18 or 1.21) as the *rotor work equation* and to Bernoulli's equation (1.5) as the *work equation*. The work equation expresses the energy changes in the flow as a result of the work done on the flow or by the flow. The rotor work equation expresses the relation between the work done by the rotor or on the rotor and the change of angular momentum in the flow

Fig. 1.8 Velocity triangle

(change of angular momentum multiplied by rotational speed). Further, we note that the rotor work equation has been derived here based on a one-dimensional flow representation (mean line representation) but that formulation for a real three-dimensional flow follows from the same principles.

1.5.3 Moment of Momentum in the Relative Frame: Forces Intervening in the Rotor Work

From a velocity triangle (Fig. 1.8) follows geometrically: $\vec{v} = \vec{u} + \vec{w}$, or $v_u = u + w_u$. The velocity triangle in Fig. 1.8 is drawn deliberately with negative w_u . It follows that

$$uv_u = u^2 + uw_u.$$

So:

$$\Delta W = u_2^2 - u_1^2 + u_2 w_{2u} - u_1 w_{1u}. \quad (1.25)$$

The Eq. (1.25) also follows from a moment of momentum balance, applied in the relative frame. Fictitious forces to be introduced are

$$\vec{Co} = -2 \vec{\Omega} \times \vec{w} \text{ and } \vec{Cf} = \Omega^2 \vec{r}.$$

The relative velocity \vec{w} has an axial component, a radial component and a tangential one. The axial component does not intervene in the Coriolis force. A tangential unit vector in the sense of the rotation may be noted as

$$\vec{l}_u = \vec{l}_\Omega \times \vec{l}_r,$$

so that

$$\vec{Co} = -2 \vec{\Omega} \times (w_r \vec{l}_r + w_u \vec{l}_\Omega \times \vec{l}_r) = -2 \Omega w_r \vec{l}_u + 2 \Omega w_u \vec{l}_r.$$

According to Fig. 1.7, $w_r = w_m \vec{l}_m \cdot \vec{l}_r$, with \vec{l}_m a unit vector in the meridional direction with positive axial and radial components. The centrifugal force does not contribute to the force moment. Neither does the radial component of the Coriolis force. The moment of momentum balance in the relative frame results in

$$\dot{m}(r_2 w_{2u} - r_1 w_{1u}) = M + M_{co}, \quad (1.26)$$

with

$$M_{co} = \int -2 \Omega w_m \vec{l}_m \cdot \vec{l}_r \rho \, dA \, dm \, r,$$

where dA is the cross-section area of an elementary annular streamtube around the average circumferential streamsurface in Fig. 1.7. The elementary length in the meridional plane is indicated by dm . So the term $\rho w_m dA$ represents the mass flow rate

through the elementary streamtube. Within the mean line representation, the result for the average streamsurface is considered to be representative for the entire flow.

We thus note $M_{co} = -\dot{m} \int 2 \Omega r \bar{l}_m \cdot \bar{l}_r dm$.

With $dm \bar{l}_m \cdot \bar{l}_r = dr$ it follows

$$M_{co} = -\dot{m} \int 2 \Omega r dr = -\dot{m} \Omega (r_2^2 - r_1^2).$$

After multiplication by Ω and division by \dot{m} , the moment of momentum equation in the relative frame results in Eq. (1.25).

Equation (1.26) may be written as

$$M = -M_{co} - M_\ell.$$

M_ℓ is the moment term associated to the turning of the relative flow (change of rw_u), in other words, the lift. The expression demonstrates, for a driven machine, that the moment required to drive the rotor must balance the moment of two forces, namely *Coriolis force* and *lift force*. In Eq. (1.25) this means that the term $u_2^2 - u_1^2$ represents the work supplied against the Coriolis force and $u_2 w_{2u} - u_1 w_{1u}$ the work supplied against the lift force. The interpretation with a driving machine is similar, but for work delivered by the Coriolis and lift forces.

The above analysis implies that two forces intervene in the rotor work. The effect of lift is the simplest to understand. For the axial pump and the axial turbine, analysed earlier (Figs. 1.2 and 1.3), it is obvious that turning of the flow within the rotor generates lift on the blades. Physically, this lift is a consequence of a pressure difference between both sides of a blade or a rotor blade channel, generated by turning the flow. We will analyse the origin of this pressure difference in Chap. 2. Figures 1.2 and 1.3 demonstrate that lift intervenes in the rotor work. In the axial examples in Figs. 1.2 and 1.3, $u_1 = u_2$, but, meanwhile, we understand that the moment of forces intervenes with work and that a change of radius affects the resulting moment.

The role of the Coriolis force in the rotor work only follows in an abstract way from the above analysis. At this stage, it is obvious that rotation induces forces in the fluid, namely the Coriolis force and the centrifugal force. Only the Coriolis force has a component in the tangential direction. This component intervenes in the moment of momentum. The concrete way rotation-induced forces intervene is by causing pressure differences between the two sides of a blade. Associated to the Coriolis force, there is a pressure difference, with a moment of the resulting rotor force around the rotation axis. This is analysed further for radial machines in Sect. 1.7 and in Chap. 3, Sect. 3.3.2.

For the time being, confusion might arise by the finding that there is a work contribution by the centrifugal force in the work and energy equations on a streamline in a rotating frame, namely expressions (1.13) and (1.14). With the above analysis it is clear that the centrifugal force does not contribute to the energy exchange between the rotor and the fluid (the rotor work), as the centrifugal force has no moment around the rotation axis. It becomes obvious from expressions (1.13) and (1.14) that the centrifugal force intervenes in the change of kinetic energy and

the pressure change (pressure-associated energy) in the flow. The centrifugal force influences the distribution of the energy forms within the rotor flow. A potential energy is associated to the centrifugal force. A change in this potential energy due to a change in radius must be compensated by a change in another energy component. Distribution of energy forms, internally within the flow, has to be distinguished from energy exchange between the flow and the rotating machine parts. The effect of the centrifugal force on the energy distribution will be discussed in the next section.

1.5.4 Energy Component Changes Caused By the Rotor Work

From the cosine rule follows (Fig. 1.8)

$$w^2 = u^2 + v^2 - 2uv_u,$$

or
$$uv_u = \frac{1}{2}u^2 + \frac{1}{2}v^2 - \frac{1}{2}w^2.$$

$$\Delta W = \frac{u_2^2 - u_1^2}{2} + \frac{v_2^2 - v_1^2}{2} + \frac{w_1^2 - w_2^2}{2}. \quad (1.27)$$

The meaning of the rotor work equation in form (1.27) becomes obvious by combining it with the energy equation. Neglecting gravitational potential energy variation over the rotor results in the energy equation in the absolute frame (1.7), in the absence of heat transfer:

$$\Delta W = \Delta h_0 = \Delta h + \Delta \frac{1}{2}v^2. \quad (1.28)$$

Combined with (1.27) it follows

$$\Delta h = \frac{u_2^2 - u_1^2}{2} + \frac{w_1^2 - w_2^2}{2}. \quad (1.29)$$

The Eqs. (1.28) and (1.29) demonstrate that work done becomes visible in two forms. For work done on the fluid, there is *kinetic energy increase* and *static enthalpy increase*. The kinetic energy increase is called the *action part* of the work, in other words, the directly visible effect. The static enthalpy increase is called the *reaction part*. The static enthalpy increase may be converted into kinetic energy by connecting a nozzle in which kinetic energy is generated (hence the term reaction). The action-reaction terminology may sound peculiar with driven turbomachines. It originates from turbines, as will be illustrated below. The concept applies to all turbomachines, however. The meaning of the static enthalpy increase becomes obvious from the work equation and the energy equation in the relative frame. In this frame all forces affecting the rotor stand still and perform no work. So we write the work equation, infinitesimally, according to (1.13):

$$d \frac{1}{2} u^2 = d \frac{1}{2} w^2 + \frac{1}{\rho} dp + dq_{irr}. \quad (1.30)$$

The energy equation according to (1.14) in the absence of heat transfer is

$$d \frac{1}{2} u^2 = d \frac{1}{2} w^2 + dh. \quad (1.31)$$

The energy equation is identical with Eq. (1.29). From the combination with the work equation it follows

$$dh = \frac{1}{\rho} dp + dq_{irr}.$$

The latter equation demonstrates that the loss-free part of the enthalpy increase due to the work done corresponds to a pressure increase.

The term $(u_2^2 - u_1^2) / 2$ is the enthalpy increase corresponding to the pressure increase generated by the centrifugal force. It is obvious that the centrifugal force generates this term by the work of the centrifugal force $d \frac{1}{2} u^2$ in the work equation (1.30). From the same equation it follows that the term $(w_1^2 - w_2^2) / 2$, infinitesimally $-d \frac{1}{2} w^2$, is the enthalpy increase corresponding to the pressure increase due to flow deceleration.

For a further clarification, we directly derive the pressure force associated to the centrifugal force (equal and opposite) as

$$-\frac{1}{\rho} \nabla p = -\Omega^2 \vec{r} \quad \text{or} \quad \frac{1}{\rho} \frac{dp}{dr} = \Omega^2 r.$$

Thus:
$$\frac{1}{\rho} dp = \Omega^2 r dr = \Omega^2 d \frac{r^2}{2} = d \frac{u^2}{2}.$$

The enthalpy increase corresponding to the pressure increase by the centrifugal force constitutes a total differential and so may be integrated from the rotor inlet to the rotor outlet, along an arbitrary path. This means that pressure increase by the centrifugal force is flow-independent and not loss-loaded. The basic reason is, as already discussed, that a potential energy is associated to the centrifugal force. The pressure field associated to the centrifugal force is thus actually static in the rotating frame. It is completely similar to the pressure field associated to the gravity force. The loss term in the work equation (1.30) is associated to the conversion of kinetic energy into enthalpy, with flow deceleration. Conversion of kinetic energy into enthalpy, which is denominated *diffusion*, is thus a process liable to losses.

1.5.5 Rotor Work in the Mean Line Representation of the Flow

It was assumed in the previous section that the expression for the rotor work (1.24), derived from a momentum balance, can be applied directly in the work and energy

equations for an average streamline through the rotor. We thus assume that the active forces, exerted to the flow by the material parts, on average intervene as represented in Fig. 1.5. This means that the work done per time unit may be considered as the scalar product of the average force and the average flow velocity. This does not follow from the reasoning with the moment of momentum balance. By applying the control volume, we need not pronounce judgment upon the details of the internal forces. We spontaneously have no objections against the use of the work expressed by (1.24) in the work equation (1.5) and the energy equation (1.6) on the basis of the fundamental laws of thermodynamics. It will be verified in Chap. 2 that the representation of the work done in Fig. 1.5 is correct for an axial machine. This verification is less feasible for a more general machine. It requires three-dimensional formulation of the conservation laws.

1.6 Energy Analysis of Turbomachines

In an energy analysis, we write work or energy balances between successive stations in a machine and we define efficiencies.

1.6.1 Mechanical Efficiency and Internal Efficiency

For a work receiving machine, the work transfer from the shaft to the fluid side of the rotor is expressed by Eq. (1.19). The efficiency of this transfer is called the *mechanical efficiency*, defined as

$$\eta_m = \frac{\Delta W}{\Delta W_{shaft}}.$$

For a work delivering machine, the work transfer from the fluid side of the rotor to the shaft is expressed by Eq. (1.20). The efficiency of the transfer, also called the mechanical efficiency, is defined as

$$\eta_m = \frac{-\Delta W_{shaft}}{-\Delta W}.$$

Up to now, the difference between the shaft work and the rotor work is the dissipation by wheel friction (q_{irr}^o), outside the flow path. In practice, shaft work is measured at the flange of the driving motor or the driven load. This means that dissipation by friction in the bearings of the shaft and the seals at the passage of the shaft through the casing are included in the definition of the mechanical efficiency.

For a work receiving machine (pump), the relation between the rotor work and the increase of the mechanical energy in the fluid (the head) may be written as

$$\Delta W = \Delta E_m + q_{irr}.$$

Here, q_{irr} is the dissipation inside the flow. The efficiency of the conversion of the rotor work (work done by the rotor on the flow) into mechanical energy increase in the fluid is called *internal efficiency*, defined as

$$\eta_i = \frac{\Delta E_m}{\Delta W}.$$

The work equation for a work delivering machine is

$$-\Delta W = -\Delta E_m - q_{irr} \quad \text{or} \quad -\Delta E_m = -\Delta W + q_{irr}$$

The internal efficiency is the ratio of the rotor work (work done by the flow on the rotor) to the mechanical energy extracted from the flow, so that

$$\eta_i = \frac{-\Delta W}{-\Delta E_m} = \frac{|\Delta W|}{|\Delta E_m|}.$$

The terminology comes from an interpretation of the heating of the fluid by the dissipation mechanisms. In simplified turbomachine analyses, heat generated outside the fluid path by wheel friction, friction in bearings and seals is supposed to be transferred to the surroundings. Heat generated internally by friction is supposed to stay in the fluid. This means that the flow, not the machine, is considered to be adiabatic (except when there is explicit heat exchange between the flow and the surroundings, as in a cooled turbine part of a gas turbine; see Chap. 11). From now on, this simplification will be assumed. The energy equation is then noted as

$$\Delta W = \Delta \left(e + \frac{1}{2} v^2 + \frac{p}{\rho} + U \right). \quad (1.32)$$

Because of the assumption of adiabatic flow, we consider q_{irr}^o as a *mechanical loss*. This means a loss with removal to the surroundings of the heat produced by the dissipation. A loss with the heat by dissipation absorbed by the fluid is called a *thermodynamic loss* or an *internal loss*. We remark that the definitions of mechanical and internal efficiencies stay valid with another interpretation of heating due to dissipation. The interpretation only influences the writing of the energy equation (1.32).

1.6.2 Energy Analysis of an Axial Hydraulic Turbine

Figure 1.9 sketches mean streamlines in the flow through an axial hydraulic turbine.

Inlet: $0 \rightarrow 1$

Absolute frame (no work): $0 = d \frac{1}{2} v^2 + \frac{1}{\rho} dp + dU + dq_{irr}.$

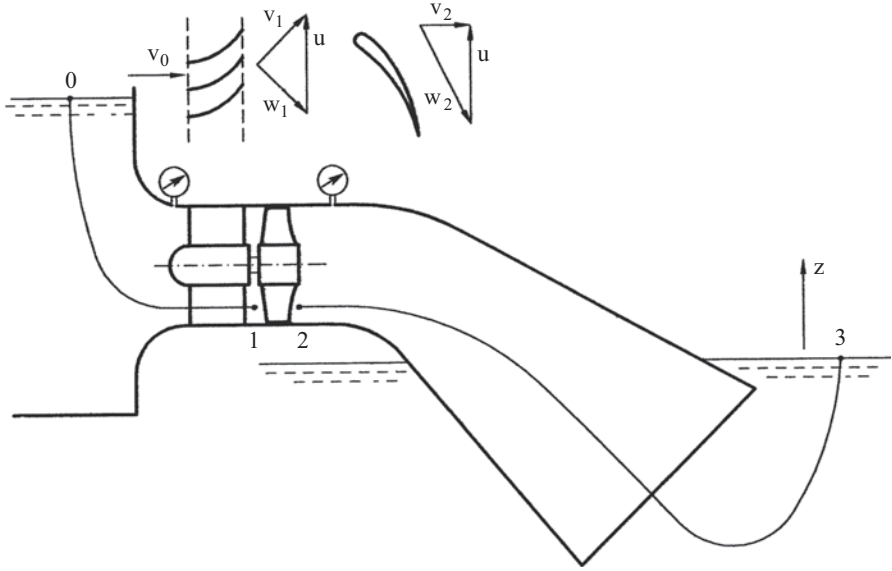


Fig. 1.9 Energy analysis of an axial hydraulic turbine

So

$$\frac{v_1^2}{2} - 0 + \frac{p_1 - p_a}{\rho} + gz_1 - gz_0 + q_{irr01} = 0,$$

or

$$g(z_0 - z_1) = \frac{v_1^2}{2} + \frac{p_1 - p_a}{\rho} + q_{irr01}.$$

The gravitational potential energy consumed is converted into kinetic energy and pressure energy, with losses. The inlet supplies the kinetic energy and pressure energy to the rotor.

Rotor: $1 \rightarrow 2$

In the absolute frame: $dW = d \frac{1}{2} v^2 + \frac{1}{\rho} dp + dU + dq_{irr}$.

So

$$\Delta W = \frac{v_2^2 - v_1^2}{2} + \frac{p_2 - p_1}{\rho} + q_{irr12},$$

or

$$\frac{v_1^2 - v_2^2}{2} + \frac{p_1 - p_2}{\rho} = -\Delta W + q_{irr12}.$$

Kinetic energy and pressure energy (= mechanical energy) are consumed in the flow in order to generate mechanical energy on the rotor ($-\Delta W$), with losses. Kinetic

energy consumption is visible in the velocity triangles ($v_1 > v_2$). The consumption of pressure energy follows from the work equation in the relative frame:

$$0 = d \frac{1}{2} w^2 + \frac{1}{\rho} dp + dq_{irr}.$$

So
$$\frac{w_2^2 - w_1^2}{2} + \frac{p_2 - p_1}{\rho} + q_{irr12} = 0,$$

or
$$\frac{p_1 - p_2}{\rho} = \frac{w_2^2 - w_1^2}{2} + q_{irr12}.$$

The relative flow accelerates ($w_2 > w_1$). Kinetic energy generation in the relative flow corresponds to pressure energy consumption.

Obviously, we also find

$$-\Delta W = \frac{v_1^2 - v_2^2}{2} + \frac{w_2^2 - w_1^2}{2}.$$

The work due to kinetic energy consumption in the absolute frame is termed the *action part*. The work generated by the acceleration of the relative flow is called the *reaction part*. The reaction part corresponds to the static enthalpy decrease: $h_1 - h_2$ (h_{0r} = constant in adiabatic flow for $u_1 = u_2$). The work done on the rotor equals the total enthalpy decrease in the flow: $h_{01} - h_{02}$ (in adiabatic flow).

The *degree of reaction* is defined as

$$R = \frac{h_1 - h_2}{h_{01} - h_{02}}, \quad (1.33)$$

with
$$h_1 - h_2 = \frac{w_2^2 - w_1^2}{2} \text{ and } h_{01} - h_{02} = \frac{v_1^2 - v_2^2}{2} + \frac{w_2^2 - w_1^2}{2}.$$

The action-reaction terminology results from the observation that a flow, in principle, may exert force on an object in two ways: by turning of the flow with constant relative velocity (*action*) and by acceleration of the flow (*reaction*), according to the sketches in Fig. 1.10. The right-hand sketch suggests the propulsion of a rocket, assuming that velocity w may be generated from an internal energy source. The velocity triangles and blade shapes with pure action ($R = 0$) and by a 50 % degree of reaction ($R = 0.5$) are sketched in Fig. 1.11, as they occur in steam turbines.

It is obvious from Fig. 1.11 that the value of the degree of reaction has a very strong influence on the shape of the velocity triangles and the rotor blade shape. In other words, the degree of reaction is a *kinematic parameter*. The effect of the choice of the degree of reaction will further be discussed at several occasions.

Draught tube: 2 → 3

Absolute frame (no work):
$$0 = d \frac{1}{2} v^2 + \frac{1}{\rho} dp + dU + dq_{irr}.$$

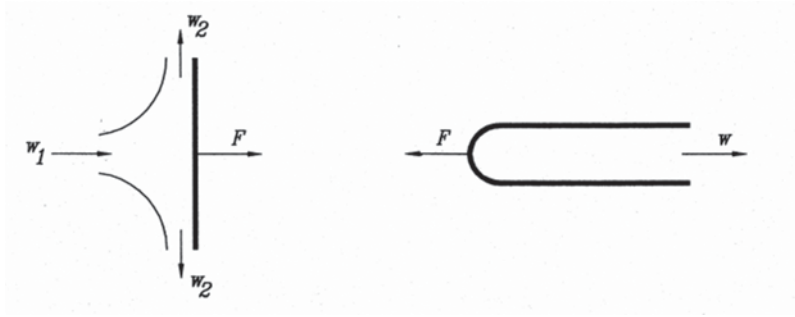


Fig. 1.10 Force by action ($w_1 = w_2$) and reaction ($Dw > 0$)

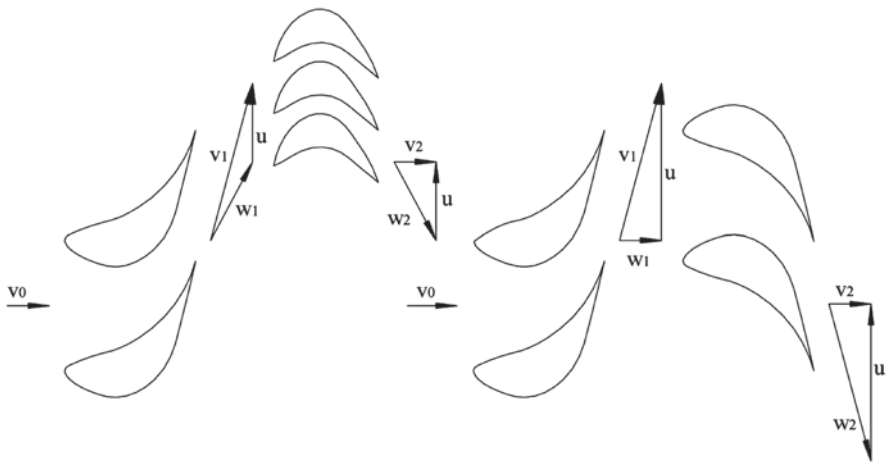


Fig. 1.11 Velocity triangles at $R = 0$ ($w_1 = w_2$) and $R = 0.5$ ($w_2 = v_1$; $v_2 = w_1$) in steam turbines

So

$$0 - \frac{v_2^2}{2} + \frac{p_a - p_2}{\rho} + g(z_3 - z_2) + q_{irr23} = 0.$$

or

$$\frac{v_2^2}{2} + g(z_2 - z_3) = \frac{p_a - p_2}{\rho} + q_{irr23}.$$

The kinetic energy and the potential energy available at the rotor outlet are used to produce pressure decrease behind the rotor and to increase in this way the pressure difference over the rotor.

The resulting three work equations are:

$$g(z_0 - z_l) = \frac{v_l^2}{2} + \frac{p_l - p_a}{\rho} + q_{irr0l},$$

$$\frac{v_1^2 - v_2^2}{2} + \frac{p_1 - p_2}{\rho} = |\Delta W| + q_{irr12},$$

$$\frac{v_2^2}{2} + g(z_2 - z_3) = \frac{p_a - p_2}{\rho} + q_{irr23}.$$

The sum is $g(z_0 - z_3) = |\Delta W| + q_{irr03}.$

The internal efficiency of the whole installation is

$$\eta_i = \frac{|\Delta W|}{g(z_0 - z_3)}.$$

For each part of the turbine, an internal efficiency may be defined, as well as the internal efficiency of the whole turbine. The draught tube is typically considered as a turbine part, but the supply duct mostly is not. Especially with a very long supply duct, it is not advisable to account its losses to the turbine. The concept of *manometric head* is introduced for this purpose. Pressure is determined by a manometer at the turbine inlet (see Fig. 1.9). As mechanical energy at the disposal of the turbine is considered:

$$\frac{v_m^2}{2} + \frac{p_m - p_a}{\rho} + g(z_m - z_3),$$

with v_m the velocity at the position of the manometer, p_m the measured pressure and z_m the geometrical manometer height. The *manometric head* H_m is then

$$gH_m = \frac{v_m^2}{2} + \frac{p_m - p_a}{\rho} + g(z_m - z_3).$$

By the term head is meant the mechanical energy expressed as a height. The manometric head H_m is lower than the geometric head $z_0 - z_3$ due to losses in the supply duct, since

$$\frac{v_m^2}{2} + \frac{p_m - p_a}{\rho} + q_{irr0m} = g(z_0 - z_m).$$

The losses in the draught tube may also be taken out by defining the mechanical energy with a manometer at the outlet of the turbine (see Fig. 1.9).

1.6.3 Energy Analysis of an Axial Pump

Inlet: $0 \rightarrow 1$

Absolute frame (no work): $0 = d \frac{1}{2} v^2 + \frac{1}{\rho} dp + dU + dq_{irr}.$

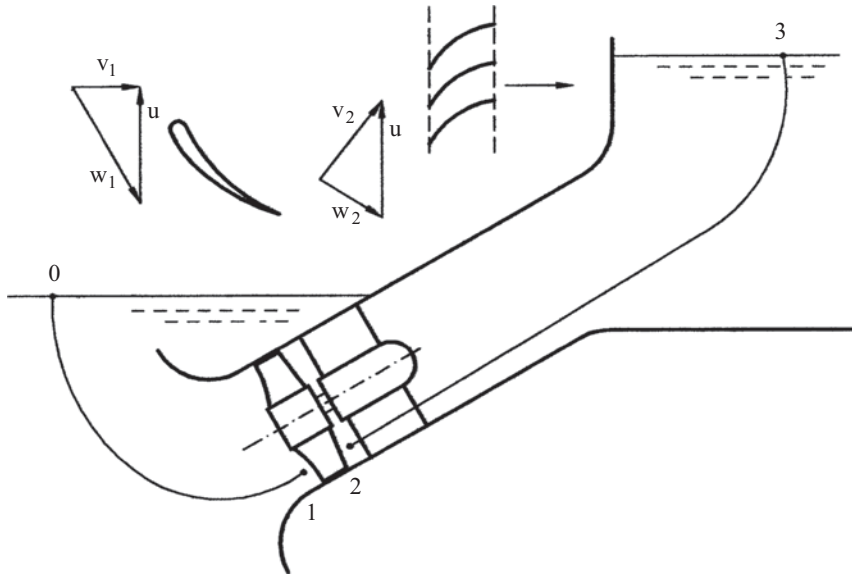


Fig. 1.12 Energy analysis of an axial pump

$$\text{So} \quad \frac{v_1^2}{2} - 0 + \frac{p_1 - p_a}{\rho} + g(z_1 - z_0) + q_{irr01} = 0,$$

$$\text{or} \quad g(z_0 - z_1) = \frac{v_1^2}{2} + \frac{p_1 - p_a}{\rho} + q_{irr01}.$$

As with the turbine, the gravitational potential energy consumed is converted into kinetic energy and pressure energy, with losses. Figure 1.12 shows a pump that is mounted below the suction level (submerged). If the pump is mounted above the suction level, with a suction pipe, $g(z_0 - z_1)$ is negative. The above expression may then be better written as

$$\frac{p_a - p_1}{\rho} = g(z_1 - z_0) + \frac{v_1^2}{2} + q_{irr01}.$$

The interpretation is then that the suction height is overcome due to pressure lowering at the suction side of the pump and that kinetic energy is generated, with losses.

Rotor: 1 → 2

$$\text{In the absolute frame: } dW = d \frac{1}{2} v^2 + \frac{1}{\rho} dp + dU + dq_{irr}.$$

$$\text{So} \quad \Delta W = \frac{v_2^2 - v_1^2}{2} + \frac{p_2 - p_1}{\rho} + q_{irr12}.$$

The work done on the fluid results into mechanical energy increase, with losses.

In the relative frame:
$$\frac{w_2^2 - w_1^2}{2} + \frac{p_2 - p_1}{\rho} + q_{irr12} = 0.$$

The kinetic energy increase in the absolute frame is visible in the velocity triangles. The pressure increase follows from the kinetic energy decrease in the relative frame.

It follows as well that
$$\Delta W = \frac{v_2^2 - v_1^2}{2} + \frac{w_1^2 - w_2^2}{2}.$$

The first part of the expression is the action part, the second one the reaction part. The work done equals the total enthalpy increase (in adiabatic flow). The reaction part of the work equals the static enthalpy increase (in adiabatic flow).

The degree of reaction is

$$R = \frac{h_2 - h_1}{h_{02} - h_{01}}.$$

Guide ring and delivery pipe: 2 → 3

In the absolute frame:
$$0 = d \frac{1}{2} v^2 + \frac{1}{\rho} dp + dU + dq_{irr}.$$

So
$$0 = 0 - \frac{v_2^2}{2} + \frac{p_a - p_2}{\rho} + g(z_3 - z_2) + q_{irr23},$$

or
$$\frac{v_2^2}{2} + \frac{p_2 - p_a}{\rho} = g(z_3 - z_2) + q_{irr23}.$$

The kinetic energy and the pressure energy available downstream of the rotor are converted, with losses, into increase of gravitational potential energy.

Addition of the three relations results in

$$\Delta W + g(z_0 - z_1) = g(z_3 - z_2) + q_{irr03},$$

or
$$\Delta W = g(z_3 - z_0) + q_{irr03}.$$

The internal efficiency of the whole installation is

$$\eta_i = \frac{g(z_3 - z_0)}{\Delta W}.$$

The losses in the pipes connected to the pump can be taken out of the definition by placing manometers at the inlet and outlet of the pump and by determining the manometric head. In the example of Fig. 1.12, the inlet is mostly considered as part of the pump. If two manometers are mounted, the *manometric head of the pump* H_m is determined by

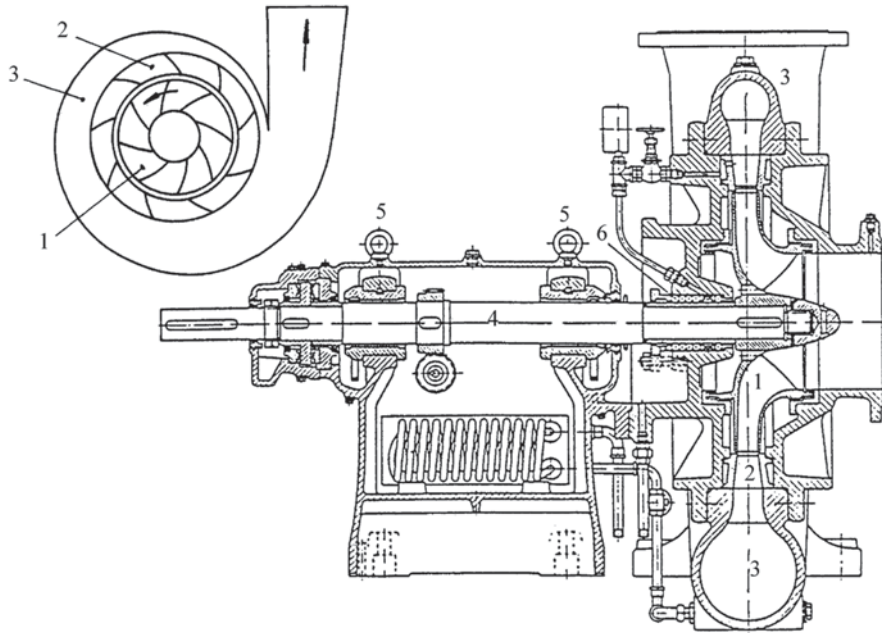


Fig. 1.13 Centrifugal pump (classical example)

$$gH_m = \frac{v_d^2 - v_s^2}{2} + \frac{p_d - p_s}{\rho} + g(z_d - z_s).$$

The subscripts *d* and *s* refer to the *discharge*/delivery and *suction* sides of the pump. The term manometric head denotes the mechanical energy rise by the pump, expressed as a height. Mostly, the term discharge side is used to denote the side by which the pump delivers the fluid. Similarly, the term *discharge pipe* is used. We will follow this practise.

1.7 Examples of Radial Turbomachines

In order to gain insight in the working principle of radial machines, we discuss two examples, first a centrifugal pump. Figure 1.13 shows the meridional section of a pump and sketches the section with the mean circumferential streamsurface. Figure 1.14 sketches the velocity triangles at the rotor inlet and outlet. The rotor is mounted in overhung to the shaft (4). With this type, the rotor suction side is free, allowing an axial water intake. Flow is turned into the radial direction within the rotor (1). There is a diffuser ring (2) and a collector (3). Further components are the bearings (5: here: sliding bearings) and the shaft seal (6: here: braided compression packing).

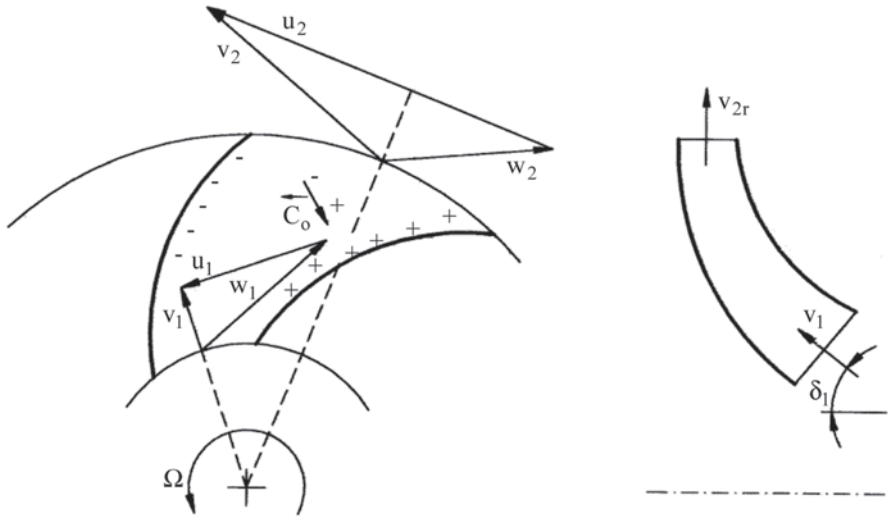


Fig. 1.14 Radial pump rotor with backward curved blades (drawn as $w_1 = w_2$)

At the rotor inlet, the absolute velocity v_1 has gained a component in the radial direction due to turning in the *suction eye* of the rotor. Theoretically, there is no component in the tangential direction, as no guide vanes have been passed through. In practice, flow is entrained upstream of the rotor blades in the suction eye, generating a small tangential component at the inlet. This is termed *spontaneous pre-swirl*. This pre-swirl does not decrease the rotor work, as it actually is caused by the torque of the rotor, influencing the upstream flow. Therefore, we draw the inlet triangle without pre-swirl. No axial velocity component is present anymore at the rotor outlet. In the example drawn, the blades at the rotor outlet are rather strongly leaning backward, compared to the rotation sense of the rotor and with an angle nearly the same as at the inlet. This rotor blade shape typically is described as *backward curved*. Within the radial rotor part, blades are straight in the axial direction. Due to the diagonal flow direction, there is some blade bending in the direction perpendicular to the mean streamsurface within the inlet part. In the mean line analysis, blade curvature perpendicular to the average streamsurface does not intervene.

The Coriolis force is $\vec{C_o} = -2 \vec{\Omega} \times \vec{w}$. The sense is as indicated in the figure. A pressure difference across a blade channel corresponds to the Coriolis force, as indicated. This generates blade forces with tangential component directed against the sense of rotation, thus causing energy transfer from the rotor to the flow. In the expression (1.25), the rotor work is $\Delta W = u_2^2 - u_1^2 + u_2 w_{2u} - u_1 w_{1u}$. The $u_2^2 - u_1^2$ part originates from the Coriolis force and is always positive for flow in centrifugal sense through the rotor ($u_2 > u_1$). The $u_2 w_{2u} - u_1 w_{1u}$ part is produced by turning of the flow, thus by lift, and may be positive or negative, dependent on the blade shape. In the example drawn, the lift term is negative ($u_2 w_{2u}$ being more negative than $u_1 w_{1u}$). In principle, the lift works in the adverse sense, as the work associated

lies in the turbine sense. To make the lift term less negative, the blades at the rotor outlet should be leaning less far backward. With a meridional velocity component, as drawn, this implies that diffusion then has to be built in ($w_2 < w_1$). It is impossible however to achieve strong deceleration in a diverging channel of limited length. As will be discussed in Chap. 2, a velocity ratio amounting to about 0.7 may be reached within optimal, stationary diffusers of limited length, i.e. about half of the kinetic energy at the inlet may be converted into pressure energy. Due to disadvantageous channel shapes within rotors, to strong changes of the shape of the cross-section and to rotation effects, the velocity ratio w_2/w_1 cannot be less than about 0.8–0.9; with as a consequence that lift cannot intervene in the pump sense. The functioning is thus essentially based on Coriolis force. The rotor has to be considered as consisting of rotating channels. The blades do not function as lifting objects.

The rotor work may also be written as

$$\Delta W = \frac{u_2^2 - u_1^2}{2} + \frac{v_2^2 - v_1^2}{2} + \frac{w_1^2 - w_2^2}{2}.$$

The term in the relative kinetic energies is not very significant in the sum. The centrifugal term corresponds to a pressure increase. As a pump is intended to increase pressure, the kinetic energy at the rotor outlet $\frac{1}{2}v_2^2$ has to be converted into pressure energy by reducing it to the kinetic energy level at the inlet $\frac{1}{2}v_1^2$. This may be achieved by a diffuser immediately downstream of the rotor. In the example of Fig. 1.13, this is an annular bladed diffuser, in which the velocity v_2 is forced towards the radial direction (tangential component decreases). Also the radial velocity component decreases due to the increase in radius and axial width. Downstream of the diffuser follows a collector in the shape of a spiral. Such a collector is mostly called a *volute*. At this stage, principal understanding of the role of the stator components downstream of the rotor is sufficient. These components will be discussed with more detail in the chapter on pumps (Chap. 8).

There is a means, despite the limitation on the rotor deceleration ($w_2/w_1 > 0.8\text{--}0.9$), to realise a positive work contribution by the lift, namely by curving the blades strongly forward at the rotor outlet, as sketched in Fig. 1.15. The term $u_2 w_{2u} - u_1 w_{1u}$ then becomes highly positive. With *backward curved* blades, work amounts to $\Delta W = u_2 v_{2u} \approx \frac{1}{2}u_2^2$ (Fig. 1.14), whereas work amounts to $\Delta W = u_2 v_{2u} \approx \frac{3}{2}u_2^2$ ($u_2 \approx 2u_1$) to $2u_2^2$ ($u_2 \approx u_1$) with *forward curved* blades. Forward curved blades generate a high kinetic energy at the outlet of the rotor. The consequence is that reduction of the velocity v_2 to the level of the velocity v_1 without significant energy dissipation is impossible. The machine, in principle, only makes sense if intended to generate velocity, in other words as a fan. This fan type will be discussed further in the chapter on fans (Chap. 3). A fan may also be designed in the way of a centrifugal pump, i.e. with backward curved blades. In that case, the machine mainly realises pressure increase and less kinetic energy increase. Such a fan is required to feed extended piping systems, in which significant losses occur. There also exist rotor shapes in between those shown in Figs. 1.14 and 1.15 (see Chap. 3).

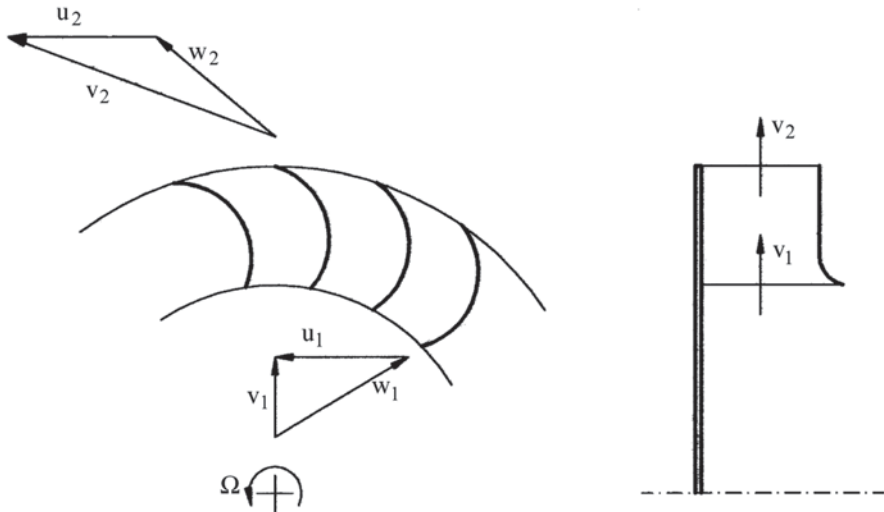


Fig. 1.15 Radial fan rotor with forward curved blades (drawn is $w_1 = w_2$)

1.8 Performance Characteristics

By a *performance characteristic* is meant a relationship between two operation quantities, such as flow rate, manometric head, power, etc., with constant other quantities. In principle, many such relations can be defined. In practice however, only a few are relevant.

With a hydraulic turbine, normally, the head is constant. The same applies to rotational speed, as the turbine typically drives a generator with a fixed rotational speed. With a constant geometry, this machine does not have any variable operation quantities. At a fixed head and rotational speed, the flow rate and power can only be varied by changing the rotor blade pitch angle (the angle of the blade chord with respect to the meridional plane) of an axial turbine (see Fig. 1.1). A characteristic may thus be: the power as a function of the rotor blade pitch angle at a constant rotational speed and a constant head.

With a pump, the rotational speed is set by the driving motor. The load is typically a piping system filling a reservoir under pressure (see Fig. 1.16). The pressure within the reservoir is variable, for instance due to the presence of an air-filled bag. With an installation for household use, it is normal to vary the reservoir pressure between 1.5 and 3 bar. A pressure sensor starts the pump when the pressure falls under the set minimum (1.5 bar) and stops the pump when pressure exceeds the maximum (3 bar). The pump thus functions at a variable manometric head. The change of manometric head affects the flow rate. The characteristic of a pump is thus normally understood to mean the relation between manometric head and flow rate at a constant rotational speed.

The form of this relation may easily be derived from the rotor work. As an example, we take the centrifugal pump in Fig. 1.14. Assume that the velocity

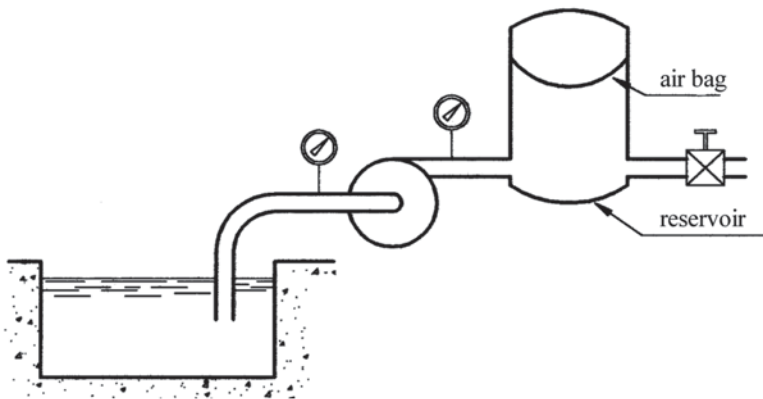


Fig. 1.16 Pump with reservoir under variable pressure

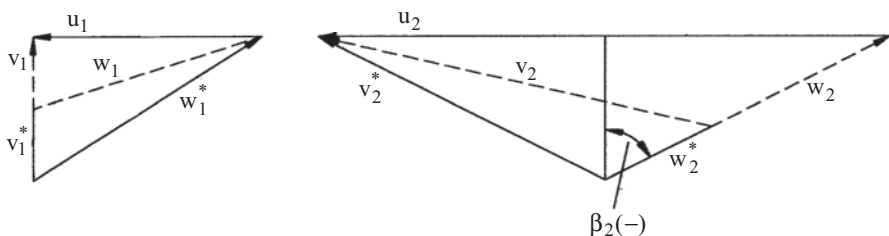


Fig. 1.17 Change of velocity triangles by flow rate decrease in a centrifugal pump; full line: design*; dashed line: decreased flow rate

triangles drawn correspond to the design flow rate. This means that w_1 is tangent to the inlet side of the rotor blades and that v_2 is tangent to the inlet side of the diffuser vanes. In that case, no inlet incidence is said to occur at the rotor and stator components. When the pump flow rate is decreased e.g. by applying a constriction to the discharge pipe, velocity triangles change as drawn in Fig. 1.17.

With decreased flow rate, the rotor work is still $u_2 v_{2u}$, with $v_{2u} = u_2 + w_{2u}$ and $\tan \beta_2 = w_{2u} / v_{2r}$ ($w_{2u} < 0$, $\beta_2 < 0$). The flow rate is proportional to v_{2r} . The relation between work and flow rate thus has the form

$$\Delta W = u_2^2 + k \tan \beta_2 Q, \quad (1.34)$$

with k being a positive constant. The relation is a descending straight line. The mechanical energy rise in the fluid is smaller than the rotor work, due to friction losses (approximately proportional to Q^2) and incidence losses. At a flow rate different from the design flow rate Q^* , the relative inlet velocity of the rotor (w_1) and the absolute inlet velocity of the diffuser (v_2) are no longer tangent to the blades or vanes. This generates a loss proportional to $(Q - Q^*)^2$ (see Chap. 3). The manometric head may be derived from the rotor work, in principle, as sketched in Fig. 1.18. The

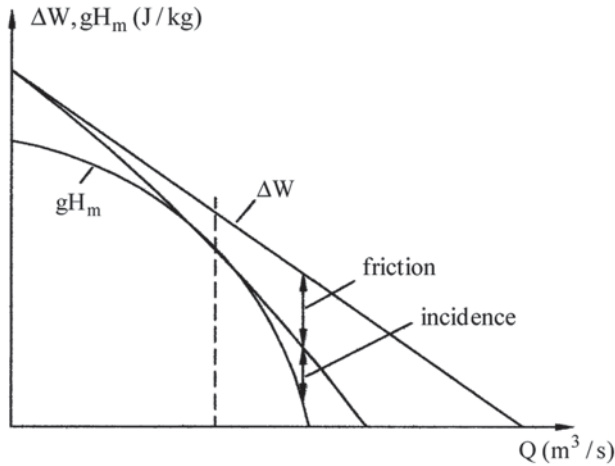


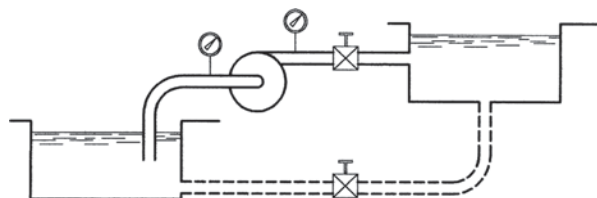
Fig. 1.18 Characteristic of a centrifugal pump (backward curved rotor blades); $\Omega = \text{constant}$

characteristic is a curve with an approximate parabolic form. The correct determination of the characteristic is somewhat more complex than sketched in Fig. 1.18, as the flow does not exactly follow the blades at the rotor outlet. So-called slip occurs. The relationship between work and flow rate therefore deviates somewhat from the purely geometrically determined relation (1.34). The slip phenomenon will be discussed in Chap. 3. The above approximate reasoning should provisionally suffice to understand that there is a functional relationship between head and flow rate.

It is common practice to consider flow rate as an independent quantity and head as a dependent one. This option is due to the common method for experimental determination of the characteristic (Fig. 1.19). The pump displaces fluid from a suction reservoir to a discharge reservoir. A valve is mounted onto the discharge pipe. Manometers are placed at the suction and discharge sides of the pump. Operation of the valve at first suggests flow rate control. The manometer readings change by this as well, of course. The manometric head is determined from these readings. A flow rate meter may be mounted additionally in the pipe for flow rate measurement. A more classic approach consists of flow rate determination by the level increase in the discharge reservoir, with a closed return pipe.

It is typical that, with a work receiving machine, the relationship between the mechanical energy rise and the flow rate at a constant rotational speed is a descend-

Fig. 1.19 Determination of a pump characteristic (used in Chap. 5)



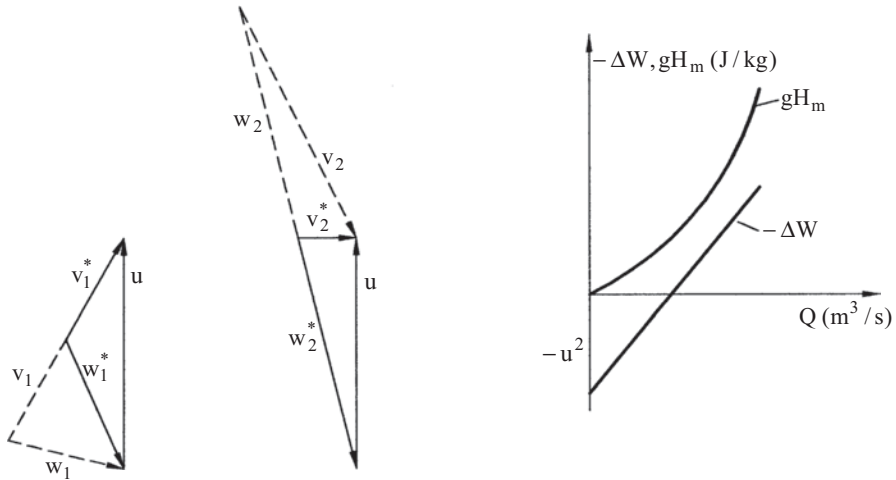


Fig. 1.20 Change of the velocity triangles with flow rate increase in an axial hydraulic turbine; full line: design (*); dashed line: increased flow rate; turbine characteristic: flow rate depending on head with constant rotational speed and constant geometry

ing curve. Figure 1.12 (axial pump) demonstrates that v_{2u} increases with flow rate decrease. The characteristic of the axial pump is thus similar to that of the centrifugal pump with backward curved rotor blades.

From a didactical point of view (not really from a practical one), it is interesting to derive the dependence of head on flow rate for a hydraulic turbine. Figure 1.20 shows the velocity triangles for the design flow rate and with flow rate increase (by increasing the head) for an axial hydraulic turbine as sketched in Fig. 1.9.

In Fig. 1.20 we notice (* indicates the design flow rate):

$$v_{lu} = v_{lu}^* \left(\frac{Q}{Q^*} \right) \quad ; \quad v_{lu} > 0,$$

$$w_{2u} = w_{2u}^* \left(\frac{Q}{Q^*} \right) \quad ; \quad w_{2u} < 0 \quad ; \quad w_{2u}^* = -u \quad ; \quad v_{2u} = u + w_{2u}.$$

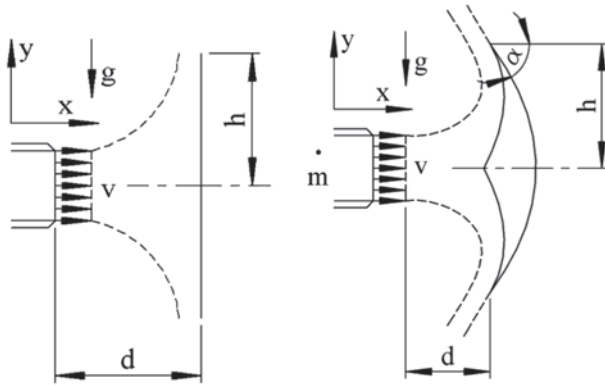
Rotor work is

$$-\Delta W = (v_{lu} - v_{2u})u = \left[v_{lu}^* \left(\frac{Q}{Q^*} \right) - u + u \left(\frac{Q}{Q^*} \right) \right] u = (v_{lu}^* + u)u \left(\frac{Q}{Q^*} \right) - u^2.$$

Figure 1.20 sketches the work and the head. The work increases linearly with the flow rate. Due to friction losses and incidence losses, the energy extracted from the flow exceeds the rotor work. The observation is that the head increases with the flow rate. Of course, a more convenient reading of the graph is saying that the flow rate increases with the head.

1.9 Exercises

1.9.1 The left figure shows a liquid jet impacting a plate perpendicularly in an open space. Use a momentum balance to determine the force on the plate in the direction of the oncoming flow. Assume that the flow, after turning, perfectly follows the plate. Assume steady flow and ignore friction. Consider gravity perpendicular to the jet, as indicated. Use a momentum balance to determine the force on the plate in the vertical direction. Note that the force approximately equals zero. Verify if the result is independent of the size of the chosen control volume. Reason that the force into the vertical direction exactly equals zero in the absence of friction on the plate.



The right figure shows a liquid jet impacting the blade of a Pelton turbine (tangential hydraulic turbine, see Chap. 9). The blade has the shape of a double spoon. The jet leaves the blade with the indicated angle α .

Determine first the force exerted on the blade into the direction of the jet when the blade stands still and assuming that gravity is perpendicular to the figure, i.e. not as indicated in the figure. Determine then the force components in vertical and horizontal directions exerted on the blade assuming that gravity is as indicated in the figure. Verify if the result is independent of the size of the chosen control volume. Note that the force in the vertical direction is very weak. May we conclude that the force exactly equals zero?

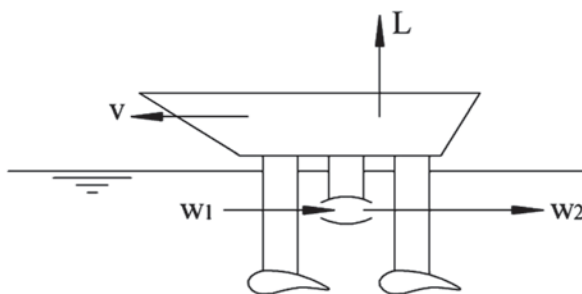
A: I: $F_x = \dot{m}v$, $F_y = -\rho gAL$, with $L \approx d - h \approx 0$.

II: $F_x = \dot{m}v(1 + \cos \alpha)$; $F_x \approx \dot{m}v(1 + \cos \alpha)$, $F_y = -\rho gAL$, with

$$L \approx d + \frac{h}{\sin \alpha} - 2h \sin \alpha.$$

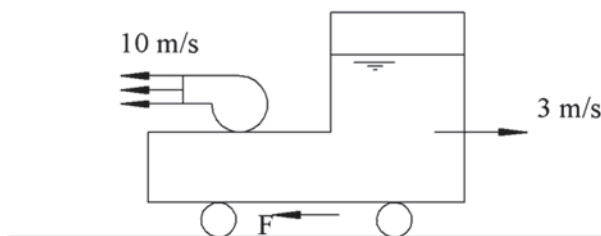
1.9.2 The figure is a sketch of a hydrofoil boat with speed $v = 20$ m/s. The mass of the boat is 100 t. The foils that keep the vessel above the surface have a lift/drag ratio $L/D = 20$. Water is sucked in by a pump and ejected through a nozzle at 45 m/s relative to the boat. Determine the mass flow rate to be handled by the

pump, ignoring the air friction on the vessel. What power should (theoretically) be supplied to the pump (i.e. ignoring losses in the pump)? What is the useful propulsive power supplied to the vessel by the jet (force times speed of the vessel)? Note that this power differs from the pump power. Explain the difference by the kinetic energy dissipated behind the vessel. Reason first with a control volume attached to the boat, i.e. in a relative frame. This is the easiest to do. Verify that the result is the same for a control volume in the absolute frame.



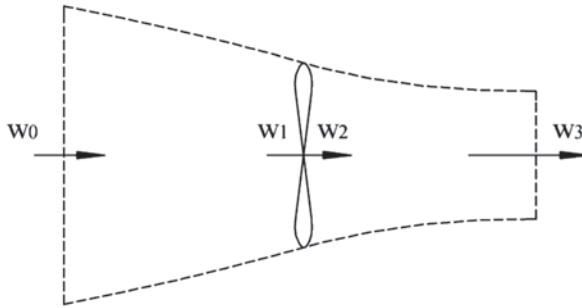
A: $P_{\text{pump}} = 1594 \text{ kW}$, $P_{\text{propulsion}} = 981 \text{ kW}$, $P_{\text{residual}} = 613 \text{ kW}$.

1.9.3 The figure shows a trolley with a water tank. The trolley moves at 3 m/s. The driving force is generated by a pump sucking water from the tank and ejecting it with a 10 m/s speed relative to the whole of the trolley, the tank and the pump, the flow rate being 2 m³/s. Determine the force exerted by the rolling resistance and the air resistance onto the trolley. Check if the same result is obtained with a control volume in the relative frame and in the absolute frame.



A: $F = 20 \text{ kN}$.

1.9.4 The figure sketches the flow through an aircraft propeller. Assume that the flying speed is 75 m/s and that the propeller accelerates the air to 120 m/s relative to the aircraft. Determine the thrust generated per m² frontal propeller area, assuming a uniform flow through the propeller. Determine, as in Exercise 1.9.2, the power to be supplied theoretically to the propeller, the useful power and the difference between them. Ignore post-swirl actually generated by the work done by the propeller on the air. Is there a substantial difference with the findings concerning the jet-propelled hydrofoil in Exercise 1.9.2? (A similar problem for a wind turbine is discussed in Chap. 10).

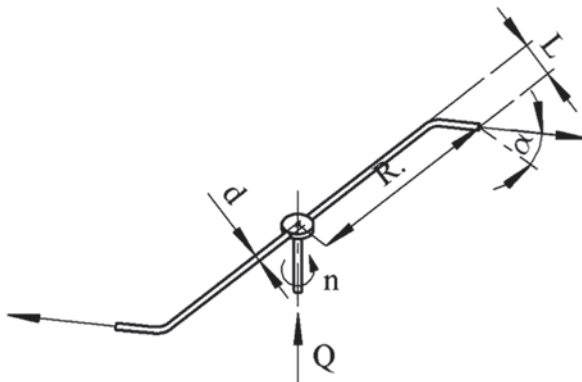


A: $P_{shaft} = 513 \text{ kW}$, $P_{propulsion} = 395 \text{ kW}$, $P_{residual} = 118 \text{ kW}$.

1.9.5 Consider the Pelton turbine of Exercise 1.9.1 once more. Determine the force exerted on the blade in the jet direction, if the blade runs with velocity $v/2$ and velocity v with respect to the nozzle. Derive the dependence of the force on the speed. Determine the power exchanged as a function of the speed. At which speed does the power attain its maximum? Explain why the power does not equal the energy flux of the water jet.

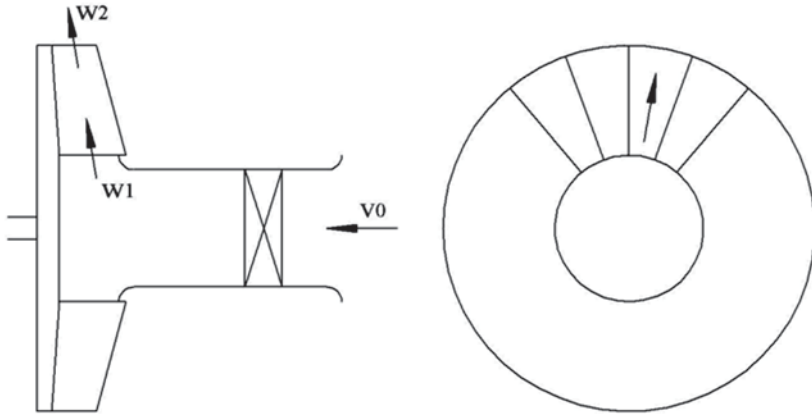
A: F_x is linearly decreasing with the blade speed, going from the force at stand still to zero for speed equal to the jet velocity. Power is at maximum at blade speed equal to half the jet velocity. The difference between the energy flux of the jet and the output power is the power associated with the kinetic energy dissipated into the atmosphere.

1.9.6 The figure shows a lawn sprinkler. The radius of the traced circle (R) is 150 mm. The diameter of the arm is 4 mm. The bent arm length (L) is 30 mm. The water spouts upward in a 30° angle to the horizontal plane. The water flow rate is 7.5 litres/min. Rotational speed amounts to 30 rpm. Determine the friction torque exerted to the lawn sprinkler shaft. Firstly, reason in the absolute frame. Then, verify the result in the relative frame. Note that the moment of the Coriolis force on the flow through the arms should be taken into account in the relative frame. What does the rotational speed become if the friction torque were halved?

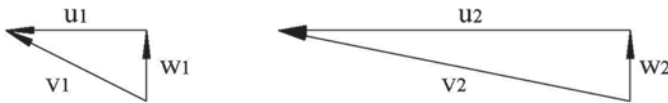


A: $M_{friction} = 71.66 \text{ Nmm}$, $n_{new} = 148.1 \text{ rpm}$.

1.9.7 The figure sketches an extraction fan with radial blades. The sucked flow gets pre-swirl by a guide vane ring, so that the flow entering the rotor is tangent to the blades. Inlet and outlet width are such that the relative velocity within the rotor is constant. Determine the formula for work done on the flow. What is the part of the kinetic energy increase and of the enthalpy increase? What is the degree of reaction? The fan is intended to remove air through the suction pipe. The velocity in the pipe generates a pressure drop. Sketch the pressure evolution through the suction pipe and the fan. Derive the required pressure rise over the fan from a pressure balance. Ignore friction losses. Analyse that there are two essential loss mechanisms with the considered application: one at the rotor inlet and another at the rotor outlet. Derive from that how the rotor shape can be made more efficient. Consider a rotor with constant meridional velocity and constant relative velocity (no internal diffusion).



A: The figure sketches the velocity triangles at the rotor inlet and the rotor outlet.



$$\Delta W = u_2 v_{2u} - u_1 v_{1u} = u_2^2 - u_1^2,$$

$$\Delta E_k = \frac{v_2^2}{2} - \frac{v_1^2}{2} = \frac{u_2^2}{2} - \frac{u_1^2}{2}, \quad \Delta E_p = \frac{u_2^2}{2} - \frac{u_1^2}{2} + \frac{w_1^2}{2} - \frac{w_2^2}{2} = \frac{u_2^2}{2} - \frac{u_1^2}{2}.$$

So: $\Delta E_p = \Delta E_k$ and $R = 0.5$.

Pressure Balance A first pressure drop occurs due to the generation of the velocity in the suction pipe v_0 . The accompanying pressure drop is $\rho v_0^2 / 2$. The acceleration in the guide vanes generates an additional pressure drop $\rho v_1^2 / 2 - \rho v_0^2 / 2$. The pressure rise by the fan is $\rho u_2^2 / 2 - \rho u_1^2 / 2$. The fan has to raise the pressure to the atmospheric pressure.

The pressure balance is: $\Delta E_p = \frac{u_2^2}{2} - \frac{u_1^2}{2} = \frac{v_0^2}{2} + \frac{v_1^2}{2} - \frac{v_0^2}{2}$.

So:
$$\Delta W = \Delta E_p + \Delta E_k = \frac{v_0^2}{2} + \frac{v_1^2 - v_0^2}{2} + \frac{v_2^2 - v_1^2}{2} \quad (1.35)$$

The work consists of three terms in kinetic energy with sum $v_2^2 / 2$. The first term is the useful term. That is the work required to compensate the pressure drop due to the velocity generation within the suction pipe. The second term is the kinetic energy rise within the stator vane ring. This increase causes a second pressure drop to be compensated by the fan. The second term is useless. The third term is the kinetic energy increase within the rotor. This is also useless, as the fan ideally only should generate a pressure rise. All kinetic energy generated within the rotor causes a larger kinetic energy dissipated into the atmosphere downstream of the rotor. The useless terms in (1.35) may be eliminated or reduced by adapting the rotor inlet and outlet, as sketched below. The blade is leaned backward at the inlet, making the stator vane ring unnecessary. The blade is leaned backward at the outlet in order to decrease the outlet velocity in the absolute frame. Constant meridional velocity and constant relative velocity are assumed (no diffusion).



$$\Delta W = u_2 v_{2u} - u_1 v_{1u} = u_2 v_{2u} = u_2 (u_2 - u_1),$$

$$\Delta E_k = \frac{v_2^2}{2} - \frac{v_1^2}{2} = \frac{(u_2 - u_1)^2}{2}, \quad \Delta E_p = \frac{u_2^2 - u_1^2}{2} + \frac{w_1^2 - w_2^2}{2} = \frac{u_2^2 - u_1^2}{2}.$$

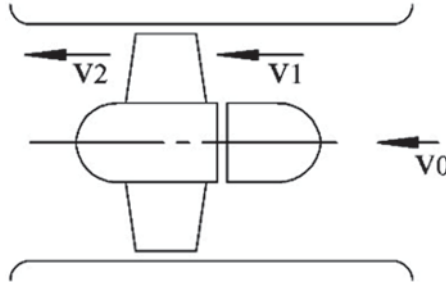
The pressure balance is now $\Delta E_p = \frac{u_2^2 - u_1^2}{2} = \frac{v_0^2}{2}$.

So:
$$\Delta W = \Delta E_p + \Delta E_k = \frac{v_0^2}{2} + \frac{(u_2 - u_1)^2}{2}. \quad (1.36)$$

The first term is the useful term once more in (1.36). The second term is the kinetic energy increase within the rotor. This term is not useful, but cannot be reduced to zero, due to the set conditions concerning constant meridional velocity and relative velocity. Expression (1.36) is obviously much more favourable than expression

(1.35). Work may further be reduced by incorporating diffusion into the rotor ($w_2 < w_1$) and by reducing the kinetic energy in a diffuser downstream of the rotor. Incorporating some diffusion into the rotor is easy and typically applied. A diffuser is a supplementary component and typically not implemented.

1.9.8 Consider the same problem as in the foregoing exercise, but with an axial fan, as sketched in the figure. Determine the power required for the application. Compare with the result from the foregoing exercise.



A: The figure sketches the velocity triangles at the inlet and the outlet. Note that, at constant meridional velocity, diffusion within the rotor necessarily occurs.



$$\Delta W = uv_{2u},$$

$$\Delta E_k = \frac{v_2^2}{2} - \frac{v_1^2}{2} = \frac{v_{2u}^2}{2}, \quad \Delta E_p = \frac{w_1^2}{2} - \frac{w_2^2}{2} = \frac{u^2}{2} - \frac{(u - v_{2u})^2}{2} = uv_{2u} - \frac{v_{2u}^2}{2}.$$

The pressure balance is $uv_{2u} - \frac{v_{2u}^2}{2} = \frac{v_1^2}{2}$.

So:

$$\Delta W = uv_{2u} = \frac{v_1^2}{2} + \frac{v_{2u}^2}{2}. \quad (1.37)$$

The first term in (1.37) is useful. The second term is the kinetic energy increase within the rotor, useless but unavoidable. We note that the expressions with the axial fan are not fundamentally different from those with the adapted radial fan in the foregoing exercise. Since with the radial fan $u_2 - u_1 = v_{2u}$, the expressions for ΔE_k and ΔW are in principle the same for both fans.

References

- Fister W (1984/1986) Fluidenergiemaschinen, Vol. 1/Vol. 2. Springer, ISBN 3-540-12864-6/3-540-15478-7
- Japikse D, Baines NC (1994) Introduction to turbomachinery. Oxford University Press, ISBN 0-933283-06-7
- Pleiderer C, Petermann H (1991) Strömungsmaschinen, 6th ed. Springer, ISBN 3-540-53037-1
- Vavra MH (1960) Aero-thermodynamics and flow in turbomachines. Wiley, no ISBN

Chapter 2

Basic Components

Abstract We learned in Chap. 1 that blades of axial machines have profiles resembling aircraft wing profiles (*aerofoils*). In machines with large spacing between blades, this resemblance is strong, as with the hydraulic turbines and pumps studied up to now. With axial compressors, gas and steam turbines, blades are positioned closer together. The blades also cause a larger flow turning. A circumferential section results in a row of blade profiles with tangential spacing comparable to, or smaller than, the largest profile dimension. We then apply the term blade row or *blade cascade*. Radial machine rotor blades principally do not function as lifting objects. The blades constitute *channels*. The blade profiles have no resemblance to aerofoils. Channel flows may be accelerating (turbines) or decelerating (pumps, fans, compressors). With decelerating or diffusion flows, avoidance of separation between flow and geometry is difficult. As we have already learned, *diffusers* also occur as stator components of turbines. Aerofoils, cascades, channels and diffusers constitute the basic components of turbomachines, which we study in this chapter.

2.1 Aerofoils

2.1.1 Force Generation

Figure 2.1 sketches the streamlines close to an aerofoil in an oncoming flow with uniform velocity v_∞ and fluid density ρ_∞ far upstream. The streamlines are intended to curve due to camber of the profile (curvature in the longitudinal direction) and due to incidence of the flow (angle difference between the oncoming flow and the profile). To grasp the effect of the curvature, the simplest is considering an observer moving along with a fluid particle. This observer then stands still relative to the flow. For the relative coordinate system with origin on the observer, with x-axis along the flow and y-axis perpendicular to it, a centrifugal force must then be introduced with a value v^2/R , perpendicular to the streamline, so along the y-axis, away from the centre of curvature (R is the radius of curvature). In the flow normal direction (y-axis) the momentum equals zero. Conservation of momentum thus means a balance of forces. This means that the centrifugal force must be kept in balance by a

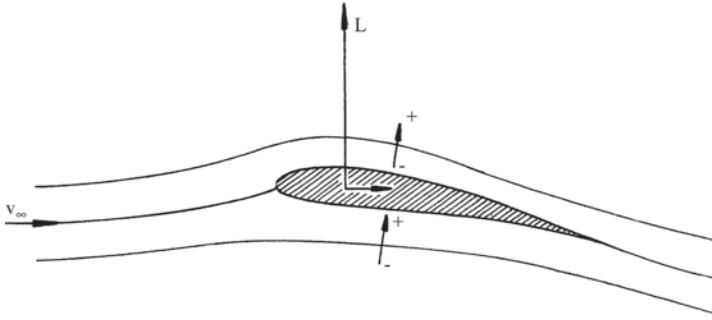


Fig. 2.1 Streamlines with flow over an aerofoil

pressure difference. The arrows perpendicular to the streamlines in Fig. 2.1 indicate the centrifugal force affecting the fluid particles. The pressure difference generated is indicated with + and - symbols. The consequence is that the pressure is lower than the distant pressure on the top side of the aerofoil, while on the bottom side it is higher than the distant pressure. It is said that a *suction side* and a *pressure side* form. The pressure difference generates a force in the upward direction, approximately perpendicular to the oncoming flow.

In fluid mechanics, it is proved that, with a lossless flow, the force on an aerofoil stands exactly perpendicular to the oncoming flow (Kutta-Joukowski theorem). In a flow with losses there is also a component in the flow direction. The perpendicular component is termed *lift* L . The component in the flow direction is termed *drag* D . These forces are usually expressed per span unit of the aerofoil (N/m). From fundamental fluid mechanics we recall that forces exerted by a flow onto objects (N), according to similitude theory, are proportional to $\rho_\infty v_\infty^2 / 2$ (= dynamic pressure, the difference between total pressure and static pressure; see Sect. 2.1.3) and to a characteristic object surface. We thus define lift coefficient and drag coefficient by

$$C_L = \frac{L}{\frac{1}{2} \rho_\infty v_\infty^2 c}, \quad C_D = \frac{D}{\frac{1}{2} \rho_\infty v_\infty^2 c}.$$

The symbol c denotes the chord length of the aerofoil, which is a measure for the largest aerofoil dimension. It approximately equals the largest distance between two points at the aerofoil surface (defined below).

An aerofoil shape (Fig. 2.2) is characterised by a camber line and a thickness distribution. The camber line is a longitudinal line, such that points on the aerofoil surface are at half the thickness set perpendicularly to both sides of it. The camber line is approximately obtained by connecting the midpoints of the inscribed circles within the aerofoil. The leading side (A) is rounded with most aerofoil shapes, causing the inscribed circle to have a finite radius there. In theoretical aerofoil represen-

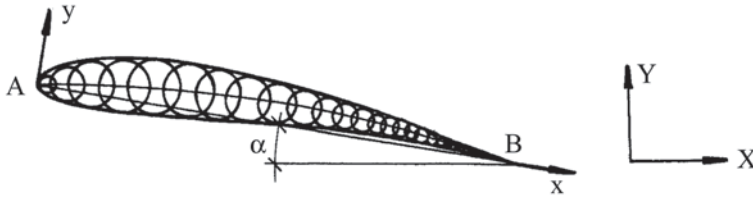


Fig. 2.2 Camber line, chord, thickness and angle of attack of an aerofoil

tations the trailing side (B) mostly has no thickness (a practical aerofoil is obtained by truncating). The *leading edge* is the final point of the camber line at the leading side and the *trailing edge* is the final point at the trailing side. The *chord* is the line segment between the leading and the trailing edges (AB).

The camber line is described by the distance to the chord (y) as a function of a coordinate (x) along the chord beginning at the leading edge and running to the trailing edge. The local thickness is commonly given as a function of the same coordinate. The angle between the chord and the oncoming flow is termed *chord angle* or *angle of attack*. Generally, chord angle means the angle between the chord and a geometric reference line while angle of attack means the angle between the chord and the oncoming flow direction. The concepts coincide with a free-standing aerofoil, but become different for an aerofoil in a machine setting. Most aerofoils have camber. As a consequence, lift is already generated with a zero value of the angle of attack. The angle of attack must then be negative in order to obtain zero lift. The position of the zero-lift defines a direction termed *zero-lift line*. The angle of attack may also be defined as the angle between the zero-lift line and the oncoming flow. The latter definition has the advantage of a zero lift with a zero value of the angle of attack. However, the zero-lift line cannot be indicated on the aerofoil a priori. From fluid mechanics it follows that this line is found with a good approximation by connecting the trailing edge to the point of maximum camber on the camber line.

2.1.2 Performance Parameters

Figure 2.3 sketches, as an illustration, the lift coefficient as a function of the angle of attack for a NACA 4412 aerofoil [1]. This aerofoil was formerly (before the contemporary common use of computational fluid dynamics techniques) typically applied in axial pumps and axial hydraulic turbines. The aerofoil shape is sketched in the figure as well. The NACA denomination refers to the classification by the National Advisory Committee for Aeronautics, the forerunner of the NASA, National Aeronautics and Space Administration. Also shown in Fig. 2.3 is the drag coefficient as a function of the lift coefficient. The tangent from the origin to the curve determines the angle of attack with maximum L/D ratio. Use of the aerofoil with this angle of attack realises maximum efficiency in most applications. The corresponding lift coefficient is about 1.00, the drag coefficient about 0.01. The lift

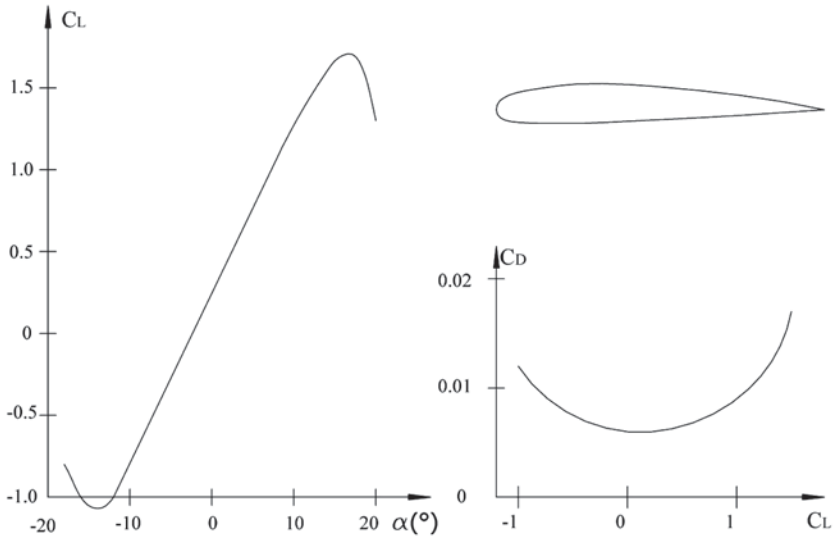
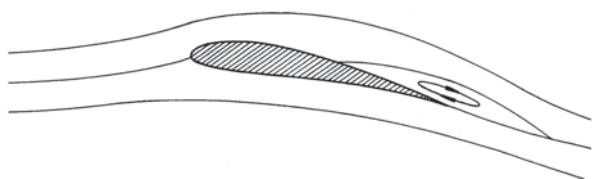


Fig. 2.3 Lift and drag coefficient for NACA 4412 at $Re = v_\infty c / \nu = 10^6$

increases with the angle of attack until an angle where the boundary layer at the suction side in the vicinity of the trailing edge separates from the surface. Beyond this angle, the lift coefficient decreases strongly and the drag coefficient increases strongly. This phenomenon is called *stall*, which means loss of proper functioning. An analogous stall phenomenon is observed with negative angles of attack, but aerofoils commonly are not designed to function well with highly negative angles of attack.

Boundary layer separation will be analysed in a following section, but one can immediately get an intuitive image of it for a very large chord angle, in particular when the profile is positioned perpendicularly to the flow. A large recirculation zone is then created downstream of the aerofoil. At the upstream side of the aerofoil, the pressure is higher than in the oncoming flow due to the flow retardation. Within the recirculation zone the pressure approximates the static pressure of the oncoming flow. The contribution to the drag by the pressure difference is termed *pressure drag*. With a weaker separation, as sketched in Fig. 2.4, pressure drag is generated

Fig. 2.4 Separated flow over an aerofoil



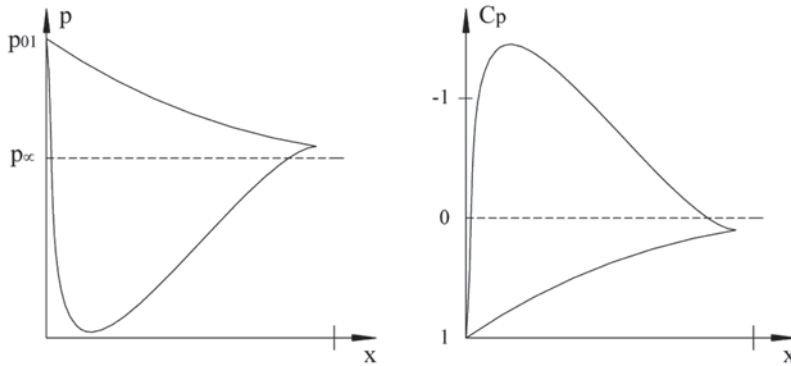


Fig. 2.5 Pressure distribution over an aerofoil with attached flow (NACA 4412)

as well. This adds to the *friction drag*. The pressure drag is the resultant in the flow direction of the pressure on the surface. The friction drag is the resultant of the shear stress on the surface. Pressure drag is rather weak with attached flow, but separation causes a strong increase. Moreover, the curvature of the streamlines at the suction side is then strongly reduced. The consequence is that the pressure minimum at the suction side is weaker than with attached flow. This explains the lift decrease after separation.

2.1.3 Pressure Distribution

The pressure distribution for optimal operation of a NACA 4412 is sketched in Fig. 2.5. At the leading edge, the velocity is near to zero and the pressure is near to the *stagnation pressure* of the oncoming flow. The stagnation pressure or *total pressure* is the pressure obtained by bringing the flow to zero velocity in an adiabatic reversible way. This means that kinetic energy is converted into pressure energy. For constant density, the stagnation pressure is $p_o = p_\infty + \frac{1}{2}\rho_\infty v_\infty^2$. The pressure is somewhat lower in the leading edge zone. The trailing edge pressure is typically slightly higher than the pressure of the oncoming flow. The pressure coefficient shown in Fig. 2.5 is defined by $C_p = (p - p_\infty) / \frac{1}{2}\rho_\infty v_\infty^2$. It is common practice to plot this coefficient with negative values to the upside in order to have the suction side at the upside of the figure. At the pressure side of the aerofoil, the pressure is uniformly decreasing. The boundary layer flow is accelerating everywhere. At the suction side, flow accelerates at the leading edge, causing a pressure drop. Already with a low aerofoil load (small angle of attack), the minimum pressure is lower than the pressure of the oncoming flow (see Fig. 2.1). From the minimum pressure point to the trailing edge, the boundary layer at the suction side is subjected to an adverse pressure gradient.

2.1.4 Boundary Layer Separation

We can obtain more detailed understanding of the flow around an aerofoil by deriving the momentum equations for an infinitesimal streamtube close to a wall. Figure 2.6 sketches such a streamtube for the suction side. We consider a flow that follows the surface, in other words, that does not separate.

The axis in flow direction is denoted by x . This direction approximately follows the surface. The normal direction is denoted by y . Shear stress on a face of the control volume is denoted by τ . The flow between the streamtube considered and the wall has a braking effect on the streamtube. The flow between the streamtube and the free flow has a driving effect. The momentum theorem in the flow direction for an infinitesimal part of the streamtube, on condition of small curvature, is

$$\rho v(dy)dv = -(dy)dp - \rho(dy)dU + (dx)d\tau.$$

From this:

$$\rho v \frac{dv}{dx} = -\frac{dp}{dx} - \rho \frac{dU}{dx} + \frac{d\tau}{dy}. \quad (2.1)$$

From now on, we assume constant density, but extension for variable density is possible. With constant density, the effect of gravity onto the pressure may be expressed by considering pressure as relative to the hydrostatic pressure. This is relevant for liquid flow. The effect of gravity may simply be ignored for gas flow. We thus simplify (2.1) to

$$\rho v \frac{dv}{dx} = -\frac{dp}{dx} + \frac{d\tau}{dy}. \quad (2.2)$$

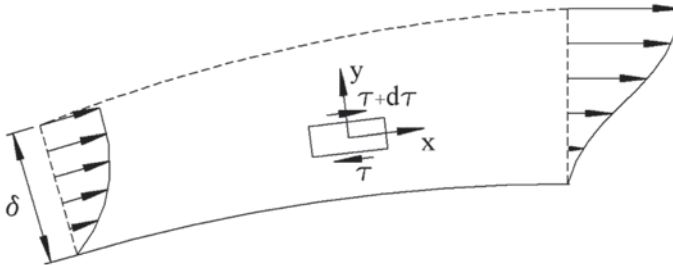


Fig. 2.6 Infinitesimal streamtube close to a wall and velocity profile evolution with an adverse pressure gradient

We first consider a flow with a zero pressure gradient. Far from the wall, the shear stress is zero. There is a certain value on the wall. So $d\tau/dy < 0$. The momentum equation demonstrates that friction reduces the velocity within the streamtube in the flow sense. The height of the streamtube thus increases in the flow sense. The same applies to the entire zone close to the wall, where flow is retarded by the wall friction. The zone affected by the wall friction is called the *boundary layer*. Its thickness is denoted by δ in Fig. 2.6. Note that this thickness cannot be determined precisely. The shear stress is partly of molecular nature due to the relation

$$\tau = \mu \frac{dv}{dy}, \quad (2.3)$$

where μ is the dynamic viscosity coefficient. We recall from fluid mechanics that friction is generated between two adjacent fluid layers with different velocity by the chaotic motion of the microscopic fluid particles (molecules or atoms) around the average macroscopic motion. Fluid particles leap from the fast layer to the slower one, where they arrive with a higher average momentum and so push forward the slower layer. Oppositely, fluid particles leaping from the slower layer to the faster one produce a braking effect. The resulting effect is described macroscopically by Eq. (2.3), with the viscosity coefficient μ as a positive quantity. According to the momentum Eq. (2.2), friction affects the velocity change with μ/ρ . We thus define the kinematic viscosity coefficient

$$\nu = \frac{\mu}{\rho}. \quad (2.4)$$

The dimension of kinematic viscosity is m^2/s . The value for water at atmospheric temperature is about $10^{-6} \text{ m}^2/\text{s}$. The value for air at atmospheric temperature and pressure is about $15 \cdot 10^{-6} \text{ m}^2/\text{s}$. So water and air are not highly viscous fluids. This results in a very thin boundary layer. It is demonstrated in fluid mechanics that, on a smooth wall without a pressure gradient, boundary layer thickness is approximately

$$\delta / x \approx 5 / \sqrt{\frac{xv_{\infty}}{\nu}}.$$

Here, v_{∞} represents the velocity far away from the wall (outside the boundary layer zone) and x the distance covered by the boundary layer. A boundary layer thickness (with laminar flow) maximally amounts to some thousandths of the covered length. It is very important to keep in mind the small thickness of a boundary layer in boundary layer analyses. When drawing a boundary layer, the thickness must

necessarily be exaggerated, which creates a false impression. Turbulent flow contains eddies (whirling flow patterns) as a result of the fragmentation due to stretching and bending of the vortices generated by shear zones. Eddies have a macroscopic size. Their motion is strongly chaotic around an average flow, similar to, but on a far larger scale, than the microscopic fluid particles. The turbulent motion thus also generates shear stress on the average flow. This stress is expressed by an eddy viscosity μ_t according to

$$\tau = (\mu + \mu_t) \frac{dv}{dy}. \quad (2.5)$$

The eddy viscosity coefficient μ_t is no fluid characteristic and depends on the local flow. It is important to realise that μ_t is a positive quantity and that it may be up to 100 times bigger than the molecular viscosity coefficient. So, due to the turbulence, the boundary layer thickness increases significantly. The thickness stays small however compared to the covered length, namely some hundredths. From the positive values of μ and μ_t and the negative value of $d\tau/dy$, we understand that the velocity within the streamtube decreases in flow sense, due to friction, but that inversion of the flow sense is impossible. Separation thus cannot be caused by the viscosity effect only.

In order to understand the role of the pressure gradient, we must also analyse the pressure variation in the normal direction. The easiest way is with a relative frame attached to a fluid particle, as used in Sect. 2.1.1, leading to a balance between the normal pressure gradient and the centrifugal force caused by the curvature of the streamline:

$$\frac{1}{\rho} \frac{dp}{dy} = \frac{v^2}{R}. \quad (2.6)$$

R is the radius of curvature. It is assumed in Eq. (2.6) that friction forces do not contribute. As is clear in Fig. 2.6, there is also shear stress on the inlet and outlet faces of the infinitesimal streamtube. A stress change in the flow direction thus contributes to the force in the normal direction. As boundary layers are very thin, with changes in the normal direction being much bigger than in the flow direction, the contribution of friction may be ignored.

A consequence of Eq. (2.6) is that the pressure distribution over an aerofoil, as sketched in Fig. 2.5, is only slightly dependent on the fluid viscosity, except maybe with very viscous fluids. Another consequence of Eq. (2.6) is an almost identical pressure variation over the various streamlines in a boundary layer, as the radius of curvature R is very large compared to the boundary layer thickness. The decrease of momentum, arising on the various streamlines according to Eq. (2.2) with an adverse pressure gradient, is thus about the same for all streamlines. Consequently, the velocity decrease is relatively stronger as the streamline is nearer to the surface.

This causes, as sketched in Fig. 2.6, the velocity profile to become more concave as the flow evolves. With a sufficiently large adverse pressure gradient, the velocity close to the profile surface may attain a very low value, causing separation downstream of this position. With the reasoning with streamtubes following the surface, as sketched in Fig. 2.6, it cannot be analysed how the transition from attached flow to separated flow exactly occurs, as the velocity within a streamtube cannot change sign. The reasoning however explains the origin of separation, which is sufficient here. We conclude that separation may occur in the trailing edge zone at the suction side, if the adverse pressure gradient is sufficiently large. We also conclude that separation cannot occur at the pressure side if the flow is everywhere accelerating. We further notice that a turbulent boundary layer has a far better resistance to separation than a laminar one. A turbulent boundary layer is much thicker than a laminar one, but turbulence generation is most intense close to the wall. With a turbulent boundary layer, the near-wall velocity gradient is much higher and thus more momentum is present near the wall than within a laminar boundary layer.

2.1.5 *Loss Mechanism Associated to Friction: Energy Dissipation*

The loss mechanism associated to friction in a boundary layer may be understood by analysing the work by friction exerted on the streamtube shown in Fig. 2.6. The bottom streamline is a stationary wall (velocity equal to zero). The overlying flow exerts positive work $(\tau + d\tau)(v + dv)$ and drives the streamtube. The underlying flow brakes by the negative work $(-\tau v)$. The net work leads to the energy equation, in the absence of heat transfer:

$$\rho(dy)v d(h + \frac{1}{2}v^2) = (\tau + d\tau)(v + dv)dx - \tau v dx,$$

or
$$\rho v \frac{dh_0}{dx} = \frac{d}{dy}(\tau v). \quad (2.7)$$

Potential energy, if relevant, is included in the enthalpy. The shear stress τ varies in the y -direction from the wall value to zero in the main flow. Velocity varies from zero to the main flow value. The τv quantity thus goes from zero to zero through a positive maximum. Thus, friction work causes a redistribution of total enthalpy within the boundary layer, but, with an adiabatic wall, the total enthalpy flux stays constant within the entire boundary layer. This follows from the integration of Eq. (2.7) in the y -direction.

The work equation associated to the momentum Eq. (2.2) is

$$\rho v \frac{d}{dx} \left(\frac{1}{2} v^2 \right) = -v \frac{dp}{dx} + v \frac{d\tau}{dy}.$$

or

$$\rho v \left(\frac{d}{dx} \left(\frac{1}{2} v^2 \right) + \frac{1}{\rho} \frac{dp}{dx} \right) = v \frac{d\tau}{dy}. \quad (2.8)$$

From now on, we assume again constant density. The work Eq. (2.8) then means that the mechanical energy $E_m = \frac{1}{2} v^2 + \frac{1}{\rho} p$ decreases due to the *displacement work* of the friction force, since $d\tau/dy < 0$.

Subtracting the work equation from the energy equation results in

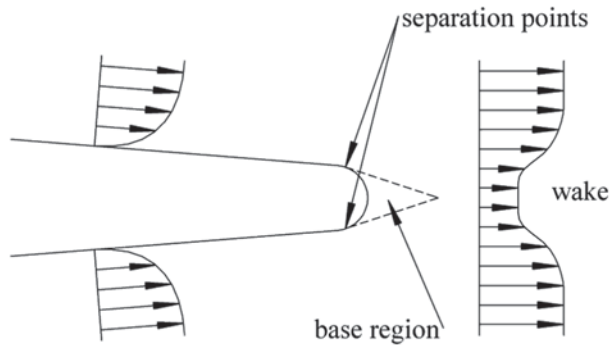
$$\rho v \frac{de}{dx} = \tau \frac{dv}{dy}. \quad (2.9)$$

The part of the work $\tau \frac{dv}{dy}$ is the *deformation work*: total work minus displacement work. This work is always positive in view of (Eq. 2.5). Friction thus results in increase of internal energy (Eq. 2.9) and decrease of mechanical energy (Eq. 2.8) with constancy of the flux of the total energy (Eq. 2.7): mechanical energy plus internal energy. The conversion of mechanical energy into internal energy is called energy dissipation.

With the boundary layer of Fig. 2.6 there is no exchange of work and heat with the surroundings. Therefore, the flux of total energy is constant and the decrease of mechanical energy is exactly equal to the increase of internal energy. So, energy dissipation may be seen in both ways. This is not a general result, however. Strictly, energy dissipation is caused by the deformation work of the friction. This may be understood by adding work done by an external force on the boundary layer in Fig. 2.6. The same work term then adds to the balance of total energy and the balance of mechanical energy. In the difference of both balances, the work term cancels. This demonstrates that actually the balance of internal energy (Eq. 2.9) determines the dissipation. This observation may cause confusion since in Chap. 1 the displacement work of the friction force resulting in mechanical energy decrease was immediately denoted as dissipation. Strictly, this is incorrect, as the deformation work is the dissipative part of the friction work. The result is correct in value, because the magnitude of the integral across the boundary layer thickness of the displacement work equals the magnitude of the integral of the deformation work, since the integral of the total work equals zero with a shear flow on a stationary wall. It is essential for this result that the friction acts on a stationary wall.

From the analysis with the differential equations it follows as well that the energy dissipation does not exactly equal the product of the shear stress at the wall and

Fig. 2.7 Merging boundary layers at a trailing edge with generation of a wake



the average velocity in a channel, as obtained in a one-dimensional analysis. This product has the correct order of magnitude, but the exact result depends on the distribution of the shear stress and the velocity gradient across a channel section. With a trapezoidal velocity profile and with an infinitesimally thin transition from core to wall, it follows that the energy dissipation integral (Eq. 2.9) equals the product of the velocity in the flow core and the shear stress at the wall.

The reasoning based on the energy Eq. (2.7) and the work Eq. (2.8) demonstrates that the wall friction affects the entire boundary layer. Energy dissipation by friction is thus no local phenomenon. Moreover, the dissipation continues downstream of the profile. Figure 2.7 illustrates how boundary layers at the suction and the pressure sides merge at the trailing edge of an aerofoil and how a wake is generated in which further energy dissipation occurs.

As mentioned above, the drag of the aerofoil is resolved into friction drag and pressure drag. Energy dissipation associated to drag may be resolved in two parts as well, termed *friction loss* within the boundary layers and *mixing loss* within the wake downstream of the aerofoil. The term mixing loss expresses the energy dissipation by the mixing of the flows from the suction side and the pressure side with each other and with the surrounding flow. Figure 2.7 makes clear that the expansion of the wake, in principle, continues up to an infinite distance from the aerofoil. So, it is very difficult to estimate the total loss by an integral of the energy dissipation within the fluid. The result of the integration is known a priori however. Let us consider, instead of a stationary aerofoil in a flow with oncoming velocity v_∞ , the motion of an aerofoil with velocity v_∞ in a stationary atmosphere. For the last case, the totally dissipated energy per time unit is $\vec{D} \cdot \vec{v}_\infty$, as all work is dissipated. Obviously, the amount must be the same for the stationary aerofoil in the steady flow. The following must thus apply (where S is a surface enclosing the aerofoil at a very large distance):

$$\vec{D} \cdot \vec{v}_\infty = \int_S (h_0 - E_m) \rho \vec{v} \cdot \vec{n} \, dS = - \int_S E_m \rho \vec{v} \cdot \vec{n} \, dS. \quad (2.10)$$

2.1.6 Profile Shapes

The optimal profile shape strongly depends on the particular application. The NACA 4412 shape used in Fig. 2.3, is, as already mentioned, rather suitable for applications in pumps and hydraulic turbines. This profile was used frequently in older designs. The intended flow deflection is small, the Reynolds number moderately high to high, i.e. in the order of 1 to $5 \cdot 10^6$ and with a high degree of turbulence within the main flow. There first is flow acceleration at the suction side, which keeps the boundary layer laminar (the laminar boundary layer becomes more stable in accelerating flow). Deceleration follows after that. With a high Reynolds number and high turbulence in the main flow, the boundary layer quickly becomes turbulent when subjected to an adverse pressure gradient (the laminar boundary layer becomes less stable in decelerating flow). This is intended, as a turbulent boundary layer better resists separation than a laminar one. An aerofoil shape with a pressure distribution as sketched in Fig. 2.5 is therefore termed a *turbulent profile*, which means that the boundary layer at the suction side is turbulent on a large part of it. The profile shape is not optimal for applications in pumps and hydraulic turbines. The predominantly turbulent boundary layer at the suction side allows a high adverse pressure gradient. Consequently, the attainable lift coefficient is high. But the drag coefficient is rather high as well, due to the higher friction than with laminar flow. Another disadvantage is the strong pressure minimum at the suction side, which may cause cavitation (local water evaporation) with some applications. Modern profile shapes have a less deep suction pressure minimum. The laminar part of the leading edge boundary layer is larger, generating a lower drag coefficient. Nowadays, these profiles are designed with computational fluid dynamics techniques.

Figure 2.8 shows an aerofoil and the accompanying pressure distribution for the middle part of a wind turbine blade [5]. The pressure distribution is completely different from the NACA 4412. Flow circumstances are here: low deflection, slight acceleration within the general flow, rather high Reynolds number, i.e. 3 – $5 \cdot 10^6$ and low turbulence in the main flow. Strong acceleration occurs at the leading edge part of the suction side, followed by a zone of weak acceleration. The boundary layer stays laminar until the end of the weak acceleration zone. This succeeds due to the low turbulence in the oncoming flow. From the beginning of the deceleration phase, the boundary layer becomes turbulent here as well. This succeeds due to the rather high Reynolds number. At first, acceleration occurs at the pressure side due to the high aerofoil thickness. Then follows a weak deceleration intended to increase the pressure difference between the pressure and the suction sides again. The obtainable lift coefficient is moderately high (~ 1.00). The drag coefficient is low (~ 0.0075), as the boundary layer at the suction side is laminar over a rather significant part. The aerofoil shape is termed a *laminar profile*. The shape is similar to profiles applied in wings of aircraft.

Present-day aerofoil profiles use the features of the profile shape of Fig. 2.8: strong acceleration followed by weak acceleration at the suction side leading edge,

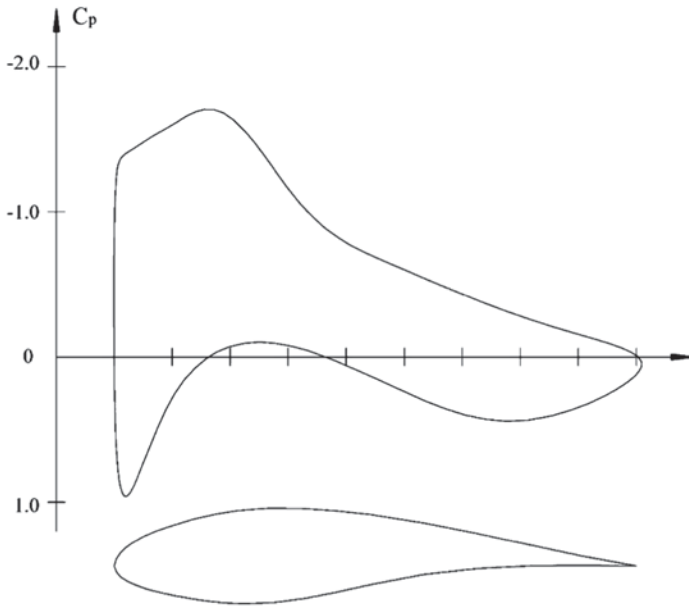


Fig. 2.8 Aerofoil shape and pressure distribution for a central part of a wind turbine blade

with a limitation of the minimum pressure; deceleration in the middle part of the pressure side in order to enhance the lift. Gradients within the zones and the extensions of the zones strongly vary from application to application. The optimum is critically determined by the Reynolds number, the mean pressure gradient in the flow (globally accelerating or decelerating flow) and the turbulence level in the core of the flow. There is no universal optimum. Determination of the optimum requires the application of advanced computational methods.

2.1.7 Blade Rows with Low Solidity

With the axial turbine or the axial pump discussed in Chap. 1, the blade profiles do not have the same performance as isolated blades, because the suction and pressure sides of neighbouring blades interact. This may cause both lift increase or lift decrease. The zero-lift direction changes and drag stays approximately the same. Figure 2.9 sketches a blade row for decelerating flow (pump, fan, compressor). The tangential distance between the blades is called *spacing* (s) or pitch. The ratio of the chord (c) to the spacing is termed *solidity* ($\sigma = c/s$). With blade systems, the term solidity generally refers to the ratio of the blade area to the flow area. An approximate blade area is typically applied, obtained by integration of the chord: $\int c dr$. With a good approximation, the zero-lift line is found by connecting the trailing edge to the point of maximum deflection on the camber line, taking the maximum

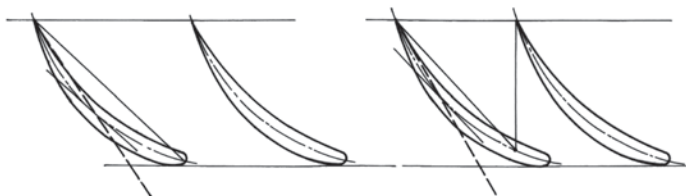


Fig. 2.9 Blade row; change of zero-lift line. Chord: full line, zero-lift line: dashed line

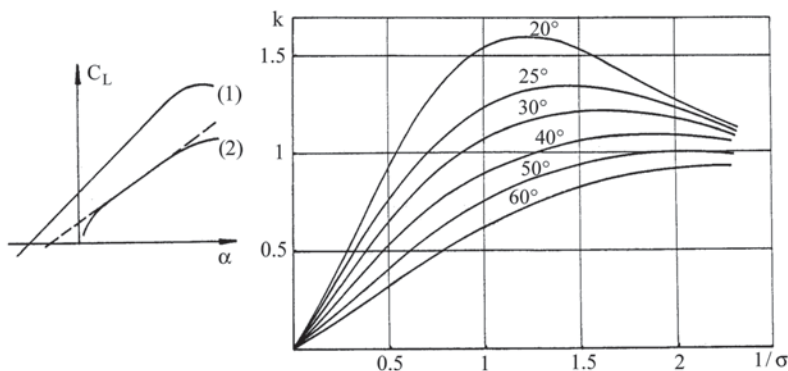


Fig. 2.10 Change of lift coefficient in a cascade. Isolated profile (1) and profile in a row (2)

on a reduced chord between the trailing edge and a point obtained by projection in the axial direction of the trailing edge of the neighbouring profile [7].

Figure 2.10 demonstrates how the lift coefficient changes. The lift coefficient shows a nearly linear variation over a broad angle of attack range. This is the range with no boundary layer separation. The slope of the lift curve changes with a factor k , plot in the figure. Results originate from measurements on various profile shapes, but all of them with a relative thickness of 8% [7]. The angle in the diagram is between the zero-lift line of the isolated profile and the tangential direction. The diagram becomes unreliable for high solidity. It may be used confidently for $\sigma = c/s < 1.3$. At higher solidity it becomes difficult to derive the blade row characteristics from the characteristics of isolated blades (see next section).

2.2 Linear Cascades

2.2.1 Relation with the Real Machine

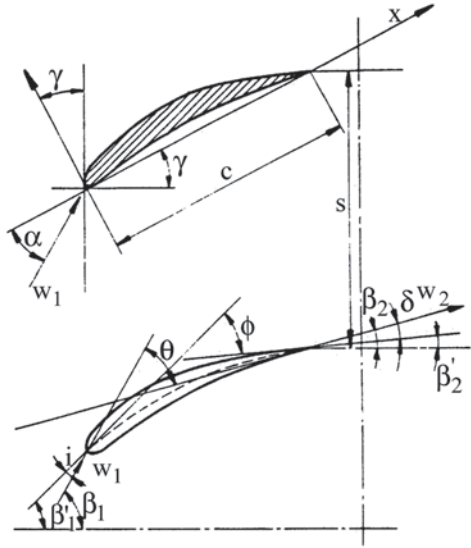
Flow within the blade passages of an axial turbomachine is three-dimensional. A two-dimensional approximation is obtained by making a cylindrical section of the

blades at the mean radius and by unrolling it into a plane. A linear cascade or blade row is built by setting up prismatic blades with the profiles obtained. In principle, an infinite number of blades are required in order to keep the periodicity of the blades in the original machine. The two-dimensional flow is representative for the real three-dimensional flow. The expressions for axial momentum are the same in both configurations. Moment of momentum with the three-dimensional flow corresponds to tangential momentum with the cascade (tangential = circumferential). Constant tangential momentum along the blade height with the linear cascade is then equivalent to constant angular momentum ($v_u r = \text{constant}$) along the radius in the real machine. This means then that the three-dimensional flow is a so-called *free vortex flow*. The term means swirling flow with constant angular momentum. In the pioneering time, axial turbomachines were built with free vortex flow because of this theoretical correspondence. They show certain disadvantages discussed later (Chap. 13: axial compressors; Chap. 15: axial and radial turbines). Present-day machines are designed with some degree of forcing of the vortex ($v_u r \neq \text{constant}$) along the radius. The deviation to the free vortex distribution is not very significant, however. With free vortex blades in a cylindrical axial turbomachine, an exact transformation exists between the flow in the machine and the linear cascade (of course with top and bottom walls added). This does no longer apply with some forcing on the vortex. For instance, no cylindrical streamsurfaces exist anymore. The analogy between the three-dimensional flow within the machine and the two-dimensional flow within the linear cascade is only met approximately. Nevertheless, studying the characteristics of linear cascades is very instructive as the flow within a linear cascade is still representative for the flow in an average cylindrical section of a real machine.

2.2.2 Cascade Geometry

The cascade is determined by the shape of the blades, their position to the axial direction and their *spacing* (tangential distance between the blades). The term *pitch* is often used for spacing, but pitch may also mean, similarly to the term with screws, the axial distance covered by the flow when it makes a full turn of 360° . This applies in particular to propellers and wind turbines with adjustable rotor blades. Then often, also the term pitch angle is used. Results are also a function of the positioning of the blades relative to the flow. The profile shape is, as with aerofoils, determined by the camber line and the thickness distribution. The profile size is determined by the chord. *Solidity* σ means the ratio of the chord to the spacing. Some characteristics are shown in Fig. 2.11. The *camber angle* ϕ is the angle difference between the tangents at the camber line on the leading and trailing edges. Profile orientation relative to the axial direction is determined by the chord angle or *stagger angle* γ . The inlet velocity w_1 forms an angle of attack α with the chord, an angle β_1 with the axial direction and an *angle of incidence* i with the tangent at the camber line on the leading edge. The angle of incidence is positive when the flow turning increases

Fig. 2.11 Cascade notation (example of decelerating flow)



by it. The outlet velocity w_2 forms with the inlet velocity w_1 an *angle of deflection* θ , with the tangent at the camber line on the trailing edge an *angle of deviation* δ and with the axial direction an angle β_2 . The angle of deviation is positive when it causes a decrease of θ .

2.2.3 Flow in Lossless Cascades: Force Components

Figure 2.12 sketches the flow through a rotor cascade with decelerating flow. We apply the fundamental laws (for a constant density fluid) to a cascade with profiles on spacing s . The flow velocities in the relative frame w have w_a into the axial direction and w_u into the tangential direction (= circumferential direction) as their components. Similarly, the force L exerted on the blades has L_a and L_u as components. The velocities w_1 and w_2 are considered sufficiently far from the cascade, so that velocity is assumed to be constant in Sections 1 and 2.

We select a right-handed coordinate frame with the x -axis in the axial direction, positive in the through-flow sense, and the y -axis in the circumferential direction, positive in the running sense of the rotor. The machine must be left turning ($\vec{\Omega} = -\Omega \vec{i}_x$) in order that the z -axis in the radial direction has the outward sense as positive sense. This is a minor complication. A right-handed coordinate frame with a right turning machine would be achieved by an x -axis in the running sense, a y -axis in the axial direction in the through-flow sense and a z -axis in the radial direction in the outward sense ($\vec{\Omega} = \Omega \vec{i}_y$). With this last convention, angles are calculated with respect to the circumferential direction and vary from 0° to 180° .

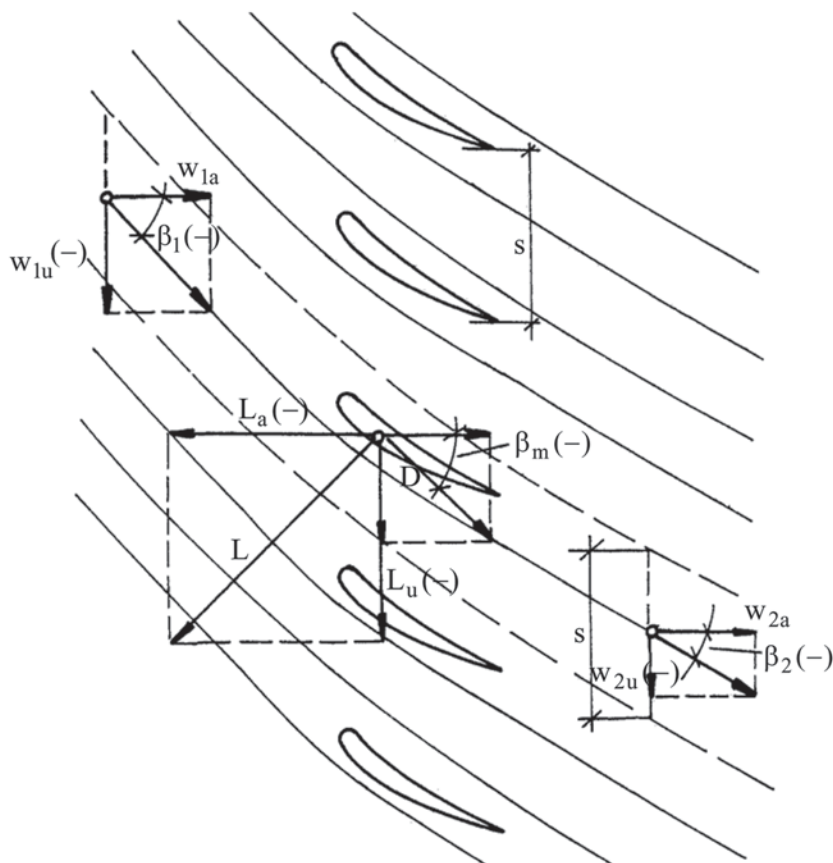


Fig. 2.12 Force exerted onto a cascade blade (rotor pump)

This choice was very often made in the past. It has the disadvantage that application of the goniometric tangent function is difficult. Due to the general use of electronic calculation devices, the first convention (axial convention) is preferred at present, with angles varying from -90° to $+90^\circ$. This convention has already been applied systematically in Chap. 1. For the entire book, we exclusively reason on left turning machines. Both left and right turning machines actually occur in practice (some illustrations concern right turning machines). More generally, we take a coordinate frame with first axis in the meridional direction (this is the tangent to the intersection of the average circumferential streamsurface with a meridional plane), positive into the through-flow sense; second axis in the circumferential direction, positive in the running sense; third axis perpendicular to the average streamsurface, positive in the outward sense.

Tangential velocity components are negative for the cascade in Fig. 2.12, with lift components L_a and L_u being negative as well. We reason in the relative frame. As centrifugal force and Coriolis force lie in the radial direction with axial machines, these forces do not intervene with momentum relations in the axial and tangential directions. The derived relations thus automatically apply to stator cascades, as we always apply the momentum laws in an algebraically consistent way. As a consequence, the derived relations also apply to cascades with accelerating flow (this will be verified later on). The pump rotor cascade in Fig. 2.12 is the most complex one to analyse (w_u , L_a and L_u being negative). That is the reason why we take it as an example.

The mass conservation law is:

$$w_{1a}s = w_{2a}s = w_a s.$$

The work equation (relative system, no losses: Eq. (2.8) with $\tau=0$) is

$$p_{01r} - p_{02r} = 0 \quad \text{or} \quad p_1 + \frac{\rho}{2} w_1^2 = p_2 + \frac{\rho}{2} w_2^2,$$

from which

$$p_2 - p_1 = \frac{\rho}{2} (w_1^2 - w_2^2).$$

With $\Delta p = p_2 - p_1$, $q_1 = \frac{\rho w_1^2}{2}$ and $w_a = w_2 \cos \beta_2 = w_1 \cos \beta_1$,

$$\text{it follows that:} \quad C_p = \frac{\Delta p}{q_1} = 1 - \frac{\cos^2 \beta_1}{\cos^2 \beta_2}. \quad (2.11)$$

The term $\Delta p/q_1$ is often denoted by C_p . A criterion for maximum cascade load with decelerating flow is: $C_p = 0.5$ ($w_2/w_1 \approx 0.7$). This results in a relation between β_1 and β_2 . For instance, corresponding values are $\beta_1 = -60^\circ$ and $\beta_2 = -45^\circ$, $\beta_1 = -55^\circ$ and $\beta_2 = -35^\circ$.

In order to apply the momentum conservation law, we consider the dashed lined contour in Fig. 2.12. It forms a control volume with two periodic streamsurfaces and two planes parallel to the cascade front. On the front and back surfaces, pressures are p_1 and p_2 . Pressure forces on the periodic streamsurfaces counterbalance. The force by the blade on the flow is $-L$.

The momentum balance in the tangential direction is

$$-L_u = \rho s w_a (w_{2u} - w_{1u}),$$

or

$$L_u = \rho s w_a (w_{1u} - w_{2u}). \quad (2.12)$$

The momentum balance in the axial direction is

$$-L_a + s p_1 - s p_2 = 0,$$

or

$$L_a = s(p_1 - p_2) = s \frac{\rho}{2} (w_{2u}^2 - w_{1u}^2). \quad (2.13)$$

The circulation around the contour in the positive sense, as periodic parts intervene with counterbalancing amounts, is

$$\Gamma = \oint \vec{w} \cdot \vec{dl} = s(-w_{1u} + w_{2u}) = s(w_{2u} - w_{1u}).$$

Combination results in

$$L_u = -\rho \Gamma w_a \quad \text{and} \quad L_a = \frac{\rho \Gamma}{2} (w_{1u} + w_{2u}). \quad (2.14)$$

The result from these formulae is that the force L is perpendicular to the velocity w_m , which has w_a and $(w_{1u} + w_{2u})/2$ as its components and that the magnitude of L is

$$|L| = \rho |\Gamma| w_m. \quad (2.15)$$

This relation is termed the Kutta-Joukowski law for cascades. It is entirely analogous to that for aerofoils, being $|L| = \rho_\infty |\Gamma| w_\infty$. The expression for aerofoils may be derived from Eq. (2.15), by keeping Γ and allowing s to increase to infinity. Then $w_1 = w_2 = w_\infty$ becomes the velocity of the parallel flow.

2.2.4 Significance of Circulation

The work equation on a streamline through the cascade is Eq. (2.2), but with $d\tau/dy=0$ in the core of the flow (negligible shear force), which we write for a rotor cascade as

$$\rho w \frac{dw}{dx} + \frac{dp}{dx} = 0. \quad (2.16)$$

The force balance in the direction perpendicular to the streamline is similar to Eq. (2.6):

$$\frac{1}{\rho} \frac{dp}{dy} = \frac{w^2}{R}. \quad (2.17)$$

Equation (2.16) may be integrated along a streamline into

$$\frac{1}{2}w^2 + \frac{1}{\rho}p = \text{constant.} \quad (2.18)$$

With the cosine rule on the velocity triangles follows

$$w^2 = u^2 + v^2 - 2uv_u.$$

Thus:
$$\frac{1}{2}v^2 + \frac{1}{\rho}p + \frac{1}{2}u^2 - uv_u = \text{constant.} \quad (2.19)$$

This means that, for constant mechanical energy of the incoming flow in the absolute frame and uniform v_u , the constant in Eq. (2.19) and thus in Eq. (2.18) is the same on all streamlines. Eq. (2.18) then also implies

$$w \frac{dw}{dy} + \frac{1}{\rho} \frac{dp}{dy} = 0. \quad (2.20)$$

Combined with Eq. (2.17), this gives

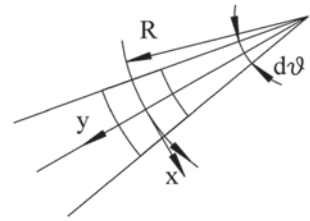
$$w \frac{dw}{dy} + \frac{w^2}{R} = 0. \quad (2.21)$$

The significance of Eq. (2.21) may be understood by calculating the circulation on an infinitesimal contour consisting of two pieces of neighbouring streamlines connected with straight segments as shown in Fig. 2.13 (x is streamline direction, y is normal direction), and by applying Stokes' circulation theorem, which is an integral theorem for the rotor of a vector quantity:

$$\oint \vec{w} \cdot d\vec{l} = \int_S (\nabla \times \vec{w}) \cdot \vec{n} dS,$$

where S is a surface spanned by the contour and \vec{n} is the unit normal vector on the surface in the sense corresponding with the sense on the contour. On the infinitesimal contour of Fig. 2.13, this gives, with R the radius of curvature of the

Fig. 2.13 Infinitesimal contour for evaluation of the rotation of the velocity vector



mean streamline and with ω the value of the rotor of the relative velocity vector in the z -direction:

$$(w + \frac{1}{2} \frac{dw}{dy} dy) (R + \frac{1}{2} dy) d\theta - (w - \frac{1}{2} \frac{dw}{dy} dy) (R - \frac{1}{2} dy) d\theta = \omega R d\theta dy,$$

or

$$\frac{dw}{dy} dy R d\theta + w dy d\theta = \omega R d\theta dy.$$

Thus

$$\frac{dw}{dy} + \frac{w}{R} = \omega. \quad (2.22)$$

With (Eq. 2.22), we understand that (Eq. 2.21) means that the rotor of the velocity vector is zero everywhere in the core of the flow. Such a flow is called *irrotational*. The meaning of the term is that the rotational speed of each fluid particle is zero, as the rotational speed is equal to half of the rotor of the velocity vector (see fluid mechanics). The consequence is that circulation is zero on every contour non-enclosing the blade and that the circulation on a contour enclosing the blade is the same for every contour around the blade. Strictly, this result is only valid for lossless flow, as the mechanical energy has to be the same for every streamline. In flow with losses, the result remains approximately valid for every contour around the blade as long as this contour does not enter the boundary layers on the blades. The contour has to cut the wake, of course, which causes a small error on the strict equality of the circulation on each contour around the blade.

2.2.5 Flow in Lossless Cascades: Work

When the cascade moves into the tangential direction at a velocity u , the absolute velocities v may be derived from u and w by constructing the velocity triangles:

$$v_{1u} = u + w_{1u}; \quad v_{2u} = u + w_{2u}; \quad v_a = w_a.$$

Formula (2.12) then becomes:

$$L_u = \rho \, s \, v_a (v_{lu} - v_{2u}).$$

The power transferred to the fluid becomes

$$P = -L_u u = \rho \, s \, v_a (v_{2u} - v_{lu}) u.$$

The power per mass flow rate unit, i.e. the work per mass unit, becomes

$$\Delta W = \frac{-L_u u}{\rho \, s \, v_a} = u (v_{2u} - v_{lu}).$$

This is Euler's formula, applied to an axial machine ($u_1 = u_2$).

It is informative to remark that the work also may be found from $-\vec{L} \cdot \vec{v}_m$ as $-\vec{L} \cdot \vec{v}_m = -\vec{L} \cdot \vec{u} - \vec{L} \cdot \vec{w}_m = -\vec{L} \cdot \vec{u}$. So, the work done on the flow by an active force, indeed, is the force multiplied with the displacement, as applied in Chap. 1. This seems to be evident at a first glance. But that is not the case, as we analyse below, for a flow with losses.

2.2.6 Flow in Cascades with Loss: Force Components

Loss results in a *total pressure drop* (Eq. 2.8), which we may express by

$$p_{01r} - p_{02r} = (p_1 + \frac{\rho w_1^2}{2}) - (p_2 + \frac{\rho w_2^2}{2}),$$

being a positive quantity. For further analysis, we assume equal loss on all streamlines. A *loss coefficient*, based on inlet dynamic pressure, is then

$$\xi_l = \frac{p_{01r} - p_{02r}}{q_l}.$$

With F the force of the flow onto the profile, then

$$\begin{aligned} F_u &= \rho \, s w_a (w_{lu} - w_{2u}) = \rho \, s \, w_a^2 (tg\beta_l - tg\beta_2), \\ F_a &= s(p_1 - p_2) = \frac{\rho s}{2} w_a^2 (tg^2\beta_2 - tg^2\beta_l) + s(p_{01r} - p_{02r}) \\ &= \rho \, s \, w_a^2 \, tg\beta_m (tg\beta_2 - tg\beta_l) + s(p_{01r} - p_{02r}), \end{aligned}$$

with

$$\operatorname{tg} \beta_m = \frac{\operatorname{tg} \beta_1 + \operatorname{tg} \beta_2}{2}.$$

The drag follows from (see Fig. 2.12):

$$\begin{aligned} D &= (F_u \bar{I}_u + F_a \bar{I}_a) \cdot (\sin \beta_m \bar{I}_u + \cos \beta_m \bar{I}_a) \\ &= F_u \sin \beta_m + F_a \cos \beta_m = s(p_{01r} - p_{02r}) \cos \beta_m. \end{aligned} \quad (2.23)$$

The drag components are

$$\begin{aligned} D_a &= s(p_{01r} - p_{02r}) \cos^2 \beta_m, \\ D_u &= s(p_{01r} - p_{02r}) \sin \beta_m \cos \beta_m. \end{aligned}$$

The lift components are

$$\begin{aligned} L_u &= \rho s w_a^2 (\operatorname{tg} \beta_1 - \operatorname{tg} \beta_2) - s(p_{01r} - p_{02r}) \sin \beta_m \cos \beta_m, \\ L_a &= -\rho s w_a^2 \operatorname{tg} \beta_m (\operatorname{tg} \beta_1 - \operatorname{tg} \beta_2) + s(p_{01r} - p_{02r}) \sin^2 \beta_m. \end{aligned}$$

The magnitude of the lift for the cascade in Fig. 2.12 ($\operatorname{tg} \beta_1 - \operatorname{tg} \beta_2 < 0$) is

$$L = \rho s \frac{w_a^2}{\cos \beta_m} (\operatorname{tg} \beta_2 - \operatorname{tg} \beta_1) + s(p_{01r} - p_{02r}) \sin \beta_m.$$

From this follows:

$$C_{Ll} = \frac{L}{q_1 c} = \frac{2}{\sigma} \frac{\cos^2 \beta_1}{\cos \beta_m} (\operatorname{tg} \beta_2 - \operatorname{tg} \beta_1) + \frac{\xi_1}{\sigma} \sin \beta_m,$$

$$C_{Dl} = \frac{D}{q_1 c} = \frac{\xi_1}{\sigma} \cos \beta_m.$$

Elimination of ξ_1 results in

$$C_{Ll} = \frac{2}{\sigma} \frac{\cos^2 \beta_1}{\cos \beta_m} (\operatorname{tg} \beta_2 - \operatorname{tg} \beta_1) + C_{Dl} \operatorname{tg} \beta_m.$$

This relation implies that the lift coefficient does not depend solely on the cascade solidity and the flow angles, but on the drag coefficient as well.

With the above formulae it should be taken into account that the β -angles are negative with the cascade considered in Fig. 2.12. This means that lift decreases due to losses. When deriving the relations, sign conventions have been applied consistently. The expressions for F_u and F_a have general validity, also for a turbine cascade ($tg\beta_1 - tg\beta_2 > 0$, $F_u > 0$, $F_a > 0$). The expression for drag remains the same with a turbine. The expression for lift, with lift being a positive quantity, becomes ($\beta_m < 0$) with a turbine:

$$C_{LI} = \frac{2 \cos^2 \beta_l}{\sigma \cos \beta_m} (tg\beta_1 - tg\beta_2) - \frac{\xi_l}{\sigma} \sin \beta_m.$$

It is remarkable that, with a given deflection in a turbine, losses cause lift increase. The different behaviour compared to the pump can be understood by analysing the four configurations shown in Fig. 2.14. The four possible combinations of the sign of the circulation and the mean tangential velocity occur. First, the correspondence of the sign combinations with Eqs. (2.14) may be verified. The tangential components of lift and drag have the same sense with pump cascades. For a given change of tangential velocity, this means given F_u , D_u decreases the magnitude of L_u . This is just the opposite with a turbine cascade.

2.2.7 Flow in Cascades with Loss: Energy Dissipation and Work by Drag Force

Equation (2.23) for drag implies

$$Dw_m = \rho s w_m \cos \beta_m \frac{p_{01r} - p_{02r}}{\rho} = \rho s w_a \frac{p_{01r} - p_{02r}}{\rho},$$

or

$$Dw_m = \dot{m} q_{irr}. \quad (2.24)$$

Equation (2.24) is similar to the formerly found expression for energy dissipation with an aerofoil Eq. (2.10). The right-hand part in Eq. (2.24) represents the difference between the mechanical energy fluxes at the inlet and outlet planes of the cascade. The term Dw_m is thus the total amount of energy dissipation. This result expresses that, with flow over a stationary cascade (we reason in the relative frame), energy dissipation equals the displacement work of the drag force exerted onto the average flow.

The finding that, for a given flow deflection, drag affects lift, is due to the contribution of the drag to the tangential velocity change. For a moving

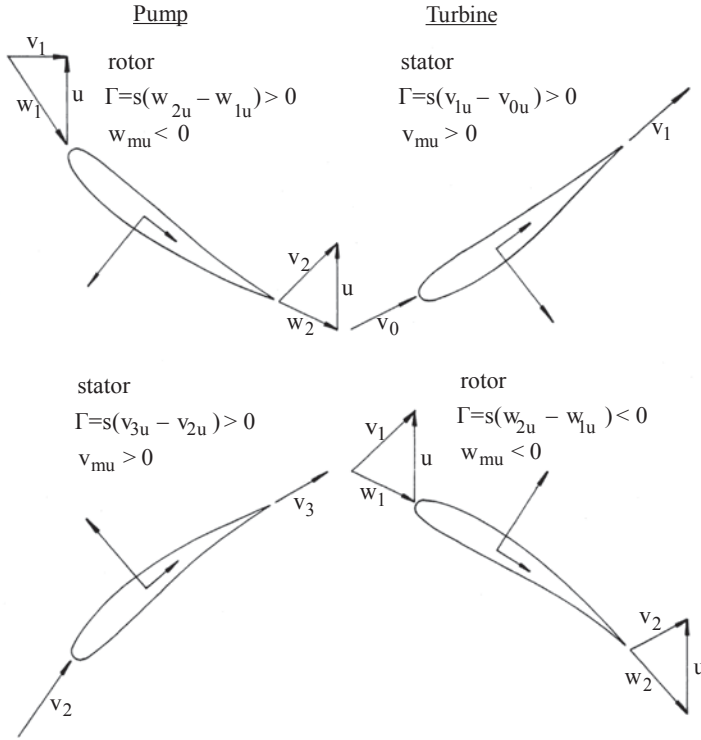


Fig. 2.14 Forces with various machine components

cascade, this means that drag contributes to the work. The work by the drag force on the fluid is $-\vec{D} \cdot \vec{u}$. Analogously to the lift, we can verify the meaning of $-\vec{D} \cdot \vec{v}_m$.

It follows that
$$-\vec{D} \cdot \vec{u} = -\vec{D} \cdot \vec{v}_m + \vec{D} \cdot \vec{w}_m,$$

with
$$-\vec{D} \cdot \vec{u} = \rho s w_a \Delta W \quad \text{and} \quad \vec{D} \cdot \vec{w}_m = \rho s w_a q_{irr}. \quad (2.25)$$

So:
$$\rho s w_a \Delta W = -\vec{D} \cdot \vec{v}_m + \rho s w_a q_{irr}. \quad (2.26)$$

Equation (2.26) again demonstrates that the total work is the sum of displacement work and deformation work. Figure 2.14 shows that the total work by the drag force is always in the sense from material parts to the fluid. A part of the work is dissipated. The displacement work $(-\vec{D} \cdot \vec{v}_m)$, corresponding to mechanical energy increase within the fluid, may either be positive or negative. Displacement work

$(-\vec{D} \cdot \vec{v}_m)$ is negative for the four configurations in Fig. 2.14. This is the situation that we intuitively expect and that is always correct for stator components. With rotor components, the displacement work of the drag force may be positive. This requires a rather high blade speed compared to the other velocity components (see Exercise 2.5.6). Equation (2.26) demonstrates that the concept of displacement work should be applied with care. Only in the case of a purely active force, without any deformation work associated, as a lift, does the displacement work equal the total work.

2.2.8 The Zweifel Tangential Force Coefficient

With an axial cascade, in principle, the component of the force on the blade useful for work is not the lift but the tangential component. It is therefore appropriate to define a coefficient on the basis of F_u as well. For a constant density fluid, the obvious reference force is $\frac{1}{2}\rho w_2^2 c_a$, with c_a the *axial chord*, as illustrated in Fig. 2.15. When losses are ignored, the pressure at the outlet is lower than the total pressure at the inlet with the amount $\frac{1}{2}\rho w_2^2$. The surface between the pressure curves on the pressure and suction sides is the magnitude of F_u . We see the relation with the reference force $(p_{01r} - p_2)c_a$. This quantity is replaced by the value for lossless constant density flow: $\frac{1}{2}\rho_2 w_2^2 c_a$ (ρ_2 is density at outlet for a compressible fluid). This allows the definition of a tangential force coefficient, expressed solely as a function of velocity quantities and the axial solidity $\sigma_a = c_a / s$, by

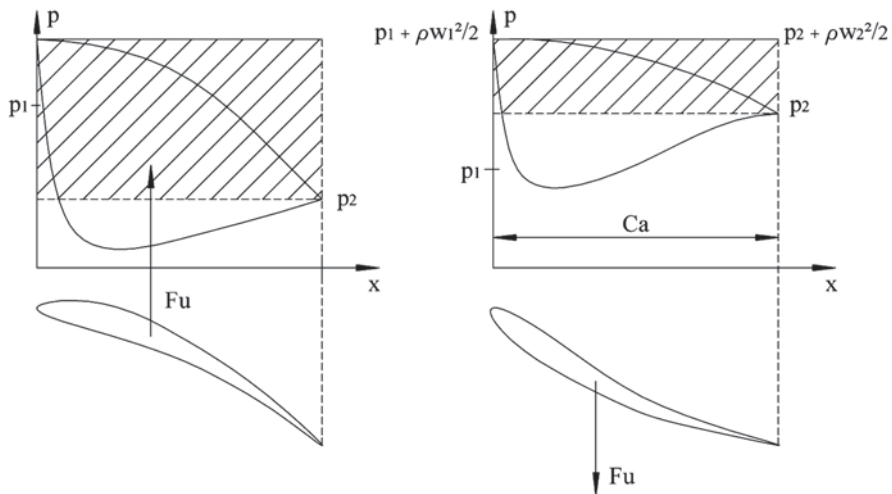


Fig. 2.15 Reference force for the tangential force; *left*: cascade with moderate flow acceleration (turbine); *right*: cascade with moderate flow deceleration (pump, fan, compressor)

$$C_{Fu} = \frac{|F_u|}{\frac{1}{2}\rho_2 w_2^2 c_a} = \frac{\rho_2 w_{2a} s |w_{1u} - w_{2u}|}{\frac{1}{2}\rho_2 w_2^2 c_a} = \frac{2|\Delta w_u| w_{2a}}{\sigma_a w_2^2}. \quad (2.27)$$

The concept of tangential force coefficient was introduced by Zweifel in the 1940s. He found that the coefficient was about 0.8 for cascades with good efficiency. The separation values were around 1.1–1.2. Good efficiency means small losses compared to the tangential force. With $C_{Fu} = 0.8$ follows an optimal value for the axial solidity by:

$$\sigma_a = \frac{c_a}{s} = \frac{2}{0.8} \frac{w_a |w_{1u} - w_{2u}|}{w_2^2} = 2.5 \frac{w_a^2 |tg\beta_1 - tg\beta_2|}{w_2^2} = 2.5 \cos^2 \beta_2 |tg\beta_1 - tg\beta_2|.$$

For a compressor with $\beta_1 = -55^\circ$ and $\beta_2 = -35^\circ$, this formula results in $\sigma_a = c_a / s = 1.22$. The chord solidity is $\sigma = \frac{c}{s} \approx \frac{c_a / s}{\cos \beta_m} = 1.78$. For a turbine with $\beta_1 = 0^\circ$ and $\beta_2 = -60^\circ$ corresponds $\sigma_a = c_a / s = 1.08$ and $\sigma = 1.43$.

The tangential force coefficient is related to the lift coefficient. Ignoring the effect of losses, the lift coefficient of a cascade is

$$L = \rho |\Gamma| w_m = \frac{1}{2} \rho w_l^2 C_{Ll} c.$$

So:

$$C_{Ll} = \frac{2|\Gamma| w_m}{w_l^2 c} = \frac{2s |w_{2u} - w_{1u}| w_m}{w_l^2 c} = \frac{2|\Delta w_u| w_m}{\sigma w_l^2}. \quad (2.28)$$

With $c_a / c \approx \cos \beta_m = w_a / w_m$ (for w_a constant), the tangential force coefficient (2.27) is

$$C_{Fu} = \frac{2|\Delta w_u| w_a s}{w_2^2 c_a} \approx \frac{2|\Delta w_u| w_m s}{w_2^2 c} = \frac{2|\Delta w_u| w_m}{\sigma w_l^2} \left(\frac{w_l}{w_2} \right)^2. \quad (2.29)$$

From the comparison between Eq. (2.28) and Eq. (2.29) follows that the tangential force coefficient is a lift coefficient, related to the outlet dynamic pressure. Zweifel's reasoning thus demonstrates that the lift coefficient with a cascade has to be related to the outlet kinetic energy.

So, for an axial cascade:

$$C_{L2} = \frac{2|\Delta w_u| w_m}{\sigma w_2^2} \approx C_{Fu} = \frac{2|\Delta w_u| w_a}{\sigma_a w_2^2}.$$

The value of the tangential force coefficient C_{Fu} with present-day, optimally functioning, turbine cascades is about 1.0–1.2. The separation value is 1.4–1.6. These values are the same for constant density and variable density fluids and do not depend on the outlet Mach number for compressible fluids. The tangential force coefficient may very reliably be applied to turbine cascades. With pump, fan and compressor cascades, application of C_{Fu} is possible as well. The optimal value is about 1.0–1.2 as well, but values show a much larger spreading than with turbines (see next section).

2.2.9 The Lieblein Diffusion Factor

With strongly decelerating cascades, the lift potential is also determined by the inlet velocity level. Therefore, the lift coefficient C_{L2} , but as well C_{L1} , is not universally applicable. Figure 2.16 shows typical velocity distributions near the blade surface (boundary layer edge) of a strongly accelerating turbine cascade and a strongly decelerating compressor cascade. The figure demonstrates that the tangential force with the turbine is strongly correlated to the outlet dynamic pressure. The correlation is much weaker with the compressor cascade, due to the strong acceleration downstream of the leading edge stagnation point, both on suction and pressure sides. Consequently, the tangential force is also determined by the value of the inlet dynamic pressure. Deceleration is limited with fans and pumps and the tangential force coefficient can be applied more reliably than with compressors. When studying axial turbines, axial fans and axial pumps, the tangential force coefficient, according to Eq. (2.29) may be applied. With compressor cascades, the concept of the *diffusion factor* is mostly used to determine the lift capacity of a cascade. This concept was introduced by Lieblein in the 1950s and there have been some variants. A diffusion factor is the ratio of the deceleration at the suction side ($w_{max} - w_2$) to a reference velocity, mostly w_1 . The diffusion factor in that sense will be discussed in Chap. 13 (axial compressors). With axial and radial fans and pumps, the concept of *local diffusion factor* may be used as well. It is the ratio of ($w_{max} - w_2$) to w_{max} .

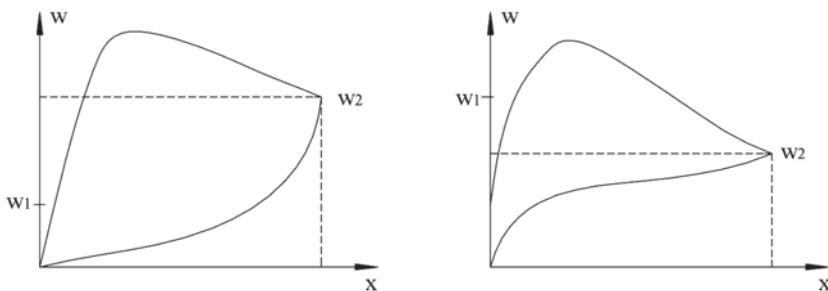


Fig. 2.16 Velocity distribution near the blade surface in a highly loaded turbine cascade (*left*) and a highly loaded compressor cascade (*right*)

A criterion for avoidance of separation is that this factor should be limited to 0.5. This means that $(w_{max} - w_2)$ must not exceed w_2 . This criterion may also be applied to estimate the lift capacity of a cascade. We will use the local diffusion factor for radial cascades in Chap. 3. So:

$$DF = \frac{w_{max} - w_2}{w_l} \quad \text{and} \quad D_{loc} = \frac{w_{max} - w_2}{w_{max}}.$$

2.2.10 Performance Parameters of Axial Cascades

The losses within the cascade are expressed by the total pressure drop $(p_{01} - p_{02})$, relative to the inlet dynamic pressure q_1 with a decelerating cascade or to the outlet dynamic pressure q_2 with an accelerating cascade. Literature offers correlations to determine loss coefficients. Methods differ for decelerating and accelerating cascades. The deviation angle δ can be determined, as well as the optimal value of the angle of incidence i . The study of these correlations exceeds the objective of the present book. We further use simple correlations. We refer to Dixon and Hall [2], Japikse and Baines [4] for more complete correlations concerning cascades.

2.3 Channels

2.3.1 Straight Channels

For a straight channel with constant cross-section area A and with fully developed flow (velocity profile does not change in flow direction), the relation between the pressure drop (denoted here by $-\Delta p$) and the shear stress on the wall is

$$A(-\Delta p) = \tau_w O L,$$

with O being the circumference and L the length of the part considered. Thus

$$\frac{-\Delta p}{\rho} = \frac{\tau_w}{\rho} \frac{O}{A} L = \frac{\tau_w}{\frac{1}{2}\rho \bar{v}^2} 4 \frac{L}{D} \left(\frac{1}{2} \bar{v}^2 \right).$$

D is the hydraulic diameter ($D = 4A/O$) and \bar{v} the average velocity. The term $-\Delta p/\rho$ represents the mechanical energy loss $-\Delta E_m$. A loss coefficient is defined by

$$\xi = \frac{-\Delta E_m}{\frac{1}{2}\bar{v}^2} = f \frac{L}{D}, \quad (2.30)$$

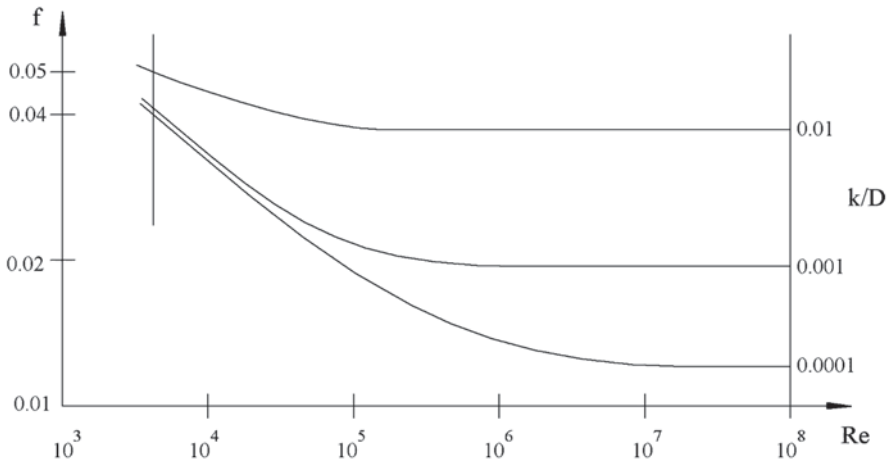


Fig. 2.17 Friction factor with circular ducts. (Moody friction factor chart)

where f is the Darcy friction factor. The Fanning friction factor is applied sometimes, defined by $\tau_w / (1/2 \rho \bar{v}^2)$. There is a ratio 4 between both factors. Figure 2.17 shows schematically the well-known Moody diagram for ducts with a circular section. The Darcy friction factor is represented. The full diagram is published in almost all books on basic fluid mechanics. It can also be found on many internet sites (look for Moody friction factor chart).

The Colebrook-White equation renders the friction factor for turbulent flows:

$$\frac{1}{\sqrt{f}} = -2 \log \left[\frac{2.51}{Re \sqrt{f}} + \frac{k}{3.7D} \right].$$

The Reynolds number is defined by $Re = \bar{v}D / \nu$, with ν being the kinematic viscosity coefficient. Roughness is represented by the equivalent sand-grain roughness k . The implicit equation may be replaced with a very good approximation (better than 1.5%) by the explicit equation of Haaland [3]:

$$\frac{1}{\sqrt{f}} = -1.8 \log \left[\frac{6.9}{Re} + \left(\frac{k}{3.7D} \right)^{1.11} \right].$$

Channels in turbomachines never have a constant cross section and a fully developed flow. It is customary however to estimate friction losses with the Moody-diagram on the basis of an average length and an average hydraulic diameter. Therefore, the applied method only gives an approximation.

2.3.2 Bends

Flow in a bend changes pressure and velocity distributions, generates adverse pressure gradients and secondary flows and the curvature affects the turbulence.

Figure 2.18 sketches the velocity distribution with an ideal fluid (frictionless). The centrifugal force due to flow curvature generates a static pressure increase at the bend outer part. Velocity is lower at the outer than at the inner part. There is an adverse pressure gradient at the entrance of the outer part and at the exit of the inner part of the bend. The effect of friction causes the velocity to be higher within the flow core than at the walls. The consequence is that the centrifugal force due to bend curvature is higher within the flow core. The difference generates two vortex flows as sketched in Fig. 2.19. This transverse flow is termed *secondary flow*. Low-energy fluid migrates from the outer part of the bend to the inner part. With 45° bends, with ratios of the radius of curvature of the bend to the diameter of 1–3, which are common values, it comes out that low-energy fluid arrives in the adverse pressure gradient zone at the bend exit. There is then a separation risk. With larger bend angles, core fluid arrives in the adverse pressure gradient zone at the bend exit. There is thus a far lower separation risk with a 90° degree bend, which is a surprising observation. Bends further affect the turbulence. Higher and lower velocity turbulent eddies occur simultaneously at a certain place. Eddies with high instantaneous velocity are subjected to high centrifugal force. These eddies migrate to the bend outer part. They create vortex motions in the boundary layer that break down into turbulence. The consequence is that turbulence at the outer part of the bend increases. Inversely, eddies with low instantaneous velocity migrate to the inner part and damp the turbulence there. This phenomenon of *turbulence migration* is clearly observed [6], but is not fully understood yet. We will describe it with the term *turbulence segregation*. A consequence of the segregation is weakening of the boundary layer at the inner part. This further increases the boundary layer separation risk at the bend inner part in the exit region.

Bend phenomena occur intensively in centrifugal rotor channels. At the inlet, flow is deflected from the axial into the radial direction. Deflection also occurs within the rotor channels, and the Coriolis force generates a similar segregation effect as the centrifugal force. A bend represents a supplementary loss, on the one hand because of increased friction within the bend, on the other by flow homogenisation downstream of the bend. By homogenisation we mean here the recovery process of the velocity profile towards an equilibrium profile adapted to the downstream channel. Velocity rearrangement of the fluid layers produces vortices that break down into turbulent eddies. These eddies interact and further break down to smaller size. The smaller the turbulent motion, the greater the impact of viscosity forces onto the motion and the greater the fraction of the energy dissipated in heat during the breakdown from larger to smaller structures. This process, causing energy dissipation, is termed the *energy cascade*. Figure 2.20 illustrates the dissipation process associated to velocity profile recovery

Fig. 2.18 Pressure and velocity distributions for flow of an ideal fluid in a bend

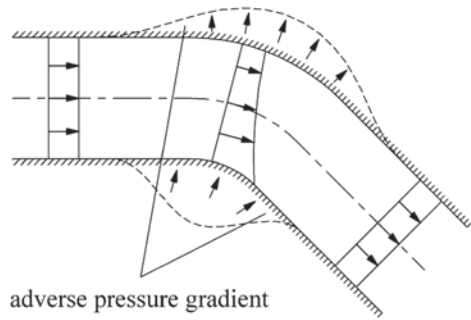
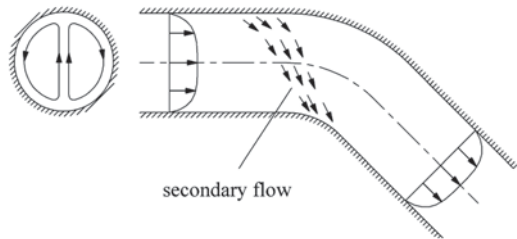


Fig. 2.19 Secondary flow; vortex motions in a cross section (*left*); secondary flow pattern near the wall (*right*)



after a sudden expansion. The recovery after a bend is similar. With a bend of 90° and $r/d = 2$, the bend loss coefficient amounts to 0.16. About half of the loss occurs in the bend itself and about half is due to homogenisation after the bend.

At the inlet of a centrifugal machine, the losses due to homogenisation are not assigned to the inlet, as the inlet is not followed by a duct in which homogenisation could occur. So, the order of magnitude of the loss coefficient due to the bend is about 0.1, but the inhomogeneous inlet flow of the rotor reduces its efficiency. In the same way, homogenisation loss downstream of the rotor is not assigned to the rotor. A mixing space may occur after the rotor. Mixing losses are calculated for this space. If there is a diffuser immediately downstream of the rotor, its efficiency is impaired due to the inhomogeneous flow. The effect of inhomogeneous inflow with a diffuser will be discussed in the next section.

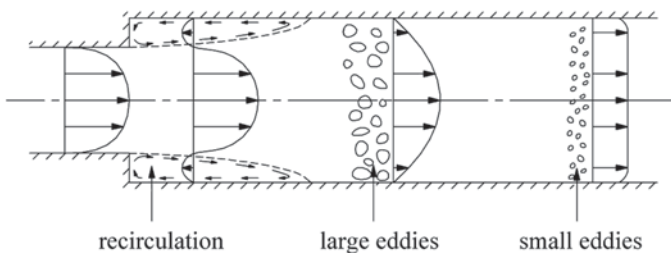


Fig. 2.20 Diffusion by sudden expansion (dump diffusion)

2.4 Diffusers

2.4.1 Dump Diffusers

Figure 2.20 sketches the flow in a sudden expansion of a channel. Flow is decelerated. A sudden expansion thus functions as a diffuser. The figure also illustrates the loss mechanism by mixing. The loss is the kinetic energy related to the velocity difference (see Exercise 2.5.4):

$$q_{irr} = \frac{(v_1 - v_2)^2}{2} = \left(1 - \frac{v_2}{v_1}\right)^2 \frac{v_1^2}{2} = \left(1 - \frac{A_1}{A_2}\right)^2 \frac{v_1^2}{2} = \xi \frac{v_1^2}{2}. \quad (2.31)$$

Diffusion by sudden expansion or dump diffusion is efficient with a rather small area ratio. For instance, $A_2/A_1 = 1.25$ gives $\xi = 0.04$. A higher area ratio is useful as well. For instance, $A_2/A_1 = 2$ gives $\xi = 0.25$. A loss coefficient with value 0.25 is not disadvantageous for a diffuser, as will be discussed below. That is why dump diffusion is applied in turbomachines, which is rather surprising at a first glance. The main advantage of dump diffusion is its realisation in a short distance.

2.4.2 Inlet Flow Distortion

Diffusers are channels where flow is decelerated and dynamic pressure is converted into static pressure. This process is called *pressure recovery*. The attainable pressure recovery or diffusion strongly depends on the uniformity of the incoming flow. Figure 2.21 compares the diffusion with uniform and non-uniform incoming flow of an ideal fluid. In both cases, 50% dynamic pressure recovery based on the average inlet velocity is intended. The figure shows the position where the 50% recovery is obtained. With the uniform flow, the corresponding velocity is $\sqrt{1 - 0.5} \approx 0.71$ times the inflow velocity and the corresponding section area is 1.41 times the inflow section area. With a non-uniform inlet, a larger area ratio is required, so a larger covered length with a given opening angle, due to the much faster velocity decrease of the slower part of the flow. At inflow, the velocities are 1.25 and 0.75 times the average velocity. The necessary reduced velocities are $\sqrt{(1.25)^2 - 0.5} \approx 1.03$ and

Fig. 2.21 Diffusion with uniform and non-uniform inlet flow

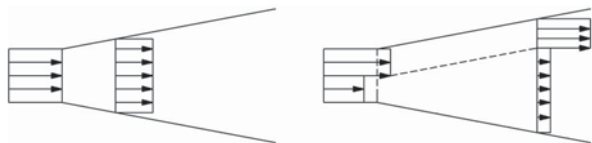
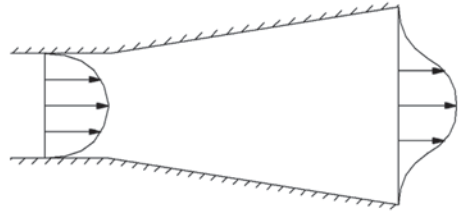


Fig. 2.22 Velocity profile evolution within a diffuser with limited length



$\sqrt{(0.75)^2 - 0.5} = 0.25$ times the average inflow velocity. The corresponding section area is 2.11 times the inflow section area. The conclusion is that disturbance of the inlet flow uniformity causes a reduction of the possible pressure recovery. Length limitation normally occurs with turbomachines, generating an inherent limitation of the pressure recovery.

Within a real flow, the velocity at the walls equals zero. The slow flow at the walls can only participate in the diffusion process when there is momentum transfer from the core flow. This transfer is due to molecular viscosity and to turbulent mixing. Both processes are coupled with energy dissipation. In the first phase of a diffusion process, strong deceleration near the walls occurs. This results in a shear stress zone moving to the centre as the fluid advances through the diffuser. Turbulence produced by the shear enhances momentum exchange. At the outlet of diffusers with a limited length, the core flow is nearly unaffected. Figure 2.22 illustrates the inhomogeneous velocity pattern at the outlet caused thereby. Velocity has only decreased little within the flow core. From that we infer that insufficient possibility for deceleration within the core flow, more than energy dissipation, constitutes the main limitation of the pressure recovery. Figure 2.22 also shows that the loss mainly consists of mixing loss downstream of the dif-

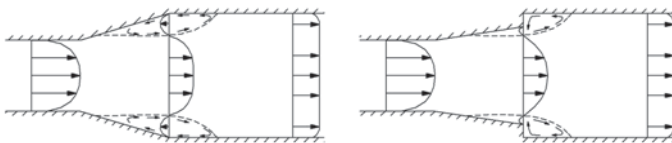
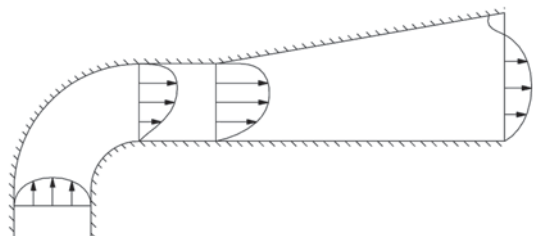


Fig. 2.23 Diffusion with separation; *left*: large separation zone; *right*: reduced separation zone by combination with sudden expansion

Fig. 2.24 Postponed diffusion after a bend and diffusion concentration on the high-energy side



fuser. The flow structure is not highly different from that with dump diffusion. Diffusion within a gradually widening channel so intrinsically is a process with high losses.

2.4.3 Flow Separation

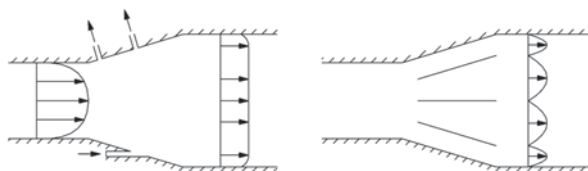
Separation occurs when the divergence of a diffuser is too strong. Pressure recovery within a diffuser with large separation is low and the exit flow is heavily deformed, with backflow at some places. Large-scale backflow is illustrated in Fig. 2.23 (left). It occurs with strong divergence and is nearly steady. The flow pattern is denominated *steady stall*. With less strong divergence, the separation is typically time dependent. Separation zones then build up repeatedly inside the diffuser and are moved out by convection. This growth and removal pattern is termed *transitory stall*. When diffusers function in transitory stall, large fluctuations in pressure recovery and outlet velocity distribution occur. A separation zone with strong backflow, as in Fig. 2.23 (left), causes large mixing losses downstream of the diffuser. It might then be more advantageous to combine a diffuser with a lower opening angle with a dump diffuser, as shown in Fig. 2.23 (right).

2.4.4 Flow Improvement

As the efficiency of a diffuser depends strongly on the uniformity of the velocity at the inlet, efficient diffusion might be impossible if the inlet velocity varies too much. Figure 2.24 shows, as an example, a diffuser downstream of a bend. It is then better to postpone the diffusion in order to reduce the distortion of the profile and to concentrate the divergence of the diffuser on the higher energy side.

Diffuser efficiency may be further improved as illustrated in Fig. 2.25. Very efficient is removal of low-energy flow at the wall by suction (Fig. 2.25 left, top wall). A somewhat similar approach is energy addition by injection in the boundary layers by tangential slots (Fig. 2.25 left, bottom wall). These techniques are applied only under special circumstances as with wind tunnel diffusers or when the fluid is drained for secondary purposes. A simple method consists in mounting guiding surfaces in a diffuser with a wide opening angle. This is mostly the only practical method to improve the outlet flow distribution (for dimensioning see 2.4.6).

Fig. 2.25 Removal of low-energy fluid (left; top wall); injection of high-energy fluid (left; bottom wall); application of guiding surfaces (right)



Mounting guiding surfaces is easy with two-dimensional diffusers, but somewhat more complex with conical diffusers.

2.4.5 Representation of Diffuser Performance

Geometrical characteristics are shown in Fig. 2.26. These are the inlet and outlet areas A_1 and A_2 , the length L and the hydraulic radius R of the inlet section (R_1 for a circle; H_1 for rectangle with high aspect ratio). A common way to represent pressure recovery is shown in Fig. 2.27 [6]. Lines of constant pressure recovery are plotted in a diagram with diffuser length to inlet radius ratio in the abscissa and the area ratio in the ordinate.

Pressure recovery is expressed with a coefficient C_p defined by

$$C_p = \frac{p_2 - p_1}{\frac{1}{2}\rho \bar{v}_1^2}.$$

The loss coefficient, in principle, is

$$\xi = \frac{p_{01} - p_{02}}{\frac{1}{2}\rho \bar{v}_1^2} = 1 - \left(\frac{\bar{v}_2}{\bar{v}_1}\right)^2 - C_p = C_{p,id} - C_p,$$

where $C_{p,id}$ is the ideal pressure recovery coefficient:

$$C_{p,id} = 1 - \left(\frac{A_1}{A_2}\right)^2.$$

For a diffuser with a free outlet, outlet kinetic energy is a loss as well, and so

$$\xi = \frac{p_{01} - p_2}{\frac{1}{2}\rho \bar{v}_1^2} = \frac{p_1 + \frac{1}{2}\rho \bar{v}_1^2 - p_2}{\frac{1}{2}\rho \bar{v}_1^2} = 1 - C_p.$$

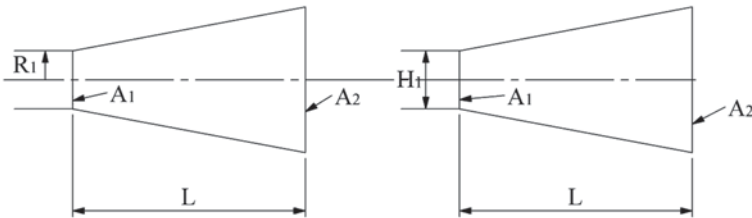


Fig. 2.26 Geometrical characteristics of diffusers

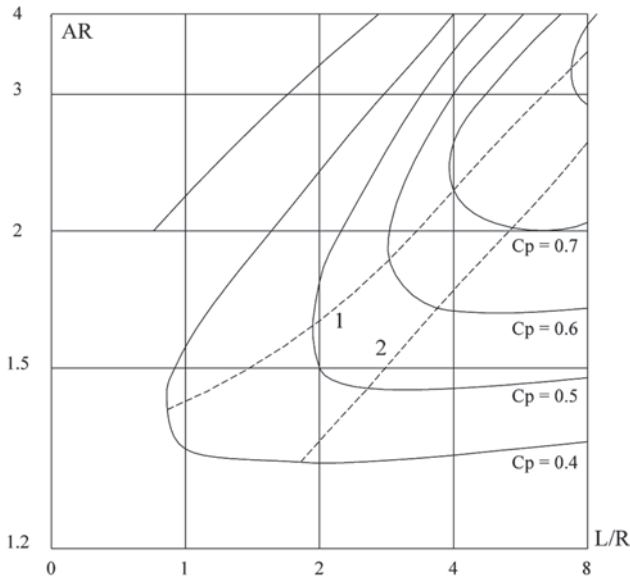


Fig. 2.27 Performance of conical diffusers with a uniform inlet profile and a free outlet; adapted from Miller [6]

The loss coefficient of a diffuser with a free outlet may be described again as $C_{p,id} - C_p$, with the ideal pressure recovery coefficient being unity.

The meaning of the dashed lines 1 and 2 in the diagram of Fig. 2.27 is that they separate the different flow regimes. In the area on the right of line 2, where the pressure recovery lines are nearly horizontal, flow is stable. With a constant area ratio, pressure recovery decreases with larger length due to increase of the friction surface. Diffusers in this area are unnecessarily long. Thus, for given area ratio, the most efficient diffusers with stable flow are just on line 2. Above line 1 steady stall occurs. For a given length, pressure recovery decreases with increasing area ratio. So, it is useless to operate a diffuser in this area. In the area between the two lines, transitory stall occurs. Most diffusers applied in practice have geometries in this region. Line 1 in Fig. 2.27 is approximately the surface ratio corresponding to minimum total pressure loss at a given length ratio (vertical tangents to the contour lines of C_p). Line 2 is approximately the length ratio corresponding to minimum total pressure loss at a given surface ratio (horizontal tangents to the contour lines of C_p). So, mostly, the lines separating the flow regimes are not drawn in a diffuser diagram and the user is supposed to know. In turbomachinery applications, where length limitation always occurs, in principle, the most efficient operation is for surface ratio corresponding to minimum total pressure loss at a given length ratio, thus on line 1. But this operation implies heavy unsteady stall or even steady stall. So, usually, for limiting oscillations, it is better to choose the geometry of a diffuser somewhere in the middle of the zone where the contour lines of pressure recovery change from horizontal to vertical direction.

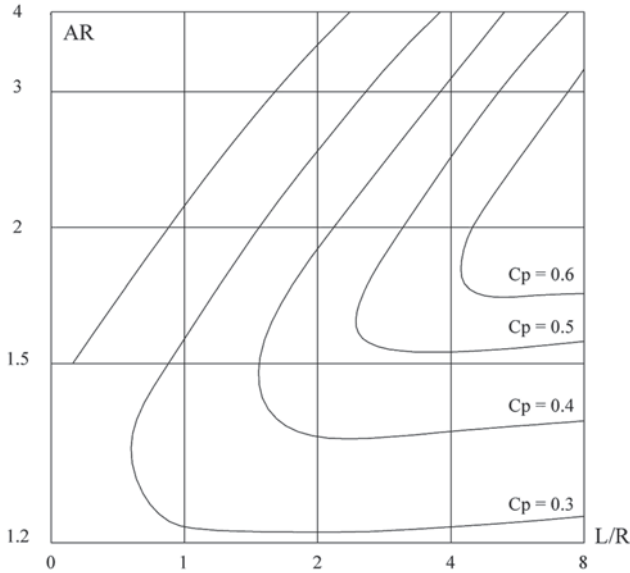


Fig. 2.28 Performance of conical diffusers with a fully developed inlet and a free outlet; adapted from Miller [6]

Figure 2.27 shows the pressure recovery with a uniform incoming flow. The corresponding diagram for a fully developed inflow is shown in Fig. 2.28 [6]. Both diagrams are valid with $Re = 10^6$. A minor correction for the change of the Reynolds number is required. Figure 2.29 shows the performance of conical diffusers connected to circular ducts at inlet and outlet, with fully developed inlet flow. For large length, the contour lines are similar to these of the previous diagrams. Differences occur with short dimensionless lengths.

The mixing after diffusion in a constant section pipe results in a static pressure increase. The length of the duct required to obtain complete mixing depends on the area ratio and the diffuser angle but typically is about 4 diameters. After the maximum pressure position, the friction factor remains somewhat higher than that of a fully developed flow during 20–50 diameters. The loss coefficient for this additional loss is about 0.1. The pressure recovery shown in Fig. 2.29 is the pressure recovery at the maximum pressure position.

2.4.6 Equivalent Opening Angle

A diffuser may be characterised by a half opening angle. For a conical diffuser, this is

$$\tan \alpha = \frac{R_2 - R_1}{L}.$$

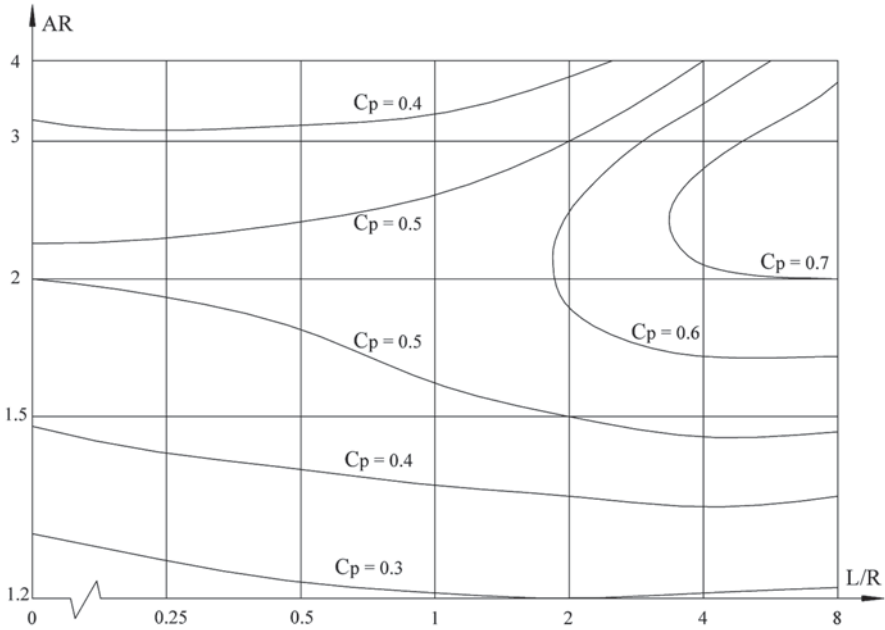


Fig. 2.29 Performance of conical diffusers incorporated in ducts; adapted from Miller [6]

For a general diffuser the same formula is used with the hydraulic radius and the term equivalent opening angle is employed. From the performance diagrams 2.27–2.28 follows that optimum operation approximately corresponds to an opening angle $2\alpha = 18^\circ$ to 8° , for the length ratio varying from small to large. If the diffuser length that is available for the desired velocity reduction, i.e. the area ratio, is too small, either a diffuser followed by a sudden expansion (Fig. 2.23) or guiding surfaces (Fig. 2.25) should be applied. The number of guiding surfaces should be determined so that the equivalent opening angle criterion is met for each partial diffuser.

2.4.7 Diffusion in a Bend

All phenomena occurring in bends and straight diffusers occur in a still more extreme form in a bent diffuser. By adding a bend immediately downstream of a diffuser, the adverse pressure gradient at the outward part of the bend entrance increases (see Fig. 2.18) and there is high risk for separation. Addition of a diffuser downstream of a bend steepens the pressure gradient at the inward part of the exit of the bend (see Fig. 2.18) and makes separation very likely. From the above

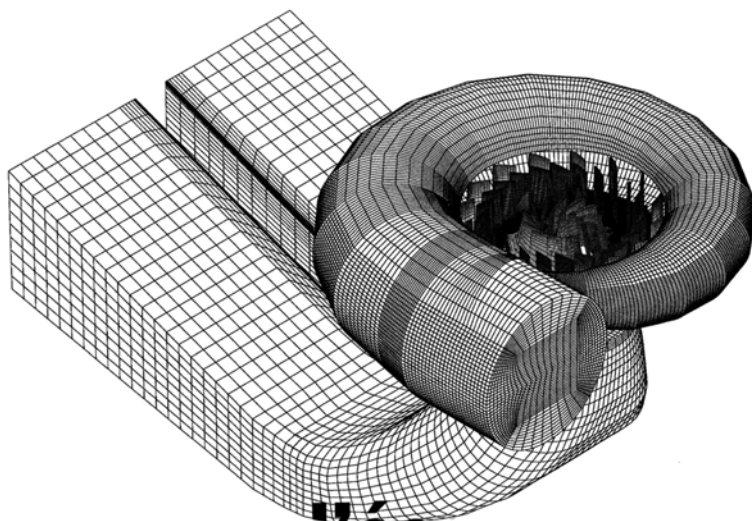
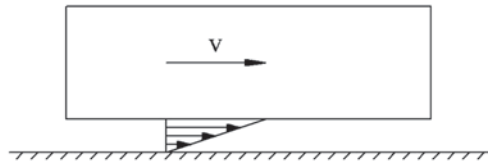


Fig. 2.30 Optimised bent diffuser of a Francis-turbine (courtesy ANDRITZ HYDRO)

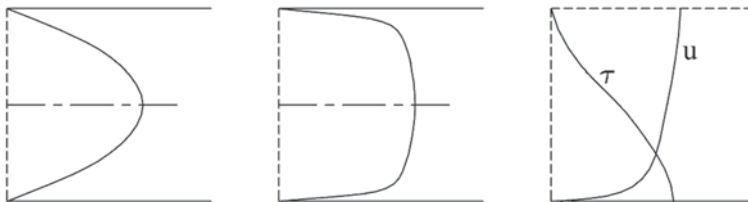
examples it is clear that diffusion within a bend is delicate. The phenomena discussed before, such as secondary flow and segregation of turbulent eddies, strongly intervene. However, a design in which bend phenomena and diffusion are well matched allows a pressure recovery that is far superior to that of a serially connected bend and a straight diffuser. The crucial aspect is useful application of secondary flow in order to bring high-energy fluid to the places with imminent separation. The optimum geometry strongly depends on the inlet conditions. The consequence is that there is no universal optimum geometry. For instance, bent diffusers are optimised for vertical shaft hydraulic turbines. Figure 2.30 shows an example (Francis turbine). A pressure recovery up to 75 % is attained. The optimisation requires computational techniques and turbulence models. At present, optimisation of stationary diffusers is very well possible. It is more difficult however for rotating diffusing channels (radial pumps and compressors), as complex secondary flow patterns intervene. Notice that a large pressure recovery requires a sufficient covered length (Fig. 2.30). Most radial pumps, fans and compressors have limited rotor channel lengths. Hence, the earlier mentioned limit of velocity deceleration ratio w_2/w_1 of about 0.8–0.9 in order to avoid separation. In some radial compressors, rotor channels with greater lengths are applied, by mounting an inducer (see Chap. 14). A velocity ratio w_2/w_1 as low as 0.6 may then be realised, but the pressure recovery is not very good, however. Figure 2.24 is intended as a practical suggestion to combine a bend with a diffuser without applying means of optimisation. It is advisable to mount the bend first, and then a duct segment with constant section (length about one diameter) in which mixing occurs by secondary flow, followed by an asymmetrically mounted diffuser.

2.5 Exercises

2.5.1. The figure sketches laminar flow between a moving block and a stationary flat wall. The block moves parallel to the wall at velocity v . There is no pressure difference in the flow direction in the space between the block and the wall. Reason that the shear stress τ within the shear layer is constant. Demonstrate that dissipated work per surface unit and per time unit equals displacement work ($v \cdot \tau$) exerted by the object onto the shear flow. Demonstrate that this result remains valid with turbulent flow.

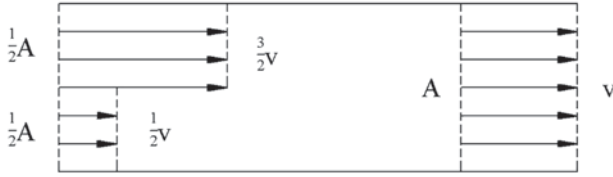


2.5.2. The left figure sketches the velocity profiles in a 2D-channel with fully developed laminar flow of an incompressible fluid ($\rho = \text{constant}$, $m = \text{constant}$). Fully developed flow means that no change of velocity profile occurs in the flow sense. Derive that the shear stress varies linearly from the wall value τ_w to zero in the channel centre. Demonstrate that the velocity profile is a parabola. Derive that the energy dissipated per wall surface unit and per time unit equals $U_m \tau_w$, with U_m being the average velocity within the channel. Note that for attaining these results nothing more is necessary than that the shear stress varies linearly along the height. So argue that the same result is attained with a turbulent profile (central figure) ($\mu_t \neq \text{constant}$). The right figure sketches the velocity and shear stress profiles with a turbulent flow of a boundary layer over a flat plate at a zero pressure gradient. The boundary layer grows. So the flow is not fully developed. The shear stress profile differs little from a linear one. So, the former result is still valid with a good approximation.



2.5.3. The figure sketches the mixing of two flows with velocities $3/2 v$ and $1/2 v$ within a 2D-channel. Both flows occupy half the section. Velocity therefore is v after complete mixing. Determine the pressure increase by complete mixing. Determine the energy dissipation by mixing per mass flow rate unit, ignoring friction.

$$A: \quad \frac{\Delta p}{\rho} = \frac{1}{2} \frac{v^2}{2}; \quad q_{irr} = \frac{1}{4} \frac{v^2}{2}.$$

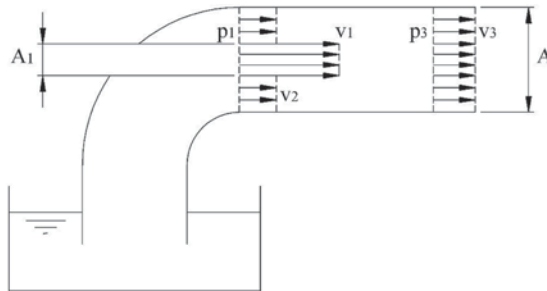


2.5.4. The figure sketches a flow with sudden expansion (dump diffusion). Determine the pressure increase and the energy dissipation per mass flow rate unit.

$$A: \quad \frac{\Delta p}{\rho} = v_1 v_2 - v_2^2 = 2 \frac{A_1}{A_2} \left(1 - \frac{A_1}{A_2}\right) \frac{v_1^2}{2}, \quad q_{irr} = \frac{1}{2} (v_1 - v_2)^2 = \left(1 - \frac{A_1}{A_2}\right)^2 \frac{v_1^2}{2}.$$



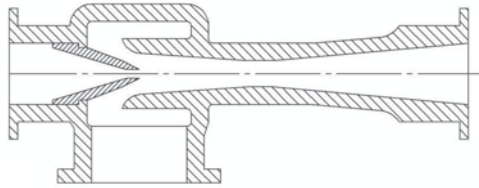
2.5.5. The figure is a sketch of a jet pump. Water is injected from an external source at velocity v_1 into a tube, driving water from the suction pipe to velocity v_2 at the injector outlet position. Determine the pressure increase in the driven flow. Determine the pump characteristic as the mechanical energy increase of the driven flow $\Delta E_{m2} = (p_{03} - p_{02}) / \rho$ as a function of its mass flow rate at given values of A_p , A and v_1 . Define surface ratio $\alpha = A_1 / A$ and velocity ratio $U = v_1 / v_2$. Take $\alpha = 0.4$ as an example and consider U as a mass flow rate measure. Define a pressure coefficient $\psi = \Delta E_{m2} / (v_1^2 / 2)$.



Study the energy exchange. An expression for the energy increase in the driven flow has already been formulated. Determine the mechanical energy decrease in the driving jet flow $(p_{01} - p_{03}) / \rho$. In most applications, the driving water for the jet is tapped from the flow in the pressure pipe. Driving water is then produced with a pump increasing the total pressure p_{03} to the total pressure p_{01} . With an ideal pump, the energy increase required exactly equals the mechanical energy decrease within the driving jet between the injection point (1) and the jet pump outlet (3). The ratio of the energy increase in the driven flow to the energy decrease in the driving flow may then be defined as the efficiency η of the jet pump. Note that this efficiency definition also applies with driving water from another origin.

Determine the efficiency η for varying α and U . Study the values of $\alpha=0.2, 0.4, 0.6, 0.8$ combined with the values of $U=0, 0.25, 0.50, 0.75, 1$. Observe that the efficiency is weakly dependent on α , but strongly dependent on U . To attain a good efficiency (better than 0.75), U must exceed about 0.6. This implies that the velocity difference between driving and driven flow at the mixing position must not be too big. This is obvious, as the loss considered is mixing loss. The driven jet must thus be highly accelerated at the position of the injector. See the geometry of a real jet pump as shown in the figure below. The velocity of the driven jet must mostly be limited in order to avoid cavitation. For instance, to $v_2 = 10$ m/s corresponds a pressure decrease in the suction pipe of $\rho v_2^2 / 2 = 50000 \text{ Pa} = 0.5 \text{ bar}$. Such a strong pressure decrease implies that the geometrical suction height must be under 5 m. Jet pumps are therefore mostly mounted below the water surface in the suction well (submerged). A pressure drop of 0.5 bar is then no problem. A diffuser beyond the mixing chamber is required as well. In the example quoted, velocity exceeds 10 m/s after mixing, but the velocity in a pipe is typically at maximum about 2 m/s. So the diffuser generates substantial losses. Attaining a considerable pressure increase with good efficiency is thus impossible.

For the study of pressure increase and mass flow rate in the driven flow, we define still other parameters. As the measure for the pressure increase, we define the ratio δ of the total pressure increase in the driven flow to the total pressure decrease in the driving flow. As the measure for the mass flow rate, we define the ratio μ of the mass flow rate of the driven flow to the mass flow rate of the driving flow. With these definitions, the efficiency is $\eta = \mu\delta$. Determine δ and μ for varying α and U . Study again the values of $\alpha=0.2, 0.4, 0.6, 0.8$ combined with the values of $U=0, 0.25, 0.50, 0.75, 1$. Observe that, for a similar efficiency, as well a low mass flow rate together with a high pressure increase as a high mass flow rate together with a low pressure increase may be chosen. The choice of the combination is mainly determined by the parameter α with only a weak effect of the value of U . Since the analysis takes neither the friction loss in the mixing chamber nor the diffuser loss into account, the velocity ratio should be chosen lower in practice than the values obtained from the analysis. Then, velocities in the mixing chamber and in the diffuser decrease. A practical value of U is about 0.5. The efficiency obtained in the analysis is about 0.65, arriving at about 0.35 in practice.



2.5.6. The figure sketches a moving linear cascade of cylindrical rods. The oncoming flow has velocity v_l . The speed of the rods is u . The ratio of the blade speed to the oncoming flow velocity is termed the *speed ratio*, being here $\lambda = u/v_l = 8$. The solidity of the cascade is $\sigma = d/s$, where d is the diameter of the rods. We choose here $\sigma = 1/8$, assuming a drag coefficient $C_D = 1$. Determine the velocity downstream of the rods. Determine the work done on the fluid. Determine mechanical energy increase within the flow and the energy dissipated. With cascade analysis it is customary to express the velocity components at the position of the cascade in proportion to the oncoming velocity and the blade speed. The axial and tangential velocity components of a driven cascade are represented by $w_a = v_l(1 + a)$, $w_{mu} = -u(1 - b)$. The factors a and b are called *interference factors*. With a linear cascade, as sketched in the figure, $a = 0$.

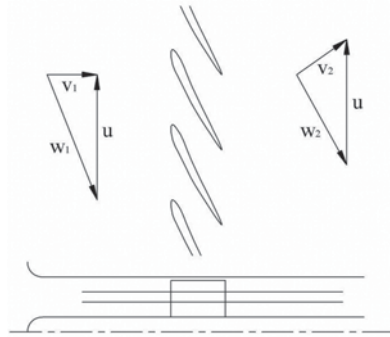
$$\mathbf{A} : b = 0.173, v_{2u} / u = 2b, \Delta W / u^2 = 2b = 0.346, \Delta E_m / u^2 = 0.053, q_{irr} / u^2 = 0.293$$



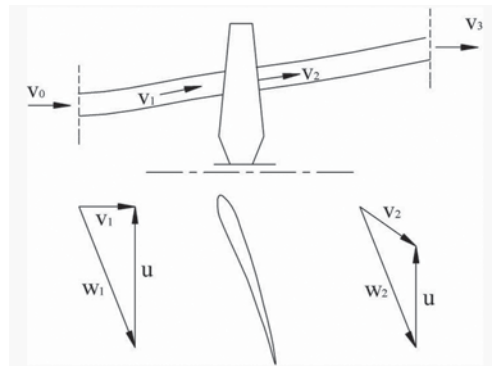
2.5.7. The figure is a sketch of an annular streamtube with an infinitesimal height through the rotor of an axial fan. The rotor blade speed within the section of the streamtube is u . As speed ratio we choose $\lambda = u/v_a = 3$, being a typical value for a half radius section (tip value $\lambda_T = 6$). Applying an interference factor, as in the previous exercise, we set $w_{2u} = -u(1 - 2b)$. The solidity of the cascade is $\sigma = c/s = 2/3$. We choose $C_L = 1$ as the lift coefficient, ignoring the drag, so $C_D = 0$. Determine the work done on the fluid. Determine the static pressure increase across the rotor. What is the degree of reaction? What is the static pressure increase obtained by the fan by addition of a stator turning the velocity into the axial direction?

$$\mathbf{A} : b = 0.152, \frac{\Delta W}{u^2} = 2b = 0.304, \frac{\Delta(p/\rho)}{u^2} = 2b - 2b^2 = 0.258,$$

$$\frac{\Delta(v^2 / 2)}{u^2} = 0.046, R = 0.848.$$



2.5.8. The figure is a sketch of an annular streamtube with an infinitesimal height through a wind turbine rotor. The velocity far upstream is v_0 . The rotor blade speed within the streamtube section is u . As speed ratio we choose $\lambda = u/v_0 = 3$, being a typical value for a half radius section (a typical tip value is $\lambda_T = 6$; see Chap. 10 on wind turbines).



Due to the power extraction, the velocity within the streamtube decreases. With interference factors, we set $v_{1a} = v_{2a} = v_0(I - a)$ en $w_{2u} = -u(I + 2b)$. Positions 1 and 2 are situated immediately upstream and downstream of the blade segment. The components of the average velocity on the blade segment are $w_{ma} = v_0(I - a)$ and $w_{mu} = -u(I + b)$. Cascade solidity $\sigma = c/s = 1/12$. We take $C_L = 1$ as the lift coefficient and ignore the drag, thus $C_D = 0$. Determine the velocity immediately upstream and downstream of the rotor within the streamtube considered. Determine the power transferred. Assume, as with the one-dimensional propeller analysis in Chap. 1 (Exercise 1.9.5), that there is symmetry in the pressure variation within the streamtube upstream and downstream of the rotor, so that the resulting pressure force onto the streamtube envelope into the axial direction equals zero.

A: The momentum balance (no pressure force in axial direction) into the axial direction on the streamtube results in

$$-L_a = \rho s v_{1a} (v_{3a} - v_0). \quad (2.32)$$

Momentum into the axial direction locally results in

$$L_a = (p_1 - p_2)s.$$

Combination gives
$$\frac{p_1 - p_2}{\rho} = v_{1a} (v_0 - v_{3a}). \quad (2.33)$$

The work equations within the streamtube upstream and downstream of the rotor are

$$\frac{p_a}{\rho} + \frac{v_0^2}{2} = \frac{p_l}{\rho} + \frac{v_l^2}{2}, \quad \frac{p_2}{\rho} + \frac{v_2^2}{2} = \frac{p_a}{\rho} + \frac{v_3^2}{2}.$$

From that:
$$\frac{p_1 - p_2}{\rho} = \frac{v_2^2 - v_l^2}{2} + \frac{v_0^2 - v_3^2}{2} = \frac{v_{2u}^2 - v_{3u}^2}{2} + \frac{v_0^2 - v_{3a}^2}{2}. \quad (2.34)$$

Combination of (Eq. 2.33) and (Eq. 2.34) results in

$$v_{1a} (v_0 - v_{3a}) = \frac{v_0 + v_{3a}}{2} (v_0 - v_{3a}) + \frac{v_{2u}^2 - v_{3u}^2}{2}.$$

Due to the radius increase within the streamtube downstream the rotor, v_u decreases. Thus, v_{3u} is smaller than v_{2u} . We ignore the difference between v_{3u} and v_{2u} here. We accept that in (Eq. 2.34) $p_1 - p_2$ becomes somewhat smaller. This is equivalent to the assumption that some losses occur within the flow downstream of the rotor. With this simplification follows

$$v_{1a} = v_{2a} = \frac{l}{2} (v_0 + v_{3a}).$$

The flow deceleration is then, as with the one-dimensional analysis, the same upstream and downstream of the rotor.

We set $v_{1a} = v_{2a} = v_0(1 - a)$, $v_{3a} = v_0(1 - 2a)$, $v_{2u} = -u(2b)$.

The energy extraction in the streamtube according to (Eq. 2.34), ignoring the difference between v_{2u} and v_{3u} , is

$$\frac{p_1 - p_2}{\rho} + \frac{v_l^2 - v_2^2}{2} = \frac{v_0^2 - v_{3a}^2}{2} - \frac{v_{2u}^2}{2} = \frac{v_0^2}{2} (4a - 4a^2) - \frac{u^2}{2} (4b^2). \quad (2.35)$$

The energy extraction according to Euler's formula is

$$\Delta W = u(v_{lu} - v_{2u}) = u(2bu). \quad (2.36)$$

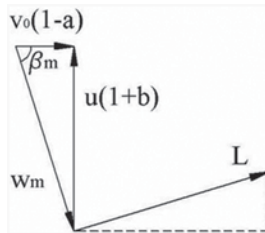
Equality of (Eq. 2.35) and (Eq. 2.36) results in

$$b\lambda^2 = a(1-a) - b^2\lambda^2. \quad (2.37)$$

The momentum balance in the tangential direction locally on the blade segment is

$$-L_u = \rho v_{la}s(w_{2u} - w_{lu}) = \rho v_{la}sv_{2u} = -\rho v_{la}s2bu. \quad (2.38)$$

The velocity triangle at the position of the blade segment is sketched in the figure:



From this:

$$L_u = L \cos \beta_m = C_L \frac{1}{2} \rho w_m^2 c \frac{v_{la}}{w_m} \quad (2.39)$$

Combination of Eq. (2.38) and Eq. (2.39) results in

$$v_{la}s2bu = \frac{1}{2} C_L c v_{la} w_m,$$

or

$$2b = \frac{\sigma C_L}{2} \sqrt{\frac{(1-a)^2}{\lambda^2} + (1+b)^2}. \quad (2.40)$$

With $\lambda=3$ and $sC_L=1/12$, (Eq. 2.37) and (Eq. 2.40) result in: $a=0.2700$, $b=0.0214$.

The power exchanged per surface unit (Eq. 2.34) is

$$\rho v_0(1-a)2bu^2 = \rho \frac{v_0^3}{2} (1-a)4b\lambda^2 = \rho \frac{v_0^3}{2} \times 0.5624.$$

2.5.9. Verify the tangential force coefficient (Zweifel) of the steam turbine cascades shown in Fig. 1.11 of Chap. 1.

A: $R=0$: stator $C_{Fu}=0.50$ (low load), rotor $C_{Fu}=0.90$ (moderate load); $R=0.50$, stator and rotor: $C_{Fu}=0.50$ (low load).

2.5.10. A cylindrical tube should undergo a diameter increase with a factor 2. For this increase, there is only a length of 1 diameter available. Design an optimum

diffuser for this application with the Fig. 2.29 diagram. What is the realisable pressure recovery?

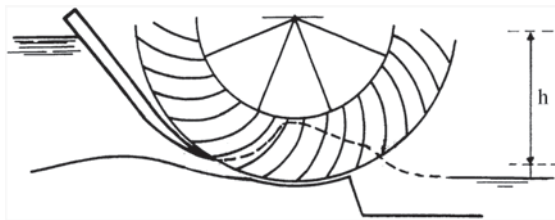
A: The most advantageous solution is a conical diffuser with an optimum opening angle (area ratio equal to 2), followed by a sudden expansion. The loss coefficient of the conical diffuser, $C_{p,id} - C_p$, is about 0.135 according to Fig. 2.29. The loss coefficient of the sudden expansion is 0.25 according to Eq. 2.31 (in reality somewhat higher due to inflow irregularity). The resulting loss coefficient based on inlet kinetic energy is $0.135 + 0.25/4 = 0.2025$. $C_{p,id} = 0.9375$. $C_p = 0.735$. This solution is more elegant than with guiding surfaces according to Fig. 2.25, which would require a very small opening angle of the partial diffusers (L/R about 16 according to Fig. 2.29). The pressure recovery of a conical diffuser with area ratio 4 is as low as for a sudden expansion: $C_p = 0.375$.

2.5.11. A diffuser with a free outlet has $L/R_i = 2$ and $AR = 1.5$. Determine, with Figs. 2.27 and 2.28, the increase of the pressure recovery coefficient when the inlet profile is transformed from fully developed into uniform.

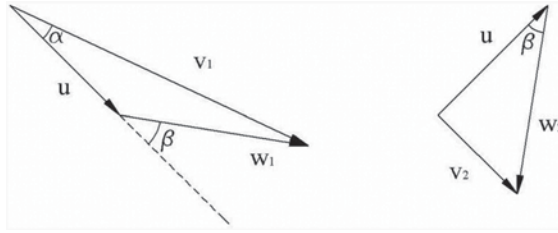
A: C_p goes from 0.45 to 0.50.

2.5.12. The figure shows a Poncelet-type waterwheel. This is an undershot waterwheel with curved blades. The water accelerates under the slide due to the height difference ($v_1^2 / 2 = gh$, ignoring losses). The direction of the water jet generated under the slide forms the angle α with the tangential direction at the periphery of the wheel. The wheel speed at the periphery (u) is allowed to vary. Magnitude and direction of the relative velocity at the wheel inlet change by this. We assume that the blade angle at inlet β is adapted so that the jet enters the wheel perfectly aligned with the blade direction (with a given machine, this condition is only correct for one operating point; thus we consider a design optimisation with a blade angle not given a priori). We assume that the water leaves the wheel at the same angle as at the inlet, so that $w_2 = w_1$.

Determine a formula for the rotor work at fixed values for v_1 and α and a variable value for u . Express the internal efficiency of the wheel, ignoring all friction losses. Determine at what peripheral speed the maximum efficiency occurs. Determine the velocity triangle at the outlet together with a formula for the outlet velocity v_2 . Interpret the efficiency attained, in other words determine which loss occurs. Conclude from the result that a small α is useful (in practice $\alpha = 15^\circ$ is applied). Is there still another apparent loss mechanism?



A: The figure sketches the velocity triangles at the inlet and the outlet of the rotor.



$$w_{1u} = v_{1u} - u = v_1 \cos \alpha - u; \quad w_{2u} = -w_{1u},$$

$$\Delta W = u(w_{1u} - w_{2u}) = 2u(v_1 \cos \alpha - u).$$

Maximum work is attained by $u = \frac{v_1 \cos \alpha}{2}$.

Maximum work is $(\Delta W)_{\max} = \frac{v_1^2}{2} \cos^2 \alpha$ with $\frac{v_1^2}{2} = gh$.

So: $\eta_i = \frac{\Delta W}{gh}$ and $(\eta_i)_{\max} = \cos^2 \alpha$.

In the inlet triangle, then $w_{1u} = \frac{v_1 \cos \alpha}{2} = u$.

In the outlet triangle, then $w_{2u} = -u$.

The outlet triangle is orthogonal: $v_{2r} = v_{1r} = v_1 \sin \alpha$.

Kinetic energy at the outlet is $\frac{v_2^2}{2} = \frac{v_1^2}{2} \sin^2 \alpha = \frac{v_1^2}{2} (1 - \cos^2 \alpha)$.

The only loss occurring within the flow is outlet kinetic energy. Therefore optimum operation corresponds to perpendicular outflow. Another loss is the downward head that is not used. The head used is somewhat lower than the geometrical head. As discussed in Chap. 1, some hydraulic turbines apply a draught tube to transform the downstream head into pressure decrease at the rotor outlet. The draught tube also functions as a diffuser and transforms a part of the outlet kinetic energy into pressure decrease at rotor outlet. Application of a draught tube is impossible with a Poncelet wheel, as the wheel runs in an open atmosphere.

References

1. Abott IH, Von Doenhoff AE (1959) Theory of wing sections. Dover Publications, ISBN 486-60586-8. NACA-aerofoil classification
2. Dixon SL, Hall CA (2014) Fluid mechanics and thermodynamics of turbomachinery, 7th edn. Elsevier, ISBN 978-0-12-415954-9. Cascade theory

3. Haaland S (1983) Simple and explicit formulas for the friction factor in turbulent flow. *J Fluids Eng* 103:89–90
4. Japikse D, Baines N (1994) Introduction to turbomachinery. Oxford University Press. ISBN 0-933283-06-7. Cascade theory
5. Knill TJ (2005) The application of aeroelastic analysis output load distributions to finite element models of wind turbines. *Wind Eng* 29:153–168
6. Miller DS (1990) Internal flow systems. Gulf Publishing Company, ISBN 0-87201-020-1. Duct systems and diffusers
7. Pfleiderer C (1961) *Die Kreiselpumpen für Flüssigkeiten und Gase*, 5th edn. Springer, no ISBN. Cascade effect on aerofoil characteristics

Chapter 3

Fans

Abstract Fans are machines to move air or a similar gas. With regard to types, there are axial, radial and mixed-flow fans. Principles for the analysis of axial turbomachines have been elaborated in the foregoing chapters, but for radial machines, only a limited theory has been developed. The fan chapter is therefore also used to complete the theory for power receiving radial machines. It is appropriate to do this with the fan. Firstly, the fan is a simple turbomachine. Further, there are various rotor shapes with radial fans (forward curved blades, radial end blades and backward curved blades), as opposed to radial pumps (only backward curved blades) and radial compressors (radial end and backward curved blades). In this chapter, we also discuss the performance evaluation of radial fans, rotor design choices with radial fans and performance of axial and mixed-flow fans.

3.1 Fan Applications and Fan Types

3.1.1 Fan Applications

A fan is a machine that moves air or a similar gas, producing a small pressure rise. A general criterion is that the total pressure ratio should not exceed 1.25 ($p_{02}/p_{01} < 1.25$). The fluid density then only changes a little. The fluid may be considered, with a good approximation, at constant density equal to the arithmetic average of the inlet and outlet values (a justification for the application of the average density is given in Chap. 4: compressible fluids). With total pressure ratios exceeding 2 ($p_{02}/p_{01} > 2$), the term *compressor* is used. It refers to a machine intended to increase the pressure of a compressible fluid. The term *blower* is typically used for intermediate machines ($1.25 < p_{02}/p_{01} < 2$), but refers also to any device that blows air with rather elevated velocity (snow blower, leaf blower, hot air blower). So, the term blower may refer to a fan with a high work input or a compressor with a low work input, mainly producing kinetic energy. There is no specific theory for blowers. Depending on the case, a blower is analysed as a fan (constant density) or as a compressor (variable density).

Fans are primarily applied to exhaust polluted air from industrial spaces, office buildings and homes. Fresh air supply, in some cases through an air conditioning

system, is an analogous application. These applications exist in quite varying dimensions. Extreme examples are fans in mines, with flow rates of the order of $500 \text{ m}^3/\text{s}$ and pressure rises of the order of 5000 Pa (two-stage axial fans). Most applications are more modest, with flow rates up to 4 to $5 \text{ m}^3/\text{s}$ and pressure rises up to 2000 Pa , i.e. power up to 10 kW (radial fans). Also low power applications are found in this sector, as cooker hood fans or fans in cars. Fans for combustion air supply or combustion gas exhaust constitute a second group. Also quite varying sizes occur here: from large steam boiler fans to small fans in home heating systems. Fans for cooling air supply, mainly fans in electronic devices and heat exchangers, constitute a third group. Some applications have a very low power, e.g. a PC fan has typically 1 W . All fan types occur. High power examples are fans for cooling air supply to surface condensers (axial fans) in electric power plants. The above application list certainly is not complete. We mention fans in vacuum cleaners and hair dryers.

3.1.2 Large Radial Fans

From about a 200 mm rotor diameter onwards, the entire machine is manufactured from steel plate. Figure 3.1 shows an example. The components are a rotor with forward curved or backward curved blades and a volute. The rotor may be directly driven by a motor. That is the simplest construction form. Figure 3.1 shows a belt driven type. The fan itself has bearings in that case. The possibility to incorporate a rotor with backward or forward curved blades into the same volute is typical. We recall (Chap. 1) that backward curved blades are mainly intended for pressure build-up, whereas forward curved blades aim at kinetic energy generation. Larger

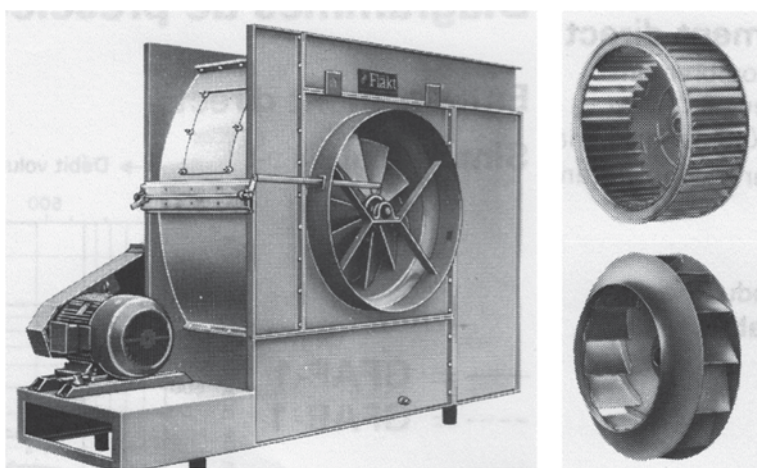
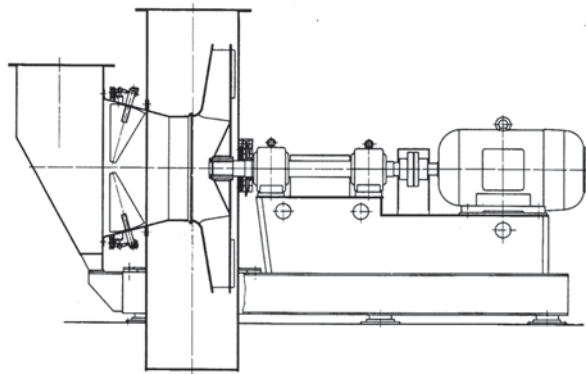


Fig. 3.1 Large radial fan with inlet guide ring. (Courtesy Fläkt Woods)

Fig. 3.2 Radial fan with inlet guide ring and directly driven shaft with bearings. (Courtesy TLT-Turbo)



machines sometimes have inlet guide vanes in the suction eye in order to influence the characteristic, as is the case with the fan in Fig. 3.1.

Figure 3.2 shows an example with separate bearings. All elements, including the rotor, are welded in larger fans.

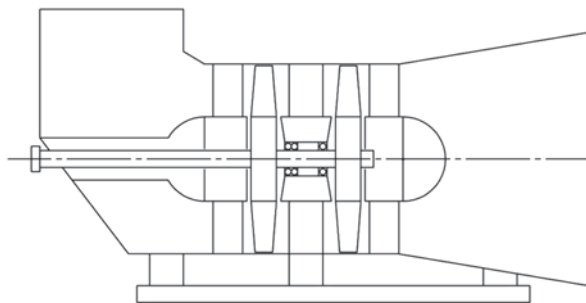
3.1.3 Small Radial Fans

Rotor and stator manufacturing from welded steel plate is difficult with a rotor diameter under 200 mm. Rotors are sometimes made from punched steel plate, with parts joined by locks and bent lips. Mould injected plastic is commonly applied. The volute may be manufactured of aluminium by casting, from plastic by injection moulding or of sheet steel by bending. The rotor is generally mounted directly onto the driving motor, often within the hub. Design examples are discussed in Sect. 3.6.

3.1.4 Large Axial Fans

Large axial fans typically have welded hubs (sometimes forged). The rotor blades have aerofoil shaped profiles and are mostly cast (aluminium). With many fans, the rotor blade angle may be changed at standstill, individually or collectively by means of a collar with lever arms, adapting the machine to a changed flow rate. The normal configuration is a rotor with a downstream stator. The number of rotor blades strongly depends on the pressure rise to be realised and may vary between 2 for a fan with a low pressure rise to the order of 20 for a fan with a high pressure rise. A high pressure rise fan is at the same time a low flow rate fan and thus has a high ratio of hub diameter to tip diameter. A low pressure rise fan typically has a low diameter ratio. Figure 3.3 is a sketch of a two-stage axial fan.

Fig. 3.3 Two-stage axial fan; flow from left to right; normal build is struts with axial inflow and outflow, followed by two stages rotor-stator



3.1.5 Small Axial Fans

Stator vanes are mostly omitted with small axial fans. The flow then contains post-swirl impairing the efficiency. The rotor is commonly mounted onto the driving motor, often with the motor in the hub. The rotor is mostly manufactured from mould injected plastic. Design examples are discussed in Sect. 3.7.

3.1.6 Cross-Flow Fans

Small power applications, such as generating an air flow with a small pressure rise, may, apart from axial fans and radial fans with forward curved blades, feature fans of a third type. Figure 3.4 shows a cross section of a so-called cross-flow fan. Air passes through the rotor twice. The stator shape determines the suction and

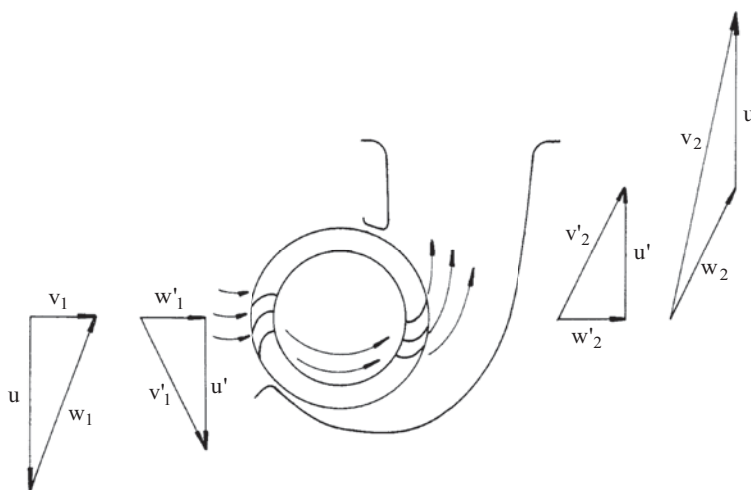


Fig. 3.4 Cross-flow fan

the discharge sides. The diameter ratio (inner diameter to outer diameter) is very high, analogous to the radial fan with forward curved blades. Velocity triangles are sketched in Fig. 3.4. Blades are radial at the inner side. Rotor work is comparable to that with a fan with forward curved blades. The degree of reaction is very low as well. The dimensions in the axial direction are nearly unlimited with this fan type, which makes it appropriate to generate a flow through a slot-shaped area. Applications are mostly generation of cooling air in electric appliances (overhead projector, copier) or a heated air jet (electric convector, blow-dryer).

3.2 Idealised Mean Line Analysis of a Radial Fan

3.2.1 Idealised Flow Concept: Infinite Number of Blades

A mean line analysis is performed in a plane perpendicular to the rotor shaft, firstly with an infinite number of infinitely thin blades. Figure 3.5 represents a meridional section and an orthogonal section of a rotor. The term *infinite number of blades* means that the flow is supposed to follow perfectly the blade geometry. This would indeed be attained with an infinite number of infinitely thin blades. The relative velocity would then be tangent to the blades at each point of the flow. The flow at the rotor inlet has no incidence and there is no friction between the fluid and the blades. An incidence-free inlet means that the flow direction coincides with the blade orientation just upstream of the inlet. In a general case, the absolute inlet

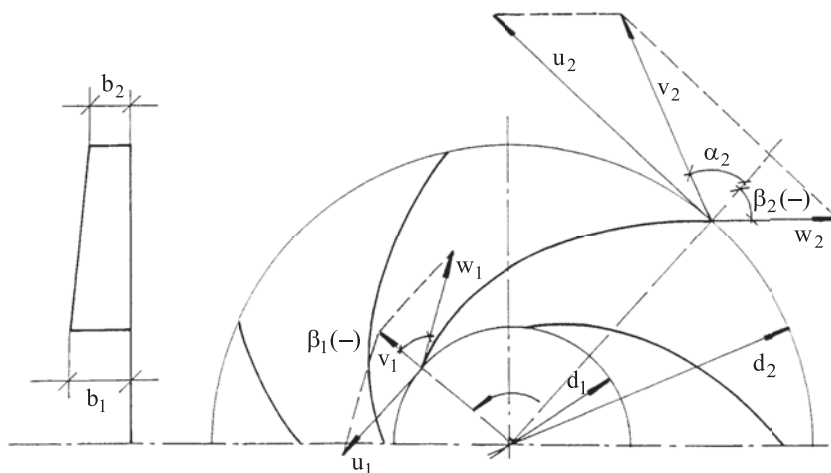


Fig. 3.5 Flow through the rotor of a radial fan; drawn for radial inlet; flow direction coinciding with blade orientation

flow direction is not perpendicular to the inlet circle and has some pre-swirl velocity v_{lu} . With most machines, no pre-swirl occurs, however. Analogous to the rotor, we assume an incidence-free inlet of the volute and no friction within the volute. Quantities related to the above defined flow get as subscripts t (theoretical flow = no losses) and ∞ (infinite number of blades). The assumptions regarding losses and flow direction coinciding with blade orientation will gradually be abandoned in further analysis steps.

3.2.2 Degree of Reaction

The degree of reaction with adiabatic flow is the ratio of the static enthalpy increase to the total enthalpy increase in the rotor. The total enthalpy increase in the rotor equals the total enthalpy increase in the machine. The static enthalpy increase is

$$h_2 - h_1 = \frac{p_2}{\rho_2} - \frac{p_1}{\rho_1} + e_2 - e_1.$$

The reversible part of this enthalpy increase is $\int \frac{1}{\rho} dp$. This follows from the entropy definition:

$$Tds = dh - (1/\rho) dp \text{ or } dh_s = (1/\rho) dp.$$

One can thus suppose that, for a small pressure increase with a compressible fluid, the isentropic enthalpy increase corresponding to the pressure increase is well approximated by

$$(h_2 - h_1)_s \approx \frac{p_2 - p_1}{\bar{\rho}},$$

with $\bar{\rho}$ being the average density. A strict justification for this approximation is presented in Chap. 13. Obviously, the relation is exact for constant density. Thus the degree of reaction may be approximated with

$$R_p = \frac{\Delta p_{rot}}{\Delta p_0}, \quad (3.1)$$

which is the ratio of the static pressure rise in the rotor to the total pressure rise in the machine.

The degree of reaction according to (Eq. 3.1) is applied in practice to fans. There is a small difference with the general definition. This is obvious, as both values

of the degree of reaction coincide for lossless flow of constant density fluid. The degree of reaction according to the general definition is strictly termed *kinematic degree of reaction* as this degree of reaction may be related to velocity components, as will be derived hereafter. There is no specific term in the fan literature for the degree of reaction according to definition (Eq. 3.1). We will use the term *pressure degree of reaction*. By the simple term degree of reaction, we will mean the *kinematic degree of reaction*. A definition of the degree of reaction, slightly deviating from the general definition is sometimes applied to other machines as well, for instance, with steam turbines (Chap. 6). Deviating definitions are always used for practical purposes. Pressure differences required to determinate the degree of reaction according to (Eq. 3.1) may be measured easily. Reliable measurement of the enthalpy differences for the general definition is impossible, as temperature differences with fans are very small. For instance, a total pressure increase of 3600 Pa corresponds to an adiabatic temperature difference of just 3 K with a density 1.20 kg/m^3 and a specific heat 1000 J/kgK . This difference cannot be measured reliably because of the effect of heat transfer.

3.2.3 Relation Between Rotor Blade Shape and Performance Parameters

The kinematic degree of reaction is given by

$$R_{t\infty} = \frac{h_2 - h_1}{h_{02} - h_{01}} = \frac{u_2^2 - u_1^2 + w_1^2 - w_2^2}{2(u_2 v_{2u} - u_1 v_{1u})}. \quad (3.2)$$

In the absence of pre-swirl,

$$v_{1u} = 0 \text{ and } w_1^2 = u_1^2 + v_1^2.$$

Then, (Eq. 3.2) becomes

$$R_{t\infty} = \frac{u_2^2 + v_1^2 - w_2^2}{2u_2 v_{2u}}.$$

In order to obtain a simple expression for the degree of reaction, we assume that the radial component of the velocity is equal at the rotor inlet and outlet. This is approximately met in real rotors and is achieved by decreasing the axial rotor width with increasing diameter.

With

$$v_1 = v_{2r} \text{ and } w_2^2 - v_{2r}^2 = (u_2 - v_{2u})^2,$$

it follows that, with $\zeta = v_{2u} / u_2$,

$$R_{t\infty} = \frac{u_2^2 - (u_2 - v_{2u})^2}{2u_2 v_{2u}} = 1 - \frac{\zeta}{2}. \quad (3.3)$$

A total pressure coefficient is defined by

$$\psi_{0,t\infty} = \frac{\Delta p_{0,t\infty}}{\rho u_2^2} = \frac{u_2 v_{2u}}{u_2^2} = \frac{v_{2u}}{u_2} = \zeta. \quad (3.4)$$

A static pressure coefficient is similarly, with $\Delta p_{rot,t\infty}$ the static pressure rise in the rotor:

$$\psi_{r,t\infty} = \frac{\Delta p_{rot,t\infty}}{\rho u_2^2} = R_{t\infty} \psi_{0,t\infty} = \zeta \left(1 - \frac{\zeta}{2}\right). \quad (3.5)$$

Equation (3.4) and Eq. (3.5) are only correct for lossless flow.

The dimensionless coefficients for the total pressure rise in the machine and for the static pressure rise in the rotor are termed *performance parameters*. They are related to the degree of reaction, which is determined by the rotor blade shape, as derived hereafter.

Figure 3.6 shows the degree of reaction and the pressure coefficients as functions of v_{2u} / u_2 . Some dimensionless outlet velocity triangles are represented. The total pressure coefficient increases with increasing v_{2u} / u_2 . The degree of reaction decreases. This implies an increase of the fraction of the rotor work used for kinetic energy rise in the flow through the rotor. The efficiency of the entire machine thus decreases when a significant part of the kinetic energy at the rotor outlet is to be converted into pressure energy downstream of the rotor. The degree of reaction is 1 for $\zeta=0$. The total pressure rise is then zero and the rotor blades are strongly curved backward. No work is done by the rotor. A machine without any rotor work is useless, of course. So, a practical minimal value is $\zeta \approx 0.2$. The degree of reaction is 0.5 for $\zeta=1$. Within the rotor, the increase of pressure energy then equals the increase of kinetic energy. The outlet part of the rotor blades is in the radial direction. There is no static pressure rise within the rotor for $\zeta=2$. Such a machine only generates kinetic energy rise. It is a pure action machine with forward curved blades and a high total pressure rise. In practice, a machine with a low degree of reaction is of little use. Most applications require some static pressure rise, and it is advisable for good efficiency to have some static pressure rise in the rotor. So, a practicable maximum value is $\zeta \approx 1.8$.

The inlet rotor blade orientation is independent of its outlet shape. Figure 3.7 schematically shows the blade shapes with *forward curved blades*, *radial end blades* and *backward curved blades*. The corresponding degrees of reaction being respectively low, 0.5 and high. So it is clear that the degree of reaction determines the rotor blade shape.

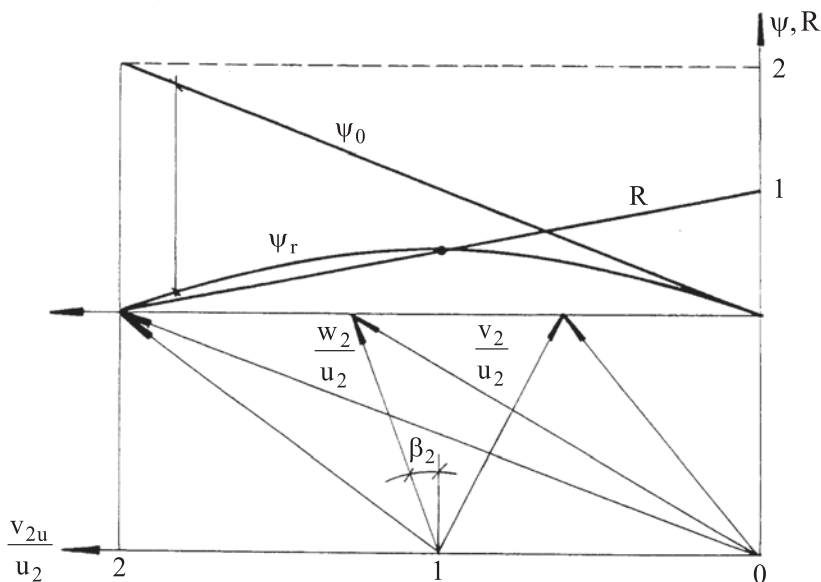


Fig. 3.6 Variation of the degree of reaction and of pressure coefficients with blade angle at the rotor outlet (β_2); the radial velocity is drawn exaggerated for clarity

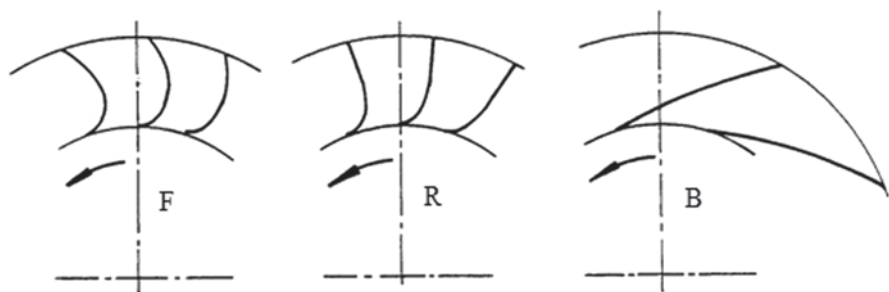


Fig. 3.7 Forward curved (F), radial end (R) and backward curved (B) blades

3.2.4 Performance Characteristics with Idealised Flow

A first characteristic represents the total pressure rise in the fan as a function of the flow rate. Their relation follows from Euler's equation. Without pre-swirl it applies that

$$\frac{\Delta p_{0,t\infty}}{\rho} = u_2 v_{2u} = u_2 (u_2 + v_{2r} \tan \beta_2) = u_2 \left(u_2 + \frac{Q}{\pi d_2 b_2} \tan \beta_2 \right). \quad (3.6)$$

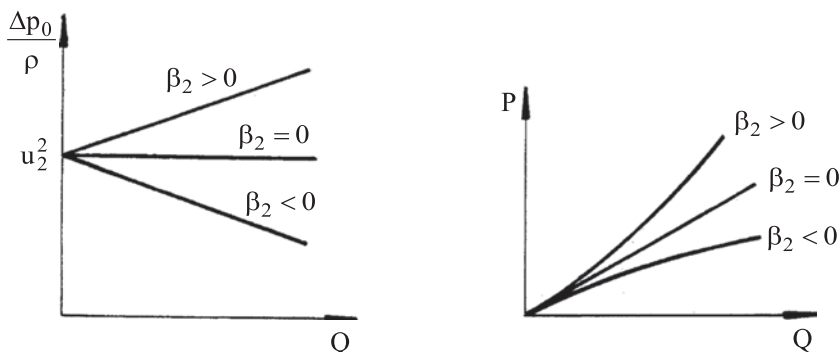


Fig. 3.8 Total pressure rise and absorbed power as a function of the flow rate with forward curved ($\beta_2 > 0$), radial end ($\beta_2 = 0$) and backward curved ($\beta_2 < 0$) blades

Equation (3.6) represents a straight line in the $(\frac{1}{\rho} \Delta p_{0,t\infty}, Q)$ -diagram (Fig. 3.8). With forward curved blades, the theoretical total pressure rise increases with the flow rate. The total pressure rise stays constant with radial end blades and it is a decreasing function of the flow rate with backward curved blades. The theoretical power $P_{t\infty}$ follows from

$$P_{t\infty} = \Delta p_{0,t\infty} Q = \rho u_2^2 Q + \rho u_2 \frac{Q^2}{\pi d_2 b_2} \tan \beta_2. \quad (3.7)$$

The relation is linear for radial end blades, quadratic and steeper than linear for forward curved blades, and quadratic and flatter than linear for backward curved blades (Fig. 3.8). The real characteristics of radial fans are discussed in Sects. 3.4 and 3.6.

3.3 Radial Fan Analysis for Lossless Two-Dimensional Flow with Finite Number of Rotor Blades

3.3.1 Relative Vortex in Blade Channels

We still consider the flow as occurring in a plane perpendicular to the shaft. The flow within a blade channel of a rotor with a finite number of blades may be considered as the superposition of two flows. The first flow is the translation flow applied until now. This flow follows the blade direction and has a uniform velocity at a given radius. The second flow is a circulation flow in the relative frame, as sketched in Fig. 3.9, showing the superposition of both flows as well. On a blade, a side forms with a higher velocity and a lower pressure (*suction side*) and another

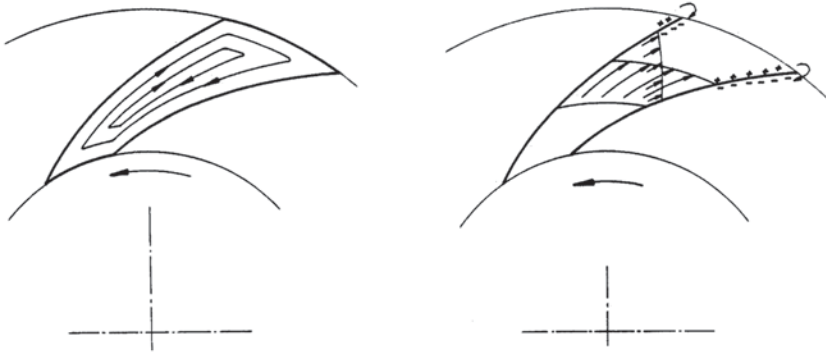
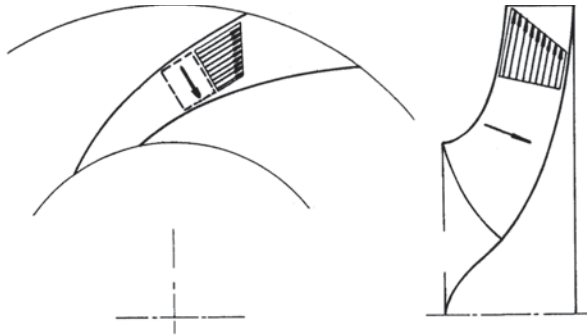


Fig. 3.9 Relative vortex motion (*left*) and superposition with the translational motion (*right*) within a blade channel of a radial rotor

Fig. 3.10 Velocity gradient by Coriolis force (*left*); by centrifugal force (*right*)



one with a lower velocity and a higher pressure (*pressure side*). The generation of suction and pressure sides has been explained in Chap. 1 as a consequence of the Coriolis force (rotation effect), but influenced by the lift force. Herewith, we understand that a rotational motion is superimposed onto the translational motion. Figure 3.10 sketches the velocity gradient generated by the Coriolis force. An analogous velocity gradient is due to the centrifugal force by streamline curvature. The figure shows the effect of curvature in the meridional plane, but the effect is similar in an orthogonal plane.

3.3.2 Velocity Difference over a Rotating Blade

We study the relative vortex motion by formulation of the momentum equations in the relative frame with Coriolis force and centrifugal force as intervening forces.

Figure 3.11 is a sketch of a streamline within an infinitesimal streamtube part through a radial rotor with backward curved blades. The streamline direction is indicated by x , the normal direction by y . The streamtube part is an infinitesimal

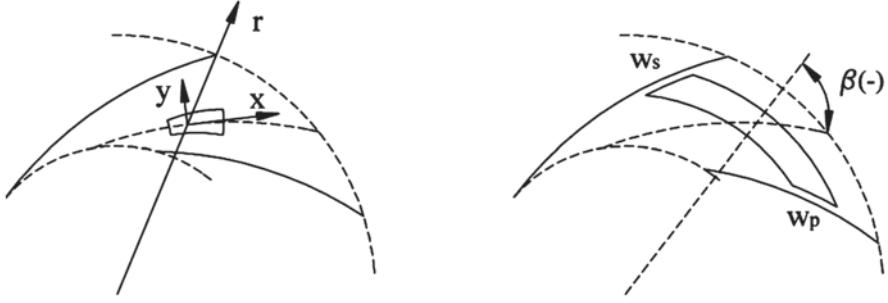


Fig. 3.11 Curved streamline and infinitesimal streamtube part (*left*); contour for determining the velocity difference over a blade (*right*)

control volume with dimension dx in flow direction and average dimension dy in the normal direction. The intervening body forces per mass unit are:

- centrifugal force by rotor rotation: $\overline{Cf} = \Omega^2 r \bar{l}_r$.
- Coriolis force by rotor rotation: $\overline{Co} = -2\Omega \times \bar{w} = -2\Omega w \bar{l}_y$.
- centrifugal force by streamline curvature for an observer attached to a fluid particle (streamline radius of curvature is R): $\overline{Cu} = \frac{w^2}{R} \bar{l}_y$.

Pressure forces onto the infinitesimal control volume in x and y directions are

$$-\frac{\partial p}{\partial x} dx dy b \quad \text{and} \quad -\frac{\partial p}{\partial y} dy dx b,$$

where b is the axial rotor width.

The x-oriented momentum balance for steady flow within the relative frame, for an observer attached to the rotor, is

$$\rho w dy b \frac{\partial w}{\partial x} dx = -\frac{\partial p}{\partial x} dx dy b + \Omega^2 r \bar{l}_r \cdot \bar{l}_x \rho dx dy b.$$

The y-oriented force balance for relative standstill of an observer attached to a fluid particle is

$$0 = -\frac{\partial p}{\partial y} dy dx b + \left(\Omega^2 r \bar{l}_r \cdot \bar{l}_y - 2\Omega w + \frac{w^2}{R} \right) \rho dx dy b.$$

The changes of r with a change of x or y are given by

$$dr = \bar{l}_r \cdot \bar{l}_x dx \quad \text{and} \quad dr = \bar{l}_r \cdot \bar{l}_y dy.$$

The balances thus become

$$w \frac{\partial w}{\partial x} = -\frac{1}{\rho} \frac{\partial p}{\partial x} + \Omega^2 r \frac{\partial r}{\partial x}, \quad (3.8)$$

$$0 = -\frac{1}{\rho} \frac{\partial p}{\partial y} + \Omega^2 r \frac{\partial r}{\partial y} - 2\Omega w + \frac{w^2}{R}. \quad (3.9)$$

The momentum balance (Eq. 3.8) is the Bernoulli equation on a streamline in the relative frame, as derived in Chap. 1. A new relation, compared to the one-dimensional analysis in Chap. 1, is the force balance in the normal direction (Eq. 3.9). The Bernoulli equation may be integrated along streamlines if ρ depends only on p . This particularly applies to $\rho = \text{constant}$. The result is ($u = \Omega r$):

$$\frac{w^2}{2} + \frac{p}{\rho} - \frac{u^2}{2} = \text{constant}. \quad (3.10)$$

From the velocity triangle follows: $w^2 = u^2 + v^2 - 2uv_u$. The constant is the same on all streamlines if the incoming flow at rotor inlet is a free vortex flow ($rv_u = \text{constant}$) with a uniform total pressure $\left(\frac{p}{\rho} + \frac{v^2}{2} \right)$. This condition is mostly met, especially when inlet guide vanes are absent. When the integration constant in Eq. (3.10) is the same for all streamlines, this relation implies

$$w \frac{\partial w}{\partial y} + \frac{1}{\rho} \frac{\partial p}{\partial y} - \Omega^2 r \frac{\partial r}{\partial y} = 0. \quad (3.11)$$

An analogous result for a compressible fluid is obtained for an isentropic flow (no entropy creation), the entropy definition being $T \nabla s = \nabla h - \frac{1}{\rho} \nabla p$. For constant entropy on the streamline, Eq. (3.8) may be integrated to

$$1/2 w^2 + h - 1/2 u^2 = \text{constant}.$$

Under analogous conditions as for an incompressible fluid, constant total enthalpy ($h_0 = h + 1/2 v^2$) and free vortex flow ($rv_u = \text{constant}$) at the inlet, the integration constant is the same on all streamlines, which implies constant entropy within the entire flow area (homentropic flow). So Eq. (3.11) applies. Combination of Eq. (3.9) and Eq. (3.11) results in

$$w \frac{\partial w}{\partial y} - 2\Omega w + \frac{w^2}{R} = 0 \quad \text{or} \quad \frac{\partial w}{\partial y} = 2\Omega - \frac{w}{R}. \quad (3.12)$$

Equation (3.12) demonstrates that the transversal velocity variation mainly originates from the Coriolis force, but that it decreases due to backward curving of the streamlines ($R > 0$). This result means, as found in Chap. 1, that rotor work decreases due to backward curving of the blades, causing negative work by the lift associated to the streamline curvature.

The significance of Eq. (3.12) may be understood, as in Chap. 2, by calculating the circulation on the infinitesimal contour formed by the edges of the infinitesimal streamtube part of Fig. 3.11 (left) and by applying the Stokes circulation theorem. On the infinitesimal contour, run in clockwise sense (negative sense according to the z -axis), this gives, with ω the value of the rotor of the velocity vector in the z -direction and $d\theta$ the slope angle variation of the infinitesimal streamline part:

$$\left(w + 1/2 \frac{dw}{dy} dy \right) (R + 1/2 dy) d\theta - \left(w - 1/2 \frac{dw}{dy} dy \right) (R - 1/2 dy) d\theta = -\omega R d\theta dy,$$

or
$$\frac{dw}{dy} dy R d\theta + w dy d\theta = -\omega R d\theta dy.$$

Thus
$$\frac{dw}{dy} + \frac{w}{R} = -\omega. \quad (3.13)$$

With Eq. (3.13), we understand that Eq. (3.12) means that the rotor of the relative velocity vector is equal to -2Ω everywhere in the flow. As the rotational speed of a fluid particle is equal to half of the rotor of the velocity vector (see fluid mechanics), this means that the relative vortex motion is such that the rotational speed of a fluid particle seen in the relative frame is exactly equal in magnitude to the rotational speed of the machine rotor. The sense of rotation of the fluid particle is opposite to the rotation sense of the machine rotor, so that the fluid particle rotation is zero in the absolute frame. This means that the relative vortex motion is an inertia reaction to the rotation of the machine rotor.

With the knowledge of the rotor of the relative velocity, the circulation may be calculated on a contour as sketched in Fig. 3.11 (right). This contour has two parts at constant radius with infinitesimal distance between each other. Calculation of the circulation allows determining the velocity difference between the suction and pressure sides of a blade at constant radius. We chose the clockwise sense on the contour. The corresponding rotation sense of the fluid particles in the relative frame is positive. The result is

$$w_s \left(\frac{dr}{\cos \beta} \right) - w_p \left(\frac{dr}{\cos \beta} \right) - (r + dr) \Delta \theta w_u(r + dr) + r \Delta \theta w_u(r) = 2\Omega r \Delta \theta dr.$$

In the expression above, w_u has to be seen as an average over the circular segment with angle variation $\Delta\theta$. Thus:

$$w_s - w_p = \Delta\theta \cos \beta \left[2\Omega r + \frac{d}{dr}(rw_u) \right]. \quad (3.14)$$

Equation (3.14) shows quantitatively that the local velocity difference over a blade has two causes: the Coriolis force and the lift force. Further insight may be gained by relating the velocity difference to the pressure difference over a blade segment by the Bernoulli equation in the relative frame. On a segment of constant radius ($u = \text{constant}$), assuming that the Bernoulli constant (Eq. 3.10) is the same on all streamlines, the relation is

$$(p_p - p_s) / \rho = \frac{1}{2} (w_s^2 - w_p^2) = (w_s - w_p) w_{mean}. \quad (3.15)$$

The velocity w_{mean} is the average of the velocities at the suction and pressure sides and may be interpreted as an average over the blade channel so that the mass flow in the channel (Z is the number of blades) is

$$\dot{m}_{channel} = \frac{\dot{m}}{Z} = \rho w_{mean} r \Delta\theta b \cos \beta. \quad (3.16)$$

Combining (Eq. 3.14, 3.15 and 3.16) results in

$$\begin{aligned} (p_p - p_s)rb &= \Delta p rb = (w_s - w_p) \rho w_{mean} r b = \dot{m}_{channel} \left[2\Omega r + \frac{d}{dr}(rw_u) \right], \\ \Delta p rb &= \frac{\dot{m}}{Z} \left[\Omega \frac{d}{dr}(r^2) + \frac{d}{dr}(rw_u) \right] = \frac{\dot{m}}{Z} \left[\frac{d}{dr}(ru) + \frac{d}{dr}(rw_u) \right]. \end{aligned} \quad (3.17)$$

Integration of this expression results in the torque transferred by the rotor:

$$M = Z \int \Delta p r b dr = \dot{m} [r_2 u_2 - r_1 u_1 + r_2 w_{2u} - r_1 w_{1u}]. \quad (3.18)$$

We recover the result already obtained in Chap. 1, that the rotor torque has contributions from the Coriolis force and from the lift force. Remark that Eq. (3.17) can be obtained directly by a moment of momentum balance on a control volume formed by the contour shown in Fig. 3.11 (right) and that the expression for the velocity difference Eq. (3.14) can be obtained from it with the Bernoulli equation in the relative frame. So, Eq. (3.14) may be derived without explicit knowledge of the value of the rotor of the relative velocity field.

3.3.3 Slip: Reduction of Rotor Work

Due to the relative vortex motion (Fig. 3.9), the average outlet flow of a blade channel deviates from the blade orientation into the sense opposite to the rotational speed. This phenomenon is termed *slip*. Figure 3.12 shows the velocity triangle at the rotor outlet with slip, compared to the velocity triangle without slip. Slip reduces the rotor work. The effect of slip may be reasoned in two ways, depending on whether the rotor can be considered as composed of channels (channel flow analysis according to Stodola) or rather as composed of individual blades with little overlap (blade load analysis according to Pfleiderer).

With the flow pattern of Fig. 3.9, Stodola (1924) assumes that the average tangential slip velocity is half of the magnitude of the velocity in the relative vortex motion:

$$\delta v_u = \delta w_u = \frac{w_s - w_{mean}}{2} = \frac{w_{mean} - w_p}{2} = \frac{w_s - w_p}{4}. \quad (3.19)$$

By w_{mean} is meant the average of the velocities on the suction and pressure sides. Since Eq. (3.19) has to be applied at the outlet of the rotor, this mean velocity is w_2 , according to the mean line flow analysis. Stodola further assumes, as a first approach, that the contribution of the lift to the velocity difference in (Eq. 3.14) may be neglected at the outlet of the rotor. This means an assumption of constant angular momentum flow at the outlet. Then

$$\delta v_u = \frac{1}{2} \Delta \theta \Omega r_2 \cos \beta_2 = \frac{\pi}{Z} \Omega r_2 \cos \beta_2 = \frac{\pi}{Z} u_2 \cos \beta_2.$$

From the velocity triangle of Fig. 3.12 it follows

$$v_{2u} = u_2 + v_{2r} \tan \beta_2 - \delta v_u = \left(1 - \frac{\pi}{Z} \cos \beta_2\right) u_2 + v_{2r} \tan \beta_2, \quad (3.20)$$

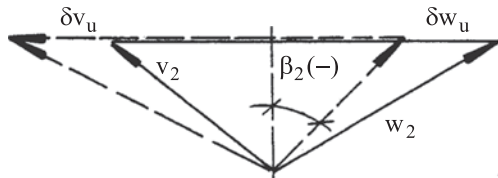
or

$$v_{2u} = \sigma u_2 + v_{2r} \tan \beta_2.$$

It appears as if it is not u_2 that is transferred by the rotor motion, but a lower velocity, denoted by σu_2 , with σ being the *slip factor*:

$$\sigma = 1 - \frac{\pi}{Z} \cos \beta_2.$$

Fig. 3.12 Effect of slip on the velocity triangle at the rotor outlet: full line with slip, dashed line without slip; the radial velocity is drawn exaggerated for clarity



This representation leads to a characteristic $1/\rho \Delta p_0$ as a function of the flow rate, parallel to the theoretical characteristic with an infinite number of blades, shifted by $(1-\sigma)u_2^2$. Stodola's reasoning holds well when blade passages strongly form channels. This always applies to pumps, but seldom to fans. A formula according to Wiesner (1967) is mostly applied with pumps. Stodola's formula has been corrected by Wiesner for curvature and friction effects with use of theoretical results by Busemann and experimental results to

$$\sigma = \left(1 - \frac{\sqrt{\cos(\beta_2^b)}}{Z^{0.7}} \right) \left(1 - \left[\frac{(r_1/r_2) - a}{1-a} \right]^3 \right), \quad (3.21)$$

with

$$a = \exp \left(-8.16 \frac{\cos(\beta_2^b)}{Z} \right),$$

where β_2^b is the material blade angle.

If necessary, we distinguish from now on between the blade angle β_2^b and the flow angle β_2 . The second factor in (Eq. 3.21) describes the overlap effect. For $r_1/r_2 < a$, the factor is put on 1. This is commonly met with pumps. For example, $\beta_2^b = -60^\circ$, $Z=6$ makes $a = (r_1/r_2)_{lim} = 0.5$. Typical is $r_1/r_2 \approx 0.4$.

The expression for the velocity difference (Eq. 3.14) is not well justified for small blade overlap. The reasoning presumes the presence of channels, so large enough solidity. The condition is noticed as the correction factor in (Eq. 3.21) intervenes for a high value of r_1/r_2 and a low value of Z . Fans with backward curved blades only have few blades and a high radius ratio (r_1/r_2), so that overlap between blades sometimes even does not exist. In case of small overlap, Pfleiderer (1924) proposes to keep the average slip velocity estimated to one fourth of the difference between the suction side and the pressure side velocities at the trailing edge, but to calculate that velocity difference from the pressure difference on the blade, using the Bernoulli relation (Eq. 3.15).

The following derivation is an adaptation of Pfleiderer's original reasoning by Eck [4], specifically for fans. The average pressure difference on the blade is determined from the rotor torque, according to

$$M = Z \int_1^2 \Delta p b r dr = Z \overline{\Delta p} M_{st},$$

where M_{st} is the static moment of the meridional section around the rotation axis and b is the local width in axial direction. The torque also follows from the moment of momentum as

$$M = \dot{m}(r_2 v_{2u} - r_1 v_{1u}) = \dot{m} \frac{\Delta W}{\Omega} = \rho v_{2r} 2\pi r_2 b_2 \frac{\Delta W}{\Omega}.$$

The pressure difference between the pressure and suction sides of a blade follows from the Bernoulli equation and is given by (Eq. 3.15). So, the velocity difference at the trailing edge between suction and pressure sides may be estimated, using the average pressure difference, by

$$\overline{\Delta p} = \rho w_2 (w_s - w_p)_2 = \frac{M}{Z M_{st}} = \frac{\rho v_{2r} 2\pi r_2 b_2}{Z M_{st}} \frac{\Delta W}{\Omega}, \quad (3.22)$$

from which:

$$\delta v_u = \frac{1}{2} \frac{v_{2r}}{w_2} \frac{\pi r_2 b_2}{Z M_{st}} \frac{\Delta W}{\Omega} = \frac{\cos \beta_2}{2} \frac{\pi r_2 b_2}{Z M_{st}} \frac{\Delta W}{\Omega}.$$

The rotor work is

$$\Delta W_t = u_2 v_{2u} - u_1 v_{1u} = \Delta W_{t\infty} - u_2 \delta v_u.$$

With Pfleiderer's reasoning, there is a relation between rotor work with and without slip according to

$$\Delta W_t = \frac{\Delta W_{t\infty}}{1 + Pf}, \text{ with the Pfleiderer factor } Pf = \frac{\cos \beta_2}{2} \frac{\pi r_2^2 b_2}{Z M_{st}}.$$

A correction for using the mean value of the pressure difference is required and a correction for friction as well. Further, to be manageable, the blade angle, and not the flow angle, must be applied. Therefore Pfleiderer adapted the formula by comparing it to experimental results and defined a *work reduction factor* as

$$\varepsilon = \frac{\Delta p_{0,t}}{\Delta p_{0,t\infty}}, \text{ with } \varepsilon = \frac{1}{1 + Pf} \text{ and } Pf = \xi \frac{r_2^2 b_2}{Z M_{st}}. \quad (3.23)$$

The coefficient ξ depends on the blade angle at the outlet and the rotor environment. Adaptation to experimental results gives

$$\xi = \lambda \left(2.5 + \frac{\beta_2^\circ}{60} \right). \quad (3.24)$$

The angle β_2° is the material blade angle, expressed in degrees (negative with backward curved blades), with

- $\lambda = 0.65$ to 0.85 for a rotor followed by a volute;
- $\lambda \approx 0.6$ for a rotor followed by a vaned diffuser;
- $\lambda = 0.85$ to 1 for a rotor followed by a vaneless diffuser.

In practice, we may approximate the integral for the determination of the static moment by

$$M_{st} = \frac{b_2 r_2 + b_1 r_1}{2} (r_2 - r_1). \quad (3.25)$$

With Pfleiderer's representation, the characteristic $1/\rho \Delta p_0$ as a function of the flow rate is a straight line that intersects the theoretical characteristic with an infinite number of blades on the abscissa (with $\beta_2 \neq 0$). This representation is simplifying and with small blade overlap, the work reduction factor certainly is flow rate dependent.

The turbomachinery literature contains many formulae for the slip factor or the work reduction factor. They all give approximate results, best workable near the design operating point. Wiesner's formula is best with high solidity rotors. Pfleiderer's formula is best with small blade overlap. However, no formula is perfect and even nowadays, research on new formulae continues. Recent proposals are by von Backström [11] and by Qiu et al. [10]. The slip factor and the work reduction factor are flow rate dependent, as shown in this last study, but it is not possible to express this dependency in a simple way.

3.3.4 Number of Blades and Solidity: Pfleiderer Moment Coefficient

When a rotor is provided with many blades, slip is small and rotor work is close to the maximum attainable. This is no optimum choice regarding efficiency, as a large blade surface implies a great friction surface. Work reduction due to slip is no loss in itself, but the effect of losses between the driving motor and the rotor (so-called mechanical losses, see Sect. 3.5.1) becomes important with a very small rotor work. So, except for cases with small rotor work, a rather significant slip is acceptable. This implies that the optimum number of blades for efficiency is mostly quite close to the minimum that is sufficient to realise an attached flow. Of course, other reasons may require a larger number. The most common reason is margin against flow separation at flow rate lower than the design flow rate (see Sect. 3.3.5).

From the flow pattern in Fig. 3.9 we learn that two criteria shall be met to avoid separation at the rotor outlet. Firstly, the number of blades must be large enough to prevent the Coriolis force and lift force from generating reversed flow at the pressure side. Secondly, blade load should not become so high that separation occurs near the trailing edge at the suction side. The pressure at the suction side and at the pressure side must become equal at a rotor blade trailing edge. So, there is always an adverse pressure gradient at the suction side trailing edge.

The velocity difference near the trailing edge follows from (Eq. 3.14), which may be written as

$$(w_s - w_p)_2 = \frac{2\pi}{Z} \cos \beta_2 \left[2u_2 + \frac{d}{dr}(rw_u)_2 \right] = \frac{4\pi}{Z} u_2 \cos \beta_2 f_R, \quad (3.26)$$

with

$$f_R = 1 + \frac{1}{2} \frac{\frac{d}{dr}(rw_u)_2}{u_2}.$$

The curvature factor, f_R , expresses the effect of the Coriolis force and the lift force (= curvature) together relative to the effect of the Coriolis force alone. This factor is difficult to estimate at the outlet of a rotor with blades with small overlap.

With (Eq. 3.26) it follows

$$w_s = w_2 + \frac{2\pi}{Z} u_2 \cos \beta_2 f_R \text{ and } w_p = w_2 - \frac{2\pi}{Z} u_2 \cos \beta_2 f_R.$$

Flow reversal at the pressure side is prevented for

$$\frac{2\pi}{Z} u_2 \cos \beta_2 f_R < w_2. \quad (3.27)$$

Prevention of boundary layer separation at the suction side may be expressed by a local diffusion factor criterion as

$$\frac{w_s - w_2}{w_s} < D_{loc} \approx 0.5 \text{ or } w_s - w_2 < \frac{D_{loc}}{1 - D_{loc}} w_2. \quad (3.28)$$

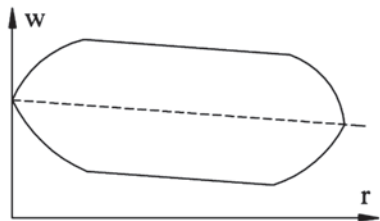
This criterion also gives result (Eq. 3.27) for $D_{loc} = 0.5$. This D_{loc} value constitutes the critical value for separation with axial cascades. Deceleration within the boundary layer at the suction side is less favourable with a centrifugal rotor, due to a strong turbulence segregation effect by the Coriolis force. Similar to the centrifugal force (Chap. 2, Sect. 2.3.2), the Coriolis force drives high-energy cores within the turbulent motion from the suction side to the pressure side. This migration effect lowers the turbulence level in the suction side boundary layer (it becomes more laminar), which weakens its capacity to withstand an adverse pressure gradient. In practice, this rather causes separation at the suction side than flow reversal at the pressure side. Therefore, we further apply criterion (Eq. 3.28) for separation at the suction side, but with w_2 in the right-hand side multiplied by the reduction factor 0.8 ($D_{loc} = 0.45$).

We note the criterion to prevent separation at the suction side as

$$C = \frac{(w_s - w_p)_2}{w_2} < C_{lim} \approx 1.6. \quad (3.29)$$

As already said, it is difficult to estimate the velocity difference near the trailing edge with a formula like (Eq. 3.26). We might set the curvature factor to unity, as in the Stodola slip reasoning, but this is certainly a quite crude assumption for fans. For pumps and compressors, the Stodola reasoning is more appropriate, which makes that (Eq. 3.26), together with (Eq. 3.29) may be used for estimating the minimum number of blades (see Chap. 14: radial compressors). For fans, a way out is using the estimate (Eq. 3.22) from Pfleiderer's reasoning based on the average pressure difference. Usually, the velocity difference over a blade in a centrifugal rotor is nearly constant as a function of the radius and the velocity distribution on the pressure and the suction sides is as sketched in Fig. 3.13.

Fig. 3.13 Sketch of velocity distribution on pressure and suction sides on the blade of a centrifugal rotor



Due to end effects at the inlet and outlet of the rotor, Pfleiderer's reasoning leads to some underestimation of the velocity difference near the outlet. With (Eq. 3.22), criterion (Eq. 3.29) becomes

$$C_M = \frac{v_{2r}}{w_2^2} \frac{2\pi r_2 b_2}{Z M_{st}} \frac{\Delta W}{\Omega} = \frac{2\pi r_2^2 b_2}{Z M_{st}} \frac{v_{2r}}{u_2} \frac{\Delta W}{w_2^2} < C_{M,\text{lim}} \approx 1.4. \quad (3.30)$$

We assume a lower limit value compared to Eq. (3.29) to take the underestimation into account. Equation (3.30) for a radial rotor is similar to the expression of the Zweifel coefficient (Eq. 2.29 in Chap. 2) for an axial cascade. The factor

$$\sigma_M = \frac{Z M_{st}}{2\pi r_2 b_2 r_2},$$

may be considered as the *moment solidity* of the meridional section, so that Eq. (3.30) may be written as

$$C_M = \frac{v_{2r}}{u_2} \frac{\Delta W}{\sigma_M w_2^2} < C_{M,\text{lim}} \approx 1.4. \quad (3.31)$$

We compare with the Zweifel tangential force coefficient:

$$C_{Fu} = 2 \frac{v_{2a} \Delta w_u}{\sigma_a w_2^2} < C_{Fu,\text{lim}} \approx 1.4,$$

with the axial solidity $\sigma_a = c_a / s$.

From now on, we call the factor C_M by Eq. (3.31) the *Pfleiderer moment coefficient* since it is based on the average pressure difference reasoning of Pfleiderer. The criterion determines the necessary solidity for avoiding boundary layer separation in a centrifugal rotor. We will assume that optimal solidity corresponds with a moment coefficient of about unity. For completeness, we should mention that Pfleiderer only had the objective to derive a formula for slip effect and not a separation criterion. The extension to a separation criterion is, however, quite obvious, as is clear from the reasoning above. Also, it should be mentioned that the separation criterion (Eq. 3.31) is not generally used in the turbomachinery literature. Mostly,

purely empirical formulae are employed for estimating the necessary rotor solidity with radial machines

The analogy between the expressions for preventing boundary layer separation with the centrifugal rotor and the axial cascade demonstrates that Eq. (3.31) also may be considered as a force coefficient. With $\overline{\Delta p}$ according to Eq. (3.22), factor C_M in (Eq. 3.31) represents:

$$C_M = \overline{\Delta p} / \rho w_2^2 = \frac{1}{2} \overline{\Delta p} / \left(\frac{1}{2} \rho w_2^2 \right).$$

As the limit value is about 1.4, a centrifugal cascade has the double load capacity of an axial one. Figure 3.13 explains this. The maximum value of the average pressure difference would be $\rho \times 2w_2 \times w_2$ if the velocity was zero near the outlet at the pressure side and the run-in and run-out zones in the pressure profile were negligibly small. An attainable value for the factor C_M thus indeed amounts to about 1.4. The double load capacity comes from the Coriolis force which allows a velocity level of about $2w_2$ on the complete suction side. A uniform level of this height cannot be obtained from lift, as is clear from Figs. 2.5, 2.8 and 2.16 (Chap. 2).

3.3.5 Number of Blades: Examples

Figure 3.14 is a sketch of 4 typical centrifugal rotor blade shapes:

- Backward curved blades: $\beta_1^b \approx -60^\circ$, $\beta_2^b \approx -60^\circ$, $r_1 / r_2 \approx 0.7$, $\beta_2 \approx -70^\circ$;
- Straight backswept blades: $\beta_1^b \approx -55^\circ$, $\beta_2^b \approx -25^\circ$, $r_1 / r_2 \approx 0.4$, $\beta_2 \approx -40^\circ$;
- Radial end blades: $\beta_1^b \approx -55^\circ$, $\beta_2^b \approx 0^\circ$, $r_1 / r_2 \approx 0.4$, $\beta_2 \approx -20^\circ$;
- Forward curved blades: $\beta_1^b \approx -30^\circ$, $\beta_2^b \approx +60^\circ$, $r_1 / r_2 \approx 0.8$, $\beta_2 \approx +45^\circ$.

Radial end blades are applied in fans, but the blade shape is mainly appropriate for high rotational speed, intended to produce large rotor work, in other words, compressor application. In the radial blade part, no bending stress by centrifugal force occurs. The inlet has to be adapted to reach the same goal there. An axial element is added, a so-called inducer (see Chap. 14: radial compressors).

We determine the minimum number of blades with (Eq. 3.31) and $\Delta W = u_2 v_{2u}$. From the velocity triangle at rotor outlet in Fig. 3.5, we derive

$$\tan \alpha_2 = \frac{v_{2u}}{v_{2r}}, \text{ or } v_{2u} = v_{2r} \tan \alpha_2 \text{ and } v_{2r} = w_2 \cos \beta_2.$$

So:

$$C_M = \frac{v_{2r} v_{2u}}{\sigma_M w_2^2} = \frac{\tan \alpha_2 \cos^2 \beta_2}{\sigma_M}.$$

By taking $b_1 r_1 = b_2 r_2$, which means constant radial velocity component in the rotor, the moment solidity may be estimated as

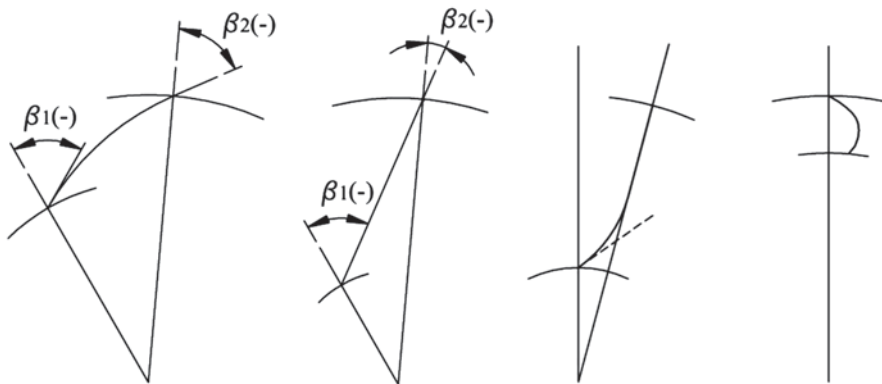


Fig. 3.14 Centrifugal rotor blade shapes: backward curved, straight backswept, radial end (inducer not drawn), forward curved

$$\sigma_M = \frac{Z}{2\pi} \left(1 - \frac{r_1}{r_2} \right).$$

From the velocity triangle at rotor outlet in Fig. 3.5, we further derive

$$\operatorname{tg} \alpha_2 = \frac{v_{2u}}{v_{2r}}, \operatorname{tg} \beta_2 = \frac{w_{2u}}{v_{2r}}, v_{2u} = u_2 + w_{2u} \text{ or } u_2 = (\operatorname{tg} \alpha_2 - \operatorname{tg} \beta_2) v_{2r}.$$

The flow coefficient and work coefficient are

$$\phi = \frac{v_{2r}}{u_2} = \frac{1}{\operatorname{tg} \alpha_2 - \operatorname{tg} \beta_2} \text{ and } \psi = \frac{v_{2u}}{u_2} = \frac{\operatorname{tg} \alpha_2}{\operatorname{tg} \alpha_2 - \operatorname{tg} \beta_2}.$$

The Pfleiderer moment coefficient may also be written as a function of the kinematic parameters:

$$C_M = \frac{\phi \psi}{\sigma_M [\phi^2 + (1 - \psi)^2]}.$$

The results are given in Table 3.1. The angle α_2 is set to 70° and C_M is set to 1.4. In the last column are given the numbers typically used in practice. For the rotor with radial end blades, the safety margin on the number of blades may seem small, but in reality the rotor has an axial part at the inlet (the inducer), which contributes to the moment solidity (see Chap. 14: radial compressors). The number of blades might be larger than given in the last column, depending on the margin that the

Table 3.1 Number of blades for the rotor shapes shown in Fig. 3.14

β_2	r_1 / r_2	ϕ	ψ	$\sigma_{M,calc}$	Z_{calc}	Z_{real}
-70°	0.7	0.182	0.500	0.230	4.82	6–7
-40°	0.4	0.279	0.766	1.152	12.06	14–16
-20°	0.4	0.321	0.883	1.733	18.15	20
$+45^\circ$	0.8	0.571	1.572	0.981	30.82	36–40

designer wants to provide for separation at the suction side and flow reversal at the pressure side at reduced flow rate. Anyhow, these phenomena cannot be avoided at very low flow rate (flow pattern of Fig. 3.9, left).

3.4 Internal Losses with Radial Fans

This section analyses internal losses with radial fans, but the discussion largely applies to radial pumps and radial compressors as well.

3.4.1 Turning Loss at Rotor Entrance

The fluid axially enters the eye of the rotor and turns 90° into the radial direction. The turning generates a loss analogous to loss in a bend. In energy measure, this loss is about 10% of the kinetic energy of the flow in the narrowest section of the suction eye.

3.4.2 Incidence Loss at Rotor Entrance

Figure 3.15 is a sketch of the inflow of a cascade (radial, axial or mixed flow), with infinitely thin blades. The blades are drawn straight, but this is not crucial for the result. The flow just upstream of the cascade is not aligned with the blades, but makes an *incidence angle* δ with them. The flow deflects from the inlet velocity w_1 to the velocity w_2 inside the blade passage with a deflection angle $\delta = \beta_1 - \beta_2$.

Continuity of the mass flow results in

$$w_1 \cos \beta_1 = w_2 \cos \beta_2.$$

The meridional component of the velocity is constant. So, the deflection velocity w_{def} is in the tangential direction. The deflection causes energy dissipation, which can be calculated from the momentum conservation equation, projected onto the β_2 direction:

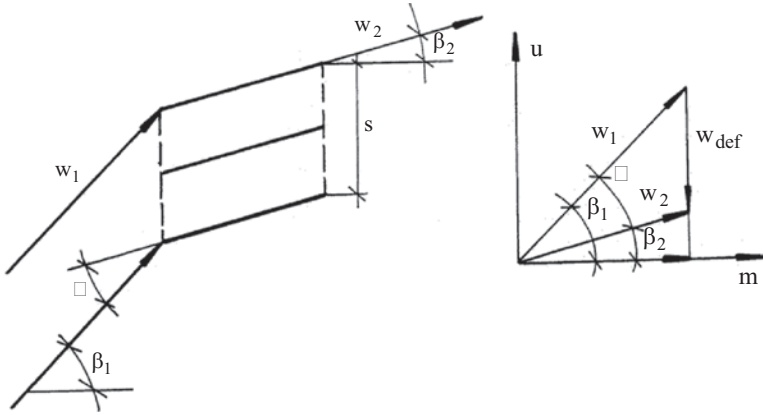


Fig. 3.15 Incidence at rotor entrance

$$\rho Q(w_2 - w_1 \cos \delta) = s(p_1 - p_2) \cos \beta_2.$$

The volume flow rate is $Q = sw_2 \cos \beta_2$ and s is the spacing of the cascade element. The momentum conservation equation thus results in

$$p_1 - p_2 = \rho w_2 (w_2 - w_1 \cos \delta).$$

The total pressure drop $-\Delta p_{0,def}$ due to tangential deflection is

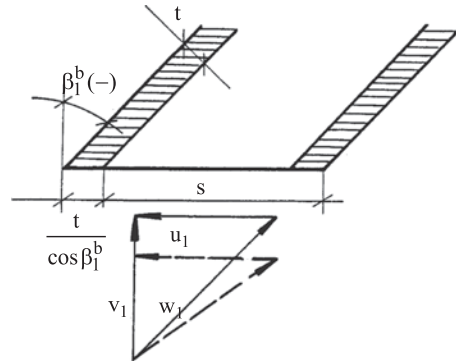
$$\frac{-\Delta p_{0,def}}{\rho} = \frac{p_1 - p_2}{\rho} + \frac{w_1^2}{2} - \frac{w_2^2}{2} = \frac{1}{2} (w_1^2 - w_2^2 + 2w_2^2 - 2w_1 w_2 \cos \delta),$$

$$\frac{-\Delta p_{0,def}}{\rho} = \frac{1}{2} (w_1^2 + w_2^2 - 2w_1 w_2 \cos \delta) = \frac{1}{2} w_{def}^2.$$

In energy measure, the loss equals the kinetic energy associated to the deflection velocity. This result is similar to that of dump diffusion. With a real cascade, the incidence loss is overestimated with the formula found, as the deflection is not sudden, but is spread over a finite length. Incidence loss follows from

$$-\Delta p_{0,def} = \mu_{def} \rho \frac{w_{def}^2}{2}, \quad (3.32)$$

Fig. 3.16 Blade thickness effect at rotor inlet; dashed line: before inlet; full line: after inlet



with μ_{def} being a coefficient of about 0.7–0.8.

3.4.3 Displacement by Blade Thickness

The blades constitute, due to their thickness t , an obstruction at the inlet of the rotor (Fig. 3.16). The flow passage width in tangential direction decreases to $s - t / \cos \beta_1^b$.

We may express the displacement effect by an *obstruction factor*: $\tau_1 = (s - t / \cos \beta_1^b) / s$. Continuity of the mass flow implies, with subscript 1 indicating the station upstream of the inlet and 1^b the station downstream of the inlet:

$$v_{1r}^b = v_{1r} / \tau_1.$$

The increase of the radial velocity component changes the direction of the relative flow. In order to prevent incidence at the inlet, the blades must be tangent to w_1^b instead of w_1 . From now on, we distinguish, if necessary, between the velocity triangles drawn immediately upstream of the inlet (station 1) and immediately downstream of it (station 1^b). The tangential velocity component in the relative frame is constant between these stations and the radial velocity component changes due to the displacement effect. A similar displacement effect occurs at the rotor outlet, with a change in radial velocity component between positions immediately upstream (station 2^b) and downstream of the outlet (station 2). Note that the slip formula, giving the relation between the tangential velocity components, must be written according to Stodola's or Pfleiderer's (for $v_{lu} = 0$) concept as

$$v_{2u} = \sigma u_2 + w_{2u}^b \text{ or } v_{2u} = \varepsilon v_{2u}^b.$$

Quantities with superscript b are calculated inside the rotor, applying the blade angle β_2^b .

3.4.4 Rotor Friction Loss and Rotor Diffusion Loss

With a rotor that can be considered as composed of blade channels, this loss may be estimated with formulae for ducts, applying an average hydraulic diameter. This is mostly appropriate for pumps. For fans, it is more realistic to apply the formulae for flow over plates with a calculation of the total friction surface. For a flow over a plate, the friction force follows from

$$F = c_f A \rho \frac{w^2}{2},$$

where the friction coefficient c_f is around 0.005. The total pressure drop is

$$\frac{-\Delta p_0}{\rho} = \frac{F w}{\dot{m}}.$$

A small diffusion mostly occurs within a rotor. The corresponding loss may be estimated by

$$-\Delta p_0 = \xi_d \rho \frac{w_1^2}{2}.$$

The loss coefficient is determined with the diffuser diagrams, but generally, this loss is extremely small.

3.4.5 Dump Diffusion Loss at Volute Entrance

A rotor with backward curved blades is customarily combined with a volute with a width strongly exceeding that of the rotor (see Figs. 3.1 and 3.2). A width ratio of 2–3 is typical and is intended to reduce the radial velocity component at the entrance of the volute. This reduction is necessary to limit the radial dimensions of the volute, as follows from the reasoning hereafter. We denote with subscript 2' the entrance conditions of the volute at radius r_2 (the outlet of the rotor is station 2).

When ignoring friction within the volute, the flow satisfies constant angular momentum:

$$v_u r = v_{2u}' r_2.$$

The volute is almost always manufactured with a constant width. The flow rate equation then reads

$$Q = 2\pi r b v_r \quad \text{or} \quad v_r r = v_{2r}' r_2.$$

Thus it follows that, in a volute with constant width, both the tangential and the radial velocity components vary inversely proportional to the radius. A streamline thus forms, in each of its points, the same angle with the radial direction. The equation of a streamline in a polar coordinate system thus reads (Fig. 3.17):

$$\operatorname{tg} \alpha = \frac{r d\theta}{dr} = \text{constant, or } dr / r = d\theta / \operatorname{tg} \alpha,$$

from which: $\ln(r / r_2) = \theta / \operatorname{tg} \alpha$.

The form of the streamline found is termed a logarithmic spiral. In order to not exert force upon the flow, the shape of the external wall of the volute shall be a logarithmic spiral. The radius ratio when passing an entire circumference is

$$\ln(r_3 / r_2) = \frac{2\pi}{\operatorname{tg} \alpha}. \quad (3.33)$$

From Fig. 3.12 it follows that the angle, by which the flow in the absolute frame leaves the rotor, may be around 70° (the radial velocity is exaggerated in the figure). The corresponding radius ratio is about 10, which is enormous. So, higher outlet angles are wanted. It is thus necessary to reduce the radial velocity component at the volute entrance. With a width ratio 3 and a rotor outlet angle $\alpha_2 = 70^\circ$ follows a volute inlet angle after the width leap $\alpha'_2 = 83^\circ$. The corresponding radius ratio is 2.16, a value still somewhat too high to be practical (see next section).

The sudden widening may be seen as dump diffusion and its loss estimated by

$$-\Delta p_0 = \rho 1/2 (v_{2r}^b - v_{2r}')^2, \quad (3.34)$$

with v_{2r}^b and v_{2r}' being the radial velocity components upstream and downstream of the width leap. With e.g. $v_{2r}' = 1/3 v_{2r}^b$ it follows that

$$-\Delta p_0 = \mu_{dump} \rho 1/2 (v_{2r}^b)^2,$$

with

$$\mu_{dump} = 4/9 \approx 0.444.$$

With Eq. (3.34), we include the effect of the blade thickness at the rotor outlet into the dump loss. Notwithstanding the high loss coefficient, the loss by width leap is never high, as the radial velocity component is not very large. The loss estimation with a sudden leap overestimates the loss at the volute entrance itself, since the flow does not suddenly occupy the available space. Figure 3.17 (middle) demonstrates that the flow enters the volute through a vortex motion. A width leap around 2.5 is ideal to give sufficient room to the swirl. A real volute cross section is sketched in Fig. 3.17 (right). It realises injection of the leakage flow into the rotor such that the boundary layer on the shroud is energised. This prevents or, at least, reduces the

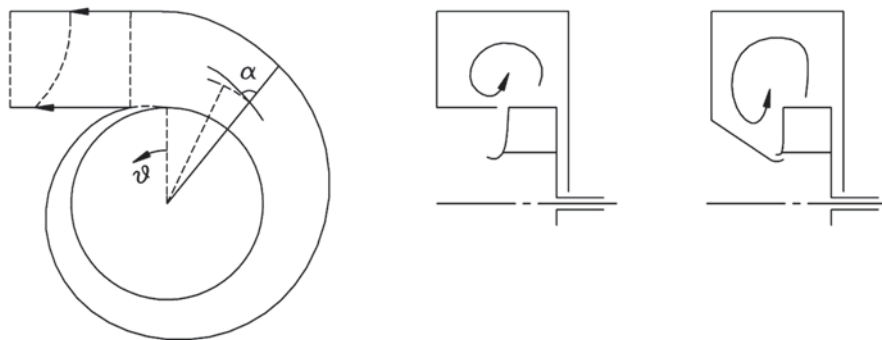


Fig. 3.17 Volute shape; *left*: flow with assumed uniform distribution over the width; *middle*: vortex motion in a meridional section; *right*: cross section in reality related to useful application of the leakage flow

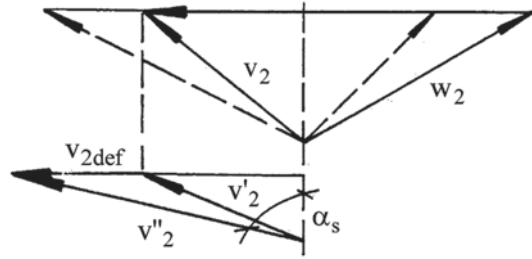
separation of the inlet flow, which has to turn 90° . The boundary layer that would separate without the injection is sucked to the wall by momentum transfer from the leakage flow. This is termed *Coandă-effect*. Figure 3.17 (left) is a sketch of a volute with the shape of the external wall being a logarithmic spiral. A clearance between the spiral and the rotor should be created by forming a so-called tongue. The tongue clearance is typically about 5 % of the rotor diameter.

Although the dump diffusion flow model for the entrance of the volute is extremely simplifying, the loss expression (Eq. 3.34) produces realistic values [4]. The loss model is also used for more streamlined volutes as in pumps and compressors [2, 6]. In reality, the larger velocity flow at the suction side of a rotor blade and the lower velocity flow at the pressure side mix while entering the volute. The resulting swirl velocity (velocity component in the meridional plane in Fig. 3.17, right) is much larger than the velocity calculated as $v_{2,r}$ in Eq. (3.34), but the associated kinetic energy is almost completely dissipated by the time that the flow reaches the outlet of the volute. This means that the dump loss formula (Eq. 3.34) is not a good estimate for the loss associated to the entrance of the volute itself, but that it becomes a good estimate if the mixing loss associated to the swirl movement in the whole of the volute is included.

3.4.6 Incidence Loss at Volute Entrance

The radius ratio of the volute, adapted to the rotor outlet flow, mostly is, notwithstanding a significant width leap, still somewhat too large to attain acceptable volute dimensions. To a radius ratio 2 corresponds a slope angle $\alpha_s = 83.7^\circ$ (the subscript s stands for scroll). A radius ratio 2 already yields workable dimensions, but many manufacturers apply a somewhat smaller radius ratio. Typically, the opening angle of the volute (α_s , but calculated tangentially) is about 5° . The corresponding radius ratio is about 1.75. This implies that the direction forced by the volute causes inci-

Fig. 3.18 *Top*: velocity triangles at the rotor outlet before and after slip (*dashed line* without slip); *Bottom*: velocity triangles at the volute inlet after the width leap, before and after tangential velocity deflection due to incidence; the radial velocity is drawn exaggerated for clarity



dence. Figure 3.18 is a sketch of the velocity triangles at the rotor outlet (absolute velocity v_2) and after the width leap (absolute velocity v'_2). A tangential deflection velocity is generated. We denote with subscript 2'' the entrance flow of the volute at radius r_2 after the tangential deflection by incidence. The incidence loss may be calculated with a formula like Eq. (3.32). Enlarging the slope angle of the volute implies that the volute is adapted to a lower flow rate than the design flow rate. The rotor and the volute now become mismatched. The above demonstrates that some degree of mismatch mostly is unavoidable.

The typical mismatch of the volute and the rotor, in the sense that the volute is adapted to a lower flow rate, implies acceleration in the volute: $v''_{2u} > v'_{2u}$. The spontaneous deceleration in the volute (Fig. 3.17, left) may completely be undone by it. Another consequence of the mismatch is enforcement of a non-uniform pressure distribution to the rotor, namely pressure decreasing in the flow sense. A pressure leap at the tongue is generated thus. The non-uniform pressure distribution causes increase of losses at the rotor outlet. In practice, it is not always obvious how to determine the angle α_s imposed by the volute. Generally [2, 6], the tangential velocity imposed by the volute to the rotor outlet v''_{2u} is calculated from the flow rate, assuming equal angular momentum between the outlet of the volute and the rotor outlet, $(rv)_3 = r_2 v''_{2u} = C$, so that $Q = C \int \frac{bdr}{r}$ at the volute outlet (Fig. 3.17, left). The loss associated to the velocity difference $v'_{2u} - v''_{2u}$ is calculated as a deflection loss.

3.4.7 Friction Loss Within the Volute

The friction loss may be estimated analogously to the friction loss in the rotor. The entire friction surface must be determined.

3.4.8 Diffusion at the Rotor Inlet

The velocity within an air transporting duct in an industrial plant may be as high as 20 m/s and even higher for short ducts (the economic velocity follows from a

balance between pipe cost and energy dissipation). In house ventilating systems, the velocity typically has to be limited to about 5 m/s because of noise generation limitation. On the suction side of a fan, velocities may be up to 30 m/s, certainly for a fan taking air directly from a large space. The meridional component of the velocity at the rotor inlet may be much lower. With $\beta_1 \approx -60^\circ$ is $v_{1m} \approx 0.6 u_1$. This implies that the order of magnitude of v_{1m} may be around 12 m/s at lower u_1 values. This requires then velocity reduction between the suction eye and the rotor inlet (inlet of the bladed part). The surface ratio (diameter suction eye $d_0 \approx$ diameter rotor inlet d_1) is approximately

$$\frac{A_1}{A_0} = \frac{4b_1}{d_1}.$$

This ratio may attain until 1.70 without the occurrence of separation. The corresponding velocity reduction is about 0.60. The Coandă-effect enables this very strong deceleration. Losses in the flow from the suction eye to the rotor inlet are approximately balanced by the energising effect of the leakage flow. So, formally, diffusion losses at rotor inlet may be neglected.

3.4.9 Flow separation at Rotor Inlet and Rotor Outlet

Centrifugal fans with straight, slightly backswept, blades or radial end blades (Fig. 3.14, second and third blade shapes), typically have separated flow at the rotor outlet, even for the design flow rate. The reason is that the deceleration ratio in the rotor, this is the velocity ratio w_2/w_1 , cannot be lower than about 0.7. For actual calculations, we assume here that this limit ratio applies between the inlet flow after rotor entrance (w_1^b) and the outlet flow before rotor exit, so before slip (w_2^b). With w_2 near to the radial direction, this limit is rapidly obtained (see the design example 7.6 in Chap. 7). The one-dimensional calculation procedure can then still be used with a flow representation of jet-and-wake type at the outlet of the rotor. This means that the flow is divided into a core flow with relative velocity equal to the limit value (called the jet) adjacent to a separation zone with very low velocity (called the wake). Physically, the wake is in the corner of the blade suction side and the shroud. In the simplest flow representation, the net through-flow velocity in the wake is set to zero (stagnant wake). The one-dimensional calculation is then applied to the jet flow through the rotor channels (see Exercise 7.7.6 in Chap. 7). With the simplest methods, slip formulae and loss formulae are used as for full through-flow (we follow this approach in Exercise 7.7.6), but corrections to the formulae are sometimes applied. With separated rotor outlet flow, the dump diffusion at the entrance of the volute is to be considered as between the core flow in the rotor channels and a uniform flow immediately downstream of the rotor outlet, filling the full width of the volute. Due to the partial filling of the rotor channels, the dump diffusion loss is much larger than with full through-flow.

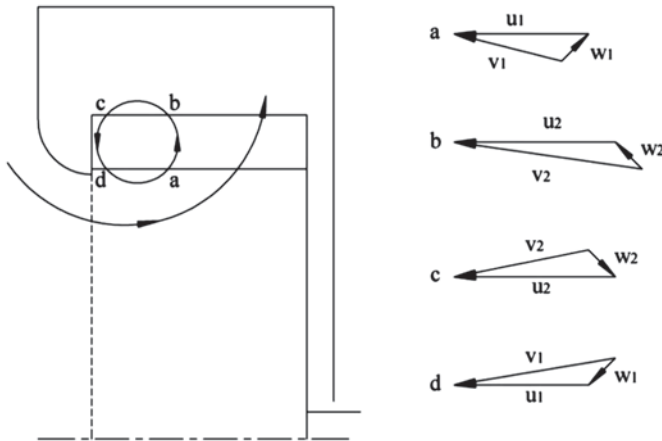


Fig. 3.19 Through-flow and recirculation flow in a rotor with forward curved blades

Centrifugal fans with forward curved blades (Fig. 3.14, fourth blade form) have recirculation flow in the rotor, also for the design flow rate. These machines have a very low degree of reaction. Therefore, they can be built with a diameter ratio d_1/d_2 close to 1 (0.85–0.9 are typical) as pressure increase by the centrifugal term, $(u_2^2 - u_1^2)/2$, does not have to be high. With a high value of the inlet diameter, the flow rate can be maximised for a given rotor diameter. Since the work coefficient is also high, centrifugal fans with forward curved blades are the most compact ones for a given duty of flow rate and total pressure rise. For this reason, this type of fan is commonly applied when space is limited. An example is car ventilation, but also home ventilation (see further discussion in Sect. 3.6). Figure 3.19 is a sketch of the flow pattern in a meridional section of a radial fan with forward curved blades, at design flow rate. Since the static pressure build-up in the rotor is small, the stabilising effect of the Coandă-flow is weak and separation of the entrance flow of the rotor cannot be avoided at the shroud. The option is then typically taken to make the width of the rotor constant and much bigger than follows from equal through-flow areas of rotor inlet and suction eye ($b_1/d_1 = 0.25$). The through-flow of the rotor can then take the space as needed, but the recirculation flow then also gets room. Figure 3.19 explains how the recirculation flow is energised in the outward radial motion (a to b: $u_2 v_{2u} - u_1 v_{1u} > 0$), how the velocity is reduced during the turning in the volute (b to c: $|v_2|_b > |v_2|_c$) with energy transfer to the through-flow, how it returns to the suction eye without energy exchange with the rotor (c to d: $u_2 v_{2u} - u_1 v_{1u} = 0$), how the velocity is reduced during the turning at the rotor entrance (d to a: $|v_1|_d > |v_1|_a$) with energy transfer to the through-flow. The energy transfer from the rotor to the through-flow by the intermediate action of the recirculation flow cannot be derived from basic conservation laws with the one-dimensional flow representation and there do not seem to be models for this effect in the fan literature. For illustration of the flow in this type of fan, we refer to Adachi

et al. [1] and Kim and Seo [7]. These studies reveal that the size of the recirculation zone is not constant over the periphery of the rotor and that the size of the recirculation zone gets larger at lower delivered flow rate. For zero net flow, the recirculation flow is the strongest and creates significant energy transfer to the fluid in the volute. For some choices of the blade angles, it is even higher than for the design flow rate.

3.4.10 *Applicability of the Loss Models*

Loss models, in the style as described above, are used with hand calculations of the performance of centrifugal fans, pumps and compressors. Modern loss correlations are mostly somewhat more complex than the formulae given above, but are inspired by the same principles [2, 4–6]. Moreover, more detailed expressions for the loss coefficients are employed, while the constant loss coefficients used here, give only an approximate value, like $\mu_i=0.7$ or $c_f=0.005$. Here, we only aim at a principal discussion. For more details, we refer to the literature cited and to a recent overview paper on loss correlations by Kim et al. [8]. In particular, this paper shows that the dump loss model and the incidence loss model for the volute entrance are still used nowadays, giving very reasonable loss estimates.

Performance evaluation with a one-dimensional flow representation, using the slip formulae of Stodola or Pfleiderer and with the loss formulae is only well justified if the flow through the rotor channels is sufficiently homogeneous in a cross section. This requirement is satisfied for centrifugal machines with backward curved blades operating not extremely far away from the design conditions. For very low flow rate, the flow in the rotor becomes a recirculation flow as shown on Fig. 3.9 (left). Such a flow cannot be analysed as a one-dimensional flow.

3.4.11 *Optimisation of the Rotor Inlet of a Centrifugal Fan*

In the design of a power receiving turbomachine for a constant density fluid, the target performance parameters are the flow rate (volume flow rate Q) and the mechanical energy rise ($\Delta p_0 / \rho$). The principal machine parameters to be determined in a first design phase are the rotor diameter (d_2) and the rotational speed (Ω). These follow from similitude considerations (see Chap. 7), implying a global optimisation, and considerations about the application of the machine. In essence, the application type determines the degree of reaction, thus the repartition of the rotor work into enthalpy increase and kinetic energy increase in the rotor (see Sect. 3.6). Once the main parameters of the machine are determined (d_2 and Ω), other parameters typically follow from local optimisation considerations. For a radial fan, without pre-swirl inlet vanes, it is generally assumed in turbomachinery theory that optimum efficiency is obtained by the minimum of the relative velocity at the entrance of the rotor. The most important loss mechanism is the mixing loss at the outlet of the rotor (dump into the volute). The second largest, but already much lower,

is the incidence loss at the entrance of the volute. The mixing loss is minimal for minimum relative velocity at outlet of the rotor (w_2). This implies minimum relative inlet velocity (w_1) and strongest possible deceleration in the rotor. The incidence loss at entrance in the volute is mostly minimal for the outlet velocity of the rotor in the absolute frame (v_2) as near to the tangential direction as possible, which again, implies minimum w_2 .

The deceleration in the eye of the rotor may be expressed by a velocity factor

$$\zeta = \frac{v_{1r}^b}{v_0} \text{ with } v_{1r}^b = \frac{Q_{rotor}}{\pi d_1 b_1 \tau_1} \text{ and } v_0 = \frac{4Q}{\pi d_0^2}.$$

Thus:

$$\zeta = \frac{Q_{rotor}}{Q} \frac{d_0^2}{4d_1 b_1 \tau_1}.$$

The diameter of the eye d_0 is somewhat smaller than the inlet diameter of the rotor d_1 and Q_{rotor} is somewhat larger than Q . Say $d_0 = 0.9 d_1$; $\eta_V = Q / Q_{rotor} \approx 0.9$ (volumetric efficiency); $\tau_1 = 0.9$ (obstruction factor), such that

$$\zeta \approx \frac{1}{4} \frac{d_1}{b_1} \text{ or } \frac{b_1}{d_1} \approx \frac{1}{4\zeta}.$$

The strongest possible deceleration between the inlet of the eye and the inlet of the rotor is about 0.60, so that $b_1 / d_1 = 0.25$ to 0.40 . Then:

$$v_{1r}^b = \frac{Q}{k\pi d_1 b_1} = 4 \frac{\zeta}{k\pi} \frac{Q}{d_1^2}, \text{ with } k = \eta_V \tau_1 \approx (0.9)^2 \text{ and } u_1 = \frac{\Omega d_1}{2}.$$

Thus:

$$(w_1^b)^2 = (v_{1r}^b)^2 + u_1^2 = a^2 (d_1^2)^{-2} + b^2 (d_1^2),$$

with $a = 4\left(\frac{\zeta}{k\pi}\right)Q$ and $b = \frac{\Omega}{2}$.

With the minimum of w_1 corresponds an optimum value of d_1 :

$$(d_1)_o = 2^{1/6} 2 \left(\frac{\zeta}{k\pi} \right)^{1/3} \left(\frac{Q}{\Omega} \right)^{1/3}. \quad (3.35)$$

The corresponding velocity components are:

$$u_1 = 2^{1/6} \left(\frac{\zeta}{k\pi} \right)^{1/3} Q^{1/3} \Omega^{2/3} \text{ and } v_{1r}^b = 2^{-1/3} \left(\frac{\zeta}{k\pi} \right)^{1/3} Q^{1/3} \Omega^{2/3}. \quad (3.36)$$

The remarkable result is that the expressions of the velocity components and the diameter d_1 are all proportional to the same factor $(\zeta / k\pi)^{1/3}$. This means that it is advantageous to set the velocity factor to the lowest possible value. The second

consequence is that the blade angle corresponding to the optimum diameter does not depend on the velocity factor. The minimum of w_l is obtained for $\tan \beta_1^b = -\sqrt{2}$, thus $\beta_1^b \approx -55^\circ$. This is, in principle, a universal result. The corresponding inlet diameter (Eq. 3.35) is, for $\zeta = 0.625$ ($b_1 / d_1 = 0.40$):

$$(d_1)_o \approx \sqrt{2} \left(\frac{Q}{\Omega} \right)^{1/3}. \quad (3.37)$$

The expressions for the velocity components become

$$(v_{1r})_o \approx \frac{1}{2} Q^{1/3} \Omega^{2/3} \text{ and } (u_1)_o \approx \frac{\sqrt{2}}{2} Q^{1/3} \Omega^{2/3}. \quad (3.38)$$

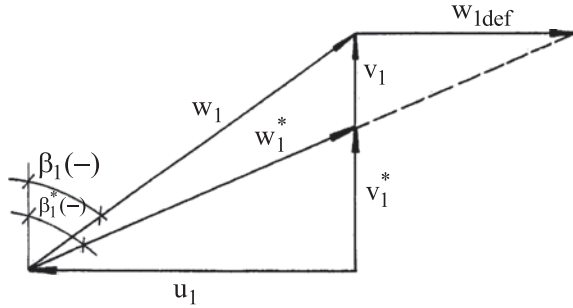
The minimum of w_1^b as a function of the diameter is quite flat. For a diameter increase of 20% or a diameter decrease of 15%, the increase of the magnitude of w_1^b is about 6%, which means 12% in rotor related losses. The corresponding blade angles are -68° and -41° . Thus $\beta_1^b = -55^\circ$ is not a strongly universal value. A 20% increase of the velocity factor from 0.625 to 0.75 causes also an increase of the magnitude of w_1^b with about 6%. In practice, the blade angle and the velocity factor may deviate from the theoretical optimum values with the purpose to match the fan to its suction duct. As already said, the through-flow velocity in a transport duct for air may be as high as 20 m/s in an industrial environment, but it may be as low as 5 m/s for noise reasons with air conditioning in rooms. The velocity at the entrance of the fan cannot deviate very much from the through-flow velocity of the suction duct. A further remark concerns pre-swirl vanes. With positive pre-swirl ($v_{1u} > 0$), the magnitude of w_1 may be considerably reduced. This would suggest that it is always very advantageous to use positive pre-swirl. With pre-swirl, however, as w_1 diminishes, more solidity is necessary in the rotor. Further, as the rotor work diminishes ($u_1 v_{1u} > 0$), a larger rotational speed is necessary to compensate for this decrease. These are factors that increase losses. This means that the principle that the minimum of w_1 approximately corresponds to maximum efficiency is only well justified for inlet flow without pre-swirl.

3.4.12 Characteristics Taking Losses into Account

Some losses are proportional to the flow rate squared: turning loss at entrance, rotor friction loss, rotor diffusion loss, loss by dump diffusion into the volute, friction loss in the volute. Incidence losses are zero with an adapted flow rate Q_* and change proportionally to $(Q - Q_*)^2$. This becomes clear from Fig. 3.20 showing the incidence at the rotor inlet. The direction indicated with β_1^* is the direction for incidence-free inlet, obtained from the blade orientation, but taking the displacement due to the blade thickness into account.

The deflection flow velocity follows from triangle similarity as

Fig. 3.20 Incidence at rotor inlet; the radial velocity is drawn exaggerated for clarity



$$\frac{w_{1def}}{u_1} = \frac{v_1 - v_1^*}{v_1^*} = \frac{Q}{Q_{*r}} - 1. \quad (3.39)$$

Further

$$-\Delta p_{0,def} = \mu_{def} \rho \frac{w_{1def}^2}{2}.$$

An analogous reasoning follows for the stator. The velocity triangles at the volute entrance are sketched in Fig. 3.21, using Stodola's slip representation.

From Fig. 3.21 it follows:

$$\frac{v_{2def}}{\sigma u_2} = \frac{v'_{2r} - v'_{2r*}}{v'_{2r*}} = \frac{Q}{Q_{*s}} - 1. \quad (3.40)$$

In Fig. 3.21, direction AC is fixed and determined by the rotor outlet angle. Direction AD is fixed as well, as a result of scaling the radial components by the surface ratio at the width leap. Direction BE is imposed by the volute. The radial velocity component v'_{2r*} has thus a fixed value, allowing to calculate the flow rate Q_{*s} .

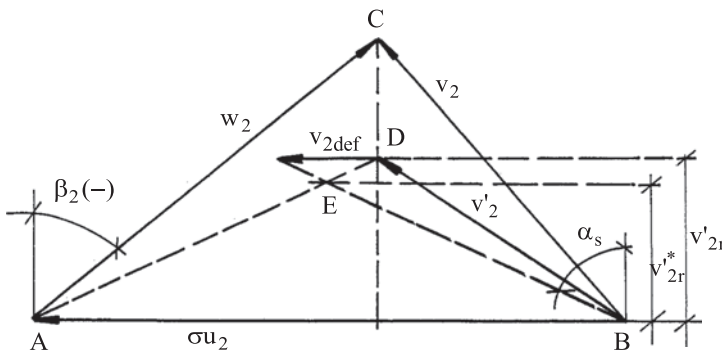


Fig. 3.21 Incidence at volute entrance; the radial velocity is drawn exaggerated for clarity

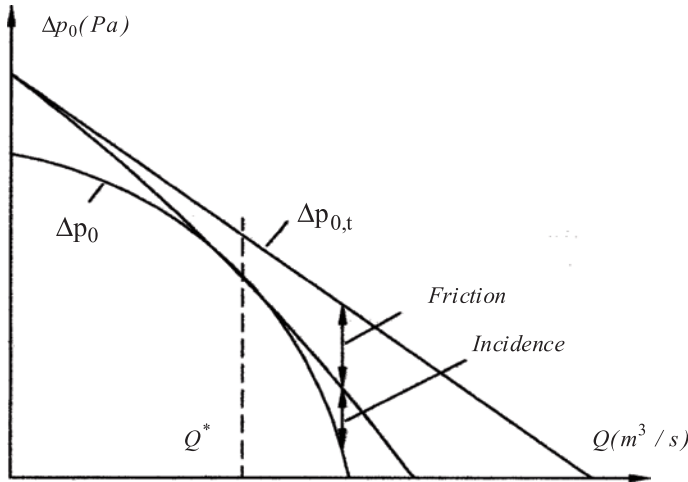


Fig. 3.22 Characteristic of a radial fan with backward curved blades

When applying Pfleiderer's slip representation, the reasoning is similar, but with a different value of Q_{*s} .

Figure 3.22 (same figure as Fig. 1.18) draws the characteristic Δp_0 as a function of the flow rate, theoretically taking slip into account (both Stodola's and Pfleiderer's reasoning lead to a linear characteristic) and obtained by subtracting friction losses (a common term for all losses proportional to the flow rate squared) and incidence losses. The representation is simplified by assuming that the volute is matched to the rotor, so that a unique design flow rate Q_* exists ($Q_* = Q_{*r} = Q_{*s}$). With this simplification, the resulting characteristic becomes a parabola, assuming constant friction loss coefficients. At zero flow rate, $\Delta p_0 \approx \rho u_2^2 / 2$ with backward curved blades. At zero net flow rate, the absolute velocity at the rotor outlet equals on average about u_2 , since the rotor flow rate is low as there is only internal leakage flow. The rotor work is approximately u_2^2 . There is nearly standstill within the volute, with incidence loss amounting to about $\rho u_2^2 / 2$. At zero net flow rate with forward curved blades, Δp_0 is much higher, due to the energy transfer by the recirculation flow within the rotor (Fig. 3.19). Δp_0 for zero flow rate is typically about the same as the design value. The resulting characteristic then typically has a maximum and a minimum (see section 3.6).

The internal efficiency is
$$\eta_i = \frac{\Delta p_0}{\Delta p_{0,t}}. \quad (3.41)$$

The internal efficiency attains its maximum at a flow rate that is lower than the design flow rate, due to part of the losses being proportional to the square of the flow rate (friction losses and diffusion losses). This phenomenon persists, even if the machine has a unique design flow rate (operating point without incidence losses in rotor and stator). Normally there is mismatch between the rotor and the stator and

no operating point exists without incidence loss in both rotor and stator. In practice, the flow rate at the operating point with maximum efficiency is often considered as design flow rate. In principle, this is not correct. Considering the operating point with incidence-free rotor inlet as design operating point is the correct attitude.

3.5 Overall Performance Evaluation

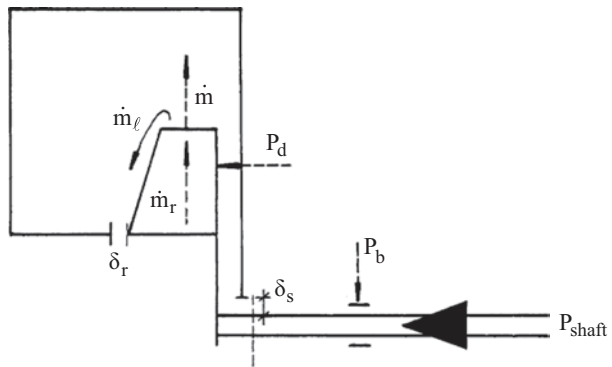
In this section, we derive the performance definitions for turbomachines, with the example of radial fans. The argumentations are generalised for constant density fluid machines.

3.5.1 Mechanical Loss

Figure 3.23 sketches a meridional section of a radial fan. The power transferred to the shaft by the driving motor is termed *shaft power* (P_{shaft}). The shaft power is not entirely transferred to the fluid, as there is mechanical loss in the bearings. The power dissipated in the bearings into heat, is conveyed into the surroundings. The outsides of the rotor shroud and rotor disc entrain surrounding fluid by friction. The energy required for this motion is taken from the shaft and dissipated into heat. Here, we consider the heat by disc friction as conveyed into the surroundings (see Chap. 1, Sect. 1.6.1), so that the disc friction loss becomes of the same nature as the bearing loss. Both are gathered in the mechanical loss, with power $P_m = P_b + P_d$. The power exchanged with the fluid within the rotor is termed *rotor power* (P_{rot}) or *internal power* (P_i). *Mechanical efficiency* is defined by

$$\eta_m = \frac{P_i}{P_{shaft}} = \frac{P_i}{P_i + P_m}. \quad (3.42)$$

Fig. 3.23 Power receiving machine



3.5.2 Leakage Loss

The clearance of the shaft passage is indicated with δ_s in Fig. 3.23. The volute fits to the rotor with clearance δ_r . Both clearances imply that the flow rate through the rotor (\dot{m}_r) exceeds the flow rate delivered by the machine (\dot{m}). The *volumetric efficiency* is defined by

$$\eta_v = \frac{\dot{m}}{\dot{m}_r} = \frac{\dot{m}}{\dot{m} + \dot{m}_\ell}. \quad (3.43)$$

In pumps, the gaps indicated in Fig. 3.23 are almost completely eliminated by sealing. The shaft sealing is typically a mechanical seal (almost without leakage) or a stuffing box (with a small leakage flow). The rotor sealing is commonly realised with wear rings. These are rings in hard materials, one on the rotor side and one on the stator side (sometimes only on the stator side; see Chap. 8: pumps), with a small gap in between them (in the order of 2‰ of the diameter) and a quite big axial width. As these rings are subjected to some wear due to the high shear stress in the fluid in the narrow gap, they have to be replaced regularly. Sealing is possible with pumps, as both the rotor and the stator have high rigidity. Sealing is impossible with fans, due to the low rigidity of plate materials. Leakage through the shaft gap is almost negligible. Leakage through the rotor gap is quite significant. The leakage flow rate depends on the gap width and on the static pressure increase within the rotor (degree of reaction). With a relative gap width of 1 % of the diameter, the leakage flow rate, with backward curved blades, may be up to 10 % of the delivered flow rate. A design according to Fig. 3.17 (right) is highly recommendable, so that the rotor leakage flow may get a useful function (energising the boundary layer on the shroud).

3.5.3 Overall Efficiency with Power Receiving Machines

The following relations apply:

$$P_{shaft} = P_i + P_m, P_i = (\dot{m} + \dot{m}_\ell) \Delta W, \Delta W = \Delta E_m + q_{irr},$$

$$\eta_g = \frac{\dot{m} \Delta E_m}{P_{shaft}} = \frac{\dot{m} \Delta E_m}{(\dot{m} + \dot{m}_\ell) \Delta W + P_m} = \frac{\dot{m}}{(\dot{m} + \dot{m}_\ell)} \frac{\Delta E_m}{\Delta W} \frac{1}{1 + P_m / P_i} = \eta_v \eta_i \eta_m.$$

The overall efficiency (global efficiency) may thus be considered as the product of three partial efficiencies.

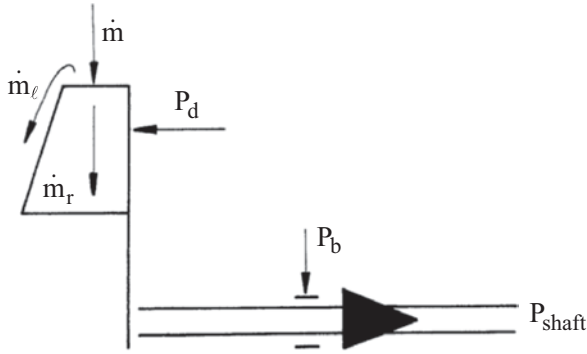


Fig. 3.24 Power delivering machine

3.5.4 Overall Efficiency with Power Delivering Machines

Figure 3.24 shows the intervening quantities. The following relations apply:

$$P_{shaft} = P_i - P_m, P_i = (\dot{m} - \dot{m}_\ell)(-\Delta W) - \Delta E_m = -\Delta W + q_{irr},$$

$$\eta_g = \frac{P_{shaft}}{\dot{m}(-\Delta E_m)} = \frac{(\dot{m} - \dot{m}_\ell)(-\Delta W) - P_m}{\dot{m}(-\Delta E_m)} = \frac{\dot{m} - \dot{m}_\ell}{\dot{m}} \frac{-\Delta W}{-\Delta E_m} \left(1 - \frac{P_m}{P_i}\right) = \eta_v \eta_i \eta_m.$$

Just as with power receiving machines, the overall efficiency may be considered as the product of three partial efficiencies.

3.6 Rotor Shape Choices with Radial Fans

The rotor shape (forward curved blades, backward curved blades) strongly affects the shape of the characteristic Δp_0 as function of Q , the value of total pressure Δp_0 and the way in which Δp_0 , at rotor level, is composed from pressure energy increase and kinetic energy increase (degree of reaction). The various rotor shapes are appropriate for various applications. Figure 3.25 (top) shows the characteristic curves at various rotational speeds for a fan with backward curved blades. The characteristic normally features a slight maximum, with the design operation point value of the total pressure rise being lower than $\rho u_2^2 / 2$. So the total pressure coefficient $\psi = \Delta p_0 / \rho u_2^2$ is lower than 0.5 (0.4 in Fig. 3.25; 0.30–0.45 being typical). For a machine with less backward leaning (straight blades, Fig. 3.14b), the characteristic features an explicit maximum with $\psi \approx 0.6$ –0.7 in the design operating point. With forward curved blades, the characteristic typically has a minimum and a maximum and ψ exceeds 1 in the design operating point. The minimum at a flow rate lower than the design value is due to the high ψ value for zero flow caused by the intense recirculation flow, as explained earlier.

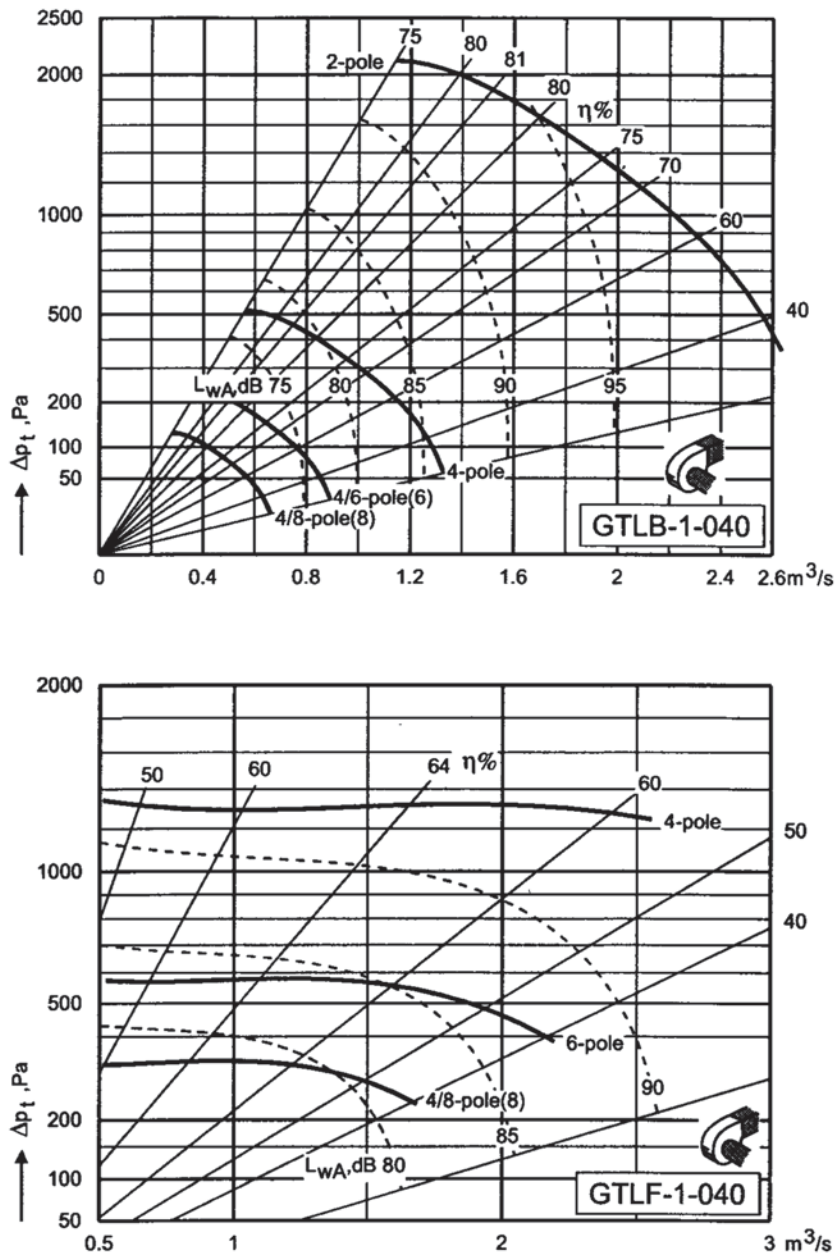


Fig. 3.25 Characteristics with a rotor with backward curved blades (*top*) and with a rotor with forward curved blades (*bottom*) in the same volute; rotors as in Fig. 3.1, rotor diameter 400 mm. (Courtesy Fläkt Woods)

Figure 3.25 shows the characteristics for rotors with backward curved and forward curved blades, fitting into the same volute. Coding 40 indicates that the rotor diameter is 40 cm. With a 2-pole driving motor, rotational speed is about 2900 rpm and with a 4-pole one it is about 1450 rpm at 50 Hz. With an equal diameter, the rotor with forward curved blades, with half the rotational speed, produces about three quarters of the pressure rise of the rotor with backward curved blades (ψ about 1.2 compared to about 0.4). Flow rates are comparable, with the inflow and outflow velocities of the fan being about the same. The rotor with forward curved blades is broader than the rotor with backward curved blades, but the through-flow does not fill the whole width, as explained before (Fig. 3.19). The outflow velocity of the rotor in the absolute frame is higher with the forward curved blades than with the backward curved blades. The ratio is about 1.5. With forward curved blades, a high velocity reduction occurs within the volute, due to tangential dump diffusion with rather high energy dissipation. With forward curved blades, the efficiency is significantly lower than with backward curved ones. The maximum efficiency with backward curved blades is about 81 %, compared to about 64 % with forward curved blades. The characteristics are very different with both rotor forms. The total pressure rise is almost independent of the flow rate with forward curved blades, but it is strongly diminishing with increasing flow rate with backward curved ones. With forward curved blades, the minimum in the characteristic may be more pronounced than in the example, depending on the blade angles chosen. In most applications, the form of the characteristic is not critical with fans. The fan load mostly consists of a duct system or a space. The total pressure rise by the fan compensates friction losses, bend losses or diffusion losses, which are all proportional to the flow rate squared. The intersection of the fan characteristic and the load characteristic is mostly about perpendicular. There is no risk of unstable operating points (see Chap. 8: pumps). But there are examples of applications with relevant form of the characteristic. Fans supplying combustion air to boilers with chain grates (coal or household waste) should feature a steep characteristic, as flow resistance of the fuel layer may vary strongly. It is advisable that this does not affect the flow rate much, which makes a fan with strongly backward curved blades suitable.

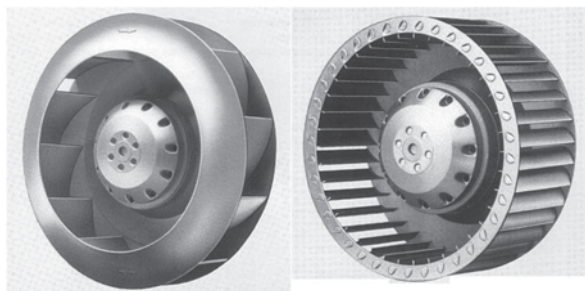
The total pressure rise value is not critical for many applications. The peripheral speed of a welded rotor may easily amount to 50 m/s. The corresponding $\frac{1}{2}\rho u_2^2$ is about 1500 Pa. With many applications, the total pressure increase needed is much lower. Typical air velocities in ducts lie around 10–20 m/s. At 16 m/s, the dynamic pressure ($\rho v^2 / 2$) is about 150 Pa. The total loss coefficient of the load thus must amount to about 10 in order to attain 1500 Pa. Note that larger peripheral speed does not create great problems. A speed of 80 m/s is easily attainable with straight back-swept blades (almost no bending stress). Such a fan thus attains ($\psi \approx 0.6$) 4500 Pa total pressure rise. Peripheral speeds until 100 m/s occur, attained by applying thicker steel plates (until 10 mm thickness) and a large number of blades (until 16).

Fan generated noise strongly increases with the rotational speed. Note that, for the Fig. 3.25 fans, with similar flow rate and total pressure rise values, the noise generated with backward curved and forward curved blades is comparable, notwithstanding the higher rotational speed with backward curved blades. A rotor with forward curved blades, with high turning and recirculation zones, is rather unfavourable

with respect to noise. The rotors with backward curved blades of Figs. 3.1 and 3.25 are manufactured very carefully with regard to noise generation. Among other things (e.g. well rounded leading edges), they feature many blades, namely 13. This is much more than strictly necessary (the forward curved blade rotor has 42 blades). Due to the high number of blades, pressure differences between pressure and suction sides are small. This strongly contributes to silent operation. A practical difference between both types is a much lower vibration level with forward curved blades, due to the lower rotational speed. The lower efficiency is less important for small power applications. Fans with forward curved blades are therefore preferred in homes. A typical type in homes is a fan incorporated into a box. The box is more or less cubic and contains a fan with forward curved blades (sometimes 2 fans) and is divided in two sections. The suction pipe of the box leads to the suction eye of the fan. The fan delivers air to the second section of the box, where dump diffusion occurs. The delivery pipe of the box is connected to this second section.

The degree of reaction is a main parameter determined by the application. It is, as discussed in Sect. 3.2, related to the blade shape. From Fig. 3.6 it follows that the total pressure rise of a pure reaction machine ($R=1$) equals zero. No work is done by the blades on the fluid, which moves purely in radial direction in the absolute frame, if no pre-swirl is applied. The shape of the workless blade follows from $v_u r = \text{constant}$, i.e. no change of angular momentum. If the blade is still more backward curved, the machine becomes a turbine. Even if centrifugal hydraulic turbines have been constructed in the past, a centrifugal form of a radial turbine is not advisable, since the centrifugal force causes pressure rise in the flow sense. A turbine is intended to utilise a pressure drop. Thus, as a principle, a radial turbine should be a centripetal machine. With β_2 between 0 and the value for $R=1$, the rotor has backward curved blades. Rotor work is rather small, but a significant part of it is used for pressure increase in the rotor. This type is appropriate if mainly intended to build up pressure. Conversion of kinetic energy into pressure by a downstream diffuser generates large losses. Large fans, with which efficiency is important, therefore exclusively have backward curved blades. Moderately backswept blade fans feature a lower relative velocity in the rotor channels for the same flow rate. Solid particles in the gas flow cause then less blade erosion. This fan type is thus appropriate for gases containing solid particles, as e.g. flue gases. It is also applied for pneumatic transport. Fans with forward curved blades enable the generation of a target total pressure rise at a low peripheral velocity. Such fans have a low vibration

Fig. 3.26 Rotors with motor incorporated into the hub. (Courtesy ebm-papst)



level and are suitable for air conditioning and hot air heating systems in homes. However, they have a low degree of reaction. The total pressure rise at the rotor level is mainly available as kinetic energy. Efficiency is impaired if a large part of the kinetic energy at rotor outlet must be converted into pressure. Such a fan is not suitable to deliver air through a large pipe system with high energy dissipation, if a lower efficiency is less acceptable.

Figure 3.26 shows rotors with backward and forward curved blades, and a motor incorporated into the hub. This is an external rotor motor: the rotor runs externally around a stator coil instead of running within a stator coil, as is more usual. Motors that are incorporated into the hub are commonly used in fans of small size. The rotors are very similar to the rotors of Fig. 3.1, but they are right-turning.

3.7 Axial and Mixed-Flow Fans

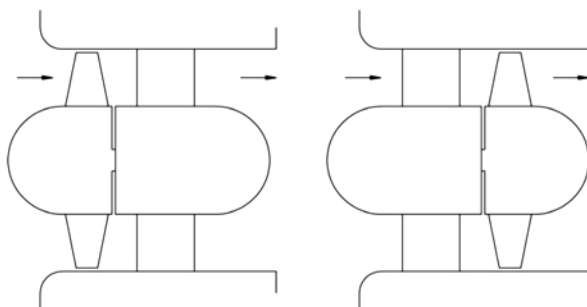
3.7.1 Degree of Reaction with Axial Fans

Figure 3.27 sketches two customary axial fan types and Fig. 3.28 sketches the corresponding velocity triangles. The first type has an outlet guide vane ring with decelerating flow, downstream of the rotor. The second type has an inlet guide vane ring with accelerating flow, upstream of the rotor. Both vane rings aim at axial flow at the machine inlet and outlet. The degree of reaction is very high, near to unity, with both types, being

$$R = \frac{\frac{w_1^2}{2} - \frac{w_2^2}{2}}{u\Delta w_u} = \frac{\frac{w_{1u}^2}{2} - \frac{w_{2u}^2}{2}}{u(w_{2u} - w_{1u})} = -\frac{w_{mu}}{u}.$$

The meaning of w_{mu} is the tangential component of the mean relative velocity. With the machine with downstream vane ring $R < 1$ (80–90%); with upstream vane ring $R > 1$ (110–120%). Most fan applications aim at pressure increase and not at velocity increase. The velocities downstream and upstream of the fan are about equal (Fig. 3.27). A high degree of reaction is desired, in principle.

Fig. 3.27 Axial fans with high degree of reaction



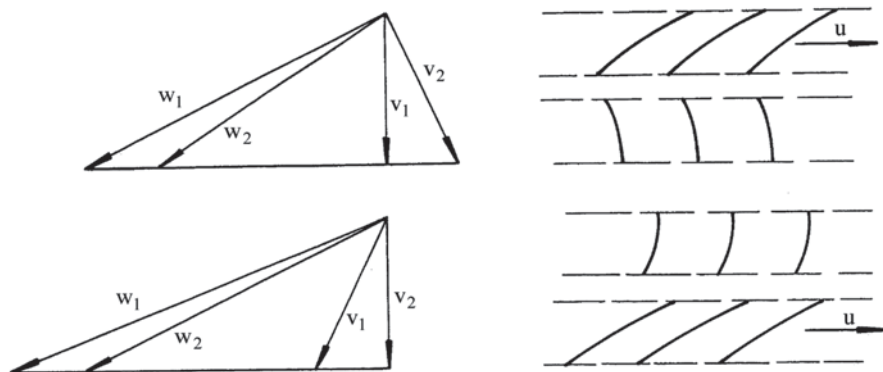


Fig. 3.28 Velocity triangles with axial fans; downstream vane ring (*top*) and upstream vane ring (*bottom*)

Differences in the performance of axial fans compared to radial ones are related to the values of total pressure rise and flow rate, relative to peripheral speed and diameter, expressed by the total pressure coefficient $\psi = \Delta p_0 / \rho u_2^2$ and by the flow factor $\Phi = Q / (u_2 \pi d_2^2 / 4)$. Figure 3.28 allows deriving that the ψ -value for axial fans is about 0.15. For radial fans, the value amounts to 0.30 (high degree of reaction) to 1.20 (low degree of reaction). The Φ -value for axial fans is of the 0.40 order, being 0.05 (backward curved blades with very narrow rotor) to 0.30 (forward curved blades with broad rotor) for radial fans. Axial fans are thus suitable for lower pressure rise, but higher flow rate.

3.7.2 Free Vortex and Non-Free Vortex Types

Figure 3.29 shows two smaller axial fan types, as typical for polluted air exhaust from a room. With the first type, the profile chord slightly increases with increasing radius. With the second type, the chord strongly increases with increasing radius and is strongly advanced with respect to the running sense (the fan in the figure is left running). The first fan is a so-called *free vortex type*. The flow meets the free vortex law, $v_u r = \text{constant}$, upstream and downstream of the rotor. With the free vortex type, work done on the fluid is constant over the radius. This is an obvious choice with multistage machines. In Chap. 13 (axial compressors) we will learn that a slight deviation from the free vortex law may be favourable, with conservation of constant work over the radius. With axial turbines (Chaps. 6 and 15) advantage is also gained if the flow deviates from the free vortex flow. Deviations from the free vortex law nevertheless remain limited with multistage machines. So, for analysis, in a first approximation, we may assume the free vortex law. The analytical advantage is then, as discussed in Chap. 2, that the three-dimensional flow within the machine is an exact transformation of a two-dimensional flow. This implies, among other things, a constant axial velocity over the radius. The three-dimensional

Fig. 3.29 Free vortex and non-free vortex axial fan types. (Courtesy ebm-papst)

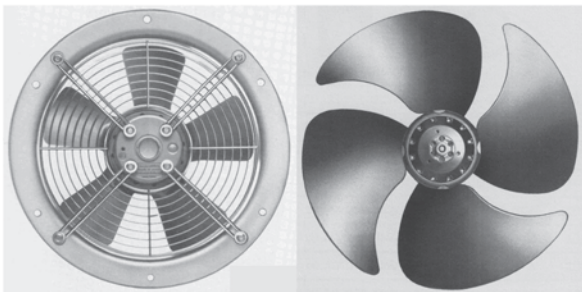
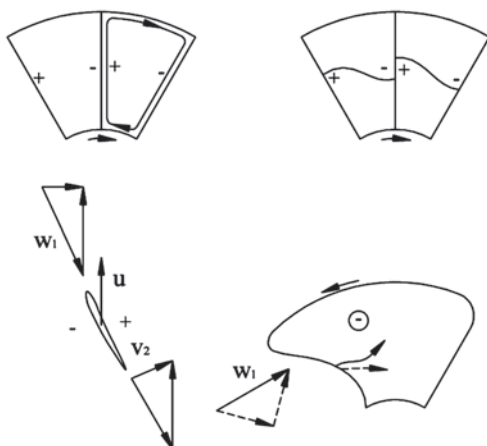


Fig. 3.30 Circulation on a contour downstream of the rotor; twist of the streamsurfaces; compensating twist by advancement of the chord at the tip



variation of flow parameters for axial machines will be analysed in Chaps. 13 and 15. When discussing the axial fan shown in Fig. 3.30 (right), certain aspects of three-dimensional flow cannot be avoided. This is done here more or less intuitively and avoids the theory of radial variation.

With a single-stage axial fan, it may be advantageous to deviate strongly from free vortex flow, namely with the objective to increase work at larger radius. This potential is not used with free vortex flow. Blade sections near the hub have a high lift coefficient and those near the top a small one. Not decreasing the lift coefficient with increasing radius and increasing the chord, the work by the fan may be strongly increased. The work is then quite inhomogeneous over the radius, but this is no principal drawback for a single-stage machine. The efficiency decreases due to the non-constant work distribution, but a special design may limit the efficiency penalty. Figure 3.30 (top, left) sketches the calculation of the circulation on a contour downstream of the rotor. When work increases with the radius, the angular momentum in the flow downstream of the rotor increases with the radius. The circulation on the contour drawn then does not equal zero:

$$\Gamma = \oint \vec{v} \cdot d\vec{S} = \int_s \vec{\omega} \cdot \vec{n} \, dS.$$

With the Stokes circulation theorem follows that rotation $\bar{\omega}$ in the axial direction is created downstream of the rotor. Streamwise rotation is normally zero with constant work. The flow downstream of the rotor always features swirl due to the presence of the tangential velocity component, but, with a free vortex blade, the rotation (ω) locally equals zero. This is the meaning of the term free vortex flow: fluid particles nearer to the shaft have higher tangential velocity, keeping a direction linked to the flow parallel to itself during the vortex motion. With non-constant work, the consequence is that a streamsurface that is cylindrical upstream of the rotor, does not remain so downstream. Figure 3.30 (top, right) shows the twisted streamsurface where fluid at the pressure side migrates to the tip and fluid at the suction side migrates to the hub. Local vortex motions created in the blade wake take a part of the kinetic energy from the core flow and dissipate it downstream of the rotor. This generates a loss mechanism associated to the twist of the streamsurfaces. Figure 3.30 (bottom) demonstrates that streamsurface twist may be compensated by advancing the chord at the tip. The relative velocity at the leading edge has a component parallel to the leading edge and a component perpendicular to it. The parallel component remains almost unaffected with flow through the rotor. The perpendicular component increases at the suction side and decreases at the pressure side. As a consequence, the relative streamlines deviate as drawn. This generates twist on the streamsurfaces, which compensates the twist by the inhomogeneous work distribution.

3.7.3 Axial Fan Characteristics; Adjustable Rotor Blades

Figure 3.31 is a sketch of the variation of the total pressure rise as a function of the flow rate. The characteristic curve has a maximum and a minimum. Figure 3.28 demonstrates that, with flow rate decrease (with same direction of v_1), the angle of attack of the flow entering the rotor increases. This increases the rotor deflection and so the rotor work. The angle of attack on the stator, if downstream, increases as well (with same direction of w_2). Flow rate decrease thus increases rotor work, but boundary layer separation occurs below a certain flow rate, within the rotor or the stator. This diminishes the total pressure rise. The total pressure rise is higher however at a very low flow rate. Recirculation flows are generated, causing a significant radius increase for the through-flow (Fig. 3.31). Due to the centrifugal force, pressure build-up arises in the flow.

The flow separation with reduced flow rate at rotor entrance and at stator entrance with a downstream stator can be removed with adjustable rotor blades. Figure 3.32 shows how by turning the rotor blades into a more tangential position and by lowering the angle of attack of the rotor blades, high incidences can be avoided at reduced flow rate. This means that by turning the rotor blades into a more tangential direction (closing the rotor) the fan is adjusted to operation at lower flow rate and lower pressure rise. In practise, with this turning some loss of efficiency occurs because the blade twist is not fully adapted anymore to the flow so that design incidence angles cannot be reached at all radii.

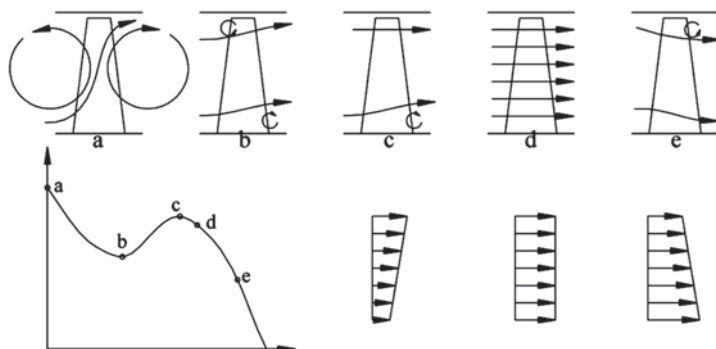


Fig. 3.31 Flow patterns through an axial fan and consequences for the shape of the characteristic curve. (Adapted from [9])

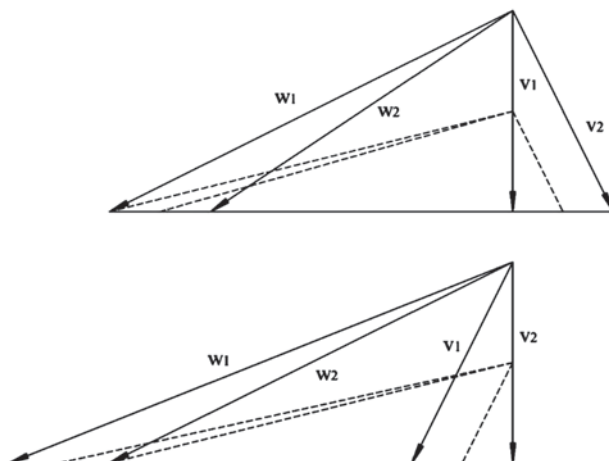


Fig. 3.32 Reduction of flow rate and pressure rise by turning rotor blades into a more tangential position; *top*: vane ring downstream of rotor; *bottom*: vane ring upstream of rotor

Similarly, by opening the rotor, characteristics can be shifted towards higher flow rate and higher pressure rise, but limited due to separation at too large angles of attack. Some larger industrial axial fans have rotor blades that are individually adjustable at standstill.

3.7.4 Mixed-Flow Fans

Some forms closely approach the axial form and others closely approach the radial form. Figure 3.33 shows the meridional section of a fan close to an axial type, with small radius change of the average flow. The corresponding velocity triangles show the axial velocity increase through the rotor by the decreasing blade height.

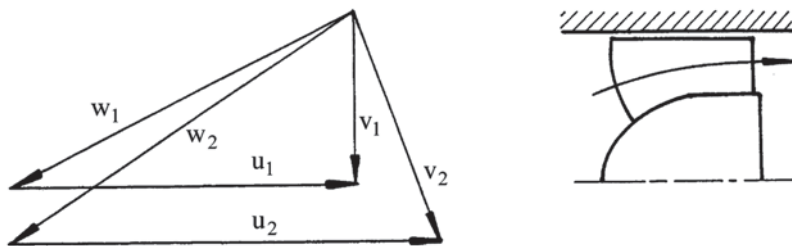
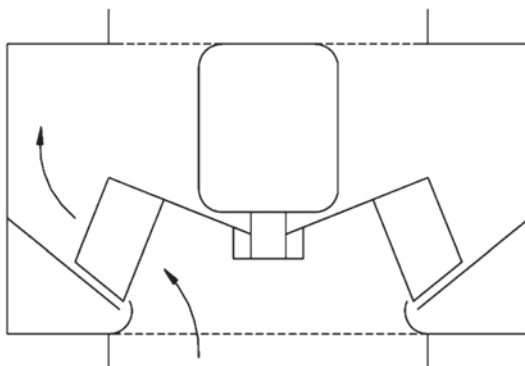


Fig. 3.33 Mixed-flow fan close to the axial form: low degree of reaction

The average blade speed increases as well, which increases the rotor work. Such a machine is, strictly spoken, a mixed-flow machine. As the blade shape remains the same as that with a purely axial machine, the machine is commonly termed as axial. In Fig. 3.33, the pressure energy rise due to the centrifugal force $(u_2^2 - u_1^2)/2$ and the pressure energy drop due to the flow acceleration $(w_2^2 - w_1^2)/2$ are comparable. Consequently, the static pressure increase in the rotor is very low. The degree of reaction of the machine is thus very low. With the example, we understand that by appropriate blade height variation in the rotor, any degree of reaction may be obtained. With a high degree of reaction fan, the total pressure coefficient related to the tip speed, amounts to about 0.15 (Fig. 3.28). With a low degree of reaction fan, this coefficient may be up to about 0.30 (Fig. 3.33), being equal to the lowest values obtained by radial fans with backward curved blades. Advantages and disadvantages with the choice of the degree of reaction are the same with axial machines and radial ones: a lower degree of reaction implies a higher rotor work, but a lower efficiency if the kinetic energy downstream of the rotor has to be converted into pressure rise. Many of these mixed-flow fans have a vaned diffuser downstream of the rotor.

Figure 3.34 is a sketch of a mixed-flow fan, with a shape close to a radial fan. This shape is chosen for fans that are incorporated into a duct. The characteristics of such a mixed-flow fan only deviate little from these of a centrifugal fan.

Fig. 3.34 Mixed flow fan close to the radial form for incorporation into a duct. (Adapted from [3])



3.8 Exercises

The list contains exercises on fans, but also on pumps and hydraulic turbines, as with the theory developed up to now, basic problems on all kinds of machines with constant density fluids can be analysed.

3.8.1 Centrifugal Pump (Idealised Flow)

A centrifugal pump has rotor internal diameter $d_1=80$ mm and external diameter $d_2=200$ mm. Blades are simply curved with width $b_1=30$ mm at the inlet and $b_2=15$ mm at the outlet. There is no pre-swirl, which results in a purely radial rotor inlet flow. Relative velocity at the rotor inlet and outlet form the angle $\beta_1=\beta_2=-60^\circ$ with the radial direction. The pump runs at 1450 rpm and pumps water ($\rho=1000$ kg/m³). Assume idealised flow, i.e. no internal losses and an infinite number of infinitesimally thin blades, with flow aligned to the blades.

1. Determine the static pressure rise across the rotor Δp_{rot} . First determine the velocity triangles and the rotor work ΔW . Verify that the sum of the pressure energy rise and the kinetic energy rise in the flow is equal to the rotor work.
2. Determine the degree of reaction R .
3. Determine the volume flow rate Q through the pump.
4. Determine the rotor power or idealised internal power P_i .

$$\mathbf{A:} \Delta W=156.78 \text{ J/kg; } (1/\rho)\Delta p_{rot}=105.69 \text{ J/kg; } R=0.674; Q=26.44 \text{ l/s; } P_i=4146 \text{ W.}$$

3.8.2 Rotor of a Centrifugal Fan (Finite Number of Blades and Internal Losses)

A centrifugal fan has rotor internal and external diameters $d_1=500$ and $d_2=750$ mm. The diameter of the rotor eye is $d_0=450$ mm. The rotor has 10 blades with thickness $t=4$ mm. Blades are simply curved with width $b_1=180$ mm at the inlet and $b_2=150$ mm at the outlet. There is no pre-swirl. Blade angles at inlet and outlet are $\beta_1^b=-60^\circ$ and $\beta_2^b=-45^\circ$. The fan runs at 1450 rpm and delivers the volume flow rate $Q=4$ m³/s ($\rho_{air}=1.2$ kg/m³). Assume that volumetric efficiency is $\eta_v=0.95$ and the incidence loss coefficient at rotor inlet is $\mu_{def}=0.80$. Apply Pfleiderer's formulae (3.23–3.25) to estimate the slip, with $\lambda=0.75$.

1. Determine the velocity triangles just upstream of the rotor inlet (station 1) and just downstream of the rotor inlet (station 1^b).
2. Determine the deceleration ratio in the rotor eye $\zeta = v_1 / v_0$.
3. Determine the tangential deflection at the rotor inlet and the corresponding incidence loss.

4. Calculate the design flow rate of the rotor. Compare with $Q=4 \text{ m}^3/\text{s}$.
5. Determine the velocity triangles just upstream of the rotor outlet (station 2^b) and just downstream of the rotor outlet (station 2).
6. Calculate the work transferred to the fluid.
7. Determine the degree of reaction.
8. Determine the rise of the total pressure rise across the rotor ignoring all losses, except the incidence loss at the rotor entrance.

A: $\zeta=0.592$; $q_{irr, incl}=46.52 \text{ J/kg}$; $Q^*=5.59 \text{ m}^3/\text{s}$; $\Delta W=1772.04 \text{ J/kg}$; $R=0.749$; $\Delta p_{0,rot}=2070.6 \text{ Pa}$.

3.8.3 Number of Blades of a Rotor of a Centrifugal Fan

Verify with the Pfleiderer moment coefficient (Eq. 3.31) that with the dimensions in Exercise 3.8.2, the number of blades is appropriate.

A: $C_M=0.960$; thus OK.

3.8.4 Volute of a Centrifugal Fan

Add a volute around the rotor of Exercise 3.8.2 with width $b_3=375 \text{ mm}$ and height at the outlet $h_3=375 \text{ mm}$. Assume a logarithmic spiral for the outer wall shape. Remark that the outlet area of the volute is 88.4% of the suction inlet area of the fan ($d_0=450 \text{ mm}$). Thus with a diffuser downstream of the volute with an area ratio 1.131 the velocity at the discharge side of the fan becomes the same as at the suction side.

1. Calculate the loss due to the radial dump at the entrance of the volute. Take into account that the complete rotor flow rate enters the volute during the dump.
2. Calculate the loss due to tangential deflection at the entrance of the volute. Assume as attenuation coefficient of this loss $\mu_{def}=0.80$.
3. Determine the rise of the total pressure across the resulting fan taking into account the dump loss at volute entrance and the incidence losses at rotor inlet and at volute inlet, neglecting all other losses.

A: $q_{irr, dump}=27.68 \text{ J/kg}$; $q_{irr, inc2}=39.33 \text{ J/kg}$; $\Delta p_0=1990.2 \text{ Pa}$.

3.8.5 Leakage Flow Rate with Centrifugal Fan

Assume in the previous Exercises 3.8.2–3.8.4 a 3 mm gap between the volute and the rotor inlet. Assume a contraction coefficient 0.90 for the gap flow. Calculate the leakage flow rate at the specified operating point and verify the estimated volumetric efficiency. Assume that the total pressure in front of the gap on the volute side is the static pressure at volute entrance after the radial dump (station 2') and that the

static pressure on the side of the rotor is the static pressure at the inlet of the rotor (station 1).

$$\mathbf{A}: Q_{leak} = 0.217 \text{ m}^3/\text{s}; \eta_v = 0.948.$$

3.8.6 Centrifugal Pump (Finite Number of Blades and Internal Losses)

A centrifugal pump has rotor internal diameter $d_i = 100$ mm and external diameter $d_2 = 180$ mm. The rotor has 8 blades with thickness $t = 2$ mm. Blades are simply curved with width $b_i = 15$ mm at the inlet and $b_2 = 10$ mm at the outlet. There is no pre-swirl. The blade angles at the inlet and outlet are $\beta_1^b = -70^\circ$ and $\beta_2^b = -60^\circ$. The pump runs at 1800 rpm and supplies the volume flow rate $Q = 17.0$ l/s ($\rho = 1000$ kg/m³). The manometric head is $H_m = 12$ m. Ignore leakage flow. Assume as mechanical efficiency $\eta_m = 0.95$ and as rotor incidence loss coefficient $\mu_{def} = 0.80$. Apply Wiesner's formula for the slip (3.20–3.21).

1. Determine the power transferred to the fluid by the rotor, the internal efficiency and the shaft power.
2. Determine the flow rate and the manometric head with an incidence-free rotor inlet, with the assumption that all internal losses, except for the incidence loss at the rotor inlet, are proportional to the flow rate squared.

$$\mathbf{A}: P_{rot} = 2494.1 \text{ W}; \eta_i = 0.802, P_{shaft} = 2625.3 \text{ W}; Q^* = 13.76 \text{ l/s}; H_m^* = 14.97 \text{ m}.$$

3.8.7 Axial Fan (Idealised Flow): Analysis on Average Diameter

The rotor of an axial fan has a hub diameter $d_h = 0.24$ m and a tip diameter $d_t = 0.48$ m. There is no pre-swirl. The inlet flow is purely axial on the quadratic average radius $r_m = 0.19$ m $\left[r_m^2 = \frac{1}{2} (r_i^2 + r_h^2) \right]$. The relative velocity forms the angle $\beta_i = -55^\circ$ to the axial direction at the rotor inlet and the angle $\beta_2 = -35^\circ$ at the outlet. Rotational speed is 2500 rpm and the air has density $\rho = 1.2$ kg/m³. Assume idealised flow, i.e. no internal losses. Assume as well that the flow on the average radius is characteristic for the entire machine.

1. Determine the velocity triangles of the flow on the average radius.
2. Determine the rotor work ΔW , the static pressure rise across the rotor Δp_{rot} and the degree of reaction R .
3. Determine the volume flow rate Q through the fan.
4. Determine the rotor power or internal idealised power P_i at design flow rate.

$$\mathbf{A}: \Delta W = 1261.2 \text{ J/kg}; \Delta p_{rot} = 1127.7 \text{ Pa}; R = 0.745; Q = 4.73 \text{ m}^3/\text{s}; P_i = 7154 \text{ W}.$$

3.8.8 Axial Fan (Idealised Flow): Free Vortex and Non-Free Vortex

Consider the axial fan from the previous exercise and assume a rotor blade shape with constant work and constant axial velocity along the radius.

1. Determine the velocity triangles at the hub and the tip.
2. Determine the degree of reaction and the work coefficient at hub and tip.
3. Verify the realisability of the fan blades by calculating the deceleration ratios w_2/w_1 and the axial chord solidities, assuming a Zweifel coefficient of unity, at hub and tip. Assume constant axial velocity in the streamtubes at hub and tip.
4. Perform the calculation once more, but now with the work ΔW proportional to the radius. Compare with constant work distribution.

A: $I: R_{hub}=0.36; \psi_{hub}=1.28; R_{tip}=0.84; \psi_{tip}=0.32; (w_2/w_1)_{hub}=0.766; (w_2/w_1)_{tip}=0.768; (\sigma_a)_{hub}=2.17; (\sigma_a)_{tip}=0.46$; **II:** $R_{hub}=0.60; R_{tip}=0.80$.

3.8.9 Inlet Guide Vane with a Centrifugal Fan

Argue that, with a centrifugal fan with backward curved blades (Fig. 3.5), the characteristic is modified by an inlet guide vane ring. Consider pre-swirl generating a tangential component of the absolute velocity in the rotation sense (closing the guide vanes) and flow rate reduction so that the direction of the relative velocity at the inlet remains the same. Observe that rotor work stays approximately the same due to the changed velocity triangle at the rotor outlet. The incidence at the volute entrance changes, but whether or not this decreases efficiency depends on the operating point. Conclude that with adjustable inlet guide vanes, in principle, characteristics may be shifted to lower or higher flow rates. In practise, there is some loss of efficiency due to incidences.

3.8.10 Change of Rotational Speed with Centrifugal and Axial Fans

Consider a centrifugal fan with backward curved blades (Fig. 3.5). Analyse the effect of the change of rotational speed. Remark that the shape of the velocity triangles is kept, if all velocity components vary proportional to the speed of rotation. Incidence angles stay the same. Conclude that similarity of the velocity triangles is obtained for flow rate proportional to rotational speed and energy rise proportional to rotational speed squared. So, similarity of velocity triangles is realised on parabolas through the origin in a map of characteristic curves. Remark that losses stay proportional to the rotor work and internal efficiency is thus maintained, provided that loss coefficients are constant. Observe that volumetric efficiency is also maintained, provided that contraction coefficients are constant. So, global efficiency is

approximately constant on similarity parabolas. Repeat the reasoning for axial fans and mixed-flow fans (velocity triangles on Figs. 3.28 and 3.33). Observe that the conclusion is the same.

3.8.11 Two-Stage Axial Fan

Consider a two-stage axial fan according to Fig. 3.3, but consider that the machine is a stator-rotor combination followed by a rotor-stator, with the intermediate vane ring made of struts not causing flow deflection. The velocity triangles are as in Fig. 3.28 (but in reversed order). Two-stage axial fans are used for rather high flow rates (above 500 m³/s), combined with a rather high pressure rise (above 4000 Pa). Such combinations cannot be realised with centrifugal fans or single-stage axial fans. Consider flow rate $Q=660$ m³/s and rise of total pressure $\Delta p_0=6500$ Pa, for rotor dimensions $d_{hub}=2.10$ m and $d_{tip}=4.20$ m at 590 rpm. Take as air density 1.25 kg/m³ and assume equal work done by both rotors. Estimate the internal efficiency $\eta_i=0.885$ and ignore leakage flow ($\eta_v=1$) and mechanical loss ($\eta_m=1$).

1. Determine the velocity triangles on the quadratic mean radius $r_m=1.660$ m $\left[2r_m^2 = r_t^2 + r_h^2\right]$.
2. Determine the degree of reaction and the work coefficient on the mean radius.
3. Assume that the fan is realised with free vortex flow. Estimate the necessary solidity at the hub of the rotor for a Zweifel coefficient of unity. Verify the deceleration ratio w_z/w_l .
4. Determine the number of blades for an axial chord equal to 20% of the blade height.

A: I: $w_{2u}=-102.58$ m/s; $R=1.14$; $(\sigma_a)_{hub}=0.70$; $(w_z/w_l)_{hub}=0.714$; $Z=22$; II: $w_{2u}=-73.93$ m/s; $R=0.86$; $(\sigma_a)_{hub}=1.30$; $(w_z/w_l)_{hub}=0.732$; $Z=41$.

Variants of the two-stage fan are manufactured. The more common design is with 2 equal stages, either stator-rotor or rotor-stator. These configurations are also possible with the sketch of Fig. 3.3. Remark that the combination stator-rotor is the most favourable with respect to necessary solidity. A special configuration is rotor-stator-rotor, also realisable with Fig. 3.3. This machine can be seen as a contraction of a rotor-stator and a stator-rotor according to Fig. 3.28 with the 2 stator vane rows merged. The machine is kinematically equivalent with the fan calculated, but with the order of the stages reversed. Another variant is a two-stage fan with contra-rotating rotors. This variant is kinematically equivalent to the previous build. There are no stator vanes, but the machine requires two shafts rotating in opposite senses. The contra-rotating version is sometimes used with smaller fans where the rotors are mounted directly on the shafts of the driving motors. It is normally not used for larger fans with external motors.

3.8.12 Axial Turbine

Consider an axial turbine according to Fig. 1.9 (Chap. 1). The outer diameter of the turbine and the supply duct diameter are 1 m. The hub diameter is 0.5 m. $n=300$ rpm, $\rho=1000$ kg/m³. On the arithmetically average radius ($r=0.375$ m), the stator deviates the flow by $+30^\circ$ with respect to the axial direction, while the rotor outflow is at -60° . The absolute flow leaves the rotor axially on the entire rotor radius. Stator vanes and rotor blades are designed for constant work and constant axial velocity along the radius.

1. Sketch the velocity triangles on the average radius (upstream and downstream of the rotor). Determine the axial velocity and the flow rate. Determine the rotor inlet angle with respect to the axial direction on the average radius.
2. Determine rotor torque and rotor power.
3. Determine the pressure on the inlet manometer (gauge pressure: relative to atmospheric pressure), assuming that the inlet manometer is on the supply duct (at a somewhat larger distance upstream of the turbine inlet than suggested by the figure) with centre of the manometer 3 m above the downward water level (tail water). Assume for the loss coefficients: stator: $\zeta=0.05$ related to the outlet kinetic energy $v_1^2/2$; rotor: $\zeta=0.05$ related to the kinetic energy of the outlet relative velocity $w_2^2/2$; diffuser $\zeta=0.50$ related to the inlet kinetic energy $v_2^2/2$ (all velocities on the mean radius).
4. Determine stator outlet angle and rotor outlet angle at the rotor periphery, measured to the axial direction.

A: $Q=4.01$ m³/s; $\beta_1=-49.1^\circ$; $P_{rot}=185.4$ kW; $p-p_a=21.56$ kPa; $\alpha_1=23.4^\circ$; $\beta_2=-66.6^\circ$.

References

1. Adachi T, Sugita N, Yamada Y (2004) Study on the performance of a Sirocco fan. *Int J of Rotating Mach* 10:415–424
2. Aungier RH (2000) Centrifugal compressors: a strategy for aerodynamic design and analysis. ASME Press. ISBN 0-7918-0093-8
3. Bleier FP (1998) Fan handbook. McGraw-Hill. ISBN 0-07-005933-0
4. Eck B (1972) Ventilatoren, 5th edn. Springer. ISBN 3-540-05600-9
5. Gülich JF (2010) Kreiselpumpen, 3th edn. Springer. ISBN 978-3-642-05478-5
6. Japikse D, Marscher WD, Furst RB (1997) Centrifugal pump design and performance, Concepts ETI. ISBN 0-933283-09-1
7. Kim K-Y, Seo S-J (2004) Shape optimization of the forward-curved-blade centrifugal fan with Navier-Stokes analysis. *J Fluids Eng* 126:735–742
8. Kim S, Park J, Choi B, Baek J (2012) Flow analysis and assessment of loss models in the symmetric volute of a turbo-blower. *J Fluids Eng* 134:011101
9. Pfleiderer C (1961) Die Kreiselpumpen für Flüssigkeiten und Gase, 5th edn. Springer. no ISBN
10. Qiu X, Japikse D, Zhao J, Anderson MR (2011) Analysis and validation of a unified slip factor model for impellers at design and off-design conditions. *J Turbomach* 133:041018
11. Von Backström TW (2006) A unified correlation for slip factor in centrifugal impellers. *J Turbomach* 128:1–10

Chapter 4

Compressible Fluids

Abstract In further chapters we will study machines that function with compressible fluids, first steam turbines (Chap. 6), then gas turbines and compressors (Chaps. 11–15). For analysis of these machines, knowledge of fundamentals of compressible fluid flow is a necessity. We study compressible fluid flow fundamentals in the present chapter, for one-dimensional steady flows. This term refers to a flow whose properties change in one single spatial direction, namely an average streamline, and that is uniform in the spatial directions perpendicular to this streamline and constant in time. The streamline need not be straight. The discussion is limited to what is strictly necessary for the fundamental analysis of turbomachines. We refer to books on fluid mechanics for a more in-depth study.

4.1 Basic Laws

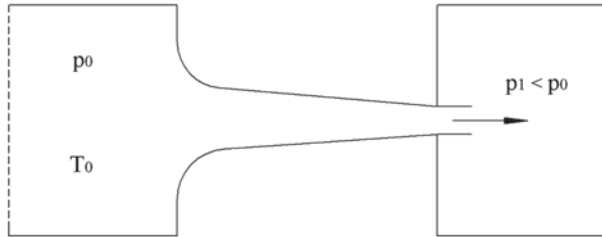
The fundamental equations for one-dimensional flows have already been derived in Chap. 1. We apply them here to compressible fluids. The one-dimensional flow is an approximation of the flow in a blade passage of a turbomachine. This approximation is not very accurate. It is primarily intended to acquire fundamental insight. Multi-dimensional effects occur in real machines. We will study them introductorily in the chapter on steam turbines. More in-depth study of multi-dimensional effects is dealt with in the gas turbine and compressor chapters. We mainly discuss turbine flow. Within most components of a turbine, flow is accelerating. A stationary channel between two spaces in which a flow accelerates is called a *nozzle*, as shown in Fig. 4.1. Nozzle flow allows analysis of the functioning of steam turbines. In the present chapter, relations are derived for accelerating flow, but most apply to decelerating flow as well.

The mass conservation equation is $\rho vA = \text{constant}$, where A is the cross-section area of the channel. Logarithmic differentiation results in

$$\frac{d\rho}{\rho} + \frac{dv}{v} + \frac{dA}{A} = 0. \quad (4.1)$$

The work equation is

Fig. 4.1 Nozzle between two spaces (0 and 1)



$$dW = d\frac{1}{2}v^2 + \frac{1}{\rho}dp + dU + dq_{irr}.$$

We consider a flow without work exchange ($dW=0$) and as yet without losses ($dq_{irr}=0$). Gravitational potential energy may always be ignored for a compressible fluid in a flow with significant pressure variation. This follows from the typical low density value (e.g. air under atmospheric conditions $\rho \approx 1.20 \text{ kg/m}^3$). Example: a 1 m height change is a change in potential energy of about 10 J/kg. The corresponding pressure change is $dp = \rho dU \approx 12 \text{ Pa}$. We simplify the work equation to

$$d\frac{1}{2}v^2 + \frac{dp}{\rho} = 0. \quad (4.2)$$

The energy equation in absence of work exchange and heat exchange is

$$0 = dh + d\frac{1}{2}v^2 + dU.$$

The influence of potential energy may be ignored again. Example: a 10 J/kg enthalpy change represents a temperature change of $dT \approx 0.01 \text{ K}$ ($c_p = 1005 \text{ J/kgK}$ for air under atmospheric conditions). We simplify the energy equation to

$$dh + d\frac{1}{2}v^2 = 0. \quad (4.3)$$

A total differential is formed in the energy equation. We therefore introduce the concept of *total enthalpy*, defined by

$$h_0 = h + \frac{1}{2}v^2. \quad (4.4)$$

The subscript 0 refers to the total value. The total enthalpy is constant in the nozzle: $h_0 = \text{constant}$.

The combination of the work equation (4.2) and the energy equation (4.3) results in

$$Tds = dh - \frac{1}{\rho} dp = 0. \quad (4.5)$$

As expected, we find that entropy is constant for reversible adiabatic flow (= without heat exchange and without losses). In order to express this second constant, we introduce the concept of *total state* or *stagnation state*. Total state refers to the state obtained by bringing to stagnation the flow in an adiabatic, reversible way. This state is indicated by the subscript 0.

From (4.5) follows
$$c_p dT = \frac{dp}{\rho},$$

and with the ideal gas law $p = \rho RT$:

$$c_p dT = RT \frac{dp}{p} \quad \text{or} \quad \frac{dp}{p} = \frac{c_p}{R} \frac{dT}{T}.$$

With $R = c_p - c_v$ and $\gamma = c_p / c_v$ this also results in

$$\frac{dp}{p} = \frac{\gamma}{\gamma - 1} \frac{dT}{T} \quad \text{or} \quad p \sim T^{\frac{\gamma}{\gamma - 1}},$$

and

$$\rho T \sim T^{\frac{\gamma}{\gamma - 1}} \quad \text{or} \quad \rho \sim T^{\frac{1}{\gamma - 1}} \quad \text{and} \quad p \sim \rho^\gamma.$$

The process is thus polytropic with exponent γ .

For a given state p, ρ, T and v , the total state follows from

$$c_p T_0 = c_p T + \frac{1}{2} v^2, \quad (4.6)$$

$$\frac{p}{p_0} = \left(\frac{T}{T_0} \right)^{\frac{\gamma}{\gamma - 1}}, \quad \frac{\rho}{\rho_0} = \left(\frac{T}{T_0} \right)^{\frac{1}{\gamma - 1}}. \quad (4.7)$$

The total state p_0, ρ_0, T_0 is constant within the nozzle and corresponds in Fig. 4.1 to the state within the first space, with an assumed stagnant fluid there.

With formulae (4.6) and (4.7), it is assumed that the gas, apart from being *ideal* ($p = \rho RT$ and h only dependent on T), is *perfect* as well, i.e. that specific heat capacities c_p and c_v are constant. In a real gas, these coefficients are somewhat temperature-dependent. For example, for a velocity change of $v=0$ to $v=300$ m/s, the kinetic energy change is 45 kJ/kg. The corresponding temperature change is about 40 K. The change of c_p over such a temperature difference is about 2–4%. So, the approximation with constant coefficients is very adequate.

For adiabatic reversible flow, the energy equation (4.6) may be written as

$$\frac{1}{2}v^2 = c_p T_0 \left[1 - \left(\frac{T}{T_0} \right) \right] = \frac{c_p}{R} \frac{p_0}{\rho_0} \left[1 - \left(\frac{T}{T_0} \right) \right].$$

With (4.7) it follows that

$$\frac{1}{2}v^2 = \frac{\gamma}{\gamma-1} \frac{p_0}{\rho_0} \left[1 - \left(\frac{p}{p_0} \right)^{\frac{\gamma-1}{\gamma}} \right]. \quad (4.8)$$

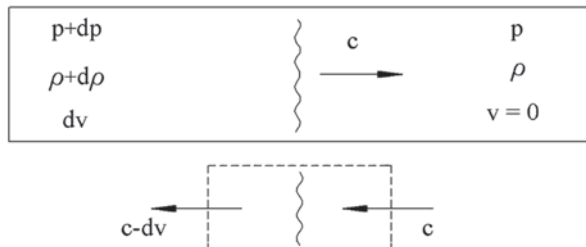
This equation is termed the Barré de Saint Venant equation. Below (Sect. 4.6), we derive a similar equation for a flow with losses. The Saint Venant equation is for a compressible fluid the equivalent of the Bernoulli equation for an incompressible (constant density) fluid.

4.2 Compressibility and Velocity of Sound

A small pressure perturbation in a compressible fluid propagates. A pressure wave is generated. The wave velocity is a function of the compressibility and may characterise it. Small pressure perturbations are called sound. The corresponding velocity is termed the *speed of sound*. Pressure waves corresponding to large pressure changes are called shock waves. Their propagation speed exceeds the speed of sound (see fluid mechanics).

Figure 4.2 represents a small pressure perturbation, propagating in a duct with a constant section, in which there is a stagnant fluid with characteristics p and ρ . The

Fig. 4.2 Sound wave propagation in a duct



propagation velocity is denoted by c . After passage of the sound wave, pressure, density and velocity become $p + dp$, $\rho + d\rho$ and dv .

We further consider a relative frame, moving along with the sound wave. The flow is steady within this frame and the laws formulated in the previous section apply. Before the wave, velocity equals c , after the wave $c - dv$.

$$\text{Mass:} \quad \frac{d\rho}{\rho} - \frac{dv}{c} = 0. \quad (4.9)$$

$$\text{Work:} \quad -cdv + \frac{dp}{\rho} = 0. \quad (4.10)$$

Elimination of dv from (4.9) and (4.10) gives

$$c^2 \frac{d\rho}{\rho} = \frac{dp}{\rho} \quad \text{or} \quad c^2 = \frac{dp}{d\rho}. \quad (4.11)$$

Isentropy (reversible adiabatic flow) means

$$p \sim \rho^\gamma \quad \text{or} \quad \frac{dp}{p} = \gamma \frac{d\rho}{\rho}.$$

$$\text{Thus:} \quad c^2 = \gamma \frac{p}{\rho} \quad \text{or} \quad c = \sqrt{\gamma \frac{p}{\rho}}. \quad (4.12)$$

The compressibility of matter is characterised by the relative volume change caused by a pressure change. The ratio of the infinitesimal pressure increase to the corresponding infinitesimal relative volume decrease is called the bulk modulus or the volumetric elasticity modulus E . For a given mass m applies $m = \rho V$, so that $d\rho/\rho + dV/V = 0$. The compressibility coefficient β , being the inverse of the bulk modulus, is

$$\beta = \frac{1}{E} = -\frac{dV/V}{dp} = \frac{d\rho/\rho}{dp}.$$

For isentropic compression it follows that

$$E = \rho \frac{dp}{d\rho} = \rho c^2.$$

Thus, velocity of sound may be used as a measure for compressibility. Low velocity of sound corresponds to high compressibility. From (4.12) and the ideal gas law, it follows that

$$c = \sqrt{\gamma RT}. \quad (4.13)$$

With an ideal gas, the velocity of sound only depends on temperature. For air under atmospheric conditions ($\gamma = 1.4$; $R = 287 \text{ J/kgK}$; $T = 288 \text{ K}$) it follows that $c = 340 \text{ m/s}$.

According to the compressibility definition, an incompressible fluid has an infinitely large elasticity modulus or an infinitely large speed of sound. No fluid is strictly incompressible, however. A liquid is compressible, but much less than a gas. For instance, water under atmospheric conditions ($p = 1 \text{ bar}$, $T = 288 \text{ K}$) has a bulk modulus $E \approx 2 \cdot 10^9 \text{ Pa}$. The corresponding velocity of sound is $c \approx 1400 \text{ m/s}$, being larger than with air, but with a ratio under one order of magnitude.

4.3 Compressibility Effect on the Velocity-Pressure Relation

For a constant density fluid the relation between velocity and pressure follows from the work equation or Bernoulli's equation (4.2), by

$$\frac{1}{2}v^2 + \frac{p}{\rho} = \text{cst} = \frac{p_0}{\rho} \quad \text{or} \quad \frac{1}{2}v^2 = \frac{p_0 - p}{\rho}. \quad (4.14)$$

For a compressible fluid, the relation is more complex and given by the Saint Venant formula (4.8). An important question for practice is in how far there is necessity to systematically use the compressible equation (4.8) for a compressible fluid like air. The answer lies in the comparison of the term $\frac{1}{2}v^2$ to the term $\frac{\gamma}{\gamma-1} \frac{p_0}{\rho_0} = \frac{\gamma}{\gamma-1} RT_0 = c_p T_0$. So, we may compare the flow velocity v to $a_0 = \sqrt{2c_p T_0}$, which is a velocity proportional to the velocity of sound $c_0 = \sqrt{\gamma RT_0}$ in stagnation conditions. For instance, for $T_0 = 288 \text{ K}$, with $R = 287 \text{ J/kgK}$ and $\gamma = 1.4$ (air), $a_0 = 760 \text{ m/s}$ ($c_0 = 340 \text{ m/s}$). In many flows, v is much smaller than a_0 , which means that the term between the square brackets in (4.8) is small. This then means that p and p_0 do not differ much, compared to p_0 itself. We may then expand (4.8) as

$$\frac{1}{2}v^2 = \frac{\gamma}{\gamma-1} \frac{p_0}{\rho_0} \left[1 - \left(1 - \frac{p_0 - p}{p_0} \right)^{\frac{\gamma-1}{\gamma}} \right] \approx \frac{\gamma}{\gamma-1} \frac{p_0}{\rho_0} \left[1 - \left(1 - \frac{\gamma-1}{\gamma} \frac{p_0 - p}{p_0} + \dots \right) \right],$$

and we recover the Bernoulli equation. This shows that for velocities that are low with respect to a_0 , the Bernoulli equation is an accurate approximation of the Saint

Table 4.1 Comparison between results of the Saint Venant and the Bernoulli equations for $T_0 = 288 \text{ K}$, $R = 287 \text{ J/kgK}$, $\gamma = 1.4$

p / p_0	0.999	0.99	0.95	0.8	0.4
$v_{SV} (m/s)$	12.860	40.732	91.747	189.042	365.060
$v_{B,\rho_0} (m/s)$	12.857	40.659	90.915	181.831	314.940
$v_{B,\rho_m} (m/s)$	12.860	40.731	91.744	188.923	361.296

Venant equation. In order to illustrate the quality of the approximation, Table 4.1 compares the results of both equations for $\rho = \rho_0$ and $\rho = \rho_m = \frac{1}{2}(\rho + \rho_0)$. Therefore, we write (4.14) as

$$\frac{1}{2}v^2 = \frac{p_0}{\rho_0} \frac{1 - (p / p_0)}{(\rho / \rho_0)}.$$

The differences between the formulae stay lower than 1 % up to velocities of about 100 m/s. The Bernoulli equation with the mean value of the density stays accurate up to 1 % for velocities up to 200 m/s and accurate up to 1 % for velocities as high as the velocity of sound. So, in practice, very often, the Bernoulli equation with constant density may be used, even for a gas. The condition is that the flow velocity has to be modest with respect to the velocity of sound. This condition is certainly met in the analysis of fans in Chap. 3. The ratio of the flow velocity to the velocity of sound is called the *Mach number*. The local Mach number is $M = v/c$. Up to a Mach number around unity, the Bernoulli equation with variable density, equal to the mean value, is accurate up to 1 %. Substitution of the Saint Venant equation by the Bernoulli equation with mean density is very convenient for fundamental analysis of compressible fluid flow and is used in the chapter on axial compressors (Chap. 13). With a liquid, a similar reasoning can be set up. Compressibility may be ignored provided that the flow velocity stays low with respect to the velocity of sound. In water, the flow velocity typically amounts to the 10 m/s order as a maximum, while the velocity of sound is about 1400 m/s. So, constant density may be assumed with a very good approximation.

With high Mach number flows, the compressible relations (4.6), (4.7), (4.8) have to be used. It is then often more convenient to write these as functions of the Mach number. The energy equation (4.6) may be written, with the use of the Mach number, as

$$\frac{T_0}{T} = 1 + \frac{v^2}{2c_p T} = 1 + \frac{\gamma R}{2c_p \gamma R T} v^2 = 1 + \frac{\gamma - 1}{2} M^2.$$

So

$$\frac{p_0}{p} = \left(1 + \frac{\gamma - 1}{2} M^2 \right)^{\frac{\gamma}{\gamma - 1}} \quad \text{and} \quad \frac{\rho_0}{\rho} = \left(1 + \frac{\gamma - 1}{2} M^2 \right)^{\frac{1}{\gamma - 1}}. \quad (4.15)$$

4.4 Shape of a Nozzle

The cross-section area evolution follows from the mass equation (4.1):

$$\frac{dA}{A} = -\frac{d\rho}{\rho} - \frac{dv}{v}.$$

The density change is linked to the pressure change by isentropy (for adiabatic reversible flow):

$$\frac{d\rho}{\rho} = \frac{1}{\gamma} \frac{dp}{p}.$$

The velocity change is linked to the pressure change by the work equation (4.2):

$$-v dv = \frac{1}{\rho} dp,$$

or

$$-\frac{dv}{v} = \frac{dp}{\rho v^2} = \frac{p}{\rho v^2} \frac{dp}{p} = \frac{1}{\gamma M^2} \frac{dp}{p}. \quad (4.16)$$

The section change is
$$\frac{dA}{A} = \frac{1}{\gamma} \frac{dp}{p} \left(-1 + \frac{1}{M^2} \right) = \frac{1 - M^2}{\gamma M^2} \frac{dp}{p}. \quad (4.17)$$

Further:

$$2 \frac{dc}{c} = \frac{dp}{p} - \frac{d\rho}{\rho} = \left(1 - \frac{1}{\gamma} \right) \frac{dp}{p},$$

and

$$\frac{dM}{M} = \frac{dv}{v} - \frac{dc}{c} = - \left(\frac{1}{\gamma M^2} + \frac{\gamma - 1}{2\gamma} \right) \frac{dp}{p}. \quad (4.18)$$

From (4.16) it follows that an expansion ($dp < 0$) always causes a velocity increase ($dv > 0$) and that a compression ($dp > 0$) reversely causes a velocity decrease ($dv < 0$). This follows also from the Saint Venant formula (4.8). Eq. (4.18) expresses that the Mach number increases by expansion and decreases by compression. From (4.17) it follows that an expansion ($dp < 0$), within a subsonic flow ($M < 1$), requires a convergent channel ($dA < 0$), while a compression ($dp > 0$) requires a divergent channel ($dA > 0$). The opposite applies to a supersonic flow: an expansion ($dp < 0$) requires a divergent channel ($dA < 0$), a compression ($dp > 0$) requires a convergent one ($dA > 0$). These relations are shown schematically in Fig. 4.3.

We first consider the flow in a convergent channel departing from a plenum as sketched in Fig. 4.1 and repeated in Fig. 4.4 (left). There is no flow when the backpressure at the outlet equals the pressure in the plenum. Flow is started when pressure is lowered and the Mach number increases in the flow sense. When the backpressure is lowered, the Mach number level in the channel increases. However,

Fig. 4.3 Expansion and compression in subsonic and supersonic flow

	$\Delta p < 0$ $\Delta v > 0$ $\Delta M > 0$	$\Delta p > 0$ $\Delta v < 0$ $\Delta M < 0$
$M < 1$		
$M > 1$		

the Mach number cannot exceed the value 1 at any place. Assuming that this would occur somewhere, the sketch in Fig. 4.3 at the right bottom demonstrates that the Mach number would decrease immediately. So, $M=1$ can maximally be attained in the outlet section of the channel. The pressure in the outlet section, corresponding to $M=1$ is termed the *critical pressure* (p_*). The corresponding state is called *critical state*. The relevant state parameters follow from (4.15) for $M=1$, being

$$\frac{T_*}{T_0} = \frac{2}{\gamma+1} \quad , \quad \frac{\rho_*}{\rho_0} = \left(\frac{2}{\gamma+1} \right)^{\frac{1}{\gamma-1}} \quad , \quad \frac{p_*}{p_0} = \left(\frac{2}{\gamma+1} \right)^{\frac{\gamma}{\gamma-1}} . \quad (4.19)$$

For $\gamma=1.4$ the corresponding numerical values are

$$\frac{T_*}{T_0} = 0.833 \quad , \quad \frac{\rho_*}{\rho_0} = 0.634 \quad , \quad \frac{p_*}{p_0} = 0.528.$$

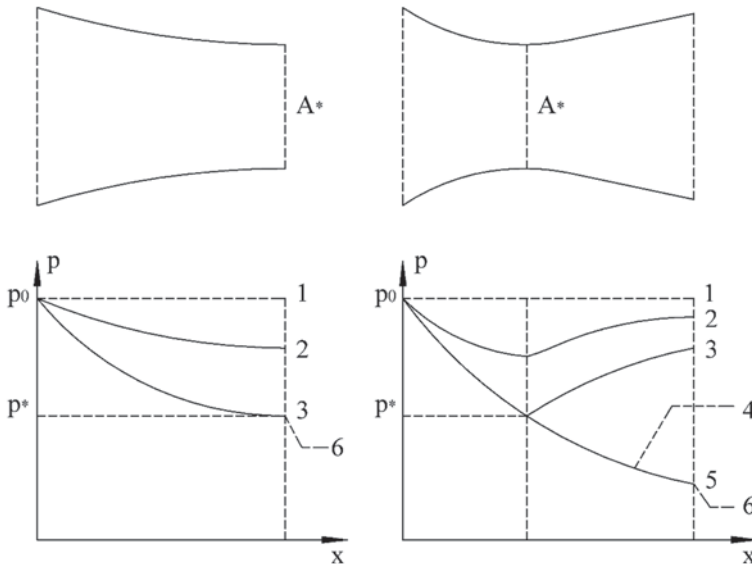


Fig. 4.4 Pressure evolution in a convergent and convergent-divergent nozzle

As long as the outlet pressure of a convergent nozzle exceeds the critical pressure ($p_3 = p_*$), the velocity in the outlet section increases as the outlet pressure decreases. With an outlet pressure equal to the critical pressure $p_3 = p_*$, a sonic state is attained in the outlet section. An additional decrease of the outlet pressure (p_6) cannot change the state within the nozzle compared to the state attained at p_3 , as the Mach number cannot exceed $M = 1$. This means that an expansion from p_3 to p_6 must occur within the space downstream of the nozzle. As the outlet pressure decreases, staying above p_3 however, the mass flow through the nozzle increases. It is blocked at the value corresponding to p_3 if pressure is lower than p_3 . Such a state is termed *choked*. The choking mass flow rate equals $\rho_* v_* A_*$.

We consider a convergent-divergent channel, as shown in Fig. 4.4 (right). From the relations demonstrated in Fig. 4.3 we learn that, with a subsonic flow within a convergent-divergent channel, the flow accelerates within the convergent part and decelerates within the divergent part. Velocity and Mach number become maximal in the throat section. The channel is said to function as a subsonic Venturi tube. Note that, if the flow enters the channel supersonically, a similar flow is possible where flow is supersonic everywhere and velocity and Mach number attain a minimum in the throat section. This is termed a supersonic Venturi tube. From the relations in Fig. 4.3 follows that subsonic flow in the convergent part may turn into supersonic flow in the diverging part. The critical state is then attained in the throat section. The backpressure p_3 in Fig. 4.4 (right) corresponds to a subsonic evolution with $M = 1$ being attained in the throat section. Pressure p_5 corresponds to a subsonic-supersonic evolution. For a backpressure between p_3 and p_5 , the corresponding pressure evolution is no longer continuous everywhere. The supersonic branch of the pressure evolution in the divergent part is followed partially or completely, followed by a discontinuous compression phenomenon (shock wave). Dependent on the pressure value p_4 , the shock wave may occur within the divergent part or downstream of the outlet section (see fluid mechanics). With backpressure p_6 lower than p_5 , there is an expansion downstream of the nozzle. In that case, the pressure evolution corresponding to p_5 is followed within the nozzle (see fluid mechanics). With a convergent-divergent nozzle, the mass flow is blocked at the choking value $\rho_* v_* A_*$, when the backpressure drops under p_3 , as the critical state is then attained in the throat. The density ρ_3 is linked to the outlet pressure by an isentropic relation. The outlet velocity v_3 is linked to the outlet pressure according to the Saint Venant formula. Expressing constant mass flow rate, this implies a non-linear equation in outlet pressure, with two solutions, namely p_3 and p_5 .

4.5 Nozzle with Initial Velocity

In the foregoing we assumed that the velocity at the nozzle inlet equals zero, with an inlet state being equal to the total state (state with subscript 0). From now on, we assume that a velocity $v_0 \neq 0$ may be present and we indicate the inlet section with the subscript 0 (state \neq total state). The above equations so must be adapted somewhat.

The energy equation is now

$$\frac{1}{2}v^2 + c_p T = \frac{1}{2}v_0^2 + c_p T_0.$$

From (4.7) follows

$$\frac{1}{2}v^2 = \frac{1}{2}v_0^2 + \frac{\gamma}{\gamma-1} \frac{p_0}{\rho_0} \left[1 - \left(\frac{p}{p_0} \right)^{\frac{\gamma-1}{\gamma}} \right].$$

So an additional term appears in the Saint Venant equation. But it is much more convenient to use the total state. We define the total state at station 0 (subscript double 0). The energy equation is then

$$\frac{1}{2}v^2 + c_p T = \frac{1}{2}v_0^2 + c_p T_0 = c_p T_{00}.$$

There is also an isentropic relation between (p, T) and (p_{00}, T_{00}) . So it follows that

$$\frac{1}{2}v^2 = \frac{\gamma}{\gamma-1} \frac{p_{00}}{\rho_{00}} \left[1 - \left(\frac{p}{p_{00}} \right)^{\frac{\gamma-1}{\gamma}} \right]. \quad (4.20)$$

4.6 Nozzle with Losses: Infinitesimal Efficiency

In case of flow with losses ($dq_{irr} > 0$), but without work or heat exchange (= adiabatic), the total temperature is still a constant of the flow. Total pressure and total density are no longer constant. For $dq_{irr} > 0$ is $T ds > 0$.

From the first equality in (4.5) it follows

$$T ds = c_p dT - RT \frac{dp}{p} \quad \text{or} \quad \frac{ds}{R} = \frac{\gamma}{\gamma-1} \frac{dT}{T} - \frac{dp}{p}.$$

From (4.7) it follows ($T_0 = cst$):

$$\frac{dp}{p} - \frac{dp_0}{p_0} = \frac{\gamma}{\gamma-1} \frac{dT}{T} \quad \text{so that} \quad \frac{ds}{R} = -\frac{dp_0}{p_0}.$$

A decrease in total pressure corresponds to an increase in entropy for adiabatic flow.

Figure 4.5 (left) sketches the h - s diagram of an expansion in a nozzle with losses between stations 0 and 1. With a quantity as p_{01} , the first subscript refers to the total state and the second to the location. Total enthalpy is constant ($h_{00} = h_{01}$) during

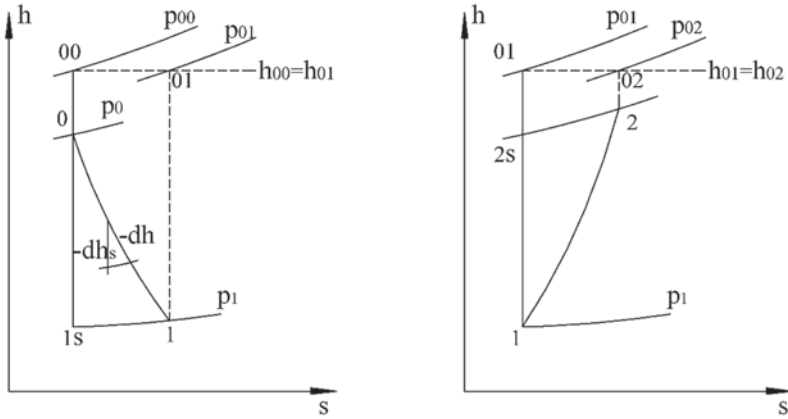


Fig. 4.5 Expansion and compression with losses: decreasing total pressure

expansion. Entropy increases due to losses, causing a decrease of the total pressure ($p_{01} < p_{00}$).

Figure 4.5 (right) shows similarly the h - s diagram of a compression with losses between station 1 and station 2. Total pressure decreases here as well, due to losses ($p_{02} < p_{01}$). We use the terms *expansion* or *compression* to indicate processes with pressure decrease or increase (here without work exchange). This terminology is typical for compressible fluids and indicates that density decreases with expansion and increases with compression.

We consider an infinitesimal part of an expansion, as sketched in the h - s diagram in Fig. 4.5 (left). We define the efficiency of this infinitesimal process (subscript ∞), using the concept of isentropic efficiency (see thermodynamics) by

$$\eta_{\infty} = \frac{-dh}{-dh_s}.$$

With $Tds = dh - \frac{1}{\rho} dp$, it follows that $dh_s = \frac{1}{\rho} dp$ and $\eta_{\infty} = \frac{\rho dh}{dp}$.

For an ideal and perfect gas:

$$\eta_{\infty} = \frac{\rho c_p dT}{dp} = \frac{p}{RT} \frac{c_p dT}{dp} = \frac{c_p}{R} \frac{dT}{dp} \frac{1}{p}.$$

Thus :

$$\eta_{\infty} \frac{dp}{p} = \frac{\gamma}{\gamma - 1} \frac{dT}{T}.$$

Assuming that $\eta_{\infty} = cst$ during the whole process, it is polytropic.

From $p \sim \rho^n$ follows $p \sim T^{\frac{n}{n-1}}$ or $\frac{dp}{p} = \frac{n}{n-1} \frac{dT}{T}$.

Thus:

$$\eta_{\infty} \frac{n}{n-1} = \frac{\gamma}{\gamma-1}. \quad (4.21)$$

From $\eta_{\infty} n(\gamma-1) = \gamma(n-1)$ it follows

$$n = \frac{\gamma}{\gamma - \eta_{\infty}(\gamma - 1)} = \frac{\gamma}{\eta_{\infty} + (1 - \eta_{\infty})\gamma}.$$

The denominator exceeds 1, since $\gamma > 1$, so follows: $n < \gamma$.

Examples: $\gamma = 1.4$, $\eta_{\infty} = 0.9$: $n = 1.346$; $\gamma = 1.3$, $\eta_{\infty} = 0.9$: $n = 1.262$.

The endpoint of the expansion (1 in Fig. 4.5, left) may be determined from the isentropic efficiency. The polytropic exponent and the *infinitesimal* or *polytropic efficiency* follow from this. The polytropic efficiency does not exactly equal the isentropic efficiency, which is slightly higher. This effect is termed *reheat effect*. We discuss it in the next section.

Taking the initial velocity into account, we obtain

$$\frac{v_0^2}{2} + h_0 = h_{00} \quad \text{and} \quad \frac{v^2}{2} + h = h_{00}.$$

Polytropic:

$$\frac{h}{h_0} = \left(\frac{p}{p_0} \right)^{\frac{n-1}{n}}. \quad (4.22)$$

Isentropic:

$$\frac{h_0}{h_{00}} = \left(\frac{p_0}{p_{00}} \right)^{\frac{\gamma-1}{\gamma}}. \quad (4.23)$$

So (4.22) x (4.23) gives

$$\frac{h}{h_{00}} = \left(\frac{p_0}{p_{00}} \right)^{\frac{\gamma-1}{\gamma}} \left(\frac{p}{p_{00}} \right)^{\frac{n-1}{n}} \left(\frac{p_{00}}{p_0} \right)^{\frac{n-1}{n}} = \left[\left(\frac{p_0}{p_{00}} \right)^{\frac{\gamma-1}{\gamma} - \frac{n-1}{n}} \right] \left(\frac{p}{p_{00}} \right)^{\frac{n-1}{n}} = C \left(\frac{p}{p_{00}} \right)^{\frac{n-1}{n}},$$

and

$$h_{00} = c_p T_{00} = \frac{c_p}{R} R T_{00} = \frac{\gamma}{\gamma-1} \frac{p_{00}}{\rho_{00}}.$$

The factor C is very close to 1.

$$C = \left(\frac{h_0}{h_{00}} \right)^{1 - \left(\frac{n-1}{n} \right) / \left(\frac{\gamma-1}{\gamma} \right)} = \left(\frac{h_0}{h_{00}} \right)^{1 - \eta_{\infty}} = \left(\frac{T_0}{T_{00}} \right)^{1 - \eta_{\infty}} \quad \text{and} \quad \frac{T_{00}}{T_0} = 1 + \frac{\gamma-1}{2} M_0^2.$$

Examples ($\eta_\infty = 0.9$): $\gamma = 1.4$; $M_0 = 0.3$: $C = 0.998$; $M_0 = 0.5$: $C = 0.995$,
 $\gamma = 1.3$; $M_0 = 0.3$: $C = 0.999$; $M_0 = 0.5$: $C = 0.996$.

Factor C may be substituted by 1 with a very good approximation, so that the Saint Venant formula, with a very good approximation becomes

$$\frac{v^2}{2} = \frac{\gamma}{\gamma - 1} \frac{p_{00}}{\rho_{00}} \left[1 - \left(\frac{p}{p_{00}} \right)^{\frac{n-1}{n}} \right]. \quad (4.24)$$

This approximation means considering a polytropic process between states 00 and 1. The approximation is obviously not adequate if inlet kinetic energy is large with respect to the enthalpy drop in the nozzle.

Similarly to (4.16), (4.17), (4.18), the flow evolution follows now from

$$\frac{d\rho}{\rho} = \frac{1}{n} \frac{dp}{p},$$

$$d \frac{1}{2} v^2 = -dh = \eta_\infty \left(-\frac{dp}{\rho} \right) \quad \text{or} \quad \frac{dv}{v} = \eta_\infty \left(-\frac{dp}{\rho v^2} \right) = \eta_\infty \frac{-1}{\gamma M^2} \frac{dp}{p}.$$

From this we obtain

$$\frac{dA}{A} = -\frac{d\rho}{\rho} - \frac{dv}{v} = \left(\frac{\eta_\infty}{\gamma M^2} - \frac{1}{n} \right) \frac{dp}{p},$$

$$\frac{dA}{A} = \frac{1}{n} \left(\frac{M_{th}^2}{M^2} - 1 \right) \frac{dp}{p} \quad \text{with} \quad M_{th}^2 = \eta_\infty \frac{n}{\gamma} = \frac{n-1}{\gamma-1}. \quad (4.25)$$

Further:

$$2 \frac{dc}{c} = \frac{dp}{p} - \frac{d\rho}{\rho} = \left(1 - \frac{1}{n} \right) \frac{dp}{p},$$

$$\frac{dM}{M} = \frac{dv}{v} - \frac{dc}{c} = - \left(\frac{\eta_\infty}{\gamma M^2} + \frac{n-1}{2n} \right) \frac{dp}{p}.$$

The last equation demonstrates that the Mach number change always has the opposite sign of the pressure change. With Venturi flow, the minima or maxima of pressure and Mach number are still attained at the throat, just as in a nozzle without losses. The throat Mach number M_{th} now plays the role of the critical Mach number. We must distinguish between subcritical flow ($M < M_{th}$) and supercritical

flow ($M > M_{th}$). The choking mass flow rate is $\rho_{th} v_{th} A_{th}$. Note that the throat Mach number is lower than 1 at choking.

State parameters in the throat at choking are

$$\frac{T_{th}}{T_{00}} = \frac{2}{n+1}, \quad \frac{\rho_{th}}{\rho_{00}} = \left(\frac{2}{n+1} \right)^{\frac{1}{n-1}}, \quad \frac{p_{th}}{p_{00}} = \left(\frac{2}{n+1} \right)^{\frac{n}{n-1}}.$$

These formulae substitute for formulae (4.19). The corresponding throat velocity follows with (4.25) from

$$v_{th} = c_{th} M_{th} = c_{00} \sqrt{\frac{2}{n+1}} \sqrt{\frac{n-1}{\gamma-1}}. \quad (4.26)$$

4.7 Isentropic and Polytropic Efficiencies

With isentropic expansion in a nozzle as sketched in Fig. 4.5 (left), the final velocity follows from

$$\frac{v_{Is}^2}{2} = h_{00} - h_{Is}.$$

In the expansion with losses, the final velocity is

$$\frac{v_I^2}{2} = h_{00} - h_I.$$

It is then obvious to define the isentropic efficiency of the expansion as

$$\eta_{ss} = \frac{v_I^2 / 2}{v_{Is}^2 / 2} = \frac{h_{0I} - h_I}{h_{0I} - h_{Is}}. \quad (4.27)$$

Such an *isentropic efficiency* is commonly used in thermodynamic analyses, but the concept is somewhat misleading. Strictly, efficiency is the ratio of the useful part of an energy conversion process to the total amount of energy processed. Expression (4.27) does not satisfy this strict definition as it is the generated kinetic energy compared to the kinetic energy that would be generated with a loss-free expansion process (isentropic). In other words, the results of two different processes are compared with each other.

The work equation for the nozzle is

$$dW = 0 = d \frac{1}{2} v^2 + \frac{1}{\rho} dp + dq_{irr}.$$

The $d \frac{1}{2} v^2$ term is the useful part of the energy conversion. This term may be integrated to $\frac{1}{2} v_I^2$, if the total state (00) is considered as the initial state. The pressure energy used to generate the kinetic energy is

$$-\Delta h_r = -\int_{00}^I \frac{1}{\rho} dp. \quad (4.28)$$

So, this term can only be determined if the path of the expansion process is known. A fundamental problem arises here since the internal details of a thermodynamic process are mostly unknown. Moreover, we wish to make a statement about the efficiency of a thermodynamic process, exclusively based on the initial and the final states. From the above, we learn that this actually is impossible for a process with a compressible fluid.

Both *isentropic efficiency* and *infinitesimal efficiency*, also called *polytropic efficiency*, are efficiency assessments, for which a process path has been agreed on for the calculation of (4.28). The isentropic efficiency corresponds to the path $00 \rightarrow I_s \rightarrow I$ (Fig. 4.5, left). To the $00 \rightarrow I_s$ part applies

$$dW = 0 = d \frac{1}{2} v^2 + \frac{1}{\rho} dp.$$

The energy used is $\frac{1}{2} v_{I_s}^2$. To the $I_s \rightarrow I$ part applies

$$dW = 0 = d \frac{1}{2} v^2 + \frac{1}{\rho} dp + dq_{irr}.$$

As this path is isobaric, there is no contribution to (4.28) and integration is possible with result

$$q_{irr} = \frac{1}{2} v_{I_s}^2 - \frac{1}{2} v_I^2. \quad (4.29)$$

The isentropic efficiency definition (4.27) corresponds to this interpretation. Dissipation during the process is considered as the enthalpy difference between states 1 and 1s:

$$q_{irr} = h_1 - h_{1s}.$$

With infinitesimal efficiency, the path is determined by defining the efficiency of an infinitesimal part, which is indisputably possible, and by assuming a constant infinitesimal efficiency on the total path. With the approximations introduced in the preceding section, the infinitesimal efficiency follows from expressions (4.24) and (4.21).

The generated kinetic energy (4.24) is

$$\frac{v_I^2}{2} = \frac{\gamma}{\gamma-1} \frac{p_{00}}{\rho_{00}} \left[1 - \left(\frac{p_I}{p_{00}} \right)^{\frac{n-1}{n}} \right]. \quad (4.30)$$

The generated kinetic energy following the isentropic path is similarly

$$\frac{v_{Is}^2}{2} = \frac{\gamma}{\gamma-1} \frac{p_{00}}{\rho_{00}} \left[1 - \left(\frac{p_I}{p_{00}} \right)^{\frac{\gamma-1}{\gamma}} \right]. \quad (4.31)$$

The integral (4.28) on a polytropic path with exponent n results in

$$-\Delta h_r = \frac{n}{n-1} \frac{p_{00}}{\rho_{00}} \left[1 - \left(\frac{p_I}{p_{00}} \right)^{\frac{n-1}{n}} \right]. \quad (4.32)$$

For $n < \gamma$, it is verified that

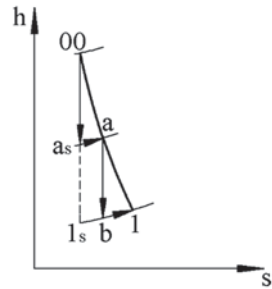
$$\frac{v_I^2}{2} < \frac{v_{Is}^2}{2} < |-\Delta h_r|.$$

So the isentropic efficiency (ratio of $\frac{1}{2}v_I^2$ to $\frac{1}{2}v_{Is}^2$) exceeds the polytropic or infinitesimal efficiency (ratio of $\frac{1}{2}v_I^2$ to $|-\Delta h_r|$). The reason why both efficiency definitions differ becomes obvious by considering a process consisting of two isentropic and two isobaric paths, as shown in Fig. 4.6.

The efficiency for the $00 \rightarrow a_s \rightarrow a \rightarrow b \rightarrow I$ path is

$$\eta = \frac{h_{00} - h_I}{(h_{00} - h_{as}) + (h_a - h_b)}.$$

Fig. 4.6 Approximation of an expansion by isentropic and isobaric paths



The slope of an isobar in a h - s diagram is $(\frac{dh}{ds})_p = T$. So, the isobars diverge in the sense that the isentropic enthalpy difference between two isobars increases with increasing entropy. So it follows: $h_a - h_b > h_{as} - h_{ls}$. This inequality expresses that a part of the loss incurred on the $a_s \rightarrow a$ path, causing heating of the gas, is recovered during the following expansion, as the isentropic enthalpy drop increases. This effect is termed *reheat effect*, meaning heating due to internal loss.

Further breakdown of the $00 \rightarrow I$ path in isentropic and isobaric parts results in a polytropic representation as a limit case. This demonstrates that, with the polytropic representation, the energy used to generate the kinetic energy (4.28) is larger than with the isentropic-isobaric process. We also understand that losses intervene in two ways with the real process: the useful result $\frac{1}{2}v_I^2$ is smaller than with the isentropic process $\frac{1}{2}v_{Is}^2$ and the energy converted to achieve this result $|\Delta h_r|$ is larger than with the isentropic process $\frac{1}{2}v_{Is}^2$.

The infinitesimal representation describes the real process better than the isentropic-isobaric representation. Both representations constitute models however, as a correct assessment of efficiency is impossible without full details of the process path. Infinitesimal efficiency has the advantage of an unchanged value when two processes are set in series, as demonstrated in Fig. 4.6. Connecting two processes in series changes the isentropic efficiency. Figure 4.6 demonstrates that the isentropic efficiency of a series of two expansions with the same isentropic efficiency generates a result with better isentropic efficiency.

The different behaviour of isentropic efficiency and polytropic efficiency also applies to expansions and compressions with work (see Chap. 11). Because of the preservation of efficiency with connection in series, use of polytropic efficiency is advisable with cycle studies. Both definitions may be used when assessing a single machine component. Isentropic efficiency is the most visual, as it implies a clear representation of losses in the h - s diagram. We therefore apply isentropic efficiency with the fundamental study of turbomachine components, as with the study of steam turbines in Chap. 6. The Saint Venant formula (4.24) is used to calculate expansion processes within steam turbine components and infinitesimal efficiency indirectly intervenes when defining the polytropic exponent.

For completeness, we mention that with a constant density fluid, there is no difference between isentropic and polytropic efficiencies. The definition of infinitesimal efficiency is still

$$\eta_\infty = \frac{-dh}{-dh_s} \quad \text{with} \quad dq_{irr} = Tds = dh - \frac{1}{\rho} dp,$$

so that

$$dh_s = \frac{1}{\rho} dp \quad \text{and} \quad \eta_\infty = \frac{-\frac{1}{\rho} dp - dq_{irr}}{-\frac{1}{\rho} dp}.$$

Further:

$$\Delta h_s = \frac{1}{\rho} \Delta p \quad \text{and} \quad q_{irr} = \Delta h - \frac{1}{\rho} \Delta p,$$

so that

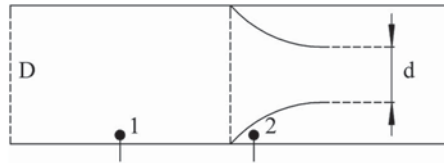
$$\eta_s = \frac{-\frac{1}{\rho}\Delta p - q_{irr}}{-\frac{1}{\rho}\Delta p}.$$

For ρ constant and η_∞ constant, the infinitesimal efficiency expression can be integrated leading to the same result as the isentropic efficiency expression.

4.8 Exercises

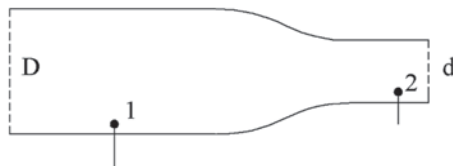
4.8.1. Air flows through a pipe with a built-in nozzle. $D = 0.40$ m, $d = 0.20$ m. Supply conditions are $p_1 = 150$ kPa, $T_1 = 300$ K. $\Delta p = p_1 - p_2 = 50$ kPa. Determine the mass flow rate, ignoring the losses within the nozzle (they are extremely low in practice) and assuming that no contraction occurs within the jet leaving the nozzle (contraction is low in practice). What is the flow rate error if the calculation is made assuming constant density determined from the upstream conditions? What is the flow rate error if the calculation is made assuming constant density determined from the average pressure in points 1 and 2 and from the temperature of the incoming flow? The calculations require derivation of mass flow rate formulae for constant density and for ideal gas (see also Exercise 4.8.5).

A: 10.71 kg/s; +26.5%; +15.5%.



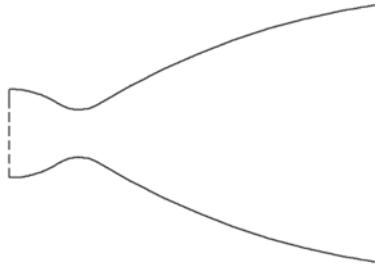
4.8.2. Air flows through a convergent pipe with diameter varying from $D = 0.40$ m to $d = 0.20$ m. Supply conditions are $p_1 = 150$ kPa, $T_1 = 300$ K. The flow ends in the atmosphere with $p_a = 100$ kPa ($T_a = 288$ K). Calculate the mass flow rate (same question as in Exercise 4.8.1, losses and contraction to be ignored). Verify that the flow state is subcritical. What is the mass flow rate at $p_1 = 200$ kPa (slightly supercritical)? What is the mass flow rate at $p_1 = 500$ kPa (strongly supercritical)? What is the mass flow rate for $\eta_\infty = 0.95$ in that last case?

A: 10.71 kg/s ($M_{th} = 0.80$); 14.85 kg/s ($M_{th} = 1$, $p_{th} = 107.26$ kPa); 37.13 kg/s (2.5 x foregoing); 35.94 kg/s ($M_{th} = 0.965$, $p_{th} = 270.45$ kPa).



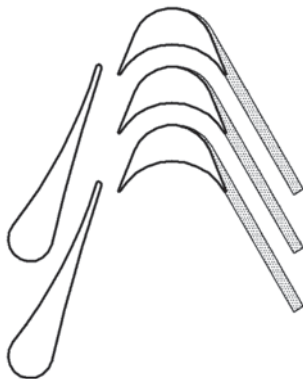
4.8.3. The figure is a sketch of a rocket nozzle. The convergent and the divergent parts are designed in such a way that the outlet flow is uniform. In practice, this is attained for absence of shockwaves in the divergent part. The section ratio outlet to throat is 25. Determine the outlet Mach number and the pressure ratio for the nozzle with isentropic air flow ($\gamma = 1.4$). An iterative procedure is necessary. Remark that the pressure ratio is very small.

A: $p/p_{00} \approx 0.00189$, $M = 5$.



4.8.4. The figure shows the section at the mean radius of the stator and the rotor of an axial turbine with zero degree of reaction. Nozzle outlet flow is supersonic. The rotor inlet flow is near to sonic ($M \sim 1$). Turbines of this type are applied to drive fuel pumps in rocket engines. The fluid is gaseous hydrogen, obtained by heating liquid hydrogen by a coil that is wound around the divergent part of the rocket nozzle (see Exercise 4.8.3). The shaded zones indicate separated flow in the rotor at the suction side trailing edge. Due to flow separation, rotor efficiency is rather low (for a definition of rotor efficiency see Chap. 6). For turbines with a very large work output, it is impossible however to attain an advantageous rotor efficiency. A low efficiency is no problem as the energy by an ideal expansion of the hydrogen is much larger than the energy required for driving the pumps. There is no separation in the turbine nozzles so that these may be calculated as lossless with a good approximation. The nozzle outlet angle is 72° . Assume a test with air ($\gamma = 1.40$) with pressure ratio $p_1/p_{00} = 0.20$. Verify the correctness of the nozzle design by calculating the tangential force coefficient of Zweifel and by determining the surface ratio of the divergent part of the nozzles. On the figure, we read: $\sigma_a \approx 0.8$; $A_l/A_{th} \approx 1.60$.

A: $C_{Fu} \approx 0.735$; thus enough solidity. The area ratio corresponding to the pressure ratio is $A_l/A_{th} \approx 1.35$; thus backpressure in the test is somewhat too high.



4.8.5. We once more study the nozzle of Exercise 4.8.1. The results obtained with the constant density formulae differ strongly from those for an ideal gas. We analyse the origin of these differences.

The relations for constant density are:

Bernoulli :
$$\frac{p_1}{\rho} + \frac{v_1^2}{2} = \frac{p_2}{\rho} + \frac{v_2^2}{2}.$$

Mass:
$$v_1 D^2 = v_2 d^2 \text{ or } v_1 = v_2 \beta^2.$$

Thus
$$\frac{p_1 - p_2}{\rho} = \frac{v_2^2}{2} (1 - \beta^4) \text{ and } \dot{m} = \rho A_{th} \frac{l}{\sqrt{1 - \beta^4}} \sqrt{\frac{2 \Delta p}{\rho}}. \quad (4.33)$$

The relations for ideal gas are:

Conservation of energy :
$$C_p T_1 + \frac{1}{2} v_1^2 = C_p T_2 + \frac{1}{2} v_2^2$$

Thus
$$\frac{v_2^2}{2} - \frac{v_1^2}{2} = C_p T_1 \left(1 - \frac{T_2}{T_1} \right)$$

Isentropy :
$$\frac{T_2}{T_1} = \left(\frac{p_2}{p_1} \right)^{\frac{\gamma-1}{\gamma}} \text{ and } \frac{\rho_2}{\rho_1} = \left(\frac{p_2}{p_1} \right)^{\frac{1}{\gamma}}. \quad (4.34)$$

Mass:
$$\rho_1 v_1 = \rho_2 v_2 \beta^2.$$

So
$$\frac{v_2^2}{2} \left[1 - \beta^4 (\rho_2/\rho_1)^2 \right] = \frac{\gamma}{\gamma-1} \frac{p_1}{\rho_1} \left[1 - \left(\frac{p_2}{p_1} \right)^{\frac{\gamma-1}{\gamma}} \right],$$

and
$$\dot{m} = \rho_2 A_{th} \frac{I}{\sqrt{1 - \beta^4 (\rho_2/\rho_1)^2}} \sqrt{2 \frac{\gamma}{\gamma-1} \frac{p_1}{\rho_1} \left[1 - \left(\frac{p_2}{p_1} \right)^{\frac{\gamma-1}{\gamma}} \right]}. \quad (4.35)$$

The expression (4.35) can be brought into form (4.33) with very good approximation as

$$\dot{m} = \rho_2 A_{th} \frac{I}{\sqrt{1 - \beta^4 (\rho_2/\rho_1)^2}} \sqrt{\frac{2 \Delta p}{\rho_m}}. \quad (4.36)$$

With (4.36), the results become very good for the data of Exercise 4.8.1. Only the last terms in (4.35) and (4.36) differ (velocity by the formulae of De Saint Venant and Bernoulli) with values 256.78 m/s (exact) and 256.24 m/s (approximate).

References

- Fox RW, Pritchard PJ, McDonald AT (2010) Introduction to fluid mechanics, 7th edn. Wiley, ISBN 978-0-470-23450-1
 Imrie BW (1973) Compressible fluid flow. Butterworth & Co, ISBN 0-408-70434-9

Chapter 5

Performance Measurement

Abstract Experimental performance analysis of turbomachines requires pressure measurement, temperature measurement and flow rate measurement at the flow side and torque and rotational speed measurement at the shaft side. The present chapter deals with the principles of the most fundamental measurement techniques for these variables and describes three laboratory set-ups for performance measurement: a hydraulic turbine, a fan and a pump. Measurement results are discussed.

5.1 Pressure Measurement

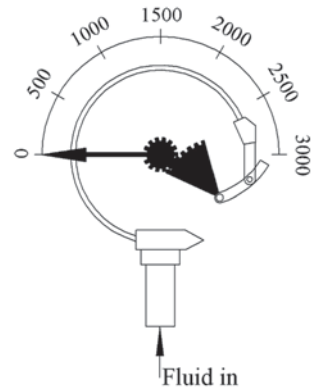
5.1.1 *The Metal Manometer*

Figure 5.1 shows a sketch. A hollow curved tube with an elliptical section is connected with the fluid (liquid or gas). The tube bends outwards due to positive pressure difference with respect to the atmospheric pressure and inwards due to negative pressure difference. The displacement of the end point of the tube is transferred to a measuring needle. The linkage allows zero and scale adjustment. The measured pressure is called *gauge pressure*, which means that it is relative to the atmospheric pressure: above (+) or below (−). Absolute pressure is determined by adding the atmospheric pressure read from a barometer. Metal manometers are not suitable for values changing quickly in time.

5.1.2 *The Pressure Transducer*

Figure 5.2 shows a sketch. Two diaphragms bend by the pressure difference with the atmosphere. In the example, the bending is detected by a strain gauge with variable electrical resistance, mounted in a Wheatstone bridge. The voltage output of the bridge is a measure of the pressure. The electronic circuit of the transducer incorporates a compensator for the temperature-related resistance change of the strain gauge. Similar pressure transducers exist with diaphragm movement detected by

Fig. 5.1 The metal manometer



the change of an electrical capacitor (1 capacitor plate moves along with the diaphragm) or by generating a piezoelectric voltage (voltage within a crystal due to strain). Capacitive measuring is mainly suitable for low pressure, piezoelectric for high pressure. There are transducers for very various pressure ranges and very various frequency responses. The voltage signal is read into a computer system through an electronic circuit board.

5.1.3 The Digital Manometer

A digital manometer functions according to the same principles as a pressure transducer. Reading out is done from a digital display. There are handheld devices with built-in transducer and display. With a handheld device, connections must be made between the device and the pressure measurement point. This is only workable for pressure measuring in air.

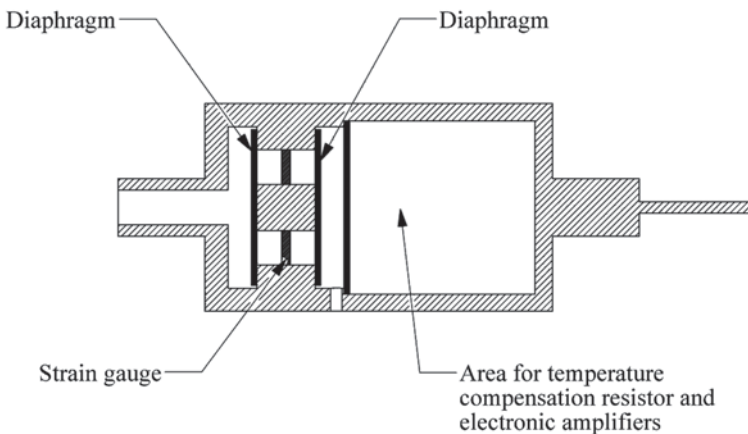


Fig. 5.2 The pressure transducer

5.1.4 Calibration of Pressure Meters

Laboratory calibration of meters of pressure above atmospheric pressure is generally performed with a device in which calibrated weights are positioned onto a piston in an oil-containing cylinder (so-called dead weight tester). Such a device is not suitable for small positive values and it cannot generate pressure below atmospheric pressure. U-shaped liquid columns are used for low positive or for negative pressures. Pressure above or below atmospheric pressure is generated in a container by means of a compressor. The pressure is derived from the height difference between the two levels in the liquid column. There are devices allowing a very precise reading of the height difference. Mostly water is used as a liquid, but also lower-density liquids. For negative or positive pressure ranges until 1 bar, a mercury column is used, as in a barometer. In a laboratory, liquid columns are used directly as well for pressure measurement in air. In an industrial environment, calibration is mostly performed by comparing with calibration manometers and with a device for the generation of positive or negative pressure. These calibration manometers are regularly checked in a calibration laboratory.

5.2 Temperature Measurement

5.2.1 The Glass Thermometer

The principle is the expansion of a liquid, mostly mercury or an alcohol, within a spherical reservoir, by the influence of temperature. Glass thermometers do not require periodical calibration, which is an advantage. Once the scale is determined, it is definitive. The use of glass thermometers is awkward because of their vulnerability. There are types with metal protective tubes.

5.2.2 The Temperature Transducer

A temperature probe is mostly based on the temperature-dependence of an electric resistance or by generating a voltage by means of a thermocouple. The variable resistance is part of a Wheatstone bridge, together with three fixed resistances. A thermocouple detects a temperature difference, typically with respect to the atmospheric temperature. This last one is then determined by a resistance measuring device. The electric signal is read into a computer system. The difference between both types is the more limited range of a resistance temperature transducer compared to that of thermocouple temperature transducer, but with a higher accuracy.

5.2.3 The Digital Thermometer

The measuring principle is the same as with the transducer, but the device features a digital display. The display may be a separate handheld device or may be mounted directly to the probe.

5.3 Flow Rate Measurement

5.3.1 Reservoir

A direct method for measuring volume flow rate is the filling of a reservoir calibrated in volume units or placed onto a balance.

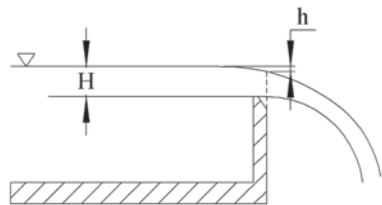
5.3.2 Flow Over a Weir

When a liquid flows over a weir, flow rate is determined by the height of the liquid surface compared to the deepest point of the weir, as is sketched in Fig. 5.3. Rectangular and triangular weirs are applied. Formulae for volume flow rate are

$$Q = \left(\frac{2}{3}\right) C_R w \sqrt{2g(H + \Delta)^3} \quad \text{and} \quad Q = \left(\frac{8}{15}\right) C_T \tan \alpha \sqrt{2g(H + \Delta)^5},$$

where w is the width of the rectangular weir, α half the angle of opening of the triangular weir and H the height of the liquid level. Coefficients C_R , C_T and Δ are determined according to standards.

Fig. 5.3 Flow over a weir



5.3.3 Pressure Drop Devices

Figure 5.4 shows a nozzle mounted within a cylindrical duct or at a duct inlet. Flow accelerates in the nozzle, causing pressure to drop. The pressure difference over the nozzle is a measure of the flow rate.

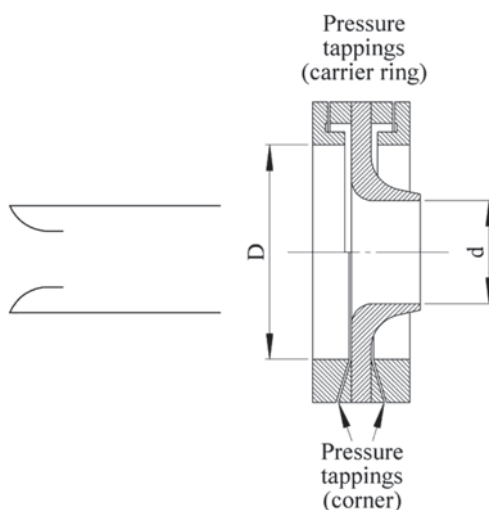
The flow rate is expressed by (4.36) (Chap. 4, Exercise 4.8.5):

$$\dot{m} = C_Q \rho_2 A_{th} \frac{1}{\sqrt{1 - \beta^4 (\rho_2 / \rho_1)^2}} \sqrt{\frac{4 \Delta p}{\rho_1 + \rho_2}}. \quad (5.1)$$

For a constant density fluid $\rho_1 = \rho_2 = \rho_m$. For a compressible fluid, the formula is accurate provided the Mach number in the throat stays moderate (say, up to Mach number about 0.75). The parameter β is the ratio of the throat diameter to tube diameter. C_Q is a coefficient taking into account the obstruction by boundary layers (see Sect. 5.7.1). For a compressible fluid, determination of ρ_1 requires the measurement of p_1 and T_1 . Velocity determination further requires the measurement of p_2 . Density ρ_2 is not determined by measuring p_2 and T_2 , but by the isentropic relation between density ratio and pressure ratio: $\rho_2 = \rho_1 (p_2 / p_1)^{1/\gamma}$.

An orifice plate (flat plate with a cylindrical orifice) or a Venturi (convergent-divergent channel) may be used instead of a nozzle. Formulae for flow rate determination are similar. For a nozzle at the duct inlet (Fig. 5.4, left), formulae are identical but with $\beta=0$ and p_1 equal to atmospheric pressure. All formulae have a flow rate coefficient C_Q , which accounts for the obstruction due to the boundary layers. Expressions for C_Q are given for standardised designs. This coefficient is

Fig. 5.4 Flow rate measurement with a nozzle; left: at the inlet; right: mounted within a duct



always somewhat lower than unity and depends on the Reynolds number of the approaching flow.

5.3.4 Industrial Mass Flow Rate Meters

Industry mostly applies mass flow rate meters with a voltage signal output appropriate to be read into a computer or on a display. Several physical principles may be applied. Turbine meters, acoustic meters, magnetic meters and vortex meters are commonly used. With a turbine meter, a turbine wheel is mounted into a casing. The rotational speed is a measure for the flow rate. Rotational speed mostly is read out magnetically (see Sects. 5.5.1 and 5.5.2). A Doppler-acoustic meter is possible with a fluid containing solid particles or bubbles larger than about 30 μm . An acoustic pulse is sent out by a piezoelectric transducer. The pulse is reflected by the particles or the bubbles and detected by a second piezoelectric transducer. The Doppler-effect modifies the frequency of the acoustic signal. Magnetic flow rate measurement is possible if the fluid is electro-conductive. The voltage generated within a conductive fluid flowing perpendicularly through a magnetic field is proportional to the flow velocity. An object is positioned in the flow with a vortex meter. Flow rate determination is based on the frequency of the vortices shed.

5.3.5 Positioning of Flow Rate Meters in Ducts

In principle, the approaching flow to a pressure drop device or a flow rate meter in a duct must be fully developed. This means a velocity profile that does not change in the flow direction. This is extremely difficult to realise in practice. Standards require approach lengths of 20–30 times the duct diameter. The approach length depends on the Reynolds number and the kind of upstream flow perturbations (e.g. number of bends passed). Smaller lengths apply when flow regulating devices, called flow conditioners, are placed upstream. These are plate systems that parallelise the flow and generate shear zones with intense turbulent mixing. Even with conditioners, the required approach lengths remain large. Flow rate measurement by an inlet nozzle, as in Fig. 5.4 (left), may be more convenient. Suction must be performed from a sufficiently large space, so that $\beta=0$ applies.

5.4 Torque Measurement

5.4.1 *Swinging Suspended Motor or Brake*

With a driven machine the driving motor may be suspended in bearings, allowing it to swing. The driving motor torque on the machine then generates a reaction torque equal to the driving torque, apart from the bearing resistance. The reaction torque is balanced with a lever arm and a force. Force determination may be performed by a balance or a force transducer. A force transducer functions like a pressure transducer. With a turbine, a brake is driven and similarly the reaction torque on the brake is measured. The brake principle may take various forms. Most obvious is an electrical generator with power supply to the grid or with dissipation by resistors. Eddy current brakes are frequently used as well. Power is then dissipated by Foucault currents and the dissipation heat is removed by cooling. Older braking systems applied friction on a drum (Prony brake) or a water ring impacting a blade system (Froude brake). These older systems are less precise and difficult to adjust.

5.4.2 *Calibrated Motor*

Swinging motor suspension cannot be applied on a driven turbomachine with integrated driving motor, as often used with smaller fans and pumps. A solution may consist in first taking off the electric motor and putting it on a test rig with a swinging suspended brake, as described above. The characteristics of the motor, together with its controller may then be determined. A frequency-controlled asynchronous motor is often used. For set frequency, torque and rotational speed are determined as a function of output power. An example is detailed in Sect. 5.7.

5.4.3 *The Torque Transducer*

This device is mounted between the shafts of the driving and the driven machine. An internal bar gets twisted by the torque transferred. Angle torsion is read out. The problem with a torque transducer is the necessity to measure the torsion in a rotating system. There are systems with strain gauges, so resistive determination, with capacitive determination and with inductive determination. The latter features four cored coils. Due to torsion, cores get deeper in two coils and less deep in the other two. The coils are mounted in a Wheatstone bridge. The set-up is similar for resistive and capacitive determination. The power supply of the bridge may be by AC, transferred at high frequency by a rotary transformer. The generated voltage is sent outside by a second rotary transformer. This type has the advantage of being contactless. Slip ring systems exist as well. With those, power supply and read-out may be by DC for resistive determination

5.5 Rotational Speed Measurement

5.5.1 *Pulse Counters*

Instruments for measuring rotational speed are called tachometers. Most function by generating and counting electric pulses. Pulse generating methods are mostly magnetic or optical. With a magnetic pulse tachometer, there is a toothed wheel in front of a magnetic transducer, which is a coil around a permanent magnet. Inductance is different depending on whether a tooth or a void is in front of the magnetic transducer. An optical pulse tachometer is a disc with holes on the rotating shaft. The light of a lamp reaches a photocell. The resistance of the photocell depends on the incidence or the absence of light. The counter transfers its result to a digital display. Handheld devices normally function with a laser beam. A reflective plate is fixed onto the shaft. The reflected beam reaches a photocell.

5.5.2 *The Speed Transducer*

The term speed transducer mostly refers to an instrument with a magnetic transducer in front of a toothed wheel. Within the coil of the magnetic transducer an alternating voltage is generated with a frequency and amplitude proportional to the rotational speed. With a digital device, pulse counting supplies the read-out to a display. With an analogous device, the variable voltage drives a needle.

5.5.3 *Electric Tachometer*

The term electric tachometer mostly refers to a DC generator producing a voltage proportional to the rotational speed.

5.6 Laboratory Test of a Pelton Turbine

5.6.1 *Test Rig*

The Pelton turbine has a rotor with 110 mm mean diameter, provided with 16 buckets. The injector has a 20 mm outlet orifice and a manually operated regulating needle. The rotor is made of accurately cast bronze and fixed on a stainless steel shaft, running in covered ball bearings. The shaft power is about 300 W at 1600 rpm, with a 21 m head and a 2.15 l/s flow rate. Specific speed $Q_s = 0.15$ (see Chap. 7 for definition of specific speed). The water is supplied by a single-stage centrifugal pump.

The maximum head and the flow rate of the pump are 24 m and 4 l/s at 2900 rpm. Pump pressure, and so turbine inlet pressure, is controlled by means of a manual valve. Flow rate is measured by a triangular weir between two reservoirs. Waves on the water surfaces are damped with bulkheads. The turbine power is adjusted with an eddy-current brake with a swinging suspended stator, kept in balance by a lever arm. The bending of the arm is measured with strain gauges in a Wheatstone bridge and is the measure for the torque. The eddy current brake excitation is set for torque adjustment.

5.6.2 Measurements

The hydraulic input power of the turbine follows from

- The mass flow rate read out on the gauge of the highest reservoir, calibrated in flow rate units (Q in l/s).
- The static pressure within the supply duct to the injector, just upstream of the turbine, read out on a metal manometer (H in m water column).
- The dynamic pressure calculated from the velocity within the supply duct to the injector, the duct diameter being 40.0 mm.

The manometric head in m water column is $H_m = H + v^2/2g$ and the hydraulic power available is $P = \rho Q g H_m$ (the height difference between the nozzle exit and the tail-water is not taken into account).

The mechanical output power of the turbine follows from

- The rotational speed measured with a magnetic tachometer. A wheel with six teeth rotates in front of a magnetic transducer and induces a voltage proportional to the rotational speed. Voltage is read out analogously from a dial with pointer. Read the 5000 rpm scale.
- The brake torque read out from the voltmeter in the Wheatstone bridge with strain gauges connected to the brake arm. Read-out is in mKp. This is the old DIN-notation for mkgf. The torque in Nm is found by multiplying by 9.81. This factor may be rounded to 10. Setting the scale to 0.4 mKp and reading it as if it were 4 Nm is a practical method.

5.6.3 Measurement Procedure

- Set the flow rate by opening the regulating needle from the fully closed position: 2, 4, 6, 8 or 10 rotations (4, 6 or 8 rotations yield the best efficiency).
- Vary the rotational speed of the turbine by adjusting the eddy current brake excitation from idle to maximum attainable load. Select eight operating points

Table 5.1 Test results for the Pelton turbine

Operating point	1	2	3	4	5	6	7	8
Rotational speed (rpm)	1900	1700	1500	1300	1100	900	700	500
Torque (Nm)	0.05	0.50	0.95	1.40	1.80	2.05	2.25	2.40

approximately evenly distributed over the rotational speed range from minimum to maximum. Read at each operating point: rotational speed, torque, flow rate (constant), head (constant).

5.6.4 Calculations

- Plot torque T (Nm) as a function of rotational speed n (rpm).
- Determine for each operating point: efficiency and speed ratio (see Chaps. 6 and 9 for definition of speed ratio). Plot efficiency as a function of speed ratio.
- Determine the speed ratio at maximum efficiency (interpolate, if necessary). Compare to the theoretical value (Chap. 9). Explain the small difference.

5.6.5 Measurement Example

- Injector needle position: 8 revolutions open.
- Static injector pressure: 11.2 m water column; Flow rate: 2.5 l/s (Table 5.1).

Answer: optimum efficiency is 0.74 at speed ratio 0.45.

5.7 Laboratory Test of a Centrifugal Fan

5.7.1 Test Rig

The design data of the fan are: $Q=0.8 \text{ m}^3/\text{s}$, $\Delta p_0=3500 \text{ Pa}$, $n=2900 \text{ rpm}$. Dimensions: $d_1=200 \text{ mm}$, $b_1=80 \text{ mm}$, $d_2=450 \text{ mm}$, $b_2=60 \text{ mm}$; 16 straight blades, $\beta_1=-57^\circ$, $\beta_2=-22^\circ$ to meridional plane. Volute: width $b_3=150 \text{ mm}$, outlet height $h_4=170 \text{ mm}$ ($b_4=150 \text{ mm}$). A description of the fan is given in Chap. 7, Sect. 7.6.

The fan is driven by a frequency-controlled asynchronous motor. The chosen frequency sets the rotational speed at zero-load. The motor slips when loaded. So the

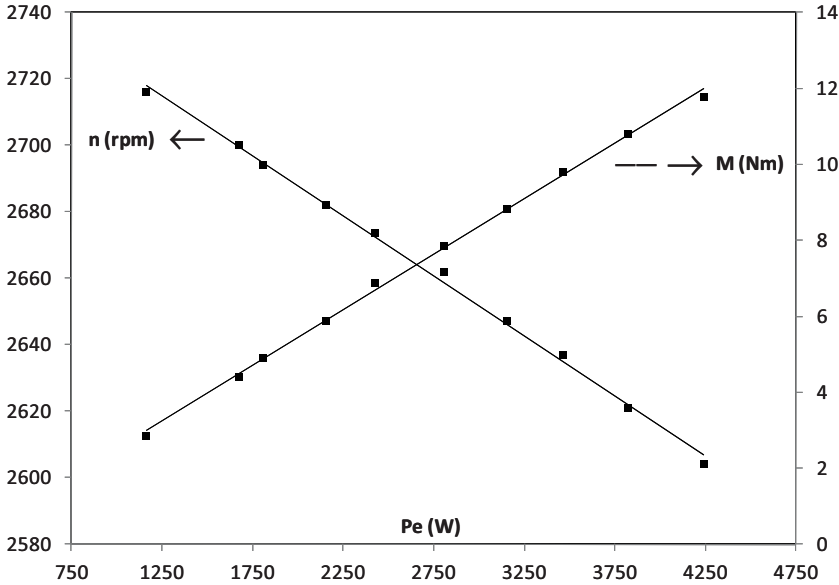


Fig. 5.5 Torque and rotational speed as a function of electric power for zero-load rotational speed 2750 rpm

characteristic is not measured at constant rotational speed. A prior mechanical measurement of the motor was done on a brake test rig. The torque and the rotational speed were measured at variable load together with the power supplied to the controller of the motor. The curves for zero-load rotational speed 2750 rpm are shown as an example in Fig. 5.5. These curves are linear with a very good approximation. With these curves so follows the torque on the shaft and the rotational speed from the measured electrical power during the test of the fan. A scale factor has to be applied to the meter for the electric power. The factor depends on the chosen voltage range (380 V) and the current range (10 A), the factor being 80 here. Characteristics for torque and rotational speed as a function of input power are given in Table 5.2 by two data couples each time.

Table 5.2 Torque and rotational speed as a function of power; chosen frequency (zero-load rpm); data couples: torque (Nm)—power (Watt) and speed (rpm)—power (Watt)

Zero-load (rpm)	Torque (Nm), power (Watt)		Speed (rpm), power (Watt)	
2000	(0, 65)	(12, 3100)	(2000, 300)	(1880, 2640)
2400	(0, 120)	(12, 3700)	(2400, 360)	(2280, 3280)
2750	(0, 165)	(12, 4225)	(2750, 400)	(2630, 3620)
3000	(0, 200)	(12, 4600)	(3000, 430)	(2880, 3900)
3200	(0, 225)	(12, 4900)	(3200, 500)	(3080, 4400)

Fig. 5.6 Fan set-up; measurement of energy rise and flow rate

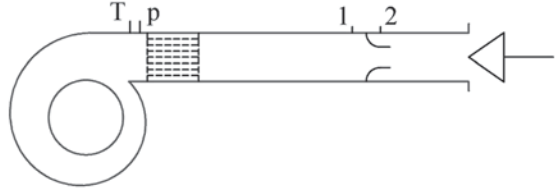


Figure 5.6 sketches the set-up for the measurement of the energy rise in the flow and the flow rate. The energy rise (mechanical energy rise) is determined from the pressure and temperature measurements p and T at the fan outlet and the pressure and temperature at inlet p_a and T_a , being atmospheric conditions. Atmospheric pressure is read on the laboratory barometer (kPa). Atmospheric temperature is read on the glass thermometer hanging next to the barometer ($^{\circ}\text{C}$). Static outlet pressure p is read with a handheld digital manometer. The measured pressure is relative to the atmospheric pressure. The laboratory has devices with Pa or kPa read-out and with mBar read-out (1 mBar = 100 Pa). Temperature T at the fan outlet is read with a resistive digital temperature meter with a probe-mounted display ($^{\circ}\text{C}$). Flow rate measurement is done with a nozzle of a standardised design according to ISO-5167, type ISA 1932 with $D = 182.9$ mm, $d = 114$ mm, $\beta = d/D = 0.6233$. Mass flow rate follows from (5.1). In order to determine the densities ρ_1 and ρ_2 , the pressures p_1 and p_2 and the temperature T_1 must be measured. Pressures p_1 and p_2 are measured with the same handheld digital manometer as used for p . We take the temperature at the fan outlet as an approximation for T_1 . This approximation is appropriate as the outlet temperature of the fan just exceeds atmospheric temperature a little and the temperature drop within the pipe between the fan and the measuring nozzle is small.

The mass flow rate formula (5.1) contains a discharge coefficient, taking into account the boundary layer obstruction in the nozzle throat:

$$C_Q = 0.9900 - 0.2262\beta^{4.1} - (0.00175\beta^2 - 0.0033\beta^{4.15}) \left(\frac{10^6}{Re_D} \right)^{1.15}.$$

The Reynolds number is $Re_D = (v_1 D \rho_1) / \mu_1 = 4\dot{m} / (\pi D \mu_1)$. Air viscosity is $\mu_1 = (17.177 + 0.0510 T_1) \cdot 10^{-6}$ Pas, with T_1 the temperature in $^{\circ}\text{C}$ ($-10^{\circ}\text{C} < T_1 < 30^{\circ}\text{C}$). The Reynolds number depends on the mass flow rate. As a consequence, determination of C_Q requires iteration. Start with $Re_D = 5 \cdot 10^5$ and one iteration is sufficient as the dependence of C_Q on Re_D is very weak.

5.7.2 *Measurements*

The input power of the fan follows from

- The torque and the rotational speed on the fan shaft determined with the characteristics of the driving motor with its controller by reading the electric input power.

The output power of the fan follows from

- The mass flow rate determined with the measuring nozzle.
- The energy rise determined from the pressure and temperature at the fan inlet and outlet. The mechanical energy rise is determined with the Bernoulli formula for density equal to the average value between inlet and outlet. The kinetic energy at the inlet is zero (atmospheric plenum). The kinetic energy at the outlet follows from the velocity at the outlet. Velocity is calculated from the mass flow rate and the density at the fan outlet, determined from p and T .

5.7.3 *Measurement Procedure*

- Select a rotational speed of 2000, 2400, 2750, 3000 or 3200 (idling rotational speed) on the frequency controller of the driving motor. Read atmospheric pressure and atmospheric temperature.
- Turn the flow control cone at the end of the measuring tube completely open. The flow rate through the fan and the electric input power are then maximal. The frequency controller has a power limiter. At an idling rotational speed of 3000 and 3200 rpm, the power limiter switches the frequency controller off with a completely open cone. Open the cone at these rotational speeds that much, that the power limiter just does not intervene. The power limiter does not intervene at other rotational speeds. Read the maximum power input. Close then the flow control cone completely, however without forcing it, and read the corresponding input power. The fan has straight blades with only moderate backward leaning. So, the energy rise is almost constant for varying flow rate and thus is the input power approximately proportional to the flow rate.
- Vary the mass flow rate by opening or closing the cone. Select eight operating points approximately evenly distributed over the power input range from minimum to maximum. When performing pressure measurements of the nozzle, it is advisable to measure the pressure upstream of the measuring nozzle and the pressure difference over the nozzle (and not the pressure downstream of the nozzle).
- Measure at each operating point: T , p , p_1 , $\Delta p = p_1 - p_2$, P_{input} .

5.7.4 Calculations

- Calculate for each operating point: \dot{m} , $\Delta p_0/\rho$ and shaft power.
- Calculate for each operating point the overall efficiency of the fan, with the shaft power as input power.
- Transform by similitude (see Chap. 7) the results for each operating point to the idling rotational speed. Apply purely kinematic similitude, so no correction for the small change of the Reynolds number. The overall efficiency is assumed constant in the conversion.
- Determine the work coefficient $\psi = \Delta W / u_2^2$ for the operating point with maximum efficiency (interpolate between the results found, if necessary) and the specific speed. Determine the rotor work from the shaft power and the flow rate, assuming that the mechanical and volumetric efficiencies equal unity. With a radial fan, mechanical efficiency is very near to unity (bearing friction and wheel friction being very low), but the volumetric efficiency may be significantly lower than unity (the gap between the volute and the rotor in the suction eye being rather large). This way, we overestimate the work coefficient (by about 10%). Evaluate the values found for the work coefficient and the specific speed.

5.7.5 Measurement Example

- Rotational speed 2750 rpm (idling value).
- Atmospheric conditions: $p_a = 100.4$ kPa, $T_a = 21.0$ °C (Table 5.3)

Answer: at 2750 rpm, the maximum energy rise (mechanical energy rise) is 2870 J/kg at mass flow rate 0.550 kg/s (weak maximum); the optimum efficiency is 0.74 at mass flow rate 0.825 kg/s (weak optimum). The energy rise at optimum efficiency is 2690 J/kg. At optimum efficiency, the energy rise coefficient is 0.64, the calculated work coefficient 0.865 (the real value presumably being about 10% lower, about 0.78). Specific speed is 0.65. Specific diameter is 3.90. These values form approximately a couple on the Cordier diagram (Chap. 7, Fig. 7.7)

Table 5.3 Test results for the fan

Operating point	1	2	3	4	5	6	7	8
T (°C)	22.5	23.2	23.6	23.7	24.0	24.6	25.7	27.4
P (kPa)	2.23	2.60	2.92	3.08	3.13	3.13	3.06	2.92
P_1 (kPa)	1.95	2.38	2.76	2.96	3.06	3.09	3.04	2.92
Δp (kPa)	3.25	2.38	1.60	1.05	0.60	0.27	0.07	0.00
P_{input} (W)	3760	3400	3000	2640	2240	1840	1480	1200

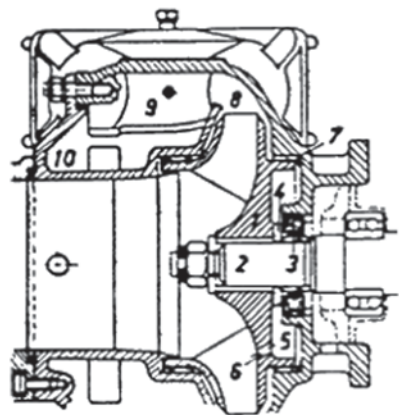
5.8 Laboratory Test of a Centrifugal Pump

5.8.1 Test Rig

The pump is a single-stage centrifugal pump with double pressure pipe, meant as a fire brigade pump (low weight, high rotational speed, high flow rate and sufficient pressure), originally driven by a small gas turbine. Figure 5.7 shows a meridional section.

The rotor (1) is mounted in overhung onto the shaft (2), running in ball bearings. The shaft is sealed with a carbon ring (3), pressed axially against a hard metal ring (mechanical seal). The axial force on the rotor is compensated by a space (5) at the back of the rotor connected to the rotor blade passages by orifices (6). Labyrinth seals (7) separate this space from the pressure side of the pump. The diffuser (9) is axial and provided with vanes. Axial diffusers are rather exceptional with centrifugal pumps. If a diffuser is required, it will regularly be a radial one. The axial type has been chosen here in order to limit the radial dimensions of the machine. The diffuser ends in the collector space (10) connected to the pressure pipes. There is no volute. Omission of the volute is also intended to limit the radial dimensions of the pump. Due to the axial diffuser and the collector space, the efficiency of the pump is rather low. The pump features are: nominal rotational speed: 4500 rpm (being maximum rotational speed as well); maximum pressure rise: 7 bar; maximum suction height: 6.7 m water column; nominal flow rate: 38 l/s; external rotor diameter: 177.5 mm; internal rotor diameter: 110 mm; axial rotor blade width at the inlet: 19 mm; number of rotor blades: 7; average blade angle at the rotor outlet relative to the meridional plane: $\beta_2^b = -58.5^\circ$. The rotor blades are doubly bent. The diffuser vane height increases in the flow sense.

Fig. 5.7 Centrifugal pump used in the laboratory test



The pump is connected to a suction reservoir with an 88.9 mm diameter pipe and to a delivery reservoir with two 63.5 mm pipes. Upstream of the delivery reservoir are two bypass pipes that are opened when this reservoir gets emptied. The pump then delivers directly into the suction reservoir. Suction and delivery pipes are provided with control valves for adjusting the suction and delivery pressures. The pump is driven by a DC motor with swinging suspended stator with lever arm connected to a balance.

5.8.2 Measurements

The hydraulic power output follows from

- The suction pressure measured by a manometer in kgf/cm^2 ($=0.981 \text{ bar}$), read as value below the atmospheric pressure.
- The delivery pressure measured by a manometer on each of the two delivery pipes in kgf/cm^2 , read as value above the atmospheric pressure.
- The height difference between manometers at suction and delivery sides. The manometers are provided with purge valves. Purging the pressure manometers guarantees that the connecting pipe is filled with water. Purging the suction manometer guarantees that the connecting pipe is filled with air. A pressure manometer thus measures the pressure in the delivery pipe at the tapping point minus the pressure corresponding to the height difference between the centre of the manometer and the tapping point. The suction manometer measures the pressure at the tapping point. The height difference to be taken into account between the manometers is the distance from the tapping point of the suction manometer to the centre of the pressure manometers. This amounts to 1.30 m.
- The flow rate by means of the calibrated delivery reservoir. The volume between the gauge glass marks is 100 l. Choose the number of measured marks in proportion to the flow rate to be measured.

Mechanical power input follows from

- The rotational speed measured with an optical pulse tachometer (disc with holes).
- The torque on the driving motor with swinging suspended stator. The scale of the balance is expressed in kgfm ($=9.81 \text{ Nm}$).

5.8.3 Measurement Procedure

- Select a rotational speed between 2000 and 2800 rpm. The driving motor is fed by a direct current controller (right part of the cabin). The rotational speed is

adjusted with a knob on the controller and is read out digitally. After adjustment, the controller keeps the rotational speed constant, independent of the motor load.

- Set six to eight points to the characteristic by constricting the delivery pipes. Keep the constriction valve on the suction side completely open. Provide for exactly equal pressures on both delivery pipes. Start the test by closing the valves on the delivering pipes. This provides maximum pressure. Then open the valves completely. This provides minimum pressure. Distribute the operating points approximately equally over pressure range. Perform the initial actions with the pump supplying to the suction reservoir. First open all valves when switching the bypass pipe valves to the suction reservoir. The position of the handles allows one single person to do this. The pump is not damaged by closing all valves suddenly, but water hammer may be generated within the delivery pipes, and this is best avoided. Let the pump deliver to the suction reservoir after flow rate measurement and empty the discharge reservoir by opening the connecting valve between the reservoirs (e.g. let in 300 l). The discharge reservoir is sufficiently large, making it impossible to overflow it. The suction pipe inlet in the suction reservoir comes out of the water with a completely filled discharge reservoir.

5.8.4 Calculations

- Determine for each operating point: flow rate, delivery pressure, suction pressure, torque. Calculate the mechanical energy rise and the overall efficiency. Plot these two parameters: $\Delta E_m = f(Q)$; $\eta = f(Q)$.
- Transform, by similitude (Chap. 7), mechanical energy rise, flow rate and efficiency to $n = 4500$ rpm. Apply Pfleiderer's formula (7.14) for correction of the overall efficiency with changing Reynolds number. Apply the correction to the overall efficiency, even though the formula is intended for the internal efficiency. We do this because we are unable to determine the mechanical efficiency and the volumetric efficiency during the test. Corrections of the head and the flow rate are applied with the formulae of Casey and co-authors (7.10–7.12). Plot the converted results: $\Delta E_m = f(Q)$; $\eta = f(Q)$.
- Determine the work coefficient and the specific speed for the operating point with maximum efficiency (interpolate between the results found, if necessary). When calculating the work coefficient, determine the rotor work from the shaft power and the flow rate, assuming that the mechanical and volumetric efficiencies equal unity. With a radial pump, the volumetric efficiency is close to unity (wear rings, labyrinth seals and shaft seals are applied to seal the rotor from the stator, both for internal and external leakage), but the mechanical efficiency may be significantly lower than unity (friction within the seals and disc friction are not negligible). We thus overestimate the work coefficient (by about 10%). Evaluate the values found for work coefficient and specific speed.

Table 5.4 Test results for the pump

Operating point	1	2	3	4	5	6	7	8
p_p (kgf/cm ²)	0.80	1.20	1.60	2.00	2.40	2.80	3.20	3.30
p_s (kgf/cm ²)	-0.72	-0.60	-0.50	-0.38	-0.28	-0.12	-0.02	0.00
T (kgfm)	4.5	4.4	4.3	4.1	3.8	3.3	2.6	2.2
Q (l/s)	42.1	38.2	33.8	29.4	25.0	17.8	8.0	0.0

5.8.5 Measurement Example

- Rotational speed 2700 rpm (Table 5.4).

Answer: at 2700 rpm the maximum energy rise (mechanical energy rise) is 336.5 J/kg with a zero mass flow rate; the optimum efficiency is 0.65 with a 25 kg/s mass flow rate. The energy rise at optimum efficiency is 275.3 J/kg. With optimum efficiency, the energy rise coefficient is 0.44 and the calculated work coefficient is 0.67 (the real value presumably is about 10% lower, so about 0.60). Specific speed and specific diameter are 0.67 and 4.57. These values form approximately a couple on the Cordier-diagram (Chap. 7, Fig. 7.7).

Chapter 6

Steam Turbines

Abstract The present chapter discusses the working principles and the construction forms of steam turbines, starting with an outline of their historical evolution. The two basic types of steam turbines are analysed. These are the impulse type and the reaction type. The chapter is also intended to formulate the general theory of axial turbines. In particular, the crucial role of the degree of reaction is discussed. Typical construction forms of large steam turbines for power stations and small turbines for industrial applications are illustrated. The chapter ends with a discussion of the shaping of blades and vanes.

6.1 Applications of Steam Turbines

A steam turbine produces shaft power by means of an enthalpy drop of steam. A special feature of steam turbines is their ability for very high power, due to the big enthalpy drop realisable per steam mass unit. Supply conditions in modern coal-fired electric power stations come to about 250 bar (25 MPa), 565 °C (supercritical). Steam expansion to a 5 kPa vacuum provides about 1500 kJ/kg when applying one reheat. This enables power generation in the 1000 MW order.

The working principles of steam turbines have been known since ancient times, but practical realisation was only achieved at the end of the nineteenth century, by Gustaf de Laval (Sweden) in 1883 and by Charles Parsons (UK) in 1884. Industrial applications started around 1920. The development of steam turbines was mainly advanced by the use of electricity as an energy carrier. From 1920, energy production was concentrated in electric power stations requiring high power driving units. Steam turbine power strongly increased in the course of time. A 1 MW turbine was a large unit in 1920. At present, units with 1000 MW power per shaft (coal) are common, whereas the biggest turbines yield a power of 1800 MW per shaft (nuclear) (see web sites of typical manufacturers Alstom, Siemens, General Electric and Mitsubishi, combined with power or energy).

Worldwide, the largest part of the electricity is produced by steam turbines. Steam is obtained by water evaporation under pressure, with solid, liquid, gaseous or nuclear fuels. The fuel is chosen depending on economic factors and environmental restrictions. Due to the low cost of nuclear fuel on the one hand but the high

investment cost of nuclear reactors on the other, nuclear power stations are used for base load. Typically, the technically highest possible turbine power (1500 MW) is opted for. Due to this high power, the steam turbine and the reactor have high thermal inertia, precluding these units from following load variations. For instance, the Chooz B unit (France) has 1500 MW power. The reactor does not allow very high inlet conditions of the steam, which are 71 bar, 287°C. There is one reheat at 10 bar until 268°C. The inlet steam is saturated and the reheat steam is only lightly superheated. This causes erosion by moisture. Fossil fuel steam turbine power stations, without gas turbines, use nearly exclusively coal, but many can use oil or gas as back-up fuel. Fossil fuel fired power stations reach very high inlet conditions, typically, as already mentioned, 250 bar, 565°C (supercritical). Inlet conditions of very modern coal units are 300 bar, 600°C (ultra-supercritical, 2 reheats). Coal units function as base load or as middle load. In the last case, it means that they partially follow the daily power consumption variation: full load during high power consumption hours, part load during low consumption hours. The need to limit thermal inertia precludes from building such units with very high power. The maximum power comes to about 800 MW, but mostly smaller units of about 400 MW are applied. Coal units of 1000 MW are base load units. Steam turbines are completely inadequate as peak units, mainly because of the thermal inertia of the steam generator. Fast-starting machines for peak load are hydraulic turbines and simple-cycle gas turbines.

Natural gas is not commonly used to fire directly a steam generator, but more typically in a combined-cycle power station. The gas is burnt in a gas turbine with outlet gases led to a recovery steam generator (no burning of fuel), which feeds a steam turbine. At present, such power stations yield the highest efficiency (net electrical efficiency about 60%). A coal fired steam turbine power station yields about 45% (the efficiency increases slightly with technical progress with an expected maximum of about 50%). A nuclear power station reaches about 35%. Combined steam and gas turbine stations are very suitable for base load, due to their very high efficiency, but they are also used for mid load because the thermal inertia of the gas turbine is small. Gas turbines are relatively small, amounting to about 400–450 MW nowadays (2014) for the largest machine (Siemens SGT5-8000H, GE 9HA, Mitsubishi M701J). Combination of one gas turbine with one steam turbine yields then about 600–700 MW. Combined units are relatively new. Gas turbine outlet gases must be sufficiently hot to produce steam at useful conditions. The outlet temperature currently amounts to about 600°C, due to the increase in inlet temperature of the turbine part, at present typically around 1500°C, enabled by progress in metallurgy and blade cooling techniques. This allows steam generation at about 565°C. Before the advent of combined units, gas turbines were exclusively applied as aircraft engines or as industrial turbines. These applications have limited power, at most 20 or 40 MW.

Steam turbines are also used as industrial machines, although decreasingly. Due to improved reliability of electric power generation and increase in available power, industrial drives are preferably electric nowadays. Steam turbines are only applied to drive machines requiring high power and turning at high rotational speed. A

typical application is drive of turbo-compressors. Drive of turbo-pumps exists also, but is less common. Opting for a steam turbine as a motor is attractive if the industrial application also needs process heat, which then can be supplied by the outlet steam from a backpressure turbine or by the extraction steam from a condenser-turbine. Cogeneration of electrical power and process heat is similar. Steam is then produced at high pressure and temperature and fed to a steam turbine driving an electric generator. The process heat is supplied by extraction steam or backpressure steam from the steam turbine. The generated electric power is consumed locally or fed into the electricity grid. Industrial steam turbines function with lower values of inlet pressure and inlet temperature than big power station steam turbines, up to a maximum of about 100 bar, 500 °C. This is due to the cost and to the need for quick adaptability of the machine load (no big thermal inertia). Dependent on the application, industrial steam turbines may differ highly in power, with the biggest around 250 MW. The biggest machines also serve in combined-cycle plants. In current cogeneration applications, steam turbines experience strong competition from gas turbines. Gas turbines burn natural gas and process steam is produced in a recovery steam generator by means of turbine outlet gas. Investment costs for gas turbines are considerably lower than for steam turbines. Waste gas from the process may also be burnt in a recovery steam generator (co-firing).

Steam turbines have had an important role in ship propulsion, but this application is nowadays extremely exceptional due to the power allowed by modern diesel engines, up till 80 MW. Large slow running diesel engines also have a higher efficiency (45%). Pressure and temperature conditions of ship propulsion steam turbines equal those of industrial steam turbines. The efficiency amounts to about 38%. At present, ships are mainly propelled by diesel engines, but gas turbines are applied for high power when available space is strongly limited: high speed battle ships, coast guard patrol boats, fast ferries and fast container ships. Some ships with gas turbines feature both gas turbines and diesel engines for propulsion. Use of the diesel engine at low speed and the gas turbine or both the gas turbine and the diesel engine for high speed is typical.

6.2 Working Principles of Steam Turbines

Present steam turbines are almost exclusively built in the axial form. The functioning is analogous with that of the axial hydraulic turbine discussed as an example in Chap. 1. A flow is generated in stator components by converting static enthalpy into kinetic energy. Mechanical work is produced by change of flow direction in the downstream rotor, i.e. by using the kinetic energy. Static enthalpy can be converted into kinetic energy during work in the rotor. A degree of reaction is then present. Even though the principle of a steam turbine is the same as for a hydraulic one, it has totally different appearance due to the nature of the fluid. The available enthalpy drop with steam is very high: of the 1000 kJ/kg order. Even under extreme circumstances, a hydraulic turbine ranks two orders lower: a 1000 m height difference

yields about 10 kJ/kg. Hydraulic turbines are always of the single-stage type for that reason. In general, steam turbines are multistage machines. Further, the low steam density allows very high flow speeds. The outlet speed at the stator blades typically amounts to about 400 m/s, even to 600 m/s. The corresponding kinetic energy is of the 100 kJ/kg order. This value also represents the order of magnitude of the enthalpy drop of a stage.

From a historical point of view, there are two steam turbine types: the impulse turbine and the reaction turbine. The impulse turbine was introduced by G. de Laval in 1883. It is a machine with no pressure drop in the rotor. The entire pressure drop and the accompanying enthalpy drop are used in the stator to produce kinetic energy. As a principle, the degree of reaction thus equals zero (correct for lossless flow; the degree of reaction is discussed in Sect. 6.7.1). Figure 6.1 (left) illustrates the functioning of a single-stage impulse turbine (sketch after Laval's original turbine). The enthalpy relations in stator and rotor are:

$$\text{Stator:} \quad h_{00} = h_1 + \frac{v_1^2}{2}, \quad (6.1)$$

$$\text{Rotor:} \quad h_{0r} = h_1 + \frac{w_1^2}{2} = h_2 + \frac{w_2^2}{2}; \quad h_1 - h_2 = \frac{w_2^2 - w_1^2}{2}. \quad (6.2)$$

We used here absence of work and heat transfer in the stator in the absolute frame and absence of work and heat transfer in the rotor in the relative frame, together

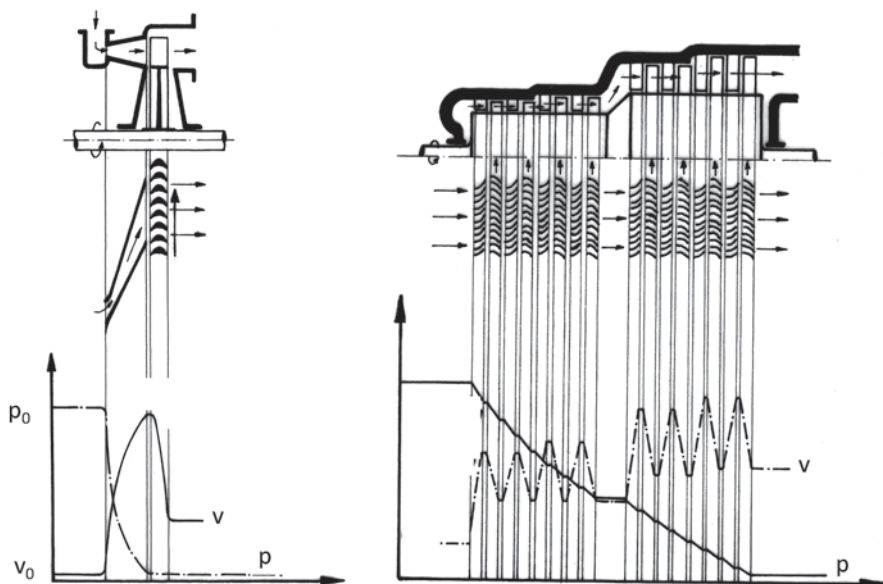
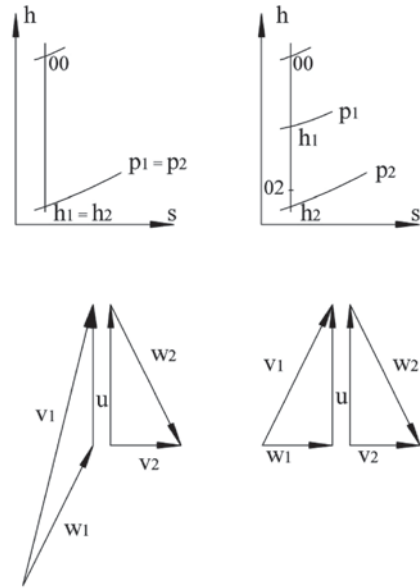


Fig. 6.1 Left: impulse turbine (single-stage example); right: reaction turbine (multistage example); sketches after the historical machines of de Laval and Parsons

Fig. 6.2 Enthalpy-entropy diagrams and velocity triangles, drawn for lossless flow with axial outlet; *left*: zero degree of reaction; *right*: degree of reaction 50 %



with $u_1 = u_2$ (Eq. 1.14 of Chap. 1). With a provisional neglect of losses, the enthalpy-entropy diagram of Fig. 6.2 (left) shows that with $p_1 = p_2$, then follows $h_1 = h_2$ and thus $w_1 = w_2$. Thus rotor work is produced only by the momentum (impulse) made available by the nozzle.

The reaction turbine was introduced by Ch. Parsons in 1884. This is a machine with a pressure drop in the rotor. Parsons' original machine had a degree of reaction of exactly 50%. This is no requirement for reaction turbines. It just was a purposeful choice. Figure 6.1 (right) illustrates the functioning of a multistage reaction turbine (sketch after Parsons' original machine). The thermodynamic relations are again (Eqs. 6.1 and 6.2).

The total enthalpy drop is: $h_{00} - h_{02} = h_1 + \frac{v_1^2}{2} - h_2 - \frac{v_2^2}{2}$.

From $R = \frac{h_1 - h_2}{h_{00} - h_{02}} = 0.5$, it follows: $h_1 - h_2 = \frac{v_1^2 - v_2^2}{2} = \frac{w_2^2 - w_1^2}{2}$.

For a stage with inlet velocity equal to outlet velocity, $\vec{v}_0 = \vec{v}_2$, rotor and stator accelerations are equal for $R=0.5$. This means that the stator blade shape and the rotor blade shape are equal, but placed symmetrically. The application of a same blade shape for both the rotor and the stator motivated Parsons to choose $R=0.5$. In Parsons' original machine all blades are prismatic and of the same cross section.

Comparison of the velocity triangles with $R=0$ and $R=0.5$ on Fig. 6.2 demonstrates that, with an equal blade speed (u), the work ($\Delta W = u \Delta v_u$) with $R=0$ is double that with $R=0.5$. This is a general rule: machines with the lowest degree

of reaction produce the largest work per stage. This was one of the reasons why Laval opted for $R=0$. The biggest possible enthalpy drop can then be handled in one stage. Parsons' machine has stator blades around the entire circumference. Laval's machine has a stator consisting of one single nozzle, which does not cover the entire circumference of the rotor. In other words, there is *partial admission* or, more in general, *partial flow*. The rotor blades only produce work when passing the nozzle. A partial admission machine can function adequately only with constant pressure in the rotor. With built-in pressure difference, the rotor blade channels not in front of the nozzle, would take flow from the nozzle. This flow cannot enter the rotor at the appropriate angle. Furthermore, each nozzle flow deviation causes angular deviations and consequently incidence losses at inlets of the rotor blade channels in front of the nozzle. Partial flow thus necessitates, in principle, constant pressure in the rotor. This was Laval's second reason to opt for $R=0$. A partial-flow machine can be built for a fraction of the power it would supply with full flow. Single-stage impulse turbines with partial admission are still built nowadays. They are mainly meant for mechanical drive. The degree of reaction is not exactly zero, but typically around $R=0.10$. This is intended to compensate rotor losses. A partial admission impulse stage is also sometimes used as first stage in a multistage machine (see Sect. 6.8.2).

A third historical steam turbine type is the radial form, represented in Fig. 6.3, introduced by the Swedish Ljungström brothers. It consists of two rotors turning

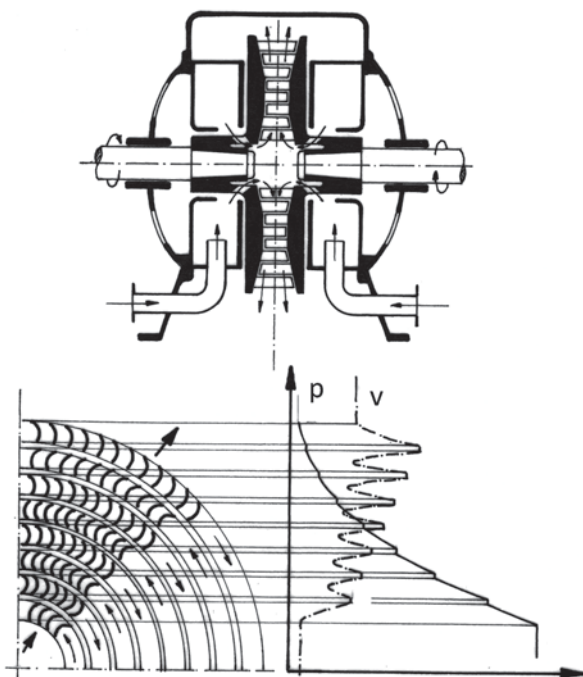


Fig. 6.3 Ljungström turbine

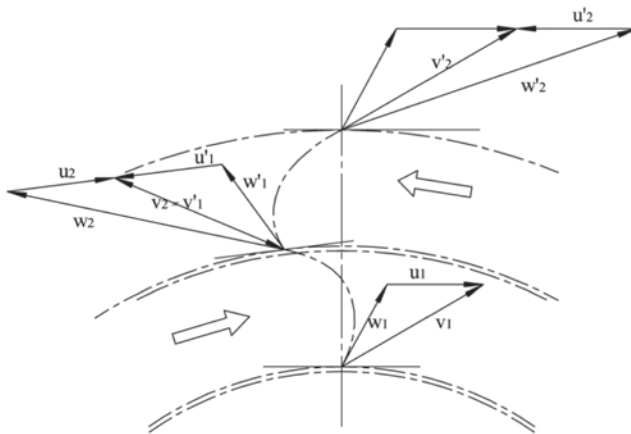


Fig. 6.4 Velocity triangles with the Ljungström turbine

in opposite senses. The flow is centrifugal through the machine. This is inadequate for a turbine, as it should be flowed through centripetally, but a centripetal design is impossible, as the very high density drop with expansion requires an outlet area much bigger than the inlet area. Velocity diagrams are shown in Fig. 6.4. The degree of reaction is near to 100 %: kinetic energy at a blade ring outlet is just somewhat higher than at the inlet. A Ljungström turbine is a very special machine, very seldom built nowadays. Important drawbacks are impossibility to cope with a high mass flow rate, big radial size and two outgoing shafts. We do not discuss this type any further.

6.3 The Steam Cycle

Figure 6.5 represents the steam cycle (Rankine cycle) in the T-s diagram, neglecting losses. The cycle demonstrated is the simple cycle without reheat and at subcritical pressure. The cycle encompasses pressure increase with slight temperature increase of the feed water (nearly undistinguishable in the diagram), heating under constant pressure, consisting of heating in the liquid phase, evaporation and superheating, isentropic expansion and condensation at constant pressure. The ratio of produced work to supplied heat is called *thermal efficiency*. This efficiency is the product of two factors: the thermodynamic cycle efficiency and the turbine efficiency. Turbine efficiency is the ratio of produced work and isentropic enthalpy drop ($h_3 - h_{4s}$) supplied by the cycle (equal to 1 in the figure). Generally, this efficiency is called *internal efficiency* (based on internal work). The best turbines yield 94–96 %. *Thermodynamic cycle efficiency* is the ratio of the isentropic enthalpy drop available for work production ($h_3 - h_{4s}$) to the heat supplied to the cycle ($h_3 - h_2$). Figure 6.5 shows this efficiency for the basic cycle. The maximum value amounts to about 45 % for

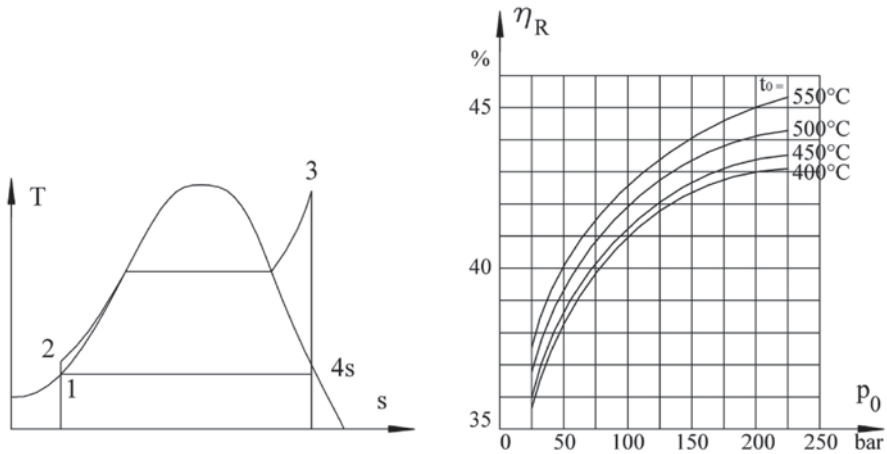


Fig. 6.5 Rankine cycle on the T-s diagram and corresponding thermodynamic efficiency

250 bar, 550°C (already supercritical). This efficiency can be increased by adding reheat and regenerative feed water heating (see thermodynamics). At 250 bar, 550°C and application of one reheat, 52% cycle efficiency is reached at present, resulting in 42% gross electric efficiency. The gross electric efficiency is the ratio of the electrical power output of the generator to the fuel power. The gross electric efficiency with state of the art technology (2014), 300 bar, 600°C and two reheats amounts to 48%. The corresponding net electric efficiency is about 43.5%. Net electric power is the power supplied by the power station. The next step, at present under development, is 375 bar, 700°C and two reheats. It should yield 53% gross efficiency. But, future units will normally be combined with CO₂ separation equipment, impairing the net efficiency.

6.4 The Single Impulse Stage or Laval Stage

For didactic reasons, we discuss a single-stage impulse turbine at first, its analysis being the simplest one. This should not convey the impression that this type prevails. Typical current designs will be discussed further down.

6.4.1 Velocity Triangles

Figure 6.6 sketches a meridional section of a steam turbine stage and a cylindrical section of a rotor blade. The velocity triangles respect proportions that are typical for impulse turbines. Angles are counted with respect to the axial direction, positive in the running sense. The coordinate system is right-handed, with x-axis in axial

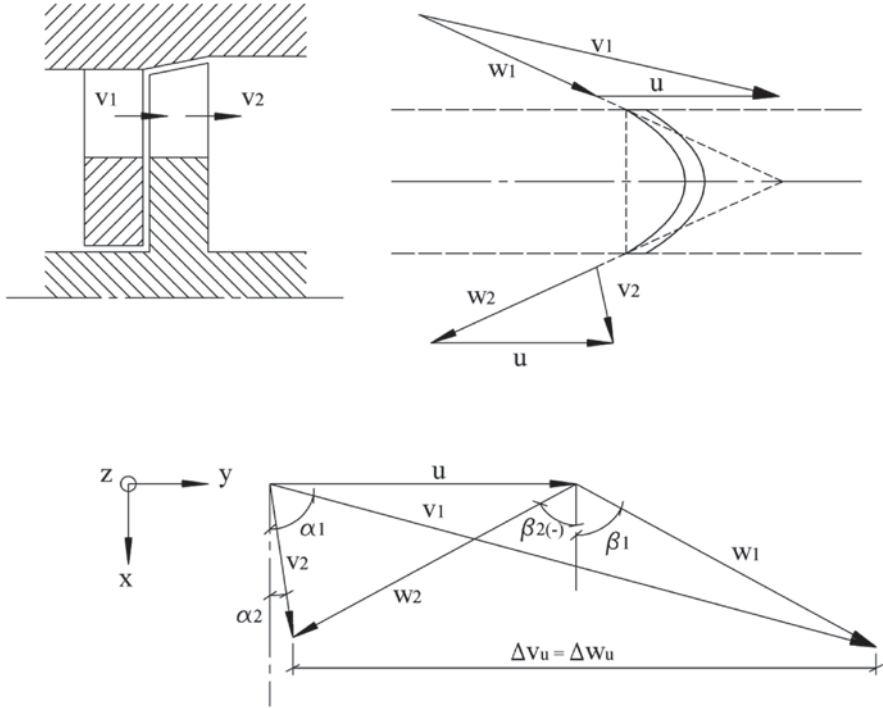


Fig. 6.6 Velocity triangles with impulse turbines ($R_s = 0$, $\psi = 1.95$; work coefficient for optimum efficiency with loss of outlet kinetic energy)

direction, positive in the through-flow sense; y-axis in tangential direction, positive in the running sense; z-axis in radial direction positive away from the shaft. A machine with positive blade speed is *left-running*: $\vec{\Omega} = -\Omega \vec{I}_x$. Flow is usually visualised top-down with axial machines. We follow this convention.

6.4.2 Work and Energy Relations

The primary relations are ($dq = 0$, $dU = 0$):

$$\text{Energy: } dW = dh + \frac{1}{2} dv^2 = dh_0,$$

$$\text{Work: } dW = \frac{1}{\rho} dp + d \frac{1}{2} v^2 + dq_{irr},$$

$$\text{Rotor work (Euler): } \Delta W = u(v_{2u} - v_{1u}).$$

Through velocity triangles it follows

$$\begin{aligned}
w_1^2 &= u^2 + v_1^2 - 2uv_{1u} \\
w_2^2 &= u^2 + v_2^2 - 2uv_{2u} \\
w_1^2 - w_2^2 &= v_1^2 - v_2^2 - 2u(v_{1u} - v_{2u}), \\
-\Delta W &= u(v_{1u} - v_{2u}) = \frac{v_1^2}{2} - \frac{v_2^2}{2} - \left(\frac{w_1^2}{2} - \frac{w_2^2}{2} \right).
\end{aligned}$$

For a turbine, we conventionally consider delivered work as positive and write:

$$\Delta W = u(v_{1u} - v_{2u}) = \frac{v_1^2}{2} - \frac{v_2^2}{2} - \left(\frac{w_1^2}{2} - \frac{w_2^2}{2} \right), \quad (6.3)$$

$$\Delta W = \Delta h_0 = h_{01} - h_{02}.$$

Then, Δh_0 represents the total enthalpy drop. From rotor work and energy it follows also

$$h_1 + \frac{v_1^2}{2} - h_2 - \frac{v_2^2}{2} = \frac{v_1^2}{2} - \frac{v_2^2}{2} - \left(\frac{w_1^2}{2} - \frac{w_2^2}{2} \right),$$

or

$$h_1 + \frac{w_1^2}{2} = h_2 + \frac{w_2^2}{2} = h_{0r} = \text{constant}.$$

We recover the result that the total relative enthalpy is constant within the rotor. This result only applies with an axial machine ($u = \text{cst}$). Within the stator $\Delta W = 0$, applies thus $h + \frac{1}{2} v^2 = h_0 = \text{constant}$.

Figure 6.7 demonstrates the processes with an impulse turbine in the h - s diagram, taking the obtained relations into account. The diagram is drawn for constant pressure in the rotor. So, we use the strict definition of an impulse turbine.

We first consider the nozzles (stator). The work equation within the stator cannot be integrated without determining the details of the expansion (see Chap. 4). Efficiency is therefore defined by comparing the result of the real expansion to that of a loss-free expansion. As isentropic nozzle efficiency we define:

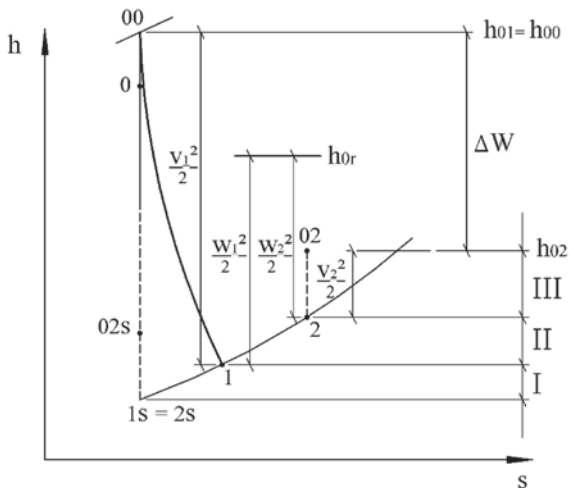
$$\eta_{ss} = \frac{v_1^2 / 2}{v_{1s}^2 / 2}, \quad (6.4)$$

with

$$\frac{v_1^2}{2} = h_{00} - h_1; \quad \frac{v_{1s}^2}{2} = h_{00} - h_{1s}.$$

Conventionally, the difference $\frac{1}{2} v_{1s}^2 - \frac{1}{2} v_1^2$ is considered as nozzle loss. This difference does not correspond exactly to the integral of dq_{irr} in the work equation. We

Fig. 6.7 h - s diagram of an impulse turbine stage; *I*: nozzle loss; *II*: rotor loss; *III*: outlet kinetic energy



recall that it has been reasoned in Chap. 4 that the conventional loss underestimates somewhat the real loss. As the real loss is practically undeterminable, because it depends on the details of the expansion path, the conventional nozzle loss is applied in the further analysis.

We define a velocity coefficient ϕ_s with

$$v_I = \phi_s v_{Is},$$

so that

$$\eta_{ss} = \phi_s^2.$$

In the rotor of an impulse turbine, $dp=0$. So the work equation can be integrated. It follows that

$$0 = 0 + d \frac{1}{2} w^2 + dq_{irr},$$

or

$$q_{irr} = \frac{w_I^2}{2} - \frac{w_2^2}{2}.$$

The decrease of the kinetic energy in the relative system thus is the loss. Rotor work (Eq. 6.3) can be written as

$$\Delta W = \frac{v_I^2}{2} - \left(\frac{w_I^2}{2} - \frac{w_2^2}{2} \right) - \frac{v_2^2}{2}. \quad (6.5)$$

The interpretation is:

$\frac{v_I^2}{2}$: kinetic energy supplied to the rotor,

$\frac{w_I^2}{2} - \frac{w_2^2}{2}$: rotor loss,

$\frac{v_2^2}{2}$: outlet kinetic energy.

It seems appropriate to define rotor efficiency by

$$\eta_r = \frac{\Delta W}{v_I^2 / 2}. \quad (6.6)$$

Such a definition is only relevant with an impulse turbine. As there is no pressure drop, the kinetic energy supplied to the rotor is the only source of work. We define a *rotor velocity coefficient* by

$$w_2 = \phi_r w_{2s} = \phi_r w_I.$$

6.4.3 Stage Efficiency Definitions

In order to define stage efficiency, we must formulate a statement about the usefulness of the kinetic energy at the stage outlet. Rotor work is first written as

$$\Delta W = \frac{v_{Is}^2}{2} - \left(\frac{v_{Is}^2}{2} - \frac{v_I^2}{2} \right) - \left(\frac{w_I^2}{2} - \frac{w_2^2}{2} \right) - \frac{v_2^2}{2}. \quad (6.7)$$

When outlet kinetic energy is completely lost, it becomes obvious from Eq. (6.7) together with Fig. 6.7 that the isentropic enthalpy drop supplied to the stage for work production is $\Delta h_s = h_{00} - h_{Is} = \frac{1}{2} v_{Is}^2$. Internal efficiency is then

$$\eta_i = \frac{\Delta W}{\Delta h_s} = \frac{\Delta W}{h_{00} - h_{Is}} = \frac{\Delta W}{h_{00} - h_{2s}} = \eta_{ss} \eta_r. \quad (6.8)$$

It becomes relatively simple to reason how this efficiency may be optimised (see Sect. 6.4.6). If outlet kinetic energy is useful, e.g. because it is supplied to a next stage, with Eq. (6.7) and Fig. 6.7, the enthalpy drop available to the stage for work production actually is $\frac{1}{2} v_{Is}^2 - \frac{1}{2} v_2^2$. This enthalpy difference may be visualised on the h-s diagram by $h_{00} - h_{02s}$, where the total state h_{02s} is obtained by adding the outlet kinetic energy to the state $I_s = 2_s$. Efficiency is then defined as

$$\eta_i = \frac{\Delta W}{h_{00} - h_{02s}}. \quad (6.9)$$

This efficiency cannot be expressed elementarily. However, if the stage is supposed to supply kinetic energy $\frac{1}{2}v_2^2$ to the next stage, it seems obvious to suppose that the stage receives a same kinetic energy: $\frac{1}{2}v_0^2 = \frac{1}{2}v_2^2$. Especially, this is satisfied when the stage inlet and the stage outlet velocities are equal in magnitude and direction: $\vec{v}_0 = \vec{v}_2$. Such a stage is called a *repeating stage*. It is a model for a stage of a multi-stage machine. For a repeating stage, (Eq. 6.9) reduces to

$$\eta_i = \frac{\Delta W}{h_0 - h_{2s}} = \frac{\Delta W}{h_0 - h_{1s}}. \quad (6.10)$$

With impulse turbines, the outlet kinetic energy is completely lost or almost completely lost in some applications. With partial admission, rotor blades not exposed to steam produce a windage flow. The fluid between the blades is driven to the periphery by centrifugal effect. This generates a circulating flow (analogous with the peripheral pump and the side-channel pump: see Chap. 8). The windage flow consumes wheel power (=windage loss). It also perturbs the outlet flow from steam-exposed blade channels and partially dissipates the outlet kinetic energy. An impulse stage with partial admission is sometimes used as a first stage in a multi-stage turbine. There is then typically a diameter reduction after this stage, intended to diminish the through-flow area in order to obtain full admission on the second and further stages. In such a case, the outlet kinetic energy in the first stage is completely lost (such a first stage will be discussed in Sect. 6.8.2). With a single-stage impulse turbine as illustrated in Fig. 6.1, outlet kinetic energy is largely a loss, as the post-connected diffuser can only recover a small amount of it. In other applications, outlet kinetic energy is fully recovered, as in full admission stages of multistage turbines. Both efficiency definitions (Eqs. 6.8 and 6.9) thus are relevant. Efficiency according to (Eq. 6.8) is called *total-to-static efficiency* as the reference enthalpy drop goes from a total to a static state: $h_{00} - h_{2s}$. Efficiency according to Eq. (6.9) is analogously called *total-to-total efficiency*. With a repeating stage the total-to-total efficiency equals a static-to-static efficiency (expression 6.10), but the latter name is not generally used.

6.4.4 Blade Profile Shape

Figure 6.8 represents the velocity triangles with a given nozzle angle α_1 and a given blade speed u . Without rotor losses, the path by which w_1 in the rotor can be turned to w_2 would be the dashed line (circle). The theoretically maximum turning, and thus maximum rotor work, is reached for a purely tangential outlet. This is practically unachievable, as there would be no axial velocity. Taking losses into account,

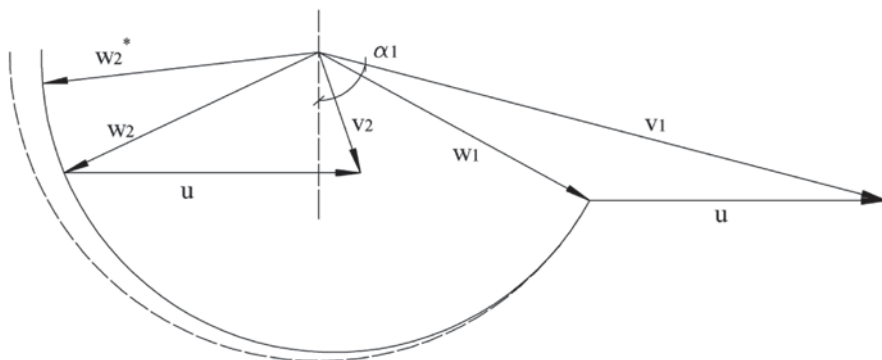


Fig. 6.8 Flow turning in the rotor of an impulse turbine

the possible turning path becomes a curve, as drawn with a full line in Fig. 6.8, with the radius decreasing as the turning proceeds. Maximum turning is reached for w_2^* , but the corresponding axial component is so small that so much turning is unachievable as well. This follows from the details of the rotor blade loading, as reasoned hereafter.

Figure 6.9 represents how to build up the profile of an impulse blade. The figure is drawn for a symmetrical blade ($\beta_2 = -\beta_1$), but the same principle applies to an asymmetrical blade. The pressure side of the rotor blade is a circular arc AB with centre O. A part of the suction side is an arc with centre O' shifted over the pitch s with respect to O, so that the pressure side of the adjacent blade A'B' has the same

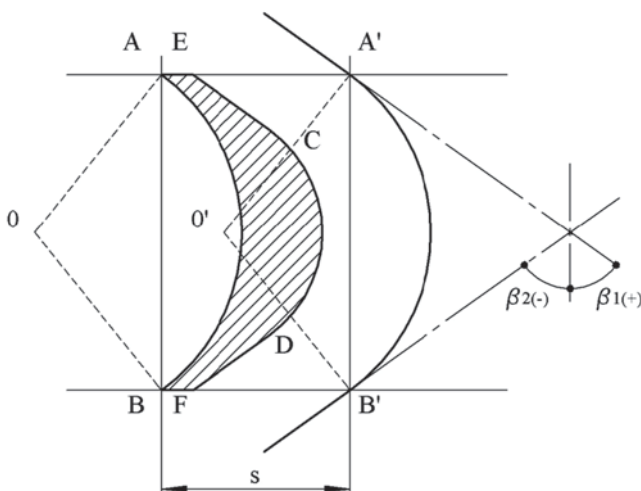


Fig. 6.9 Traditional design of an impulse blade with high rotor inflow velocity; the blade may be rounded at the leading edge for sufficiently low Mach number

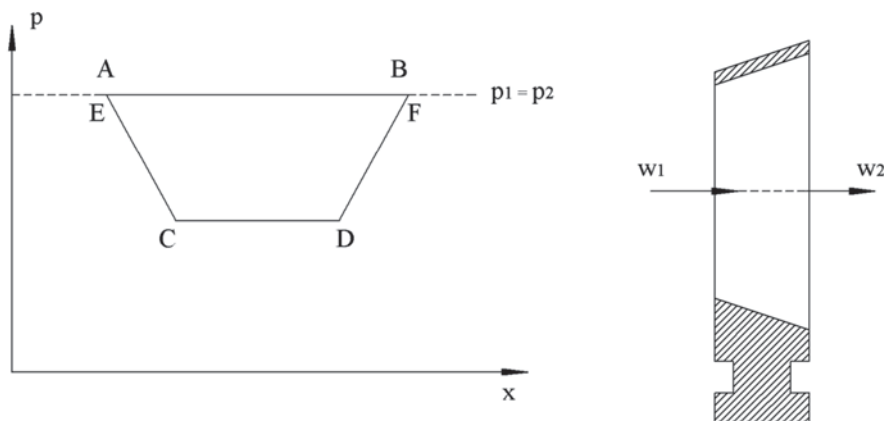


Fig. 6.10 Pressure distribution with a traditional impulse blade in a cylindrical section (*left*); meridional section through the blade (*right*)

centre O' . Suction side parts EC and DF are drawn straight in the figure, parallel with the inlet and outlet flow directions. The flow in the channel part $A'B'CD$ has circular streamlines with centre O' . Thus, in absence of losses, the flow satisfies the free-vortex law with constant angular momentum around the centre O' . This means that the streamline $A'B'$ is under constant pressure, namely inlet pressure and outlet pressure. The CD part is under constant pressure as well, but at a lower value than the common inlet and outlet pressure. Pressure decreases in flow direction in the EC part and it increases in the DF part. The pressure distribution at the suction and pressure sides is drawn in Fig. 6.10. The transition parts EC and DF are drawn straight, but the pressure variation on these parts normally is not exactly linear. The exact form is determined by the geometrical form of parts EC and DF in Fig. 6.9, but the possibility to deviate from linear geometrical forms and linear pressure variation is limited.

As is typical, the load capacity of the blade profile is determined by the adverse pressure gradient on the suction side near the trailing edge. But, the pressure diagram in Fig. 6.10 is very unfavourable with regard to load capacity. For a given pressure gradient DF, the force generated by the blade (surface of the pressure diagram) increases if a stagnation point is built in at the blade leading edge AE. However, realisation of a stagnation point presupposes that the velocity w_1 is not too high, in other words has a Mach number that is sufficiently lower than unity. This is the problem in most cases. Mostly, the nozzle outlet velocity v_1 is supersonic. The rotor inlet velocity w_1 is lower, but typically has a Mach number near unity. It is not possible to build up a stagnation point for high-subsonic flows without generating high losses by shock waves. So, only for sufficiently low inflow Mach number, the leading edge may be rounded. Independent of the leading edge shape (with or without stagnation point), it is clear that there is a pressure difference between the suction and pressure sides of a rotor blade, also in an impulse turbine. There is thus always deceleration at the suction side trailing edge.

Even with a symmetrical blade form, as represented in Fig. 6.9, axial velocity decreases from inlet to outlet ($w_{1a} > w_{2a}$) due to losses. Further, the fluid density decreases somewhat due to heating at constant pressure by losses ($\rho_1 > \rho_2$). Both effects cause the need of a diverging meridional shape of the blade (Fig. 6.10, right). At the periphery and the hub, the section area increase causes flow curvature in the meridional plane. The associated pressure decrease on the concave side of the streamsurfaces adds load to the boundary layer at the suction side trailing edge. This implies that for a symmetrical blade, the divergence of the meridional section is close to the possible maximum. In practice, $\beta_2 = -\beta_1$, i.e. a symmetrical blade, is mostly opted for. At most only a few degrees of deviation from symmetry are possible. Henceforth we take $\beta_2 = -\beta_1$ for the further analysis.

6.4.5 Loss Representation

Loss coefficients are defined with compressible fluids in the same style as introduced for constant density fluids in Chaps. 2 and 3. Two definitions are common. A loss coefficient associated to the loss representation of the nozzles in Fig. 6.7 is

$$\xi = \frac{\frac{1}{2}v_{1s}^2 - \frac{1}{2}v_1^2}{\frac{1}{2}v_1^2} = \frac{h_1 - h_{1s}}{h_{01} - h_1}. \quad (6.11)$$

The loss may also be expressed through the decrease of the total pressure as

$$\omega = \frac{p_{00} - p_{01}}{p_{01} - p_1}. \quad (6.12)$$

The coefficient (Eq. 6.11) is called the *energy loss coefficient* or the *enthalpy loss coefficient* and (Eq. 6.12) the *pressure loss coefficient* or *total pressure loss coefficient*. For constant density, there is no difference between the coefficients because the difference between total pressure and static pressure is then density multiplied with kinetic energy. For a compressible fluid, there is a difference which increases with Mach number (see Exercise 6.10.1). The pressure loss coefficient is most convenient in experiments. For fundamental analysis of machine components, the energy loss coefficient is the most convenient. Variant forms of the definitions are often used. The denominator in (Eq. 6.11) may be replaced by $\frac{1}{2}v_{1s}^2 = h_{00} - h_{1s}$ (we denote this coefficient with ξ_θ). The denominator in (Eq. 6.12) may also be $p_{00} - p_1$ (we denote this coefficient with ω_θ).

For the rotor in Fig. 6.7, the enthalpy loss coefficient is

$$\xi = \frac{h_2 - h_1}{h_{0r} - h_2} = \frac{h_2 - h_1}{\frac{1}{2}w_2^2}, \quad (6.13)$$

with the outlet kinetic energy as reference term.

Enthalpy loss coefficients may be obtained with Soderberg's loss correlation (1949), adapted by later researchers [3, 6]. We use here the simplified version by Hawthorne [6]. It represents the losses in an accelerating cascade with optimal solidity (Zweifel's formula 2.27 in Chap. 2) as a fraction ξ of the outlet kinetic energy, with

$$\xi = \xi_1 + \xi_2 \quad \text{with} \quad \xi_1 = 0.025 \left(1 + \left(\frac{\delta^0}{90}\right)^2\right) \quad \text{and} \quad \xi_2 = 3.2 \left(\frac{c_a}{h}\right) \xi_1, \quad (6.14)$$

where δ^0 is the turning of the flow within the cascade in degrees. The coefficient ξ_1 determines friction losses on the blades, with factor 0.025 for a Reynolds number equal to 10^5 , based upon hydraulic diameter and outlet velocity. With a lower Reynolds number, the factor is somewhat higher. Coefficient ξ_2 determines the friction losses in the end wall boundary layers and the losses by secondary flows (discussion of secondary flows in Sect. 6.9.1). The aspect ratio is the ratio of blade height h to axial width c_a . Henceforth we will take aspect ratio = 4 as an example. The loss formula is intended for subsonic flow. If need be, losses by shock waves have to be added. Clearance losses are not included either. We will use Soderberg's formula for losses in the rotor too, although the formula is meant for cascades with a general acceleration. We do this for reasons of simplicity as the objective of the discussions hereafter on optimisation of the efficiency is only to derive global tendencies. For more complete, but much more complex, loss correlations, we refer to Lewis [6], Moustapha et al. [7], Korpela [4] and Dixon and Hall [3].

6.4.6 Optimisation of Total-to-Static Efficiency

According to Eq. (6.8), optimisation of the total-to-static efficiency means, with given $h_{00} - h_{1s}$, the maximisation of the rotor work $\Delta W = u(w_{1u} - w_{2u})$. The tangential velocity change, with given u , increases with the nozzle angle α_1 (Fig. 6.8). But constructional realisability precludes from opting for α_1 near to 90° . The value of α_1 typically is at maximum 72° to 75° . We take $\alpha_1 = 75^\circ$.

With a symmetrical blade,

$$w_{2u} = -\phi_r w_{1u}, \quad w_{2a} = \phi_r w_{1a},$$

and

$$\Delta W = u(w_{1u} - w_{2u}) = u(1 + \phi_r)w_{1u}.$$

With

$$w_{1u} = v_{1u} - u = \phi_s v_{1s} \sin \alpha_1 - u,$$

it follows that

$$\Delta W = (1 + \phi_r)u(v_{1u} - u).$$

Work has, for constant ϕ_r , a parabolic variation in u , and reaches a maximum for

$$u = u_o = \frac{v_{lu}}{2} = \frac{\phi_s v_{ls} \sin \alpha_l}{2}.$$

The value of the maximum is

$$(\Delta W)_o = (1 + \phi_r) u_o^2 = \left(\frac{1 + \phi_r}{2}\right) \phi_s^2 \sin^2 \alpha_l \frac{v_{ls}^2}{2}.$$

The maximum efficiency value is

$$(\eta_i)_o = \frac{(\Delta W)_o}{\Delta h_s} = \left(\frac{1 + \phi_r}{2}\right) \phi_s^2 \sin^2 \alpha_l.$$

This result is somewhat approximate because the rotor velocity coefficient varies slightly with varying blade speed.

Applied to the nozzle for $\delta = \alpha_l = 75^\circ$, Soderberg's formula results in $\xi = 0.0763$, for aspect ratio = 4.

$$\text{With } \xi_s \frac{v_l^2}{2} = \frac{v_{ls}^2}{2} - \frac{v_l^2}{2},$$

$$\text{it follows that } \eta_{ss} = \frac{1}{1 + \xi_s} = 0.929 \text{ and } \phi_s = \frac{1}{\sqrt{1 + \xi_s}} = 0.964.$$

We define the velocity obtained by the enthalpy drop Δh_s converted loss-free in kinetic energy, i.e. $v_s^2 / 2 = \Delta h_s$, as an *energy reference velocity* v_s of the stage. This velocity is called the *spouting velocity*. With an impulse turbine is $v_{ls} = v_s$. We call *speed ratio* the ratio of the blade speed to the spouting velocity:

$$\lambda = u / v_s.$$

The optimum speed ratio with an impulse turbine is

$$\lambda_o = \frac{\phi_s \sin \alpha_l}{2} \approx 0.465.$$

With $\alpha_l = 75^\circ$ corresponds $\beta_l \approx 62^\circ$. Rotor loss can be expressed, with $w_2 = \phi_r w_l$, by

$$\frac{w_l^2}{2} - \frac{w_2^2}{2} = \left(\frac{1}{\phi_r^2} - 1\right) \frac{w_2^2}{2} = \xi_r \frac{w_2^2}{2},$$

from where: $\phi_r = \frac{I}{\sqrt{I + \xi_r}}$.

With $\Delta\beta = 124^\circ$, it follows according to Soderberg that $\xi = 0.1304$, from where $\phi_r = 0.941$. The corresponding optimum efficiency with $\phi_r = 0.941$ is

$$(\eta_i)_o = \frac{I + \phi_r}{2} \phi_s^2 \sin^2 \alpha_I \approx 0.84.$$

The loss formula enables the analysis of the nozzle angle influence. For $\alpha_I = 80^\circ$ follows $\phi_s = 0.962$, $\lambda_o = 0.475$, $\beta_I = 70.5^\circ$, $\phi_r = 0.930$, $(\eta_i)_o = 0.866$. This example demonstrates that the largest possible α_I -angle is advantageous for efficiency. Axial velocity decreases with a larger nozzle angle. This implies a lower flow rate through the machine, which might constitute a drawback for some applications. Even if the flow rate limitation is acceptable, the nozzle angle cannot be increased until 80° . The accompanying blade cannot be materialised. About 75° is the highest achievable nozzle angle.

Figure 6.6 represents the velocity triangles with optimal operation for $\alpha_I = 75^\circ$. The outlet velocity v_2 deviates from the axial direction in the running sense. Some rotor asymmetry, in the sense of $|\beta_2| > \beta_I$, increases efficiency. This is applied in practice. The outlet velocity is then approximately axial and the efficiency amounts to about 0.85.

It is common practice to express the *work coefficient* of a stage, also called *stage loading coefficient*, by

$$\psi = \frac{\Delta W}{u^2}.$$

A similar coefficient is defined with the isentropic enthalpy drop supplied to the stage (here: total-to-static). The isentropic enthalpy drop is often called the *isentropic head* and even shortly the *head*. So, the term head is used, similarly as with a constant density fluid, to express the work capacity of the fluid.

The *head coefficient* is

$$\psi_s = \frac{\Delta h_s}{u^2}.$$

With $\Delta W = \eta_i \Delta h_s$, it follows that $\psi = \frac{\eta_i}{2\lambda^2}$ and $\psi_s = \frac{I}{2\lambda^2}$.

For a Laval stage, the optimum value of the work coefficient is $\psi_o \approx 1.95$. The optimal value of the head coefficient is $(\psi_s)_o \approx 2.30$.

6.5 The Pressure-Compounded Impulse Turbine or Rateau Turbine

6.5.1 Principle

Pressure compounding is connecting stages in series with a pressure drop in each of them. The objective is to distribute the enthalpy drop over a number of stages so that the enthalpy drop per stage becomes tractable. In the previous section we learned that the work coefficient of an impulse stage with loss of outlet kinetic energy amounts to about 1.95. The blade speed acceptable for a turbine depends on steam temperature. At a temperature of the 500°C order, it may amount to about 200 m/s. This rather low value comes from the use of relatively cheap steel materials. At the end of the expansion, near to the vacuum, steam temperature decreases to about 50°C and the blade speed at mean radius may increase to about 400 m/s. For 200 m/s is $\Delta W \approx 1.95 \times (200)^2 \text{ J/kg} \approx 75 \text{ kJ/kg}$. For 400 m/s is $\Delta W \approx 300 \text{ kJ/kg}$. Figure 6.11 represents the serial connection of impulse stages in a so-called Rateau turbine. The first stage is fed by nozzles mounted on a distributor chamber (often called steam chest). Steam thus enters the turbine casing at a lower temperature and a lower pressure than those of the steam supplied. The distributor is a relatively small chamber, more advantageously subjected to pressure load than the much larger turbine casing. From the second stage onward, nozzles are mounted in stator discs, called *diaphragms*, sealed to the shaft with labyrinth rings with very small clearance. In an impulse stage, the whole pressure drop is in the stator. The role of the diaphragms is to reduce the clearance surface around the shaft. Rotor blades rows need not be sealed to the casing, as there is no pressure drop in the rotor.

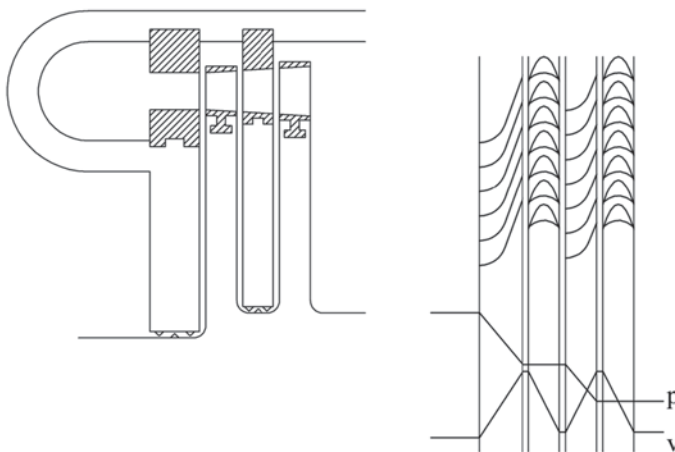


Fig. 6.11 Pressure compounding (*serial connection*) of impulse stages

6.5.2 Efficiency

The serial connection of the stages provides outlet kinetic energy recovery. The repeating stage efficiency is rendered by (Eq. 6.10). The enthalpy drop over the stage (total-to-total or static-to-static) is $h_o - h_{1s}$ (Fig. 6.7). Nozzle velocity is

$$\frac{v_I^2}{2} = \phi_s^2 \left[\frac{v_s^2}{2} + \frac{v_2^2}{2} \right] \quad \text{with} \quad \frac{v_s^2}{2} = h_o - h_{1s}.$$

According to Fig. 6.6 it follows that, with symmetrical rotor blades:

$$v_{Iu} = v_I \sin \alpha_I, \quad v_{Ia} = v_I \cos \alpha_I, \quad w_{Iu} = v_{Iu} - u, \\ v_{2a} = \phi_r v_{Ia}, \quad w_{2u} = -\phi_r w_{Iu}, \quad v_{2u} = u + w_{2u}, \quad \eta_i = \frac{2u(v_{Iu} - v_{2u})}{v_s^2}.$$

The motivation for using symmetrical blades is the same as with a single-stage impulse turbine. Velocity components relative to v_s and the internal efficiency can be determined iteratively from the foregoing relations, for a given nozzle angle α_I , and given speed ratio $\lambda = u / v_s$. Iterations start with $\phi_s = \phi_r = 1$. Flow angles are determined after a first calculation, loss coefficients (Soderberg) follow and thus also rotor and stator velocity coefficients. Values of $v_{Iu} / v_s, v_{2u} / v_s$ and η_i as functions of λ , with $\alpha_I = 75^\circ$, are given in Table 6.1.

Table 6.1 Internal efficiency as a function of speed ratio for an impulse turbine stage with outlet kinetic energy recovery (Soderberg eq. with AR=4; $\alpha_I = 75^\circ$)

$\lambda = u / v_s$	η_i	v_{Iu} / v_s	v_{2u} / v_s
0.40	0.8557	0.952	-0.117
0.50	0.9027	0.965	0.062
0.54	0.9134	0.975	0.129
0.55	0.9154	0.978	0.146
0.60	0.9225	0.995	0.226
0.65	0.9260	1.015	0.303
0.68	0.9271	1.029	0.348
0.70	0.9275	1.039	0.377
0.72	0.9276	1.050	0.406
0.74	0.9275	1.061	0.434
0.77	0.9271	1.078	0.476
0.80	0.9264	1.096	0.517
0.85	0.9245	1.127	0.584
0.90	0.9219	1.161	0.649
1.00	0.9152	1.233	0.775

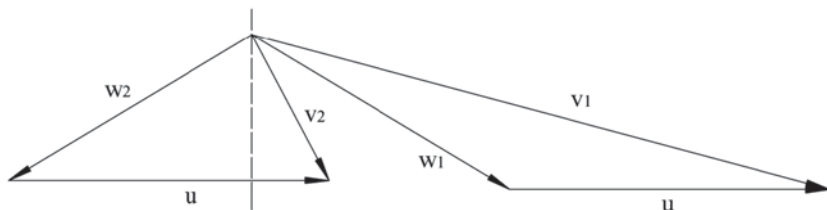


Fig. 6.12 Velocity triangles for impulse turbine with outlet kinetic energy recovery: $\lambda=0.54$ ($R_s=0$, $\psi=1.56$; work coefficient for optimum efficiency)

The optimum speed ratio changes onto a much higher value compared to optimisation with outlet kinetic energy loss: from 0.47 to 0.72, but the meaning of the reference velocity v_s is not the same in both cases. With equal pressure levels, v_s is lower here. This partially explains the higher value of λ . The ratio of the outlet kinetic energy to the enthalpy drop is about 25% with $\lambda=0.72$. Thus, this difference cannot be the only cause of a much higher speed ratio at optimum efficiency. The efficiency is almost 9 percentage points better: it increases from 84% to almost 93%. The efficiency increase comes from the outlet kinetic energy recovery. The optimum speed ratio shifts to a higher value, since rotor and stator turnings then decrease, and the loss coefficients with them. The outlet kinetic energy increases, but this is not a penalisation now. For the same reason, the nozzle outlet angle does not have to take the maximum technically realisable value. We assume here the rather high value of $\alpha_l=75^\circ$, because this leads to low axial velocity and hence large height of the blades. This is appropriate for flow with high steam density as in the high-pressure part of the turbine. But actually, the nozzle angle may be optimised too (see Chap. 15). The optimum as a function of speed ratio is very weak so that the speed ratio may be strongly reduced without significant reduction of the internal efficiency. The efficiency decreases with about one and a half percentage point with a speed ratio lowered until 0.54. The work coefficient is higher with a lower speed ratio. The turbine may then be built with fewer stages, which results in lower disc friction loss. The consequence is that the speed ratio for optimum overall efficiency (leakage and disc friction included) is much lower than that for optimum internal efficiency. The foregoing argumentation does not allow the determination of the precise value of the optimum speed ratio. We may assume that it is around 0.54. The velocity triangles are drawn in Fig. 6.12 with $\lambda=0.54$ (compare to Fig. 6.6). The work coefficient is $\psi = \eta_i / 2\lambda^2 \approx 1.56$.

6.6 The Velocity-Compounded Impulse Turbine or Curtis Turbine

Velocity compounding means that steam from the nozzles is used in several rotor blade rows, without pressure drop in the components downstream of the nozzles. Figure 6.13 illustrates the principle. Having worked in a first blade row, steam is

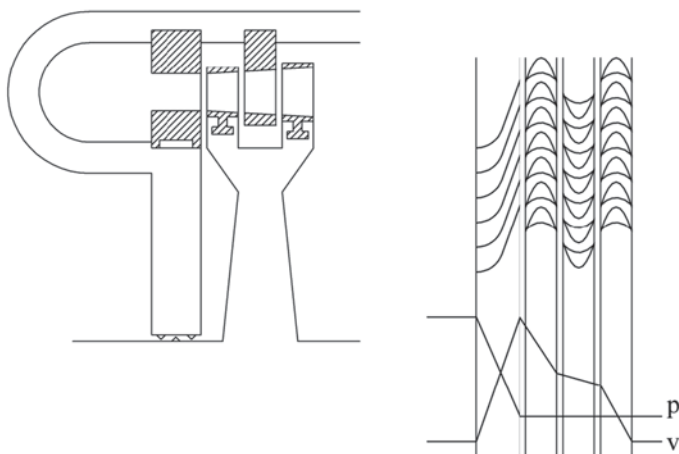


Fig. 6.13 Velocity compounding: Curtis turbine

turned by stator vanes without any pressure drop, so that it can be supplied to a second blade row running in the same sense as the first one. Therefore, the two rotor blade rows can be mounted together on the same wheel. The kinetic energy from the nozzles is reduced in two partial stages. This explains the term velocity compounding. This turbine type was patented in 1895 by C.G. Curtis.

Figure 6.14 represents the velocity triangles. The velocity component v_{1u} must be about 4 times as big as the blade speed u to make the flow kinematically possible. For the same reasons as with the Laval turbine, rotor blades and inverting stator vanes must be symmetrical.

The tangential outlet velocity of the first rotor blade row is

$$v_{2u} = w_{2u} + u = -\phi_{r1}(v_{1u} - u) + u.$$

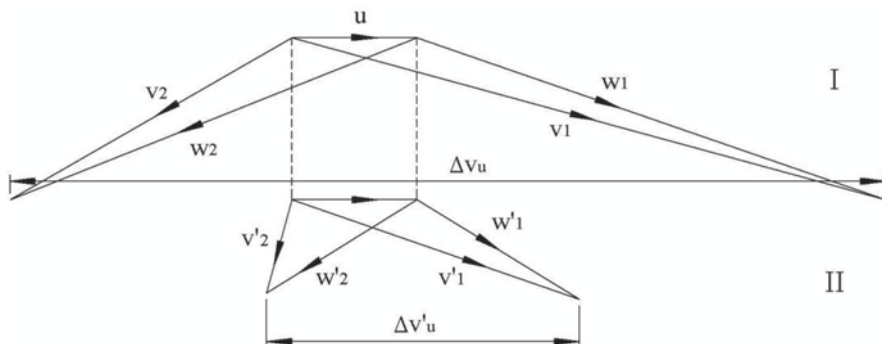


Fig. 6.14 Velocity triangles with a Curtis turbine

The work in the first rotor blade row is

$$\Delta W_1 = u(v_{1u} - v_{2u}) = (1 + \phi_{r1}) u(v_{1u} - u).$$

The tangential inlet velocity of the second rotor blade row is

$$v'_{1u} = -\phi_{inv} v_{2u} = \phi_{inv} [\phi_{r1} (v_{1u} - u) - u].$$

The work in the second rotor blade row is

$$\Delta W_2 = (1 + \phi_{r2}) u(v'_{1u} - u).$$

The total work is

$$\Delta W = (1 + \phi_{r1}) u(v_{1u} - u) + (1 + \phi_{r2}) u(\phi_{inv} \phi_{r1} v_{1u} - \phi_{inv} \phi_{r1} u - \phi_{inv} u - u).$$

With assumed equal velocity coefficients, this expression is reduced to

$$\Delta W = (1 + \phi) u[(1 + \phi^2) v_{1u} - (\phi^2 + \phi + 2) u].$$

With constant ϕ , the work variation is, as with the Laval stage, parabolic in u . Maximum work is attained for

$$u = \frac{1 + \phi^2}{2(\phi^2 + \phi + 2)} v_{1u} = \frac{1 + \phi^2}{2(\phi^2 + \phi + 2)} \phi_s \sin \alpha_1 v_s.$$

With $\alpha_1 = 75^\circ$, $\phi_s = 0.965$ and $\phi = 0.94$ follows $\lambda_o \approx 0.230$

$$\text{and } (\eta_i)_o = \frac{\Delta W_o}{v_s^2 / 2} = 2(1 + \phi) \lambda_o \left[\frac{1 + \phi^2}{2} \phi_s \sin \alpha_1 \right] \approx 0.785.$$

The corresponding work coefficient is $\psi_o = \frac{\Delta W}{u^2} = \frac{\eta_i}{2\lambda_o^2} \approx 7.40$.

The optimum speed ratio of the Curtis stage is thus about half of that of the Laval stage (0.230 against 0.466). The work coefficient is about 3.8 times as big (7.40 against 1.95). The foregoing derivations may be refined by calculating the velocity coefficients depending on the turnings in the blade rows. This affects details of the results obtained, but not the overall conclusion. The efficiency of a Curtis stage is lower than that of a Laval stage, basically because the conversion of the nozzle kinetic energy causes three losses, respectively in the first rotor blade row,

the inverting stator vane row and the second rotor blade row. Rotor work is about 4 times higher than with the Laval stage. The Curtis principle can be extended to 3 and more rotor blade rows. For $\alpha_I = 90^\circ$ and taking no losses into account, the following relations are optimal:

$$\text{Laval: } v_{Iu}/u = 2, \psi = 2, \lambda_o = 1/2.$$

$$\text{Curtis 2: } v_{Iu}/u = 4, v'_{Iu}/u = -v_{2u}/u = 2, \psi = 6 + 2 = 8, \lambda_o = 1/4.$$

$$\begin{aligned} \text{Curtis 3: } v_{Iu}/u &= 6, v'_{Iu}/u = -v_{2u}/u = 4, \\ v''_{Iu}/u &= -v'_{2u}/u = 2, \psi = 10 + 6 + 2 = 18, \lambda_o = 1/6. \end{aligned}$$

Curtis stages with three rotor blade rows have never been used in practice, because the efficiency is even much lower than with two rotor blade rows. We will discuss the application of a Curtis stage with two rotor blade rows in Sect. 6.8.2, but Curtis stages are only very exceptionally applied in modern machines.

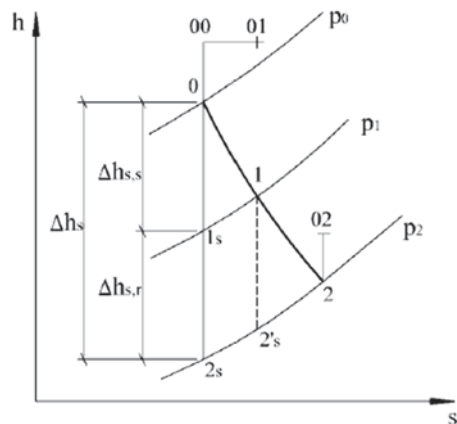
6.7 The Reaction Turbine

6.7.1 Degree of Reaction

Figure 6.15 represents the h-s diagram of a turbine stage with a degree of reaction around 50%. The degree of reaction we used until now is defined by

$$R = \frac{h_1 - h_2}{h_{01} - h_{02}}, \quad (6.15)$$

Fig. 6.15 h-s diagram of a reaction turbine



with

$$h_1 - h_2 = \frac{w_2^2}{2} - \frac{w_1^2}{2},$$

and

$$h_{01} - h_{02} = u(v_{1u} - v_{2u}) = u(w_{1u} - w_{2u}).$$

With an assumed constant axial velocity (approximately met), it follows that

$$R = \frac{w_{2u}^2 - w_{1u}^2}{2u(w_{1u} - w_{2u})} = -\frac{w_{2u} + w_{1u}}{2u} = -\frac{w_{mu}}{u}.$$

This degree of reaction can thus be expressed as a function of the velocity components and is therefore named the *kinematic degree of reaction*.

There is a second definition of the degree of reaction, called *thermodynamic degree of reaction*, expressed with static enthalpy drops on the isentropic process:

$$R_s = \frac{\Delta h_{s,r}}{\Delta h_s} = \frac{\Delta h_{s,r}}{\Delta h_{s,s} + \Delta h_{s,r}}. \quad (6.16)$$

The two definitions of degree of reaction are equal for a repeating stage with lossless flow. With losses and with degrees of reaction not near to 0 or 1, $R \approx R_s$. For degrees of reaction near 0 or 1 the difference is more significant. For instance, $R_s = 0$ but $R < 0$ for a stage with constant pressure in the rotor. We will also use the term *isentropic degree of reaction* to refer to R_s . The reason for using definition (Eq. 6.16) is the same as with fans (definition of the pressure degree of reaction): precise determination of the kinematic degree of reaction is not possible in practise due to typically rather large errors with temperature measurements.

6.7.2 Efficiency

Figure 6.16 represents velocity triangles for 50% degree of reaction.

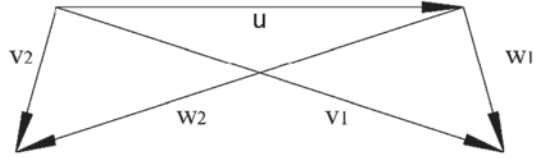
According to Fig. 6.15, the following applies for the stator blades with a repeating stage, using isentropic efficiency:

$$\begin{aligned} \frac{v_1^2}{2} &= \eta_{ss} \left[\frac{v_2^2}{2} + (1 - R_s) \Delta h_s \right], \\ \frac{v_{1u}^2}{2} + \frac{v_a^2}{2} &= \eta_{ss} \left[\frac{v_{2u}^2}{2} + \frac{v_a^2}{2} + (1 - R_s) \Delta h_s \right], \\ v_{1u} &= \sqrt{\eta_{ss} [v_{2u}^2 + v_a^2 + (1 - R_s) v_s^2] - v_a^2}. \end{aligned} \quad (6.17)$$

It is obvious that the positive root should be chosen.

$$w_{1u} = v_{1u} - u$$

Fig. 6.16 Velocity triangles for a turbine with degree of reaction of 50% ($R=0.50$, $\psi=1.20$; ψ is larger than the value $\psi=0.95$ for optimum efficiency)



$$w_{1u} = v_{1u} - u.$$

Ignoring the enthalpy increase by the divergence of the isobars, it applies that:

$$\begin{aligned} \frac{w_2^2}{2} &= \eta_{sr} \left[\frac{w_1^2}{2} + R_s \Delta h_s \right], \\ w_{2u} &= -\sqrt{\eta_{sr} (w_{1u}^2 + v_a^2 + R_s v_s^2) - v_a^2}. \end{aligned} \quad (6.18)$$

The negative root should be chosen in this case.

$$v_{2u} = w_{2u} + u, \quad \eta_i = \frac{2u(v_{1u} - v_{2u})}{v_s^2}.$$

Iterative determination of the velocity components relative to v_s , with given R_s and λ , is quite simple. We take $\alpha_I = 72^\circ$ as an example. We start iterations with $v_{2u} = 0$, $\eta_{ss} = 1$, $\eta_{sr} = 1$. After a first calculation, we determine the flow angles and the loss coefficients with Soderberg's formula. Stator and rotor efficiency follow from $\eta_{ss} = 1/(1 + \xi_s)$, $\eta_{sr} = 1/(1 + \xi_r)$. Table 6.2 represents the results for $R_s = 0, 0.25, 0.50$ and 0.75 .

Values in bold in Table 6.2 are those with optimum internal efficiency and with a lower speed ratio corresponding to one and a half percentage points lower efficiency. Maximum efficiency is obtained with $R_s = 0.5$. The reason is that the velocity triangles then are symmetrical with each other, as can be derived from Fig. 6.16. Losses are quadratic in the outlet velocities of rotor and stator, which leads to minimum sum of losses with symmetrical velocity triangles. As from the former analysis for $R_s = 0$, we observe that the speed ratio can be decreased substantially compared to the optimum, without great loss of internal efficiency. The number of stages is lower at a lower speed ratio. Turbines with degree of reaction significantly above zero are constructed as drum turbines (see the later Figs. 6.20 and 6.21). But even with drum turbines, wheel friction loss is lower with fewer stages: shorter rotor, less friction surface in between stages. So, optimum overall efficiency is reached at a lower speed ratio than at optimum internal efficiency. As an estimate for the optimum, we can adopt once more a decrease of internal efficiency with one and a half points. The global results from Table 6.2 are summarised in Table 6.3. Also shown is the performance at $\lambda = 0.60$ and for axial inlet and outlet. Note that the results for $R_s = 0$ do not accord completely with those in Table 6.1. Stator angles are slightly different and axial velocity is constant in the present analysis. The blade is thus non-symmetrical.

Table 6.2 Internal efficiency as a function of speed ratio with varying degree of reaction; $a = v_{Iu} / v_s$, $b = v_{2u} / v_s$ (Soderberg correlation $AR=4$; $\alpha_I = 72^\circ$)

$R_s=0.0$				$R_s=0.25$			
λ	η	a	b	λ	η	a	b
0.40	0.8605	0.959	-0.117	0.50	0.8898	0.830	-0.060
0.45	0.8836	0.960	-0.022	0.55	0.9042	0.834	0.012
0.50	0.9006	0.968	0.068	0.60	0.9149	0.841	0.079
0.53	0.9080	0.975	0.119	0.62	0.9182	0.845	0.104
0.60	0.9184	0.998	0.233	0.65	0.9223	0.852	0.142
0.65	0.9218	1.019	0.310	0.70	0.9371	0.865	0.203
0.70	0.9232	1.044	0.385	0.75	0.9301	0.880	0.260
0.72	0.9232	1.055	0.414	0.80	0.9318	0.898	0.312
0.75	0.9230	1.072	0.456	0.87	0.9325	0.926	0.390
0.80	0.9217	1.102	0.526	0.90	0.9324	0.939	0.421
0.90	0.9166	1.169	0.659	1.00	0.9303	0.986	0.521
$R_s=0.50$				$R_s=0.75$			
λ	η	a	b	λ	η	a	b
0.60	0.9070	0.678	-0.078	0.60	0.9150	0.519	-0.244
0.65	0.9187	0.678	-0.028	0.64	0.9220	0.508	-0.212
0.70	0.9280	0.681	0.019	0.70	0.9284	0.495	-0.168
0.75	0.9348	0.687	0.063	0.75	0.9316	0.488	-0.134
0.80	0.9393	0.694	0.106	0.80	0.9338	0.483	-0.101
0.85	0.9418	0.702	0.148	0.85	0.9354	0.480	-0.070
0.90	0.9428	0.712	0.188	0.90	0.9364	0.479	-0.041
0.94	0.9430	0.721	0.219	0.95	0.9369	0.480	-0.013
1.00	0.9423	0.736	0.264	0.97	0.9369	0.481	-0.002
1.05	0.9411	0.749	0.301	1.05	0.9361	0.485	0.039
1.10	0.9396	0.764	0.336	1.10	0.9348	0.488	0.063

Table 6.3 Internal efficiency with varying degree of reaction

R_s	$\lambda_o (-1.5\%)$	η_o	b_o	$\eta (\lambda=0.60)$	$\lambda (b=0)$	$\eta (b=0)$
0	0.53	0.908	0.119	0.918	0.46	0.888
0.25	0.62	0.918	0.104	0.915	0.54	0.902
0.50	0.70	0.928	0.019	0.907	0.68	0.925
0.75	0.64	0.922	-0.212	0.915	0.97	0.937

Conclusions are:

- Optimum overall efficiency is reached with $R_s=0.5$ and the corresponding speed ratio $\lambda \approx 0.70$. Inlet and outlet flow are very near to the axial direction.
- For a somewhat lower speed ratio, as $\lambda=0.60$, internal efficiency is at its lowest at $R_s=0.5$. This shows that the optimum in the efficiency variation is very weak.
- With axial inlet and outlet, optimum speed ratio increases with the degree of reaction.

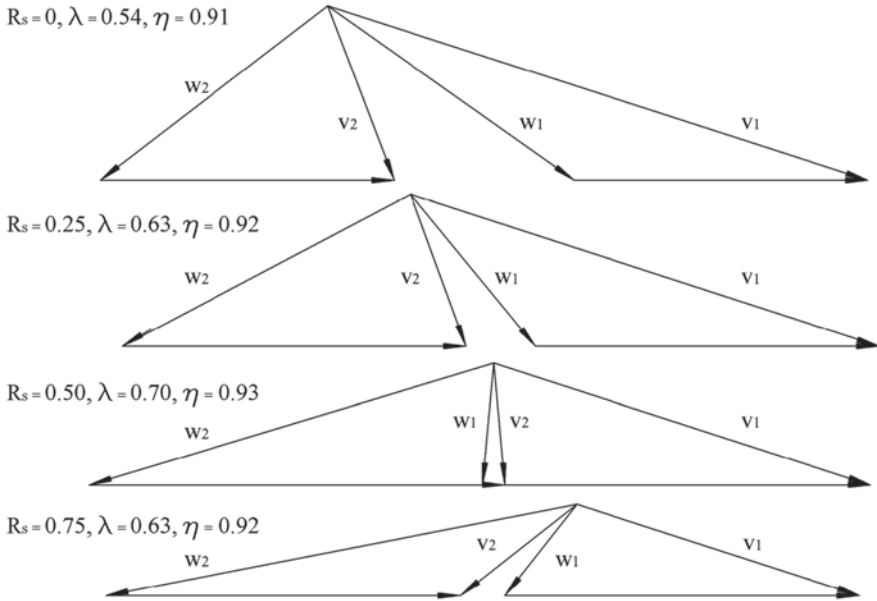


Fig. 6.17 Velocity triangles with optimum efficiency ($\alpha_I = 72^\circ$)

Velocity triangles at maximum overall efficiency (optimum internal efficiency -1.5%) are sketched in Fig. 6.17 (drawn for the same value of v_s). The maximum efficiency depends only very weakly on the degree of reaction, but the shape of the rotor blades depends very strongly on the degree of reaction. The highest efficiency is reached with $R_s = 0.50$, however. The corresponding work coefficient $\psi = (\eta_i / 2\lambda^2) \approx 0.95$ and at optimum, the inlet and outlet velocities of the stage are near to axial. This is very convenient, as it enables a turbine without special first and last stages. The internal efficiency is lower with a lower degree of reaction, but the corresponding work coefficient is higher. This results in fewer stages, causing smaller wheel friction loss. Leakage is also smaller with a low degree of reaction when the machine is made as a disc turbine, as shown in Fig. 6.11 (but disc friction with a disc turbine is higher than with a drum type). The main part of the pressure drop occurs in the stator. By mounting stator blades in diaphragms, the leakage surface in the stator can be reduced. A degree of reaction above zero requires sealing at the tip of the rotor blades (Fig. 6.11 represents an impulse turbine). We discuss rotor tip sealing in Sect. 6.8.1. Disc friction and leakage make that the overall efficiency with low degree of reaction is not always lower than with 50% degree of reaction (see Sect. 6.8.1). Figure 6.18 presents the velocity triangles with axial inlet and outlet. At low degree of reaction, there is a small efficiency loss compared to the optimum as with the triangles in Fig. 6.17.

The foregoing results have historically led to two radically different design options. For some applications, manufacturers choose for $R_s = 0.50$ and accompanying $\lambda = 0.7$ ($\psi = 0.95$). This option is made for maximum efficiency and axial inlet and

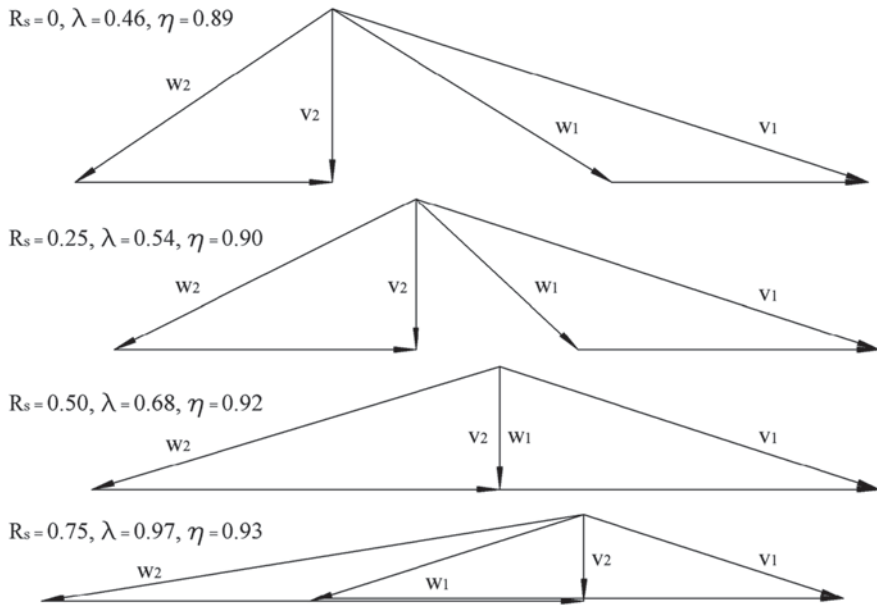


Fig. 6.18 Velocity triangles with axial inlet and outlet ($\alpha_1 = 72^\circ$)

outlet flow. For other applications, the choice is a low degree of reaction, namely $R_s \approx 0.10$ – 0.15 and corresponding $\lambda \approx 0.57$ ($\psi \approx 1.40$). In principle, such a turbine yields a somewhat lower efficiency (about one percentage point), but it can be designed with fewer stages than a turbine with $R_s = 0.50$. The types are denoted with the names *reaction turbine* and *impulse turbine*. The term reaction turbine implies a degree of reaction around 50%. The term impulse turbine implies zero degree of reaction or a low degree of reaction $R_s = 0.10$ – 0.15 . As discussed earlier, the blade shape is disadvantageous with $R_s = 0$ (Figs. 6.9 and 6.10), even if rounding of the leading edge is possible. With a degree of reaction somewhat above zero, the rotor blade becomes asymmetrical and creation of a leading edge stagnation region increases its load capacity. In modern reaction type turbines, the degree of reaction is not exactly 50% at the mean radius. Modern optimisation methods are numerical. The degree of reaction is a parameter that is optimised. It varies somewhat from stage to stage and varies also with the radius in a given stage. Moreover, blade shapes are three-dimensional (see Sect. 6.9)

6.7.3 Axial Inlet and Outlet

From the foregoing analysis follows that the inlet and outlet flows of an optimised stage are near to the axial direction. A priori assumption of axial outlet velocity enables a very simple analysis of the axial turbine.

Rotor work is then $\Delta W = u(v_{1u} - v_{2u}) = uv_{1u}$.

The kinematic degree of reaction is

$$R = \frac{\frac{1}{2}w_2^2 - \frac{1}{2}w_1^2}{\Delta W} \quad \text{or} \quad 1 - R = \frac{\frac{1}{2}v_1^2 - \frac{1}{2}v_2^2}{\Delta W}.$$

With axial outlet and constant axial velocity through the rotor is $v_2 = v_{1a}$, so that

$$1 - R = \frac{v_{1u}^2}{2uv_{1u}} \quad \text{or} \quad R = 1 - \frac{1}{2} \frac{v_{1u}}{u}. \quad (6.19)$$

The work coefficient is

$$\psi = \frac{\Delta W}{u^2} = \frac{v_{1u}}{u}. \quad (6.20)$$

Expressions (Eqs. 6.19 and 6.20) are similar to the expressions obtained with the analysis of a radial fan in Chap. 3. Assumptions for the fan were: inlet velocity in the meridional plane and constant meridional component of the velocity in the rotor. The assumptions are similar here. From (Eqs. 6.19 and 6.20) it follows

$$\psi = 2(1 - R). \quad (6.21)$$

So, a low degree of reaction corresponds to a high work coefficient and vice versa. For $R=0$ is $\psi=2$. For $R=0.5$ is $\psi=1$. For $R=1$ becomes $\psi=0$.

Further it follows $\lambda^2 = \frac{u^2}{2\Delta h_s} = \frac{\eta_i}{2\psi}$,

$$\text{or, with } \eta_i \approx 0.92: \quad \lambda = \frac{\sqrt{\eta_i} / 2}{\sqrt{1 - R}} \approx \frac{0.48}{\sqrt{1 - R}}. \quad (6.22)$$

This expression approximately reproduces the results shown in Fig. 6.18:

$R=0$, $\lambda=0.48$; $R=0.25$, $\lambda=0.55$; $R=0.50$, $\lambda=0.68$; $R=0.75$, $\lambda=0.96$.

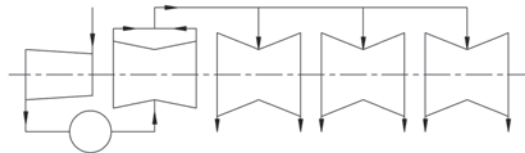


Fig. 6.19 Possible lay-out of a large steam turbine for a coal-fired power station: one single flow HP, one double-flow IP part and three double-flow LP parts (*some machines have two LP parts*); reheat between HP and IP parts

6.8 Steam Turbine Construction Forms

6.8.1 Large Steam Turbines for Power Stations

Figure 6.19 sketches the lay-out of a steam turbine in the 1000 MW order for typical steam conditions 250 bar/565 °C/565 °C for use in coal-fired power stations. The machine has 5 parts: a high-pressure part (HP), an intermediate-pressure part (IP) and 3 low-pressure parts (LP). The high-pressure part has a single flow. There is a reheat after the HP part. The intermediate part and each low-pressure part have two flows. Multiplication of the number of flows as the expansion advances is necessary, because of the strong decrease of steam density.

Figures 6.20 and 6.21 show longitudinal sections of HP and IP parts of reaction type (degree of reaction around 50%). An example of an LP part is shown later (Fig. 6.27). Note the steam extractions (the outlet of the IP part is not visible). The parts have a double casing. The inner casing encompasses two halves with a horizontal split. The parts of the inner casing are joined by shrink rings with the HP turbine. This is a traditional method that is less chosen at present, because of the time-consuming assembling and disassembling with inductive heating for expansion of the shrink rings. The inner and outer casings of the IP turbine have horizontal splits as well, but parts are joined by bolts (not visible in the figure; see the later Fig. 6.28). Figure 6.22 represents an inner casing with shrink rings.

Fig. 6.20 HP part of a large steam turbine. (Courtesy Alstom)

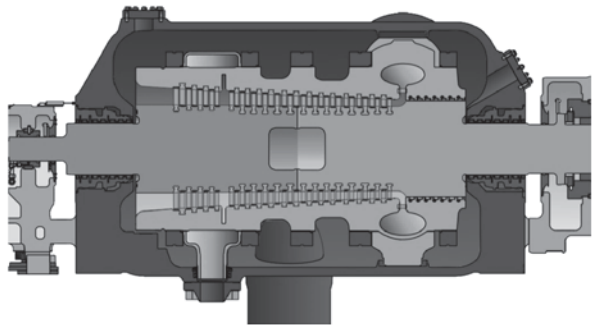


Fig. 6.21 IP part of a large steam turbine. (Courtesy Alstom)

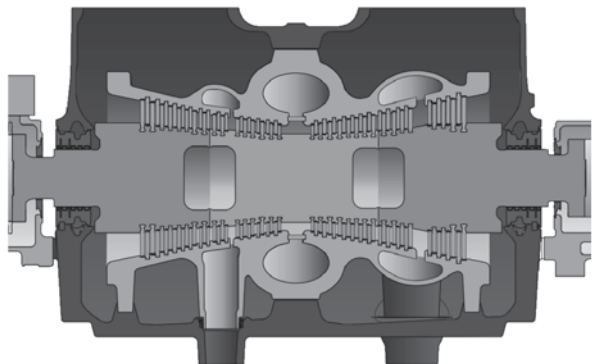


Fig. 6.22 Inner casing of a HP part with *shrink rings*. (Courtesy Alstom)

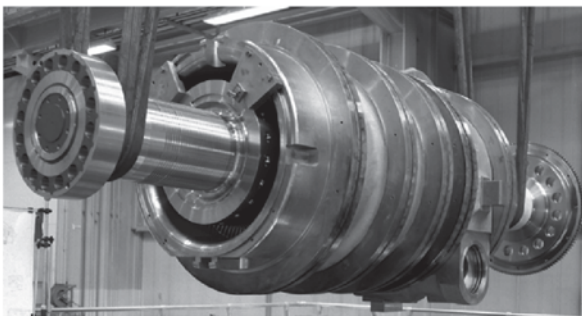


Fig. 6.23 Inner casing of a HP part with *countersunk bolts* and outer casing of *barrel type*. (Courtesy Siemens Energy)

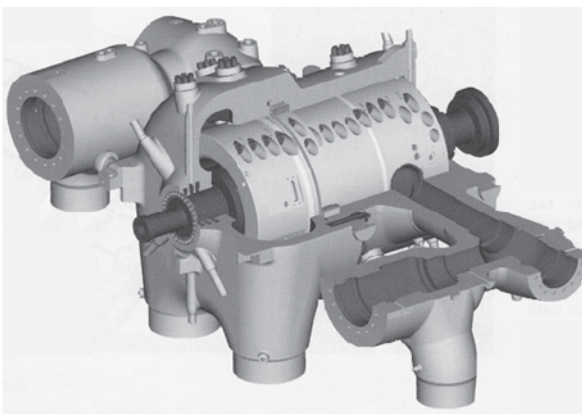


Figure 6.23 shows a build with the two inner casing halves joined by countersunk bolts. With the first form, the outer casing has a horizontal split. The outer casing with the second form is a so-called barrel type. It encompasses two parts joined with a radial split. Both builds aim at a minimal outer casing size. An inner casing with a horizontal split, used with an HP part as well (see further: Fig. 6.28) and customary with an IP part, requires some more space because of the bolt heads.

The double casing construction with HP and IP parts is meant to bring the outlet pressure between the two casings. This does not reduce the pressure difference between the inside and the outside of the machine, but replacing a very thick shell by two thinner ones is advantageous as regards to thermal stresses. These are the stresses due to unequal heating, especially delicate during starting and stopping of the turbine. As regards strength of the outer casing of the HP section, it is important to limit the casing dimensions. Stator casings are manufactured from high-grade steels. An HP inner casing is customarily made of a 12% Cr and 1–1.5% Mo cast steel. Critical outer casing parts and the central rotor part are made of this steel as well. Other parts of the outer casing and the rotor are manufactured from cast steel with less Cr, typically 10%. The casings are cast. HP and IP rotor parts are traditionally forged from an ingot and joined by welding, as on Figs. 6.20 and 6.21. The modern tendency is to compose the rotor from more parts. The construction of these parts is then easier, but there are more welds.

With reaction blading, there is an axial force on the rotor in the through-flow sense. In the double-flow parts of Fig. 6.19, the axial forces in the opposite flow senses balance each other. With the single flow HP part, the axial force is balanced by an equilibrium piston. This is the cylindrical part at the right-hand side of the rotor of Fig. 6.20, sealed at its periphery with labyrinth combs. The steam pressure after the first stator row is at one side and the pressure at the outlet of the HP part at the other side (the equilibrium piston is also visible in Fig. 6.29).

With HP and IP turbines, blades are mounted into tangential slots. With LP parts, tangential slots are applied for the first stages and axial slots for the last ones (see further, Fig. 6.27). Figure 6.24 represents tangential slot mounting. Rotor blades have a so-called hammer root. A cavity is required for mounting the blade roots into the tangential slots. It is filled afterwards with a bolted metal piece. Mounting of stator vanes does not require roots, as represented in Fig. 6.24, but there are variants where roots are applied to stator vanes. Figure 6.24 also shows that blades and vanes may be shrouded with cover bands fitting to labyrinth combs. There are variants with combs on the cover bands and with smooth casing or smooth rotor parts. Mostly, cover bands are formed by blade heads, as shown in Fig. 6.25. The rotor blades represented in Fig. 6.25 (right) have so-called fir tree roots.

Figure 6.26 shows the rotor of a combined HP-IP part of a large steam turbine of impulse type of the 1000–1500 MW order for use in nuclear power stations. In the example, the HP side of the combined part has 9 stages and the IP part has 4 stages (flows in opposite sense). Depending on the power, the turbine may have two LP parts (1000 MW order) or 3 LP parts (1500 MW order). An LP rotor is shown in Fig. 6.27. Steam conditions with a nuclear power station are significantly lower than with a coal-fired plant. The values of Chooz-B (France) are 71 bar, 287 °C at HP inlet (saturated steam); 10.1 bar, 268 °C at IP part inlet (superheated) and 3.3 bar at LP part inlet. There is moisture separation and reheat between the HP and IP parts. Because of the rather low supply pressure, the HP-IP part can be made with a single casing. Blades are quite long in the HP-IP part. This comes from the necessity for a large flow rate, as the enthalpy drop of the steam over the entire turbine is rather low. So, big through-flow areas are necessary. The tip diameter of the last stage may be as big as 6 m. Therefore, turbines in nuclear power stations run at

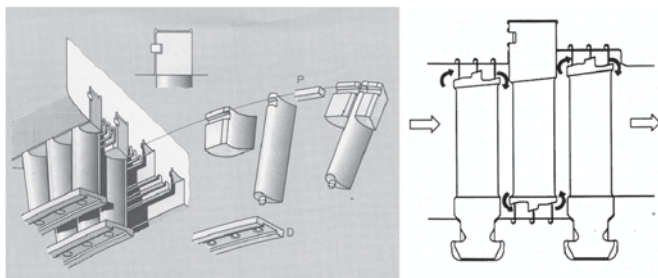


Fig. 6.24 Rotor and stator blade mounting in tangential slots. (*Left*: courtesy Alstom; *right*: from Havakechian and Greim 1999; permission by SAGE Publications)

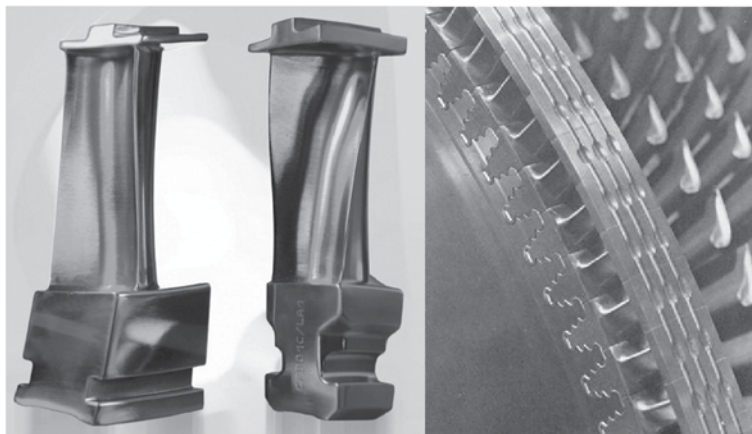
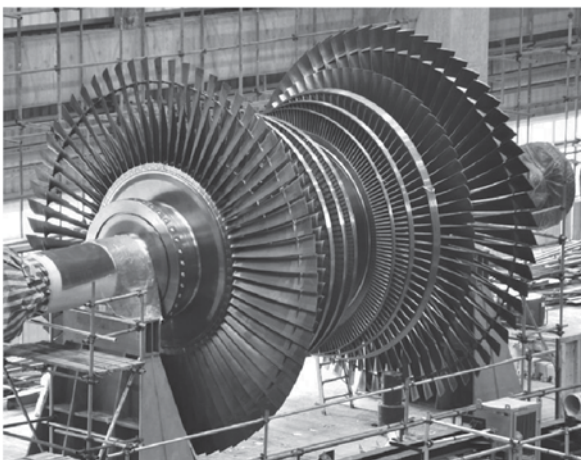


Fig. 6.25 *Left: IP part stator vane (shown upside down) and rotor blade with integrated cover bands and tangential mounting as on Fig. 6.24; right: rotor blades with integrated cover band and axial slot mounting on the wheel of an impulse type first stage. (Courtesy Alstom)*

Fig. 6.26 Rotor of the combined HP-IP part of a large impulse type steam turbine. (Courtesy Alstom)



Fig. 6.27 Rotor of the LP part of a large steam turbine. (Courtesy Alstom)



so-called half speed: 1500 rpm in a 50 Hz system. Rotor rows in the HP-IP part have cover bands, composed by blade heads. In the HP-IP part, the degree of reaction is very low at the hub, but it increases towards the periphery (Sect. 6.9.2 discusses the increase of the degree of reaction with radius). So, saying that the HP and IP parts are of impulse type means that the degree of reaction is very low at the hub, but the degree of reaction is not very low on the average radius. In the LP-parts of the turbine, the degree of reaction is also low at the hub, but it is near to 90% at the casing in the last stage (see Exercise 6.10.5).

The LP part of Fig. 6.27 is from a steam turbine of a nuclear power plant. The general appearance of an LP part of a coal-fired plant is similar, but the diameters are smaller and the rotational speed is 3000 rpm in a 50 Hz system. In the last stage of the LP turbine in Fig. 6.27, rotor blades have reinforcing elements, touching each other (so-called snubbers). These elements are intended to increase the stiffness of the rotor (higher eigenfrequencies), but cause aerodynamic losses. The snubbers are necessary in the example because the blades are very long. Last stage blades in LP parts of coal-fired power stations are shorter and made with large chord at the root, making reinforcements unnecessary. The last two LP part stages have no cover bands. The blades are very long. Thus, the clearance between the rotor and the casing is, relatively seen, very small. Clearance loss is relatively low. Moreover, cover bands cannot be applied to the last stages for reasons of strength. The blade tip speed is at the highest level there. A cover band would unacceptably contribute to the centrifugal force. In the example shown, the blade speed at the circumference of the last stage is about 530 m/s. Rotors in the LP part of steam turbines for a nuclear power station may be made by discs shrunk on a shaft (1500 rpm in a 50 Hz system). With coal-fired plants, the construction is typically by welding forged parts, as for HP and IP parts (3000 rpm in a 50 Hz system). Casings are made from welded steel plates. Blades are mounted with axial slots in disc type rotors. With the drum type rotor of Fig. 6.27, the blades of the first four stages are mounted with tangential slots. The slots are axial with the last two stages (curved for the last stage).

Figure 6.28 represents the impulse type VHP module (very high pressure) of a large steam turbine for a coal-fired power station with ultra-supercritical steam conditions. The machine has two reheats. Steam conditions are 285 bar and 580°C/580°C/580°C. The machine has a very-high-pressure part (VHP), a high-pressure part combined with an intermediate-pressure part, a double-flow intermediate-pressure part and two LP parts, each with two flows. In the VHP part, steam expands from 285 to 78 bar. The VHP section has an inner and an outer casing, both with horizontal splits. The figure shows the nozzles incorporated in diaphragms. At low degree of reaction, pressure drop occurs for the largest part across the stator. It is then advantageous to reduce the diameter of the hub sealing of the stator vane ring. For very high steam density, lower clearance losses may compensate the intrinsically somewhat lower internal efficiency, compared to reaction stages. As a result, the overall efficiency of an impulse type turbine part may even be higher for high steam density.

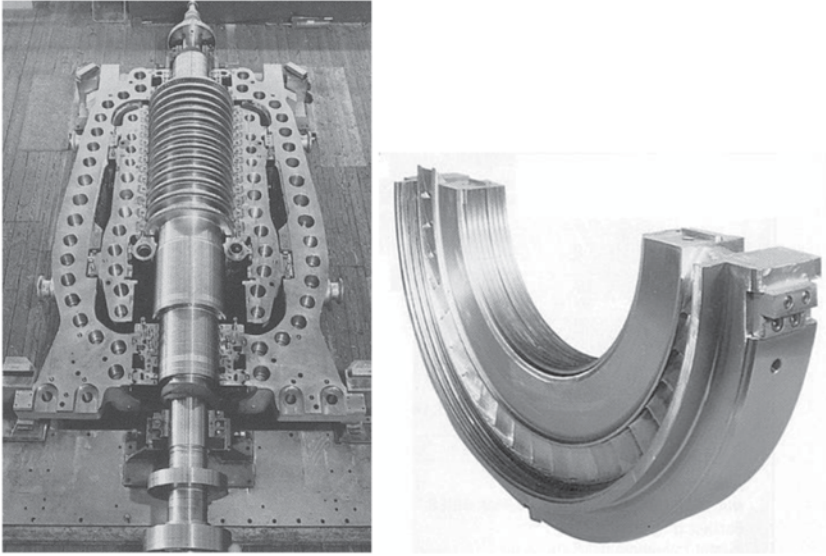


Fig. 6.28 Impulse type VHP part of a large steam turbine for an ultra-supercritical coal-fired power station; nozzle diaphragm. (Courtesy Alstom)

6.8.2 Industrial Steam Turbines

Figure 6.29 represents an industrial condenser turbine of reaction type, with steam extractions. Variants exist with backpressure. The turbine shown has an equilibrium piston at the left-hand side in the figure. Such turbines are single-casing machines with power ranging from as low as 100 kW (single-stage; low admission pressure) to around 250 MW with admission pressure up to about 150 bar. Applications are mechanical drive of turbo-compressors (natural gas pipelines) and large pumps

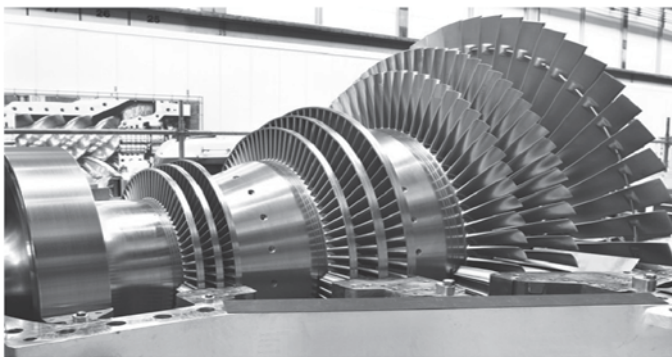


Fig. 6.29 Industrial steam turbine of reaction type; equilibrium piston on the *left-hand side*. (Courtesy MAN Diesel & Turbo)

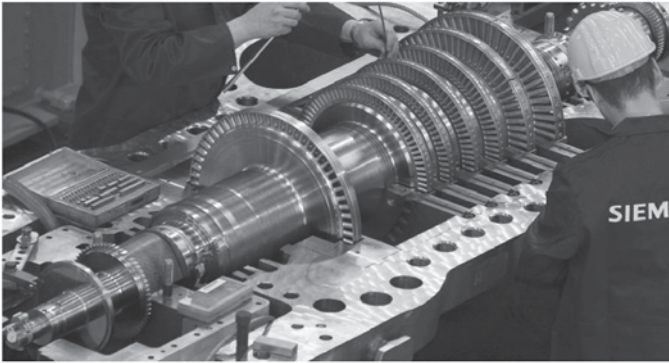


Fig. 6.30 Industrial steam turbine of impulse type. (Courtesy Siemens Energy)

(feed-water pumps in power plants) and combined steam-and-gas turbine power stations (as condenser turbines and for power of the 100–200 MW order).

Figure 6.30 represents a small industrial turbine of impulse type. The turbine has a first stage with partial admission. A partial-admission impulse type first stage also occurs with larger turbines. With a rather low turbine power and a rather high steam supply pressure, it is normally impossible to design the first stage with full admission. Blade height must be sufficient in order to reach acceptable efficiency of the flow through the rotor and the stator. At a low blade height, friction area is large compared to through-flow area. Especially the effect of the end boundary layers (on hub and shroud) becomes important. The most efficient flow with a turbine is obtained for a large aspect ratio: height-to-chord ratio. Customarily, blade heights are not made less than about 25 mm.

Partial admission, however, impairs stage efficiency. A windage flow originates from the centrifugal force in rotor channels without through-flow. This circulating flow consumes power. Further, flow is less efficient in flowed rotor channels, as there is a start-up and a run-out phenomenon. The windage flow also interferes with the outlet flow, reducing the efficiency of the outlet kinetic energy recovery in the next stage. All these losses imply that, mostly, full admission from the second stage is aimed at. This normally requires a diameter reduction to make the through-flow area sufficiently small, as in Fig. 6.30. In the second and further stages, the degree of reaction may then be kept low, as in Fig. 6.30, but it may also be around 50%. With all stages of impulse type, the axial force on the rotor is small. An equilibrium piston is then not necessary and a thrust bearing suffices.

With small power machines, full flow may stay impossible after a first impulse stage, even with a strong diameter reduction. Historically, a Curtis stage was then chosen as first stage. Since a Curtis stage produces four times as much work as a Laval stage at the same blade speed, a much higher pressure drop is possible. It becomes then easier to achieve full admission on the second and further stages. Nowadays, this possibility is not used anymore, because of the

lower efficiency of a Curtis stage compared to a Laval stage. Normally, it is more efficient to feed a steam turbine at a somewhat lower pressure. This reduces cycle efficiency, but allows higher turbine efficiency. The optimum of the product must be aimed at.

6.9 Blade Shaping

6.9.1 HP and IP Blades

Figure 6.31 sketches a cylindrical section of a stator vane row in the HP part of a steam turbine with subsonic outlet velocity, the pressure distribution on the vanes on the mean radius and the variation of the outlet angle along the height (angle to the tangential direction). The pressure distribution allows deducing that the outlet Mach number is about 0.5. The average outlet angle is 71° . The variation of the outlet angle follows from the presence of secondary flow. Secondary flow is defined as the flow caused by interaction between the core flow within the vane row and the boundary layers on the hub and casing end sides (the end walls). The core flow is called the primary flow (a precise definition is given in Chap. 13). Figure 6.32 illustrates the development of a passage vortex, in the same way as discussed in Chap. 2 for a curved duct. As the velocity in the core flow is larger than in the end

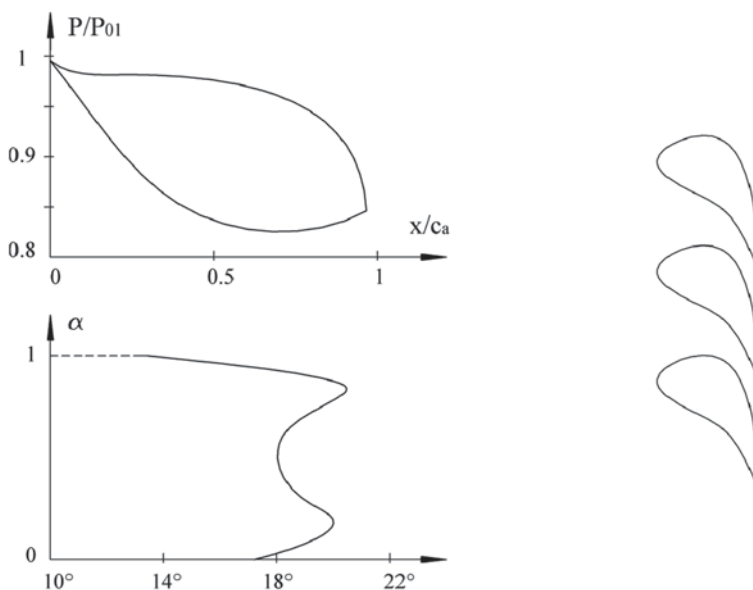


Fig. 6.31 Cross section of a stator cascade (*right*); mid-plane pressure distribution; outlet flow angle along the height. (Courtesy Siemens Energy)

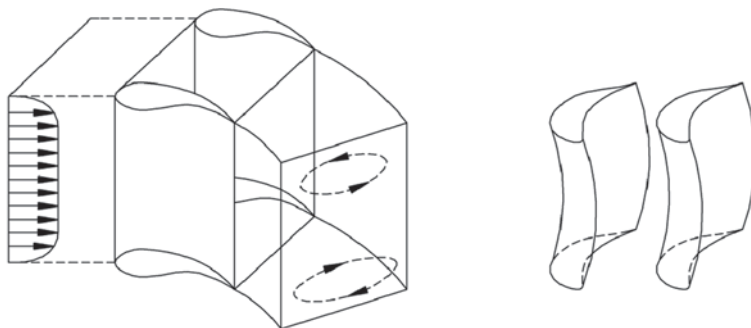


Fig. 6.32 Passage vortex generation; bowing of vanes (*or blades*) reducing profile loss in the end wall zones and intensity of the passage vortex

boundary layers, the centrifugal force by the flow turning is stronger. The difference in centrifugal force causes a double vortex flow, where the parts together are denominated the *passage vortex*. The interaction between the primary flow and the end wall boundary layers generates additional vortex structures, not represented in the figure. These will be discussed further in Chap. 13. The whole of these vortices is denominated *secondary flow* and the passage vortex is its main component. In the end wall boundary layers, the passage vortex pushes the through-flow more into the tangential direction and pushes it more into the axial direction just above the end wall boundary layers. The secondary flow causes outlet flow non-homogeneity. The flow homogenises downstream of the vane row with a corresponding mixing loss. With rather low-height vanes, as typical in the HP part of a steam turbine, and to a somewhat lower degree in the IP part, losses in the boundary layers on the end walls and losses due to the secondary flow cause a serious loss increase for the vane row.

The losses due to the presence of the end wall boundary layers are reduced by bending the vanes, as represented in Fig. 6.32. This bending is called *bowing*. In the end zones, the suction side is turned to the centre of the vane passage. The consequence is that a streamline in the end boundary layer, near the suction side of the vane, is pushed towards the centre of the passage at the vane row entrance. In principle, there is an inverse effect at the pressure side, but the displacement possibility of a streamline is limited there due to the acute angle of the vane. One expects that the streamline in the end boundary layer, near the suction side of the vane, which moves towards the centre of the passage at the vane row entrance, would return towards the end wall at the vane row exit. In reality this does not fully happen because the passage vortex is formed in approaching the exit plane of the vane row. The passage vortex hinders this return (see the rotation sense in Fig. 6.32). A first net effect is an increase of the acceleration at the suction side of the vane somewhat more to the centre of the blade passage and a reduction of it in the end zone. The consequence is decrease of the profile loading, and so the primary loss (the loss due to the boundary layers on the vane), in the end wall zone. This is beneficial, as the profile loss in the end wall zone is high. The consequence is also that the profile loading increases somewhat away from the end wall. This means that the profile

has to be adapted for this higher load. In principle, a somewhat larger chord is necessary, but change of the profile shape is also possible. A second net effect is that some mass flow is displaced from the end wall boundary layer towards the centre of the vane channel. By this shift, the intensity of the passage vortex diminishes and it spreads over a larger spanwise distance. So, the non-homogeneity of the outlet flow is lower and mixing losses downstream of the vane row decrease. From the foregoing arguments one understands that bowing may be beneficial, but it should not be too strong as by bowing, the flowed surface (so-called wetted area) increases and by the spanwise load variation vortices are formed in the wake of a vane (trailing vortices). It means that the actual optimisation of the bowing is quite delicate. Also, introducing bowing on a vane row changes the inflow conditions of the downstream blade row. So, the optimisation of a complete stage or even a number of stages has to be considered. Concave bending at the suction side is advantageous with rotor blades as well, for the same reasons as for stator vanes. For a discussion on the different loss mechanisms, we refer to the overview paper by Denton [2]. A recent experimental analysis of the effects of bowing in low aspect ratio turbine stages is by Rosic and Xu [8]. An example of the optimisation of a steam turbine HP stage is by Lampart and Hirt [5]. This last study shows that 3D shaping of HP and IP stages may lead to an efficiency gain, but the possible gain is rather limited, typically 0.5 percentage points with respect to the straight stacked blades and vanes. With the three-dimensional vane and blade shaping, the efficiency in steam turbine HP and IP parts reaches about 94 % and 96 %. Better efficiency is achieved within IP parts because of the lower effect of secondary losses.

6.9.2 LP Blades

The LP section of a large steam turbine is provided with long blades. Secondary losses therefore do not play an important role. The problem with LP blades is the large variation of the degree of reaction as a function of the blade height. Flow is very tangential at the stator outlet. This induces a strong centrifugal force in the space between stator and rotor, causing an important pressure gradient with high pressure at the casing and a low pressure at the hub. Flow is almost axial at the stator inlet and at the rotor outlet and there is no radial pressure gradient. The pressure gradient in between the stator and the rotor necessarily causes a high degree of reaction at the casing and a low one at the hub. The enthalpy drop over the stage should be approximately the same at all radii and thus the speed ratio increases from the hub to the casing. The consequence is a natural correspondence between the variation of the speed ratio and the variation of the degree of reaction, in the sense that the speed ratio does not differ much from the optimal value appropriate for the degree of reaction, as shown in Fig. 6.18. So, Fig. 6.18 represents the variation tendency of the velocity triangles from hub to casing, where typically $R_s \approx 0.15$ at the hub, and the degree of reaction increases with the radius. The longest blades nowadays achieve $R_s \approx 0.85$ at the casing. The maximum blade length amounts to about 1.20 m with a 2.00 m hub diameter (turbines at 3000 rpm: coal-fired) and

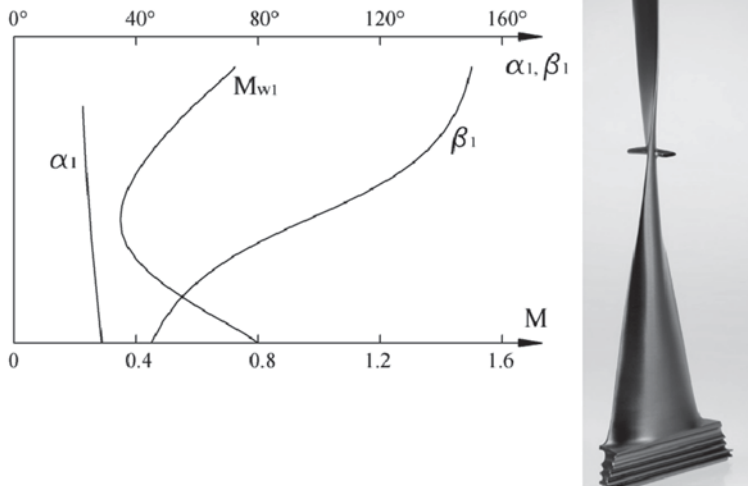


Fig. 6.33 Flow angles and Mach number for the final stage of an LP part of a large steam turbine with straight stacking of blade sections (*angles to tangential direction*); *right: rotor blade*. (Courtesy Alstom)

1.80 m with a 3.00 m hub diameter (turbines at 1500 rpm: nuclear). The triangles in Fig. 6.18 are drawn with a constant axial velocity in the rotor. In reality, axial velocity increases from inlet to outlet because of the density drop. At the stage outlet, the axial velocity is about constant over the radius. At the rotor inlet, the axial velocity is higher at the hub and smaller at the casing (for realistic triangles, see Fig. 6.38 in the exercise section). Figure 6.18 (also Fig. 6.38) demonstrates that the rotor blade profile strongly changes from hub to tip, with a strong turning at the root and a very weak one at the tip. Figure 6.33 sketches the variation of the flow angles at stator outlet and rotor inlet and the Mach number at rotor inlet for the final stage of a large steam turbine with straight stacked vanes and blades (data provided by Alstom). A rotor blade is also shown in Fig. 6.33.

The problem with very long blades is that the Mach number at rotor inlet is large at the hub and at the casing, and may approach unity. This generates shock waves (see fluid mechanics), with associated shock loss. Therefore, a final stage in an LP part is adapted in order to minimise shock loss. The other stages in the LP part and the stages in the HP and IP parts also show variation of the degree of reaction with the height. Therefore rotor blades are twisted (see Fig. 6.25). This variation does not cause high Mach number problems at the hub and the casing, however. There only arises a problem in the final stage of an LP section.

Three adaptations reduce the rotor inlet Mach number at the hub and the casing. The traditional one is setting the stator blade outlet more axial at the hub (opening the vanes) and setting it more tangential at the casing (closing the vanes). The

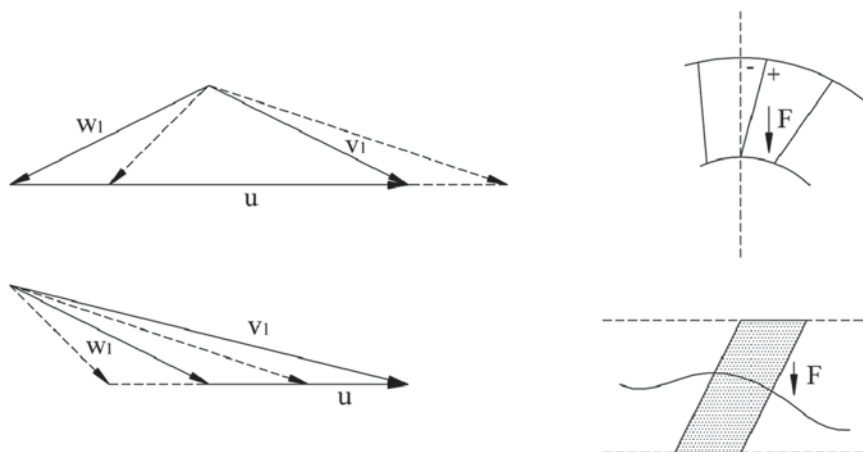


Fig. 6.34 Mach number reducing adaptations at the hub and the casing at rotor inlet: (1) opening of the nozzles at the hub and closing them at the casing, (2) lean within the orthogonal plane, generating pressure force toward the hub, (3) sweep within the meridional plane, generating pressure force toward the hub

changes in velocity triangles are demonstrated in Fig. 6.34 (left). The Mach number decrease of the relative flow at rotor inlet is obvious. The feasibility of this adaptation presumes an appropriate adjustment of the pressure distribution to the altered velocity distribution. This actually happens, but we do not prove this here (the study requires an analysis of radial equilibrium, which is discussed in Chap. 13). The vane angle adaptation decreases the variation of the degree of reaction from hub to casing. The flow rate increases near the hub and decreases near the casing. The stator outlet angle has a geometric limit, around 75° to the meridional plane. The adaptation thus inevitably causes a smaller stator angle at the hub than practically attainable and thus a smaller stage work than physically possible. Normally, this is no drawback, as the stator angle is not set at its maximum geometric value in order to allow a larger flow rate (see Fig. 6.33). A change in the variation of the degree of reaction may also be attained by exerting a radial force against the centrifugal force. Figure 6.34 (top, right) demonstrates that inclining the stator vanes within the orthogonal plane, denoted with *lean*, generates a radial force, directed inward, due to pressure differences between pressure and suction sides of the vanes. This can also be achieved by inclining within the meridional plane, denoted with *sweep* (Fig. 6.34, bottom, right). Sections more towards the casing get the expansion later, creating a higher pressure level on the same axial position. Combination of lean and sweep results in a rather complex 3D-shape of the stator vane, as shown in Fig. 6.35. For a recent example of optimisation of a steam turbine LP stage, we refer again to Lampart and Hirt [5]. The obtained improvement by 3D stacking with respect to straight stacking is more than 2.4%.

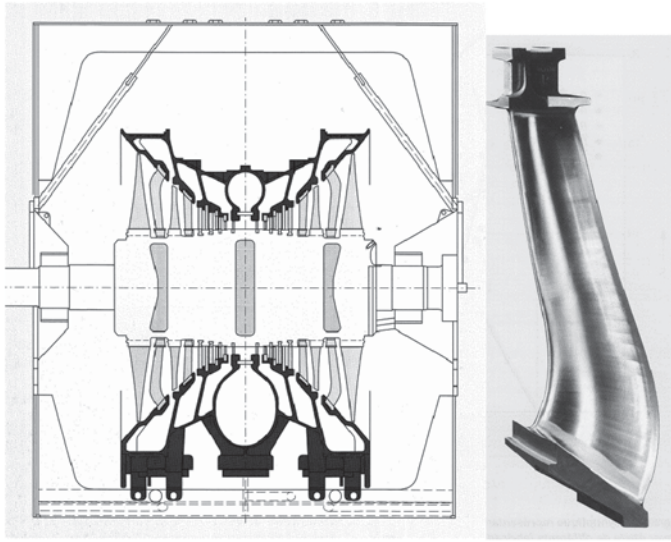


Fig. 6.35 3D-shape of the stator vane of the final stage in the LP part of a steam turbine. (Courtesy Alstom)

The adaptations discussed above are to a certain degree applied in all reaction stages, but not leading to such extreme shapes as in the last stage. The motivation is reducing the degree of reaction at the casing, which is advantageous for the reduction of leakage losses. Thanks to aerodynamic optimisation, the efficiency in the LP part of a turbine yields about 92 % for dry flow. In reality, condensation reduces the efficiency to about 90 %. The efficiency of an entire large steam turbine comes to about 92.5 % (HP 94 %, IP 96 %, LP 90 %).

6.10 Exercises

6.10.1. Compare the energy loss coefficient (Eq. 6.11) and the pressure loss coefficient (Eq. 6.12) applied to the expansion of air ($\gamma=1.4$) in a nozzle with infinitesimal efficiency 0.9 for varying outlet Mach number $M_1=0.25, 0.50, 1$ and 2. Ignore the kinetic energy at the inlet of the nozzle. Use the formulae of Chap. 4. Observe that the energy loss coefficient decreases weakly with increasing Mach number (the energy loss coefficient is linked to the isentropic efficiency: $\xi = 1/\eta_s - 1$ and $\xi_0 = 1 - \eta_s$) and that the pressure loss coefficient increases quite strongly with increasing Mach number. Remark that the Mach number influence on the pressure loss coefficient may be neutralised by using the logarithm of pressure instead of pressure (such a modified coefficient is then linked to the polytropic efficiency). Remark that the polytropic efficiency can be obtained in an experiment by measurement of the kinetic energy and calculation of the polytropic enthalpy

drop with formula (4.32). The polytropic exponent follows from fitting a polytropic pressure-temperature relation through the states at start and end of the process. A similar procedure can be used with a rotor or a stage when the work is determined by the Euler formula and measurement of velocity components.

6.10.2. In basic analysis of turbomachines, adiabatic flow is supposed, but a real flow is seldom perfectly adiabatic. The definitions of isentropic efficiency and loss coefficients are all based on adiabatic flow. Use of these notions is therefore often problematic in practise. Study the influence of heat transfer on the example of nozzle flow of an ideal gas with p_{00} and T_{00} as inlet conditions and p_1 as backpressure (the h-s diagram for adiabatic flow is Fig. 4.5). Assume distributed heat transfer proportional to the enthalpy drop according to $dq = \kappa(-dh)$, with constant κ , positive for heat addition to the nozzle and negative for heat removal. The equations for work and energy are (work is zero):

$$dW = d\frac{1}{2}v^2 + \frac{1}{\rho}dp + dq_{irr}, \text{ or } d\frac{1}{2}v^2 = -\frac{1}{\rho}dp - dq_{irr},$$

$$dW + dq = dh + d\frac{1}{2}v^2, \text{ or } d\frac{1}{2}v^2 = -dh + dq = (1 + \kappa)(-dh).$$

The work equation allows the introduction of the infinitesimal efficiency in the same way as with adiabatic flow: $d\frac{1}{2}v^2 = \eta_{\infty}(-\frac{1}{\rho}dp)$. With this relation substituted in the energy equation, it follows that, for ideal gas and constant values of heat capacity, η_{∞} and κ , the expansion process is polytropic with coefficient:

$$\frac{n}{n-1} = \frac{1+\kappa}{\eta_{\infty}} \frac{\gamma}{\gamma-1}.$$

Derive the formulae for generated kinetic energy, converted pressure energy, $-\Delta h_r$, and enthalpy drop $-\Delta h$, analogous to the formulae (4.30) and (4.32) for adiabatic flow. With constant coefficients, the following relations hold:

$$\frac{1}{2}v_1^2 = \eta_{\infty}(-\Delta h_r), \quad \frac{1}{2}v_1^2 = (1 + \kappa)(-\Delta h).$$

Thus, in an experiment, kinetic energy can be measured and η_{∞} and κ can be determined in average sense. Verify by comparison with adiabatic flow for $\kappa = 0.20$ and $\kappa = -0.20$, together with $\eta_{\infty} = 0.90$, that the generated kinetic energy is not much affected by heat transfer. Verify for pressure ratios $p_{00}/p_0 = 1.20, 1.50$ and 2 (A: the difference with adiabatic flow for pressure ratio 2 is $+1.45\%$ for $\kappa = 0.20$ and -2.13% for $\kappa = -0.20$). So, in an experiment, the measured kinetic energy may be taken as the value for adiabatic flow with only little error. But the measured value can be corrected to adiabatic flow with the determined values of η_{∞} and κ . A similar correction can be done for rotor work when the work is determined by the Euler formula and measurement of velocity components.

6.10.3. Superheated steam can accurately be represented as an ideal gas with a specific heat ratio γ around 1.30. Wet steam deviates quite strongly from an ideal gas. Nevertheless, the most essential ideal gas relations can be used. These are, for an expansion process in a nozzle (Fig. 4.5), the polytropic relation between density and pressure $\rho / \rho_{00} = (p / p_{00})^{1/n}$ and the relation between enthalpy and pressure

$$h_{00} - h = \frac{\gamma}{\gamma - 1} \frac{p_{00}}{\rho_{00}} \left[1 - \left(\frac{p}{p_{00}} \right)^{\frac{n-1}{n}} \right].$$

These relations can be fitted very accurately to an isentropic expansion in the wet steam region. Verify first for the density-pressure relation. Take as an example an isentropic expansion starting from saturated vapour at 6 bar until 0.5 bar. Calculate density for the pressure levels 3.5, 2, 1 and 0.5 bar. Use steam tables from a book on thermodynamics or from a website. A basic Mollier-diagram for water-steam can be found on: http://www.engineeringtoolbox.com/mollier-diagram-water-d_308.html. Steam properties may be calculated with:

<http://www.spiraxsarco.com/resources/steam-tables.asp>. The starting point of the expansion defines the entropy. Values of specific volume (inverse of the density), entropy and enthalpy are obtained by linear interpolation as a function of the dryness factor (also called steam quality: ratio of the mass fraction of vapour to the mass of the mixture of saturated liquid and saturated vapour). (A: the specific heat ratio γ is 1.1334 for a fitting to the 5 data couples). Verify then that the enthalpy-pressure relation is very accurately satisfied with the obtained value of the specific heat ratio. Observe that the ideal gas law $p = \rho RT$ is not well satisfied (R is not a constant), but remark that the ideal gas law can easily be avoided in the calculation of the expansion of a nozzle. Consider subsequently the polytropic efficiency $\eta_{\infty} = 0.90$ for characterisation of irreversibility. Verify that couples of density and enthalpy calculated on the polytropic expansion correspond very well with real steam data for the pressure levels used before.

6.10.4. Figures 6.26 and 6.27 represent the HP-IP rotor and an LP rotor of the Arabelle impulse type steam turbine of Alstom. The machine is built with two LP parts for electric power 900 MW–1400 MW and with 3 LP parts for 1300 MW–1700 MW. The machines are not strictly unique and are adapted somewhat to the particular application. We consider here Flamanville 3 (France) with 1750 MW electric power, which is the largest turbine up to now. The steam conditions are: inlet at 75 bar, 290 °C (saturated) with expansion to 11 bar in the HP part; moisture separation and reheat on 11 bar to 275 °C (superheated); condenser pressure is 46 mbar. Mass flow at turbine inlet is 2500 kg/s (lower flow rate in IP and LP parts) and rotational speed is 1500 rpm. For the last stage, the tip diameter and hub diameter are 6.00 and 2.50 m (blade length is 1750 mm). The hub diameter of the first stage in the HP part is 1.75 m (the hub diameter varies slightly in the HP-IP part). The corresponding blade speeds are 471.24, 196.35 and 137.45 m/s. The blade speed in the HP part is very low, causing a low stage work. The reason is that the shafts of the HP-IP part and the 3 LP parts are coupled inline to drive a single generator (so called tandem-compound machine). A more comfortable blade speed at the hub of the HP-IP part would be the double speed, being about 275 m/s,

reached by the rotational speed 3000 rpm. Such an arrangement, sometimes chosen by other manufacturers, requires two shafts driving each a generator (so-called cross-compound machine).

Determine the number of stages in the HP part, assuming that the degree of reaction is 10% at the hub and that the hub diameter is 1.75 m. Design the hub section of the first stage of the HP part with zero degree of reaction (Laval stage). The real machine has a small positive degree of reaction at the hub, but we take zero degree of reaction for the ease of computation. Take $\alpha_1 = 75^\circ$.

A: $(\Delta h_s)_{stage} \approx 38 \text{ kJ/kg}$, $(\Delta h_s)_{HP-part} \approx 340 \text{ kJ/kg}$: 9 stages (see Fig. 6.26). There is recovery of outlet kinetic energy of the stage. So, calculation of the velocity triangles requires iteration. Assuming a repeating stage and symmetrical rotor blades, the velocity triangles result in $\beta_1 = -\beta_2 = 60.83^\circ$. For determination of the blade shape, according to Fig. 6.9, we take $\beta_1 = -\beta_2 = 60^\circ$. We denote the inner and outer radii of the blade channel by r_1 and r_2 and the channel width by $b = r_2 - r_1$. The height of the stator vanes at outlet = height of the rotor blades at inlet $\approx 183 \text{ mm}$. We choose the axial chord of the rotor blades equal to 100 mm (we may scale afterwards) and the minimum blade thickness to 2 mm.

The Zweifel tangential force coefficient set to unity is

$$C_{Fu} = \frac{2sw_{2a}\Delta w_u}{c_a w_2^2} = 1.$$

Ignoring losses: $\Delta w_u = -2w_{2u} = 2w_2 |\sin \beta_2|$ (in reality somewhat larger) and ignoring blade thickness: $s = b / \cos \beta_2$ (in reality somewhat larger) and $c_a = 2r_2 |\sin \beta_2|$. Inserting these expressions, the Zweifel coefficient becomes:

$$C_{Fu} = \frac{2sw_2 \cos \beta_2 2w_2 |\sin \beta_2|}{c_a w_2^2} = 4 \frac{b \cos \beta_2 |\sin \beta_2|}{\cos \beta_2 2r_2 |\sin \beta_2|} = 2 \frac{b}{r_2}.$$

Another way for deriving the maximum acceptable width of the rotor blade channel is by a local diffusion factor applied to the decelerating part of the suction side boundary layer in Fig. 6.10 (part DF):

$$D_{loc} = \frac{w_{max} - w_2}{w_{max}} < 0.5.$$

w_{max} is the maximum velocity at the suction side, being $r_2 w_2 / r_1$ according to the free vortex flow. The expression of the local diffusion factor becomes:

$$D_{loc} = \frac{r_2 / r_1 - 1}{r_2 / r_1} = \frac{r_2 - r_1}{r_2} = \frac{b}{r_2}.$$

Both $C_{Fu} = 1$ and $D_{loc} = 0.5$ lead to $b/r_2 < 0.5$. In practice, the upper limit is taken as $b/r_2 = 0.4$, leading to $r_2 = 2.5b$ and $r_1 = 1.5b$. This means that the channel width may be at maximum half of the radius of curvature of a mean streamline. This rule is sometimes called Brilling's rule [1].

The channel width becomes $b = 23.09$ mm, rounded to 23 mm. Taking the blade thickness at the tips 2 mm, leads to a pitch of 50 mm. The number of blades becomes 110. Figure 6.34 shows the rotor blade geometry. The leading edge is rounded because the inlet Mach number is well below unity. A straight part is added to the blades at the trailing edge. The final axial chord is 90 mm.

We begin dimensioning the nozzle vanes with an outlet width of 23 mm (=width of the rotor blade passages). With thickness 2 mm, the pitch is then 96.6 mm and the corresponding number of vanes is 57. The number of rotor blades 110 is too close to $2 \times 57 = 114$. So, we reduce the number of vanes to 48, for instance. Pitch is then 115.5 mm. The outlet width becomes 28 mm. With a Zweifel coefficient of unity, the corresponding axial chord is 58 mm. We take this value as a basic value (we may scale afterwards). Figure 6.37 shows the construction of a preliminary nozzle vane shape. The blade thickness in the trailing edge zone is set to 2 mm. Point E is chosen on the pressure side. The camber line EF is a curve with angle of the tangent linearly varying as a function of axial distance (x) from 0° to 75° . This is a parabola with equation $y/x_E = (tg\alpha_1/2)(x/x_E)^2$. A thickness distribution and a leading edge zone are added. The locations of points C and E are varied in order to obtain a smooth profile. The resulting axial chord is 70 mm, which brings the Zweifel coefficient on 0.825.

The geometries of Figs. 6.36 and 6.37 may serve as initial geometries in a CFD package for optimisation of the vane and blade shapes. Comparison with the shape shown in Fig. 6.31 reveals that the geometrically determined shape of Fig. 6.37 is rather far away from an optimised shape. But the optimum shape strongly depends on exit angle and outlet Mach number.

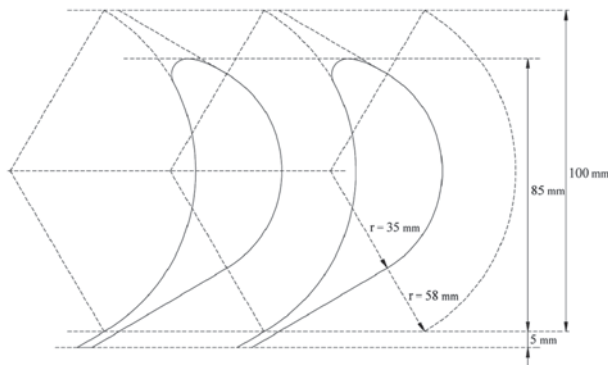


Fig. 6.36 Rotor blade profile; initial shape

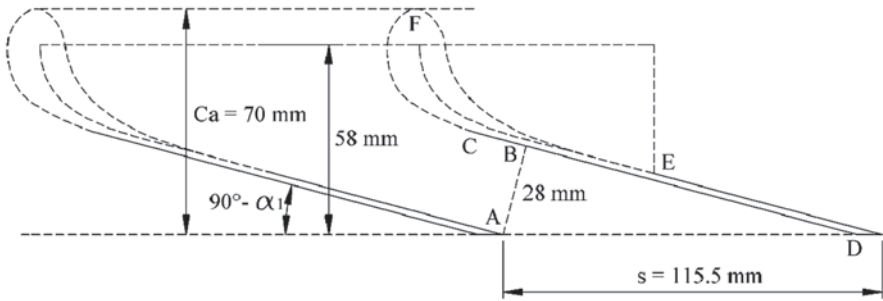


Fig. 6.37 Stator vane profile; subcritical flow; initial shape

6.10.5. Design the last stage of the LP part of the Arabelle turbine described in the previous exercise.

- a. Determine the number of stages necessary in the expansion from 11 bar, 275 °C to 46 mbar. Take as hub diameter of the first IP-stage 2.50 m (Fig. 6.26) and assume a degree of reaction of 10%. Consider also 10% degree of reaction for the hub part of the last stage and take again as hub diameter 2.50 m (Fig. 6.27). Take into account that the hub diameter increases somewhat in the successive stages of the IP part and then decreases in the successive stages of the LP part, Compare with the number of stages in Figs. 6.26 and 6.27 (4+5).

A: The isentropic enthalpy drop of the IP part+LP part is 875 kJ/kg. For $R = 10\%$, the isentropic enthalpy drop in the first and last stages is about 77 kJ/kg. With this value, the number of stages is 11.4. The number of stages may certainly be reduced to 10, taking into account the larger diameter in the middle stages. In reality, there are 9 stages. These look somewhat more loaded than optimal.

- b. Determine the variation of the velocity as a function of the radius in the space between the stator and the rotor for the last stage of the LP part. Consider constant total enthalpy over the radius downstream (and upstream) of the stator vanes. Take as stator outlet angle 70° , constant over the radius (this is lower than the geometric maximum of about 75° in order to enlarge the mass flow). Estimate the stator loss coefficient with the formula of Soderberg, ignoring secondary loss. Take as simplification that streamsurfaces are cylindrical (radial velocity component equal to zero), such that there is equilibrium between the radial pressure gradient and the centrifugal force (so-called simple radial equilibrium). Derive that the tangential velocity varies according to $v_{lu} \sim r^{-a}$, with $a = (\phi_s \sin \alpha_1)^2$, where ϕ_s is the velocity coefficient of the nozzle vanes. Neglect the difference between infinitesimal and isentropic efficiency such that $\eta_\infty = \phi_s^2$.

A: Cylindrical stream surfaces: force equilibrium:

$$\frac{1}{\rho} \frac{dp}{dr} = \frac{v_{lu}^2}{r}.$$

Constant enthalpy downstream of nozzle vanes ($v_{lr} = 0$):

$$h_0 = h_1 + \frac{1}{2}v_{1u}^2 + \frac{1}{2}v_{1a}^2.$$

Constant vane angle: $\tan \alpha_1 = v_{1u}/v_{1a}$.

Combination of the above, with the derivative of the enthalpy equation in the radial direction:

$$\frac{dh_0}{dr} = 0 = \frac{dh_1}{dr} + \left(1 + \frac{1}{\tan^2 \alpha_1}\right) v_{1u} \frac{dv_{1u}}{dr}.$$

Loss in the stator according to Soderberg:

$$\xi = 0.025 \left[1 + \left(\frac{\delta^\circ}{90} \right)^2 \right], \text{ with } \delta^\circ = \alpha_1 = 70^\circ, \phi_s = 1 / \sqrt{1 + \xi} = 0.9805.$$

Infinitesimal efficiency of the nozzle vanes:

$$\eta_\infty = (-dh) / \left(-\frac{1}{\rho} dp \right) \text{ thus } \frac{dh}{dr} = \eta_\infty \frac{1}{\rho} dp.$$

Downstream of the nozzle vanes: $\frac{dh_1}{dr} = \eta_\infty \frac{1}{\rho} \frac{dp_1}{dr} = \eta_\infty \frac{v_{1u}^2}{r}$.

Combination with the enthalpy equation:

$$0 = \eta_\infty \frac{v_{1u}^2}{r} + \frac{1}{\sin^2 \alpha_1} v_{1u} \frac{dv_{1u}}{dr} \text{ or } \eta_\infty \sin^2 \alpha_1 \frac{v_{1u}}{r} + \frac{dv_{1u}}{dr} = 0.$$

This equation is satisfied for $v_{1u} \sim r^{-a}$, with $a = \eta_\infty \sin^2 \alpha_1$. We take $\eta_\infty = \phi_s^2 : a = 0.8490$.

- c. For equal work on all radii and axial outlet of the stage, the tangential component of the stator outlet velocity should vary according to $v_{1u} \sim r^{-1}$. Thus with perfect axial outlet at the hub and $v_{1u} \sim r^{-a}, v_{1u}$ at the casing is larger than according to $v_{1u} \sim r^{-1}$ and v_{2u} is positive. In order to reach axial outlet in the mean sense, with the objective of minimising the tangential kinetic energy at the outlet, v_{2u} has to be set to a negative value at the hub. This can be obtained by enlarging somewhat the work coefficient. For $R=0.10$, the speed ratio for axial outlet is:

$$\lambda = \frac{u}{v_s} = \frac{0.48}{\sqrt{1-R}} \approx 0.50, \text{ thus } \psi_s = \frac{\Delta h_s}{u^2} = \frac{1}{2\lambda^2} \approx 2.$$

We choose for $R_s = 0.10 : \psi_s = 2.20$. This change lowers somewhat the efficiency at the hub.

- d. Determine the velocity triangles at the hub for $R_s = 0.10$ and $\psi_s = 2.20$. Take constant axial velocity at the hub ($v_{1a} = v_{2a}$). Consider a repeating stage. The isentropic degree of reaction is then $R_s = (h_{1s} - h_{2s}) / (h_0 - h_{2s})$. With $u = 196.35$ m/s and $\psi_s = 2.20 : \Delta h_s = 84.82$ kJ/kg. We round to 85 kJ/kg and dis-

tribute as $\Delta h_{ss} = h_0 - h_{1s} = 76.5$ kJ/kg and $\Delta h_{sr} = h_{1s} - h_{2s} = 8.5$ kJ/kg. Calculate the last stage without consideration of the recovery of the outlet kinetic energy in the diffuser downstream of the last stage. This means that it is assumed that the magnitude of the axial velocity downstream of the stage has been chosen already. In reality, the optimisation of the outlet velocity determines the value of the nozzle angle. So, it is assumed here that $\alpha_I = 70^\circ$ is the result.

A: The calculations require iteration.

$$\beta_I = 53.2^\circ, \beta_2 = -57.4^\circ; R = 0.081; \Delta W = u(v_{1u} - v_{2u}) = 79.45 \text{ kJ/kg};$$

$$\eta_{tt} = 0.935.$$

- e. Determine the velocity triangles as a function of the radius, taking into account: $v_{1u} \sim r^{-a}$, $v_{1a} = v_{1u}/\tan \alpha_I$, $v_{1s} = v_I/\phi_s$, $\Delta h_{ss} = \frac{1}{2}v_{1s}^2$, $\Delta h_s = 85$ kJ/kg and $\Delta h_{sr} = \Delta h_s - \Delta h_{ss}$. Take as inflow velocity of the stator the value of v_{2a} at the hub. Calculate loss coefficients with the formula of Soderberg, ignoring secondary loss. Take as approximation that v_{2a} is constant along the radius. With this last assumption, a mass flow balance is not necessary. This can be used afterwards to determine the height of the streamtubes at inlet and outlet of the rotor. Calculate for the values of radius: $r = 1.25, 1.60, 2.15$ m, 3.00 m.

A: the results are shown in Table 6.4 and the velocity triangles in Fig. 6.38.

6.10.6. Design a small industrial steam turbine with 3000 rpm rotational speed. Steam at turbine inlet is at 100 bar and 500 °C. Take as flow rate $\dot{m} = 100$ kg/s (calculations can easily be adapted for another flow rate). The inlet stator angle is $\alpha_I = 75^\circ$. Design the turbine such that the expansion is realised until 25 bar back-pressure. Achieve this in 3 different ways: 1) by Curtis stages; 2) by Laval stages (Rateau turbine); 3) as a reaction turbine with 50% isentropic degree of reaction. Make the calculations for axial inlet and outlet. Take the following technical limitations into account: at 500 °C, blade speed must not exceed about 200 m/s; blade height should be minimally about 25 mm for ideal functioning.

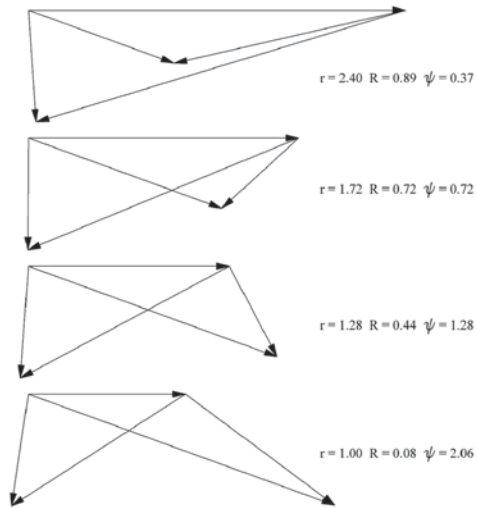
- a. Determine the main features and dimensions: the number of stages required; the average diameter (possibly different per stage); the blade height (possibly different per stage); the velocity triangles of the first stage; the h-s diagram of the first stage with an indication of losses; the internal power of the first stage.

A: Curtis: 1 stage, $h = 25$ mm, $\theta \sim 2 \times 90^\circ$; Laval: 4 stages, $h_I = 25$ mm,

Table 6.4 Blade of the last stage of an LP part

r	u	v_{1u}	v_{1a}	w_{1u}	w_{2u}	v_{2u}	η_{tt}	R	ψ
m	m/s	m/s	m/s	m/s	m/s	m/s	—	—	—
1.25	196.4	382.9	139.4	186.5	-217.5	-21.1	0.933	0.08	2.06
1.60	251.3	310.5	113.0	59.2	-261.4	-10.0	0.948	0.44	1.28
2.15	337.7	241.6	87.9	-96.1	-338.7	-0.9	0.964	0.72	0.72
3.00	471.2	182.1	66.3	-289.2	-461.7	9.6	0.956	0.89	0.37

Fig. 6.38 Velocity triangles for the last stage of the LP part



$\theta_l \sim 2 \times 80^\circ$, $h_4 = 25$ mm, $\theta_4 = 360^\circ$; 50% reaction: 7 stages, $h_l \sim 15$ mm (ideal minimum height cannot be obtained).

b. Design the nozzles and the rotor blades. Take the Curtis stage as an example.

A: Curtis: $Z_s = 32$, $b_{throat} = 12$ mm, $b_l = 15.5$ mm. $Z_r = 150$, $c_a \approx 35$ mm, $b_l = 7.45$ mm. The rotor blades may be drawn as in Fig. 6.34, except that the leading edge should stay sharp as the inlet Mach number is above unity. The stator vanes may be drawn as in Fig. 6.37, but the nozzle channels are convergent-divergent here: see Fig. 6.39. The positions of the points B, C and E should be chosen such that the resulting profile is smooth.

6.10.7. Figure 6.40 is a sketch of a Girard turbine. It is an axial hydraulic turbine of impulse type developed around 1850. The rotor turns in the atmosphere. Therefore, pressure at the rotor inlet and outlet is atmospheric pressure. The zero pres-

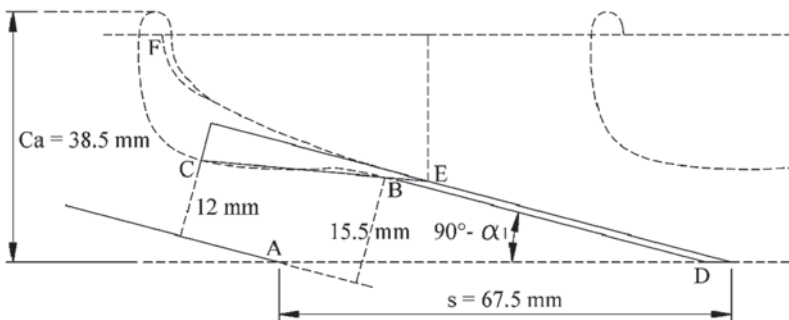


Fig. 6.39 Stator vane profile; supersonic flow; initial shape

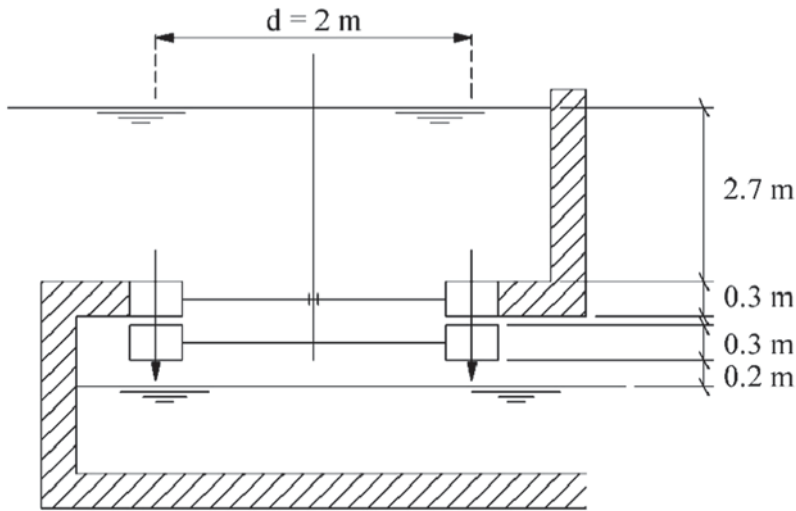


Fig. 6.40 Girard turbine (*impulse turbine*)

sure difference across the rotor makes the analogy with a Laval impulse type steam turbine. The Girard turbine can be analysed similarly. The only essential difference comes from the gravitational potential energy in the rotor, which creates a slight acceleration such that the kinematic degree of reaction becomes slightly positive, where it is slightly negative with a Laval turbine.

Analyse the flow through the Girard turbine with a mean line representation of the flow (one-dimensional representation). Assume admission over 360° to the stator. Take as outlet angle of the nozzle vanes $\alpha_1 = 60^\circ$ and consider the operating point with exact axial outlet of the rotor, seen in the absolute frame: $\alpha_2 = 0^\circ$. Determine losses in stator and rotor cascades with Soderberg's formula. Take the aspect ratio of vanes and blades (height to axial chord) equal to unity. Assume constant axial component of the velocity in the rotor.

- Determine axial and tangential components of the absolute velocity at the outlet of the stator vanes. Derive the outlet velocity from the work equation in the stator. The height difference between the water surface in the water chamber and the outlet of the stator vanes is 3.00 m.
- Determine the blade speed such that the absolute velocity at rotor outlet is in the axial direction. Derive this speed from the work equation in the rotor. Pay attention to the small acceleration in the rotor. The consequence is that rotor blades cannot be exactly symmetrical for constant axial velocity. The computation requires iteration for the loss coefficient of the rotor. A starting value may be determined from a computation ignoring rotor loss. The height difference between inlet and outlet of the rotor is 0.30 m. Ignore the small gap between stator and rotor.

- c. Determine the rotor work and the internal efficiency. The height difference between the outlet of the rotor and the downward water level is 0.20 m. The head supplied to the machine is $3.00\text{ m} + 0.30\text{ m} + 0.20\text{ m} = 3.50\text{ m}$.
- d. Split the rotor work into the action and reaction parts. Determine the degree of reaction. Observe that it is a low positive number.
- e. Determine the speed ratio. Calculate the spouting velocity from the supplied head of 3.50 m.
- f. Make the balance of the rotor work, the losses in stator and rotor, the kinetic energy at outlet and the downward head. The sum of the energy terms should be equal to the supplied mechanical energy. Determine the fraction of the outlet kinetic energy in the balance. Observe that outlet kinetic energy is the largest part of the losses.
- g. Determine the number of stator vanes and rotor blades from a Zweifel coefficient value of 0.8.
 $\mathbf{A} : v_{la} = 3.575\text{ m/s}, v_{lu} = 6.191\text{ m/s}, u = 3.213\text{ m/s}, \Delta W = 19.892\text{ J/kg},$
 $\eta_i = 0.579, R = 0.0365, \lambda = 0.388,$ outlet kinetic energy is 18.61 % of the supplied mechanical energy, $Z_s = 23, Z_r = 50$.

References

1. Balje OE (1981) Turbomachines: a guide to design, selection and theory. Wiley, ISBN 0-471-06036-4
2. Denton JD (1993) Loss mechanisms in turbomachines. J Turbomach 115:621–656
3. Dixon SL, Hall CA (2014) Fluid mechanics and thermodynamics of turbomachinery, 7th edn. Elsevier, ISBN 978-0-12-415954-9
4. Korpela SA (2011) Principles of turbomachinery. Wiley, ISBN 978-0-470-53672-8
5. Lampart P, Hirt L (2012) Complex multidisciplinary optimization of turbine blading systems. Arch Mech 64:153–175
6. Lewis RI (1996) Turbomachinery performance analysis. Wiley, ISBN 0-470-23596-9
7. Moustapha H, Zelesky M, Baines C, Japikse D (2003) Axial and radial turbines. Concepts NREC, Wilder. ISBN 0-933283-12-0
8. Rosic B, Xu L (2012) Blade lean and shroud leakage flows in low aspect ratio turbines. J Turbomach 134:031003

Chapter 7

Dynamic Similitude

Abstract The present chapter discusses the concept of similitude, which means that two machines may be similar in the sense that there exist proportionality factors for geometry, velocities and forces. The performance characteristics of one of the machines can then be derived from the known characteristics of the other. The concept forms the basis of the initial design of a turbomachine, which means the determination of main parameters as the rotational speed, the size and some geometric ratios. In this chapter, we discuss the theory of dynamic similitude and some applications, including the basic design of a radial fan.

7.1 Principles of Dynamic Similitude

7.1.1 Definition of Dynamic Similitude

Two flows are dynamically similar when they are geometrically similar, when velocities at homologous points have the same direction and have a constant ratio and when forces at homologous points have the same direction and have a constant ratio. In other words, flows are dynamically similar when similitude is as well geometric, kinematic and dynamic.

With the simplest flows, i.e. steady flows with incompressible fluids in a stationary geometry, dynamic similitude implies kinematic similitude, as the velocity field unambiguously results from the integration of the force field. Further, kinematic similitude implies geometric similitude, as streamlines unambiguously result from the integration of the velocity field. Therefore, the term dynamic similitude is applied to the common denomination of the three elements within similitude. Henceforth we simply use the term similitude. The notion dynamic similitude is limited to the flow itself. Apart from fluid transport itself, other transport phenomena may occur within a flow. Heat transport is an example. The notion of similitude may be extended to these phenomena. Additional transport phenomena are not directly relevant for the fundamental study of turbomachines. For turbomachines, work by a rotor is an additional phenomenon compared to simple flows. In the present chapter, the similitude study is limited to constant density fluids. An extension to compressible fluids is made in Chap. 15.

7.1.2 Dimensionless Parameter Groups

Similar lengths have a constant ratio within similar flows. Similar velocities have a constant ratio as well. As velocity is a length divided by time, the combination of velocity and length implies that similar time intervals have a constant ratio. Analogously, from the constant ratio of forces and from the equality of a force to a mass times a length divided by the square of a time ($N = \text{kgm/s}^2$), it follows that similar masses have a constant ratio. The fundamental quantities, i.e. length, mass and time, by which all mechanical quantities may be expressed, thus show a constant ratio at homologous points within similar flows. The consequence is that a *dimensionless group of parameters* formed by combining quantities describing the flow must have the same value in homologous points. For example, pressure has the same dimension as the product of a density (kg/m^3) and the square of a velocity (m^2/s^2). A dimensionless pressure coefficient (7.1) thus has the same value at homologous points within similar flows, with p_r being a reference value for pressure, e.g. inlet pressure:

$$C_p = \Delta p / \rho v^2 = \frac{p - p_r}{\rho v^2}. \quad (7.1)$$

Example (7.1) demonstrates that dimensionless groups of parameters necessarily are formulated as

$$\pi = A^a B^b C^c \dots, \quad (7.2)$$

with $A, B, C \dots$ being the parameters and a, b, c, \dots exponents. The exponents are integers in the example, but this is not absolutely necessary, as broken powers of dimensionless parameter groups are dimensionless as well. The term π -group is often used for a dimensionless group.

7.1.3 Similitude Conditions

We take flow of a constant density fluid within a stationary channel as an example to derive how similitude conditions may arise. The quantities describing the flow are geometry, velocities and forces. We consider a second flow being similar to the first one, as sketched in Fig. 7.1. For similitude, ratios of length, mass and time must be equal. If we choose a length unit, a mass unit and a time unit that are characteristic for the flow (intrinsic units) and if we express the equations describing the flow with this unit system, the resulting number equations must be identical for both flows. This allows the identification of similitude conditions.

As unit of length e_ℓ we take e.g. the inlet width L . As velocity unit we take e.g. the inflow velocity $e_v = V$. From a consistent system of units follows a time unit:

$$e_v = \frac{e_\ell}{e_t} \rightarrow e_t = \frac{L}{V}.$$

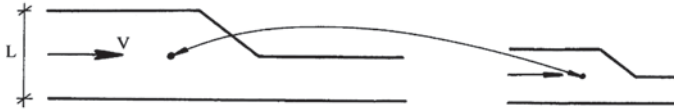


Fig. 7.1 Similar flows and intrinsic units

The mass unit may be determined by choosing the fluid density as the density unit: $e_\rho = \rho$. As $e_\rho = e_m / e_\ell^3$, a mass unit follows with a consistent unit system.

The flow equations are

$$\nabla \cdot \vec{v} = 0, \quad \frac{\partial \vec{v}}{\partial t} + \vec{v} \cdot \nabla \vec{v} + \frac{1}{\rho} \nabla p = -g \vec{I}_z + \nu \nabla^2 \vec{v}.$$

The pressure unit is adopted because of consistency as $e_p = e_\rho e_v^2 = \rho e_v^2$.

The dimensionless equations follow from

$$\vec{v} = [\vec{v}] e_v, \quad t = [t] e_t, \quad \nabla = [\nabla] \frac{1}{e_\ell}, \quad \dots,$$

with quantities between brackets being dimensionless.

The momentum equation becomes:

$$\left[\frac{\partial \vec{v}}{\partial t} \right] \frac{e_v}{e_t} + [\vec{v} \cdot \nabla \vec{v}] \frac{e_v^2}{e_\ell} + \left[\frac{1}{\rho} \nabla p \right] \frac{e_p}{\rho e_\ell} = -g \vec{I}_z + \nu \left[\nabla^2 \vec{v} \right] \frac{e_v}{e_\ell^2}.$$

Dimensional factors within the left-hand term are all $e_v^2 / e_\ell = V^2 / L$. By multiplication with L/V^2 we obtain a dimensionless equation with the right-hand term:

$$-\frac{gL}{V^2} \vec{I}_z + \frac{\nu}{VL} \left[\nabla^2 \vec{v} \right].$$

Two dimensionless groups are formed, that must have the same value for both flows considered. Note that the continuity equation does not cause similitude conditions because of its homogeneity. Similitude conditions are expressed by

$$\text{Re} = \frac{VL}{\nu} = \text{constant (Reynolds)}, \quad \text{Fr} = \frac{V}{\sqrt{gL}} = \text{constant (Froude)}.$$

The similitude conditions may be interpreted as conditions that *forces of different origins must have a fixed ratio*. We distinguish (acceleration is interpreted as inertia force):

$$\frac{\partial \vec{v}}{\partial t} + \vec{v} \cdot \nabla \vec{v} \quad + \quad \frac{1}{\rho} \nabla p \quad = \quad -g \vec{I}_z \quad + \quad \nu \nabla^2 \vec{v}$$

inertia force *pressure force* *gravity force* *viscous force*.

So: Re = inertia force/viscosity force, Fr^2 = inertia force/gravity force. If the pressure unit had not been chosen a priori as ρV^2 because of the consistency of the unit system, a third similitude condition would become

$$Eu = e_p / \rho V^2 \text{ (Euler) = pressure force / inertia force.}$$

For instance, we could have chosen the pressure difference over the channel as pressure unit. This would constitute a principal error. This means that the Euler number is not a similitude condition. But it is a dimensionless group. Consequently, for all flows that are similar with each other (= family of similar flows), there must be an unambiguous relation of the form:

$$Eu = \frac{\Delta p}{\rho V^2} = f(Re, Fr).$$

All other possible dimensionless groups are also functions of Re and Fr .

The above example implies that similitude conditions are created with a general flow problem because of the requirement that *forces of different origins must have a fixed ratio*. In the same way, *velocities of different origins must have a fixed ratio*. With turbomachines, there are always two velocities of different origins: the through-flow velocity and the blade speed. In a general flow problem, there are dynamic and kinematic similitude conditions.

7.1.4 Purpose of Similitude Analysis

Similitude analysis demonstrates that a dependent parameter cannot depend individually on the independent parameters of a problem. The relation must necessarily apply between a *dimensionless group containing the dependent parameter and dimensionless groups of independent parameters*. Similitude analysis thus reduces the number of degrees of freedom of the relations. The result demonstrates that a physical relation cannot depend on the unit system chosen to measure the variables. Therefore, it is advantageous to determine the dimensionless groups uniting the independent parameters when performing a flow analysis, either experimentally or numerically.

Similitude is mostly applied with keeping geometry constant, i.e. the geometric factor constitutes the unit. The degrees of freedom are then only kinematic and dynamic. Formulating a problem as in Fig. 7.1 in a dimensionless form generates the solution for an arbitrary inflow velocity (kinematic) and an arbitrary density (dynamic) in one effort. So, ∞^2 problems are analysed in one effort. Strictly, even ∞^3 are, as the solution also applies to each geometrically similar problem, but the extension to geometrically similar problems mostly has no practical relevance (except with reduced scale models, see Sect. 7.4.5).

7.1.5 Dimensional Analysis

The above reasoning demonstrates that considering similar flow problems means exactly the same as the dimensionless formulation of a flow problem. Dimensional analysis is herewith a tool to determine the independent dimensionless groups without much prior physical knowledge. The only prerequisite is the ability to list the independent parameters. In the above example these are:

Fluid	ρ, μ (or $\nu = \mu/\rho$)
Geometry	L
Kinematic	V
Dynamic	g

Apart from that, the intervening fundamental dimensions must be listed. These are found in the unit list of the MKSA-system, being length, mass and time for the flow problem considered. It is obvious now that five independent parameters with three fundamental dimensions only allow the formation of two independent dimensionless groups. A dimensionless group has the form $\Pi = \rho^a \nu^b L^c V^d g^e$. The dimension of the group is verified with Table 7.1.

Being dimensionless requires compliance with the following conditions:

$$\begin{aligned} -3a + 2b + c + d + e &= 0 \\ a &= 0 \\ -b - d - 2e &= 0. \end{aligned}$$

The system of three homogeneous equations in five variables allows ∞^2 solutions. This corresponds to 2 independent groups. Determination of these groups is not unambiguous. It is customary to take only one ‘clearly acting’ factor per group. For example, we may opt for a group containing ν but not g and for a second group containing g but not ν .

The first group is found by $b=1$ and $e=0$, from which $d=-1$, $a=0$, $c=-1$:

$$\Pi_1 = \frac{\nu}{LV}.$$

Each power of this group is satisfactory as well, so that we can take VL/ν .

The second group is found by $b=0$ and $e=1$, from which $d=-2$, $a=0$, $c=1$:

$$\Pi_2 = \frac{Lg}{V^2} \quad \text{or} \quad \frac{V}{\sqrt{gL}}.$$

The general result is that there are $m-n$ dimensionless groups with m independent parameters and n fundamental dimensions. This result constitutes the Vachy-Buckingham theorem, often called the π -theorem.

Table 7.1 Dimension table of a parameter group formed by the independent parameters of the flow problem of Fig. 7.1

	ρ	ν	L	V	g
L	-3	2	1	1	1
M	1				
t		-1		-1	-2
	a	b	c	d	e

7.1.6 Independent and Dependent Parameter Groups

The listing of problem-describing parameters requires a certain understanding of the problem. For instance, we know that the performance of a turbomachine with a constant density fluid is determined by the change of the mechanical energy $E_m = p/\rho + \frac{1}{2}\nu^2 + gz$. So ΔE_m must be specified as a single parameter. If the three components of ΔE_m were specified apart as parameters, an Euler number and a Froude number would appear as incorrect in the similitude conditions.

7.1.7 Dimensionless Parameter Groups in Turbomachines with a Constant Density Fluid

For a pump (or fan), a possible set of independent parameters is

Fluid	ρ, ν
Geometry	D (Relevant rotor diameter)
Operating point	Ω, \dot{m}

The relevant diameter D is normally the outer diameter of the rotor. To determine the operating point, we assume a rotational speed enforced by the driving motor and a flow rate regulated by valves. The head is then a dependent parameter. Remark that rotational speed and head may be considered as independent and flow rate as dependent. It is important to understand that two parameters determine the operating point. There are three fundamental dimensions: L, M, t . Consequently, there are $5 - 3 = 2$ independent dimensionless groups. These may be determined by means of a dimensional analysis, analogous with the first example. Acting factors must be chosen for that. They may be ν and Ω . On the base of the insight we meanwhile acquired, these groups can be formed directly, as the problem encompasses a dynamic similitude condition (associated to viscosity) and a kinematic similitude condition (associated to rotational speed).

A measure for the through-flow velocity is $V = \frac{\dot{m}}{\rho D^2}$.
A Reynolds number may thus be formed as

$$Re = \frac{VD}{\nu} = \frac{\dot{m}}{\rho D \nu} = \frac{\dot{m}}{D \mu} = \frac{Q}{D \nu}. \tag{7.3}$$

The tip speed of the rotor follows from $u = \frac{\Omega D}{2}$.

The kinematic similitude condition thus results in the group

$$\phi = \frac{V}{u} = \frac{2\dot{m}}{\rho D^3 \Omega}.$$

It is customary to omit numerical factors and to take

$$\Phi = \frac{\dot{m}}{\rho \Omega D^3} = \frac{Q}{\Omega D^3} \quad (\text{flow factor}). \quad (7.4)$$

A dependent group, based upon the mechanical energy change is

$$\psi = \frac{\Delta E_m}{u^2} \text{ or } \Psi = \frac{\Delta E_m}{\Omega^2 D^2} \quad (\text{head factor}). \quad (7.5)$$

It would be hazardous to introduce the mechanical energy rise in the form of a manometric head H_m , expressed as a height. By lack of attention, a group H_m/D could be formed, which has no physical meaning.

Henceforth, dimensionless groups formed by externally visible parameters as Q , ΔE_m , Ω and D will be denoted by capitals. Groups that are based on internal parameters will be denoted by lower-case letters. For instance, the ratio of an axial velocity component (with axial machines) or a radial component (with radial machines) to a blade speed by

$$\phi = \frac{v_a}{u} \quad \text{or} \quad \phi = \frac{v_{r2}}{u_2}.$$

Such a quantity is officially called flow coefficient (not flow factor). For a dimensionless representation of work, a work coefficient is defined by

$$\psi = \frac{\Delta W}{u^2}.$$

The dimensionless groups ϕ and ψ , based on internal parameters, have already been applied spontaneously in earlier chapters. The verbal distinction between internal and external dimensionless groups, as introduced here, is commonly not applied in practice. The terms flow factor and flow coefficient are mostly used indistinctly, as the terms work factor and work coefficient. Head factor and head coefficient are used as well. Introduction of numerical factors into dimensionless groups sometimes occurs. A flow factor may be defined as $\Phi' = Q / \left(\frac{\pi D^2}{4} \frac{\Omega D}{2} \right)$ and a head factor as $\Psi' = 2\Delta E_m / (\Omega D / 2)^2$. This requires some attention. For the determination of the Reynolds number according to (7.3), the through-flow velocity has been

chosen as a base. The blade speed may be chosen, leading to $Re = \Omega D^2/\nu$. The last expression is even commonly favoured.

7.1.8 Strong and Weak Similitude Conditions

Not all mathematically determined similitude conditions have an equal practical relevance. This is demonstrated by the friction factor in circular ducts, as shown in Fig. 2.17 of Chap. 2. With a given relative roughness, the friction factor becomes independent of the Reynolds number for a sufficiently high value of the Reynolds number. The physical reason is that, at a high Reynolds number, the (laminar) sub-layer at the wall becomes so thin that the roughness peaks of the wall directly affect the core flow. Friction is then determined only by roughness and not by viscosity. This example demonstrates that, in case of a high Reynolds number, this number is not a practical condition for similitude anymore. In turbomachines with low viscosity fluids such as water ($\nu \approx 10^{-6} \text{ m}^2/\text{s}$) or air ($\nu \approx 15 \cdot 10^{-6} \text{ m}^2/\text{s}$), the Reynolds number is mostly so high (order of magnitude of some hundred thousands) that it does not constitute a practical condition for similitude in a first approach. A limited correction for the influence of the Reynolds number is sometimes necessary (see below).

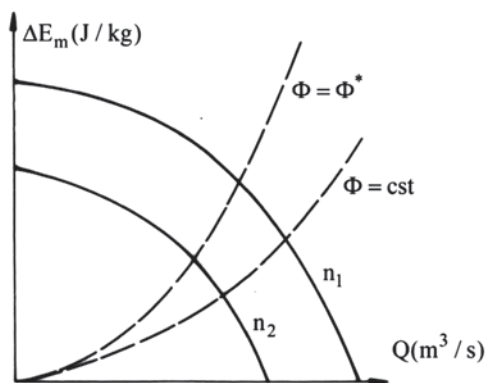
Analogous behaviour occurs with the Mach number for flows of compressible fluids. The Mach number is the ratio of the flow velocity to the speed of sound. The finite propagation velocity of sound waves results from the compressibility of the fluid. In an incompressible fluid, this velocity (theoretically) is infinitely high. This demonstrates that, with a sufficiently low Mach number, this number does not constitute a practical similitude condition. We refer to Chap. 4, where it has been demonstrated that, with Mach numbers until about 0.3, the Bernoulli and Saint Venant equations give the same results with a good approximation.

7.2 Characteristic Numbers of Turbomachines

7.2.1 Definition of a Characteristic Number

A characteristic turbomachine number is a dimensionless combination of parameters taken from *flows with optimum efficiency*. Such a number is unique for the machine and for geometrically similar machines. It characterises the shape of the machine. We should first reason the relevance of such a definition. Therefore we consider the Q-H curve of a driven turbomachine with a constant density fluid (pump or fan), as sketched in Fig. 7.2. From the foregoing we know that, with neglect of the influence of the Reynolds number, the only similitude condition is the constancy of the flow factor $\Phi = Q/\Omega D^3$. The head factor $\Psi = \Delta E_m/\Omega^2 D^2$ is then a dependent parameter. With a change in rotational speed, all flows meeting constant Φ are similar with each other. For these flows, Ψ is constant as well. The flow rate

Fig. 7.2 Similar flows at varying rotational speed for a pump or a fan



in these flows changes proportionally to the rotational speed. The energy rise is proportional to the square of the rotational speed. So, all flows on a parabola through the origin in Fig. 7.2 are similar with each other. These similar flows have the same (internal) efficiency, as the latter is a dimensionless group. One of the parabolas ($\Phi = \Phi^*$) thus corresponds to the flows with optimum efficiency. As a consequence, the corresponding values of the flow factor Φ and the head factor Ψ are unique for the machine (and similar ones). These numbers are thus characteristic numbers for the machine shape.

The above reasoning leading to the similarity parabolas implies that the Q-H curves of a driven turbomachine with a constant density fluid all coincide at various rotational speeds, if rendered dimensionless in the form Ψ as a function of Φ . The latter is correct only if the effect of the Reynolds number is negligible (see Sect. 7.4.1 on effect of the Reynolds number).

7.2.2 Specific Speed and Specific Diameter

Two other numbers are customarily constructed from the numbers $\Phi (= \Phi^*)$ and $\Psi (= \Psi^*)$, containing respectively Ω but not D and D but not Ω . These numbers are denominated *specific speed* (Ω_s) and *specific diameter* (D_s). The diameter is eliminated from Φ and Ψ by the combination

$$\frac{\Phi^2}{\Psi^3} = \frac{Q^2}{\Omega^2 D^6} \cdot \frac{\Omega^6 D^6}{\Delta E_m^3} = \frac{\Omega^4 Q^2}{\Delta E_m^3},$$

resulting in

$$\Omega_s = \frac{\Omega \sqrt{Q}}{(\Delta E_m)^{3/4}}. \quad (7.6)$$

The rotational speed is eliminated by the combination

$$\frac{\Phi^2}{\Psi} = \frac{Q^2}{\Omega^2 D^6} \cdot \frac{\Omega^2 D^2}{\Delta E_m} = \frac{Q^2}{D^4 \Delta E_m},$$

resulting in

$$D_s = \frac{D(\Delta E_m)^{1/4}}{\sqrt{Q}}. \quad (7.7)$$

Each family of similar flows within a turbomachine is characterised by a certain value of Ω_s and D_s . The specific speed and the specific diameter of the machine are the values for flows with optimum efficiency. The numbers Ω_s and D_s are more convenient numbers than Φ^* and Ψ^* , as a machine is designed for target values of Q and ΔE_m . So the specific speed determines the corresponding rotational speed. The specific diameter determines the corresponding diameter and as a consequence, the machine dimensions. According to the similitude theory, only one dimensionless group is independent. Generally, the specific speed is preferred. The three values applied in this group, flow rate, energy change and rotational speed can always be correctly established externally. A rotor diameter can only be approximately determined externally, which implies that an exact determination of the numbers Φ^* , Ψ^* and D_s is unfeasible without information about the real value of the rotor diameter.

An interpretation of Ω_s and D_s follows from considering a reference machine, yielding the required flow rate and the required energy change with $\Phi=1$ and $\Psi=1$. The rotational speed and the diameter of the reference machine meet $\Omega_r D_r^3 = Q$ and $\Omega_r^2 D_r^2 = \Delta E_m$, resulting in

$$\Omega_r = \frac{(\Delta E_m)^{3/4}}{\sqrt{Q}} \text{ and } D_r = \frac{\sqrt{Q}}{(\Delta E_m)^{1/4}}.$$

So:

$$\Omega_s = \frac{\Omega}{\Omega_r}, \quad D_s = \frac{D}{D_r}.$$

The adjective ‘specific’ follows from this interpretation. More general terms are *speed number* and *diameter number*. These terms are sometimes used. Numerical factors are sometimes included into the definitions of Ω_s and D_s , namely when this also applies to Φ and Ψ . The former definitions of Φ' and Ψ' imply for the rotational speed and the diameter of the reference machine:

$$\Omega'_r = \sqrt{\pi} \frac{(2\Delta E_m)^{3/4}}{\sqrt{Q}} \quad \text{and} \quad D'_r = \frac{2\sqrt{Q}}{\sqrt{\pi}(2\Delta E_m)^{1/4}}.$$

Speed number (σ) and diameter number (δ) are then defined by

$$\sigma = \frac{\Omega}{\Omega'_r} = \frac{\Omega \sqrt{Q}}{\sqrt{\pi}(2\Delta E_m)^{3/4}} \approx 0.335 \Omega_s,$$

$$\delta = \frac{D}{D'_r} = \frac{\sqrt{\pi} D (2\Delta E_m)^{1/4}}{2\sqrt{Q}} \approx 1.054 D_s.$$

Generally, the notions specific speed, specific diameter, speed number and diameter number are applied as defined here.

$$\text{We further note that } \sigma \delta = \frac{\Omega D / 2}{\sqrt{(2\Delta E_m)}} = \frac{u}{V_e} = \lambda,$$

with V_e being an energy reference velocity. The ratio λ is called *speed ratio*. This notion has already been used in the foregoing chapter.

The foregoing expression is also

$$\Omega_s D_s = \frac{\Omega D}{\sqrt{\Delta E_m}} = \lambda 2\sqrt{2} = \frac{I}{\sqrt{\Psi}}. \quad (7.8)$$

This expression demonstrates again that, if desirable, speed ratio or head factor may be used as a shape parameter, instead of specific speed. Speed ratio (see Chap. 6) or work coefficient (see Chap. 3) are sometimes more visual.

Older technical literature concerning pumps and hydraulic turbines often uses a dimensional form or specific speed, mostly noted as n_s or n_q , defined by

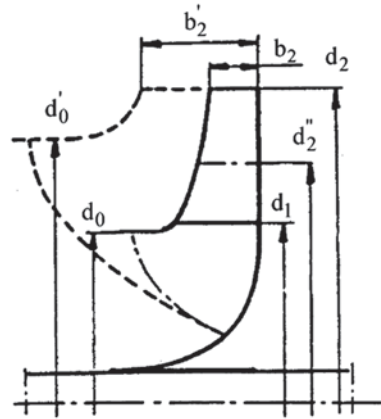
$$n_s = \frac{n\sqrt{Q}}{H_m^{3/4}},$$

where the units of n , Q and H_m are rpm, m³/s and m. This number is not dimensionless and proportional to Ω_s according to $[n_s] \approx 53 [\Omega_s]$.

7.2.3 Relation Between Characteristic Numbers and Machine Shape

In the foregoing sections we reasoned in an abstract way that the numbers Φ^* , Ψ^* , Ω_s , D_s and λ characterise the shape of a machine. We reason now more concretely by means of the specific speed (7.6). The mechanical energy change ΔE_m is, through the internal efficiency, linked to the rotor work $\Delta W = u_2 v_{2u} - u_1 v_{1u}$. We now consider a given machine, namely a pump, the meridional section of which is rendered by the full lines in Fig. 7.3. This machine has a certain specific speed. The specific speed may be increased in different ways. A first way is keeping the rotational speed constant, keeping the velocity triangles constant and increasing the flow rate. In this case, the mean inner and outer diameters of the rotor stay the same. A higher flow rate with the same velocity components requires a larger rotor width. This may result in the dashed form in Fig. 7.3. A second way is keeping the flow rate constant, keeping the velocity triangles constant and increasing the rotational speed Ω . The mean inner and outer diameters of the rotor then must decrease. The corresponding

Fig. 7.3 Specific speed increase of a centrifugal pump in two ways



outer diameter in Fig. 7.3 thus may be the diameter indicated by d'_2 and the resulting meridional section the dash-dotted form. Since the flow rate and the velocities are unchanged, the diameter of the suction eye d_0 remains unchanged. Increasing the original specific speed to the same new value in the two ways described makes the dashed shape and the dash-dotted shape geometrically similar.

If the specific speed is increased strongly in the second way (constant d_0), but combined with diminishing the rotor work, a diagonal shape and finally an axial shape are obtained, as shown in Fig. 7.4. From this reasoning ensues that *specific speed is a shape parameter at which low values correspond with radial forms and high values with axial forms*. The other numbers are shape parameters as well in the same way. The magnitude evolution of these numbers may be reasoned by noting that, at a given rotational speed Ω and diameter d_2 , an axial form has a high flow rate and a low energy rise, whereas a radial form has a low flow rate and a high energy rise. Figure 7.5 renders four pump rotor shapes with their corresponding specific speed values (source: [7]). We further elucidate the relation between meridional shape and shape parameters in the next section.

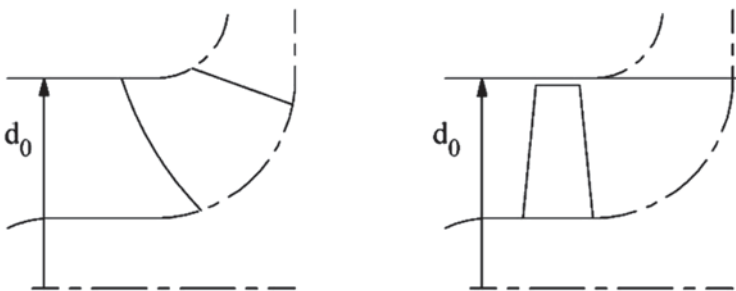


Fig. 7.4 Diagonal shape (mixed flow) and axial shape attained by specific speed increase

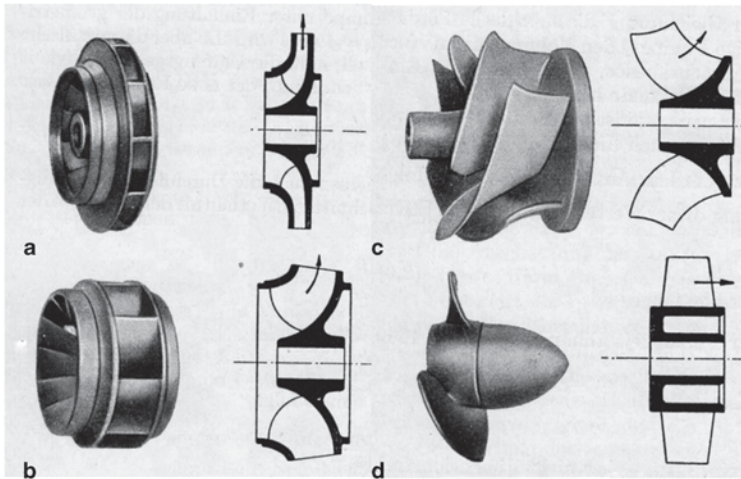


Fig. 7.5 Pump rotor shapes. **a** $\Omega_s = 0.2\text{--}0.7$; **b** $\Omega_s = 0.7\text{--}1.5$; **c** $\Omega_s = 1.5\text{--}3$; **d** $\Omega_s = 2.5\text{--}6$. (From [7]; permission by Springer)

7.2.4 Design Diagrams

Flows with optimum efficiency may be determined for a given turbomachine. The shape parameters (characteristic numbers) take a certain value with these flows. Ω_s and D_s may be determined that way. The same Ω_s and D_s values may also correspond to the optimum flows in a machine with a slightly different shape (a strong deviation is not possible). The optimum efficiencies for both machines are not the same then. So, there is a shape corresponding to the maximum efficiency for each combination of Ω_s and D_s . A diagram rendering the maximum possible efficiency for given values of Ω_s and D_s may be drawn as sketched for single-stage compressors and pumps in Fig. 7.6 (source: [2]). For the compressors, the volume flow rate is determined with the inlet density and the head with the isentropic enthalpy rise. In principle, such a diagram may be composed by studying all machines on the market and by including each time the machine with the best efficiency for given Ω_s and D_s at optimum flows. But this is unfeasible in practice. Diagrams of the Fig. 7.6 kind occurring in the literature are always calculated. The calculation method is normally verified for only a limited number of test machines, making the diagrams only partially reliable (see also Sect. 7.4.1: effect of Reynolds number and Sect. 7.4.2: effect of relative roughness).

One machine shape yielding maximum efficiency corresponds to a chosen specific speed. In the Fig. 7.6 diagram, a line may be drawn rendering the corresponding values of the specific diameter. This line is called the *Cordier line*. Note that optimisation for a given specific diameter would generate another line. Optimisation is however always implemented for a given specific speed. As a function of specific speed, there is always an absolute maximum efficiency attained at about

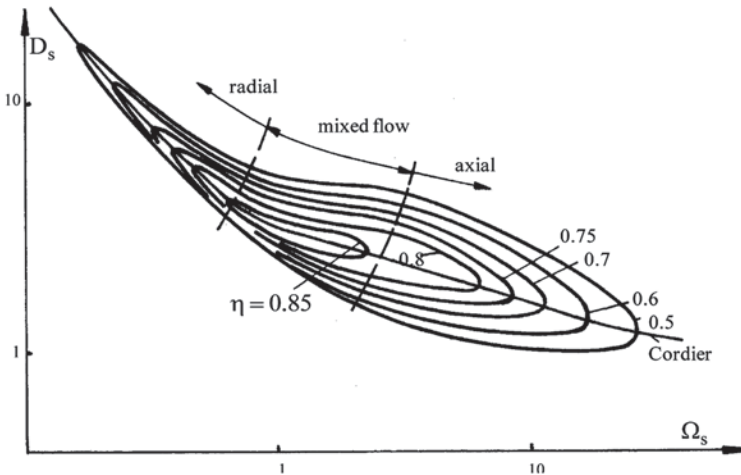


Fig. 7.6 Maximum attainable efficiency for single-stage compressors and pumps at given Ω_s and D_s . (Adapted from [2])

$\Omega_s = 1$ (diagonal form). Low specific speed machines have a lower efficiency, as their channels are long and narrow, causing increased friction losses. High specific speed machines have a lower efficiency, as rotor work then gets low, causing increased relative weight of losses.

Pump design starts from the specification of the flow rate and the energy rise. The choice of a rotational speed that optimises the specific speed may be attempted. From $\Omega = \Omega_s \Delta E_m^{3/4} / \sqrt{Q}$ emerges that, with a high head and a low flow rate, the corresponding rotational speed may be high and may become unrealisable. For a pump driven by an electric motor, the maximum rotational speed at 50 Hz power supply amounts to about 2900 rpm (asynchronous motor). In such a case, a sub-optimal specific speed might be opted for. The opposite occurs with a low head and a high flow rate. The optimum rotational speed might be too low to be realisable in practice. Synchronous rotational speeds are fractions of 3000 rpm and currently can be: 3000, 1500, 1000 and 750, asynchronous rotational speeds being about 3% lower. A gearbox between the motor and the machine may be opted for. The reasoning demonstrates that the choice of rotational speed is a priority. This also applies to other turbomachines. For this reason, optimisations are always implemented for a given specific speed. When no solution with an acceptable efficiency can be found within a design diagram, series connection or parallel connection shall be taken into consideration (see Sect. 7.5).

The Cordier line that can be drawn in a $\Omega_s - D_s$ diagram is universal, with a good approximation, for all turbomachines (Cordier 1953). Figure 7.7 sketches this universal diagram. There is a difference between driven (pumps, compressors) and driving (turbines) machines (source: [5]). The diagram concerns machines with full through-flow. An additional degree of freedom is generated with partial through-flow. The diagram is always to be applied when designing a turbomachine, but

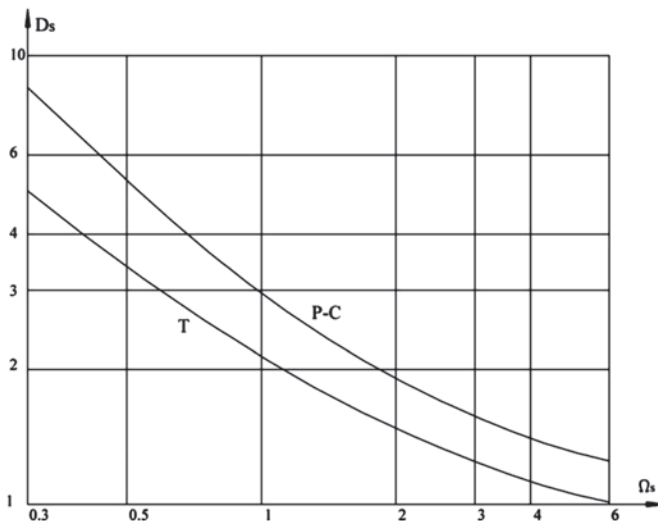


Fig. 7.7 Universal Cordier diagram: turbines (*T*), pumps and compressors (*P-C*). (Adapted from [5])

it should be mentioned that turbomachines are not always designed for optimum efficiency.

7.2.5 Shape of Characteristic Curves

Turbomachine characteristics have a shape depending on the value of the specific speed. We illustrate this for pumps. In Chap. 1 we learned that rotor work may be written as the sum of three kinetic energy difference terms:

$$\Delta W = \frac{u_2^2 - u_1^2}{2} + \frac{v_2^2 - v_1^2}{2} + \frac{w_1^2 - w_2^2}{2}.$$

The lower the specific speed, the more radial-type the meridional shape and the more dominant the centrifugal term (first term) is in the rotor work. This term does not vary with the flow rate. The consequence is that the lower the specific speed, the flatter the head is as a function of the flow rate and the flatter the efficiency is as a function of the flow rate. This is illustrated in Fig. 7.8, based on pump characteristics published in the books of Pfleiderer [9] and Dietzel [4]. At a high specific speed, the energy rise as a function of the flow rate typically has a maximum and a minimum. This is due to circulating flows with operation at very low net flow rate, as sketched in Fig. 7.9. With mixed flow and axial machines, the consequence is an increase of the centrifugal term in the rotor work at very low flow rate. Circulating flows at inlet and outlet occur with purely radial rotors as well, but do not influ-

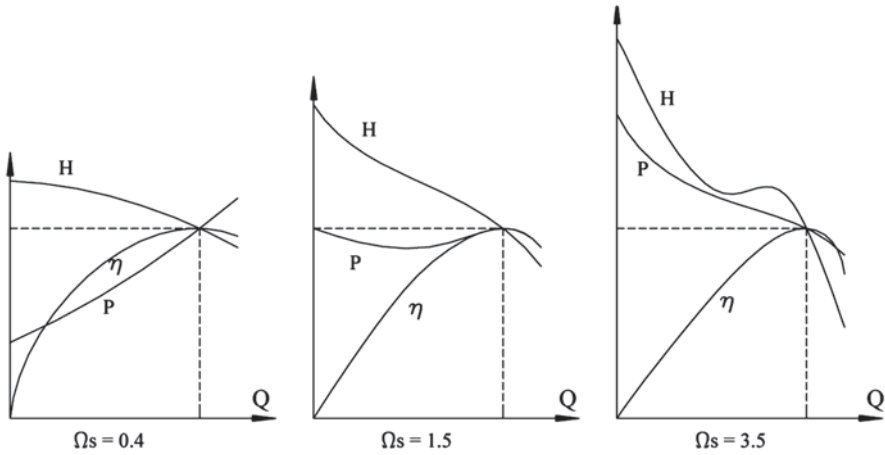


Fig. 7.8 Change of shape of performance characteristics of pumps with change of specific speed; head H , power P , efficiency η

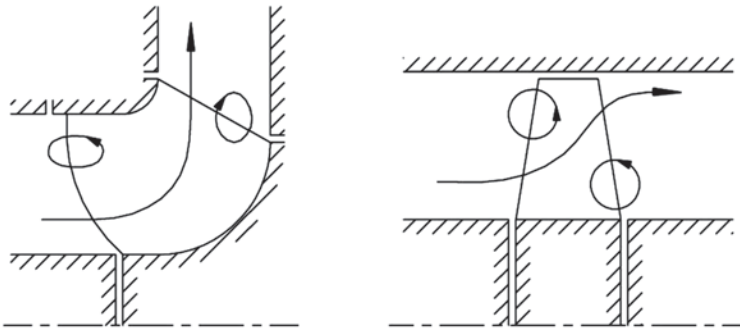


Fig. 7.9 Circulating flows with operation at very low net flow rate in mixed flow and axial pumps. (Adapted from [9])

ence much the energy rise in the through-flow with backward inclined or backward curved blades (there is large influence with forward curved blades: see Fig. 3.19 in Chap. 3).

7.2.6 Power Specific Speed

The internal power (rotor power) is the product of mass flow rate and rotor work. Thus, specific speed may also be written as

$$\frac{\Omega \sqrt{P_i}}{(\Delta E_m)^{5/4} \sqrt{\rho}}.$$

For hydraulic turbines, a *power specific speed* is defined by

$$\Omega_{sp} = \frac{\Omega \sqrt{P_{shaft}}}{(gH_m)^{5/4} \sqrt{\rho}},$$

with P_{shaft} the power measured at the shaft and H_m the manometric head. This form of specific speed is commonly used, as flow rate determination with a hydraulic turbine is not easy. Rotational speed, head and shaft power are the externally measurable quantities. The power specific speed is, strictly speaking, not a dimensionless group of flow quantities. The internal power should be used for that, as mechanical losses do not follow the similitude laws of flows. Since internal power is not directly measurable and mechanical efficiency is extremely close to unity, shaft power is used.

7.3 Application Example of Similitude: Variable Rotational Speed with a Pump

We consider a pump application as sketched in Fig. 7.10.

The energy rise between the pressure side (p) and the suction side (s) of the pump is

$$\Delta E_m = \frac{p_p - p_s}{\rho} + \frac{v_p^2 - v_s^2}{2} + gh_m,$$

where h_m (machine) is the height difference between the pressure and suction flanges. The required energy increase follows from the load of the pump. Work equations for the suction and the discharge pipes are

$$\frac{p_a}{\rho} + 0 + 0 = \frac{p_s}{\rho} + \frac{v_s^2}{2} + gh_s + q_{irr,s},$$

$$\frac{p_p}{\rho} + \frac{v_p^2}{2} + 0 = \frac{p_a}{\rho} + 0 + gh_p + q_{irr,p}.$$

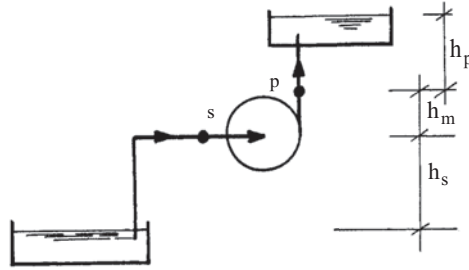
The sum of both expressions makes

$$\frac{p_p}{\rho} - \frac{p_s}{\rho} + \frac{v_p^2}{2} - \frac{v_s^2}{2} = g(h_s + h_p) + q_{irr,sp},$$

or

$$\Delta E_m = gh_{geo} + q_{irr,sp}.$$

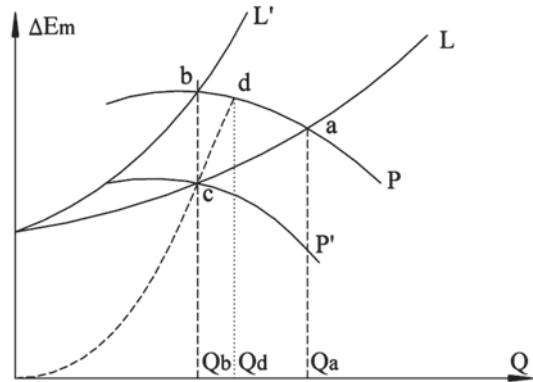
Fig. 7.10 Pump between suction and discharge reservoirs



Here, h_{geo} is the geometric height difference between the levels in the suction and discharge reservoirs. The required energy rise as a function of the flow rate is denominated the *load characteristic*. Pump and load characteristics are sketched in Fig. 7.11. The load characteristic has a static part, which is the value at zero flow rate and a dynamic part which increases approximately with the square of the flow rate. The dynamic part is typically denoted by the term *head loss*, meaning the dissipation of mechanical energy due to loss mechanisms. The intersection of both characteristics determines the operating point of the pump. When designing the installation, a pump with an optimum operating point close to the target operating point should be chosen. Also, the pipe dimensions should be optimised in the sense that a balance should be made between the energy cost by dissipation within the pipes and the investment cost of the pipes, taking their expected life time into account. A typical example of an installation according to Fig. 7.10 is water distribution. The application may be large scale with a water distribution company, small scale with the water supply to a horticulture farm and very small scale with home distribution of rain or well water. The discharge reservoir is not necessarily built as suggested in the figure, namely an open reservoir at a height. Often, closed pressurised reservoirs are applied. This makes no energetic difference, however. The load characteristic keeps the shape as in Fig. 7.11.

Assume that the installation is designed for flow rate Q_a supplied by the pump to the discharge reservoir. Water distribution from the discharge reservoir mostly shows a very strong flow rate variation, typically from zero to a maximum value. The pump in Fig. 7.10 is not intended to follow these flow rate changes. The pump functions around the operating point (a), as indicated in Fig. 7.11, with a discharge reservoir level fluctuating between a minimum and a maximum (or, equivalently, the pressure in the closed reservoir fluctuating between a minimum and a maximum). Thus, the load characteristic (L) of the pump in Fig. 7.11 is not fixed, but fluctuating. The pump is switched on when the reservoir level reaches a minimum and is switched off when the level reaches a maximum. Determination of the design operating point thus requires a study of the frequency distribution of the flow rates extracted from the discharge reservoir. This study determines the design flow rate of the pump and the capacity of the discharge reservoir.

Fig. 7.11 Operating point; pump characteristic P , load characteristic L



There are pump applications similar to the one in Fig. 7.10, where a large capacity of the discharge reservoir is unwanted, or where even no reservoir is wanted. Pumps in chemical plants or pumps for hot water distribution in central heating systems are examples. Such pumps must allow flow rate variation. The classical solution is constricting the discharge pipe through a control valve, shifting the load characteristic in Fig. 7.11 from L to L' . The flow rate is then reduced from Q_a to Q_b . There are possibly control valves on various branches in the pipe system, as typical with thermostatic valves on individual radiators of a central heating system. The constricting method is disadvantageous from an energy point of view. With larger systems it is therefore advisable to make the rotational speed of the pump adjustable and to reduce the pump characteristic to P' by reducing the rotational speed. The required rotational speed may be calculated by considering a similitude parabola through the origin and through point c . This intersects the pump characteristic P in point d .

The required rotational speed follows from $\frac{n_c}{n_a} = \frac{Q_b}{Q_d}$.

With larger pumps, it may make sense to adapt the operating point in this way. This requires rotational speed control onto the driving motor. A frequency controlled asynchronous motor is the most current system. Optimising the system and the control strategy can sometimes become quite complicated, as often a combination of buffer capacity, constricting valves and rotational speed control is required. Variable rotational speed is mainly interesting from an energetic point of view, when the static head (gh_{geo}) in the load characteristic is low. The operating points are then close to a similitude parabola. A typical example is water circulation within a central heating system. Central heating circulators for somewhat larger applications are nearly always provided with adjustable rotational speed motors as a standard nowadays. Currently there is an evolution towards permanent magnet motors with a wet rotor (see Chap. 8, Sect. 8.7.3 on canned pumps). Fan applications have a very small static head as well. Fans are therefore almost always equipped with adjustable rotational speed motors, typically frequency controlled asynchronous motors.



Fig. 7.12 *Left* domestic pump group with large reservoir and fixed speed; *right* small reservoir and variable speed (Courtesy Wilo)

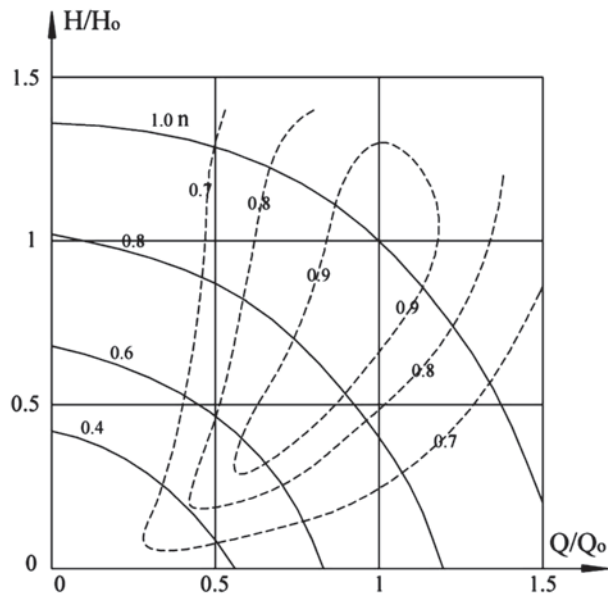
Even if energy considerations are of low relevance, as with home distribution of rain and well water, pumps with variable rotational speed are applied. The control strategy is quite simple then, namely keeping discharge pressure constant and switching off at zero flow. Variable rotational speed pumps have the advantage that only a very small buffer reservoir is needed, which is just meant for detecting pressure. At present, both systems with variable rotational speed and very small reservoir and systems with fixed rotational speed and a larger reservoir are marketed, with the variable rotational speed system getting increasingly popular. The larger reservoir system indeed easily shows deficiencies. The buffer capacity comes from water stored in a rubber bellows, enclosed in the air-filled reservoir. Air leaks from the reservoir and bellows rupture are current flaws. Figure 7.12 shows the two types of domestic pump groups.

7.4 Imperfect Similitude

7.4.1 Effect of Reynolds Number with the Same Fluid

With operation at low flow rate, the Reynolds number may become small. By the mere application of the kinematic similitude condition, similitude is not entirely correct. Especially, efficiency diminishes when the Reynolds number is reduced to small values. For example, in the field of the characteristics of a centrifugal pump for various rotational speeds, as sketched in Fig. 7.13, the efficiency contours only follow the similitude parabolas in the centre of the diagram. At a low flow rate,

Fig. 7.13 Efficiency contours of a centrifugal pump. (Adapted from [4])

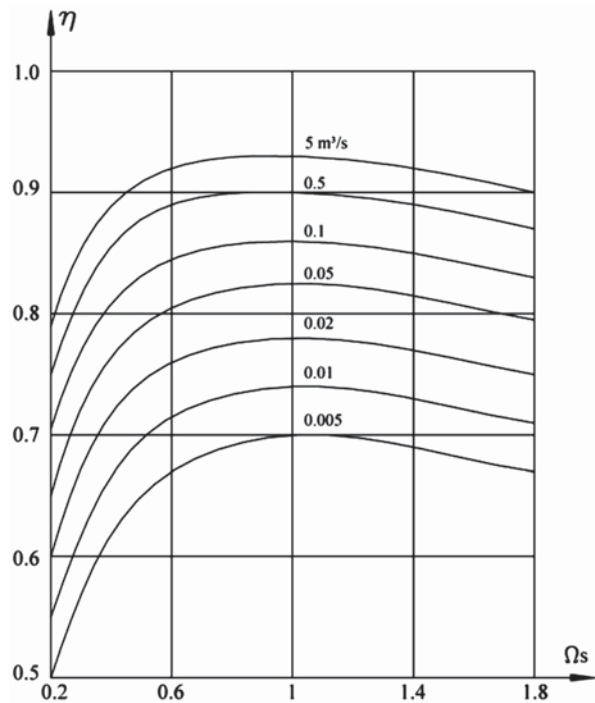


curves close due to the Reynolds number effect. Curves close as well at a high flow rate. Another phenomenon occurs there. Velocities increase at a high flow rate. As a consequence, the pressure at the suction side of the pump drops. Vapour bubbles are generated when the pressure gets lower than the vapour pressure within the fluid. This phenomenon is called *cavitation*. The vapour bubbles occupy space, causing the fluid to accelerate with higher friction losses. This affects efficiency compared to the value expected from kinematic similitude. The Reynolds number influence occurs with fans, but not the cavitation effect. So, efficiency contours stay open for high flow rate.

7.4.2 Effect of Relative Roughness

With higher Reynolds number ($Re > 10^5$) and higher relative roughness ($k/D > 10^{-3}$), the friction factor in the Moody diagram (Fig. 2.17 in Chap. 2) is mainly determined by the relative roughness. In some turbomachines, relative roughness is very low and roughness only has a very limited effect on the performance parameters. Centrifugal fans are examples. These machines are made from smooth rolled steel sheets and mostly have rather large dimensions (industrial fans: 0.5 to about 2 m). Hydraulic turbines are other examples. The rotors of these machines are cast, but they are sufficiently large (diameter from 1 to 10 m) to allow finishing by milling and grinding. Pump parts are cast and pump dimensions are mostly rather limited (rotor diameters from 0.1 to 0.5 m), precluding final polishing. Absolute roughness with pumps is approximately constant. Pump dimensions thus effect efficiency,

Fig. 7.14 Effect of machine size on efficiency with pumps (Worthington diagram). (Adapted from [10])



with lower efficiency for smaller pumps. So, a diagram such as Fig. 7.6 cannot have general validity. The diagram is calculated for an average machine size. To exemplify this aspect, Fig. 7.14 (source: [10]) renders the internal efficiency with pumps depending on specific speed at various machine sizes. This diagram, known as the Worthington diagram, is found in nearly every book on pumps. Note that machine size has no effect on the specific speed for which optimum efficiency is attained. In other words, the universal Cordier diagram keeps its validity.

7.4.3 Effect of Viscosity

Pump characteristics are mostly available for water. Use of a more viscous fluid impairs the performance because of larger friction losses (head and efficiency decrease) and larger flow displacement by boundary layers (flow rate decreases). Almost all books on pumps contain a nomogram by the Hydraulic Institute in New York [8], allowing corrections for increased viscosity. It can also be found on many internet sites (look for Hydraulic Institute viscosity correction chart). The entries of the chart are the flow rate and the head for the viscous fluid, together with the fluid viscosity. The outputs are correction factors for flow rate (C_Q), head (C_H) and efficiency (C_E). The correction relations are $Q_{vis} = C_Q Q_w$, $H_{vis} = C_H H_w$, $\eta_{vis} = C_E \eta_w$. The

relations allow calculating the flow rate and head with water (subscript w), from which the pump can be chosen. With the known efficiency in water, the efficiency with the viscous fluid can be estimated. Quite often in chemical industry the same pump or compressor is used with various fluids. Performance is normally determined by the manufacturer with water and air as fluids. Calculating the expected performance with another fluid is very important for the manufacturer because of the guarantee to be given to a user. Therefore, a calculation method for radial compressors was worked out by a group of manufacturers [3, 11]. The procedure is quite rational and may be applied to pumps too, although it has not been developed specifically for pumps.

The proposed correction factor for internal efficiency is

$$\frac{1-\eta_i}{1-\eta_{it}} = \frac{0.3+0.7 f / f_{\infty}}{0.3+0.7 f_t / f_{\infty}}. \quad (7.9)$$

In this formula, f is the friction factor from the Moody diagram (Fig. 2.17) and f_{∞} is the friction factor for very high Reynolds number for the same relative roughness. The formula presumes that 30% of the losses do not depend on the Reynolds number. The subscript t refers to the test result with air. To determine the Reynolds number, an average velocity of $0.5 u_2$ within the rotor and the stator is assumed, as well as an average hydraulic diameter of rotor and stator channels being $2 b_2$. So $Re = (u_2 b_2) / \nu$. The Moody diagram applies an equivalent sand-grain roughness (k). The technical roughness of a surface, called arithmetic roughness, is the average value of the deviation to an average surface:

$$R_a = \frac{1}{\ell} \int_0^{\ell} |y| dx.$$

Roughness values must be determined within the rotor on a blade, on the hub disc and the shroud, near the rotor outlet, and within the stator on the sidewalls and in the centre of a vane (in the case of a vaned diffuser), near the stator inlet. An average value is determined. With equivalent sand-grain roughness is meant the diameter of closely packed sand grains resulting in the same skin friction. The ratio to the arithmetic mean roughness is around 10 for values of the arithmetic roughness lower than about $20 \mu\text{m}$ [1]. So, we may assume

$$\varepsilon = \frac{k}{D_h} = \frac{10 R_a}{2 b_2} = 5 \frac{R_a}{b_2}.$$

It is assumed that half of the efficiency change affects the energy rise, by

$$\frac{\Delta E_m}{\Delta E_{mt}} = 0.50 + 0.50 \frac{\eta_i}{\eta_{it}}, \quad (7.10)$$

and the other half the work by

$$\frac{\Delta W}{\Delta W_i} = 0.50 + 0.50 \frac{\eta_{it}}{\eta_i}. \quad (7.11)$$

It is further found that the flow rate and the energy rise are related as with a rotational speed change, according to

$$\frac{Q}{Q_i} = \sqrt{\frac{\Delta E_m}{\Delta E_{mi}}}. \quad (7.12)$$

Corrections applied to flow rate and energy rise imply a correction of the kinematic similitude condition. This means that, with different fluids, operation points with optimum efficiency do not exactly correspond according to kinematic similitude. From the quoted study emerges that the calculation method is very accurate on condition that the loss change $(1 - \eta_i)$ is limited to about 20%.

Possible values for compressors are $u_2 = 300$ m/s; $d_2 = 400$ mm; $b_2 = 20$ mm; $R_a = 2 \mu\text{m}$ (milled surfaces); $\nu = 15 \cdot 10^{-6} \text{ m}^2/\text{s}$ (air). This results in $Re = (u_2 b_2)/\nu = 4 \cdot 10^5$, $\varepsilon = 5R_a/b_2 = 5 \cdot 10^{-4}$. A point in the transition area (both effect of Re and ε) corresponds in the Moody diagram. Possible values with pumps are $u_2 = 30$ m/s; $d_2 = 200$ mm; $b_2 = 10$ mm; $R_a = 20 \mu\text{m}$ (smooth sand cast surfaces); $\nu = 10^{-6} \text{ m}^2/\text{s}$ (water), resulting in $Re = (u_2 b_2)/\nu = 3 \cdot 10^5$, $\varepsilon = 5R_a/b_2 = 10^{-2}$. The point in the Moody chart is in the rough surfaces area (no effect of Re). A point within the transition area is obtained with a fluid that is ten times as viscous (light oil).

7.4.4 Rotor Diameter Reduction: Impeller Trimming

The rotor diameter may be reduced by turning on a lathe in order to lower the head of a pump (impeller trimming). When designing a pump installation, it would be a mere coincidence if an exactly appropriate pump were found with a manufacturer. In general, a pump with a slightly too high head shall be chosen. The head may then be diminished by reduction of the rotor diameter. This way, a manufacturer can cover a certain head and flow rate range with the same pump. Figure 7.15 renders an application field for a given pump type. The meaning of the coding is the diameter of the suction pipe combined with the rotor diameter. When trimming, normally only the blade tips are cut. The hub disc and the shroud, if any, often must be kept, as they contribute to the rotor sealing and the guiding of the fluid to the post-connected stator. Assuming that trimming does not change the rotor blade outlet angle, which is normally met with a good approximation, flow rate and energy rise change according to $Q \sim u_2 \sim d_2$, $\Delta E_m \sim u_2^2 \sim d_2^2$, on the basis of kinematic similitude on the outlet velocity triangle. Similitude is not perfect however. A decrease of the blade length diminishes the work done on the fluid. In other words, the slip between flow and geometry increases. This causes the energy rise to be lower than predicted by the simple reasoning. Furthermore, flow rate reduction at a constant rotational speed generates incidence at the rotor inlet and the post-connected stator. So, the

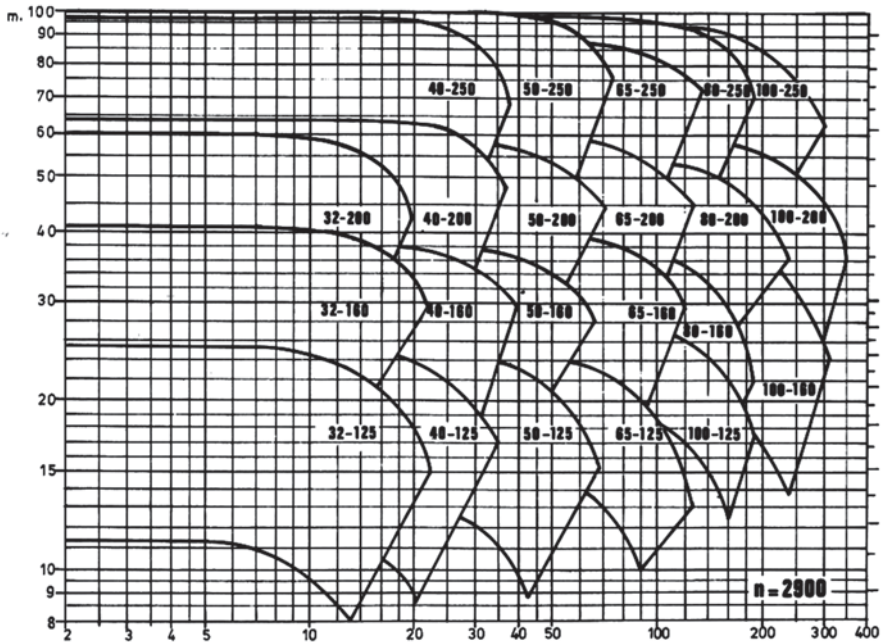


Fig. 7.15 Application field of a single-stage centrifugal pump type. (Courtesy Johnson pump, SPX Flow Technology)

efficiency diminishes somewhat. Due to the combined effects of slip increase and incidence, the rotor must be trimmed down less than predicted by the simple similitude reasoning. A reduction factor has to be applied to the theoretical diameter decrease. This factor depends somewhat on the specific speed. An average value is about 0.75 [9].

7.4.5 Reduced Scale Models

When developing large dimension machines (hydraulic turbines, large pumps), tests are sometimes performed on a reduced scale model. When using the same fluid, the Reynolds number diminishes. In addition, perfect geometric similitude is impossible due to no constant relative roughness and no constant relative clearance values. As most machines are manufactured with the same techniques (e.g. casting) or the same machine tools, wall roughness typically is of the same order of magnitude. So, absolute roughness is approximately constant and relative roughness is not. Clearances are typically kept as small as possible, requiring a certain minimum value to be workable. Further, there is never an exact geometric similitude as some parts (e.g. blades) have a minimum thickness imposed by the production technique. In order to take into account the Reynolds number decrease and the increase of relative

roughness, the relative clearances and the relative thicknesses, so-called *model laws* can be applied. Model laws are inspired by the finding that $1 - \eta$ is proportional to the friction losses and that these, according to the Moody diagram, vary within the transition area with the Reynolds number to a power between -0.25 and -0.1 . Clearly, the exponent is a rough estimate. Thus, model laws have a weak foundation and should not be overvalued.

Moody's model law for hydraulic turbines is

$$\frac{1 - \eta}{1 - \eta_0} = \left(\frac{D}{D_0} \right)^{-0.05} \left(\frac{Re}{Re_0} \right)^{-0.2}. \quad (7.13)$$

Pfleiderer's model law for centrifugal pumps is

$$1 - \eta = \left(1 - \left[\frac{1 - 70 / D^{1.5}}{1 - 70 / D_0^{1.5}} \right] \eta_0 \right) \left(\frac{Re}{Re_0} \right)^{-0.1}. \quad (7.14)$$

In the first formula, D is the rotor diameter. In the last formula, D is the diameter of the suction eye, expressed in mm. The subscript 0 refers to the model. Both formulae encompass a correction on the effect of the Reynolds number in order to take the imperfect geometric similitude into account. For pumps, Re is determined with the peripheral rotor speed ($Re = u_2 d_2 / \nu$), for turbines with the spouting velocity ($Re = \sqrt{2gH_m} d_2 / \nu$).

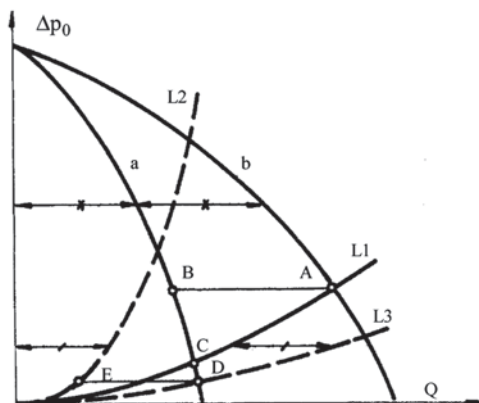
7.5 Series and Parallel Connection

If no single-rotor machine with an acceptable rotational speed can be found for a particular combination of energy change and flow rate, series or parallel connection may be considered. Connection may occur within the same machine. Series connection of rotors increases the overall energy exchange. Parallel connection increases the flow rate. These internal connections are common with pumps. They will be studied in the chapter concerned. Internal series connection is very common with compressors, steam and gas turbines. Series or parallel connection of separate machines may be chosen to enable a flexible use of the machine group.

7.5.1 Parallel Connection of Fans

Figure 7.16 shows the flow rate addition of two parallel connected identical fans. Flow rate is doubled with the same energy rise. With the load characteristic LI (typically no static part with fans), the operating point is B for an individual fan. If

Fig. 7.16 Parallel connection of two identical fans



one of the fans would break down, with reverse flow impeded, the other fan would operate in point C. Impeding reverse flow with fans is often complicated because of the large dimensions of the ducts. Assuming that $L2$ is the resistance characteristic of a freely turning fan with reverse flow, the load of the working fan then consists of two parallel connected resistances: the duct with characteristic $L1$ and the fan with resistance characteristic $L2$. Characteristic $L2$ must, as concerns the working fan, be plotted toward the side with positive flow rates. The working fan thus has a load characteristic $L3$, found by adding the abscissas of $L1$ and $L2$. The operating point of the working fan is now D, while a flow rate corresponding to E flows back through the freely turning fan.

When the fans have different characteristics (strongly different characteristics a and a' in Fig. 7.17), the characteristic of the parallel connection is again found by adding flow rates. BF represents the resistance characteristic of the working small fan, when fluid is forced to flow back. If backflow through the small fan is not impeded, the resulting characteristic is BCDE. If no reversed flow is possible (non-return valve), ADE is the resulting characteristic.

Parallel operation becomes more difficult with fans having a minimum and a maximum in their characteristic. Parallel connection of two identical fans with forward curved blades (Fig. 7.18) results in several possible branches for the characteristic of the parallel connection. Certain load characteristics intersect the system characteristic at several points. The fans in parallel connection may shuttle then between several operating points (exceptional behaviour).

7.5.2 Parallel Connection of Pumps

With parallel connected pumps, typically head losses (H_{lp}) and geometric heads (H_l) are different in the different parallel paths. Figure 7.19 shows an example with two pumps. The parallel operation may be studied by determining the difference of the

Fig. 7.17 Parallel connection of two fans with largely different dimensions

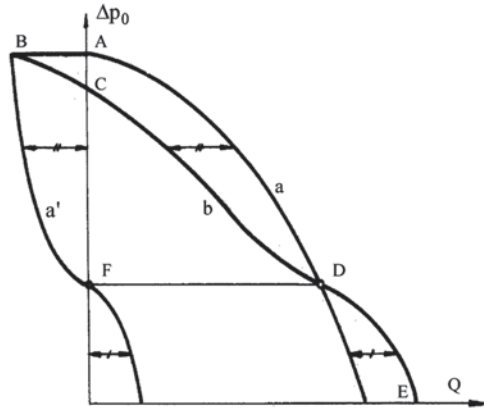
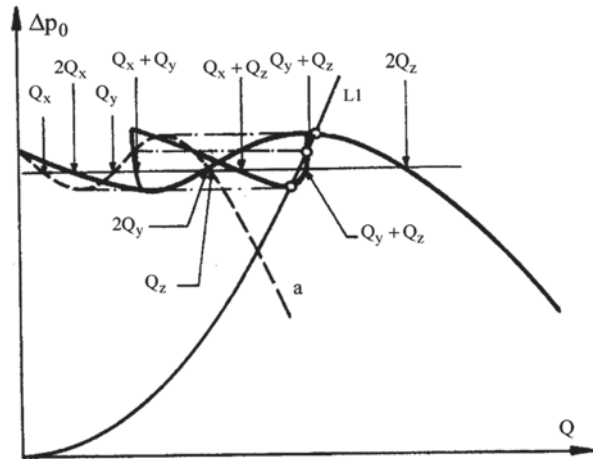


Fig. 7.18 Parallel connection of identical fans with a minimum and a maximum in the characteristic



head produced by a pump (P1) and the head consumed by the connected pipe (L1) between the suction reservoir and the node in the network (N). The thus obtained net characteristic of the left-hand branch is denoted by B1 in Fig. 7.19. The characteristic of the parallel connection of the two branches may then be determined as before, i.e. by summing the flow rates of the net characteristics B1 and B2 for equal head. The load on the resulting characteristic is the branch from the node N to the discharge reservoir.

7.5.3 Series Connection of Fans

When two fans are connected in series (different characteristics a and a' in Fig. 7.20), the characteristic of the series connection is found by adding the pressure

7.6 Turbomachine Design Example: Centrifugal Fan

This book aims at fundamental understanding of turbomachines. Design of turbomachines requires, in principle, more in-depth study, but design of a rather simple machine, such as a radial fan, is achievable with the material provided herein. As an example, we choose the fan of the laboratory test in Chap. 5. Design data for the fan are $Q=0.8 \text{ m}^3/\text{s}$ and $\Delta p_0=3500 \text{ Pa}$. We immediately mention that attaining a total pressure rise of 3500 Pa is rather challenging. From the fan chapter we learned that a head coefficient of a radial fan with backward curved blades can attain about $\psi=0.5$. With $\rho \approx 1.20 \text{ kg/m}^3$ air density it follows:

$$\psi = \frac{\Delta p_0 / \rho}{u_2^2} = 0.5 \rightarrow u_2 \approx 75 \text{ m/s}.$$

So, the required peripheral speed is rather high.

The design starts from the Cordier diagram as given in Fig. 7.7. In specialised literature, such a diagram is complemented with geometric data as diameter ratio (d_1/d_2) and width to diameter ratio (d_2/d_2) as functions of specific speed [6, 9]. These supplementary data are not strictly necessary however. The couple on the Cordier line, leading to the maximum possible speed of about 2900 rpm is $\Omega_s = 0.70, D_s = 3.80$. This results in $d_2=0.46 \text{ m}$, $n=2966 \text{ rpm}$, which we may reduce somewhat to $d_2=0.45 \text{ m}$, $n=2900 \text{ rpm}$, so $u_2=68.33 \text{ m/s}$. The required ψ then becomes 0.625.

With (3.37), for maximum deceleration in the rotor eye ($b_1/d_1 = 0.40$):

$$(d_1)_o = \sqrt{2} \left(\frac{Q}{\Omega} \right)^{1/3} = 0.195 \text{ m}.$$

We take $d_1=0.20 \text{ m}$. Then: $v_1 = 1/2 \Omega^{2/3} Q^{1/3} = 20.97 \text{ m/s}$. With $d_0=0.18 \text{ m}$:

$$v_0 = \frac{4Q}{\pi d_0^2} = 31.43 \text{ m/s}.$$

The value of v_0 is acceptable, because a typical duct

velocity may be up to 20 m/s, but with direct aspiration from the atmosphere, the inflow velocity may be as high as 30 m/s. The through-flow velocity of the rotor cannot be much lower than 20.97 m/s, because then $v_1/v_0 = 0.667$, which is quite low. So, in principle, we accept the value of v_1 .

$$Q_{\text{rotor}} = \pi d_1 b_1 \tau_1 v_1^b \approx Q / 0.9.$$

With $\tau_1 \approx 0.90$ it follows that $b_1=75 \text{ mm}$. But with $b_1/d_1=0.40$ we obtain $b_1=80 \text{ mm}$. We choose $b_1=80 \text{ mm}$. This lowers somewhat v_1 to $v_1^b = 19.65 \text{ m/s}$. The velocity ratio $v_1^b/v_0 = 0.625$ is still realisable (0.60 is the limit value).

$$u_1 = 30.37 \text{ m/s}; v_1 = Q_{\text{rot}} / (\pi d_1 b_1) = 17.68 \text{ m/s}; w_1 = \sqrt{u_1^2 + v_1^2} = 35.14 \text{ m/s}.$$

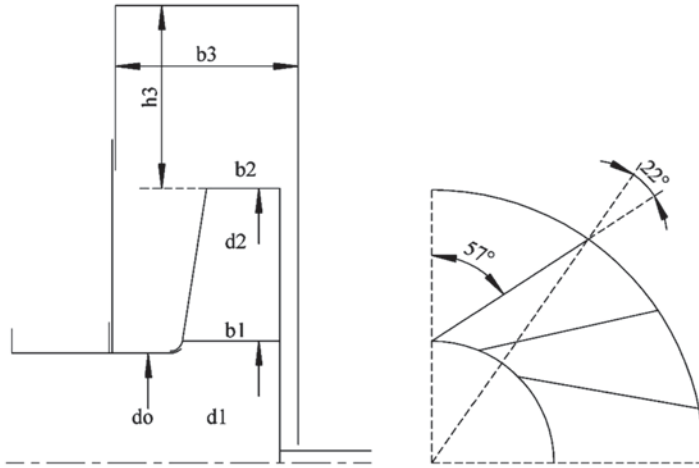


Fig. 7.21 Meridional and orthogonal sections of the rotor

$$\frac{\Delta p_0}{\rho} = 2917 \text{ m}^2 / \text{s}^2.$$

Then: $\tan \beta_1^b = -u_1 / v_1^b : \beta_1^b \approx -57^\circ$. This value then differs somewhat from the theoretically optimum value (-55°). With $\eta_i \approx 0.85 : \Delta W = 3432 \text{ J/kg}$; then $\psi = \frac{\Delta W}{u_2^2} = 0.735$ and $\Delta W = u_2 v_{2u}$, thus: $v_{2u} = 50.22 \text{ m/s}$. With an estimate of the work reduction factor of 0.80, we obtain $(v_{2u})_{\text{geo}} = 62.78 \text{ m/s}$.

Suppose that we can realise the deceleration ratio $w_2/w_1 = 0.70$. Then: $w_2 = 24.60 \text{ m/s}$, $v_{2u} = 50.22 \text{ m/s}$, $w_{2u} = -18.11 \text{ m/s}$, $w_{2r} = 16.65 \text{ m/s}$. These results seem acceptable, since with $v_1 = 17.68 \text{ m/s} : v_{2r}/v_1 = 0.94$.

Geometrically: $(w_{2u})_{\text{geo}} = -5.55 \text{ m/s}$, $v_{2r}^b = Q_{\text{rot}} / (\pi d_2 b_2 \tau_2) = 17.47 \text{ m/s}$, thus $\beta_2^b \approx -17.6^\circ$. The rotor blades can only be swept moderately backward. We knew this already, as $\psi = 0.735$ is quite high. With straight blades, to $\beta_1^b = -57^\circ$ corresponds $\beta_2^b = -22^\circ$ (see Fig. 7.21). So, we can opt for straight backward inclined blades. The fan might then realise somewhat less total pressure rise than the target value, because the blade outlet angle is somewhat too big in magnitude. If it later turns out to be necessary, we may enlarge the outlet diameter somewhat.

Width at outlet: $Q_{\text{rotor}} = \pi d_2 b_2 v_{2r} : b_2 = 38 \text{ mm}$. We take $b_2 = 40 \text{ mm}$.

$$C_M = \frac{w_{2r} v_{2u}}{\sigma_M w_2^2} \approx 1.0, \text{ which gives } \sigma_M \approx 1.38, \text{ with } \sigma_M = \frac{Z M_{st}}{2\pi r_2 b_2 r_2}.$$

$M_{st} = \int b r dr = \frac{b_1 r_1 + b_2 r_2}{2} (r_2 - r_1) : Z = 16.5$. We take $Z = 16$. Choice of plate thickness: $t = 3 \text{ mm}$.

We can now correct the velocity triangles, using improved values of the obstruction factors. At this stage, we still take $\eta_v = 0.90$ and $\eta_i = 0.85$.

Inlet triangle

$$\beta_1^b = -57^\circ, \tau_1 = \frac{\pi d_1 - Zt / \cos \beta_1^b}{\pi d_1} = 0.860,$$

$$v_1^b = \frac{Q}{\pi d_1 b_1 \tau_1 \eta_v} = 20.40 \text{ m/s};$$

$$u_1 = 30.37 \text{ m/s}; v_1 = \tau_1 v_1^b = 17.68 \text{ m/s}; w_1 = 35.14 \text{ m/s}.$$

Outlet triangle:

$$\beta_2^b = -22^\circ, \tau_2 = \frac{\pi d_2 - Zt / \cos \beta_2^b}{\pi d_2} = 0.963,$$

$$v_{2r}^b = \frac{Q}{\pi d_2 b_2 \tau_2 \eta_v} = 16.32 \text{ m/s}; v_{2r} = \tau_2 v_{2r}^b = 15.72 \text{ m/s}.$$

Slip:

$$\psi = \lambda \left(2.5 + \frac{\beta_2^0}{60} \right) = 0.75 \times (2.5 - 0.367) = 1.60;$$

$$Pf = \frac{\psi}{Z} \frac{2b_2 r_2^2}{(b_2 r_2 + b_1 r_1)(r_2 - r_1)} = 0.191, \varepsilon = \frac{I}{1 + Pf} = 0.840,$$

$$(v_{2u})_{geo} = u_2 + v_{2r}^b \tan \beta_2^b = 61.74 \text{ m/s}; v_{2u} = \varepsilon (v_{2u})_{geo} = 51.86 \text{ m/s}.$$

Thus: $\Delta W = 3544 \text{ J/kg}; \Delta p_o = \eta_i \rho \Delta W = 3614 \text{ Pa}.$

For the scroll, we first try a width leap of 2.5 (standard value): $b_2' = 100 \text{ mm}$. The radial velocity is then $v_{2r}' = Q / (\pi d_2 b_2') = 5.66 \text{ m/s}$; with $v_{2u} = 51.86 \text{ m/s}; \alpha_2 = 83.77^\circ$. This angle is somewhat too small for a compact scroll. The tangential angle is optimally around 5° , thus $\alpha_2 \approx 85^\circ$. With $\alpha_2 = 85^\circ$:

$$\ln \left(\frac{r_3}{r_2} \right) = \frac{2\pi}{\tan \alpha_2} \rightarrow \frac{r_3}{r_2} = 1.733 \rightarrow r_3 = 390 \text{ mm}; h_3 = r_3 - r_2 = 165 \text{ mm}.$$

The velocity at the outlet of the scroll is then on average $(b_2' = b_3): Q / (h_3 \times b_3) = 48.48 \text{ m/s}$. This velocity is too high. In order to reach the same velocity level as at the entrance, the outlet section must be equivalent to a circle with diameter 180 mm. This may be realised with $b_3 = h_3 = 150 \text{ mm}$ and then a divergent part to $h_4 = 170 \text{ mm}, b_4 = 150 \text{ mm}$. We try $b_2' = b_3 = 150 \text{ mm}$.

$$\text{Then: } v_{2r}' = 3.77 \text{ m/s}, \alpha_2 = 85.84^\circ: \frac{r_3}{r_2} = 1.579 \rightarrow r_3 = 355 \text{ mm}.$$

With $h_3 = 150 \text{ mm}$, we enlarge radius r_3 to 375 mm. The theoretical flow rate at the scroll outlet, with $v_u r = \text{constant}$, is $\int_{r_2}^{r_3} \frac{v_{2u} r_2}{r} b_3 dr = 0.894 \text{ m}^3/\text{s}$. The actual flow rate is about 10% smaller due to boundary layer obstruction. So, the scroll is correct.

We take a tongue clearance of about 10% of the radius: about 22.5 mm. The opening angle of the scroll is calculated for the first sector of 30° with $b_3 = b_2$, because the flow expansion by the width leap cannot be sudden. This way, the tongue clearance becomes 20 mm. For the rest of the scroll, the full width is used, but the scroll is made somewhat larger than calculated with the logarithmic spiral.

The width leap to the scroll becomes quite large: 40 mm/150 mm. Common practice is then to widen the rotor at the outlet, for instance to 60 mm. Then, the strongest possible deceleration is realised in the rotor, but at rotor outlet the flow is then separated. We may accept that a velocity reduction of 0.7 is possible between the inlet flow just after rotor entrance and the outlet flow just before rotor exit, so before slip. Enlargement of the rotor width at outlet is commonly used with fans with slightly backward leaning blades or forward curved blades. For forward curved blades, typically the outlet width is taken equal to the inlet width, because the diameter ratio is near to unity (see Fig. 3.19). Figures 7.21 and 7.22 show the geometry. A final calculation of the performance of the fan can now be made (see Exercise 7.7.6).

7.7 Exercises

7.7.1. Reason that, with a radial fan or pump, the similitude laws with a change of rotational speed, $Q \sim n$, $\Delta p_0 \sim n^2$, stay valid in the presence of incidence at the rotor and the scroll inlets.

7.7.2. $Q = 0.20 \text{ m}^3/\text{s}$, $H_m = 30 \text{ m}$, $\eta_{\text{global}} = 0.75$ are measured at a pump with $n = 1450 \text{ rpm}$. The fluid is water with $\nu = 10^{-6} \text{ m}^2/\text{s}$. Determine flow rate, head and efficiency of the pump when doubling the rotational speed for a similar flow. Assume a volumetric efficiency and a mechanical efficiency of respectively 1 and 0.9 and assume that these values do not change. Correct the internal efficiency for imperfect similarity by means of Pfleiderer's formula (7.14). Correct head and flow rate according to the formulae of Casey and co-authors (7.10–7.12). Consider the method of Casey et al. (7.9) as an alternative for the efficiency correction. Assume $R_a = 20 \mu\text{m}$ for that. Determine an approximation for the rotor diameter and the rotor width at outlet assuming a work coefficient 0.4 and a flow angle -70° at the rotor outlet. Note that the correction on efficiency is small with (7.14) and that it even becomes smaller with (7.9).

A: $H_m = 120.80 \text{ m}$, $Q = 0.401 \text{ m}^3/\text{s}$, $d_2 \approx 400 \text{ mm}$, $b_2 \approx 26.5 \text{ mm}$.

7.7.3. Consider the pump of the previous exercise once more. Take as approximations for rotor diameter and rotor width at outlet 400 mm and 25 mm. Determine for $n = 1450 \text{ rpm}$ the head and the flow rate for operation with a light oil with $\nu = 200 \cdot 10^{-6} \text{ m}^2/\text{s}$ in the operating point homologous to $Q = 0.20 \text{ m}^3/\text{s}$ and $H_m = 30 \text{ m}$ with water. Correct for imperfect similitude with the formulae of Casey and co-authors (7.10–7.12). Use the formula of Haaland to describe the Moody diagram (Sect. 2.3.1 in Chap. 2).

A: $H_m = 28.83 \text{ m}$, $Q = 0.196 \text{ m}^3/\text{s}$.

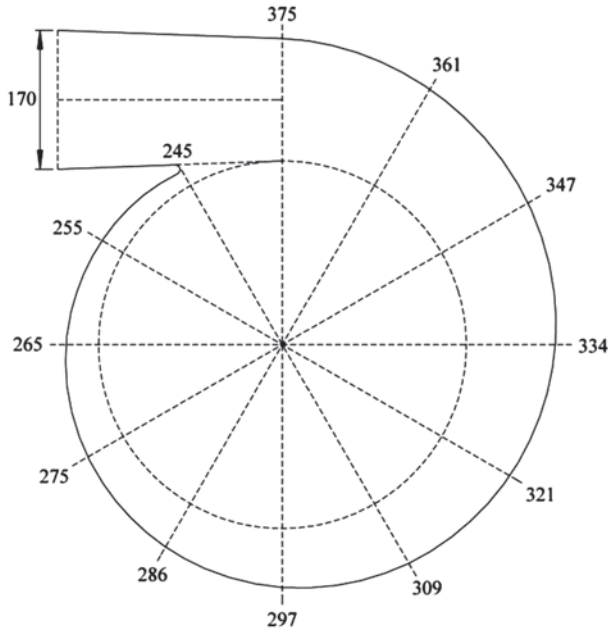


Fig. 7.22 Orthogonal section of the volute

7.7.4. A 1/10 scale model should be built of a hydraulic turbine with 40 MW shaft power, 50 m manometric head, 100 rpm rotational speed and overall efficiency 0.90. The available head in the laboratory is 6 m. Determine the rotational speed of the model, the expected flow rate and the shaft power, with similar flow. Correct the efficiency for imperfect similitude by means of Moody's formula (7.13). Apply the correction to the overall efficiency, in other words assume volumetric and mechanical efficiencies both equal to unity. Correct power and flow rate by the method of Casey et al. (7.10–7.12). Note that head and work have to be switched in these formulae for use with turbines. Observe that the efficiency correction is quite big with a 1/10 scale ratio.

A: $H_m = 6.0$ m, $Q = 0.292$ m³/s, $n = 333.8$ rpm, $\eta = 0.780$, $P = 13.42$ kW.

7.7.5. A throttle valve connected in series with a pump is a traditional way of flow rate adjustment, as discussed in Sect. 7.3. An alternative way is fitting a bypass line to the pump connecting the discharge side to the suction side with the throttle valve in the bypass line. The net flow rate of the pump is then reduced by circulating part of the flow rate. Determine the net characteristic of the pump combined with the valve in both cases. Observe that with the valve in series the net head is mainly reduced for high flow rate while with the valve in parallel the net head is mainly reduced for low flow rate.

7.7.6. Calculate flow rate and total pressure rise in the design point of the fan rendered in Figs. 7.21 and 7.22 with the methods of Chap. 3. Compare with the target values $Q = 0.80$ m³/s and $\Delta p_0 = 3500$ Pa at 2900 rpm.

- Consider that, at the design operating point, the inlet flow of the rotor is aligned with the blade direction after the flow has entered. Determine the design rotor flow rate under this condition.
- Take into account that the deceleration in a rotor channel cannot be stronger than 0.70. Interpret that this applies to the inlet flow after rotor entrance (w_1^b) and the outlet flow before rotor exit, so before slip (w_2^b). Observe that the deceleration limit is reached. Take as flow model a core flow with uniform flow velocity (w_2^b) at the pressure side of a rotor channel and a zero flow velocity zone at the suction side (jet and stagnant wake model). Assume that Pfleiderer's work reduction factor formulae (Chap. 3: 3.23–3.25) apply to the core flow. Determine rotor work with this assumption.
- Consider the dump diffusion at the entrance of the volute as between the core flow in the rotor channels and a uniform flow immediately downstream of the rotor outlet, filling the full width of the volute. Due to the partial filling of the rotor channels, the dump diffusion loss is considerably larger than with full through-flow.
- Calculate the leakage flow between the volute and the rotor inlet assuming that the total pressure at the volute side of the gap is the static pressure at the volute entrance after dump diffusion (station 2') and that the pressure at the rotor side of the gap is the inlet pressure of the rotor (station 1). Ignore contraction in the leakage flow. Assume that the gap width is 2 mm.
- Calculate the incidence loss at the entrance of the volute assuming that angular momentum is conserved between the volute inlet, after tangential deflection due to incidence (station 2'), and the volute outlet (station 3). The velocity distribution at the volute outlet follows from the net flow rate.
- Determine the total pressure rise of the fan taking into account the dump diffusion loss and the incidence loss at volute entrance. Neglect the other losses. This leads to some overestimation of the total pressure rise. Take as density $\rho = 1.20 \text{ kg/m}^3$.

A: $Q_{\text{rotor}} = 0.853 \text{ m}^3/\text{s}, \epsilon_{\text{Pfleiderer}} = 0.816, \Delta W = 3290.1 \text{ J/kg},$
 $q_{\text{irr}}^{\text{dump}} = 180.27 \text{ J/kg}, (\Delta p/\rho)_{\text{gap}} = 2086.5 \text{ J/kg}, Q_{\text{leak}} = 0.0763 \text{ m}^3/\text{s}, \eta_v = 0.911,$
 $Q_{\text{net}} = 0.777 \text{ m}^3/\text{s}, q_{\text{irr}}^{\text{incid}} = 4.75 \text{ J/kg}, \Delta p_0 = 3726 \text{ Pa}, \eta_i = 0.944.$

The calculated flow rate is somewhat lower than the target value. The calculated pressure rise is larger than the target value, but the inlet loss in the rotor eye and friction losses are not taken into account. The internal efficiency should decrease until 0.887 for obtaining the target value of the total pressure rise.

7.7.7. Calculate flow rate and total pressure rise in the design point of the fan rendered in Figs. 7.21 and 7.22 from the measured values at 2750 rpm (Chap. 5). Scale the laboratory test results from 2750 rpm to 2900 rpm with kinematic similitude, assuming that efficiency is unchanged.

A: The scaled measured values of flow rate and total pressure rise at the best efficiency operating point are $0.725 \text{ m}^3/\text{s}$ and 3590 Pa . The best efficiency flow rate is

always somewhat lower than the design flow rate. With the flow rate at the design operating point estimated at 10% higher than at optimum efficiency, the estimated design flow rate is $0.80 \text{ m}^3/\text{s}$. The corresponding interpolated value of the total pressure rise is 3470 Pa. The obtained values of flow rate and total pressure rise are very near to the target values.

References

1. Adams T, Grant C, Watson H (2012) A simple algorithm to relate measured surface roughness to equivalent sand-grain roughness. *Int J Mech Eng Mechatron* 1:66–71
2. Balje OE (1981) *Turbomachines: a guide to design, selection and theory*. Wiley, ISBN 0-471-06036-4
3. Casey MV (1985) The effects of Reynolds number on the efficiency of centrifugal compressor stages. *J Eng Gas Turbines Power* 107:541–548
4. Dietzel F (1980) *Turbinen, Pumpen und Verdichter*. Vogel Verlag, ISBN 3-8023-0130-7
5. Dubbel H (2001) *Taschenbuch für den Maschinenbau*, 20th edn. Springer, ISBN 3-540-67777-1
6. Eck B (1972) *Ventilatoren*, 5th edn. Springer, ISBN 3-540-05600-9
7. Fuchslocher-Schulz H (1967) *Die Pumpen*, 12th edn. Springer, (no ISBN)
8. Hydraulic Institute standards for centrifugal, rotary and reciprocating pumps. The Hydraulic Institute, New York
9. Pfleiderer C. (1961) *Die Kreiselpumpen für Flüssigkeiten und Gase*, 5th edn. Springer (no ISBN)
10. Pfleiderer C, Peterman H (1991) *Strömungsmaschinen*, 6th edn. Springer, ISBN 3-540-53037-1
11. Strub LA, Casey MV et al (1987) Influence of the Reynolds number on the performance of centrifugal compressors. *J Turbomach* 109:541–544

Chapter 8

Pumps

Abstract The fundamentals of pump operation have been fully treated in the foregoing chapters. Three particular aspects are discussed in the present chapter. The first is evaporation of the fluid in liquid state when the pressure inside the pump becomes lower than the vapour pressure. Cavities with vapour then emerge and the phenomenon is generally described as cavitation. The second concerns starting up. Priming is necessary. This is filling the pump and the suction pipe with the liquid to be pumped. The third topic is the intersection of the pump characteristic with the load characteristic, which mostly has a large static part. The intersection does not necessarily result in a stable operating point. Cavitation, priming and stability are discussed in the present chapter. Further topics are some aspects concerning shaping of the components, construction and special applications.

8.1 Cavitation

8.1.1 Cavitation Phenomenon and Cavitation Consequences

Cavitation occurs when a liquid evaporates locally with generation of a vapour cavity due to static pressure decrease under vapour pressure. The vapour pressure of a liquid strongly depends on temperature and may be very low at atmospheric temperature. At 15 °C, the vapour pressure of water is about 2 kPa. It is nevertheless possible that such a low pressure is attained at the entrance of a pump. Intervening phenomena are decrease of static pressure due to suction height, pressure drop by losses and pressure drop by dynamic effects.

Cavitation mainly has two consequences. First, there is erosion. Cavitation-generated vapour bubbles are conveyed by the flow and condense at places where the static pressure again exceeds the vapour pressure. This occurs in a fast collapse, termed *implosion*. The colliding edges of a cavity generate strong liquid jets impacting on material walls. The material surface crumbles locally and pits are formed that gradually may grow into perforations. The phenomenon is termed *pitting*. Fatigue-resisting materials resist cavitation erosion the best. When cavitation is unavoidable, it is advisable to manufacture the pump from a stainless steel type, e.g. 18/8

chrome-nickel steel. But cavitation leading to erosion is mostly prevented. Ship propellers are exposed to the same phenomenon, but the difference with pumps is that the vapour bubbles can easily be kept away from material surfaces. So cavitation does not necessarily result in cavitation erosion.

Vapour bubbles hardly affect the flow with incipient cavitation (beginning of cavitation), so that the performance characteristics do not change. Developed cavitation, i.e. with significant vapour bubble zones, affects the flow. The through-flow velocity is locally enlarged by the obstruction by the vapour bubbles and the flow direction is changed. Both effects result in higher losses. Pump efficiency and head decrease with developed cavitation.

8.1.2 *Types of Cavitation*

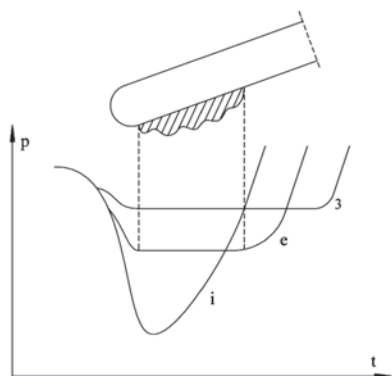
With flow over free-standing hydrofoils or over convex bends in walls, incipient cavitation mostly occurs at some distance from the material walls. Several types may be distinguished: bubble cavitation, sheet cavitation, cloud cavitation and vortex cavitation. Bubble cavitation refers to individual bubbles within the fluid. These bubbles originate around nuclei of dissolved air mixed with vapour. Bubbles joining together to a larger zone are termed sheet or cloud cavitation, depending on whether the zone adopts the form of a thin surface or rather of a full space. Vortex cavitation arises within the low-pressure core of tip vortices. In that case, bubbles join to lines following the vortex core. Cavitation within the tip vortex of a ship propeller blade is a typical example. With cavitation by bubbles, whether or not joining in lines, sheets or clouds, the presence of cores with gas and vapour is crucial. Gases, as air, do not completely dissolve in water. Cores, called nuclei, are generated due to surface tension. The pressure within a core exceeds the pressure in the surrounding fluid because of surface tension. The smaller the radius of a (spherical) core, the larger the pressure difference is. Gas in the core is mixed with an amount of vapour from the fluid. Cavitation starts when cores strongly expand due to evaporation of the fluid. Therefore, due to surface tension, the pressure around a core must be below the vapour pressure, as vapour pressure, by definition, is the pressure with which the liquid evaporates in equilibrium with the vapour, i.e. with a very large contact surface, so without the effect of surface tension. The required pressure difference under vapour pressure approximately amounts, at 20°C in water [4], to: 1 bar with core radius 1 μm , 0.1 bar with core radius 10 μm , 0.01 bar with core radius 100 μm . In the presence of only small cores, tension must be exerted on the liquid before cavitation bubbles can be generated. Cores are rather large in industrial water, with the radius of the largest cores typically in the 30 μm order. The required pressure difference below the vapour pressure is then not very high, about the magnitude of the vapour pressure itself. One could say that cavitation occurs with pressure in the liquid approximately equal to zero pressure. The exact pressure within the liquid at which cavitation occurs is termed the critical pressure (critical regarding cavitation). This value applies under

static conditions. Inertia and viscous effects intervene as well within a flow. These generate delay between the location where the critical pressure is reached and the location of bubble formation. The equation describing the radius of a bubble, as a function of surface tension and viscous forces, is known as the Rayleigh-Plesset equation [1, 4]. It allows the calculation, with numerical methods, of bubble generation, if the critical pressure is known. The liquid state determining the critical pressure is termed *water quality*. It mainly concerns the size of the largest cores and the thermodynamic state, first of all the temperature. The critical pressure is rather difficult to predict, which makes the calculation of bubble cavitation (and derived forms) a quite delicate matter.

The study of incipient cavitation (bubble cavitation) is not crucial with pumps and hydraulic turbines, as incipient cavitation neither causes erosion nor performance decrease. For these phenomena to occur, a significantly large cavitation zone is required. A large zone is always attached to the suction side of a blade and, therefore, the term *attached cavitation* is used. With an attached cavitation bubble, it may be assumed that the pressure within and around the bubble is vapour pressure with no interfering effect of surface tension. The occurrence of cavitation thus becomes independent of water quality. Henceforth we assume that cavitation occurs as soon as the local pressure attains the vapour pressure. This is a justified assumption for developed cavitation. Further, we may assume that the vapour pressure at the cavitation bubble has the same value as at the pump inlet. This is a good assumption for a cold fluid. For a fluid near evaporation, the vapour pressure at the cavitation zone may significantly be lower than at the pump entrance because the latent heat necessary for vaporisation lowers the local temperature.

Figure 8.1 sketches the pressure distribution in absence of cavitation on the leading zone of a rotor blade of a centrifugal pump with zero incidence. The leading edge is mostly an ellipse with a 2/1 radius ratio, followed by a constant thickness zone. The minimum value of the pressure coefficient $(C_p)_{min} \approx -1$ at zero incidence. When the leading edge features a better hydrodynamic profile, which is possible with large centrifugal pumps, acceleration at the leading edge, and so pressure

Fig. 8.1 Suction side pressure distribution on the leading edge zone of a blade profile of a centrifugal pump; *i* in absence of cavitation (or at incipient cavitation); *e* with a bubble that large that erosion occurs; 3 with a bubble causing performance drop



drop, may be lower. Thus the value of $(-C_p)_{min}$ at zero incidence may fall until about 0.5. With axial pumps, blades always feature a hydrodynamic profile and the $(-C_p)_{min}$ value may be similarly low. Additional acceleration occurs with positive incidence, increasing $(-C_p)_{min}$ by 0.2–0.3 per degree of incidence until a limit value is attained when the flow separates, which occurs at 5–6° incidence. In case of negative incidence, suction may occur at the leading edge of the pressure side and $(-C_p)_{min}$ may increase rather strongly. The $(-C_p)_{min}$ change is thus very strong with the variation of incidence. Figure 8.1 also sketches the pressure distribution in the presence of a large cavitation bubble. There is vapour pressure within the bubble, levelling out the minimum in the pressure profile. A bubble that is sufficiently big for causing erosion typically features a $(-C_p)_{min}$ plateau value around 0.3. This value increases somewhat at positive incidence (flow rate lower than design). When the cavitation zone expands so much that it obstructs the through-flow, pump performance is affected. Head and efficiency decrease. With a flow rate smaller than the design value, obstruction becomes noticeable when the separation zone extends into the throat of the blade passage. The corresponding value of $(-C_p)_{min}$ is typically about 0.15 [6]. With a flow rate larger than the design value, obstruction already becomes noticeable with a smaller cavitation zone, but the corresponding $(-C_p)_{min}$ is of the same order of magnitude. The cavitation zone in Fig. 8.1 is highly unsteady in reality. Fluid parts are continuously entering and evaporating and fluid parts also continuously leave the zone and implode.

8.1.3 Cavitation Assessment: Cavitation Number and Required Net Positive Suction Height

Two concepts are applied for assessing cavitation risk and cavitation degree.

The cavitation number is a pressure coefficient using the pressure and the velocity of the oncoming flow, like a pressure coefficient for description of the pressure distribution on a blade:

$$\sigma = \frac{p_l - p_v}{\frac{1}{2} \rho w_l^2}. \quad (8.1)$$

Vapour pressure is denoted with p_v . Pressure and velocity just upstream of the pump rotor inlet are p_l and w_l . The cavitation number is an internal quantity, which, strictly, cannot be determined by external measurements. The pressure at the pump inlet is in practice used as an approximation of p_l . There is a small difference with the pressure just upstream of the rotor inlet due to inlet losses. The velocity w_l can be determined with a good approximation by

$$w_l^2 = u_l^2 + v_l^2, \quad (8.2)$$

where u_l stands for the blade speed at rotor inlet and v_l follows from the flow rate and the through-flow area. The pressure p_l for which there is incipient cavitation on the blade determines a critical value of the cavitation number:

$$\sigma_i = \frac{(p_l - p_v)_i}{\frac{1}{2}\rho w_l^2}. \quad (8.3)$$

The subscript i indicates incipient cavitation. The value of σ_i may be determined from the pressure distribution on the rotor blade. The pressure coefficient is

$$C_p = \frac{p - p_l}{\frac{1}{2}\rho w_l^2} \text{ so } \sigma_i = -(C_p)_{\min}. \quad (8.4)$$

As argued in the previous section, incipient cavitation is not very relevant. We study erosion cavitation. The corresponding value of the cavitation number is $\sigma_e \approx 0.3$. In view of the blade speed in (8.2), it is obvious that the tip section normally is the most critical. With axial pumps, the hub zone may be critical as well, due to the acceleration around the leading side of the hub.

The concept of NPSH (*net positive suction head*) is applied as externally determinable quantity. By definition, NPSH is the difference between the total pressure at the suction flange and the vapour pressure, expressed in height. When the difference is expressed in energy, the term NPSE (net positive suction energy) is used. When determining the pressure at the suction flange, it is corrected to the centre of the rotor inlet. By this, NPSH becomes approximately independent of the exact position of the pressure reading point.

$$NPSE = gNPSH = \frac{p_s}{\rho} + \frac{v_s^2}{2} - \frac{p_v}{\rho}. \quad (8.5)$$

The subscript s refers to the suction flange. When defining NPSH, total pressure is applied, as dynamic pressure is also available as protection against cavitation. In order to avoid cavitation, NPSH should take a minimum positive value, indicated with NPSH required: $NPSH_r$. The subscript r stands for *required*. This minimum value follows from the summation of the pressure changes between the suction flange and the location with minimum pressure on the rotor blades. The total pressure at the rotor inlet is lower than the total pressure at the pump inlet, due to losses within the inlet section:

$$\frac{p_s}{\rho} + \frac{v_s^2}{2} = \frac{p_l}{\rho} + \frac{v_l^2}{2} + \xi \frac{v_l^2}{2}. \quad (8.6)$$

The loss coefficient ξ is low, typically about 0.1. The pressure drop between the rotor inlet and a location on the rotor blade is determined by the pressure coefficient:

$$-C_p = \frac{p_l - p}{\frac{1}{2}\rho w_l^2}. \quad (8.7)$$

When cavitation occurs on the location considered, pressure equals the vapour pressure. We may then replace $-C_p$ with σ according to (8.1). The NPSH value required to avoid cavitation should meet

$$NPSH > NPSH_r \quad \text{with} \quad gNPSH_r = (1 + \xi) \frac{v_l^2}{2} + \sigma \frac{w_l^2}{2}. \quad (8.8)$$

The NPSH value is always positive and that feature is referred to in the terminology. The highest, and thus most critical value of NPSH, is attained for the most unfavourable combination of v_l and w_l . With a centrifugal pump, the most unfavourable combination is at the casing.

Henceforth we reason with centrifugal pumps. The hub side may be most critical with axial pumps. This complicates the reasoning, but the results derived hereafter may be applied qualitatively to axial pumps as well. We reason with a pump with supply to the suction eye in line with the shaft, as in Fig. 1.13 of Chap. 1. The reasoning is the same for a mixed-flow pump (see the further Fig. 8.12) or for an axial pump (see Fig. 1.3 in Chap. 1) with a similar suction eye. We note the highest value of $NPSH_r$ as

$$gNPSH_r = \lambda \frac{v_l^2}{2} + \sigma \frac{w_l^2}{2}, \quad (8.9)$$

with $w_l^2 = u_l^2 + v_l^2$ and $u_l = \frac{\Omega d_l}{2}$,

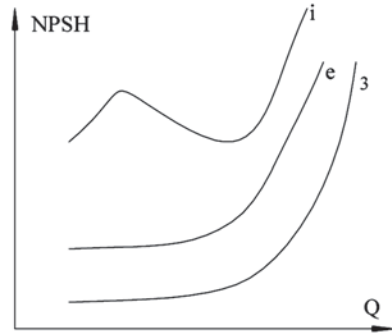
where d_l is the diameter of the rotor inlet at the casing or the rotor shroud. The value of $\lambda \approx 1.1$. The velocity v_l at the corresponding position may be estimated from the velocity v_0 at the inlet of the eye of the rotor by a velocity factor:

$$\xi = \frac{v_l}{v_0} \quad \text{with} \quad v_0 = \frac{4Q}{\pi d_o^2}.$$

Thus:
$$v_l = 4 \left(\frac{\xi}{k\pi} \right) \frac{Q}{d_l^2}. \quad (8.10)$$

We take here into account that the leakage flow in a pump is negligible. The diameter of the suction eye of the rotor is denoted with d_o . The factor k is the square of the ratio (d_o/d_l) , typically about $(0.9)^2$. If the shaft passes through the suction eye, this factor must also take into account the obstruction by the hub around the shaft. With (8.10), we use a similar notation as we did with the optimisation of the inlet of the rotor of a radial fan (Sect. 3.4.10). Generally, the velocity factor ξ is unity in a pump

Fig. 8.2 Variation of $NPSH_i$, $NPSH_e$ and $NPSH_3$



(see next section). For the study of incipient cavitation, the cavitation number σ_i must be introduced. This number significantly changes with incidence. The NPSH value corresponding to start of erosion is denoted with $NPSH_e$. In practice, the effect on performance is mostly determined with a criterion of 3% head drop due to cavitation. We indicate the corresponding value with $NPSH_3$. The σ -values are $\sigma_e \approx 0.3$ and $\sigma_3 \approx 0.15$. $NPSH_1$ (1% decrease) is sometimes used as well.

Figure 8.2 sketches the variation of $NPSH_i$, $NPSH_e$ and $NPSH_3$ [2, 3]. The deviating variation of $NPSH_i$ at very low flow rate is due to circulating flow at the pump inlet. Typically, manufacturers only publish curves of $NPSH_3$ in their catalogues, as this quantity can easily be determined experimentally. The value of $NPSH_i$ may only be determined reliably the optical way. This is feasible when the pump inlet is observable through transparent parts, especially manufactured for this purpose. Measuring of $NPSH_e$ cannot be performed easily. It requires long duration operation of a pump and damage observation. A pump user should know that the $NPSH_e$ value may significantly exceed the $NPSH_3$ value. Individual manufacturers do not supply precise information concerning this aspect. It is commonly advised to keep a safety margin of 0.5 m on the value of $NPSH_3$. This margin is mostly not sufficient to prevent erosion. Complete prevention of erosion may require a safety factor of about 2 on the $NPSH_3$ value, according to the European association of manufactures [2], since σ_e is about twice as high as σ_3 (see exercise 8.8.2).

8.1.4 Optimisation of the Inlet of a Centrifugal Pump Rotor

With operation in the design point, coefficients λ and σ in expression (8.9) for $NPSH_r$ have a fixed value. $NPSH_r$ may easily get minimised [9]. First, we remark that the NPSH value cannot be improved by introducing pre-swirl, since λ is larger than σ . Formula (8.9) takes the form

$$2gNPSH_r = ax^{-2} + bx,$$

with $x = d_I^2$, $a = (\lambda + \sigma) 16 \left(\frac{\zeta}{k\pi} \right)^2 Q^2$, $b = \frac{\sigma \Omega^2}{4}$.

The optimum follows for $x_o^3 = \frac{2a}{b}$. Thus:

$$(d_I)_o = \left(128 \frac{\lambda + \sigma}{\sigma} \right)^{1/6} \left(\frac{\zeta}{k\pi} \right)^{1/3} \left(\frac{Q}{\Omega} \right)^{1/3}. \quad (8.11)$$

With optimisation to erosion with $\lambda \approx 1.1$ and $\sigma \approx 0.3$ it follows, for $\zeta = 1$:

$$(d_I)_o \approx 2.125 \left(\frac{Q}{\Omega} \right)^{1/3}. \quad (8.12)$$

The corresponding NPSH_r value is

$$(gNPSH_r)_o = \left(\frac{2a}{b} \right)^{1/3} \left(\frac{3b}{4} \right) = \left(128 \frac{\lambda + \sigma}{\sigma} \right)^{1/3} \left(\frac{\zeta}{k\pi} \right)^{2/3} \left(\frac{3\sigma}{16} \right) \Omega^{4/3} Q^{2/3},$$

or $(gNPSH_r)_o \approx \frac{1}{4} \Omega^{4/3} Q^{2/3}. \quad (8.13)$

This result allows the definition of a specific speed, termed *suction specific speed*:

$$\Omega_{ss} = \frac{\Omega \sqrt{Q}}{(gNPSH_r)^{3/4}}. \quad (8.14)$$

From (8.13) it follows that the optimum suction specific speed is about 3 for $\lambda = 1.1$ and $\sigma = 0.3$. The shape of the velocity triangle at the inlet is fixed for minimum NPSH_r. From (8.12) it follows that the corresponding u_I and v_I are

$$u_I = \frac{\Omega d_I}{2} \approx 1.063 \Omega^{2/3} Q^{1/3} \text{ and } v_I = \frac{4\zeta Q}{k\pi d_I^2} \approx 0.348 \Omega^{2/3} Q^{1/3}.$$

Hence: $(tg\beta_I)_o = -(u_I / v_I)_o = -2 \sqrt{\frac{\lambda + \sigma}{\sigma}} \approx -3.05$, from which $\beta_I \approx -72^\circ$.

The remarkable result is that the optimum blade angle does not depend on flow acceleration or deceleration at the inlet of the rotor (factor $\zeta/k\pi$). It should be noticed that the obtained value is the blade angle at the casing. On the average radius, the magnitude of the angle may be lower (if there is radius variation). The pump inlet may also be optimised with respect to losses. A similar reasoning as with NPSH applies, but with λ and σ representing loss coefficients. For $\lambda = 0.1$ and $\sigma = 0.1$ (losses

at the inlet of the rotor), the blade angle is $\beta_l \approx -63^\circ$. Some researchers argue, similarly as with radial fans, that optimum internal efficiency is attained by minimisation of the relative speed w_l at the tip [7, 10]. The corresponding values then are $\lambda=0$ and $\sigma=1$ and the blade angle becomes $\beta_l \approx -55^\circ$ (as with the radial fan). With a smaller magnitude of the blade angle corresponds a higher through-flow velocity. The rotor inlet is thus narrower with optimisation for losses instead of cavitation. Optimisation for losses is possible with uncritical cavitation, which is the case for the second and following stages in a multistage pump.

The results achieved allow deriving what typical values of blade speed and inflow speed may be. We assume, as an example, $u_2 = 30\text{ m/s}$ (attained with $d_2 = 200\text{ mm}$ and $n=2900\text{ rpm}$). With moderately backward curved blades, v_{2u} may amount to about 20 m/s . Rotor work is then 600 J/kg . With an internal efficiency of 0.8 , the head amounts to 48 m . With a diameter ratio 0.4 , $u_l = 12\text{ m/s}$. To $\beta_l = -72^\circ$ corresponds $v_l = 3.9\text{ m/s}$. This is a rather high speed, much higher than what is typically chosen for a suction pipe, being $2\text{--}2.5\text{ m/s}$. So, normally, a convergent duct part just upstream of the pump is required (so-called suction nozzle). The through-flow velocity may be increased after the first stage in a multistage pump. For the example, the blade angle corresponding to 5 m/s is -67° . The example demonstrates that, mostly, a blade angle in the order of -63° or -55° cannot be chosen. A high through-flow velocity is sometimes possible, in case of direct suction as with the axial pump in Fig. 1.3. The example also shows that deceleration between the inlet of the eye of the rotor (velocity v_θ) and the inlet of the blades of the rotor (velocity v_l) is not a realistic option. One might deduce from (8.13) that deceleration ($\zeta < 1$) would be beneficial for reduction of the NPSH_r . This is not a correct conclusion, however, as deceleration would mean a substantial increase of the entrance loss, so a higher value of λ . This means that with a pump, the optimum value of the velocity factor ζ , in principle, is unity (in some pumps there is a slight acceleration). So, there is a big difference here with fans.

8.1.5 Net Positive Suction Head of the Installation

The total pressure at the suction flange results from the pressure within the suction reservoir minus the pressure drop by the suction height and the head loss within the suction pipe. From the work equation between the suction reservoir and the suction flange follows

$$\frac{p_r}{\rho} + 0 + 0 = \frac{p_s}{\rho} + \frac{v_s^2}{2} + gH_s + q_{irr,s}.$$

H_s is the suction height, positively calculated when the centre of the rotor inlet is above the liquid level of the suction reservoir. The pressure in the reservoir, above the liquid surface, is represented by p_r , which mostly equals atmospheric pressure. The NPSH supplied to the pump by the installation is called the available value and is denoted by NPSH_a . Its value is

$$gNPSH_a = \frac{p_r}{\rho} - gH_s - q_{irr,s} - \frac{p_v}{\rho}. \quad (8.15)$$

At atmospheric pressure in the reservoir ($p_r=101.3$ kPa) and water at 15°C ($p_v=1.7$ kPa), $(p_r-p_v)/\rho g$ represents about a 10 m height. As a consequence, the geometric suction height certainly cannot exceed 10 m.

In order to avoid cavitation, the available NPSH should exceed the required NPSH. With (8.14), the NPSH required may be noted as

$$(gNPSH_r)_o = (\Omega_s / \Omega_{ss})^{4/3} (gH_m). \quad (8.16)$$

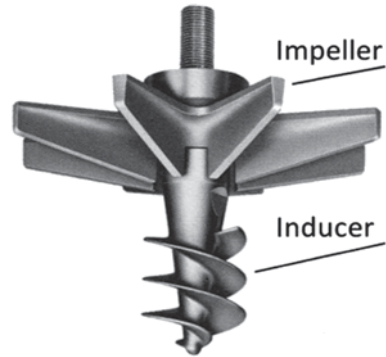
The required NPSH decreases for a given head, if specific speed decreases. With (8.16) and $\Omega_{ss}=3$, it follows that $NPSH_r$ for a pump with a low specific speed (e.g. $\Omega_s=0.4$), is about 2 m (for $H_m \sim 30$ m) to 3 m (for $H_m \sim 45$ m). Taking into account suction pipe losses, this implies that the suction height may amount to 6–7 m. This result applies to pumps operating at design flow rate.

8.1.6 Increasing the Acceptable Suction Height

In case of difficulties with the suction height, there are some obvious measures, as increasing the diameter of the suction pipe in order to diminish the head loss (increasing $NPSH_a$) or choosing a pump with a lower specific speed (decreasing $NPSH_r$). These measures raise costs: larger ducts and a larger pump.

It may occur that avoiding cavitation is impossible with a pump with the usual suction specific speed ($\Omega_{ss} \approx 3$). Some special designs with a higher suction specific speed exist. The factor σ has the greatest effect on $NPSH_r$, as emerges from (8.13). E. g. for $\sigma=0.1$ and $\lambda=1.1$, the factor in (8.13) becomes 0.10 instead of 0.25. This gives a result better than halving $NPSH_r$, with the corresponding $\Omega_{ss}=5.3$. Decreasing the blade load at the inlet implies, in principle, an increase of the number of rotor blades. But this generates an adverse effect with pumps with a low specific speed (being the most advantageous ones regarding $NPSH_r$), as the flow velocity increases due to increased displacement effect. This may be solved by mounting a helical rotor upstream of the radial rotor, as shown in Fig. 8.3. This helical rotor is termed an *inducer*. The helix features a very large blade surface, allowing generation of a significant force with a small pressure difference between pressure and suction sides. The pressure build-up within the inducer should be sufficiently high in order to avoid cavitation within the downstream centrifugal rotor. With an inducer, Ω_{ss} may be raised to about 7. The inducer shown in Fig. 8.3 has one blade, but types exist with several blades. There are also types with the inducer integrated into the impeller, which then means that the inducer blades continue smoothly into some of the blades of the post-connected centrifugal rotor.

Fig. 8.3 Series connection of inducer and impeller. (courtesy Sundyne)



8.2 Priming of Pumps: Self-Priming Types

The rotor work per mass unit, given by Euler's formula, is independent of the fluid. The corresponding pressure increase is proportional to the density. Density is about 1000 kg/m^3 with water. With air, it is about 1.20 kg/m^3 under atmospheric conditions. The ratio between them is about 800. If a pump features a 40 m water column head, it yields $40/800 \text{ m} = 50 \text{ mm}$ water column in air. This pump can, with a rotor running in air, raise water within the suction pipe by 50 mm. Normally, this does not allow the water to reach the pump, which implies that the pump fails to be self-starting. In order to start operation, the pump and the suction pipe have to be filled with water. This preparation is called *priming*, which literally means making ready for operation. This is normally done at the first operation of a pump when there is a foot valve at the bottom end of the suction pipe. Even with a foot valve, air may enter the suction pipe and the pump at standstill due to loss of tightness of the foot valve. So, it is often necessary that air can be removed from the suction pipe. Jet and water-ring vacuum pumps are sometimes applied with large pumps. Some pumps realise the evacuation of the air themselves. These are called *self-priming*. Four types are described below.

8.2.1 Side Channel Pump

This is the most classic self-priming pump (Fig. 8.4). It may be single-stage or multistage. An open rotor with many radial blades turns between two stator walls. One wall has an inlet port A, the other one an outlet port B, both near the shaft. At a larger distance from the shaft, each wall features an incomplete ring-shaped channel C or D, starting and deepening gradually at the place of the inlet port and becoming shallower and disappearing at the place of the outlet port (the pump also functions with one side channel). With a first operation, the pump is filled with water. By rotor

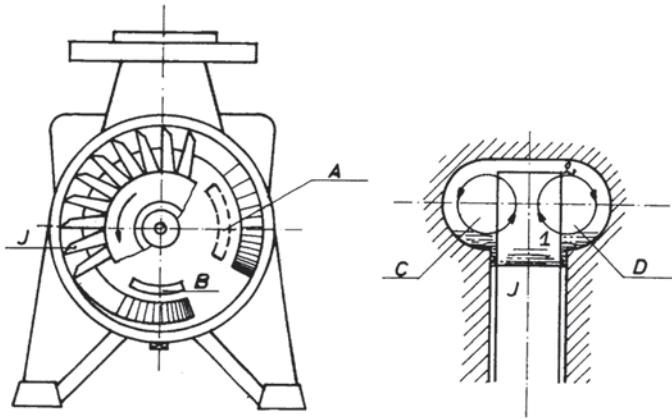


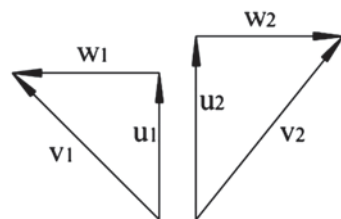
Fig. 8.4 Side channel pump

rotation, a liquid ring is formed, becoming less thick in the radial direction as the side-channel is wider. In the zone where the side channel widens, the volume enclosed by the hub, the blades and the liquid ring increases, which generates suction of air through the inlet port A. In the zone where the side channel becomes narrower, the enclosed volume decreases, causing air discharge through the outlet port B. During air evacuation from the suction pipe, the machine functions as a volumetric compressor. When the rotor is completely filled with water, turbomachine operation starts. There is then a continuous connection between the inlet port and the outlet port through the side channel(s). Figure 8.4 demonstrates that a helical flow is generated within the side channels as a consequence of the centrifugal force in the spaces between the blades. The inlet (1) and outlet (2) velocity triangles during motion in and out the rotor are sketched in Fig. 8.5. The triangles take into account that the outflow of the rotor is in the axial direction (blades aligned with the shaft) and that kinetic energy is transformed into pressure energy in the side channel. The consequence is that the inflow of the rotor is approximately in the axial direction.

Rotor work is

$$\Delta W = u_2 v_{2u} - u_1 v_{1u} = u_2^2 - u_1^2. \quad (8.17)$$

Fig. 8.5 Velocity triangles at the inlet and the outlet in the through-flow of the rotor of a side channel pump ($u_1 < u_2$)



When the flow rate through the pump is lower, the pitch of the helical motion within the side channels becomes lower. Work (8.17) is done each time water is passing through the rotor. So, the head increases strongly when the flow rate diminishes. Efficiency is low, due to the short turns of the flow, leakage losses and friction losses within the water ring. The head of a side channel pump is 4–10 times higher than that of a common centrifugal pump with the same peripheral speed, as the water flows repeatedly through the rotor. Side channel pumps are designed for the $0.03 < Q_s < 0.6$ range. Their efficiency may maximally attain 50%. A rather low efficiency is no drawback with small power applications, as a small centrifugal pump does not attain a high efficiency either.

8.2.2 *Peripheral Pump (regenerative pump)*

The wet operation of this pump (Fig. 8.6) is identical to that of the side channel pump and the Q-H characteristic is similar. The capacity to evacuate air from the suction pipe is due to splattering of water within the space around the blades. This creates an air-water emulsion with a density sufficient to be pumped. At the outlet side of the pump, air and water are separated. In the pump shown, this is done by a cyclone pipe. Centrifugal force drives the water to the outside. The air is evacuated to the discharge pipe by the cyclone core. The water flows back to the rotor. The cyclone is not essential. Air-water separation is also realised within a sufficiently large vent chamber. As opposed to the side channel pump, the peripheral pump does not function as a compressor during air evacuation. The discharge pipe should allow spontaneous evacuation of the air. If not, fitting a bypass line in order to discharge air to the outside during air evacuation may be necessary. The peripheral pump features a better efficiency than the side channel pump.

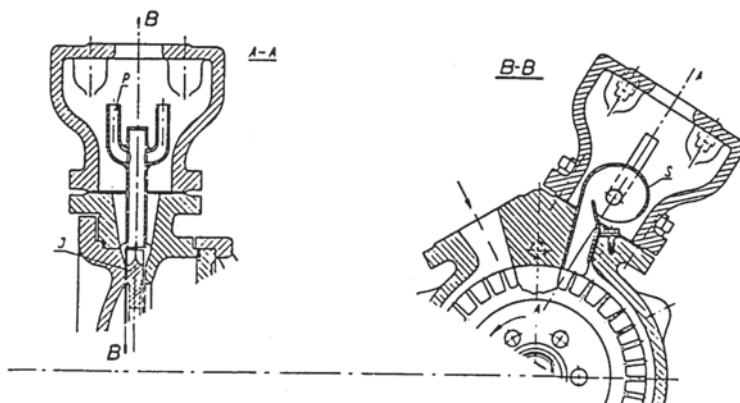


Fig. 8.6 Peripheral pump

8.2.3 Self-Priming Centrifugal Pump

The splattering principle with generation of an emulsion may be applied to a centrifugal pump with a classical rotor form as well. Fig. 8.7 shows two examples. A self-priming pump requires permanent presence of water within the pump casing. Liquid, present at standstill, should not flow back to the suction pipe. Therefore, the suction pipe is positioned above the rotor and fitted with a non-return valve. Also, this liquid should not, at the pump start, be drained away through the discharge pipe. An air-water separator (A) is incorporated into the pump house for that purpose. The separator is a large space in which the pumped emulsion comes to an almost standstill, allowing the air to escape from the water. The air leaves the pump through the discharge pipe and the water drops back to the bottom of the pump house and is led to the rotor. As for the peripheral pump, the discharge pipe should allow spontaneous evacuation of the air. With the pump of Fig. 8.7 (left), liquid enters the rotor through an orifice B in the volute. Wet operation is that of a common centrifugal pump, with the exception of a small flow rate through the orifice (may be in one sense or the other). The type shown in Fig. 8.7 (right) is self-priming as well, without an orifice. This is due to the double volute. The rotor-mixed emulsion is drained through the internal volute and the separated water flows back through the external volute. Backflow through an orifice in the volute (Fig. 8.7, left) or the outer branch of the volute (Fig. 8.7, right) is delicate, however. The weight of the back flowing water should be sufficient to attain flow against the head realised by the emulsion. Self-priming pumps are frequently used in agricultural applications, with open rotors and few blades (Fig. 8.7, right), but with a backflow orifice that directly carries the water upon the rotor. This results in very efficient splattering. The drawback is some circulating flow in wet operation. The pumps presented are suitable for contaminated liquids, but the particles should, of course, not be larger than the backflow orifice and the volute throat.

Fig. 8.7 Self-priming centrifugal pump; *left*: with backflow through an orifice; *right*: with back-flow through the external part of a double volute; d indicates the discharge side

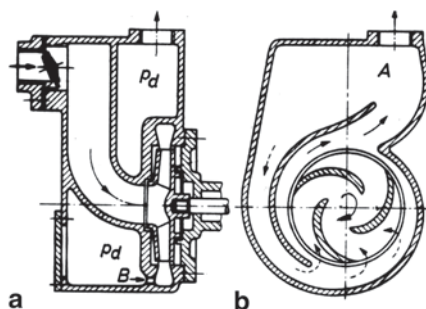
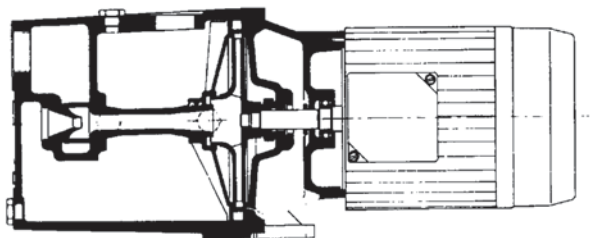


Fig. 8.8 Jet pump. (courtesy Johnson pump; SPX Flow Technology)



8.2.4 Jet Pump

This pump is by far the most used in household applications. The principle is that a water jet pump is internally mounted upstream of a centrifugal rotor. The water leaving the rotor runs into a pump house that is connected to the nozzle. The water jet entrains the air from the suction pipe. Wet operation is similar. The jet pump and the centrifugal rotor are connected in series, which allows attaining a higher head. Cavitation cannot occur in the centrifugal rotor but may occur in the suction chamber or the mixing chamber of the jet pump (Fig. 8.8).

8.3 Unstable Operation

Unstable operation points may occur for flow rates lower than the flow rate at the maximum of the Q - H characteristic. When a pump delivers through a pipe without head loss into a reservoir from which a fixed flow rate is extracted, all operating points at the left of the maximum are unstable (Fig. 8.9). The load characteristic is a horizontal line in that case (only static head). When filling the reservoir, the operating point passes the right curve branch from A to B. Assume that the flow rate delivered by the pump to the reservoir equals the flow rate extracted from it in point B. Point B is a stable operating point. This may be verified by exerting a perturbation, e.g. a decrease of the flow rate extracted from the reservoir during a short period of time. The level within the reservoir rises then, which causes the flow rate delivered by the pump to decrease. This causes the level within the reservoir to decrease and the operating point to return to its original position. But point C, positioned at the left of the maximum, is an unstable operating point. When the flow rate extracted from the reservoir decreases during a small period of time, causing a rise of the reservoir level, the flow rate delivered by the pump increases and the operating point moves away from its original position. In this case, the operating point moves to the maximum. With a short duration increase of the flow rate extracted from the reservoir, the operating point moves towards point D. As a consequence, operating point C cannot be reached.

With Q_c being the flow rate extracted from the reservoir, the operating point, during filling, passes the right curve branch from A to M. At the maximum of the characteristic, the flow rate supplied by the pump still exceeds the flow rate

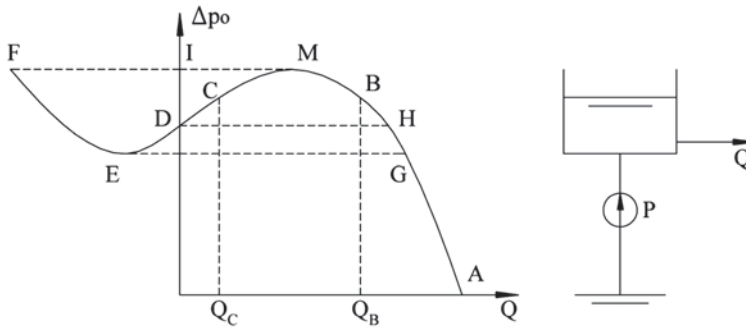


Fig. 8.9 Unstable operation of a pump

extracted from the reservoir. So the reservoir level keeps rising. One moment later, there is no longer an intersection with the characteristic for $Q > 0$. But there is an intersection with the continued characteristic for $Q < 0$. This branch represents the head by the pump when flow is forced through the pump against the normal flow sense. The operating point thus leaps over onto point F. This intersection is stable (may be verified by perturbation analysis). At the operating point F, the reservoir discharges through its delivery pipe and through the pump. So the reservoir level sinks. The operating point moves from F to E. The reservoir still keeps discharging at the minimum E. The next moment there is no longer an intersection for $Q < 0$. The operating point leaps onto point G. The reservoir level then rises again, which implies that the GMFE cycle keeps running and point C is never attained. If a non-return valve is provided in the suction pipe, the flow rate cannot turn negative. The cycle is then HMID.

When taking losses into account, the head imposed on the pump by the reservoir and the pipes rises with increasing flow rate. Further, the flow rate extracted from the reservoir normally increases when the level in the reservoir increases. Taking these dependencies into account, one sees that the separation point between stable and unstable operating points is not the maximum in the characteristic, but a point with a somewhat lower flow rate. To be entirely sure that no unstable operating point can occur with pumps, the Q - H characteristic must not feature any maximum. This assumes sufficient backward curving of the blades. The slip intervenes here as well. With fewer rotor blades, slip is larger and the characteristic curve is steeper. With the load characteristic commonly found in fans, i.e. a parabola through the origin, no unstable operating points occur. A final remark concerns the shape of the cycle around an unstable operating point. In Fig. 8.9 it is assumed that the operating point jumps suddenly between branches while conserving head. In reality, the jump takes some time and the reservoir level sinks in the transition from M to F and rises in the transition from E to G. This causes the flow rate range in the cycle to be smaller than sketched in Fig. 8.9. The range is the smaller the smaller the capacity of the reservoir is.

8.4 Component Shaping

8.4.1 Simply and Doubly Curved Blades in Radial Rotors

The simplest pump rotor shape has simply curved blades (Fig. 8.10), meaning that all orthogonal sections are equal. Inlet and outlet angles follow from the velocity triangles. The blade shape at intermediate points should be determined so that the through-flow area of a rotor channel increases gradually and that the channel is not unnecessarily curved. The blade camber line is often a circular arc, meeting the directions at the inlet and the outlet. If this curve does not satisfy the requirements, another shape must be chosen. An example is a curve like a logarithmic spiral, but with $tg\beta$ linearly varying with the radius, according to (8.18). The equation may be integrated analytically.

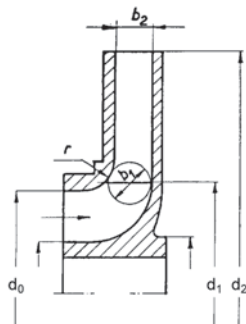
$$\frac{rd\theta}{dr} = tg\beta = \frac{tg\beta_2(r-r_1) + tg\beta_1(r_2-r)}{r_2-r_1}. \quad (8.18)$$

We further consider the case, shown in Fig. 8.11, where circumferential streamsurfaces are not orthogonal due to change of width, but with β -angles being identical on a given radius. The angle β_1 is projected into the orthogonal plane to a value β'_1 (angles are considered here with respect to the tangential direction) as

$$tg\beta'_1 = tg\beta_1 \cos \varepsilon_1. \quad (8.19)$$

If the inlet edge of the rotor blades is parallel to the rotation axis, and the inlet velocity has the same value at all points, β_1 is constant, but β'_1 varies. For the flow to enter without incidence, the blade should be doubly curved. Figure. 8.11 represents this shape in a projection onto an orthogonal plane. Doubly curved blades are also re-

Fig. 8.10 Simply curved blade



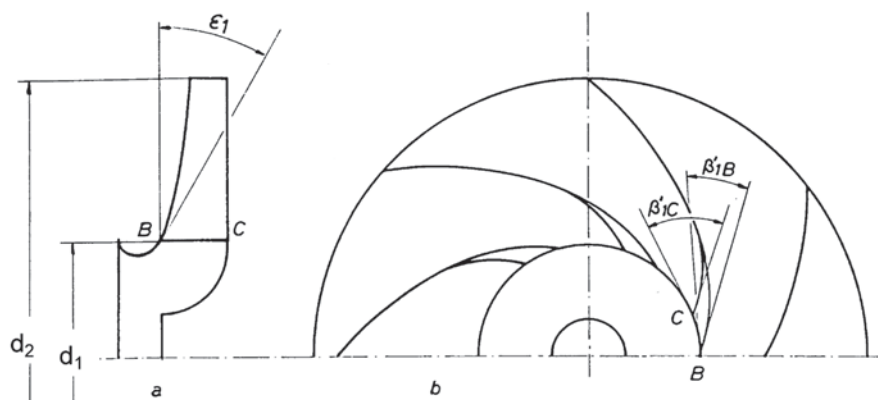


Fig. 8.11 Doubly curved blades at rotor inlet with constant radius. (angles with respect to the tangential direction; right running rotor)

quired when the blades are extended into the suction eye, which means that the radius of the inlet edge is not constant. The β_i -angle then also varies along the inlet edge.

8.4.2 Mixed-Flow and Axial Pumps

Blade extension into the suction eye is required for larger values of the specific speed. Non-extended blades then become broader and shorter, impairing the guidance of the flow. Extension lengthens the blades and also reduces cavitation sensitivity, as the relative velocity decreases. So blades are extended into the suction eye and become doubly curved from $\Omega_s \approx 0.6$ onward. Due to a big difference in the length of the streamlines, the outlet edge of a blade cannot be kept parallel to the shaft from $\Omega_s \approx 1.25$ onward (change in radius and deviation from the meridional plane). This way, a mixed-flow pump is obtained. At a further increase of specific speed, it is advantageous to omit the rotor shroud. The reason is that the relative velocity becomes larger than the absolute one. So, there is less friction without shroud. Mixed-flow open rotor pumps are applied with a specific speed of about 1.5–3. A radial diffuser followed by a volute or an axial diffuser (Fig. 8.12) may be mounted downstream of the rotor. With further specific speed increase, the outlet diameter becomes equal to the inlet diameter, resulting in an axial rotor, followed by an axial diffuser. This type is applied for specific speeds above about 2.5. So, the application field of axial pumps partially overlaps the field of mixed-flow pumps.

8.4.3 Pump Inlet

This part conveys the liquid to the suction eye of the pump rotor. A straight duct in line with the shaft constitutes the best solution. It can only be applied when

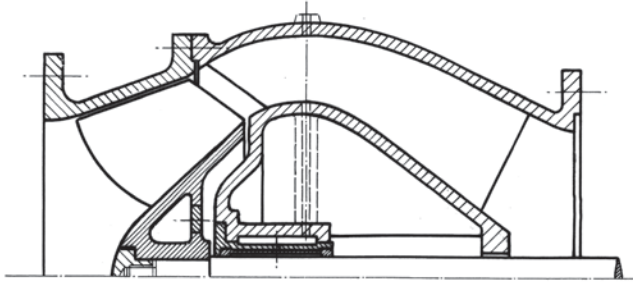


Fig. 8.12 Mixed-flow pump

no bearing is required at the suction side. This is possible with many single-stage pumps (see Fig. 1.13 in Chap. 1). A bearing may be mounted on a bend at the suction side, but the bend impairs the flow uniformity at the rotor entrance and takes up a lot of space. Therefore, an inlet bend is seldom used, sometimes with larger axial pumps. With centrifugal pumps, a volute-shaped suction chamber is mostly applied, requiring less axial length. Figure 8.13 sketches an orthogonal and a meridional section of the suction chambers of a double-suction pump. A double-suction rotor is a form of internal parallel connection (see further Fig. 8.19). The volute shape of the suction chambers is not complete. Part of the flow is led directly to the suction eye of the rotors. The pre-swirl of the inlet flow may be corrected by vanes in a stator inlet part to the rotor.

8.4.4 Pump Outlet

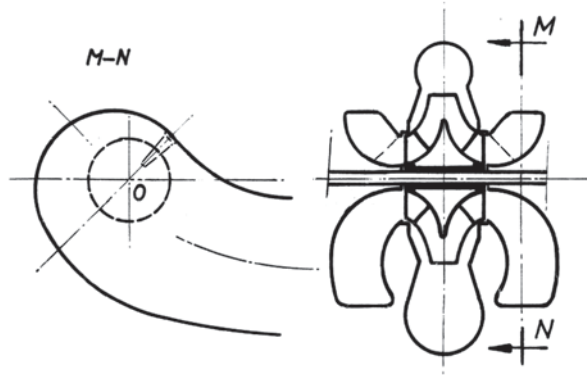
Fluid is conveyed from the rotor to the discharge pipe or to the next stage and kinetic energy is converted into pressure. The first function is mostly realised by a volute followed by a linear diffuser (see further Fig. 8.15). The kinetic energy conversion may also be done upstream of the volute with a vaned or a vaneless diffuser ring. These elements are discussed below.

8.4.5 Vaneless Diffuser Rings

A vaneless diffuser ring consists of two circular surfaces forming the diffuser walls. The axial width (b) may be constant or vary with the radius r . Assuming that no external forces affect the fluid, the flow has constant angular momentum:

$$v_u r = cst. \quad (8.20)$$

Fig. 8.13 Volute-shaped suction chambers with a double-suction rotor



The mass flow imposes

$$2\pi r b v_r = \text{cst.} \quad (8.21)$$

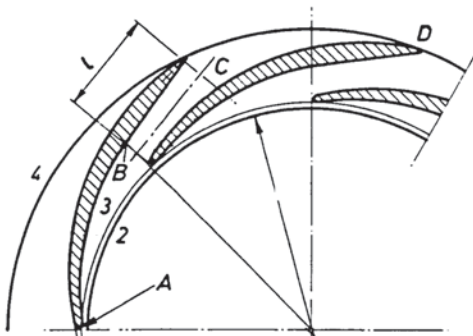
For $b = \text{constant}$, it follows that

$$\tan \alpha = \frac{v_u}{v_r} = \text{cst.} \quad (8.22)$$

Within a diffuser with a constant width, streamlines are logarithmic spirals. The velocity magnitude decreases inversely with the radius. When the difference between the inlet velocity and the outlet velocity is great, i.e. when much kinetic energy has to be converted into pressure energy, the external diameter of the vaneless diffuser becomes large. Due to the long streamlines, friction losses become high. These friction losses may still increase at a flow rate below the design value: the angle α then increases and streamlines lengthen. When the width increases with the radius, streamlines are even longer than with parallel walls. So, vaneless diffusers are only suitable to convert low amounts of kinetic energy.

8.4.6 Vaned Diffuser Rings

In case of parallel diffuser sidewalls: $v_r r = \text{cst.}$ A faster diffusion compared to the vaneless diffuser is achieved if v_u decreases faster. This requires exertion of tangential forces onto the fluid by means of diffuser vanes. The vanes are mounted more radially than the streamlines with vaneless diffusers. With vaned radial diffusers, two nearby vanes only overlap over a limited length (Fig. 8.14). Diffusion mainly occurs within the widening section BC of the channels formed by two adjacent vanes. The wall AB, constituting the supply to the overlap section, principally is a logarithmic spiral. Similarly, the wall CD is also of logarithmic spiral form. The final vane shape and the optimum number of vanes follow from optimisation, which nowadays typically is a CFD-optimisation. Mostly, the number of diffuser blades is

Fig. 8.14 Vaned diffuser ring

one more than the number of rotor blades. When operating in off-design conditions, the flow angle at the inlet of the diffuser differs from the vane angle, with flow separation as a possible consequence. At a high flow rate the fluid must strongly accelerate in order to pass through the throat area B. So, a pressure drop occurs upstream of position B. Its magnitude may exceed the pressure rise downstream of B. So, it may occur that, from a certain flow rate onward, higher than the design flow rate, the vaned diffuser generates a pressure drop instead of a pressure rise.

8.4.7 Volute

Figure 8.15(left) sketches a volute fitting immediately to the rotor. There is no diffuser ring in between the rotor outlet and the volute inlet. This type is frequently used, mainly with smaller pumps. Velocity reduction is realised in a post-connected linear diffuser. If an internal diffuser ring is mounted, the following discussion stays valid, however.

A volute collects the liquid leaving the rotor and conveys it to the discharge pipe. For the design flow rate, the volute imposes a uniform backpressure to the rotor. At a flow rate below the design value, deceleration occurs within the volute and at a

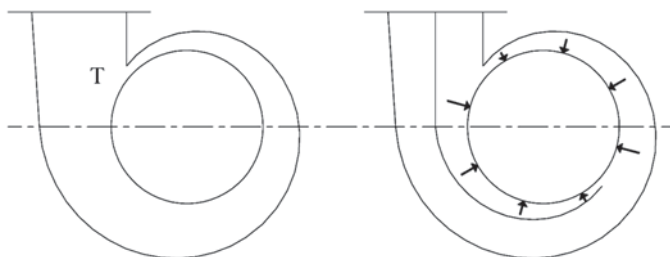
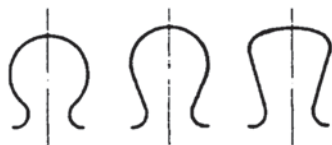
**Fig. 8.15** Single volute (*left*) and double volute (*right*) for attenuation of non-uniformity in off-design conditions

Fig. 8.16 Cross section profiles of pump volutes

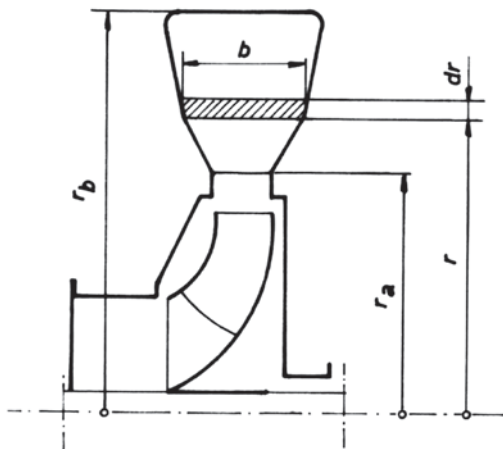


flow rate above the design value, acceleration occurs. The backpressure is then non-uniform, impairing the rotor efficiency. A second drawback may be a high bearing load due to the radial force on the shaft. Both drawbacks are attenuated by mounting two partial volutes (Fig. 8.15, right), instead of one volute.

In principle, a volute could consist of two parallel walls at distance equal to the rotor outlet width, and an external wall with logarithmic spiral shape. This form is disadvantageous since the volute then takes much radial space and the transition from the rectangular final section towards a circular outlet becomes very long. The radial dimension is diminished by enlarging the width immediately after the volute inlet (Fig. 8.16). Remark that with symmetrical volute cross sections, as typically used, two vortex motions are formed by the entrance flow.

The volute is a channel with a chosen meridional section shape (Fig. 8.17), the area of which gradually increases to take up the inflowing fluid. In theory, the volute begins with zero section area. But a tongue is incorporated (T in Fig. 8.15) in order to limit vibrations and noise generated by the outlet flow from the rotor channels, periodically hitting the opposite wall. An exaggerated tongue clearance, however, causes a circulating liquid ring, impairing the efficiency. In theory, the flow within a volute should meet constant angular momentum, $v_u r = cst$, as no external forces affect the fluid. A volute is preliminary calculated this way, but with through-flow sections enlarged by about 20% to take boundary layers and secondary flows into account. The final design is carried out by CFD-optimisation. The variation of the

Fig. 8.17 Section area determination of a volute



external volute wall, with a chosen section profile (Fig. 8.17), follows from constant angular momentum as

$$dQ = v_u dA = \frac{C}{r} b dr, \text{ with } v_u r = C,$$

and the flow rate through a section on the position angle ϕ as

$$Q_\phi = \frac{\phi}{2\pi} Q = C \int_{r_a}^{r_b} \frac{b dr}{r},$$

which results in $r_b = f(\phi)$.

8.4.8 Return Channels

In multistage pumps, the liquid must be led from the diffuser ring outlet diameter to the smaller diameter of the suction eye of the next stage. With radial rotors, the liquid turns 180° in the meridional view, between the diffuser and the return channel. This usually occurs within a ring-shaped, vaned or vaneless chamber with a constant cross section. If this space features vanes, the liquid follows continuous channels from the diffuser (with vanes) until the suction eye of the next stage. This is the best solution from a flow point of view, but requires more complicated castings. As the velocity within the channels has to decrease, their cross section area should increase. Therefore, it is usually not possible to provide the return channels with parallel side walls. Further, the area increase must run gradually in order to prevent boundary layer separation. This often necessitates vanes with a variable thickness. The return vanes end radially or are somewhat more curved ($\varepsilon = 5^\circ$) in order to compensate for the flow deviation. The vane shape is determined by methods applying to rotor blades. Remark that continuous diffuser and return channels are standard design practice with mixed-flow stages connected in series (Fig. 8.12).

8.5 Internal Parallel and Series Connection Of Rotors

8.5.1 Reason for Internal Parallel or Series Connection

At pump design, flow rate, head and rotational speed are known. Flow rate and head are imposed by the application. The rotational speed follows from the choice of the specific speed. At a first design stage, a specific speed is chosen for optimum efficiency. The optimum value is about unity. A deviation from this choice is mostly required to attain a rotational speed that is suitable for a driving motor. If the specific

speed becomes too high or too low, parallel or series connection has to be applied. Internal forms of parallel or series connection are discussed below.

8.5.2 *Internal Parallel Connection of Rotors*

Internal parallel connection is normally done with 2 rotors forming a double-suction rotor (Fig. 8.19), with volute-shaped suction chambers and a common spiral case outlet. Double-suction rotors have the additional advantage that no axial force is exerted on the shaft (see Sect. 8.6.5). Double-suction pump casings are made with an axial split (plane containing the shaft). In practise, this is mostly a horizontal split, since typically these pumps are mounted with a horizontal shaft (Fig. 8.19). Suction and discharge pipes are connected to the lower part of the casing in order to allow easy opening of the pump for maintenance.

8.5.3 *Internal Series Connection of Rotors: Multistage Pumps*

Internal series connection results in a multistage pump (Fig. 8.20). Each stage encompasses a rotor, a diffuser and internal return channels. Rotors should be mounted as close as possible to each other in view of shaft rigidity. Return channels thus feature short bends. This impairs the efficiency. In the traditional design, called a ring-section pump (Fig. 8.20), the pump is composed of a series of discs, axially tightened by bolts. The vaned diffuser and the return channels are cast in a disc (Fig. 8.18). During the assembly, stator and rotor elements are slid alternately onto the shaft. With this construction, all rotors face in the same sense so that there is a resulting axial force on the shaft (see the further discussion in Sects. 8.6.5 and 8.6.6). For balancing the axial force, rotors may be mounted in groups with

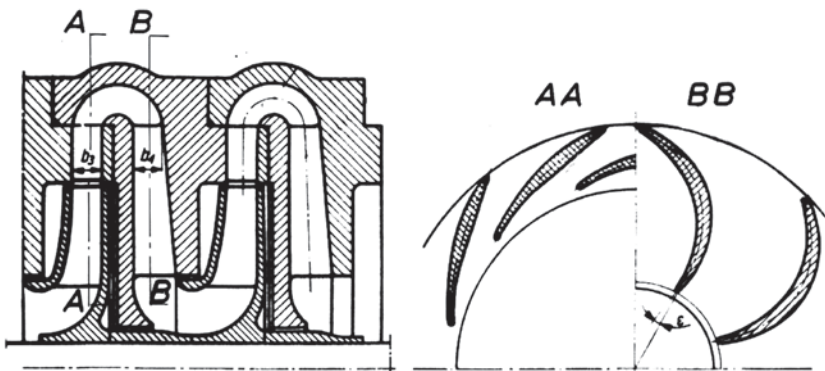


Fig. 8.18 Return channels in multistage centrifugal pumps

opposing sense. For instance, a six-stage pump may be divided into two parts with three rotors in the same sense. After a first group of rotors, the liquid is then collected by a volute and led by a conduit to the suction eye of the first rotor of the second group. Such pumps are made with an axial split casing and very often, the connecting conduit is integrated in a casing part (realised by a connection in the cast piece). In some pumps, more than two groups of rotors are used.

8.6 Constructional Aspects

8.6.1 *Rotor*

The rotor is mostly cast, exceptionally welded. Small rotors for pure water are manufactured from bronze (CuSn) because of the small allowed wall thickness (minimum 3 mm). Plastics are sometimes applied. Larger rotors are mostly manufactured from cast iron. Cast iron and bronze may be applied for peripheral speeds up to about 50 m/s. Beyond this speed, alloyed steels are applied and chromium steel up to about 90 m/s (for comparison: fans 110 m/s and compressors 450 m/s max.). The choice of the material is often determined by the characteristics of the liquid to be pumped, temperature, pressure, presence of solid materials and corrosion resistance. Manufacturing the moulds may be complex with doubly curved blades or narrow channels. Sometimes the lost wax process has to be applied, or casting must be performed in dies in order to get a smooth finish. The surface condition is very important in view of rotor efficiency. It is often impossible to finish the surfaces, as they are inaccessible to tools. Axial pump blades can be finished with a digital milling machine.

8.6.2 *Stator*

The stator of a single-stage single-suction pump mostly consists of a rear part with a shaft passage and a volute and a front part with an internal suction tube. Single-stage pumps with double suction often feature a stator with a horizontal split (Fig. 8.19). Dependent on the fluid pressure, stators are manufactured from cast iron, cast steel or alloyed cast steel (chrome steel). Forged steel is appropriate for high pressures and temperatures.

8.6.3 *Shaft Sealing*

Shaft sealing may be done with a stuffing box or a mechanical seal. In a stuffing box, packing rings are pressed around the shaft with a gland (Fig. 8.20). A packing

Fig. 8.19 Axially split casing double-suction pump. (courtesy Sulzer)

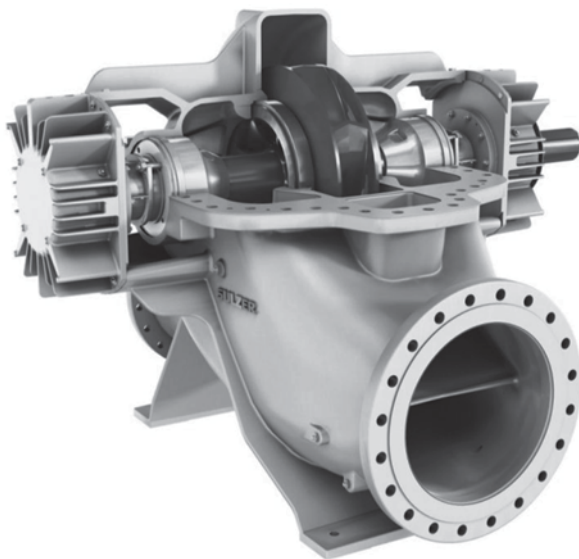
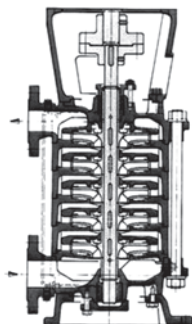


Fig. 8.20 Multistage vertical pump. (courtesy ANDRITZ)



is a braided rope, mostly manufactured from teflon and graphite. It is appropriate for circumferential speeds under 20 m/s and pressures under 15 bar. A small leakage flow should be allowed for lubrication and for removing friction heat. If the pumped liquid contains solid particles, it may be advantageous to rinse the packing rings with pure liquid from an external source. This rinsing prevents the solid particles from penetrating into the packing. The rinse water is pressed into the seal through a ring with radial perforations, placed halfway the stuffing box. Liquid injection may be useful as well if the pump is operated with a suction pressure lower than atmospheric pressure, to prevent air intake. The injection liquid may then be tapped from

the pressure side of the pump. A mechanical seal consists of two rings with polished surfaces sliding over each other, one of them being linked to the stator, the other one to the rotor, pressed together by a spring (applied in the pump of Fig. 8.19). The rings are normally manufactured from metal, but feature a coating. One ring has a soft coating (e.g. carbon), the other one a hard one (e.g. silicon carbide or tungsten carbide). A liquid film should be formed between the rings for lubrication. This liquid mostly evaporates partly. A mechanical seal is not completely tight. Mechanical seals are applied for sliding speeds up to 60 m/s and pressures up to 450 bar.

8.6.4 Bearings

Rotational speed, load, required life and required rigidity determine the choice of the type of bearing. Ball bearings and roller bearings of various types are applied, always with one of the bearings for balancing the axial force (e.g. an angular contact ball bearing or tapered roller bearing). Oil-lubricated sliding bearings are applied in case of high rotational speeds, large dimensions and heavy loads.

8.6.5 Axial Force Balancing with Single-Stage Pumps

Rotors with one-sided suction exert an axial force on the shaft, oriented to the suction side. If the force is not very significant, it may be balanced by a ball or a roller bearing, in other cases by a thrust bearing. Another solution consists in generating a hydrostatic balancing force, as explained hereafter and in the next section. Fig. 8.21 shows that the rotor is subjected to rotor outlet pressure (p_p) on the back of the rotor disc and on the front of the shroud. In the rotor eye, the pressure is suction pressure (p_s). The resulting axial force is approximately

$$F_{ax} = (A_e - A_s)(p_p - p_s), \quad (8.23)$$

with A_e the eye area and A_s the cross section area of the shaft, if the shaft passes through the suction eye. In case of an overhung rotor, (8.23) becomes:

$$F_{ax} = (A_e - A_s)p_p - A_e p_s. \quad (8.24)$$

Both expressions are approximate. The pressure on the back of the rotor is not constant. Dragged by the rotor disc, the liquid outside the rotor is subjected to centrifugal force, which generates a pressure gradient. By the turning of the flow within the suction eye, suction pressure is not constant, either.

When two rotors are mounted onto the same shaft, with their suction eyes directed into opposite senses, the axial force is completely neutralised when both rotors operate in parallel. With rotors operating in series, a significant reduction

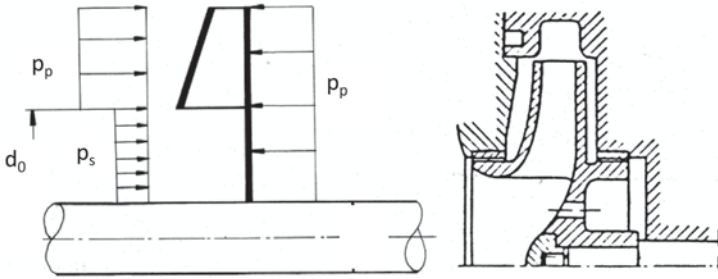


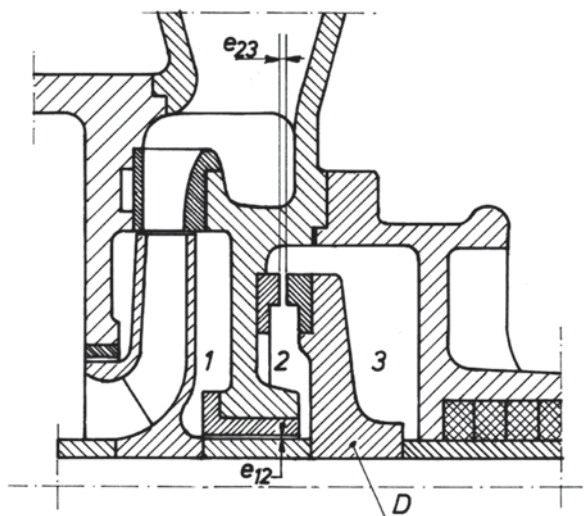
Fig. 8.21 Generation of axial force (*left*) and rotor balance chamber (*right*)

of the resultant axial force is obtained, also outside design conditions. For an individual rotor, the axial force may be largely balanced by a chamber made as shown in Fig. 8.21 (right). The chamber is separated from the rotor outlet area by a collar on the rotor disc fitting with a clearance seal (small gap) to a wear ring on the casing (there is a very small leakage flow). The balance chamber is put on suction pressure by drilling holes in the rotor disc (most common procedure) or by an external pipe connecting the chamber to the suction part of the pump. In the first case, the leakage flow perturbs the main flow somewhat. Remark that also a clearance seal with wear ring is used to separate the outlet area of the pump rotor from the suction eye (there is also a small leakage flow).

8.6.6 Axial Force Balancing with Multistage Pumps

Changing the suction sense of some rotors is a solution, but it complicates the construction of the pump. A balance chamber may be provided on each one-sided rotor. But with multistage pumps, a single balance disc is generally applied (Fig. 8.22). This disc D is mounted onto the shaft in between two chambers (2 and 3). Chamber 3 is connected to the suction part of the pump by an external pipe. The outlet pressure of the last rotor in chamber 1 is reduced to an intermediate pressure in chamber 2 by flow through the clearance e_{12} . A pressure difference is maintained between chambers 2 and 3 by flow through the clearance e_{23} . The balancing disc exerts, with the pressure difference $p_2 - p_3$, an axial force with the sense opposite to the axial force on the rotors. Axial force compensation requires appropriate disc diameter and clearance dimensions. The balancing disc relieves the high-pressure sealing around the shaft, but generates leakage. The balance disc is self-adjusting, when the shaft is movable in the axial direction (sliding bearings or roller bearings). The clearance width e_{23} is then variable. As clearance e_{12} is fixed, p_2 decreases when the shaft moves to the right, i.e. when the axial force exerted onto the rotors decreases. Wear rings on both sides of the gaps have to be replaced when these wear out. In principle, the disc can only be used with pure liquids.

Fig. 8.22 Balance disc for a multistage pump



8.6.7 Wear Rings

Clearance seals are used in pumps for separating the outlet area of the rotor from the suction eye and for forming chambers for balancing the axial force. The clearances are very small, typically of the order of 1.5–2% of the diameter in order to keep the leakage flow small. Although there is theoretically no metal contact, the surfaces of the clearances wear due to the high shear stress in the leakage flow. Therefore, often on both sides of the gap, rings in hard metal are placed. These rings are called wear rings. When the leakage flow becomes too large (two to three times the design value), these rings are replaced. In many pumps, there are no wear rings on the impeller side (Figs. 8.21 and 8.22), which makes the pump more reliable. The casing wear rings may then be replaced together with the impeller. Often, this is feasible since the time between necessary replacements may be very long, of the order of several years, and the impeller blades also wear over such a long time. It is also possible to replace the casing wear ring by a slightly thicker version and reduce the diameter of the corresponding collar on the impeller by turning on a lathe.

8.7 Special Pumps

Pumps are manufactured in many variants. It is not the objective of this book to discuss the different builds. Practical information may be obtained from the websites of manufacturers or from books on practical aspects like the ones of Karassik and McGuire [8] and Girdhar and Moniz [5]. In this section, a limited choice is made of some special cases.

8.7.1 Borehole Pumps

The main requirement is a small external diameter in order to lower the pump into a borehole pipe. Therefore, the pump is always of the multistage type, even with relatively low head. Mixed-flow stages according to Fig. 8.12 are connected in series. The pump may be driven by a motor mounted on top of the borehole pipe, through a long shaft, borne in rubber bearings, lubricated and cooled by the pumped liquid. When this liquid contains too many solid particles, the bearings may be mounted in a separate tube, filled with pressurized water or oil. Mostly, the motor is submersible, connected directly to the pump. The motor is traditionally a wet rotor squirrel cage motor (see below: canned pump). The smallest diameter amounts to about 60 mm.

8.7.2 High-Pressure Pumps

High-pressure pumps are used, for instance, as boiler feed pumps (pressure up to 300 bar) or in chemical plants. Avoiding leakage of ring-section pumps, composed of rings tightened with external bolts may then be difficult, especially when the fluid is also hot. For such applications, the ring sections are often mounted in a second cylindrical tube casing. Inlet and outlet parts are connected to the envelope of the second casing and the rings are pressed by end plates fitted to the cylindrical casing. These pumps may be opened without disconnecting the pipes. Another possibility for a high pressure pump is an axially split casing.

8.7.3 Sealless Pumps: Circulation Pumps, Chemical Pumps

Circulation pumps are used with steam generators with forced circulation and domestic heating boilers. The head is generally low, but pressure and temperature may be very high. Pumps with the shaft passing to the exterior and conventional shaft seals may lead to large leakage. With some applications as circulation pumps for domestic use and chemical pumps, leakage is just not allowed. Sealless pumps are commonly applied, with liquid penetrating around the rotor of the driving electric motor (Fig. 8.23). The traditional motor is a squirrel cage induction motor with stator windings isolated from the rotor with a non-magnetic can. The pumped liquid lubricates the sliding bearings. Due to the can, the gap between the stator winding and the rotor is rather large, which impairs efficiency. A modern evolution is application of permanent-magnet synchronous motors. These have higher efficiency as the gap size is then not very critical.

Another kind of sealless pump is realised with a magnetic coupling formed by permanent magnets on both ends of a split shaft (Fig. 8.24). Canned motor pumps and magnetic drive pumps are often applied for pumping chemicals, as complete avoidance of leakage is then necessary.

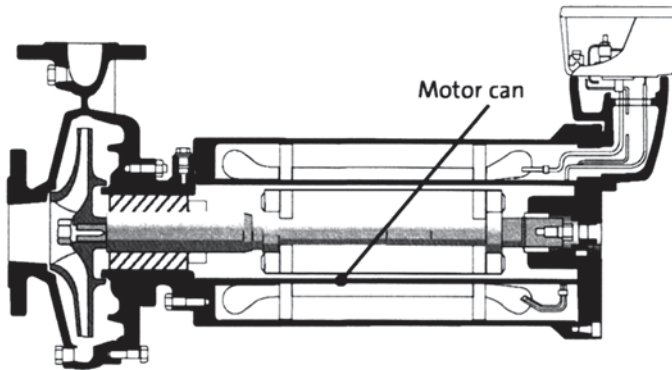


Fig. 8.23 Canned motor chemical pump. (courtesy Grundfos)

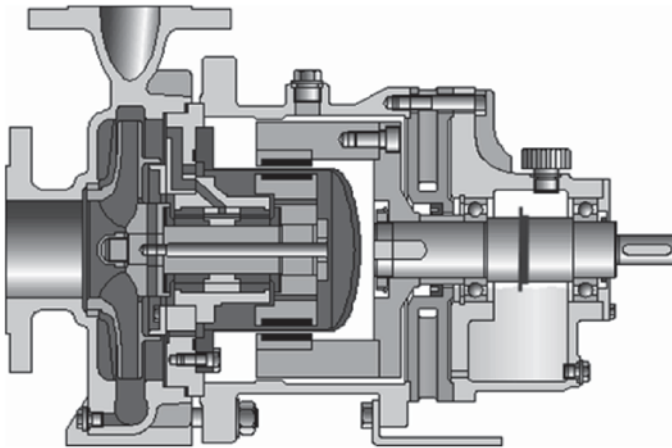


Fig. 8.24 Magnetic drive chemical pump. (courtesy Klaus Union)

8.7.4 Slurry Pumps

Clogging of the rotor channels must be avoided by providing large passages. Open impellers with one or two blades are applied (Fig. 8.25). Vaned or vaneless diffuser rings are not used because of the clogging risk. A ring-shaped stator channel with constant cross section around the rotor is typical. If a volute is used, the tongue must leave sufficient clearance to allow the passage of the largest solid particles. Packing seals are rinsed with pressurised clean water in order to prevent sand entrance. The presence of solid elements in the pumped liquid decreases the pump performance. This is also the case after strong wear, which may be reduced by using wear-resistant materials.

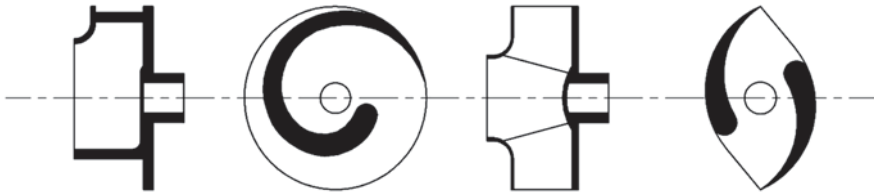


Fig. 8.25 Rotor shapes with slurry pumps

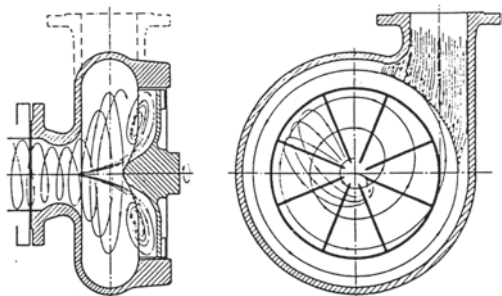
8.7.5 Pumping of Solid Materials

Solid materials, mixed with a liquid, can easily be pumped with special pumps. For pumping sand and gravel, as with dredge pumps, pumps are quite conventional ones, except that passages are large and wear-resistant materials are used. Also, the performance of these pumps is lower than with pure water. But pumping fruit, potatoes and even fish is possible with a pump with sufficiently large impeller passages of the types of Fig. 8.25. A pump for the same purpose is a vortex pump as sketched in Fig. 8.26. The pump has a recessed open impeller and a large distance between the blades and the stator walls. The traditional rotor has pure radial blades which create a vortex motion in a constant cross section stator. The working principle is the same as with the side channel or the peripheral pump (Fig. 8.5). The efficiency may amount to about 60 %. Modern types often have backward curved blades. This improves efficiency as part of the rotor work comes from functioning as a conventional centrifugal pump.

8.7.6 Vertical Submerged Pumps

On ships, limitation of floor space is more stringent than limitation of height. Therefore, vertical pumps are typically used. Figure 8.20 is an example, but pumps are often submersible and placed in a high cylindrical container with a rather small diameter. So, these pumps resemble borehole pumps, but have a bigger diameter.

Fig. 8.26 Vortex pump



Multistage pumps with mixed-flow rotors and with radial rotors exist. Also single-stage pumps with radial, mixed-flow and even axial rotors are employed. The suction pipe is connected to the upper part of the container, but the suction part of the pump is near the bottom, so that the inlet pressure is much higher than the pressure in the suction pipe. This may increase the available net positive suction height with several meters. A similar arrangement is used with condensate extraction pumps in thermal power stations, as the fluid is near to vapour pressure. Similar arrangements may also be used for the same reason in chemical plants.

8.7.7 *Partial Emission Pumps*

Such a pump is meant for high head and small flow rate. The traditional type has a rotor with pure radial blades turning at high rotational speed in a constant cross section stator chamber (Fig. 8.27). The discharge is through a diffuser with small cross section area, placed tangentially to the stator chamber. The entrance of the diffuser only allows outlet flow of the rotor over a fraction of its periphery. This partial emission feature realises the low flow rate. Some pumps of this type are made with an inducer as shown in Fig. 8.3. A small-scale example is the pump for water spraying on the windshield of a car. Some pumps look similar but have backward curved blades as with conventional centrifugal pumps. This improves the efficiency. Their peripheral speed is much lower. These are pumps for very small flow rate, but they do not realise a very high head.

8.7.8 *Pumps for Viscous Fluids*

Pumps for viscous fluids do not differ strongly from pumps for low viscosity fluids. Blade passages are typically somewhat wider and the efficiency is lower (see Chap. 7). Centrifugal pumps maintain an acceptable efficiency up to viscosities in the order of $150 \cdot 10^{-6} \text{ m}^2/\text{s}$ (150 times the viscosity of water), corresponding to an averagely viscous machine oil. Operation stays possible up to $500 \cdot 10^{-6} \text{ m}^2/\text{s}$. Channel

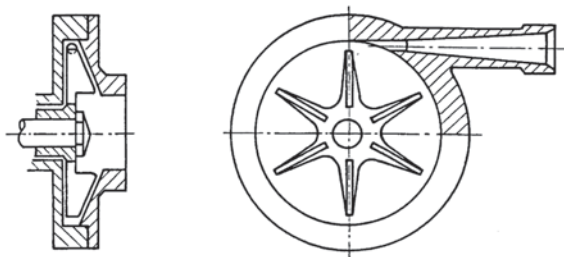


Fig. 8.27 Partial emission pump

impeller pumps, in the form as used with slurry pumps (Fig. 8.25, right) may even be used up to $1000 \cdot 10^{-6} \text{ m}^2/\text{s}$.

8.8 Exercises

8.8.1 Looking up Pump Characteristics

With the following web site, pump manufacturers may be identified: <http://www.pumps-directory.com>. Search for a particular type of pump. With this information, one may consult the web site of a manufacturer. Some manufacturers provide information on the characteristics of some of their products. One may learn on practical aspects of pumps with the information provided by manufacturers. One manufacturer offers free access to a pump handbook with material that complements very well the present chapter on pumps and the previous chapter on similitude. Search for Grundfos pump handbook. The result is: http://net.grundfos.com/doc/webnet/mining/_downloads/pump-handbook.pdf.

8.8.2 Verification of an NPSH-Value

On the web sites of some pump manufacturers, characteristic curves may be found, including the variation of the required NPSH as a function of the flow rate. Make the choice of a pump and verify the required NPSH at the design flow rate against the value obtained from $\Omega_{ss} = 3$ according to Eq. (8.16). In the Grundfos pump handbook, an example of a set of pump characteristics is discussed at the very beginning of the book in Sect. 1.1.2. We may read the data for the flow rate at optimum efficiency. These are: flow rate $Q = 70 \text{ m}^3/\text{h}$, head $H = 42 \text{ m}$, power $P = 10 \text{ kW}$, efficiency $\eta = 80\%$, $\text{NPSH}_r = 3 \text{ m}$. First, we may verify the efficiency. The rotational speed is not mentioned, but we may guess the value by considering the possible range of specific speed of single-stage centrifugal pumps, since the head is a typical value of such a pump. Verify that $n = 2900 \text{ rpm}$ leads to $\Omega_s = 0.463$. We take this value, since the rotational speed of $n = 1450 \text{ rpm}$ leads to an unlikely low value. Calculate the required NPSH with Eq. (8.16) for $\Omega_{ss} = 3$. The result is $\text{NPSH}_r = 3.478 \text{ m}$. This means that about 0.5 m safety margin has to be provided with respect to the value obtained by the manufacturer from measurement of 3 % head drop. This value is the typical safety margin advised by manufacturers. Since $\Omega_{ss} = 3$ is the optimum value for incidence-free flow, normally a safety margin of 0.5 m cannot be sufficient for avoiding cavitation erosion. It looks wise to provide an NPSH value of 4 m for the considered case, but a safety factor of 2, as recommended by Europump [2], seems exaggerated.

References

1. Brennen CE (2013) *Hydrodynamics of pumps*. Cambridge University Press. ISBN 978-1-107-40149-5
2. Europump (1999) *NPSH for rotodynamic pumps*. Europump guide to advanced pumping technology, nr. 1. Elsevier. ISBN 1-85617-356-9
3. Europump (2000) *Operating rotodynamic pumps away from design conditions*. Europump guide to advanced pumping technology, nr. 3. Elsevier. ISBN 1-85617-372-0
4. Franc JP, Michel JM (2004) *Fundamentals of cavitation*. Kluwer Academic Publishers. ISBN 1-4020-2232-8
5. Girdhar P, Moniz O (2005) *Practical centrifugal pumps*. Elsevier. ISBN 0-7506-6273-5
6. Gülich JF (2010) *Kreiselpumpen*, 3rd. edn. Springer. ISBN 978-3-642-05478-5
7. Japikse D, Marscher W, Furst RB (1997) *Centrifugal pump design and performance*. Concepts ETI. ISBN 0-933283-09-1
8. Karassik IJ, McGuire JT (1991) *Centrifugal pumps*, 2nd edn. Chapman & Hall. ISBN 0-412-06391-3
9. Pfleiderer C (1961) *Die Kreiselpumpen für Flüssigkeiten und Gase*, 5th edn. Springer (No ISBN)
10. Tuzson J (2000) *Centrifugal pump design*. Wiley. ISBN 0-471-36100-3

Chapter 9

Hydraulic Turbines

Abstract In this chapter, we discuss the different types of hydraulic turbines for electric power plants. We analyse their main characteristics in order to understand in which range of head and flow rate they can be used efficiently. We also discuss bulb turbines for tidal energy plants and reversible pump-turbines for pumped storage plants.

9.1 Hydraulic Energy

Hydraulic energy becomes available by water flow between two places with a difference in altitude. Hydraulic turbines convert the gravitational potential energy in mechanical energy. This mechanical energy is in practice merely used for electricity generation. Natural altitude differences are very seldom just serviceable. In most cases, a water reservoir is built by erecting a dam in a river. In high mountain areas, a supply pipe connects the reservoir with a power station at a much lower altitude. The available head then strongly exceeds the dam height. With most rivers, however, the power station can only be built within the dam or very near to it and the available head is lower than the dam height. With plain rivers, the dam normally enables shipping traffic in combination with a lock system. Available heads may thus strongly differ: from the 1000 m order to some few meters. It is obvious that lower heads imply higher investment costs per unit of power. The minimal economically applicable head is about 4–5 m.

River water originates from rain or snow at higher altitudes. This is caused by water evaporation at lower altitudes, by rise and condensation in the colder atmosphere at higher altitudes. The energy source with this process is the sun. Hydraulic energy is thus part of a thermal cycle using solar energy. Throughout the world there is about 700.000 MW installed hydraulic power (2014). About 15% of all electricity is generated by means of hydraulic energy and about 25% of the practically exploitable hydraulic energy potential is already in use. Most of the potential is already used in Europe and North America. Notwithstanding some big plants in Asia and South America, there still is a significant unused potential.

Hydraulic turbines may strongly vary in size. The typical power is 100–400 MW, but there also exist 4–5 MW turbines and even much smaller ones. Hydraulic power

stations with power under 10 MW are classified as small ones and those with power not exceeding 1 MW are called micro power stations. At present, the second biggest power station is the Itaipu plant at the Brazil-Paraguay border with 14,000 MW installed power, 20 turbines of nominal power 700 MW, nominal head 118 m, surface area of the reservoir about 1350 km². The biggest power station is the Three Gorges plant on the Yangtze river in China with 22,500 MW installed power, 32 turbines of nominal power 700 MW and 2 smaller turbines of 50 MW, nominal head 81 m, surface area of the reservoir about 1000 km²

9.2 Hydraulic Turbine Types

9.2.1 Large Turbines (> 10 MW)

At present, three types are used for larger applications.

A *Pelton turbine*, as drawn in Fig. 9.1, is an impulse turbine (zero loss-free degree of reaction) with an injector (nozzle) generating a jet of water. This jet propels a runner turning in the atmosphere. Blades have the shape of a double spoon. Figure 9.1 represents a machine with a horizontal shaft and one injector. Up to two injectors may be applied with a horizontal shaft (one propelling the bottom side, as shown, and one propelling vertically downwards). Up to two wheels may be mounted onto the same shaft (one on both sides of the generator). A Pelton turbine may also be built with a vertical shaft. Up to six injectors may be applied with a vertical shaft.

A *Francis turbine*, represented in Fig. 9.2, is a radial machine with a medium to high degree of reaction (0.55–0.75). With the turbine shown, water is supplied by a volute (also called spiral casing). This is a typical design (a water chamber may be applied with small turbines). The water flows through guide vanes, adjustable for flow rate control. The vanes can be closed down to a zero flow. The rotor usually

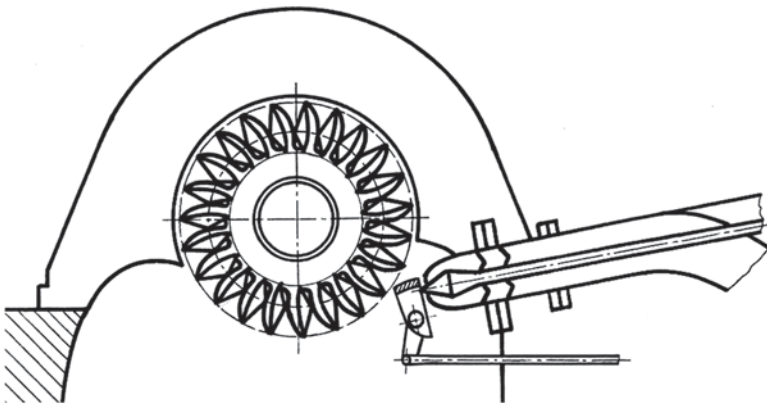


Fig. 9.1 Pelton turbine with horizontal shaft and one injector

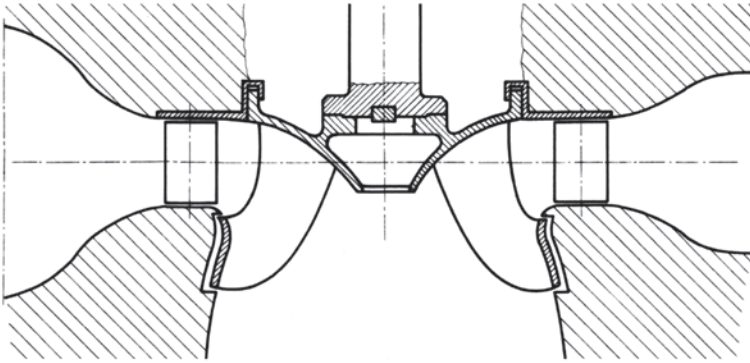


Fig. 9.2 Francis turbine (high specific speed type); adjustable stator vanes

has 12–16 blades. The inflow of the rotor is radial (no axial velocity component), but the outflow is approximately axial (small radial velocity component). Such a rotor is called radial. With a radial rotor, rotor blades cannot be adjusted. Strongly different rotor forms are used (see further below). Downstream of the rotor is a draught tube. With the type represented, the draught tube is modelled in the concrete structure. It can also be made of steel.

A *Kaplan turbine*, represented in Fig. 9.3, is an axial machine with a high degree of reaction (0.75 and higher). The turbine shown has a volute supply and a radial stator with adjustable vanes. Upstream of the adjustable stator vanes, there are fixed stator vanes that play a role in supporting the structure. These are called stay vanes and are often also employed with Francis turbines. The rotor is flowed through axially and has adjustable blades. Downstream of the rotor is a draught tube. Flow rate control is mainly achieved by positioning the rotor blades. Stator vanes play only a minor role (see further). Stator vanes can, as with the Francis turbine, be completely closed in order to reduce the flow rate to zero. Large turbines are mounted vertically and have a volute, as represented in Fig. 9.3. Small turbines (see Chap. 1) may be mounted with an inclined shaft and may be designed with an axial stator and axial water supply. Medium and small machines may be made with a horizontal shaft as well (see further: bulb turbines). The rotor usually has 4–6 blades. Kaplan turbines sometimes are described as propeller turbines due to the resemblance of the rotor to a ship propeller. There also exist mixed-flow rotor forms with adjustable rotor blades. Mixed-flow machines have a lower degree of reaction than axial machines and have properties in between those of Francis and Kaplan turbines.

Hydraulic turbines are of single-stage type, due to their very low specific energy. For example, the specific energy corresponding to a 1000 m head is $gH \approx 10,000 \text{ J/kg} = 10 \text{ kJ/kg}$, whereas the order of magnitude with gas turbines and steam turbines is 1000 kJ/kg. With complete energy use in a nozzle, as with a Pelton turbine, 10,000 J/kg leads to the velocity $v \approx 140 \text{ m/s}$. The optimal blade speed is then about 70 m/s (degree of reaction = 0, speed ratio analogous with an impulse type steam turbine). With a 2 m diameter, the corresponding rotational speed is about 670 rpm. This is a rather low value. Typical rotational speeds with Pelton turbines

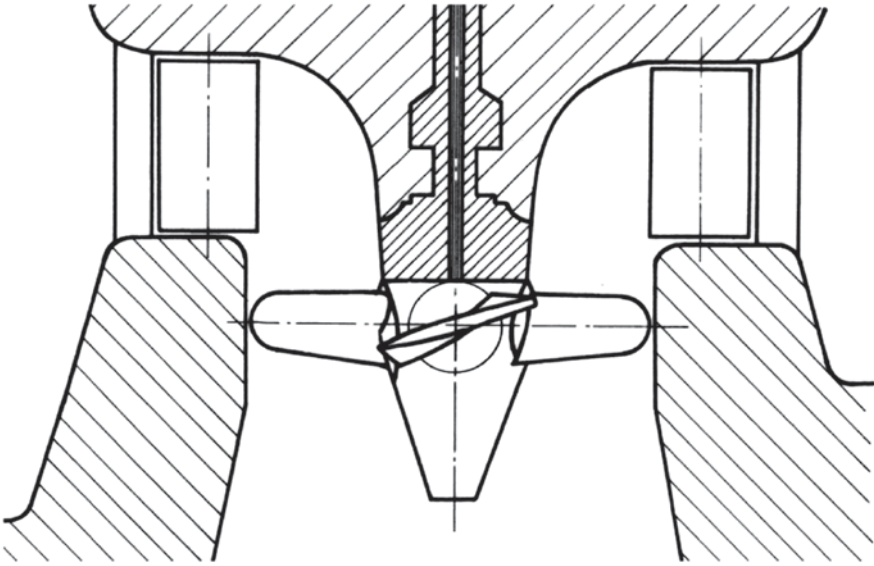


Fig. 9.3 Kaplan; adjustable rotor blades and stator vanes

thus amount to 500, 427, 375 rpm, with lower rotational speeds as heads get lower. With Pelton turbines, rotational speeds become impracticable at low heads, but, of course, the smaller the turbine, the lower the head may be.

The example demonstrates the irrelevance of multi-stage hydraulic turbines and shows that lower heads require much higher rotational speeds than with impulse-type machines. As we will study further, the relation between the degree of reaction and the optimal speed ratio with hydraulic turbines is the same as with steam turbines. Lower heads thus require turbines with a medium degree of reaction (Francis turbine). Still lower heads require a high degree of reaction (Kaplan turbine). Figures 9.1, 9.2, 9.3 further reveal that, at equal sizes, Kaplan turbines handle the highest flow rates and Pelton turbines the lowest ones. The head-flow combinations mean that a Pelton turbine has a low specific speed: $\Omega_s = \Omega \sqrt{Q} / (gH)^{3/4}$. Values range from about 0.05–0.165 with a single-injector turbine. Specific speed ranges from about 0.30–2.10 with Francis turbines, whereas Kaplan turbines cover a 1.65–6.00 range (see further). The specific speed range from 0.165 to 0.30 is covered by multi-injector Pelton turbines. Figure 9.4 represents the range of application for the various types ($n_q \approx 50 \Omega_s$). The term bulb/tube turbine refers to axial machines with an axial stator and axial water supply.

9.2.2 Small Turbines (<10 MW)

The three types of large machines are applied with small-scale applications as well. The term small scale may refer to a turbine generating some few MW, but also to

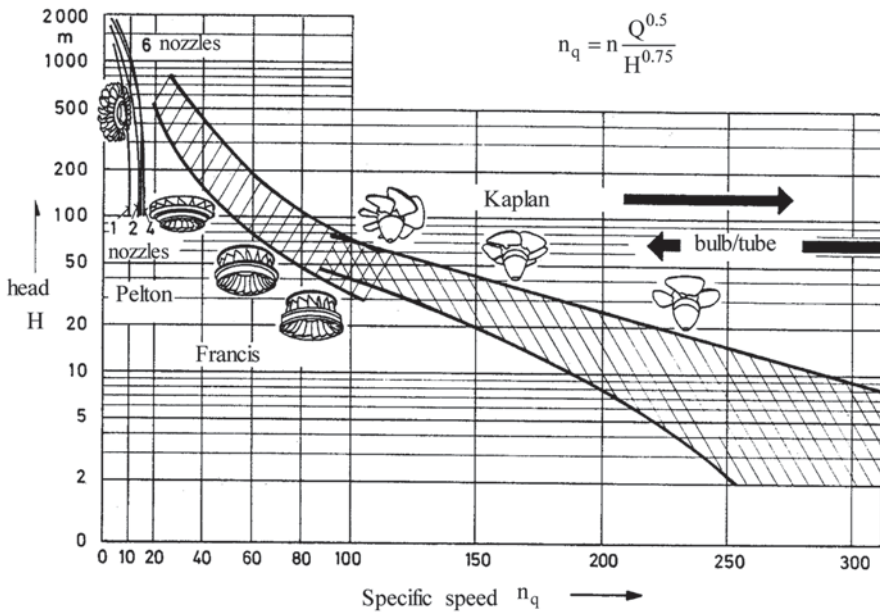
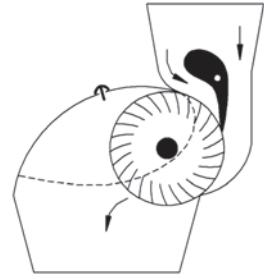


Fig. 9.4 Range of application for various types of hydraulic turbines. (From [1]; permission by Vogel Verlag); $n_q \approx 50 \Omega_s$

one yielding only some tens of kW. The diagram in Fig. 9.4 does not always apply anymore then. It is obvious that a Pelton turbine may be used with a 10 m head if dimensions are sufficiently small. In the calculation example, the same rotational speed is obtained with a 10 m head and a 0.2 m diameter. Small Pelton turbines for high head exist as well. Pelton turbines are rather easily made with small dimensions. Small Francis and Kaplan turbines are only possible for low head. As already mentioned, Francis turbines may be simplified by using a water chamber for lower head (applicable up to a 4–5 m head). For low power, an axial turbine is mostly integrated in a pipe as a so-called tube turbine. Small axial turbines mostly have a fixed stator, as the flow rate is mainly determined by the position of the rotor blades (see further below). Machines with fixed rotor blades and adjustable stator vanes exist as well. There are also small axial machines with fixed rotor blades and fixed stator vanes. No flow rate variation is then possible (at a constant head and a constant rotational speed).

Apart from the three types discussed, there is a cross-flow type, mostly referred to as a Banki-turbine (after its inventor). Figure 9.5 represents a section. The functioning is similar to that of a cross-flow fan (Chap. 3), but turbine-wise. Blades have a radial direction at the inside. Relative velocities at the rotor inlet and outlet are identical. As a result, the degree of reaction is zero. Cross-flow turbines are a further development of undershot water wheels. The machine has a draught tube enabling recovery of the downward head. The rotor partially runs in air. A sniffer valve is

Fig. 9.5 Cross-flow turbine

provided to supply air, as air is entrained in the draught tube. Cross-flow turbines can be constructed very easily, but their efficiency is significantly lower than that of other hydraulic turbine types, namely about 80 % compared to about 90 %.

9.3 Pelton Turbines: Impulse Turbines

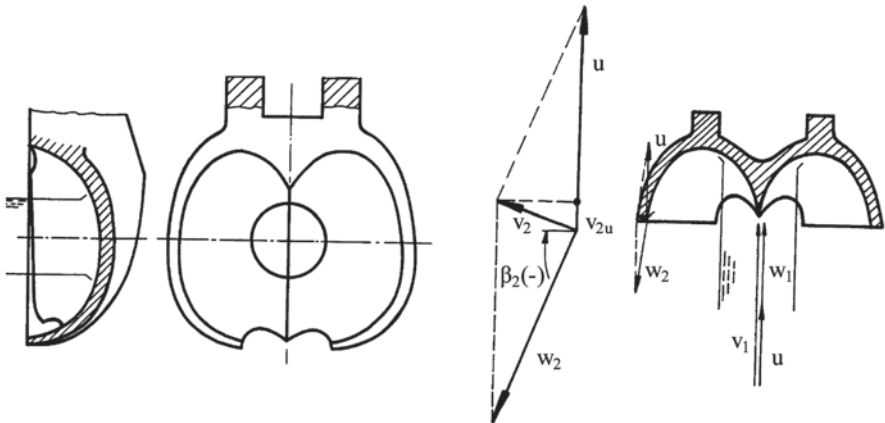
9.3.1 Performance Characteristics

Figure 9.6 sketches the flow over the rotor buckets of a Pelton turbine (the term bucket is typically used).

The inlet velocity v_1 has the same direction as the blade speed u :

$$w_1 = v_1 - u.$$

The top angle of the central ridge of the bucket does not equal zero, generating a small incidence component at the rotor inlet. The incidence loss is integrated in the

**Fig. 9.6** Flow over a Pelton turbine bucket

rotor loss coefficient. At the outlet, the relative speed w_2 forms an angle β_2 with the shaft direction. The flow angle is approximately equal to the outlet blade angle. From the outlet blade angle follows ($\beta_2 < 0$, $\beta_2 \approx -80^\circ$):

$$v_{2u} = u + w_{2u} = u + w_2 \sin \beta_2,$$

$$\Delta W = u(v_{1u} - v_{2u}) = u(w_1 - w_2 \sin \beta_2).$$

The jet velocity is $v_1 = \phi_s \sqrt{2gH_m}$, with ϕ_s being a velocity coefficient, taking nozzle and volute (if present) losses into account. H_m is the manometric head, determined with a manometer at the injector inlet. By writing v_1 as above, the downward head between the injector nozzle and the tail water is not included in the manometric head, which is a typical practice. Since there is no possibility for confusion, we represent the manometric head by H from now on. Let $\phi_r = w_2/w_1$ be a velocity coefficient, taking rotor blade losses into account. We obtain then

$$\Delta W = u(v_1 - u)(1 - \phi_r \sin \beta_2).$$

Rotor work varies parabolically as a function of blade speed u with a maximum at $u = v_1 / 2 = \frac{1}{2} \phi_s \sqrt{2gH}$. The optimal speed ratio is ($\phi_s \approx 0.97$):

$$\lambda = \frac{u}{\sqrt{2gH}} = \frac{1}{2} \phi_s \approx 0.48. \quad (9.1)$$

Nozzle efficiency may be formulated as

$$\eta_s = \frac{v_1^2 / 2}{gH} = \phi_s^2 \approx 0.94,$$

and rotor efficiency as

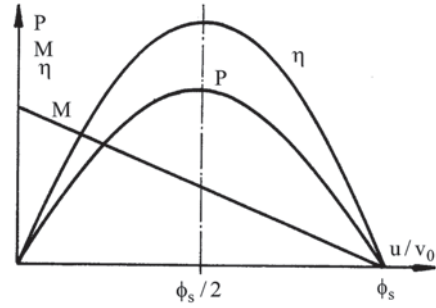
$$\eta_r = \frac{\Delta W}{v_1^2 / 2} = 2(1 - \phi_r \sin \beta_2) \frac{u}{v_1} \left(1 - \frac{u}{v_1}\right).$$

The optimum rotor efficiency is

$$\eta_{r,o} = 2(1 - \phi_r \sin \beta_2)^{1/4} \approx 0.97.$$

Assumed hereby is that $\phi_r \approx 0.96$ and $\beta_2 \approx -80^\circ$.

Fig. 9.7 Power, torque and efficiency as a function of speed ratio with a pelton turbine



Overall (global) efficiency is $\eta_g = \eta_s \eta_r \eta_m$.

From the foregoing values and a mechanical efficiency of about 0.98, it follows that the overall efficiency at optimum speed ratio is about 0.90. It even might be better in practice, namely up to 0.92.

Rotor power is $P_{rot} = \dot{m} \Delta W$.

Shaft power P_{shaft} equals rotor power multiplied by mechanical efficiency.

Figure 9.7 represents the variation of power and efficiency, as a function of the blade speed u and the variation of the torque exerted on the rotor by the fluid. The torque is calculated by dividing rotor power by angular velocity:

$$M = \dot{m} r (1 - \phi_r \sin \beta_2) (v_1 - u).$$

The torque is a linear function of the speed. It decreases from the maximum value at $u=0$ to zero for $u=v_1$. The maximum speed that may be reached by the turbine blades, as far as the turbine is not driven, thus equals double the design speed. If the turbine were designed to resist a centrifugal force four times as high as the design centrifugal force, no damage could occur if the turbine runs idling. Pelton turbines are not built so strong for reasons of cost. A protective device for limiting over-speed thus must be incorporated. The foregoing conclusions rest on an assumed constant mechanical efficiency. Mechanical losses mainly occur by wheel friction. These change with the cube of the rotational speed and thus strongly increase with increasing speed. As a consequence, the optimum speed ratio is somewhat lower than derived here, namely about 0.45–0.47, with lower values for turbines with a lower power (one injector, smaller injector diameter). The maximum speed with an idling turbine (runaway speed) equals about 1.8 times the design speed.

9.3.2 Specific Speed

We take the notation d for the outlet diameter of the nozzle and D for the diameter of the rotor at the jet centre line. The flow rate is obtained by

$$Q = v_l \frac{\pi d^2}{4} = \phi_s \sqrt{2gH} \frac{\pi d^2}{4}.$$

The rotational speed is derived from the blade speed by

$$\Omega = \frac{2u}{D}.$$

$$\text{Thus: } \Omega_s = \frac{\Omega \sqrt{Q}}{(gH)^{3/4}} = \frac{u}{\sqrt{2gH}} \sqrt{\phi_s \pi} 2^{3/4} \frac{d}{D}.$$

With the optimum speed ratio $\lambda = u / \sqrt{2gH}$ of about 0.48 and $\phi_s = 0.97$:

$$\Omega_s \approx \sqrt{2} \frac{d}{D}. \quad (9.2)$$

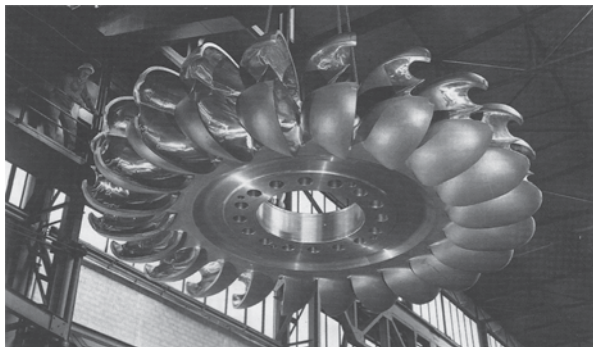
For best flow conditions, the d/D value lies between about 1/16 and 1/8. Small d/D values generate long jets with a large contact surface with the air compared to the cross section. This causes a relatively high friction and drop formation. High d/D values generate jets with bad flow guidance by the buckets. In practice d/D can vary from about 1/24 to 1/8, with low d/D values resulting in machines with a lower efficiency.

There is a constructional limit to the specific speed because of the centrifugal load on the buckets. With increasing Ω_s at constant Q and H values, D must increase. The centrifugal force on a bucket is $m\Omega^2 r$. The mass of the bucket (m) stays constant since the mass only depends on d , so on Q and v_l , which both are constant. Further $u = \Omega r$ must be constant, as v_l is constant and u/v_l as well. The centrifugal force is thus proportional to Ω . If Ω_s increases, D must decrease, because of $\Omega_s \sim d/D$. The machine diameter D cannot decrease below a minimum value determined by the circumferential length required for mounting the buckets since their size and number are determined by flow requirements. The required mounting length increases with the head, as forces on the buckets increase proportionally to the head. Table 9.1 lists the maximum values of d/D and Ω_s as functions of the head, according to Vivier [3]. These values apply to larger units (10–60 MW). With smaller turbines, the limitations caused by the centrifugal load may already occur with lower head. The foregoing discussion applies to turbines with one rotor and one injector. With z_1 rotors with z_2 injectors each, the flow rate is multiplied by $z_1 z_2$ and thus the specific speed with $\sqrt{z_1 z_2}$.

Table 9.1 Maximum values of d/D and Ω_s depending on head for pelton turbines

H (m)	400	600	1000	1500	2000
$(d/D)_{\max}$	1/8	1/10	1/14	1/19	1/24
$(\Omega_s)_{\max}$	0.165	0.130	0.095	0.070	0.055

Fig. 9.8 Pelton turbine rotor. (Courtesy ANDRITZ HYDRO)



9.3.3 Determination of the Main Dimensions

Flow rate and head are imposed by the application. Specific speed is chosen with regard to the strength limitations from the centrifugal load. Specific speed is mostly chosen as high as possible in order to achieve relatively high and electrically serviceable rotational speeds (428, 500, 600 rpm). With a relatively high flow rate, several rotors and several injectors may be needed. The jet velocity follows from

$$v_j = \phi_s \sqrt{2gH},$$

where $\phi_s = 0.96\text{--}0.98$. The diameter of the injector throat follows from:

$$Q = \frac{\pi d^2}{4} v_j,$$

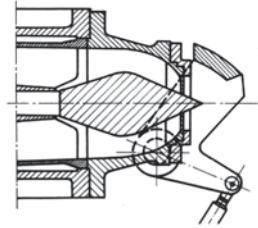
with Q the flow rate per injector. All bucket dimensions are subsequently derived from the jet diameter. The condition for maximum efficiency, $u / v_j \approx 0.48$, determines the blade speed and thus the rotor diameter. The number of blades depends on the condition that at least one blade must receive the jet. When a blade leaves the jet, the following one shall have entered with some overlap.

Figure 9.8 shows a rotor. Rotors are mostly manufactured of stainless steel because of good resistance of this material to erosion. Other erosion-exposed parts are made of stainless steel as well. The cut-out at the tip of the buckets is intended to enable a smooth transition of the water jet from one bucket to the next one.

9.3.4 Flow Rate Control and Over-Speed Protection

Adjustment of the flow rate, and thereby power at constant head, is achieved with a needle influencing the through-flow area of the injector (Fig. 9.9). Care must be taken for too abrupt changes of the position of the needle. The closing time should

Fig. 9.9 Adjusting needle and jet deflector with a pelton turbine



be sufficiently long (typically 15–30 s) in order to avoid water hammer in the supply duct. If a fast flow rate reduction is required with a sudden turbine load decrease, a jet deflector is used. The deflector is turned between the injector and the buckets. This takes at most a few seconds. The deflected jet causes strong erosion of the surrounding parts. This device should thus only be applied in anticipation of flow rate adjustment by a slow movement of the needle.

9.4 Francis and Kaplan Turbines: Reaction Turbines

9.4.1 Shape of the Velocity Triangles: Kinematic Parameters

Figure 9.10 is a sketch of the velocity triangles at rotor inlet and outlet for an average streamline. A radius ratio $u_2/u_1 = 0.5$ is assumed as an example. This corresponds to a medium specific speed Francis turbine. Five parameters are required to determine the shape of the velocity triangles. For the inlet triangle these may be: flow coefficient $\phi = v_{1m}/u_1$ and tangential speed coefficient $\zeta = v_{1u}/u_1$. One of these parameters may be replaced by the stator vane angle α_1 . For the outlet triangle they may be: radius ratio $m = u_2/u_1$, ratio of the meridional component of the velocities v_{2m}/v_{1m} , velocity ratio w_2/w_1 . One of the parameters may be replaced by the outlet angle α_2 . Parameters determining the shape of the velocity triangles are called kinematic parameters. In Fig. 9.10, the three kinematic parameters determining the outlet velocity triangle are: $\alpha_2 = 0$, $v_{2m}/v_{1m} = 1$, $w_2/w_1 = 1$. That this

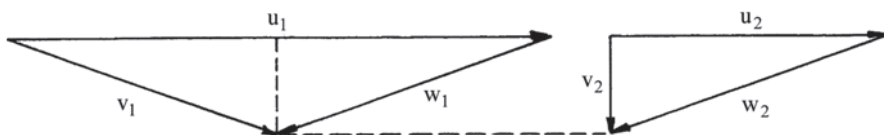


Fig. 9.10 Velocity triangles at rotor inlet and outlet with Francis turbines (in principle); $m = u_2/u_1 = 0.50$

choice is reasonable, although not optimal, may be demonstrated by considering the losses and deriving some guidelines for optimisation.

9.4.2 Optimisation of the Velocity Triangles

Losses first occur in the distributor components. These are the volute and the adjustable guide vanes. Flow is accelerating in these parts, causing only small losses, namely of the 5% order of the kinetic energy at the stator outlet ($v_1^2/2$). We represent the distributor losses by $\xi_s \frac{1}{2} v_1^2$ with $\xi_s \approx 0.05$. The spaces in between blades in the rotor constitute channels. Loss is mainly caused by friction and may be represented by $\xi_r \frac{1}{2} w_2^2$, where again the order of magnitude of the loss coefficient is a few percent: $\xi_r \approx 0.05$. The loss representation is acceptable, unless the rotor would have diffusion ($w_2 < w_1$). In that case, diffusion loss should be added. Incorporating diffusion is possible, but it is contrary to turbine functioning. So we do not expect it. Kinetic energy at the rotor outlet ($v_2^2/2$) is not completely lost, as the draught tube also functions as a diffuser. Recovery of this kinetic energy is limited to about 75%, however. The outlet loss is thus very high and dominantly determines the optimisation. Diffuser loss is represented by:

$$q_{irr,d} = \xi_d \frac{1}{2} v_2^2 \quad \text{with} \quad \xi_d \approx 0.25.$$

As diffuser loss is dominant, measures have to be taken to minimise the kinetic energy at the rotor outlet. This first implies that the outlet velocity should be oriented axially, as drawn in Fig. 9.10. Moreover, the value of v_2 must be kept low. This implies a low flow coefficient v_{1m}/u_1 . As a consequence, the stator inlet angle α_1 must be rather large. This cannot be exaggerated, as a greater α_1 means a larger turning in the distribution elements and thus larger losses. It also implies greater through-flow areas, which increases friction surfaces in both the rotor and the stator. An exact value for the stator angle α_1 cannot be determined with a simple reasoning. The whole optimisation should be studied for that. In real Francis turbines, α_1 varies between about 60 and 75°. 70° is applied in Fig. 9.10.

Work may thus be represented by

$$\Delta W = gH - \sum q_{irr} = gH - \xi_s \frac{v_1^2}{2} - \xi_r \frac{w_2^2}{2} - \xi_d \frac{v_2^2}{2}. \quad (9.3)$$

Kinematic parameters should follow from minimising the sum of the losses. With the relation (9.3), it is impossible to perform an exact optimisation, if fixed loss coefficients are assumed. But some guidelines may be derived from it.

Given the dominance of outlet losses, we may assume an axial outlet flow ($\alpha_2 = 0$). With regard to the reduction of the outlet loss, it is clearly advantageous to choose the ratio of the meridional components v_{2m}/v_{1m} below 1. v_2 is reduced by

that, but the required outlet area then increases. We therefore provisionally assume the ratio as 1, but we keep in mind that a reduction is advantageous, if feasible. The velocity ratio $w_2/w_1 = I$, principally, is not optimal. If, at given v_{2m} , acceleration is incorporated, the flow turning in the rotor increases. This implies an increase of the work by the lift force. Work by the Coriolis force equals $u_1^2 - u_2^2$. The work by lift force equals $u_1 w_{1u} - u_2 w_{2u}$. Note that the lift work is negative with the triangles in Fig. 9.10. It may be made less negative, even positive, by incorporating acceleration. This enables a reduction of the number of blades, resulting in a smaller friction surface. A greater turning increases the rotor loss coefficient, however, and greater outlet velocity increases losses as well. Thus, acceleration and turning should not be too big. Incorporating some acceleration in order to prevent a negative contribution to the work by the lift force, even making it somewhat positive, is thus advantageous.

9.4.3 Degree of Reaction and Speed Ratio

We assume an axial outlet velocity in order to minimise outlet losses. We also assume constant meridional velocity components. Thus it follows

$$\Delta W = u_1 v_{1u} - u_2 v_{2u} = u_1 v_{1u},$$

$$R = \frac{\frac{u_1^2 - u_2^2}{2} + \frac{w_2^2 - w_1^2}{2}}{u_1 v_{1u}} \quad \text{or} \quad 1 - R = \frac{\frac{v_1^2 - v_2^2}{2}}{u_1 v_{1u}}.$$

Thus:

$$R = 1 - \frac{1}{2} \frac{v_{1u}}{u_1}.$$

The work coefficient is

$$\psi = \frac{\Delta W}{u_1^2} = \frac{u_1 v_{1u}}{u_1^2} = \frac{v_{1u}}{u_1}.$$

Thus:

$$\psi = \frac{v_{1u}}{u_1} = 2(1 - R). \quad (9.4)$$

The speed ratio is

$$\lambda = \frac{u_1}{\sqrt{2gH}} = \frac{u_1}{\sqrt{2\Delta W}} \sqrt{\eta_i} = \frac{\sqrt{\eta_i}}{\sqrt{2}\sqrt{\psi}} = \frac{\sqrt{\eta_i}}{2\sqrt{1-R}}.$$

With $\eta_i \approx 0.92$ (optimal efficiency), it thus follows

$$\lambda \approx 0.48 / \sqrt{1-R}. \quad (9.5)$$

The relations (9.4) and (9.5) are very universal. They are compatible with the Pelton turbine result (9.1). They are also compatible with the findings for steam turbines in Chap 6. Conditions for achieving relation (9.5) are assumption of an axial outlet flow and a constant meridional component of the velocity. In real machines these conditions are very well met. Note that relation (9.4) was also obtained by the analysis of radial fans in Chap. 3. With the relation (9.4), the degree of reaction may be read from the velocity triangles. For example, in Fig. 9.10 velocity triangles are drawn with $v_{1u}/u_1 = 0.5$. The corresponding degree of reaction is $R=0.75$. From this we learn that the degree of reaction is a kinematic parameter. We may apply it instead of the tangential velocity coefficient. Note that work coefficient (9.4) and speed ratio (9.5) are kinematic parameters as well.

9.4.4 Velocity Triangles with Varying Degree of Reaction

Figure 9.11 renders velocity triangles at degrees of reactions varying from $R=0.55$ to $R=0.85$, with realistic proportions based on parameter variations from the books of Vivier [3] and Dietzel [1]. There is a limited flow turning and some acceleration in the rotor. Ratios of meridional components are put to 0.85, 0.90, 0.95 and 1.00 at degree of reaction 0.55–0.85 in order to render the tendencies. The theoretical expression of the degree of reaction (9.4) has been used. A variable meridional

Fig. 9.11 Velocity triangles at varying degrees of reaction

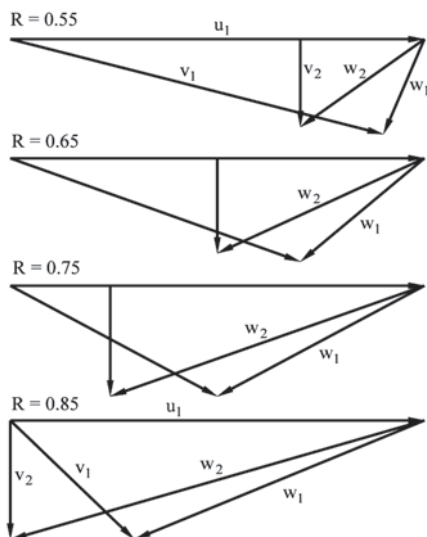


Table 9.2 Stator angles as a function of degree of reaction with Francis and Kaplan turbines

R=0.55	R=0.65	R=0.75	R=0.85
$\alpha_1 = 75^\circ$	$\alpha_1 = 70^\circ$	$\alpha_1 = 60^\circ$	$\alpha_1 = 45^\circ$

velocity component causes some deviation of the real degree of reaction. A higher degree of reaction implies less freedom to decrease v_2 with respect to v_{lm} . Constant mass flow rate then requires an increase of the outlet area. This is more difficult with a diameter ratio near to 1 (see Fig. 9.12). With degrees of reaction 0.55 and 0.65, the work by lift has been put exactly to zero: $u_1 w_{1u} - u_2 w_{2u} = 0$; it is difficult to avoid negative values. With the degree of reaction of 0.75, u_2 was determined by interpolation between the values of the other cases. The part of the lift work comes out at 15 %.

Realisation of a Francis turbine with a degree of reaction under $R=0.55$ is possible. Rotor turning must be high in that case in order to obtain a sufficient outlet diameter. This impairs the efficiency. Therefore, turbines with a low degree of reaction are not used in practice. The flow coefficient v_{lm}/u_1 increases somewhat with an increasing degree of reaction. The value varies from 0.23 to 0.27 with Francis turbines (this is approximately constant). This ratio changes more strongly with Kaplan turbines, namely $v_{lm}/u_1 \approx 0.30$ – 0.40 with a degree of reaction varying from 0.75 to 0.90. A rudimentary argumentation cannot demonstrate that this is optimal. Approximate stator angle values are given in Table 9.2.

9.4.5 Specific Speed and Meridional Shape of Francis Turbines

With $\Omega_s = (\Omega \sqrt{Q}) / (gH)^{3/4}$, we express Ω and Q as functions of geometric parameters. With b_1 being the stator vane height at the stator outlet and d_1 the rotor inlet diameter:

$$\Omega = \frac{2u_1}{d_1} = \frac{2 \times 0.48}{d_1 \sqrt{1-R}} \sqrt{2gH},$$

and

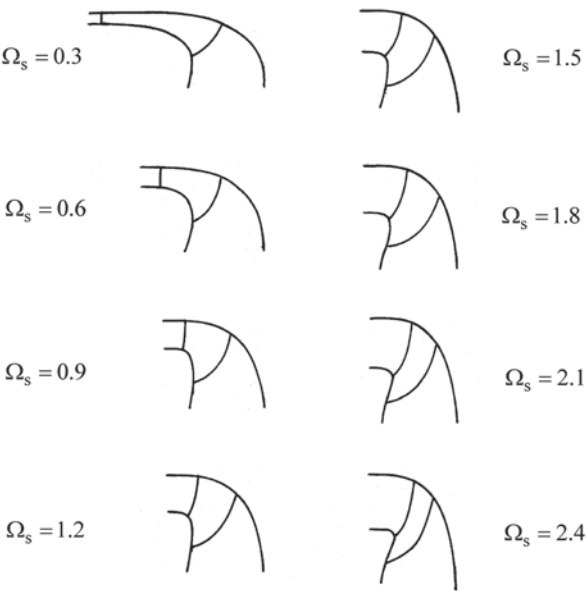
$$Q = \pi d_1 b_1 v_{lm} = \pi d_1 b_1 0.25 \frac{0.48}{\sqrt{1-R}} \sqrt{2gH},$$

where we applied $v_{lm}/u_1 \approx 0.25$.

After substitution we obtain

$$\Omega_s \approx \frac{1}{(1-R)^{3/4}} \sqrt{\frac{b_1}{d_1}}.$$

Fig. 9.12 Meridional section shape depending on specific speed with Francis turbines. (Adapted from Vivier [3])



This expression demonstrates that the ratio b_l / d_l and the degree of reaction must increase in order to increase specific speed. As demonstrated in the previous section, the diameter ratio increases with increasing degree of reaction. These influences explain the meridional shapes shown in Fig. 9.12. Just as with pumps with doubly curved blades, blade shapes may be designed by means of streamtubes, drawn in a meridional section. The exact blade shape is not discussed any further here. Blade design requires a study of the equilibrium of the various streamtubes and the flow turning in each streamtube. The study results in the chord, the inlet angle and the outlet angle of the blade segment in each streamtube. On the base thereof the blade may be drawn (with the so-called Kaplan method).

In order to give an idea of the efficiency variation with Ω_s , Table 9.3 lists some characteristic data based on the books of Vivier [3] and Dietzel [1]. The values

Table 9.3 Degree of reaction and outlet kinetic energy with Francis and Kaplan turbines

Francis							
Ω_s	0.3	0.6	0.9	1.2	1.5	1.8	2.1
R	0.53	0.56	0.59	0.64	0.68	0.72	0.75
$v_2^2 / 2gH$	0.025	0.035	0.050	0.075	0.090	0.100	0.105
Kaplan							
Ω_s	2	3	4	5			
R	0.80	0.85	0.88	0.90			
$v_2^2 / 2gH$	0.16	0.25	0.34	0.43			

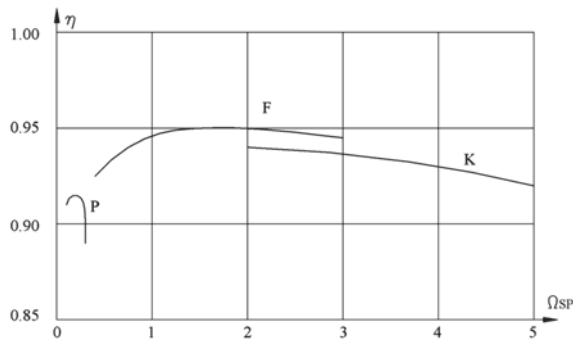


Fig. 9.13 Internal efficiency as a function of specific speed

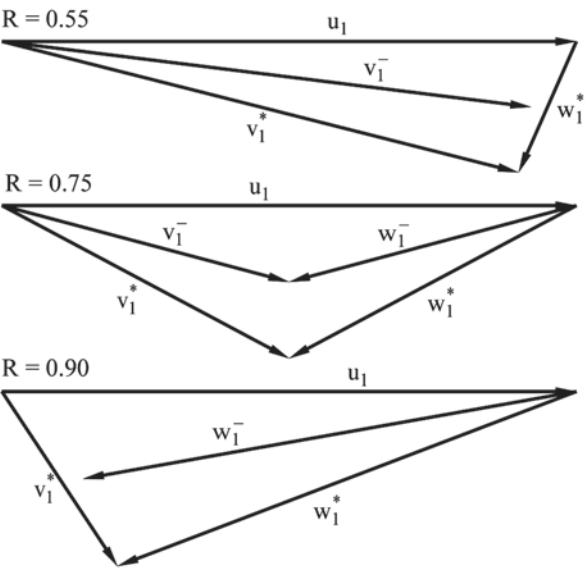
in Table 9.3 establish that the kinetic energy to be recovered in the draught tube proportionally gains importance with increasing specific speed. This is a factor impairing the efficiency at large specific speed. On the other hand, with a low specific speed, the blade surface in the rotor is large, causing large friction losses. Efficiency thus has a maximum as a function of specific speed. Figure 9.13 renders the variation (adapted from [2]). Efficiency is at its highest at about $\Omega_s = 1.5$. The maximum overall efficiency with Francis turbines is about 93.8% (Itaipu). The corresponding internal efficiency is 95.1%, with 98.6% generator efficiency. Specific speed is limited by cavitation risk, as $v_2^2 / 2gH$ increases with Ω_s . For given head, the pressure at rotor outlet thus decreases with Ω_s , which explains the maximum specific speed as a function of the head in Fig. 9.4.

9.4.6 Flow Rate Control with Reaction Turbines

Figure 9.14 sketches the inlet velocity triangles at the $R=0.55$, $R=0.75$ and $R=0.90$ degrees of reaction. The figure demonstrates how a change of a stator angle hardly causes any incidence on the rotor at $R=0.55$. The flow rate of the turbine may thus be controlled efficiently by adjusting the stator vanes only. A medium degree of reaction $R=0.75$ requires adjustment of both stator and rotor angles to prevent incidence. The rotor angle cannot be adjusted in Francis turbines (but there exist diagonal machines with adjustable rotor blades). Serious incidence at rotor inlet therefore occurs in case of flow rate change imposed by angle adjustment of the stator vanes. The angle of both stator vanes and rotor blades is adjustable in Kaplan turbines. With a high degree of reaction $R=0.90$, the flow rate can be controlled efficiently by only adjusting the rotor angle. Adjustment of the stator angle is not strictly required. Only a small incidence occurs. Incidence velocity is then the tangential distance between the end point of vector w_1^- and the direction of v_1^* .

Figure 9.15 renders efficiency versus flow rate for the various turbine types. The Pelton turbine has a very flat efficiency curve. The dependency is stronger with the

Fig. 9.14 Sensitivity to rotor or stator angle changes for reaction turbines



Francis turbine, increasing with specific speed from 0.5 to 2. The Kaplan turbine with adjustable stator vanes and rotor blades also has a rather flat efficiency curve. The dependency on flow rate increases if only the rotor blades are adjustable. The

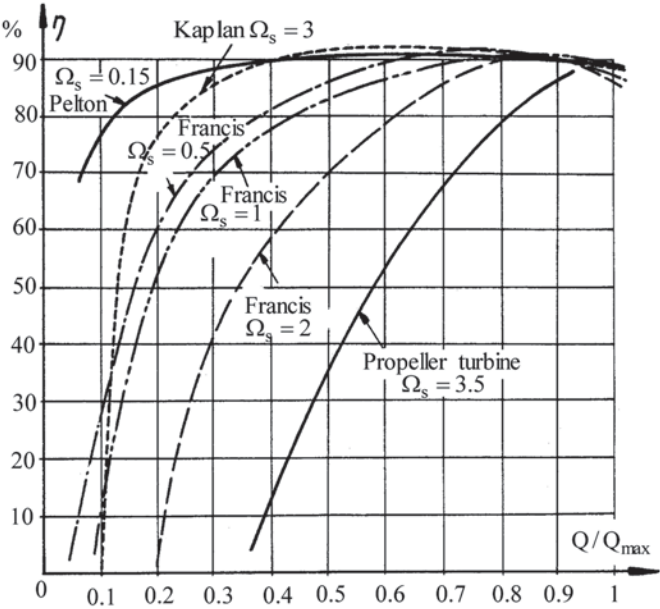


Fig. 9.15 Efficiency versus flow rate of the various turbine types. (Adapted from [3])

variation with the Kaplan turbine with $\Omega_s = 3$ and only adjustable rotor blades is comparable to that of a Francis turbine with $\Omega_s = 1$ (not explicitly shown). An axial turbine with adjustable stator vanes, but fixed rotor blades (called propeller turbine in the figure), has a very sharp efficiency variation.

9.4.7 Examples (Figs. 9.16, 9.17)

Fig. 9.16 Francis turbine rotor $\Omega_s \approx 1$. (Courtesy ANDRITZ HYDRO)

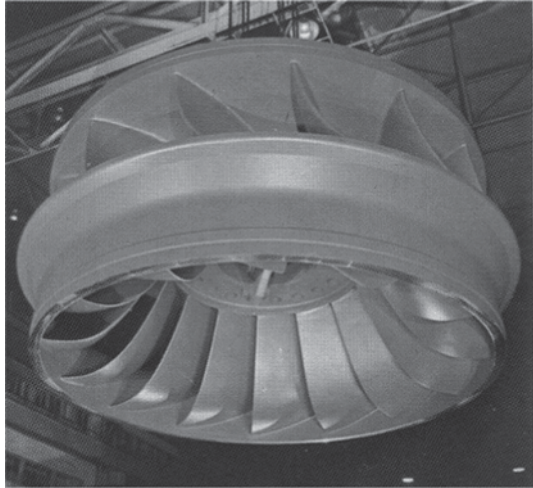
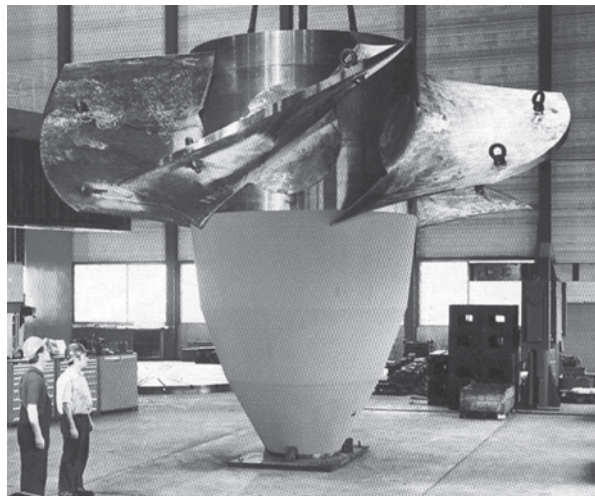


Fig. 9.17 Kaplan turbine rotor $\Omega_s \approx 3$. (Courtesy ANDRITZ HYDRO)

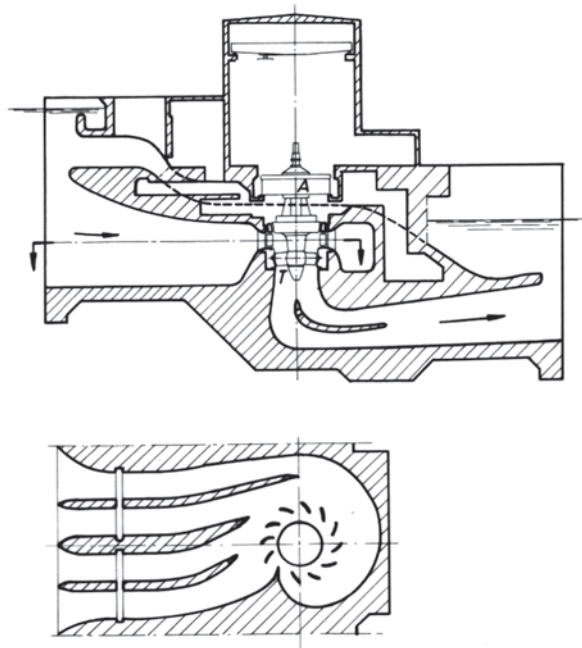


9.5 Bulb and Tube Turbines

Kaplan turbines for low head are mostly mounted with a vertical shaft, with the generator above the tail water line (Fig. 9.18). The generator is indicated by A (alternator) and the turbine by T. With low-head applications, the supply channel to the turbine is broad. Only part of the flow rate is guided to the rotor with a volute. The other part is admitted directly. Uniform flow distribution requires an appropriate stay vane ring. The quite strong changes of flow direction, especially in the draught tube, cause relatively high losses when head is low. For low head, a horizontal shaft of the turbine-generator group, aligned with the axis of the channel that connects both dam sides is more advantageous (Fig. 9.19). The generator (A) is positioned under the water surface then, which requires mounting in a watertight casing. The bulb that is formed that way is fixed to the channel walls with the profiled struts C. The bulb also houses the adjusting mechanism for the stator vanes D. The bulb is accessible through a shaft E (also profiled), through which power cables run. The axial turbine rotor with adjustable blades (R) is situated downstream of the bulb.

Bulb turbines are also applied to exploit tidal energy. A river estuary is closed with a dam containing a series of bulb turbines. At low tide at the sea side, turbines run with a through-flow in the estuary-sea sense. This is the normal through-flow sense. At high tide at the sea side, turbines run in the sea-estuary sense. Rotor blades and stator vanes are turned by $\sim 180^\circ$ for that, and the sense of rotation is reversed. This impairs the efficiency somewhat. Parts a and b in Fig. 9.20 represent the vane

Fig. 9.18 Kaplan turbine with low head



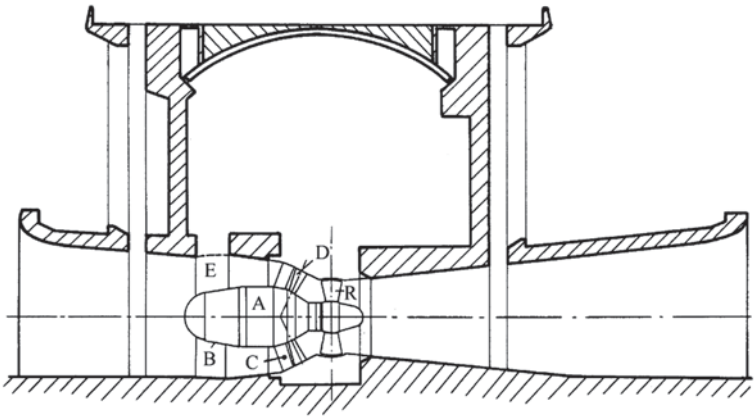


Fig. 9.19 Bulb turbine with low head

and blade positions corresponding with turbine operation in both senses. In periods of small difference in level, it may be profitable to pump in the sense as during the previous turbine phase. This operation allows an increase of available energy for the following turbine phase. Both turbine and pump functions can be performed by the same bulb machine. Leaving the stator vanes in their original position, turning

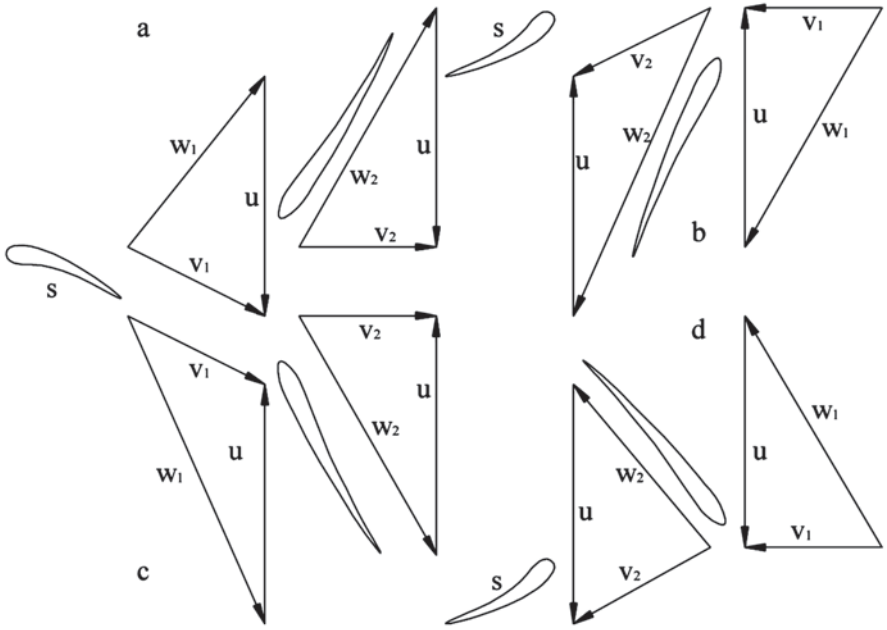


Fig. 9.20 Velocity triangles for turbine operation in normal sense (a), and reverse sense (b), and for pump operation in normal sense (c), and reverse sense (d)

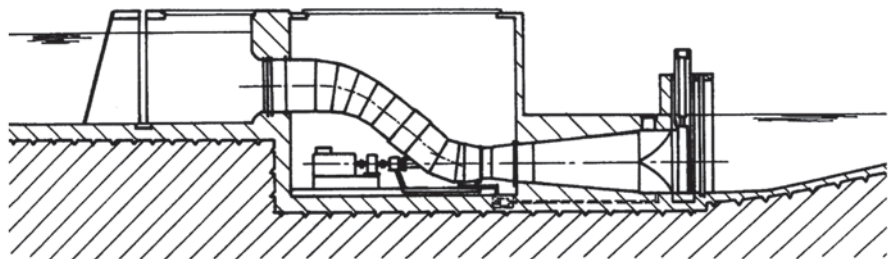


Fig. 9.21 Tube turbine

the rotor blades into a position that is approximately mirrored with respect to the meridional plane and reversing the sense of rotation create pump operation in the estuary-sea sense. The positions are shown on part c of Fig. 9.20. Starting from these positions, turning the stator vanes and rotor blades about 180° and reversing the rotation sense creates pump operation in the estuary-sea sense, as shown on part d in Fig. 9.20. Note that pump operation is obtained as well with blade positions in part a in Fig. 9.20, with a reverse sense of rotation. Pumping then occurs in the sea-estuary sense. But leading edges and trailing edges are then not adapted to the flow, which strongly impairs the efficiency. Pump operation as sketched in parts c and d of the figure is somewhat less efficient than the original turbine operation. The torsion of the blades is fixed. Blades may be positioned correctly for an average flow, but positions are not fully correct for all streamtubes.

Pump operation also allows converting electric energy into hydraulic energy by pumping water during periods of low electricity consumption. This then implies functioning as a pumped storage plant. In France, the Rance tidal power/pumped storage plant (near Mont Saint-Michel) was established according to this principle (24 groups of 10 MW).

Small size plants (10–500 kW) use bulb turbines with an angled gearbox in the bulb. The generator stands above the tail water level. Small applications also allow housing the turbine in a bended tube, with a shaft passing to the outside and a generator that may be placed in a watertight cellar (Fig. 9.21). Tube type turbines are completely axial ($u_1 = u_2$). The degree of reaction is thus very high. Flow rate control is normally only by adjusting the rotor blades.

9.6 Reversible Pump-Turbines

Pumped storage plants first accumulate hydraulic energy by pumping water during periods of low electricity consumption. Water is then led to turbines during peak periods. Pumped storage plants differ in some aspects from the combination of a standard hydraulic power plant and a pump station. This is mainly the case when the four basic components (pump, motor, turbine, generator) are reduced to three (pump, turbine and motor-generator) or even two (reversible pump-turbine and

motor-generator). The disadvantage of the three-machine combination is that the pump is idling during turbine operation, and vice-versa. This disadvantage may be avoided by disconnecting either the turbine or the pump. In practice, only the pump shaft is provided with a coupling, as the pump has much more friction loss than the turbine (the pump is typically multistage and the turbine is single-stage). The common shaft of the three machines may be mounted either horizontally or vertically. With a vertical shaft, the electric machine is at the top, the turbine in the middle and the pump at the bottom. This is in view of the priming of the pump and its larger sensitivity to cavitation. With a combined motor-generator and a combined pump-turbine, two machines are sufficient for the pumped storage plant. The main advantage is then saving of investment cost (25–40% on machines and 20–30% on the whole plant). The design of a rotor that can be efficient both for a turbine and for a pump is not obvious, however. The discussion of bulb turbines already revealed that an axial hydraulic machine may function both as a turbine and as a pump. The same applies, in principle, to a radial machine. Figure 9.22 renders optimal shapes for turbine and pump rotors. The differences are caused by the different slip effect and by the limitation of the deceleration in the pump rotor. A rotor serving both purposes must be a compromise between both shapes and be relatively close to the optimal pump rotor shape. Figure 9.22 shows the combined machine. When functioning as a pump, the suction eye resembles the outlet side of a turbine. There are fewer

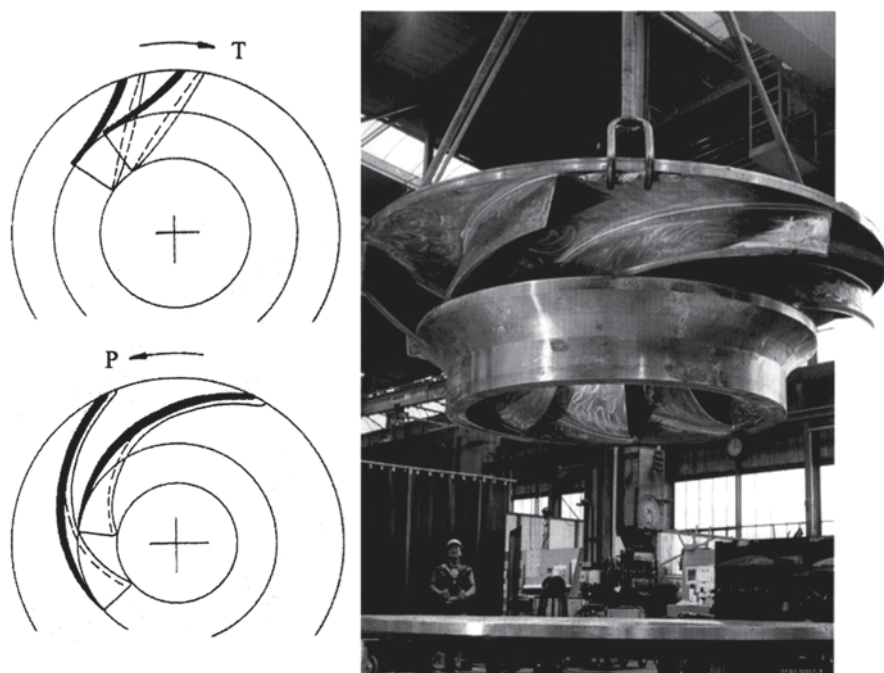


Fig. 9.22 Pump-turbine; *left*: optimal individual pump and turbine shapes; *right*: combined pump-turbine rotor. (Courtesy ANDRITZ HYDRO)

blades than would be typical with a Francis turbine. The following disadvantages of a two-machine plant may be mentioned. Pump and turbine efficiency are lower than with a three-machine plant. Transition from pump to turbine operation or vice versa requires inverting the sense of rotation, causing an interruption of the operation. Due to the slip effect, optimum pump operation requires a higher rotational speed than optimum turbine operation. This is traditionally achieved by pole change in the motor-generator. In modern plants, an asynchronous machine with variable speed is often applied. This is a so-called doubly fed machine with a wound rotor connected to the grid through a frequency converter (see next chapter on wind turbines). Variable rotational speed also improves the efficiency at a variable level difference between the reservoirs. This increases the pump-turbine cycle efficiency to about 80 %, where without variable speed it is around 75 %.

9.7 Exercises

9.7.1. The Pelton turbine rotor, shown in Fig. 9.8, is from the San Carlos hydraulic plant in Colombia. The features are: head 587 m, power per turbine 175 MW, rotational speed 300 rpm, (outer) rotor diameter 4100 mm, six injectors per rotor. Assess the suitability of these features, given the overall efficiency $\eta=91\%$.

A: The diameter corresponding to the optimal speed ratio is 3.18 m, being 77.5 % of the outer diameter. This seems good. Specific speed per injector is 0.11.

9.7.2. Calculate the internal efficiency of the Francis turbines of which the velocity triangles are sketched in Fig. 9.11. Take as loss coefficient for the diffuser $\xi_d=0.25$ and determine the loss coefficient of the distributor and the rotor from Soderberg's formula for aspect ratio 4: $\xi = 0.045(1 + (\delta^\circ / 90)^2)$, with δ° the flow turning in degrees. Study the distribution of the losses, especially the value of rotor losses compared to diffuser losses. Compare efficiency values to those rendered in Fig. 9.13.

A: Diffuser losses are dominant at a low degree of reaction (low specific speed). With a high degree of reaction (high specific speed), rotor losses exceed diffuser losses (remarkable!). Calculated efficiency corresponds to Fig. 9.13 for specific speed above two. Calculations overestimate the efficiency at low specific speed. Friction losses in stator and rotor are underestimated by taking the aspect ratio equal to four because of the narrow distributor and rotor channels. Results strongly improve by taking the correct aspect ratio into account, according to formula 6.14 in Chap. 6.

9.7.3. Argue, by extrapolating the kinematic features rendered in Fig. 9.11, that a Francis turbine with $R=0.50$ is possible. Note that this requires a small ratio of the outlet diameter to the inlet diameter. Draw the velocity triangles.

9.7.4. Argue, starting from the velocity triangles rendered for the Kaplan turbine in Fig. 9.11, how efficiency evolves when the flow coefficient ($\phi = v_{2a} / u_1$) increases. Velocity triangles are sketched for $\phi=0.30$. Reason for $\phi=0.30$, $\phi=0.40$, $\phi=0.50$. Calculate loss coefficients with Soderberg's formula.

A: Efficiency decreases with increasing flow coefficient.

9.7.5. Calculate that the lift force part in the rotor work amounts to 15% for the Francis turbine with $R=0.75$, of which the velocity triangles are represented in Fig. 9.11. Determine the diameter ratio (d_2/d_1) with a 50% lift force part. Note that the diameter ratio strongly increases and that rotor flow turning increases.

A: The diameter ratio is 0.87.

9.7.6. Argue that for the Francis turbine with $R=0.65$, of which the velocity triangles are represented in Fig. 9.11, very low incidence is generated when the flow rate is halved by closing the stator vanes. Assume that the internal efficiency is unaffected, so that the rotor work remains the same. Remark the strong post-swirl, which causes an efficiency drop. Does this efficiency drop increase or decrease the incidence at the rotor inlet? How is the incidence affected if the degree of reaction is lowered to $R=0.55$?

A: The incidence is very low. The incidence increases by the efficiency drop. A lower degree of reaction implies lower incidence.

9.7.7. Argue that for the Kaplan turbine with $R=0.85$, of which the velocity triangles are represented in Fig. 9.11, very low incidence is generated when flow rate is halved by closing the rotor blades. Assume that the internal efficiency is unaffected, so that the rotor work remains the same. Note the strong post-swirl decreasing the actual efficiency. Does this efficiency drop increase or decrease the incidence at the rotor inlet? How is the incidence affected, if the degree of reaction increases to $R=0.90$?

A: The incidence is very low. The incidence increases by the efficiency drop. A higher degree of reaction implies lower incidence.

9.7.8. The Francis turbine rotor, represented in Fig. 9.16, is from the Karakaya power plant in Turkey. Features are $H=156.7$ m, $n=150$ rpm, $P_e=340$ MW, $d_1=5400$ mm, $b_1=1200$ mm. Assess the suitability of the shape rendered in Fig. 9.16. The overall efficiency $\eta=93.5\%$.

A: The calculated specific speed is about 1. The ratio of width to diameter corresponds to Fig. 9.12.

9.7.9. The Kaplan turbine rotor, represented in Fig. 9.17, is from the Jebba power plant in Nigeria. Features are $H=29.3$ m, $n=93.75$ rpm, $P_e=102.7$ MW, $d_{outer}=7100$ mm. Assess the suitability of the shape rendered in Fig. 9.17. The overall efficiency $\eta=92\%$.

A: The calculated specific speed is 2.75.

9.7.10. Argue that, with a reversible Francis type pump-turbine, as rendered in Fig. 9.22, the rotational speed in pump operation must be larger than in turbine operation for good efficiency in both modes, because of the slip effect. Reason with $\beta_1=\beta_2=60^\circ$. Estimate the rotational speed ratio for a rotor with six blades and determination of the slip with Wiesner's formula (Chap. 3 formula 3.21).

9.7.11. The internal efficiency of the Girard turbine studied in Exercise 6.10.7 of Chap. 6 is only about 58%. The main reason is the quite large kinetic energy at the rotor outlet. The efficiency may be improved by mounting the rotor in a cylindrical tube and adding a bent diffuser in the style of Fig. 9.18. Due to suction by the downward head and the pressure recovery in the diffuser, a pressure drop is then

created over the rotor. Proper functioning thus requires mounting a sealing between the shroud of the rotor and the cylindrical tube.

Analyse the transformed machine with an unaltered stator. This means that the pressure at the outlet of the stator (or inlet of the rotor) remains atmospheric pressure and that the outlet velocity of the stator does not change. Assume a pressure recovery coefficient of the diffuser equal to 0.60. Consider again the operating point with exact axial outlet of the rotor.

- Determine the expression for the pressure at the outlet of the rotor (= inlet of the diffuser). Due to the suction by the downward head and the pressure recovery in the diffuser, this pressure is lower than atmospheric pressure. The pressure difference may be expressed in energy measure by $(p_a - p_2)/\rho$. Calculate this value.
- Determine the blade speed such that the absolute velocity at outlet of the rotor is in the axial direction. This computation requires iteration for the loss coefficient of the rotor. Determine the loss coefficient with Soderberg's formula (Eq. 6.14 in Chap. 6) with aspect ratio equal to 1. A starting value may be determined from a computation ignoring rotor loss. For the pressure difference over the rotor, the height difference of 0.30 m between inlet and outlet of the rotor has to be taken into account.
- Determine the rotor work and the internal efficiency. The head supplied to the machine is still 3.50 m. Observe the much improved efficiency.
- Split the rotor work into the action and reaction parts. Determine the degree of reaction. Observe that it is now much higher than with the Girard turbine.
- Determine the speed ratio. Calculate the spouting velocity from the supplied head of 3.50 m.
- Make the balance of the rotor work, the losses in stator, rotor and diffuser. The sum of the energy terms should be equal to the supplied mechanical energy. Observe that, with respect to the Girard turbine, the rotor loss has increased but that the diffuser loss is much lower than the sum of the losses due to outlet kinetic energy and downward head.

$$\mathbf{A:} \quad v_{1a} = 3.575 \text{ m/s}, \quad v_{1u} = 6.191 \text{ m/s}, \quad u = 4.065 \text{ m/s}, \quad \Delta W = 25.168 \text{ J/kg}, \\ \eta_i = 0.733, \quad R = 0.239, \quad \lambda = 0.491.$$

9.7.12. Results of the previous exercise are that the efficiency improves much by adding the diffuser and that the speed ratio increases due to the increased degree of reaction. The speed ratio may be increased further by opening the stator vanes. Analyse the effect of opening the vanes from $\alpha_1 = 60^\circ$ to $\alpha_1 = 45^\circ$ and $\alpha_1 = 30^\circ$. Keep the axial velocity. The consequence is that the flow rate is unchanged.

- Determine axial and tangential components of the absolute velocity at the outlet of the stator vanes.
- Determine the expression for the pressure at the outlet of the stator. This pressure is higher than atmospheric pressure. The pressure difference may be expressed in energy measure by $(p_1 - p_a)/\rho$. Calculate this value.

- c. Repeat the steps (a) to (e) of the previous exercise. Observe that the efficiency increases by opening the stator vanes to $\alpha_I = 45^\circ$, but that it decreases with respect to this value by further opening to $\alpha_I = 30^\circ$. This shows that there is an optimum stator vane angle.

$$\mathbf{A}: v_{Ia} = 3.575 \text{ m/s}, \quad v_{Iu} = 3.575 \text{ m/s}, \quad u = 7.405 \text{ m/s}, \Delta W = 26.430 \text{ J/kg}, \\ \eta_i = 0.770, \quad R = 0.758, \quad \lambda = 0.892.$$

$$\mathbf{A}: v_{Ia} = 3.575 \text{ m/s}, \quad v_{Iu} = 2.064 \text{ m/s}, \quad u = 11.322 \text{ m/s}, \Delta W = 23.369 \text{ J/kg}, \\ \eta_i = 0.681, \quad R = 0.909, \quad \lambda = 1.366.$$

References

1. Dietzel F (1980) Turbinen, Pumpen und Verdichter. Vogel Verlag, ISBN 3-8023-0130-7
2. Dixon SL, Hall CA (2014) Fluid mechanics and thermodynamics of turbomachinery, 7th edn. Elsevier, ISBN 978-0-12-415954-9
3. Vivier L (1966) Turbines hydrauliques et leur régulation. Albin Michel, Paris, no ISBN. Rather old book, but still relevant for theory, application and design of hydraulic turbines

Chapter 10

Wind Turbines

Abstract In this chapter, we discuss the different types of wind turbines and the basic technical aspects of large wind turbines for electricity generation. We analyse the performance of wind turbines and discuss their adaptation to a wind regime.

10.1 Wind Energy

Wind is air circulation in the terrestrial atmosphere as a consequence of irregular warming by the sun. Wind energy systems use the kinetic energy of the wind. We generally speak of a Wind Energy Conversion System (WECS). Mostly, a system for electricity generation encompasses a wind turbine rotor, a gearbox, a generator and a tower. The term Wind Turbine (WT) is commonly used to name the whole.

A particular feature of wind energy is its very diffuse character. The yearly average wind speed at 50 m height along the West European coast between Brittany and Denmark is about 7 m/s (about 8.5 m/s at 100 m height). Optimum energy yield is typically obtained by designing the system such that maximum power on the generator (called rated power) is reached at a wind speed (called rated wind speed) about 50 % higher than the yearly average speed (see Sect. 10.4: wind regime). The energy flux of the undisturbed wind through a plane surface (area A) perpendicular to the wind direction is (mass flow rate \times kinetic energy):

$$P_0 = \rho A v \frac{1}{2} v^2 = \frac{1}{2} \rho v^3 A. \quad (10.1)$$

To $\rho = 1.2 \text{ kg/m}^3$ and $v = 12.5 \text{ m/s}$ corresponds about 1200 W/m^2 . A wind energy system converts nearly 45 % of that (see Sect. 10.3: performance). This results in a net power density of about 500 W/m^2 . A rated power of 1 MW requires a through-flow surface of about 2000 m^2 , corresponding to a circle with a diameter of about 50 m. This demonstrates that large power wind energy conversion systems require great dimensions.

10.2 Types of Wind Energy Conversion Systems

10.2.1 Drag Machines

There is a difference between machines where power results from lift (perpendicular to the relative velocity) or from drag (in the direction of the relative velocity). A simple example of a drag machine is the cup anemometer (Fig. 10.1). The principle is that the cup whose concave side is facing the wind is subjected to a greater force than the cup that faces the wind with its convex side. There are many forms of such machines. Rather common is the Savonius rotor (Fig. 10.1) (Savonius 1924).

Drag machines have three major disadvantages. First, the average blade speed cannot exceed the wind speed. That results in low rotational speeds, except for very small machines. This is very disadvantageous for many applications. Further, the efficiency is low. Efficiency is expressed by a power coefficient:

$$C_p = \frac{P}{\frac{1}{2}\rho v_0^3 A}, \quad (10.2)$$

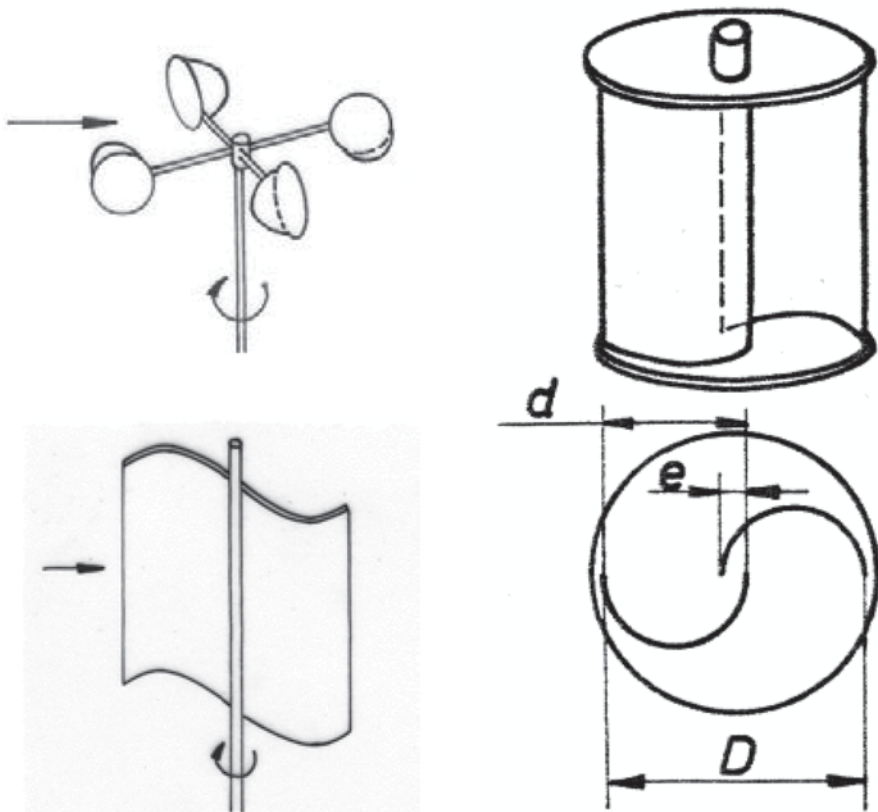


Fig. 10.1 Drag machines; *top left*: cup anemometer; *right*: Savonius rotor

where P is the power produced by the machine, v_0 the undisturbed wind speed and A is the through-flow area perpendicular to the wind direction. The through-flow area is the area covered by the rotating parts of the machine. As already mentioned, and as we will analyse further, the power coefficient of a modern lift-based wind energy conversion system amounts to about 0.45. For a drag machine this is much lower, typically around 0.20, due to large forces contrary to the sense of rotation and thus dissipating energy. The third disadvantage with drag machines is their large solidity. The term solidity means the ratio of the blade surface to the through-flow area. With drag machines, solidity typically exceeds unity. Drag machines are only rarely applied and only for low-power applications. An example is the Savonius rotor on the roof of vehicles to drive a fan in the interior.

10.2.2 High-Speed Horizontal-Axis Turbines

The most common type is an axial turbine with force generation by lift. The rotor is sketched in Fig. 10.2. The axis is approximately horizontal with turbines of this kind, hence their name. Wind velocity at the place of a rotor blade (v) is reduced compared to the free wind velocity (v_0). The wind velocity also deviates somewhat from the original direction (not rendered in Fig. 10.2). From the velocity triangle follows the origin of lift (L) with a component in the sense of rotation. With such machines, blade speed (u) may be much higher than wind speed. Tip speed ratio is commonly defined by

$$\lambda = u_r / v_0, \quad (10.3)$$

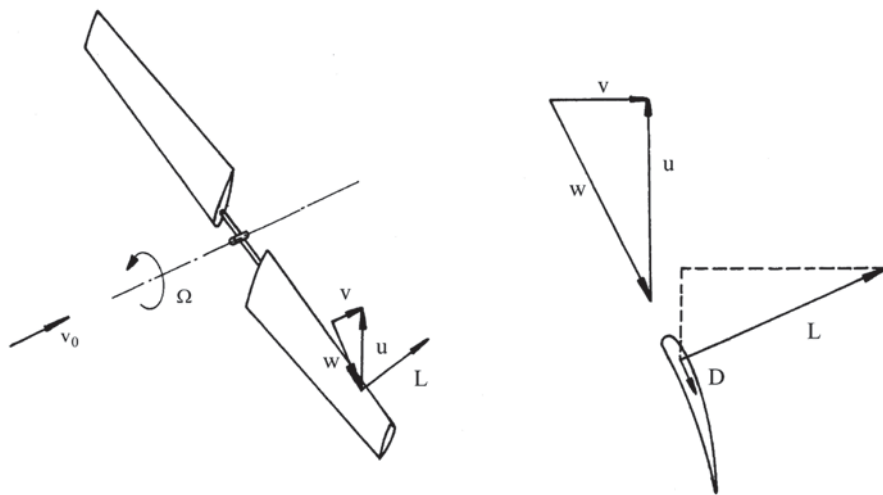


Fig. 10.2 Working principle of a horizontal-axis wind turbine (HAWT)

Fig. 10.3 Horizontal-axis wind turbine: E126. (Courtesy Enercon)



where u_T is the blade speed at the rotor tip. A typical value with optimum operation is about 6. The triangle drawn is thus representative for a section in the inner part of the rotor. With an axial machine, the rotor blade drag force causes energy dissipation. This drag is small compared to the lift.

Figure 10.3 represents a front view of a three-blade horizontal-axis wind turbine for electricity generation. The rotor diameter is 127 m. It is one of the biggest machines existing nowadays (manufacturer Enercon). The rated power is 7.58 MW for locations with a high average wind speed (10 m/s at hub height).

Table 10.1 Dimensions of horizontal-axis wind turbines

500 kW	$D=39$ m	2000 kW	$D=72$ m
750 kW	$D=45$ m	2500 kW	$D=80$ m
1000 kW	$D=52$ m	4500 kW	$D=112$ m
1500 kW	$D=63$ m	6000 kW	$D=125$ m

Most turbines have three rotor blades. At present (2014), machines of the 3 MW order are standard. All manufacturers are developing machines of the 5–6 MW order and larger. There is a strong tendency to even larger power. Larger machines are principally cheaper per unit of power. Further, at greater hub height, the average wind speed is higher. The current dimensions are listed in Table 10.1 (for an average wind speed of 7 m/s at 50 m height). For off-shore or coastal area installation, the hub height approximately equals the rotor diameter (higher wind speed near the surface than for an inland location). For inland locations, the hub height is larger. Mostly, machines are installed in a group, called a wind farm. Prevention of too strong mutual interference requires a spacing of about 5 diameters. When arranged in a square matrix (more advantageous arrangements are possible), a wind turbine occupies a $25D^2$ ground area. This yields 13.1 MW/km² with 500 kW machines and 14.8 MW/km² with 1000 kW machines. The more advantageous value with larger machines is due to the greater hub height and thus to a higher average wind speed. Until a decade ago, some large turbines had two blades because of cost. Two blades with a greater average chord cost less than three blades with a smaller average chord. At present, large turbines have three blades. A three-blade machine turns more steadily than a two-blade one. Fluctuation of power as a result of a greater wind force on an upper blade and a lower wind force on a lower blade is much smaller with a three-blade rotor. Larger dimensions require better power constancy.

10.2.3 Technical Aspects of Horizontal-Axis Wind Turbines for Electricity Generation

Rotor blades are manufactured of glass fibre reinforced polyester or epoxy (epoxy is much lighter than polyester). Carbon fibre is applied in critical areas. Blade profiles vary strongly over the span. At the tip, only a low lift coefficient is required because of the high relative velocity, but a very low drag coefficient is important. The profile required is similar to that of an aircraft wing, i.e. a laminar profile, but sensitivity for contaminants should be low. Toward the hub, a very high lift coefficient is required and a low drag coefficient is less important, i.e. a turbulent profile. The profiles near the hub are no standard NACA turbulent profiles, but profiles with an increased lift coefficient by means of aft-loading (significant pressure difference in the rear part; see Chap. 2, Fig. 2.8). Along the whole span, profiles with a great

relative thickness are necessary, typically 17% at the tip to 35% at the hub, because of strength. The blades are rigidly fixed to the hub, but have a high bending flexibility. With two-blade turbines, articulated rotors are typically applied. The rotor hinges then around an axis perpendicular to the turbine shaft. This enables absorption of the force difference due to the higher wind velocity on the upper blade and the lower wind velocity on the lower one. The rotor has a small cone angle in order to reduce the bending moment on the hub. The centrifugal force moment thus compensates the blade force moment. Sufficient clearance from the tower requires a tilt angle of the shaft (small slope compared to the horizontal direction).

The rotor shaft is borne in a nacelle housing the gearbox (if present) and the generator. The rotational speed depends on the turbine size and is about 25 rpm with a 1000 kW turbine and about 18 rpm with a 2500 kW turbine. The tip speed varies from about 60 to 75 m/s with 40–80 m diameter rotors. The rotor is mostly set upwind of the tower. Downwind types hardly ever occur anymore. A downwind rotor follows spontaneously changes in wind direction, but a big disadvantage is that the rotor blades turn through the wake of the tower. This causes efficiency loss and serious fatigue load. Upwind rotors are preferred therefore. They require an active yaw mechanism. The nacelle is on top of the tower, mostly on a gliding ring on shoes with synthetic covering and with an internal gear, driven by a yaw motor and controlled by the wind direction detected with a vane on the nacelle. Computer control is applied, as sudden changes of wind direction shall not be reacted to immediately. A brake is applied to spare the yaw mechanism. The tower is usually a steel tube tower. Large towers may have a concrete lower part. Small systems sometimes use a lattice tower.

Figure 10.4 represents the section of a nacelle of a turbine with blade pitch control. It is a two-blade turbine of 500 kW that is no longer manufactured. Its parts are: hub cover, pitch control mechanism (the pitch angle is the angle of the blade chord with the axial direction on a reference radius), gearbox, generator, mechanical brake, gliding ring for yaw movement, yaw motor.

At wind speed above the rated value, the available wind power exceeds the maximum generator power. The power possibly yielded by the rotor must then be reduced. There are two common systems to achieve this: *pitch control* and *stall control*. Because of the lower blade speed near the hub (see velocity triangle in Fig. 10.2), the relative velocity is lower as well. Equal energy capture in all streamtubes requires a constant product of the blade speed and the tangential component of the lift. Relative velocity is high at the tip, so that generation of the required lift needs only a small chord and a small angle of attack. A large chord and a great angle of attack are required at the hub. Thus the blade is close to the tangential direction near the tip, but at the hub it is much nearer to the axial direction. Due to the variation of the angle of attack with the radius, the torsion of the blade is lower than the angle variation of the relative velocity. Blade torsion typically amounts to about 10° . As the angle of attack is already very high at the hub in rated conditions, a small increase of the wind velocity causes separation at an unaltered blade

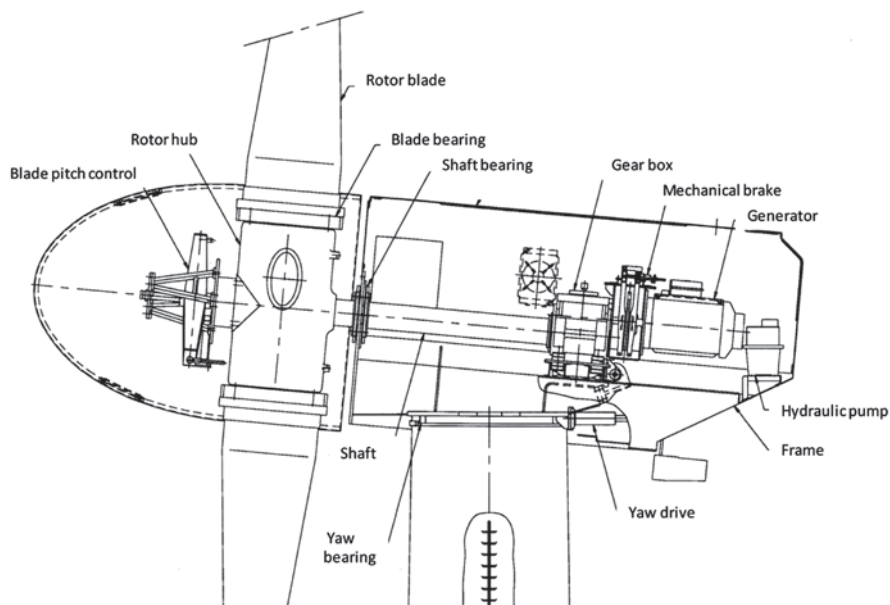


Fig. 10.4 Parts of a HAWT nacelle. (Courtesy Vestas)

chord angle and blade speed. As wind velocity increases, the separation zone grows towards the tip. Thus, there is a spontaneous power limitation with increasing wind speed at a constant rotational speed. A blade may be designed appropriately, so that the power is approximately limited to the rated power with wind speeds exceeding the rated value. This is called *stall control*. With *pitch control*, the blade is turned towards the axial direction at higher wind velocities, causing a decrease of the angle of attack over the whole span. Pitch control requires rotor blade mounting to the hub by means of a bearing. A lever mechanism is incorporated into the turning hub or the individual blades are provided with pitch motors. The advantage with pitch control is that the rotor may be made powerless by positioning the blades aligned with the wind direction. This is called feathering the blades. Feathering is applied in stormy weather. The wind turbine is switched off from a certain wind speed (typically 25 m/s, see Sect. 10.4) by feathering the rotor. In feathered pitch position at standstill, rotor blade stresses are minimal. With stall control, the rotor is stopped in stormy weather by means of a mechanical brake. Mechanical stress on the rotor blades is then much higher than on a feathered rotor, but no strong problem arises with wind turbines up to the 1 MW order, in a moderate climate. Larger wind turbines are provided with pitch control or with *active stall control*. Stall control as described up to now is called *passive stall control*. There is also an active stall control system. Power limitation at higher wind speeds is achieved by

stall, but the blade angle is adjusted such that the power gets exactly limited to the rated power. This system is applied with wind turbines turning at fixed rotational speed (see further: fixed and variable rotational speed) of the 1–2 MW order. In this power range, an exactly limited generator power is important, just as feathering in stormy weather is important too. Why active stall control instead of pitch control is preferred with certain turbines is explained in the further discussion of fixed and variable rotational speed.

For the case that connection to the grid would be interrupted, it shall be possible to stop the turbine at full speed. Machines with pitch control and active stall control are provided with a mechanical brake on the fast shaft of the gearbox (more advantageous than on the slow shaft). This brake also serves as a parking brake, i.e. to keep the rotor in standstill with very low wind speed. Additionally, pitch control is applied to decrease rotor power. Pitch control is much slower than the brake however. Turbines with passive stall control may be provided with a second brake on the slow shaft. With passive stall control there is always an aerodynamic brake as well. This functions by setting the rotor blade tip perpendicularly to the blade speed, reducing the power to a low value. In all cases, there is the possibility to turn the rotor 90° out of the wind, as an ultimate measure, by means of the yaw mechanism. At very low wind velocities (lower than the cut-in speed, see Sect. 10.4), the rotor is immobilised by the brake. A turbine with stall control is switched on by releasing the brake. The rotor then starts spontaneously. This is possible if the design value of the tip speed ratio is not too large. No problem arises with values up to $\lambda=6$ at optimum rotor operation, corresponding to $\lambda=4.5$ at rated wind velocity (see paragraph 10.4). Rotors with higher design tip speed are normally not self-starting because the blades are mounted more tangentially. A turbine with pitch control does not start when releasing the brake. The blades must be turned away from the feathered position.

With the simplest systems, the generator is an asynchronous machine. Pole changing is very often applied, allowing the generator to turn at lower speed with low wind velocities. With a fixed rotational speed, the optimum power coefficient is only reached at one single wind speed. In order to optimise the energy yield, this wind speed shall be about 75 % of the wind speed for rated power (see Sect. 10.4: wind regime). At a fixed rotor blade pitch, as with stall control (pitch always fixed with passive stall control and with power lower than rated with active stall control), the yield is lower than with pitch control where the rotational speed may be kept optimal through a certain wind speed range (see Sect. 10.4: wind regime). Pitch control cannot easily be applied with a fixed speed generator. The wind speed always has fluctuations, growing at higher average wind speed. Pitch control cannot be realised so fast that it neutralises gust effects on torque and power. Many turbine parts are thus subjected to fatigue and power may fluctuate strongly. The gust problem is obviously most important at high wind speed. Stall controlled turbines (both actively and passively) are much more tolerant to gusts, that partly are absorbed by increase and decrease of the rotor stall area. With higher power, a variable rotational speed is more advantageous to improve the energy yield and to attenuate the fatigue load on the rotor blades and on the gearbox (if present). Turbines above about 2 MW are

provided with variable rotational speed and pitch control. Variable rotational speed turbines partly absorb gusts by the instantaneous variation of the rotational speed as a response to the variable rotor force. Rotor inertia is thus used to buffer gusts.

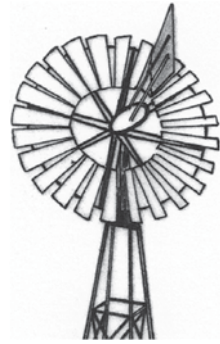
Three generator concepts are used. The first system is a squirrel cage asynchronous generator with fixed rotational speed (except for slip variation). A main electrical disadvantage with asynchronous generators is their inability to generate reactive power. Capacitors are applied to compensate reactive power consumption. The second system is an asynchronous generator with a frequency controlled wound rotor, connected to the grid (so-called doubly fed machine). Due to the frequency control, the rotor magnetic field rotates with adjustable speed. The machine behaves like a synchronous generator with a rotational speed governed by the frequency difference between the stator and the rotor. A speed range of about $\pm 30\%$ compared to the synchronous speed (i.e. the speed corresponding to the grid frequency) is typical. At a sub-synchronous rotational speed, grid power flows to the rotor. At a super-synchronous rotational speed, rotor power flows to the grid. A $\pm 30\%$ speed change requires a frequency converter power of $\pm 30\%$ of the stator power. The third system is a synchronous generator connected to the grid through a frequency converter, converting the entire power. A typical $\pm 30\%$ speed change is also possible with this type. Both wound rotor generators with electronic excitation and permanent magnet generators are applied. Synchronous generators can have a large number of pole pairs, and thus can turn at low speed so that a gearbox may be unnecessary (direct drive). The nacelle must then be very wide. Large wind turbines may be made with direct drive (e.g. Enercon E112: diameter 112 m, 4.5 MW, speed range 8–13 rpm, synchronous generator with a large number of poles), applying a one-stage planetary gearbox and a permanent magnet synchronous generator (e.g. Multibrid M5000: diameter 116 m, speed range 5.9–14.8 rpm, transmission 1:9.92, synchronous generator with 28 poles) or a three-stage gearbox with an asynchronous generator with rotor frequency control (e.g. REpower 5M: diameter 126 m, speed range 6.9–12.1 rpm, transmission 1:97, six-pole asynchronous generator). The direct drive system needs a wide nacelle (the diameter of the generator of the E126 of Fig. 10.3 is 12 m). The system with the three-stage gearbox requires a long nacelle (Fig. 10.4). The nacelle of the mixed concept with a one-stage gearbox and a multi-pole generator is the most compact one.

Much simpler turbines are used in small-scale applications (200 W–10 kW). Very small turbines have high rotational speed, enabling a direct coupling to the generator. These are mostly generators with permanent magnets. Small turbines are not computer-controlled. They are normally power-limited by turning out of the wind (see next section).

10.2.4 Low-Speed Horizontal-Axis Wind Turbines

For pumping, often a type as sketched in Fig. 10.5 is used. The working principle is identical to that of the previously discussed type, but the solidity is much larger. The

Fig. 10.5 Low-speed horizontal-axis wind turbine for pump drive



solidity of a horizontal-axis wind turbine for power generation is in the 0.06–0.08 order. The solidity of the machine represented in Fig. 10.5 is about 0.5. With a greater solidity, the maximum power extraction from the wind is reached at a lower blade speed and the power coefficient is lower (see Sect. 10.3: performance). A high torque is obtained, as required for pump driving. Turbines of this type are applied on locations where electric power supply is difficult, as on meadows and fields. Dimensions are limited. The rotor is kept in the wind by a vane. It is turned partially out of the wind at high wind speed. This may be realised by mounting the rotor onto a frame with a hinge and a spring. The rotor is turned either upwards or sideways by the axial force on the rotor or by the force on a plate perpendicular to the wind (systems are not represented on Fig. 10.5).

10.2.5 Vertical-Axis Wind Turbines

Figure 10.6 represents a type with straight prismatic blades and a vertical shaft. A horizontal section is shown, with one blade in four positions. In the upwind and

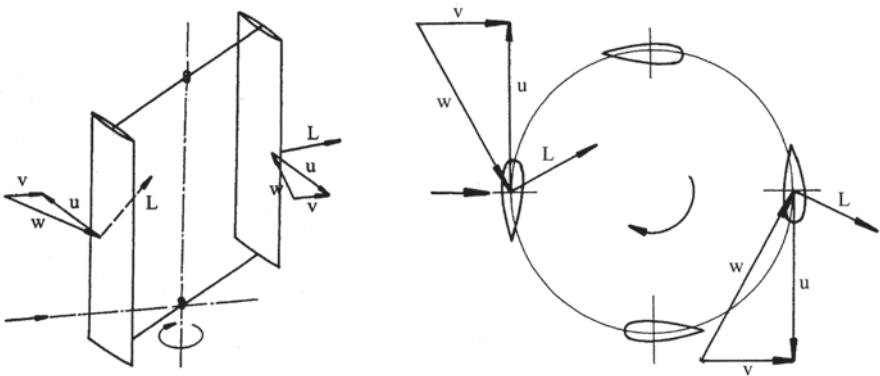


Fig. 10.6 Vertical-axis wind turbine with straight blades (VAWT)

downwind positions, the velocity triangles imply a lift force with a tangential component in the sense of the blade speed. No lift is generated in the other two positions. The force on a rotor blade changes cyclically with this type. At least three rotor blades are required to achieve a constant torque. Vertical-axis wind turbines have as main advantages that they are principally insensitive to wind direction and that the load may be coupled at ground level. A major disadvantage is that the turbine is not self-starting when the blade position is fixed. For that reason, sometimes, a vertical-axis wind turbine is combined with a Savonius rotor. Self-start may be achieved with prismatic blades by mounting these blades on pivots and by controlling their angle through rods. A simple mechanism is joining the rods in a point downstream of the shaft (Fig. 10.7). This point is set by a vane. The centrifugal force causes large bending moments in vertical-axis wind turbines with straight blades. Turbine dimensions must be limited, therefore. The maximum blade length is about 15 m. This limitation may be overcome by bowing the blades into a troposkin shape ('troposkin' is Greek for rotating rope). With this shape, only traction force occurs as a result of centrifugal force and gravity. This kind of turbine is commonly named a Darrieus turbine (Darrieus 1931). A two-blade example is sketched in Fig. 10.7. Darrieus turbines are not self-starting. The largest turbine ever built had a height of 96 m, a diameter of 64 m and yielded 4 MW.

The fluctuating lift with vertical-axis wind turbines impairs the efficiency compared to that of horizontal-axis wind turbines, as there is drag, even with low lift. Further, straight-blade turbines always need drag generating struts. Upper and lower areas do not perform well with a troposkin shape. Due to the low blade

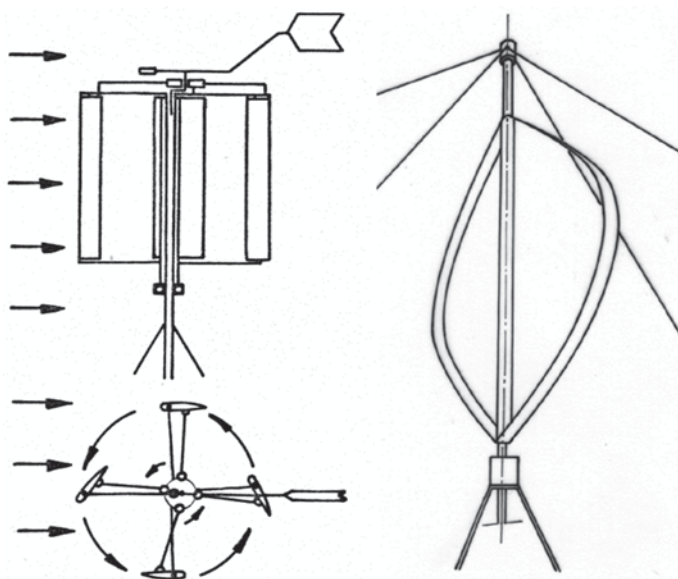


Fig. 10.7 Vertical-axis wind turbines; *left*: control mechanism with straight blades; *right*: troposkin shape

speed, these blade parts cyclically enter in stall. The velocity triangles in Fig. 10.6 demonstrate that, at maximum lift ($\alpha \approx 12.5^\circ$), the ratio of the blade speed on the equator to the local wind speed is about 4.5. With the deceleration of the wind at the turbine, the speed ratio based on the free wind speed is about 3. VAWTs thus typically run much slower than HAWTs. Power limitation with wind speeds exceeding the rated value cannot be realised adequately with a VAWT. There is a spontaneous mechanism of progressive stall with the troposkin shape, but it is impossible to limit the power to an approximate constant value as with a stall-controlled HAWT. A straight-blade VAWT cannot be limited in power by simple means. Machines with adjustable blade slope have been proposed, enabling decrease of the through-flow area, but these are mechanically vulnerable. Due to the lower power coefficient and the intrinsic difficulty of power limitation, VAWT types are only applied for small power.

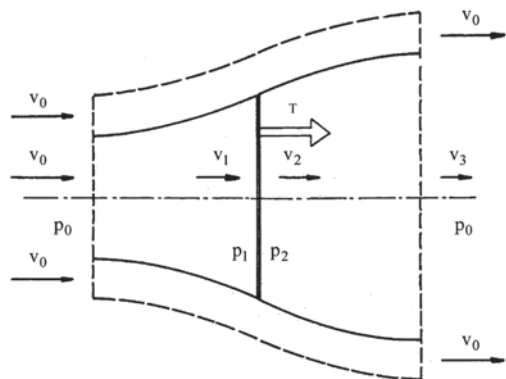
10.3 Wind Turbine Performance Analysis

10.3.1 Momentum Analysis (Single Streamtube Analysis)

The simplest flow model represents the rotor of a horizontal-axis wind turbine as a disc with uniform distribution of flow parameters just upstream and just downstream of the rotor. This is called an actuator disc. A streamtube though the rotor is considered with flow parameters which only change in the direction perpendicular to the disc, so that the flow is rendered one-dimensionally. Swirl behind the turbine and losses in the flow are neglected. Figure 10.8 sketches the flow through the turbine.

Far upstream of the turbine, wind velocity is v_0 , and pressure is p_0 . The flow is retarded by the disc, so that the velocity v_1 just upstream of the rotor is lower than v_0 and consequently pressure p_1 is higher than p_0 . Just downstream of the turbine, velocity v_2 equals velocity v_1 (continuity), but pressure p_2 is lower than p_1 . Thus, the

Fig. 10.8 One-dimensional streamtube through a horizontal-axis wind turbine



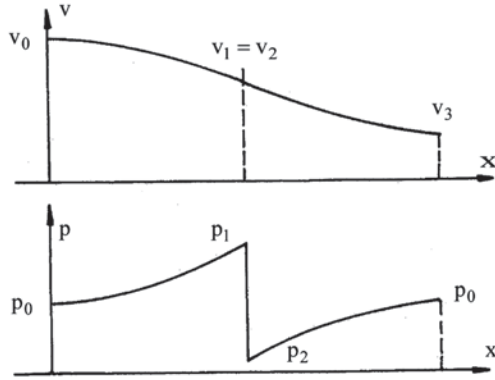


Fig. 10.9 Velocity and pressure variation with a one-dimensional flow representation

pressure difference $p_1 - p_2$ expresses the energy extraction from the flow. Downstream of the turbine, pressure increases again to p_0 , which decreases the velocity to v_3 . The evolution of velocity and pressure are represented in Fig. 10.9.

The relation between velocity and pressure follows from the work equations upstream and downstream of the disc (work = 0):

$$\frac{p_0}{\rho} + \frac{v_0^2}{2} = \frac{p_1}{\rho} + \frac{v_1^2}{2}, \quad \frac{p_2}{\rho} + \frac{v_2^2}{2} = \frac{p_0}{\rho} + \frac{v_3^2}{2},$$

from which by addition: $\frac{p_2}{\rho} + \frac{v_0^2}{2} = \frac{p_1}{\rho} + \frac{v_3^2}{2}$,

or

$$\frac{p_1 - p_2}{\rho} = \frac{1}{2}(v_0^2 - v_3^2). \quad (10.4)$$

The force on the rotor disc is

$$T = A(p_1 - p_2). \quad (10.5)$$

The momentum balance on the streamtube, with the force $-T$ exerted on the flow, is

$$\dot{m}(v_3 - v_0) = -T, \quad (10.6)$$

where $\dot{m} = \rho v_1 A$ is the mass flow rate through the rotor disc.

When writing (10.6), it is assumed that the resultant force of the pressure distribution on the envelope of the streamtube equals zero. That supposes a symmetrical distribution of velocity and pressure in Fig. 10.9. This assumption may be avoided by applying a second, sufficiently wide, streamtube around the streamtube passing

through the rotor, allowing the assumption that there is atmospheric pressure p_0 on the envelope of the outer tube (Fig. 10.8). There is no work in the second streamtube. As a consequence, the outlet velocity is v_0 . A momentum balance on both streamtubes together results in (10.6), without any further assumptions.

Combination of (10.4), (10.5) and (10.6) results in

$$T = \rho v_1 A (v_0 - v_3) = A (p_1 - p_2) = \frac{1}{2} A \rho (v_0^2 - v_3^2),$$

$$v_1 = \frac{v_0 + v_3}{2}.$$

so that

This means that flow deceleration is symmetric, i.e. as much before as behind the rotor.

The velocity decrease is expressed by an interference factor a , so that

$$v_1 = v_0(1 - a), \quad v_3 = v_0(1 - 2a).$$

Power extracted from the flow is

$$P = \dot{m}(\frac{1}{2}v_0^2 - \frac{1}{2}v_3^2) = \rho A v_1 \frac{1}{2}(v_0^2 - v_3^2).$$

The power coefficient is

$$C_P = \frac{v_1}{v_0} [1 - (\frac{v_3}{v_0})^2] = (1 - a)(4a - 4a^2) = 4a(1 - a)^2. \quad (10.7)$$

The power coefficient reaches a maximum for $a = \frac{1}{3}$, with maximum value

$$C_{P, \max} = \frac{16}{27} = 0.593. \quad (10.8)$$

The obtained maximum value is called the Betz-limit. It represents the approximate upper bound of the power coefficient of a wind turbine. The derivation is well applicable to a horizontal-axis wind turbine, but the result applies, by extension, to any wind energy system, as only momentum and energy relations are used.

The force upon the actuator disc follows from (10.6) in a dimensionless form:

$$C_T = \frac{T}{\frac{1}{2} \rho v_0^2 A} = 2 \frac{v_1}{v_0} (1 - \frac{v_3}{v_0}) = 2(1 - a) 2a.$$

From $a = \frac{1}{3}$ follows:

$$C_T = \frac{8}{9} = 0.889.$$

A completely tight, plane plate, placed perpendicularly to the wind has a drag coefficient of 1.28. So, the working wind turbine takes up an axial force of about 70 % of the force exerted on a tight, plane plate. This puts a very large load on the rotor and the supporting tower.

It subsequently appears with (10.7) that not all energy that passes uninhibitedly through the frontal surface of a wind energy system can be captured. As the flow retards when capturing its kinetic energy, the mass flow passing through the rotor disc decreases. There is thus an optimal retardation, found to be $a = \frac{1}{3}$ according to the preceding derivation.

The preceding theory is generally known as ‘Momentum Theory’ or ‘Rankine-Froude Actuator Disc Theory’ (Rankine 1865; Froude 1889; Betz 1920).

10.3.2 Multiple Streamtube Analysis

The analysis in the preceding section may be refined by considering a series of concentric annular streamtubes with an infinitesimal thickness and by writing the momentum and work relations for each streamtube. With this analysis, the rotation effect behind the rotor may be taken into account. A wind turbine example was already studied in Chap. 2, Exercise 2.5.8. Figure 10.10 represents an infinitesimal streamtube. The figure also renders the velocity triangles immediately upstream and downstream of the rotor disc. At the position of the rotor disc, the axial velocity component is represented by $(1-a)v_0$. There is no tangential velocity component immediately upstream of the rotor. The tangential velocity component immediately downstream of the rotor is represented by $-2bu$.

The pressure variation in the streamtube may be assumed symmetrical. The momentum balance in axial direction stays then the same as in the preceding analysis:

$$dT = dA(p_1 - p_2) = \rho v_0(1-a) dA(v_0 - v_{3a}),$$

with $dA = 2\pi r dr$.

With $v_{3a} = (1-2a)v_0$, it follows that

$$\frac{p_1 - p_2}{\rho} = v_0^2 (1-a) 2a. \quad (10.9)$$

The work equation in the relative system between the positions just upstream and downstream of the rotor is

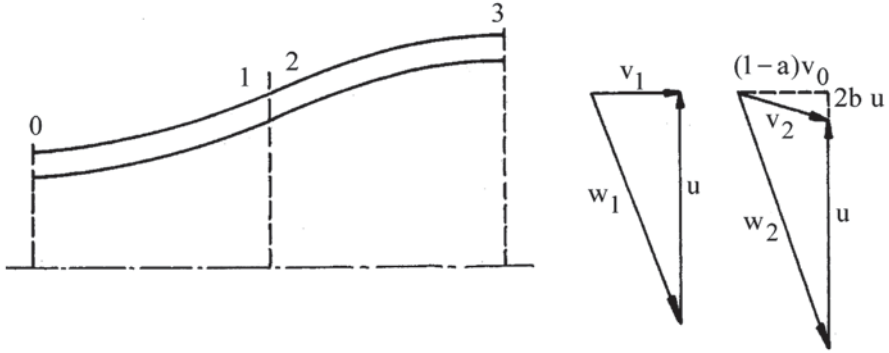


Fig. 10.10 Streamtube with infinitesimal thickness through a horizontal-axis wind turbine

$$\frac{p_1}{\rho} + \frac{v_{1a}^2}{2} + \frac{u^2}{2} = \frac{p_2}{\rho} + \frac{v_{2a}^2}{2} + (1+2b)^2 \frac{u^2}{2},$$

or

$$\frac{p_1 - p_2}{\rho} = 2b(1+b)u^2. \quad (10.10)$$

Combination of (10.9) with (10.10) produces b as a function of a :

$$b(1+b)\lambda_r^2 = a(1-a), \quad (10.11)$$

with λ_r the local speed ratio: $\lambda_r = u / v_0$.

Work (power) gained from the streamtube is given by Euler's formula:

$$dP = \rho dA v_0 (1-a)(2bu^2),$$

meaning with (10.11):

$$dP = \rho dA v_0^3 \frac{2a(1-a)^2}{1+b}. \quad (10.12)$$

Expression (10.12) replaces expression (10.7) on an infinitesimal basis. Expression (10.7) is recovered for $b=0$ (no post-swirl) and $a=\text{constant}$ over the radius.

The power (10.12) may be optimised for each streamtube, giving

$$\frac{(1-a)^2 - 2a(1-a)}{1+b} - \frac{a(1-a)^2}{(1+b)^2} \frac{db}{da} = 0,$$

or

$$\frac{db}{da} = \frac{(1+b)(1-3a)}{a(1-a)}. \quad (10.13)$$

Expressions (10.11) and (10.13) together determine the optimal variation of the factors a and b as functions of λ_r . The solution is (10.11), together with

$$b = \frac{1-3a}{4a-1}.$$

Table 10.2 shows the results. The optimum interference factor a is now smaller than $1/3$ and decreases as λ_r decreases. Interference factor b increases as λ_r decreases.

These factors enable the determination of the power by integrating (10.12). The result depends on $\lambda_T = u_T / v_0$, as shown in Table 10.3, according to Hunt [2]. The resulting value of C_P is smaller as λ_T is smaller. This result shows the influence of the post-swirl. As the design tip speed is lower, swirl behind the rotor is stronger. This impairs the power coefficient by the kinetic energy related to the tangential velocity component. Without taking losses into account, the best turbine is obtained for the highest speed ratio.

10.3.3 Blade Element Analysis

The rotor blade may be designed by calculating the blade element force for each infinitesimal streamtube. Figure 10.11 represents the velocity triangle at the rotor disc, where the tangential interference factor is b . The figure shows the lift and drag forces. The axial and tangential components of the resulting force exerted by the blade elements may be expressed as functions of lift, drag and flow angle ϕ .

The following relations apply:

$$\tan \phi = \frac{(1-a)v_0}{(1+b)u} = \frac{1-a}{(1+b)\lambda_r},$$

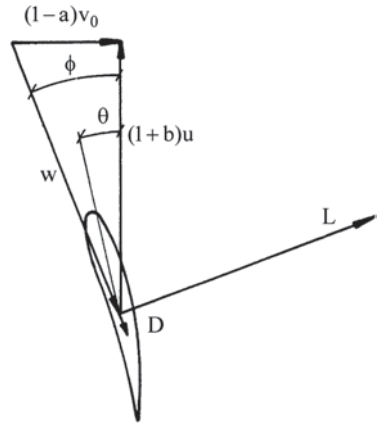
Table 10.2 Interference factors in multiple streamtube analysis

λ_r	a	b
0	0.25	∞
0.157	0.27	2.375
0.374	0.29	0.812
0.753	0.31	0.292
2.630	0.33	0.031
∞	$1/3$	0

Table 10.3 Power as a function of tip speed ratio from multiple streamtube analysis

λ_T	0.5	1	2	5	10
C_P	0.288	0.416	0.512	0.570	0.593

Fig. 10.11 Velocity triangle at the rotor disc



$$\begin{aligned} dX &= dL \cos \phi + dD \sin \phi, & dY &= dL \sin \phi - dD \cos \phi, \\ dL &= \frac{1}{2} \rho w^2 C_L c \, dr, & dD &= \frac{1}{2} \rho w^2 C_D c \, dr. \end{aligned}$$

C_L and C_D are the lift and drag coefficients and c is the local chord. The axial and tangential components of the force exerted are related to momentum changes in the axial and tangential directions. This enables expressions for the interference factors as functions of lift and drag coefficients, flow angle ϕ and local chord c . By way of a simplification, it is mostly assumed that the drag force does not intervene in the momentum relations and the work. The expressions from the preceding Sect. (10.9–10.13) then keep their validity.

With the interference factors follows the local flow velocity v . This may be considered as the sum of the free wind velocity v_0 and an induced velocity v_i . The induced velocity has the direction of the lift, as a result of (10.11). Knowledge of the interference factors, also called induction factors, enables determination of the power with a given rotor geometry, i.e. chord c and pitch angle θ as functions of radius and given relations for C_L and C_D as functions of the angle of attack $\alpha = \phi - \theta$. Average induction factors within the streamtube, as derived in the preceding section, and local induction factors at the place of a blade section shall be distinguished. Their relation is derived from the induction of vortices associated to the lift. The difference between average and local factors becomes particularly important at blade tips. Calculation of that difference is, therefore, commonly called correction for tip losses.

The power gained from the wind is still rendered by integrating (10.12). The net power is calculated by subtracting the power dissipated by the drag. The representation as described here implies by (10.11) and (10.12) that only lift determines the influence of the rotor on the flow and the energy exchange. The drag force is then considered as solely dissipative. As mentioned before, this representation is an approximation (see also Chap. 2, Sect. 2.2.7).

For known relations of C_L and C_D as functions of the angle of attack, the performance of a wind turbine may be optimised. The relevant derivation is similar to that

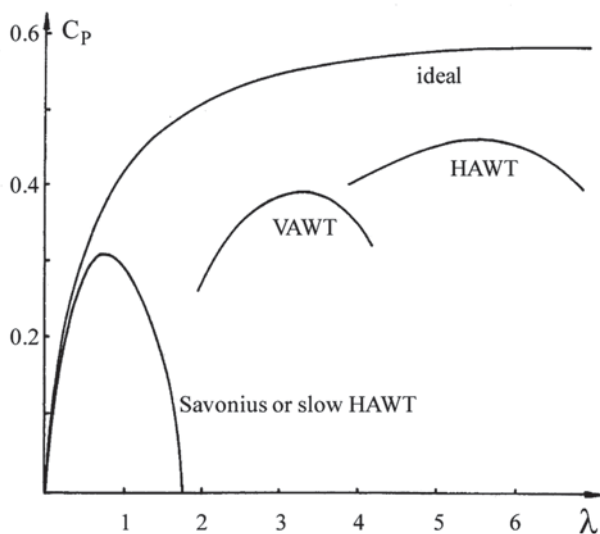


Fig. 10.12 Power coefficient with various wind turbine types. (Adapted to [2])

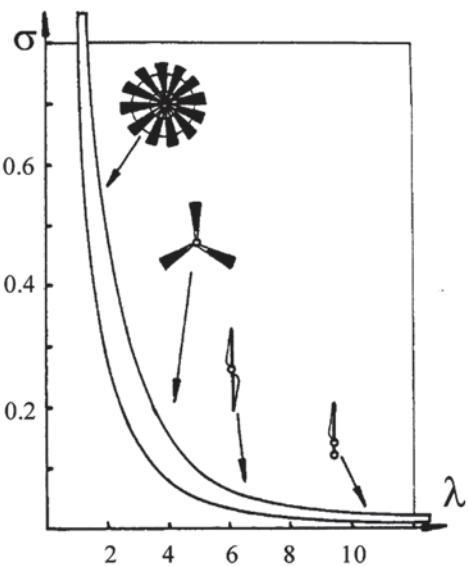
in the preceding section, but the expressions are more complicated and the solution can only be found by means of numerical iteration. We do not discuss this here and refer to Hunt [2] and Freris [1] for a complete derivation. Figure 10.12 represents the result of the optimisation of a HAWT at $\lambda_T = 6$. The resulting C_p is 0.45 (shaft power). The figure also shows the performance of a Darrieus rotor and a Savonius rotor. There are similar analysis techniques, based on multiple streamtubes for vertical-axis wind turbines [2]. The actual performance of a HAWT is not very sensitive to the design tip speed ratio, on condition that it is sufficiently high, i.e. in the $\lambda_T = 6-8$ order. With optimisation for a very high tip speed ratio, e.g. exceeding 10, there is performance loss due to the increasing effect of rotor drag losses.

Figure 10.13 represents the solidity corresponding to the design tip speed ratio. The lower the design tip speed ratio, the higher the torque yielded by the wind turbine is and the larger the corresponding blade surface is.

10.4 Adaptation to a Wind Regime

Figure 10.14 sketches a histogram with 1 m/s velocity classes. It is typical for the wind at 50 m height at a location on the West European seashore. The histogram shows the probability $P(v_i)$ that a certain wind speed occurs. The yearly average wind speed is about 7 m/s. Also shown is a distribution indicated with $P(v_i^3)$, which is the distribution of the energy density (energy flux through a unit surface). The meaning of the distributions is

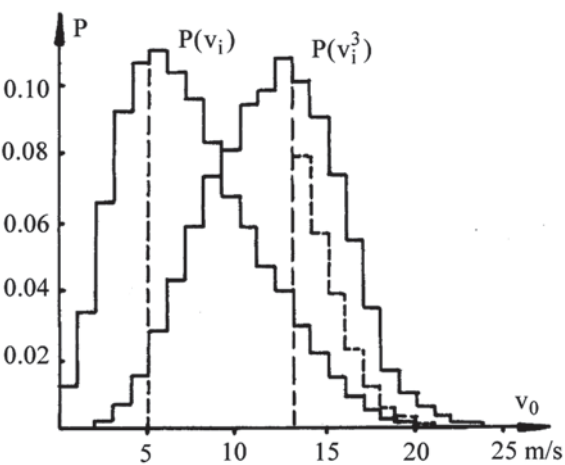
Fig. 10.13 Relation between solidity and design tip speed ratio. (Adapted to [2])



$$P(v_i) = \frac{\text{number of hours with wind velocity } v_i \text{ in a year}}{\text{number of hours in a year (8760)}},$$
$$P(v_i^3) = \frac{\text{yearly energy in the wind at velocity } v_i}{\text{total yearly energy in the wind}}.$$

The shape of the wind energy distribution is completely different from the shape of the wind velocity distribution, since the cubic power of the velocity has a strong effect. The energy average velocity is about 12 m/s.

Fig. 10.14 Distribution of wind speed and wind energy flux



The following wind speeds may be determined.

- *Cut-in speed.* This is the wind speed under which the wind turbine is not operated, because the energy yield is too low to justify wearing the system. The value typically amounts to 4–5 m/s. The example takes 5 m/s.
- *Rated speed.* The power is limited to the value corresponding to this wind speed. From this speed onwards, the generator produces at its maximum power, called rated power, and the wind energy flux is not completely used. The rated speed is determined by balancing the yield against the cost. In Fig. 10.14, this velocity is 13 m/s. A dashed line indicates the energy captured above the rated wind speed.
- *Cut-out speed.* This is the wind speed above which the turbine is stopped in order to avoid damage. Together with wind speed, wind unsteadiness increases. In the example, the cut-out speed is 25/s. The available energy above this speed is very small.

Figure 10.15 shows the variation of the power coefficient and the power of a 4.5 MW turbine as an example. Cut-in speed is 3 m/s and rated wind speed is 13 m/s. Within the 3–6 m/s wind speed range, the turbine turns at the minimum generator speed (–30%). Pitch changes with wind velocity. The speed ratio is optimal within the 6–10.5 m/s velocity range. From 10.5 m/s onwards, the generator turns at maximum speed (+30%) and the C_p value decreases with increasing wind velocity. From 13 m/s wind speed onwards, power is limited to 4500 kW.

The wind speed histogram (Fig. 10.14) demonstrates that the wind turbine is stopped during about 30% of time; it turns below rated wind speed during 60% of time and above rated wind speed during 10% of time. The yearly yield corresponds to about 30% of the yield of a wind turbine producing at rated power during the whole year. This ratio is called capacity factor. It can also be expressed in hours. A capacity factor around 3000 h is typical, somewhat less at inland locations and

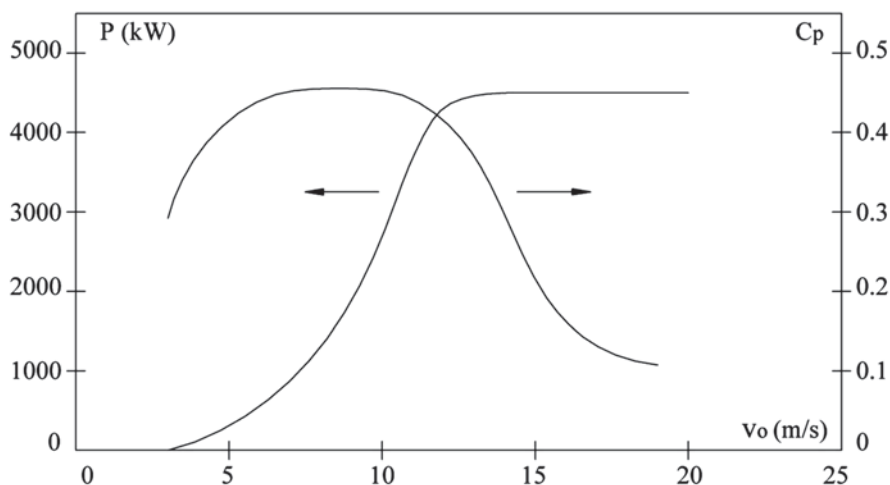


Fig. 10.15 Power coefficient and power of E112 (Enercon)

somewhat more at off-shore locations. The preceding description demonstrates that a wind turbine must be adapted to the wind regime of its location. There are differences between off-shore locations, coast locations and inland locations. Manufacturers offer wind turbines with the same rotors, but with different generators and tower heights, the greatest tower height being applied inland.

References

1. Freris LL (1990) Wind energy conversion systems. Prentice Hall. ISBN 0-13-960527-4
2. Hunt VD (1981) Wind power: a handbook on wind energy conversion systems. Van Nostrand Reinhold. ISBN 0-442-27389-4

Chapter 11

Power Gas Turbines

Abstract A gas turbine is a turbomachine composed of a compressor part, a part with heat supply to the compressed gas and a turbine part in which the hot gas expands. The present chapter discusses gas turbines for mechanical power generation. These are machines with an outgoing shaft, meant to drive a load. The largest market sector of such machines is electrical power generation, but machines for driving compressors and pumps in industrial plants and for driving large vehicles and ships also are examples. We discuss the working principles of the components of power gas turbines in the present chapter. As electric power generation is the largest sector of application, we choose components of such machines for illustrations. The main purpose of the chapter is the discussion of the overall performance of power gas turbines. Performance analysis is a matter of thermodynamic modelling and is not strongly linked to a particular application.

11.1 General Concept and Components

11.1.1 Definition of a Gas Turbine

The general definition of a gas turbine is given above. Figure 11.1 shows a scheme of a gas turbine with an outward shaft driving a load. The machine is thus intended for mechanical power generation. The general term for such a machine in the present book is *power gas turbine*, but this term does not universally refer to the broad category of gas turbines with an outgoing shaft. The most likely is that the term is understood as a gas turbine driving a generator in an electric power plant. Gas turbines for power plants form the largest market sector of gas turbines with an outgoing shaft. They also are the biggest machines with power nowadays (2014) up to 450 MW. There is no unique term to indicate gas turbines for power plants. They are sometimes called land-based gas turbines, but the term *industrial gas turbine* is applied as well. The term industrial gas turbine for power generation is sometimes used with the purpose to distinguish from industrial gas turbines for mechanical drive, which form a second subcategory. This term refers to a gas turbine in an industrial plant driving a rotating machine requiring high power. Mostly this is a compressor. Less common is drive of a big pump. Power gas turbines are further

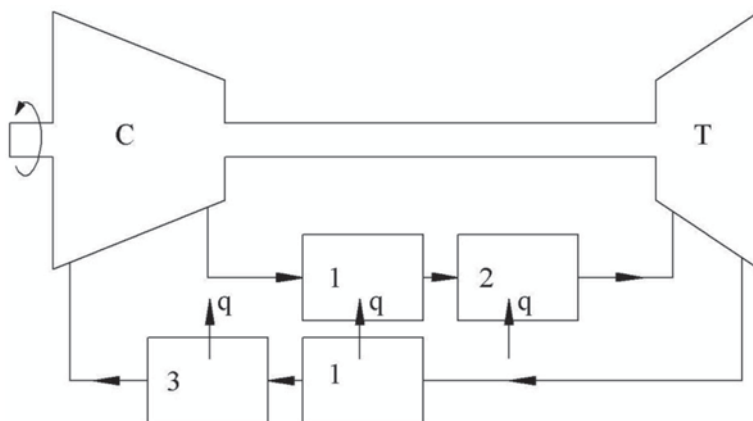


Fig. 11.1 Scheme of a power gas turbine

used to drive vehicles, ships, propeller aircraft and helicopters. Gas turbine driven vehicles are large power vehicles, as off-highway trucks, excavators, tanks and train locomotives. Also ships requiring high propulsive power in limited available space are gas turbine driven. This applies mainly to fast container ships, fast ferries, coast guard patrol boats and military ships like frigates and torpedo ships. Gas turbines are also applied for aircraft propulsion. These are commonly called *aero gas turbines*. Gas turbines for larger aircraft do not feature an outgoing shaft. The turbine part drives a compressor part and a part for thrust generation by acceleration of air, termed *fan*. The combustion gas leaving the turbine part is applied to generate thrust as well. Aero gas turbines are discussed in Chap. 12. The term aero gas turbine is commonly applied to all turbines for aircraft propulsion, including outgoing shaft machines for driving the propeller of a propeller aircraft or a helicopter rotor.

Figure 11.1 represents a closed cycle gas turbine. The gas delivered by the compressor is heated by two heat exchangers. Heat exchanger 1 extracts heat from the exhaust gas of the turbine. Heat from an external source is added in heat exchanger 2. The gas leaving the turbine part is further cooled by heat exchanger 3, using an external cooling source. The closed cycle is rarely applied. The cycle is mostly open, which then means that the compressor takes air from the atmosphere and that the exhaust gas of the turbine, having passed through heat exchanger 1, is discharged into the atmosphere. In that case, there is no heat exchanger 3. In an open cycle, heat exchanger 2 is always a combustion chamber, where the air is heated by internal combustion. The gas passing through the cycle is converted from air into a combustion gas. The atmosphere interferes as a component with the open cycle. The exhaust gas is cooled in the atmosphere and combustion products are regenerated by the flora of the earth. Many gas turbines do not feature a heat exchanger 1, as sketched in Fig. 11.1. In its simplest form, the gas turbine consists of a compressor part, a combustion chamber and a turbine part. The cycle is then termed a *simple cycle*. Heat exchanger 1, if present, may take two forms. The term *recuperator*

means a heat exchanger with heat transfer through metal walls. The term *regenerator* refers to a device with a rotating tube matrix of ceramic material, with the hot and cold gas alternately flowing through it.

Figure 11.1 suggests a machine with a single shaft. Most power gas turbines for electricity generation are built this way, but multi-shaft machines exist as well. A typical gas turbine for traction (vehicle, ship, propeller aircraft) has two turbine parts. Then, the high pressure part drives the compressor and the low pressure part drives the external load. The machine is divided into a *gas generator*, encompassing the compressor, the combustion chamber and the HP turbine and a *power turbine*, with different rotational speeds of both shafts. The gas generator turns at a rather high rotational speed, whereas the power turbine turns at a lower speed, adapted to the load. For traction, the torque as a function of speed is advantageous. At a fixed fuel flow rate, the power generated by the gas generator and supplied to the power turbine is constant. So, the product of the torque and the rotational speed on the outgoing shaft is then approximately constant. Some machines have a gas generator with two parts (we discuss the reason in the next section): compressor split into two parts and turbine split into two parts. The machine then has three shafts. A compressor part connected to a turbine part is called a spool. With multi-shaft machines, the shafts are mostly concentric, with the outgoing shaft, as on Fig. 11.1, at the compressor side. This is no general rule, but most applications benefit from an outgoing shaft at the cold side of the machine.

11.1.2 Comparison with Other Thermal Engines

Gas turbines show similarities, but differences as well, with reciprocating internal combustion engines and steam turbines. Within a reciprocating engine, the gas completes also a cycle of compression, heating by combustion and expansion, but the difference is that the stages of the cycle occur within the same space, but at different times. By alternating cold and hot stages, the thermal load on the walls is lower at a given combustion temperature. Reciprocating engines thus allow higher combustion temperatures. Further, the combustion happens for a large part under a constant volume. A high combustion temperature is then very advantageous for efficiency. The combustion in a gas turbine is at constant pressure. The consequence is that the simple-cycle efficiency does not depend much on the combustion temperature (see Sect. 11.3.3). Both machine types reach comparable efficiencies at present. With a simple cycle, the efficiency of a gas turbine amounts to about 40%. This is lower than the efficiency of a diesel engine, about 45%, but some extensions, analysed later, allow efficiency improvement with gas turbines. With both machine types a high combustion temperature is important for a high power density, or power per volume occupied. For this aspect, gas turbines have a very significant advantage over reciprocating engines, as flow through a gas turbine is continuous and occurs at high speed, with a through-flow Mach number of the order of 0.5. Large state-of-the-art land-based gas turbines feature about 1500 °C as inlet temperature of the turbine part and develop about 400 MW power. The dimensions

are approximately: diameter 5 m and length 13 m. A diesel engine with these dimensions only attains about 10 MW.

A high temperature at the combustion chamber outlet creates great technological problems for the combustor and the turbine. The melting temperature of the materials for the combustor and the turbine blades and vanes is about 1350 °C. With regard to sufficient strength and avoidance of creep, the highest allowable metal temperature of turbine blades is about 900 °C. Combustor and turbine parts thus need intensive cooling and protection against the hot gas. The technological gas turbine design is strongly determined by cooling and heat protection aspects, which we discuss below.

Gas turbines share similarities with steam turbines, with cycles running very analogously for both machines. The main difference is that the steam turbine feed pump replaces the gas turbine compressor. With regard to efficiency potential, this is very advantageous for the steam turbine. A pressure increase of 250 bar (typical pressure in a steam cycle) in water requires, with 90% efficiency, about 27.5 kJ/kg. A compression with pressure ratio 20 (typical for a gas turbine for electricity generation) requires about 460 kJ/kg for air at 288 K at compression start (one may verify with the formulae of Sect. 11.2: $R \approx 288 \text{ J/kg}$, $c_p \approx 1000 \text{ J/kg}$, polytropic efficiency 0.90). An expansion with the same pressure ratio starting at 1350 °C yields about 940 kJ/kg ($R \approx 288 \text{ J/kg}$, $c_p \approx 1250 \text{ J/kg}$). The power consumed by the pump is almost negligible with a steam turbine. The power of the compressor with a gas turbine is about half the power produced by the turbine part. This proportion is nearly the same for other pressure ratios. Global gas turbine efficiency is thus very sensitive to the efficiency of the components.

11.1.3 Example of a Power Gas Turbine

Figure 11.2 shows a large gas turbine for electrical power generation. It is a so-called *heavy duty type* machine, which means a very robust design meant for long production time per year (continuous operation is possible) and long periods between overhaul (typically 20,000 h). These machines are built for high power (from about 50 MW to about 450 MW). They are heavy, but this is no drawback for stationary land-based use. The compressor and turbine components are axial. The type shown is a version of the Siemens SGT6-5000F (Siemens Energy). The power is 208 MW at 3600 rpm (for use at 60 Hz), with compressor pressure ratio 17 realised with 16 stages (pressure ratio per stage is about 1.20). The turbine has four stages, with three of them cooled. For other examples, we refer to the websites of the main manufacturers (search for Siemens, Alstom, General Electric, Mitsubishi, in combination with gas turbines or energy). E.g., the most recent version of the SGT6-5000F reaches 232 MW with pressure ratio 18.9 in 13 stages.

The compressor is composed of discs. These are visible on Fig. 11.2. Also visible on the figure is how the compressor blades are attached to the discs by roots

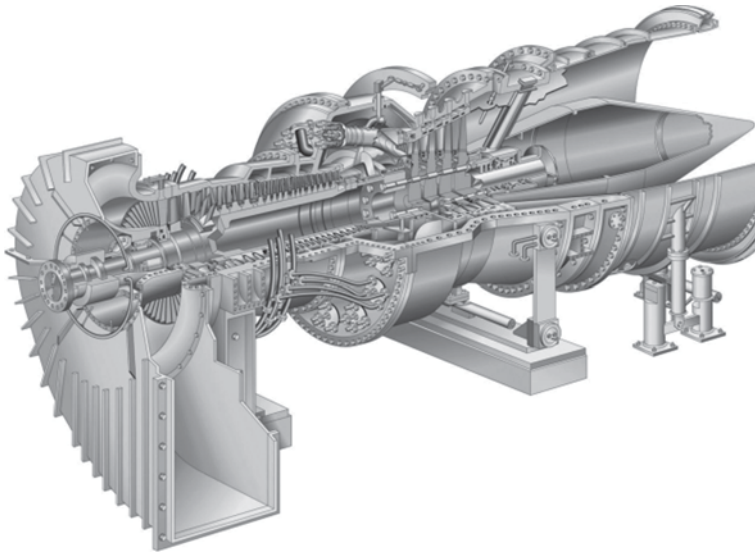


Fig. 11.2 Power gas turbine. (Siemens SGT6-5000F; courtesy Siemens Energy)

inserted in slots (see also further Fig. 11.4). The discs are connected to each other by teathed annular zones and tightened with bolts. The construction of the turbine is similar, but the fixing of the blades is with fir tree roots (multiple contact surfaces). The shaft is realised by adding hollow tubes to the connected discs.

A second category of machines meant for electricity production is the *aero-derivative type*. These machines are derived from aero gas turbines for thrust generation, by replacing the fan (front of the machine) by a compressor stage and by replacing the end part of the low-pressure turbine (rear of the machine) by adapted turbine stages. Such machines are offered by aero gas turbine manufacturers as a second product line. The machines are light (required for aero use) and have a pressure ratio typically around 40, so much higher than with a typical heavy duty gas turbine (see Chap. 12). They also have multiple shafts (two or three). The compressor is split into a low-pressure (LP) and a high-pressure (HP) part. In two-shaft machines, the turbine is split into two parts, with the HP turbine driving the HP compressor and the LP turbine driving the LP compressor and the external load on the cold end side of the machine (compressor side). In three-shaft machines, the turbine is split into three parts: the HP part drives the HP compressor, the intermediate-pressure part (IP) drives the LP compressor and the LP part drives the external load, either at the cold end side or at the hot end side of the machine. Typical manufacturers are Rolls Royce and General Electric (see websites; search for the name of the manufacturer combined with the term *aero-derivative*). Aero-derivative machines have limited power (range from about 5 MW to about 50 MW; there is one type with 100 MW). They are used for electricity generation, but typically not in large power stations, but very often in industrial plants requiring large

electric power (order of several tens of MW). Typical plants are off-shore oil or gas platforms, desalination plants and refineries. These machines are also used for mechanical drive of compressors and pumps in such plants. Adapted machines for ship propulsion exist (see the websites; search for Rolls Royce or General Electric, in combination with the term marine gas turbines). Manufacturers of gas turbines for power generation typically also offer heavy duty machines of smaller power for electricity generation in industrial plants or mechanical drive (search for small heavy duty gas turbines) and there are manufacturers who only make such smaller machines (e.g. MAN Diesel and Turbo).

11.1.4 Compressor Part

Figure 11.3 sketches the blade profiles and the velocity triangles at mean radius of an axial compressor. The shaft direction is horizontal in the figure. Figure 11.4 is a view on the rotor of the compressor of the SGT6-5000F. As usual, we employ the term *blade* in a rotor and the term *vane* in a stator, but the term blade refers to both in a general sense. A compressor stage consists of a rotor followed by a stator, but, typically, the inlet flow direction deviates from the axial direction. This means that the compressor has an inlet guide vane ring. The deviation is mostly about 15° in the rotation sense. By this deviation, the magnitude of the relative velocity at rotor inlet diminishes, for a given tangential velocity change. This is normally needed to reduce the Mach number of the relative inlet velocity. The major limitation of a compressor is the velocity reduction in the rotor (ratio w_2/w_1) and the stator (v_1/v_2 for a repeating stage), which has to stay above 0.7 (approximately) in order to avoid

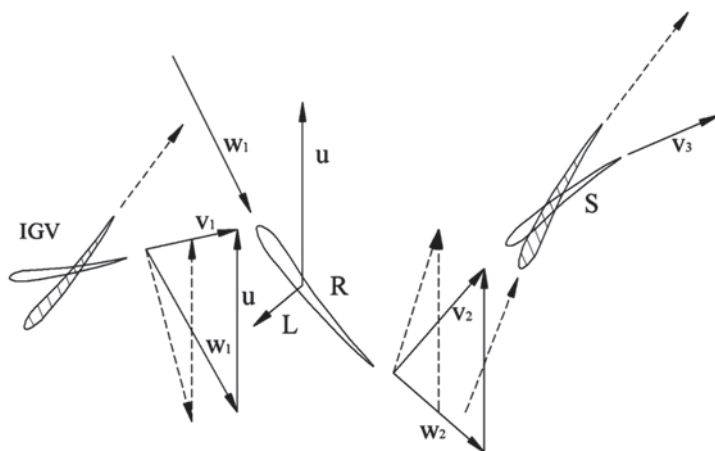
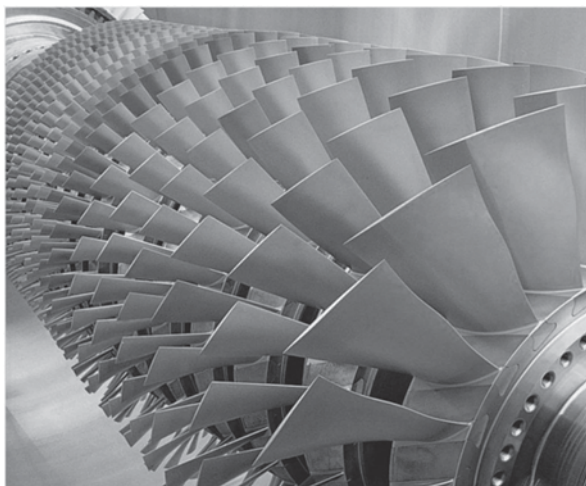


Fig. 11.3 Blade and vane profiles and velocity triangles of an axial compressor; *full lines*: design flow rate; *dashed lines*: reduced flow rate

Fig. 11.4 Compressor rotor of the SGT6-5000F. (Courtesy Siemens Energy)



flow separation. The consequence is that the flow turning in both stator and rotor is limited, which limits the work coefficient ($\psi = \Delta W / u^2$, thus $\psi = \Delta w_u / u = \Delta v_u / u$) to about 0.4 on the mean radius. Therefore, the blade speed is chosen as high as possible. In a heavy duty machine, it is typically somewhat less than 300 m/s on the mean radius (say 280–300 m/s). The precise value depends on the size of the machine and the rotational speed (300 m/s corresponds to a diameter of 1.91 m at 3000 rpm). The blade speed is near to the sonic speed, but below it (in air at 288 K, the speed of sound is 340 m/s). The inlet velocity of the rotor is approximately the same (Mach number around 0.85). So, the limitation of the blade speed comes from keeping inflow velocities just subsonic and is not caused by strength limitations (for more detailed discussion, see Chap. 13). The vanes and blades in a compressor are commonly made of alloys of steel with chromium and cobalt. With respect to strength, the blade speed at mean radius may be close to 400 m/s. The magnitude of the stage work is quite sensitive to the choice of the blade speed. With 280 m/s corresponds about 30 kJ/kg, but with 300 m/s it is already about 36 kJ/kg. A pressure ratio of 17 starting with air at 288 K requires about 420 kJ/kg. This means 14 stages of 30 kJ/kg. A pressure ratio of 20 requires about 460 kJ/kg and can be realised with 13 stages of 36 kJ/kg.

Usually, the angular position of the inlet guide vanes of a compressor can be adjusted to adapt the machine to lower mass flow rate than the design mass flow rate. The SGT6-5000F of Fig. 11.2 has an adjustable guide vane ring. A close look at the figure reveals the pivot of the vane in the upper position, linked by a lever arm to a ring, allowing collective adjustment of the vane angles. With some compressors also the stator vane angles of a number of stages at the front are adjustable, up to about one fourth of the total number of stages (typically three or four stages). Such stages are often called *variable geometry stages*. The SGT6-5000F shown in Fig. 11.2 only has adjustable inlet vanes, but the most recent version has three rows of variable stators. With variable geometry front stages, the compressor may

be adapted better for mass flow rate lower than the design value. We can easily understand the need for adjustable inlet guide vanes. It is somewhat more difficult to understand the benefit of a number of front stages with adjustable stator vanes for reduced load operation of the gas turbine (reduced mass flow rate).

During start-up of a compressor with many stages, the density rise from the first stage to the last stage is less than at design conditions. For a constant density fluid, the shape of the velocity triangles of the stages does not change when the stages maintain their flow coefficient and their work coefficient. So, at a reduced rotational speed, the shape is maintained for an operating point that obeys kinematic similitude. With a compressor, due to equal mass flow rate in successive stages, the reduced density rise causes deviations with increased through-flow velocity in the rear stages and decreased through-flow velocity in the front stages. Figure 11.3 shows that by lowering the through-flow velocity, with unchanged flow direction at outlet of the rotor (w_2) and unchanged flow direction at outlet of the stator (v_1), because these directions are imposed by the blades and the vanes, the incidences at rotor and stator inlet increase. Flow turnings in rotor and stator increase, which means that the stage work increases with diminished flow rate. But, big incidence may lead to flow separation. When this happens, the work diminishes, which then typically leads to impossibility to bring the gas turbine to full speed. There are several remedies for the stall in the first stages of a compressor during start-up. First, part of the flow after a few stages may be blown off through valves and led to the turbine part. A second way is splitting the compressor in parts and so making several spools. The objective is limiting the number of connected stages in a compressor part. The compressor has to be split into two or three parts, depending on the pressure ratio. Splitting the compressor is typically done with aero-derivative turbines, but is not typical with heavy duty machines. With large gas turbines for electricity generation, it is advantageous with respect to the precision of the rotational speed control to use only one shaft. Mostly, stall is avoided by adjustable stator vanes. Figure 11.3 shows that by turning the stator vanes more to the tangential direction (hatched profiles), both the incidences at stator and rotor inlet decrease. This allows starting up of the gas turbine.

With only the inlet guide vane ring adjustable, starting up of the gas turbine becomes possible, because avoiding stall in the first stage obviously is the critical action. When a compressor has multiple variable geometry front stages, it means that part-load operation of the gas turbine has been optimised. The output power of a gas turbine is diminished by reducing the fuel flow rate. In order to understand the consequence for the mass flow rate, one has to know that the turbine normally operates with a mass flow rate very near to the choked value or even on the choked value (for a detailed discussion, see Chap. 15). The choking mass flow rate is proportional to the density at turbine inlet and the velocity of sound at turbine inlet. The product of these quantities is proportional to the pressure and inversely proportional to the square root of the temperature. So, a reduced fuel flow rate causes, in first instance, lowering of the turbine inlet temperature and thus increased mass flow rate through the turbine. Increased mass flow rate means for the compressor, at fixed rotational speed as in a single-shaft machine, reduced pressure ratio (the

characteristic is lower work with increased flow rate). Of course, the turbine reacts to this change in pressure by a lower mass flow rate. So, it not easy to determine with simple means what the precise outcome is of pressure ratio and mass flow rate at reduced load, but it is sufficient here to understand (at least believe) that the mass flow rate increases and the pressure ratio decreases. The detailed study of the change of the operating point of a gas turbine with changing load is not easy and becomes even more complex when the gas turbine has many degrees of freedom, as multiple spools and variable geometry on the compressor. This detailed study is far above the objectives of the present book and we refer to specialised books [3, 7]. Higher air flow rate at part load reduces the efficiency of the compressor. Lower fuel flow rate and higher air flow rate at part load reduces the fuel-air ratio in the combustion chamber. The fuel-air ratio is always low in a gas turbine, in the sense that full mixing of fuel with air leads to a mixture that is much too lean for stable combustion. This makes the operation of the combustion chamber delicate (see discussion in a further section). Variation of the fuel-air ratio with load makes the realisation of good combustion, which means keeping low the noxious combustion products (CO and NO_x), more difficult. So, it is better for compressor efficiency and for combustion chamber performance that the mass flow rate is reduced at part load and that the fuel-air ratio stays approximately constant. This then means approximately constant turbine inlet temperature, but reduced pressure ratio [7]. The mass flow rate may be reduced by variable stator geometry in the front stages of the compressor. As Fig. 11.3 shows, the mass flow is reduced by turning the stator vanes more towards the tangential direction. By the same action, the stage work may also be reduced (lower flow turnings in rotor and stator). This leads then to a reduced pressure ratio. By doing this in a number of stages, the mass flow rate through the compressor is reduced, but also the density rise is reduced. This makes that in further stages the discrepancy between the through-flow velocity in design conditions and at reduced load may become sufficiently small so that variable stator geometry becomes unnecessary. In principle, the part load efficiency benefits from more stages with adjustable stator vanes, but at the other hand, leakage in the stator parts increases which diminishes the efficiency, also in design conditions. So, a practical optimum is with not many variable geometry stages.

11.1.5 Turbine Part

Figure 11.5 sketches the blade and vane profiles and the velocity triangles at the hub of an axial turbine. A turbine stage consists of a stator (with *vanes*) followed by a rotor (with *blades*). As with steam turbines, we may use the term *nozzle* for the channels formed by the stator vanes. Figure 11.6 is a view on the rotor of SGT6-5000F. The back part is the turbine with four stages. Vanes and blades in a heavy duty gas turbine are similar to those in the first stages of an LP part of a steam turbine. But, typically, the through-flow velocity and the work coefficient are larger (see

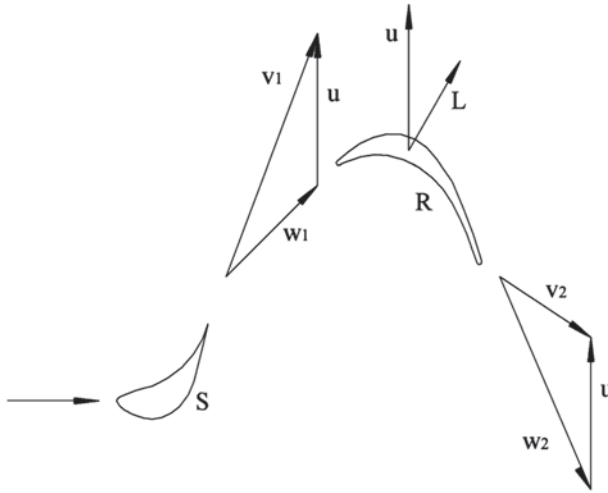


Fig. 11.5 Vane and blade profiles and velocity triangles of an axial turbine ($\psi=2$, $\phi=0.6$, $R=0.4$)

Chap. 15). The reason is realisation of large power per unit of volume and limitation of blade and vane surfaces that need cooling and hot gas protection. The work coefficient is typically above 2 at the hub ($\psi \approx 2.20$). In Fig. 11.5, the kinematic parameters are: $\psi=2$, $\phi=v_a/u=0.6$, R (degree of reaction) $=0.4$. The blade speed is typically around 350 m/s at the hub (this value comes from strength limitations). So, the stage work is about 250 kJ/kg ($\psi \approx 2.20$). With a compressor pressure ratio until

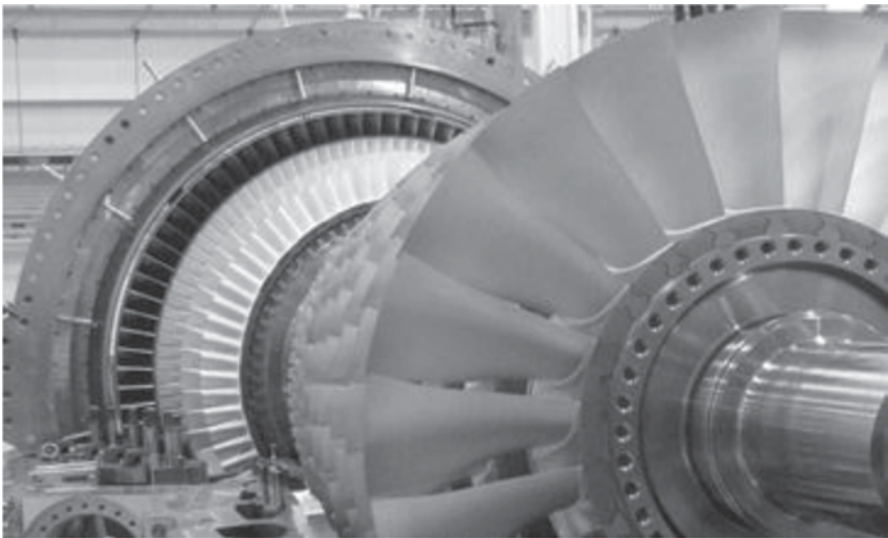


Fig. 11.6 Rotor of the SGT6-5000F. (Courtesy Siemens Energy)

20, four stages suffice in the turbine part (enthalpy drop is about 980 kJ/kg). With a compressor pressure ratio 40, five stages are needed (verify with the formulae of Sect. 11.2).

The interior parts of the combustion chamber and the first stages of the turbine are exposed to the hottest combustion gas. These parts therefore need cooling and shielding from the hot gas. Heat shielding is done with a *thermal barrier coating* (TBC). This is a layer of 100–400 μm thickness of ceramic material, formed by a vapour deposition process of a mixture of zirconium and yttrium. It can withstand very high temperatures and has an extremely low heat conduction coefficient (in the order of 1 W/mK). This layer creates a temperature difference of 100–300 °C. The ceramic layer is attached to a metal bond layer of about 100 μm thickness, formed by an alloy of nickel, cobalt, chromium, aluminium and yttrium, which itself covers the blade metal. The intermediate layer, or bond coat, serves as an elastic layer between the blade metal and the ceramic top coat. In between the bond coat and the top coat, a small oxide layer grows due to the high temperature and this oxide has a role in binding the two coats to each other. The white surface material of the blades of the first three stages in Fig. 11.6 is the ceramic layer. The metal materials for combustors, turbine blades and vanes are alloys of nickel, chromium and cobalt (nickel-base super-alloys; melting temperature about 1350 °C). The blades of the first stage are typically cast with temperature controlled cooling such that a blade forms a *single crystal*. This very expensive technique is necessary for obtaining maximum strength. The blades of the second stage are subjected to lower temperatures. These blades are typically cast with a less delicate cooling technique in a *directionally solidified* form, which means that the blade is composed of several crystals, but all in the longitudinal direction. Blades of non-cooled stages may be cast conventionally, leading to a large number of crystals with borders in all directions.

Cooling of the first stages of the turbine part of a gas turbine (stator and rotor parts of stages 1 and 2 and the stator of stage 3 of the SGT6-5000F in Fig. 11.2) is normally realised by air bleeds on the compressor. This air is led to the interior of the hollow stator vanes and rotor blades of the turbine, typically by external conduits in a land-based gas turbine and by internal perforations in an aero gas turbine. For rotor cooling, the air has to be brought into perforations of the rotor discs through slip ring sealed chambers. Three cooling principles are often combined. Figure 11.7 (left) sketches sections through a rotor blade. First, there is *convection cooling* by the air flowing through the internal passages. Heat transfer is enhanced by ribs in the broader passages and by pins in the narrower ones. A large fraction of the air is exhausted at the tip of the blade to provide cooling of the casing. A small fraction is exhausted at the trailing edge of the blade. By perforations between the front convection cooling channel and a channel at the leading edge, jets are formed impinging at the internal side of the trailing edge. This way of cooling is called *impingement cooling*. Impinging jets perpendicular to the surface realise a much higher heat transfer than flow aligned to the surface, as with convection cooling. This more intense cooling is very advantageous at the leading edge, where the heat load is the largest. *Film cooling* may be added. The air is led to the blade surface by holes, typically with an angle of about 30° to the surface, forming a protective film.

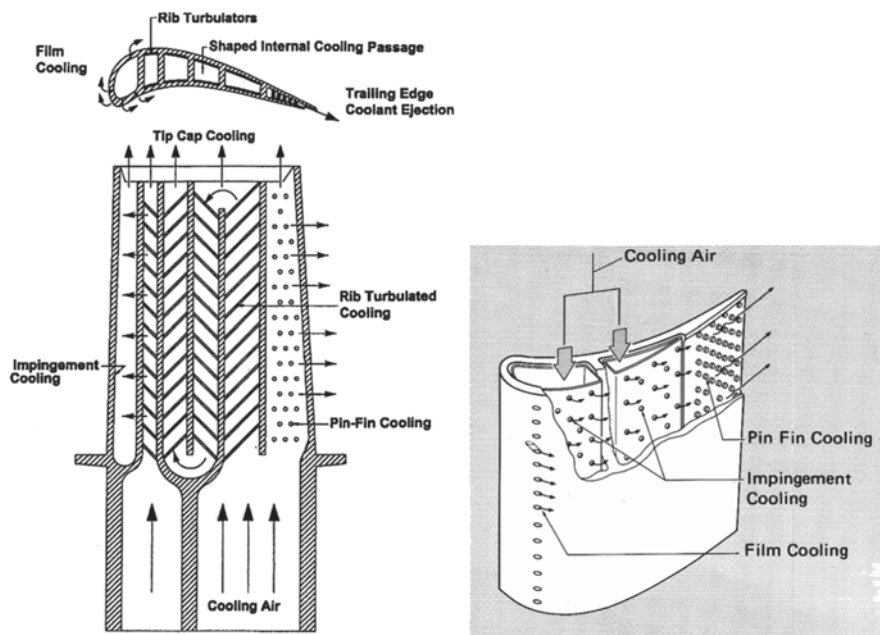
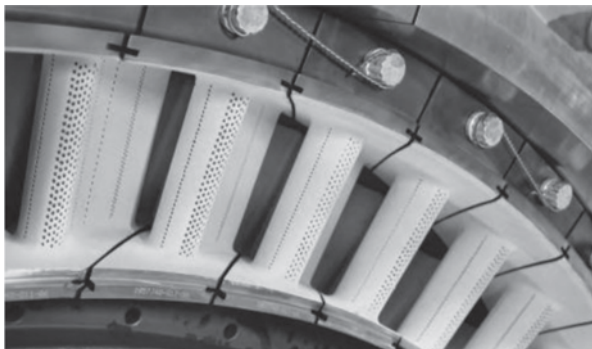


Fig. 11.7 Rotor blade with convection cooling, impingement cooling and film cooling (*left*; from Fu et al. [6]; permission by ASME); stator vane with impingement cooling by inserts and film cooling. (*right*; courtesy Mitsubishi-Hitachi)

With stator vanes, the same principles may be used as for rotor blades, but more intense cooling is reached by using inserts, as shown on Fig. 11.7 (right), so that impingement cooling is realised over a large fraction of the vane surface. Inserts are often used with first row stator vanes (e.g. SGT6-5000F). Figure 11.8 shows the cooling film holes in stator vanes.

Fig. 11.8 Film cooling holes in stator vanes. (Courtesy Siemens Energy)



11.1.6 Combustion Chamber

A combustion chamber has an outer shell, mostly cylindrical, as in Fig. 11.2, not exposed to the heat of the combustion, and an inner part which confines the combustion gas. The outer part has to withstand the pressure difference between the interior of the gas turbine and the external atmosphere. The inner part is generally called the *liner*, which means that it functions as a lining or an inner surface. The inner part has to withstand the heat of the combustion and therefore must be cooled. With large machines, there are two types of combustion chambers. With the *can-annular* form, as in Fig. 11.2, the inner part is composed of a number of approximate cylindrical cans (16 for the SGT6-5000F in Fig. 11.2) placed in the outer annular space. The individual liners are connected with tubes so that one liner can ignite another. A second possible form is *annular*, which then means that the inner part is annular. The typical fuel for a gas turbine for electricity generation is natural gas. For this fuel, the cans of a can-annular combustion chamber typically contain 6–9 burners. The annular combustion chamber has a large number of burners. For instance, the GT26 of Alstom has an annular combustion chamber with 84 burners. A first advantage of the annular combustion chamber is lower friction surface, resulting in a somewhat lower pressure drop in the combustion chamber. The second advantage is a more homogeneous temperature profile at turbine entrance. The disadvantage is that it is more difficult to keep the combustion process stable. Small or medium size gas turbines often have combustion chambers of can type, which means a number of cylindrical cans, each with a cylindrical liner. Land-based gas turbines typically have so-called reverse flow combustion chambers. This means that the flow coming from the compressor inverses direction, as in Fig. 11.2, before it enters the internal parts of the combustion chamber. The through-flow velocity of the compressor is of the order of 150 m/s (about half of the blade speed on the mean radius). The allowable velocity at the position of the combustion itself is of the order of 15 m/s. Realisation of the big velocity reduction is the easiest with a reverse flow chamber. Gas turbines for propulsion always have a straight through-flow combustion chamber, because the frontal area has to be minimised. The cooling and the heat protection of the liner or liners follow the same principles as with turbine blades. The most common is convection cooling by air flowing over the exterior liner surface and a thermal barrier coating on the interior surface. But impingement cooling of cans, requiring then a shell with holes around the cans, is also employed. With annular liners, other systems are film cooling of the inner surfaces (see Chap. 12, Sect. 12.6.3) and heat protection by ceramic tiles covering the metal surface.

Figure 11.9 sketches a longitudinal section of a somewhat simplified and unified version of the burner system used, with some variants, in can-annular combustion chambers by many manufacturers (Siemens, General Electric, Mitsubishi). A number of equal burners are positioned around a more complex central

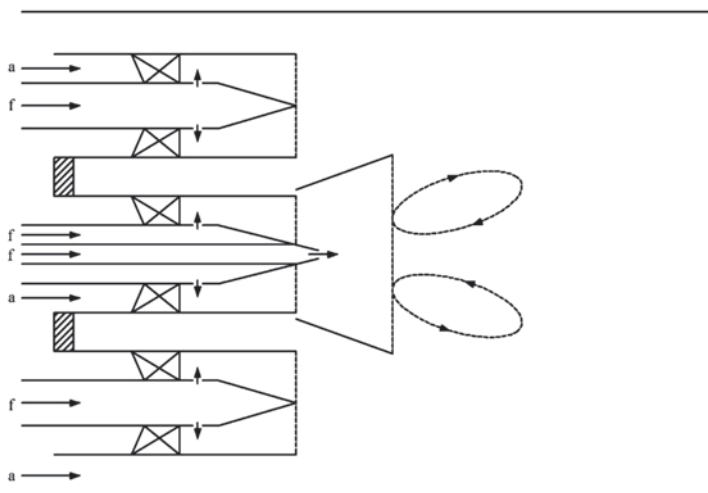


Fig. 11.9 Longitudinal section of a simplified Dry Low Emissions burner system (*DLE*) for a can-annular combustion chamber

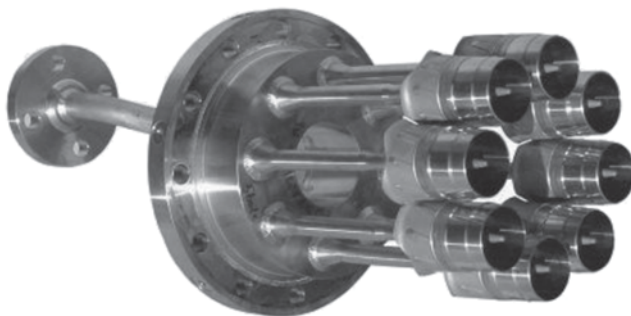


Fig. 11.10 Peripheral burners of a DLE system. (Courtesy Siemens Energy)

one, called the *pilot burner*. Figure 11.10 is a picture of eight peripheral burners, without the pilot burner. Burners are constructed for low production of noxious combustion products, which are nitrogen oxides (NO_x) and carbon monoxide (CO). NO_x forms by reactions at high temperature between nitrogen and oxygen of the air. CO forms by incomplete combustion due to lack of oxygen. For low production of both, the combustion principles are *lean premixing* and *staged combustion*. Traditional organisation of combustion is injecting pure fuel into air. The (gaseous) fuel then diffuses into the air and a flame front forms where the gas-air composition is about stoichiometric. The flame is then very stable but the

combustion temperature is high and much NO_x is formed. By mixing fuel and air prior to combustion into a lean mixture, the combustion temperature is much lower, so that much less NO_x is formed. The drawback is then that much CO is formed due to incomplete combustion. It is therefore essential for completing the combustion that air is added in a second stage to the combustion gas. The difficulty with premixed combustion is that the combustion may be quite unstable for a mixture with composition near to the lean flammability limit (there is also a rich limit, but this one is not relevant here).

The burner system of Fig. 11.9 is started by injecting pure fuel through the central pipe of the pilot burner. The mixture that forms by diffusion is ignited by a spark and a diffusion flame is formed, which is very stable. From a small load on, the pure fuel stream is stopped and replaced by a premixed flow, but with a composition sufficiently richer than the lean flammability limit, so that stable combustion is possible. The premixing is realised by swirling the air flow and injection of the fuel through holes in the hollow swirl vanes (or holes downstream of the vanes as in Fig. 11.9). The mixture passes a cone. Due to the swirl and the deceleration of the flow, a low pressure zone forms in the centre of the flow. By the low pressure, combustion gas is sucked from downstream so that a circulating flow pattern is formed (Fig. 11.9). The conveyed hot combustion gas ignites the oncoming mixture. The stabilisation and ignition process is called *swirl stabilisation* and is used in many industrial burners. The peripheral burners with premixing of fuel and air into a very lean mixture, under the lean flammability limit, are started in stages. In case of eight peripheral burners, the stages may be a first group of four burners, followed by another four, as load increases. This mixture burns as it reaches the stable pilot flame. Air is added downstream of the primary combustion zone through slots or holes in the liner surface in order to allow the further combustion of the formed CO (second stage of the combustion). More air is added further downstream (dilution air). With can liners, there are transition tubes which bring the combustion gas to the turbine inlet. Also these transition tubes have to be cooled. The air used for convection cooling of these tubes is mixed in just before the turbine inlet. The same principles are used in other combustion systems, but the technical realisation may be different from described above. In particular, with an annular combustion chamber, all burners are equal. A possible realisation is then a burner in the style of the pilot burner of Fig. 11.9, with a second ring of swirl vanes around it with injection of fuel forming a very lean mixture (e.g. Siemens, Alstom). The basic ingredients are always: gas injection in a swirling air flow, swirl-stabilisation of the flame, and staging of the combustion air. This technology is commonly denoted by the term dry low NO_x (DLN) or dry low emissions (DLE). With the most advanced systems, nowadays (2014), the production of NO_x and CO can be kept below 9 ppm over a broad range of the load. Alternative techniques for reducing NO_x are injection of water or steam in the combustion chamber. These wet techniques are sometimes used with smaller gas turbines, but not with large turbines that run almost continuously.

11.2 Thermodynamic Modelling

At the inlet and the outlet of a compressor or expander, flow is mostly homogeneous and steady with a good approximation. This is not the case at the inlet or the outlet of a stage. For a stage we assume averages over the inlet area and outlet area as representative states. As unsteadiness originates from rotor revolution, such averages are steady at constant rotor speed. We wish to assess stage efficiency only using the average inlet and outlet states.

11.2.1 *Isentropic Efficiency with Adiabatic Compression or Expansion*

For assessing the efficiency of a compressor or a turbine stage, we consider steady flow between the average states at inlet and outlet. To a streamline in the absolute frame applies:

Energy equation:

$$dW + dq = d \frac{1}{2}v^2 + dh + dU, \quad (11.1)$$

Work equation:

$$dW = d \frac{1}{2}v^2 + \frac{1}{\rho}dp + dU + dq_{irr}, \quad (11.2)$$

where dW is the elementary work done on the fluid and dq the elementary heat supplied to it. The gravitational potential energy is denoted by U . Further, dq_{irr} is the heat by irreversibility (dissipation). Firstly, we consider adiabatic processes, i.e. $dq=0$.

The energy equation is a total differential and thus can be integrated. The work equation forms a total differential if ρ is only a function of p . A special case meeting this condition is $\rho=\text{constant}$. The reversible part of the work done on the fluid is then $\Delta \frac{1}{2}v^2 + \Delta p/\rho + \Delta U$ and the quantity $E_m = \frac{1}{2}v^2 + p/\rho + U$ is called the *mechanical energy*, the sum of kinetic energy, pressure potential energy and gravitational potential energy (see Chap. 1). Historically, the term *head* is used for the mechanical energy divided by the gravity acceleration g , so expressed in metres. But with machines receiving or delivering work, it is more convenient to use the term head for the difference of mechanical energy across a component or across the machine, so expressed in J/kg. We have used the term head in this sense in previous chapters and we will continue this terminology. From the difference between the work equation and the energy equation it follows $dq_{irr} = dh - 1/\rho dp$. For constant density, the dissipated part of the work is then Δe , with e the internal energy. Since internal energy cannot be a source of work in a constant density fluid, the efficiency

definition is then simple. The efficiency of a machine with work done on a fluid, i.e. a pump, equals the ratio of the useful part of the work to the total work and the useful part of the work is the head. Assessment of the efficiency becomes more difficult with a compressible fluid. Integration of the work equation requires a way to determine a unique dependence between ρ and p . The traditional solution consists in considering a lossless flow and comparing its performance with the flow with losses. With $dq_{irr}=dh-1/\rho dp=0$ it follows $Tds=dh-1/\rho dp=0$. Thus the lossless flow is isentropic. For an isentropic flow, ρ is a unique function of p and integration of the work equation is possible.

We first notice that the change of gravitational potential energy for a gas is negligible with the processes that we analyse. E.g. for $\Delta z=1$ m is $\Delta U=g \Delta z=9.81$ J/kg. Converted into enthalpy, this means for $c_p=1005$ J/kgK (air): $c_p \Delta T=\Delta U$ or $\Delta T \approx 0.01$ K. Further we apply the concept of *total state* or *stagnation state*. This is the state attained by bringing the flow to zero velocity in a reversible adiabatic way. We note this state with the subscript 0; especially $h_0=h+\frac{1}{2}v^2$. With the concept of total enthalpy and ignoring the small changes in gravitational potential energy, Eqs. (11.1) and (11.2) become

$$dW = dh_0 = dh + d\frac{1}{2}v^2, \quad (11.3)$$

$$dW = \frac{1}{\rho} dp + d\frac{1}{2}v^2 + dq_{irr}. \quad (11.4)$$

Figure 11.11 sketches a compression and an expansion in the h - s diagram.

With a compression with the same starting point and the same final pressure, the isentropic process requires less work. Efficiency can thus be defined by

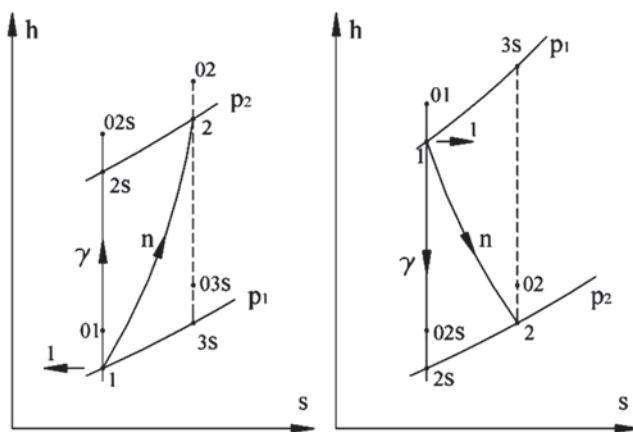


Fig. 11.11 h - s diagram for compression and expansion

$$\eta_s = \frac{h_{02s} - h_{01}}{h_{02} - h_{01}} = \frac{\Delta W_s}{\Delta W}. \quad (11.5)$$

For an expansion, Eqs. (11.3) and (11.4) are written as

$$\begin{aligned} -dh_0 &= -dW, \\ -\frac{1}{\rho} dp - d\left(\frac{1}{2}v^2\right) &= -dW + dq_{irr}. \end{aligned}$$

The isentropic expansion with the same starting point and the same final pressure extracts more work from the fluid and efficiency can be defined as

$$\eta_s = \frac{h_{01} - h_{02}}{h_{01} - h_{02s}} = \frac{-\Delta W}{-\Delta W_s}. \quad (11.6)$$

Henceforth, the final points 02 and 02s will be positioned on the same isobar p_{02} in schematic representations. This is strictly spoken incorrect, as isobars in the h - s diagram diverge with increasing entropy.

Expressions (11.5) and (11.6) define the so-called *isentropic total-to-total efficiency*. The work is compared to the total enthalpy change of an isentropic process with the same starting point and the same final pressure. The isentropic total enthalpy change is termed *isentropic head*. So, it is assumed that the isentropic head is the *mechanical energy*, meaning the maximum available enthalpy difference for work generation by the fluid (see Chap. 1, Sect. 1.4.4). For an expansion, this is correct, but for a compression the available enthalpy difference at the end of the compression is higher due to the divergence of the isobars. It is $h_{02} - h_{03s}$ in Fig. 11.11, left. The isobars diverge in an h - s diagram, since $(dh/ds)_p = T$. Therefore, it seems appropriate to define an isentropic efficiency of a compression process based on the re-expansion isentropic head $h_{02} - h_{03s}$. We denote this efficiency by the term *isentropic re-expansion efficiency*:

$$\eta_{sre} = \frac{h_{02} - h_{03s}}{h_{02} - h_{01}}. \quad (11.7)$$

When the kinetic energy at the end of a compression is not useful, a *total-to-static efficiency* is defined by

$$\eta_s = \frac{h_{2s} - h_{01}}{h_{02} - h_{01}} \text{ or } \eta_{sre} = \frac{h_2 - h_{03s}}{h_{02} - h_{01}}. \quad (11.8)$$

Analogously, for a turbine, the total-to-static efficiency is

$$\eta_s = \frac{h_{01} - h_{02}}{h_{01} - h_{2s}}. \quad (11.9)$$

The isentropic efficiencies are no efficiencies in the strict thermodynamic sense. Efficiency is, by strict definition, the ratio of the useful part of the work to the total work with a given process. But, a compressible fluid does not allow a precise definition of the useful part, as this would require detailed knowledge of the real process path in the h - s diagram. This path is not defined as the real process is unsteady and moreover, the objective is to define efficiency solely using the states at the start and the end of the process. Efficiencies defined here are *quality numbers*, as they compare the work from two processes, namely that of a lossless steady process and that of the real one. Strictly spoken, such a quality number is termed *effectiveness*, but the two concepts are not distinguished in practice, so that we henceforth will use the term isentropic efficiency.

11.2.2 Reheat Effect

The problem with the efficiency assessment of a compression or an expansion is the heating of the fluid by the losses. This causes a shift of a state point in the h - s diagram to the right side, for a given pressure. The divergence of the isobars thus increases the enthalpy difference available for work by the fluid, exactly in the same way as an enthalpy difference increase by external heating. This implies that part of the work dissipated is recoverable. On the other hand, the work required to continue compression or to recompress after expansion increases. This effect is termed *reheat effect*.

In further analysis, we assume that the kinetic energy change for the overall process is negligible, so that we may state that $d \frac{1}{2} v^2 = 0$. The total-to-total efficiency may then be noted by comparing static states. To a compression and an expansion respectively apply

$$\eta_s = \frac{h_{2s} - h_1}{h_2 - h_1}, \quad \eta_{sre} = \frac{h_2 - h_{3s}}{h_2 - h_1} \quad \text{and} \quad \eta_s = \frac{h_1 - h_2}{h_1 - h_{2s}}.$$

We then speak of isentropic efficiency, without any further specification.

In order to study the reheat effect, we first consider the series connection of two compressions with the same isentropic efficiency, as sketched in Fig. 11.12, left.

The isentropic efficiencies are equal:

$$\eta_{s1} = \frac{h_{2s} - h_1}{h_2 - h_1} = \eta_{s2} = \frac{h_{3s} - h_2}{h_3 - h_2}.$$

The isentropic efficiency of the entire compression is lower:

$$\eta_s = \frac{h_{3ss} - h_1}{h_3 - h_1} = \frac{h_{3ss} - h_{2s} + h_{2s} - h_1}{h_3 - h_2 + h_2 - h_1}.$$

This follows from the divergence of the isobars: $h_{3s} - h_2 > h_{3ss} - h_{2s}$.

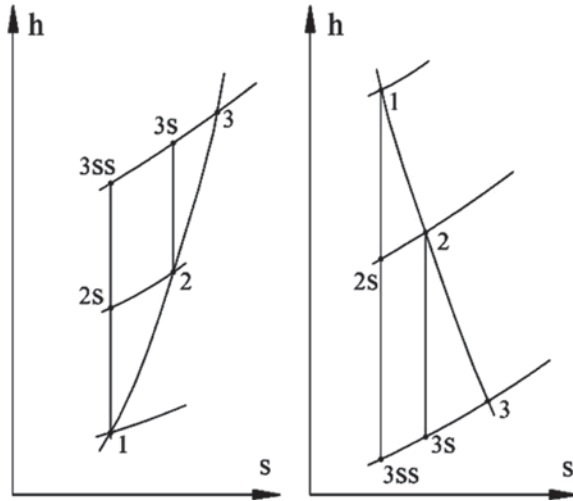


Fig. 11.12 Series connection of compressions and expansions

An opposite effect occurs with series connection of two expansions with the same isentropic efficiency (Fig. 11.12, right):

$$\eta_{s1} = \frac{h_1 - h_2}{h_1 - h_{2s}} = \eta_{s2} = \frac{h_2 - h_3}{h_2 - h_{3s}}.$$

The isentropic efficiency of the entire expansion is greater:

$$\eta_s = \frac{h_1 - h_3}{h_1 - h_{3ss}} = \frac{h_1 - h_2 + h_2 - h_3}{h_1 - h_{2s} + h_{2s} - h_{3ss}}.$$

This follows from the divergence of the isobars: $h_{2s} - h_{3ss} < h_2 - h_{3s}$.

Part of the energy dissipation of the first expansion is recovered with the second expansion. On the other hand more work is required for a recompression from the final point 3.

Series connection of compressor stages with equal isentropic efficiency results in an isentropic efficiency of the entire compression lower than the isentropic efficiency of the components. For the isentropic re-expansion efficiency, the result is higher efficiency of the series connection. With series connection of turbine stages the result is also higher isentropic efficiency of the series connection. So, isentropic efficiency is unsuitable for the study of the effects of changing the pressure ratio in gas turbine cycles.

11.2.3 Infinitesimal Efficiency; Polytropic Efficiency

The problem caused by the reheat effect can be avoided by defining efficiency on an infinitesimal base. The relations for a compression are (with $d \frac{1}{2} v^2 = 0$):

$$dW = dh, \quad dW = \frac{1}{\rho} dp + dq_{irr}.$$

For an infinitesimal part of the process, efficiency, in strict thermodynamic sense, is

$$\eta_{\infty} = \frac{dh_s}{dh} = \frac{\frac{1}{\rho} dp}{dh}.$$

This is termed *small stage efficiency* or *infinitesimal efficiency*. The subscript ∞ indicates that the complete process is thought as being composed of an infinite number of infinitesimal parts. With an ideal gas, we further have, with $p = \rho RT$, $dh = c_p dT$:

$$\eta_{\infty} = \frac{RT dp}{c_p p dT} = \frac{\gamma - 1}{\gamma} \frac{dp/p}{dT/T}.$$

With constancy of the specific heat ratio (perfect gas) and η_{∞} over the entire compression follows

$$\frac{dp}{p} = \eta_{\infty} \frac{\gamma}{\gamma - 1} \frac{dT}{T}. \quad (11.10)$$

The process thus is polytropic with exponent n ($p \sim \rho^n$):

$$\frac{n}{n-1} = \eta_{\infty} \frac{\gamma}{\gamma-1} \quad \text{or} \quad \eta_{\infty, comp} = \left(\frac{n}{n-1} \right) / \left(\frac{\gamma}{\gamma-1} \right). \quad (11.11)$$

In the h - s diagram (Fig. 11.11, left) we see that $n > \gamma > 1$, so

$$\frac{n}{n-1} < \frac{\gamma}{\gamma-1}, \quad \eta_{\infty} < 1.$$

For example: $\gamma = 1.4$, $\eta_{\infty} = 0.95$, $n = 1.430$; $\gamma = 1.4$, $\eta_{\infty} = 0.9$, $n = 1.465$.

Integration of (11.10) results in:

$$\frac{\gamma-1}{\gamma} \ln(p_2 / p_1) = \eta_{\infty} \ln(T_2 / T_1).$$

The similar result for an isentropic process is

$$\frac{\gamma-1}{\gamma} \ln(p_2 / p_1) = \ln(T_{2s} / T_1).$$

So:

$$\eta_{\infty} = \frac{\ln(T_{2s}) - \ln(T_1)}{\ln(T_2) - \ln(T_1)} = \frac{\ln(h_{2s}) - \ln(h_1)}{\ln(h_2) - \ln(h_1)}.$$

The obtained efficiency is termed *polytropic efficiency*. By convention it may also be applied to entire stages and the entire compressor by

$$\eta_p = \frac{\ln(h_{02s}) - \ln(h_{01})}{\ln(h_{02}) - \ln(h_{01})}. \quad (11.12)$$

Assuming that the compression can be represented as polytropic, we calculate for an ideal and perfect gas (Fig. 11.11, left) the following quantities.

Isentropic work (*isentropic head*):

$$\Delta h_s = \int_1^{2s} \frac{1}{\rho} dp = \frac{p_1}{\rho_1} \int_1^{2s} \frac{\rho_1}{\rho} d\left(\frac{p}{p_1}\right) = \frac{p_1}{\rho_1} \int_1^2 \left(\frac{p}{p_1}\right)^{\frac{1}{\gamma}} d\left(\frac{p}{p_1}\right) = \frac{\gamma}{\gamma-1} \frac{p_1}{\rho_1} \left[\left(\frac{p_2}{p_1}\right)^{\frac{\gamma-1}{\gamma}} - 1\right].$$

Reversible part of the work (*polytropic head*):

$$\Delta h_r = \int_1^2 \frac{1}{\rho} dp = \frac{p_1}{\rho_1} \int_1^2 \left(\frac{p}{p_1}\right)^{\frac{1}{n}} d\left(\frac{p}{p_1}\right) = \frac{n}{n-1} \frac{p_1}{\rho_1} \left[\left(\frac{p_2}{p_1}\right)^{\frac{n-1}{n}} - 1\right].$$

Work available with isentropic re-expansion (*isentropic re-expansion head*):

$$\Delta h_{sre} = \int_2^{3s} -\frac{1}{\rho} dp = -\frac{\gamma}{\gamma-1} \frac{p_2}{\rho_2} \left[\left(\frac{p_1}{p_2}\right)^{\frac{\gamma-1}{\gamma}} - 1\right].$$

With

$$\rho_2 = \rho_1 \left(\frac{p_2}{p_1}\right)^{1/n},$$

$$\begin{aligned} \Delta h_{sre} &= -\frac{\gamma}{\gamma-1} \frac{p_2}{\rho_1} \left(\frac{p_2}{p_1}\right)^{\frac{1}{n}} \left(\frac{p_1}{p_2}\right)^{\frac{\gamma-1}{\gamma}} \left[1 - \left(\frac{p_2}{p_1}\right)^{\frac{\gamma-1}{\gamma}}\right] \\ &= \frac{\gamma}{\gamma-1} \frac{p_1}{\rho_1} \left(\frac{p_2}{p_1}\right)^{\frac{1}{n}} \left[\left(\frac{p_2}{p_1}\right)^{\frac{\gamma-1}{\gamma}} - 1\right]. \end{aligned}$$

Total work:

$$\Delta h = C_p(T_2 - T_1) = C_p T_1 \left(\frac{T_2}{T_1} - 1\right) = \frac{\gamma}{\gamma-1} \frac{p_1}{\rho_1} \left[\left(\frac{p_2}{p_1}\right)^{\frac{n-1}{n}} - 1\right].$$

Table 11.1 Comparison of efficiency definitions of a compression with $\eta_\infty = 0.9$ and $\gamma = 1.4$

	$r = p_2/p_1 = 2$	$r = 10$	$r = 40$
$\eta_s = \Delta h_s / \Delta h$	0.8898	0.8641	0.8398
$\eta_\infty = \Delta h_i / \Delta h$	0.9000	0.9000	0.9000
$\eta_{sre} = \Delta h_{sre} / \Delta h$	0.9096	0.9296	0.9442

Results for $\eta_\infty = 0.9$ and $\gamma = 1.4$ are shown in Table 11.1. For a given infinitesimal efficiency, the difference with the other efficiencies increases with the pressure ratio. Isentropic efficiency decreases with increasing pressure ratio. The efficiency based on re-expansion work increases with increasing pressure ratio.

Infinitesimal efficiency may be introduced in the same way for an expansion. We note (with $d \frac{1}{2} v^2 = 0$):

$$-dh = -dW, \quad -\frac{1}{\rho} dp = -dW + dq_{irr}.$$

Infinitesimal efficiency is defined by

$$\eta_\infty = \frac{-dh}{-dh_s} = \frac{-dh}{-\frac{1}{\rho} dp} = \frac{-c_p dT}{-RT(dp/p)} = \frac{\gamma}{\gamma - 1} \frac{(-dT/T)}{(-dp/p)}.$$

So:

$$\eta_{\infty,exp} = \left(\frac{\gamma}{\gamma - 1} \right) / \left(\frac{n}{n - 1} \right). \quad (11.13)$$

In the h-s diagram (Fig. 11.11, right) we see that $n < \gamma$, so

$$\frac{n}{n - 1} > \frac{\gamma}{\gamma - 1}, \quad \eta_\infty < 1.$$

For example: $\gamma = 1.4$, $\eta_\infty = 0.95$, $n = 1.373$; $\gamma = 1.4$, $\eta_\infty = 0.9$, $n = 1.346$.

Further:

$$\eta_p = \frac{\ln(h_{01}) - \ln(h_{02})}{\ln(h_{01}) - \ln(h_{02s})}. \quad (11.14)$$

Assuming that the expansion can be represented as polytropic, we calculate for an ideal and perfect gas (Fig. 11.11, right) the following quantities.

Isentropic work (*isentropic head*):

$$\begin{aligned} \Delta h_s &= \int_1^{2s} -\frac{1}{\rho} dp = \frac{p_1}{\rho_1} \int_1^{2s} -\frac{\rho_1}{\rho} d\left(\frac{p}{p_1}\right) = \frac{p_1}{\rho_1} \int_1^2 -\left(\frac{p}{p_1}\right)^{\frac{1}{\gamma}} d\left(\frac{p}{p_1}\right) \\ &= \frac{\gamma}{\gamma - 1} \frac{p_1}{\rho_1} \left[1 - \left(\frac{p_2}{p_1}\right)^{\frac{\gamma - 1}{\gamma}} \right]. \end{aligned}$$

Table 11.2 Comparison of efficiency definitions of an expansion with $\eta_\infty = 0.9$ and $\gamma = 1.4$

	$r = p_2/p_1 = 1/2$	$r = 1/10$	$r = 1/40$
$\eta_s = \Delta h / \Delta h_s$	0.9087	0.9269	0.9405
$\eta_{\infty} = \Delta h / \Delta h_r$	0.9000	0.9000	0.9000

Reversible part of the work (*polytropic head*):

$$\Delta h_r = \int_1^2 -\frac{1}{\rho} dp = \frac{n}{n-1} \frac{p_1}{\rho_1} \left[1 - \left(\frac{p_2}{p_1} \right)^{\frac{n-1}{n}} \right].$$

$$\text{Total work: } \Delta h = c_p (T_1 - T_2) = \frac{\gamma}{\gamma-1} \frac{p_1}{\rho_1} \left[1 - \left(\frac{p_2}{p_1} \right)^{\frac{n-1}{n}} \right].$$

Results for $\eta_\infty = 0.9$ and $\gamma = 1.4$ are shown in Table 11.2. The conclusion is similar to that of a compression.

The practical application of polytropic efficiency implies two minor difficulties. This efficiency cannot be read directly from an h - s diagram and may only be calculated directly for an ideal and perfect gas with formulae (11.11) and (11.13). Polytropic efficiency may be calculated for a general gas with the logarithmic formulae (11.12) and (11.14), which then implicitly represent the gas in an averaged way as ideal and perfect. There is no real problem when studying gas turbine cycles. Air is an ideal gas ($p = \rho RT$, $R = 287 \text{ J/kgK}$ for dry air). Air is no perfect gas. Its heat capacity is pressure-independent, but increases with temperature. The same applies to a combustion gas, as we discuss in the next section.

Taking variable c_p and R into account with numerical simulations does not constitute an essential problem. A polytropic representation is not used then, but only the definition of infinitesimal efficiency. With an expansion this is $-dh = -\eta_\infty \frac{1}{\rho} dp$. The expansion path is divided into intervals. For each interval, the relation with average values of c_p and R is integrated. This has to be done iteratively, starting with the values at the beginning of the interval. The provisional value for h at the end of the interval is applied to determine T with a tabulated relationship $h = h(T)$. From this emerge provisional values of c_p and R at the end of the interval. Iteration is done a few times. As c_p and R only slightly vary, two or three iterations suffice in practice. This allows a very simple determination of the end point of an expansion with given η_∞ . The opposite operation, with a given end point and seeking the infinitesimal efficiency is more difficult. It requires iteration on the value of the infinitesimal efficiency. Calculations for compressions run analogously.

11.2.4 Thermodynamic Properties of Air and Combustion Gas

Dry air is a mixture of the following components in mass fractions:

$$0.7553 \text{ N}_2 + 0.2314 \text{ O}_2 + 0.0128 \text{ Ar} + 0.0005 \text{ CO}_2.$$

Table 11.3 Gas constant and heat capacity of gases relevant with combustion

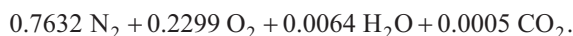
	R (J/kgK)	C_p (J/kgK)			C_p/R	
		0 °C	500 °C	1500 °C	0 °C	1500 °C
N ₂	295.31	1026	1057	1150	3.47	3.89
O ₂	259.83	908.4	979.1	1071	3.50	4.12
H ₂ O	461.52	1858	1976	2302	4.03	4.99
CO ₂	188.92	820.5	1016	1195	4.34	6.33

At 1 bar, 15 °C, 60 % relative humidity, air contains a 0.0064 mass fraction of water. Air composition then becomes



Henceforth we assume this air composition with detailed simulations.

Fuel is a mixture of carbon and hydrogen, spread over several chemical compounds. O₂ in air is consumed by combustion with generation of H₂O and CO₂. The ratio between the Ar and N₂ fractions in the air remains constant. Therefore, it is customary to combine the Ar with the N₂ and denote it then as N₂ from air. We so note the air composition as



The properties of the relevant gases are listed in Table 11.3, with N₂ from air (Source: [1]). The heat capacity C_p is the integral value, which means that the enthalpy difference between 0 °C and the temperature indicated is this value of C_p , multiplied with the temperature difference.

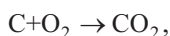
For air follows

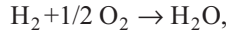
$$R = 0.7632R_{\text{N}_2} + 0.2299R_{\text{O}_2} + 0.0064R_{\text{H}_2\text{O}} + 0.0005R_{\text{CO}_2},$$

$$C_p = 0.7632C_{p\text{N}_2} + 0.2299C_{p\text{O}_2} + 0.0064C_{p\text{H}_2\text{O}} + 0.0005C_{p\text{CO}_2}.$$

This results in $R=288.2$ J/kgK; $C_p=1004.2, 1045.0, 1139.2$ J/kgK, at 0, 500, 1500 °C. The gas constant is somewhat higher than for dry air, which is 287.1 J/kgK. The heat capacity increases with temperature. For N₂ and O₂, $C_p/R=\gamma/(1-\gamma)$ is about 3.5 at low temperature (0 °C) and 4 at high temperature. These values are 4–4.3 and 5–6.3 for respectively H₂O and CO₂. So C_p/R increases with temperature and increases also by the generation of combustion products. For air in the range 0–500 °C, C_p is about 1025 J/kgK. The corresponding value of γ is about 1.39. So, we may assume this value of γ , together with $R=288$ J/kgK for hand calculations with compressors.

The chemical combustion equations are





So, 1 kg C forms 3.664 kg CO₂ and consumes 2.664 kg O; 1 kg H forms 8.937 kg H₂O and consumes 7.937 kg O.

For a fuel with mass fractions c carbon and h hydrogen and a fuel-air ratio f (kg/kg), the composition of the combustion gas for $(1+f)$ kg is

$$0.7632 \text{ N}_2 + [0.2299 - (h \times 7.937 + c \times 2.664)f] \text{ O}_2 \\ + (0.0064 + h \times 8.937 \times f) \text{ H}_2\text{O} + (0.0005 + c \times 3.664 \times f) \text{ CO}_2.$$

The gas constant follows from

$$(1+f)R = 288.2 - (h \times 7.937 + c \times 2.664) \times 259.83 \times f \\ + h \times 8.937 \times 461.52 \times f + c \times 3.664 \times 188.92 \times f \\ = 288.2 + (h \times 2062.33 + c \times 0.016) \times f.$$

With $h=0.13974$, $c=0.86026$ this becomes $(1+f)R=288.2+288.2f$.

The composition of a liquid fuel is always near $h=0.14$ and $c=0.86$. So, the gas constant of the combustion gas is approximately that of air, independent of the fuel-air ratio.

For heat capacity follows analogously, for $h=0.14$, $c=0.86$:

$$(1+f)C_p(0^\circ\text{C}) = 1004.2 + 1819.6f, \\ (1+f)C_p(500^\circ\text{C}) = 1045.0 + 2342.7f, \\ (1+f)C_p(1500^\circ\text{C}) = 1139.2 + 3002.0f.$$

For $f=0.03$, as an example, it follows: $C_p=1027.9$, 1082.8 , 1193.5 J/kgK, at 0 , 500 , 1500°C .

We take, as an example, combustion in air following a compression with pressure ratio 20 and $\eta_{oc}=0.9$, starting from $T_a=288$ K ($\gamma=1.39$).

$$\text{For air: } \frac{\gamma}{\gamma-1} = \frac{C_p}{R} = 3.564. \text{ Thus: } \frac{n}{n-1} = \eta_\infty \frac{\gamma}{\gamma-1} = 3.208.$$

$$\left(\frac{T_2}{T_1}\right)^{\frac{n}{n-1}} = \frac{p_2}{p_1}, \text{ from which } T_2 = 733 \text{ K} = 460^\circ\text{C}.$$

The thermal combustion equation is:

$$C_{pa}(T_2 - T_r) + f C_{pf}(T_f - T_r) + f H_L(T_r) = (1+f)C_{pg}(T_3 - T_r).$$

The subscripts a , f and g refer to air, fuel and combustion gas. H_L is the lower heating value of the fuel, determined at the reference temperature T_r , which often is $T_r=288\text{ K}$, the standard temperature at sea level (sometimes 25°C is used). The lower heating value of a liquid fuel is around $H_L=42,000\text{ kJ/kg}$. The temperatures T_2 and T_3 are upstream and downstream of the combustion chamber. The heat content of fuel may be ignored. The values of C_{pa} and C_{pg} are averages over the temperature ranges. It follows that

$$f = \frac{C_{pg}(T_3 - T_r) - C_{pa}(T_2 - T_r)}{H_L(T_r) - C_{pg}(T_3 - T_r)}.$$

We assume as approximate values of the heat capacities 1025 kJ/kg for air and 1150 kJ/kg for the combustion gas. It follows, for $f=0.03$:

$$1025(733 - 288) + 0.03 \times 42 \cdot 10^6 = 1150 (T_3 - 288).$$

The gas temperature at the combustion chamber outlet is $T_3=1718\text{ K}=1445^\circ\text{C}$. A correct temperature determination requires iteration with corrected heat capacity values. The example demonstrates that the fuel-air ratio is at maximum about 0.03 in practise, as the gas temperature 1500°C is about the maximum turbine inlet temperature used nowadays (2014).

For the example, the average heat capacity of the combustion gas over the range $500\text{--}1500^\circ\text{C}$ is

$$C_p = (1193.5 \times 1500 - 1082.8 \times 500) / 1000 = 1248.9\text{ J/kgK}.$$

The corresponding value of γ is 1.30. So, we may use $\gamma=1.30$ together with the gas constant $R=288\text{ J/kgK}$ as representative values with hand calculations in the turbine part of a gas turbine. Remark that the average C_p in the range $0\text{--}1500^\circ\text{C}$ is 1193.5 J/kgK for $f=0.03$. The corresponding value of γ is 1.318. So, we may use $\gamma=1.32$ together with $R=288\text{ J/kgK}$ as representative values for hand calculation of the enthalpy in the combustion chamber.

With gaseous fuels as natural gas (CH_4), the gas constant of the combustion gas differs somewhat from the value of air. For pure CH_4 , 12.011 kg C goes together with $2 \times 2.0159\text{ kg H}$, which means $c=0.749$; $h=0.251$. Then:

$$(1 + f)R = 288.2 + 517.7f.$$

The lower heating value of natural gas is around $50,000\text{ kJ/kg}$. This implies a fuel-air ratio around 0.025 for T_3 around 1500°C . For $f=0.025$: $R=292.8\text{ J/kgK}$. Real natural gas also contains higher hydrocarbons, as C_2H_6 , and also N_2 and CO_2 , causing a lower gas constant, so that there is little difference with 288.2 J/kgK . With the combustion gas composition corresponding to pure CH_4 , $C_p=1100\text{ J/kgK}$ and 1213 J/kgK at 500 and 1500°C for $f=0.025$. The average value in the range $500\text{--}1500^\circ\text{C}$ is 1268 J/kgK . Taking into account that an actual value is somewhat lower due

to presence of N_2 and CO_2 components, we still may use $R=288$ J/kgK together with $\gamma=1.30$ for hand calculations of the expansion in the turbine and together with $\gamma=1.32$ for determination of the fuel-air ratio in the combustion chamber.

11.2.5 Heat Capacity Representation

The integral heat capacity of a gas as a function of temperature may be expressed, with good accuracy, by a polynomial, according to

$$C_p = A + B\left(\frac{T}{1000K}\right) + C\left(\frac{T}{1000K}\right)^2 + D\left(\frac{T}{1000K}\right)^3.$$

Mean square fitting to the values of the integral heat capacity between 0°C and the temperature T , in $^\circ\text{C}$, for values between 0 and 1500°C per 100°C [1] leads to the results in Table 11.4. The error of the fitted polynomials is lower than 2 %. The differential heat capacity $c_p = dh/dT$ is given by

$$c_p = A + 2B\left(\frac{T}{1000K}\right) + 3C\left(\frac{T}{1000K}\right)^2 + 4D\left(\frac{T}{1000K}\right)^3.$$

11.2.6 Cooled Expansion

Vanes and blades are cooled within the HP part of the turbine. This has to be taken into account when describing the expansion. Two phenomena intervene, namely cooling of the through-flow and mixing of the cooling air into the expanding gas. In order to model the cooled expansion we here use a method with the cooling distributed over the expansion, analogous to the distribution of the energy dissipation in the polytropic description. This way of simulation is, with many variants, commonly applied in the literature. There is an enormous literature on the topic. We refer to a few examples [2, 4, 8, 10]. The simulation methodology used here contains some simplifications with respect to what typically is done.

For an infinitesimal expansion, the work equation (with no change of kinetic energy) reads

$$-\frac{1}{\rho} dp = -dW + dq_{irr}. \quad (11.15)$$

Table 11.4 Polynomial fitting of heat capacity (coefficients in J/kg)

	A	B	C	D
N_2	1026.3	26.5	91.2	-36.3
O_2	906.8	155.2	-18.3	-8.4
H_2O	1856.6	156.4	199.5	-70.7
CO_2	821.0	502.5	-254.3	57.1

Infinitesimal efficiency is defined by

$$-dW = \eta_{\infty} \left(-\frac{I}{\rho} dp \right). \quad (11.16)$$

The heat removed from the main flow by cooling may be noted for an entire stage as

$$-\Delta Q = A_b \alpha (\bar{T}_g - \bar{T}_b), \quad (11.17)$$

where A_b is the blade surface, α the heat transfer coefficient ($\text{W/m}^2\text{K}$) and $(\bar{T}_g - \bar{T}_b)$ the average temperature difference between the gas and the blades. The heat removed may be compared with the stage work according to

$$-\Delta W = \dot{m}_g \psi u^2,$$

where \dot{m}_g is the gas mass flow rate (kg/s), ψ the work coefficient of the stage and u the blade speed. The gas flow rate may be noted by $\dot{m}_g = \rho v A_g$, with ρ and v representative values of density and through-flow velocity and A_g the through-flow area. The ratio of the heat removed to the work done is

$$\frac{-\Delta Q}{-\Delta W} = \left(\frac{A_b}{A_g} \right) \frac{\alpha}{\rho v \bar{c}_{pg}} \frac{I}{\psi} \frac{(\bar{T}_g - \bar{T}_b)}{u^2}.$$

The surface ratio is typically around 8. The Stanton number $St = \alpha / \rho v \bar{c}_{pg}$ is around 0.005 for convective heat transfer in a flow along a flat plate, with \bar{c}_{pg} the heat capacity at \bar{T}_g [4]. We define $\kappa = \frac{A_b}{A_g} St \frac{I}{\psi} \frac{\bar{c}_{pg}}{u^2}$. With $\psi \approx 2$ and blade speed 300 m/s at the hub, it follows that $\kappa \approx 0.3 \times 10^{-3} \text{ K}^{-1}$.

By distributing the work and the cooling over the expansion, we may assume the differential equation:

$$\frac{-dq}{-dW} = \kappa (T_g - T_b), \quad (11.18)$$

with $-dq$ and $-dW$ heat removed and work done per mass unit for an infinitesimal part of the expansion and T_g and T_b local gas and blade temperatures. To word the meaning of the heat coefficient, κ may be expressed in J/kJK , so about 0.3 J/kJK .

With state-of-the-art machines the tolerable blade temperature $T_b \approx 900^\circ\text{C}$. The value of the heat transfer coefficient κ is lower than estimated up to now. The resistance to heat transfer increases strongly by applying a protective ceramic coating onto the blades (TBC: *Thermal Barrier Coating*) and by using film cooling. Due to these measures, the value of κ may be halved to about 0.15 J/kJK . It is immediately obvious that the thermal barrier coating constitutes an additional thermal resistance. Some reasoning is required to understand that a cooling film may be considered as

an additional resistance too. Heat transfer between gas and blades (11.17) may, with an adapted definition of the heat transfer coefficient, be noted as

$$-\Delta Q = A_b \alpha (\bar{T}_{aw} - \bar{T}_b), \quad (11.19)$$

with \bar{T}_{aw} the mean adiabatic wall temperature. This is the temperature the wall would adopt in absence of heat transfer. It approximately equals the gas temperature at a low velocity, but non-negligible heating by friction occurs at high velocity. The adiabatic film cooling effectiveness may be defined as

$$\eta_f = \frac{\bar{T}_g - \bar{T}_{aw}}{\bar{T}_g - \bar{T}_e}. \quad (11.20)$$

This effectiveness then expresses how much the adiabatic wall temperature decreases compared to the gas temperature, due to the protection by the film, as a fraction of the temperature difference between the gas \bar{T}_g and the cooling air \bar{T}_e leaving the ejection holes. It is a realistic approximation that the temperature of the cooling air entering the film equals the blade temperature, due to the intense contact between cooling air and blade within the ejection holes. We so may assume $\bar{T}_e = \bar{T}_b$ and thus combine (11.19) and (11.20) into

$$-\Delta Q = A_b \alpha (\bar{T}_g - \eta_f (\bar{T}_g - \bar{T}_b) - \bar{T}_b) = A_b \alpha (1 - \eta_f) (\bar{T}_g - \bar{T}_b).$$

From this reasoning emerges that film cooling decreases the heat transfer between gas and blade. Film cooling efficiency may amount up to 30 %, so that film cooling reduces the heat transfer to about 70 %. In combination with a thermal barrier coating, κ may be halved so that the resulting value is about 0.15 J/kJK.

The expansion of the cooled stage is represented by the h-s diagram in Fig. 11.13 (left). The 12' part is the expansion with distributed cooling. The 2'2" part renders the temperature drop by mixing and the 2"2 part is the pressure drop by mixing.

In order to calculate the expansion through a turbine, the entire pressure drop is divided into sufficiently small intervals. In Fig. 11.13 a pressure interval corresponds to the pressure difference $p_1 - p_2$. This interval is considered as a stage. This fictitious stage has a pressure drop that is much lower than a stage in reality. With a first iteration, the pressure difference $p_1 - p_2'$ may be set equal to $p_1 - p_2$. On the 12' path, the energy equation is noted as

$$-dh = -dW - dq = -dW (1 + \kappa (T_g - T_b)), \quad (11.21)$$

and

$$-c_{pg} dT_g = \eta_\infty \left(-\frac{RT_g dp}{p} \right) (1 + \kappa (T_g - T_b)). \quad (11.22)$$

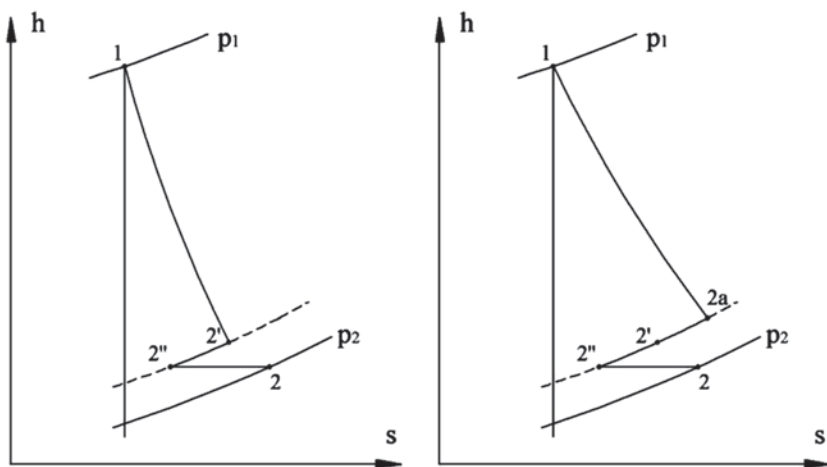


Fig. 11.13 Expansion with cooling and mixing of cooling air and gas; *left*: simultaneous cooling and expansion on the 12' path; *right*: adiabatic expansion followed by cooling

The Eqs. (11.16) and (11.18), together with the gas law, are applied to obtain (11.21) and (11.22). c_{pg} is the differential value of the specific heat. Equations (11.21) and (11.22) may be integrated exactly. The resulting expressions are rather complex and do not allow an immediate interpretation. Approximate integration with an average value of the factor $1 + \kappa(\bar{T}_g - T_b)$ therefore is more convenient. This factor only changes little over a small pressure interval. Approximate integration of (11.22) results in

$$\frac{T_{2'}}{T_1} = \left(\frac{p_{2'}}{p_1} \right)^{\frac{R\eta_{\infty}}{\bar{c}_{pg}}(1 + \kappa(\bar{T}_g - T_b))}. \quad (11.23)$$

The average temperature during expansion and the average specific heat appear in the formula. Now, the interpretation of result (11.23) becomes rather simple. The relation is polytropic and the exponent increases by cooling. This implies that, for a given pressure interval, the final temperature with cooling is lower than without cooling. With (11.23) follows the enthalpy difference over the pressure interval:

$$-\Delta h = \bar{c}_{pg}(T_1 - T_{2'}) = \bar{c}_{pg}T_1 \left(1 - \frac{T_{2'}}{T_1} \right). \quad (11.24)$$

With an approximate integration according to the same principle, (11.21) results in

$$\frac{-\Delta W}{-\Delta h} = \frac{1}{1 + \kappa(\bar{T}_g - T_b)} \text{ and } \frac{-\Delta q}{-\Delta h} = \frac{\kappa(\bar{T}_g - T_b)}{1 + \kappa(\bar{T}_g - T_b)}. \quad (11.25)$$

With (11.23), (11.24), (11.25), work follows from

$$-\Delta W = \bar{c}_{pg} T_1 \frac{1 - \left(\frac{p_{2'}}{p_1}\right)^{\frac{R\eta_\infty}{\bar{c}_{pg}}(1+\kappa)(\bar{T}_g - T_b)}}{1 + \kappa(\bar{T}_g - T_b)}. \quad (11.26)$$

We take as an example $p_1/p_{2'} = 2$, which is a large ratio (approximately the value of an entire stage in reality). With $\bar{T}_g - T_b = 1300 - 900^\circ\text{C}$ and $\kappa = 0.3 \text{ J/KgK}$ it follows $\kappa(\bar{T}_g - T_b) \approx 0.120$. For $R\eta_\infty/\bar{c}_{pg} \approx 0.200$ the factor of $\bar{c}_{pg} T_1$ in the right-hand side of (11.26) then is 0.1284. This value may be compared to the result of an adiabatic flow, obtained for $\kappa = 0$, being 0.1294. There is less than 1% difference. The same applies to the exact integration of (11.21) and (11.22). This implies that there is a quasi-complete compensation between the increase of the enthalpy drop on the 12' path in Fig. 11.13 (left) by the cooling and the consequence that the work is a fraction of this enthalpy drop. But, strictly, the work diminishes a little by cooling.

So, for almost the same final result, a cooled expansion may be represented by an adiabatic expansion with work, followed by a cooling without work. These processes are sketched in Fig. 11.13 (right). The 1-2a path is the adiabatic expansion. The 2a-2' path is the temperature decrease by blade cooling. The 2'-2'' path is the further temperature decrease by mixing the ejected cooling air with the gas and the 2''-2 represents the pressure drop by mixing. It is not necessary to determine the intermediate temperatures. The final temperature T_2 directly results from a mixing equation, for which the cooling air mass flow rate must be known. The cooling air mass flow rate follows from a heat balance with the blade seen as a heat exchanger:

$$-\Delta Q = -\dot{m}_g \Delta q = \dot{m}_c c_{pc} (T_e - T_c), \quad (11.27)$$

with \dot{m}_c the cooling mass flow rate, c_{pc} the specific heat of the cooling air, T_c the temperature of the cooling air at entrance of the blade and T_e the end temperature of the cooling air. The specific heat is the average value for air over the $T_e - T_c$ range. The temperature T_e follows from $T_e - T_c = \varepsilon (T_b - T_c)$, with ε the effectiveness of the cooling. The effectiveness is about 0.5 with convection cooling and about 0.7 with combined cooling by convection and impingement. With the assumption $T_e = T_b$, already used above for film cooling, the effectiveness of film cooling is set to 1. Equation (11.27) is completed by $-\Delta Q$ from (11.18) into

$$-\Delta Q = -\dot{m}_g \Delta q = \dot{m}_g \kappa (\bar{T}_g - T_b) c_{pg} (T_1 - T_{2a}) = \dot{m}_c c_{pc} (T_e - T_c), \quad (11.28)$$

with \bar{T}_g and c_{pg} average values over the $T_1 - T_{2a}$ temperature range. From (11.28) follows, with use of the effectiveness ε , the cooling air mass flow rate as

$$\delta = \frac{\dot{m}_c c_{pc}}{\dot{m}_g c_{pg}} = \left(\frac{\kappa}{\varepsilon}\right) \frac{(\bar{T}_g - T_b)(T_1 - T_{2a})}{(T_b - T_c)}. \quad (11.29)$$

The thermal mixing equation determining T_2 reads:

$$\dot{m}_g c_{pg} (T_{2a} - T_2) + \dot{m}_c c_{pc} (T_c - T_2) = 0. \quad (11.30)$$

This implies

$$T_2 = \frac{T_{2a} + \delta T_c}{1 + \delta}. \quad (11.31)$$

The heat capacities in (11.30) do not exactly equal those in (11.29), but we neglect the small differences. As a result thereof, calculation of the work and the final temperature of the expansion becomes very simple.

Assuming that the cooling air does not contribute any momentum to the main flow, the decrease of the momentum flow rate within the main flow, thus the decelerating force, is $\nu \dot{m}_c$, with ν the average through-flow velocity just before mixing. The corresponding pressure drop is $-dp A_g$, with A_g the through-flow area. The gas flow rate is $\dot{m}_g = \rho \nu A_g$. So:

$$-dp = \frac{\dot{m}_c}{\dot{m}_g} \rho \nu^2 \quad \text{or} \quad -\frac{dp}{p} = \frac{\dot{m}_c}{\dot{m}_g} \frac{\rho \nu^2}{p} = \frac{\dot{m}_c}{\dot{m}_g} \gamma M^2,$$

where M is the Mach number of the flow just before mixing. The mixing occurs nearby the trailing edge, i.e. where the Mach number is close to 1. The pressure loss thus ensues from

$$\frac{p_{2'} - p_2}{p_2} = \frac{\dot{m}_c}{\dot{m}_g} \gamma M^2 = \delta \mu \quad \text{with} \quad \mu = \frac{c_{pg}}{c_{pc}} \gamma M^2. \quad (11.32)$$

We may assume $M \approx 0.8$, so that $\mu \approx 0.85$. In reality, the cooling air supplies some momentum to the main flow. This moderates the pressure loss coefficient, with a realistic value about $\mu \approx 0.7$ [4].

11.2.7 Compression with Extraction

The calculation of the cooled turbine cannot be separated from the calculation of the compressor from which the cooling air is extracted. In practice, there are only a few extractions (2–3). In order to become independent of the precise position of these extractions, the extractions are distributed here over the compression. This is achieved by dividing the entire pressure interval in the compressor and the turbine into an equal number of subintervals. This is done according to a power series, so that the pressure ratio of the fictitious stages always is the same. We choose e.g. as many stages as the overall pressure ratio amounts to (40 stages at pressure ratio 40). Due to the pressure drop in the combustion chamber, corresponding points

on the compressor path feature a somewhat higher pressure than on the turbine path. We consider this pressure difference as necessary to bring the cooling air from the compressor to the turbine. It is e.g. assumed in a first iteration that 90 % of the air aspirated by the compressor is supplied to the combustion chamber, i.e. 10 % of the air is used as cooling air. For a given air flow rate into the combustion chamber, the fuel flow rate required to attain a specified turbine inlet temperature (TIT) can thus be determined. The specific heat and the gas constant for the first expansion stage can be determined that way. Cooling air is mixed with the gas at the end of each stage. The gas composition changes and adapted values of specific heat and gas constant are determined. The procedure is repeated for the further fictitious turbine stages until the gas temperature reaches the allowable blade temperature. From that point, calculations are performed without cooling, i.e. with $\kappa=0$. When the expansion has been fully calculated, the air flow rate to be extracted from the compressor at the various pressure levels is known. The air flow rate supplied to the combustion chamber is recalculated and the foregoing procedure repeated until convergence is attained. Thereafter, the power input to the compressor and the power output by the turbine are calculated, taking the mass flow rates in the various stages into account.

11.3 Performance of Simple-Cycle Power Gas Turbines

11.3.1 Idealised Simple Cycle

In a simple-cycle gas turbine, the flow passes in sequence through a compressor, a combustion chamber and a turbine. The main loss with this cycle is thermal in the sense of unused heat in the exhaust gas of the turbine. Thermodynamic losses range in second order. They encompass work dissipated into heat within the compressor and the turbine and the work loss by cooling of the turbine. Mechanical losses in the work transfer from the turbine to the compressor and to the external load range in third order. To estimate the influence of the various losses, we first analyse a cycle with only thermal loss, i.e. $\eta_{\infty c} = \eta_{\infty t} = \eta_m = 1$ and $\kappa=0$ and with unchanged fluid in the cycle.

Atmospheric conditions: p_0, T_0 .

Compressor (1→2): $r = p_{02} / p_{01} = p_{02} / p_0$,

$$W_c = c_p (T_{02} - T_{01}) = c_p T_{02} \left(1 - \frac{T_{01}}{T_{02}}\right) = c_p T_{02} \left(1 - r^{-\frac{\gamma-1}{\gamma}}\right).$$

Combustion chamber (2→3): $\Delta Q = c_p (T_{03} - T_{02})$.

We adopt the simplification that there is no change in mass flow rate and in heat capacity of the gas.

Turbine (3 → 4):
$$W_t = c_p (T_{03} - T_{04}) = c_p T_{03} (1 - r^{-\frac{\gamma-1}{\gamma}}).$$

The work output is

$$\Delta W = W_t - W_c = c_p (T_{03} - T_{02}) (1 - r^{-\frac{\gamma-1}{\gamma}}). \quad (11.33)$$

The *thermal efficiency* is the ratio of the power output to the power supplied by the fuel:

$$\eta_t = \frac{\Delta W}{\Delta Q} = 1 - r^{-\frac{\gamma-1}{\gamma}}. \quad (11.34)$$

This theoretical efficiency does not depend on the turbine inlet temperature. The result is significantly different from the efficiency of real simple-cycle gas turbines. For instance, with $r=20$ and $r=30$, for $\gamma=1.40$ (dry air), the theoretical efficiencies are 0.575 and 0.622. Efficiencies of real machines are about 0.395 (e.g. Siemens SGT5-4000F, $r \approx 18$, $T_{03} \approx 1350^\circ\text{C}$; representative for a heavy duty machine) and 0.415 (e.g. General Electric LM6000, $r \approx 29.5$, $T_{03} \approx 1250^\circ\text{C}$; representative for an aero-derivative machine). The much lower efficiency in reality is mainly due to the change of the gas composition in the combustion chamber and to the compressor and turbine efficiencies, as we analyse in the next section.

For later discussions, it is important to remark the quite important influence of the exponent in the efficiency expression (11.34). From now on, we will use the term exponent in the pressure-temperature relation, as the exponent in the polytropic relation of form

$$\frac{p_b}{p_a} = \left(\frac{T_b}{T_a} \right)^e.$$

For isentropic flow, the exponent is $\gamma / (\gamma - 1) = C_p / R$. For dry air at 0°C , $\gamma=1.40$ and the exponent is 3.5. For a combustion gas $\gamma \approx 1.30$ and the exponent is around 4.333. The theoretical efficiencies for $r=20$ and $r=30$ become for $\gamma=1.30$: 0.499 and 0.544. These values are significantly lower than for $\gamma=1.40$. This observation is already an indication that the efficiency of the simply cycle decreases by the conversion of air into combustion gas. This is one of the aspects that we study in the next section.

11.3.2 Simple Cycle with Component Efficiencies and Different Heat Capacities of Air and Combustion Gas

Extending the previous analysis for the efficiencies of the compressor and the turbine parts is quite simple. It is also easy to take into account the larger value of

the heat capacity of the combustion gas with respect to that of air, if constant values of heat capacities are used. The adapted relations are listed hereafter. The subscripts *a* and *g* refer to the air and the combustion gas. The subscripts *c* and *t* refer to the compressor and the turbine.

Compressor (1 → 2):

$$W_c = c_{pa}(T_{02} - T_{01}) = c_{pa}T_{01}\left(\frac{T_{02}}{T_{01}} - 1\right) = c_{pa}T_{01}\left(r^{\frac{R}{\eta_{\infty c}c_{pa}}} - 1\right).$$

Turbine (3 → 4):

$$W_t = c_{pg}(T_{03} - T_{04}) = c_{pg}T_{03}\left(1 - r^{\frac{-\eta_{\infty t}R}{c_{pg}}}\right).$$

Combustion chamber (2 → 3):

$$\Delta Q = c_{pg}(T_{03} - T_{01}) - c_{pa}(T_{02} - T_{01}). \quad (11.35)$$

We adopt the simplification that there is no change in mass flow rate. The inlet temperature of the compressor is taken as the reference temperature for the lower heating value of the fuel, which comes from the point of view that heating is meant for increasing the work capacity of the fluid, already realised by the compression.

The efficiency is

$$\eta = \frac{\frac{c_{pg}}{c_{pa}} \frac{T_{03}}{T_{01}} \left(1 - r^{\frac{-\eta_{\infty t}R}{c_{pg}}}\right) - \left(r^{\frac{R}{\eta_{\infty c}c_{pa}}} - 1\right)}{\frac{c_{pg}}{c_{pa}} \left(\frac{T_{03}}{T_{01}} - 1\right) - \left(r^{\frac{R}{\eta_{\infty c}c_{pa}}} - 1\right)}. \quad (11.36)$$

In principle, the values of the differential heat capacities of the combustion gas in the combustion chamber equation and the turbine equation have to be different, as these are averages over a different temperature range. For the combustion chamber $\gamma \approx 1.32$ and for the turbine $\gamma \approx 1.30$. We take here an average, which then means $c_{pg} / R \approx 4.25$. For the compressor, we take $\gamma = 1.40$, so that $c_{pa} / R = 3.50$. Table 11.5 illustrates the influence of the different parameters. The temperature ratio T_{03} / T_{01} is set at 5 and 6, corresponding to T_{03} equal to 1440 K (= 1167 °C) and 1728 K (= 1455 °C) with T_{01} equal to 288 K. The first part of Table 11.5 reproduces the results obtained by the analysis of the previous section. The second part illustrates the efficiency drop caused by the increase of the heat capacity due to the combustion. The reduction factor of the efficiency is about 85 %. The results also show that efficiency becomes somewhat dependent on the temperature ratio. The efficiency benefits from a higher temperature at the turbine inlet. The third part

Table 11.5 Influence on efficiency of the simple cycle of gas properties and component efficiencies according to the simplified expression (11.36)

$c_{pd}/R=3.50, c_{pg}/R=3.50; \eta_{xc}=\eta_{xt}=1$	$r=20$	$r=30$	$r=40$
$T_{03}/T_{01}=5$	0.575	0.622	0.651
$T_{03}/T_{01}=6$	0.575	0.622	0.651
$c_{pd}/R=3.50, c_{pg}/R=4.25; \eta_{xc}=\eta_{xt}=1$			
$T_{03}/T_{01}=5$	0.490	0.529	0.533
$T_{03}/T_{01}=6$	0.494	0.535	0.561
$c_{pd}/R=3.50, c_{pg}/R=4.25; \eta_{xc}=\eta_{xt}=0.9$			
$T_{03}/T_{01}=5$	0.387	0.403	0.405
$T_{03}/T_{01}=6$	0.409	0.435	0.448
$c_{pd}/R=3.50, c_{pg}/R=4.25; \eta_{xc}=\eta_{xt}=0.8$			
$T_{03}/T_{01}=5$	0.239	0.202	0.144
$T_{03}/T_{01}=6$	0.295	0.291	0.274

of Table 11.5 illustrates the combined effect of the component efficiencies and the change of the gas composition. The efficiency decreases considerably due to component efficiencies. The values obtained are very near to the values for real machines (e.g. the SGT5-4000F and the LM6000 used in the previous section). This observation means that the supplementary effects due to variability of the gas properties and due to cooling remain quite limited (see next section). The fourth part of Table 11.5 illustrates the very low global efficiency with lower efficiencies in the compressor and the turbine. The dramatic reduction of the global efficiency proves the need for high component efficiencies.

11.3.3 Simple Cycle with Component Efficiencies, Cooling and Variable Gas Properties

Figure 11.14 shows the efficiency of the simple cycle obtained with the simulation methodology explained in Sect. 11.2. The infinitesimal efficiencies of the compressor and the turbine are set at 90%. Further parameters are: pressure drop in the combustion chamber: 4%; thermal efficiency of the combustion chamber: 98%; mechanical efficiency of the work transfer of the turbine to the compressor and the external load: 99%. The fuel is pure CH_4 with lower heating value 50 MJ/kg. The energy balance of the combustion chamber is written in the same way as (11.35):

$$\Delta Q = f H_L = (1 + f) c_{pg} (T_{03} - T_{01}) - c_{pa} (T_{02} - T_{01}). \quad (11.37)$$

This means that the reference temperature of the lower heating value is the total temperature at the inlet of the compressor and that any energy that has been supplied to the gaseous fuel by heating it and compressing it is absorbed in the definition of the

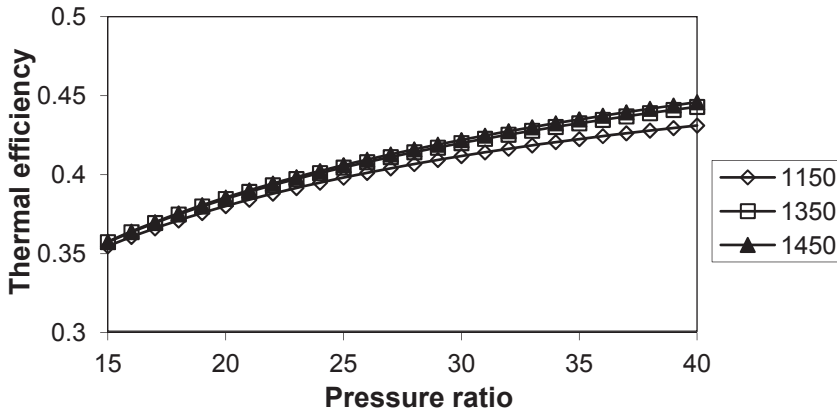


Fig. 11.14 Efficiency of a simple-cycle gas turbine (CH_4 , $\text{TIT}=1150\text{--}1450\text{ }^\circ\text{C}$)

lower heating value. The heat exchange coefficient in the turbine is set to $\kappa=0.15\text{ J/kJK}$. Film cooling is assumed with heat exchanger effectiveness $\varepsilon=1$. This means that we consider very advanced thermal protection and cooling. We notice the obvious influence of the pressure ratio. The efficiency increases with the pressure ratio in the indicated range ($r=15\text{--}40$). The increase does not continue indefinitely. This means that there is a pressure ratio for maximum efficiency, but this maximum occurs far above $r=40$. The obtained efficiencies are somewhat lower than obtained in the previous section. This is due to the turbine cooling (this was also verified by simulations with $\kappa=0$; results not shown). The small improvement of the efficiency with increasing turbine inlet temperature (TIT) in absence of cooling, observed in the previous section, is almost completely neutralised by the cooling. This means that TIT has almost no influence on obtainable efficiency. For this result, the heat transfer in the turbine has to be sufficiently small. It was verified by simulations with a larger value of the heat exchange coefficient, namely $\kappa=0.3\text{ J/kJK}$, that the efficiency at larger TIT becomes smaller than at lower TIT (results not shown). So, high TIT is not essential for high efficiency. The benefit of high TIT is mainly high work output, as we illustrate with a further figure.

The results shown in Fig. 11.14 are very realistic. This may be verified with the two machines which we already used as examples (SGT5-4000F and LM6000). The correspondence for other machines is similar, but the global efficiency is quite sensitive to the efficiencies of the compressor and turbine components, as already became clear in the previous section. Modern gas turbines have component efficiencies somewhat above 0.90 and older ones may have lower component efficiencies, although improved blade shapes, when they become available, are also implemented in older types of machines. The global efficiency is also somewhat dependent on the fuel composition. Simulations with kerosene, the fuel of aero-engines, represented as $\text{C}_{12}\text{H}_{24}$ (diesel oil is near to $\text{C}_{12}\text{H}_{23}$), show an efficiency decrease of about 2%

(results not shown). This is mainly due to the higher fuel-air ratio as a consequence of the lower heating value 43 MJ/kg.

The efficiency results of Fig. 11.14 are obtained with cooling air extracted from the compressor, as in most machines. Further, it is assumed that there is no pre-cooling of this air by an external heat exchanger before supplying it to the turbine. In some machines such pre-cooling is implemented. Cooling may also be realised with an externally provided fluid. In particular, machines exist with *steam cooling*. The choice for this cooling fluid comes from applications in combined-cycle systems (see Sect. 11.4.4). The heat capacity of steam is higher than that of air, which, principally, lowers the necessary cooling flow rates. Further, the heat absorbed by the steam may be used in the steam cycle. However, there are some drawbacks with steam too. Steam has to be led into the machine, but also led out of it. This is possible, but is somewhat complicated for rotor parts. Further, film cooling cannot be used. This increases the heat transfer between the hot gas in the turbine and the blades and the vanes ($\kappa=0.20$ J/kJK instead of 0.15 J/kJK) and decreases the heat exchanger effectiveness of the blades and the vanes ($\varepsilon=0.7$ instead of 1). Simulations with cooling with an external fluid have as a result that the global efficiency of the simple cycle is slightly lower than with cooling by air from the compressor (results not shown). But these are results assuming that the heat transferred to the cooling fluid is useless. Taking into account that the heat may contribute to a second cycle, one may conclude that there is a small advantage with steam cooling in a combined-cycle application. We will come back to closed loop steam cooling with the discussion of combined cycles in Sect. 11.4.4.

Figures 11.15, 11.16, 11.17 and 11.18 show specific power, turbine outlet temperature (TOT), fuel flow rate and cooling flow rate obtained by simulation with pure CH_4 as fuel. The results with kerosene as fuel differ slightly. For instance, specific power is about 4–5 % lower with kerosene. The specific power is expressed as the power per unit of mass flow rate of the exhaust gas. The increase of the specific power with the combustion temperature is obvious. The specific power has a weak maximum as a function of pressure ratio, around pressure ratio 15–20. An important observation for practise is that with respect to specific power, it is not useful to choose the pressure ratio too high. Heavy duty gas turbines have typically a pressure ratio in the order of 20. The simple-cycle efficiency (Fig. 11.14) is then not at maximum, but these machines are typically used in combined-cycle power stations and the optimum efficiency with combined cycles occurs at lower pressure ratio (see Sect. 11.4.4). It is difficult to verify precisely the realism of the simulation results for specific power, because specific power is strongly dependent on TIT and the value of TIT is never precisely known for real machines. Further, the results are somewhat dependent on fuel composition. Examples of heavy duty gas turbines, with TIT around 1350 °C, are: Siemens SGT5-4000F producing 292 MW at $r=18$ with 685 kg/s exhaust mass flow and TOT=577 °C (the specific power is 426.3 kJ/kg); Mitsubishi M701F, producing 312 MW at $r=17$, with 720 kg/s exhaust mass flow and TOT=597 °C (the specific power is 433.3 kJ/kg). An example of an aero-derivative turbine is General Electric LM6000 producing 42.9 MW at $r=29.5$,

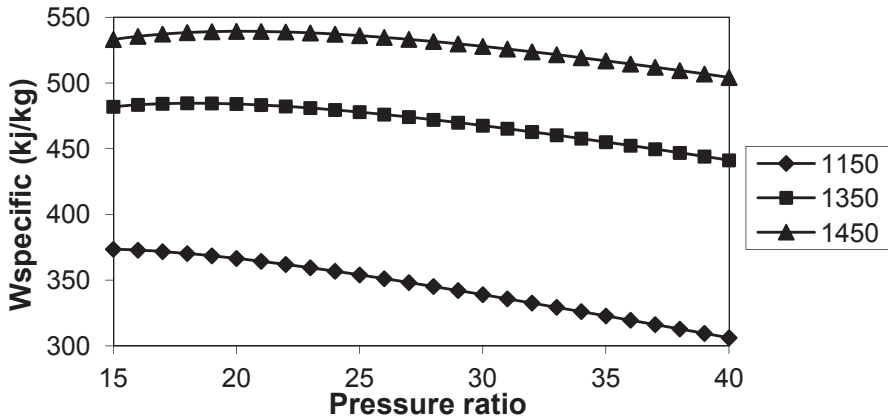


Fig. 11.15 Specific power of a simple-cycle gas turbine (CH_4)

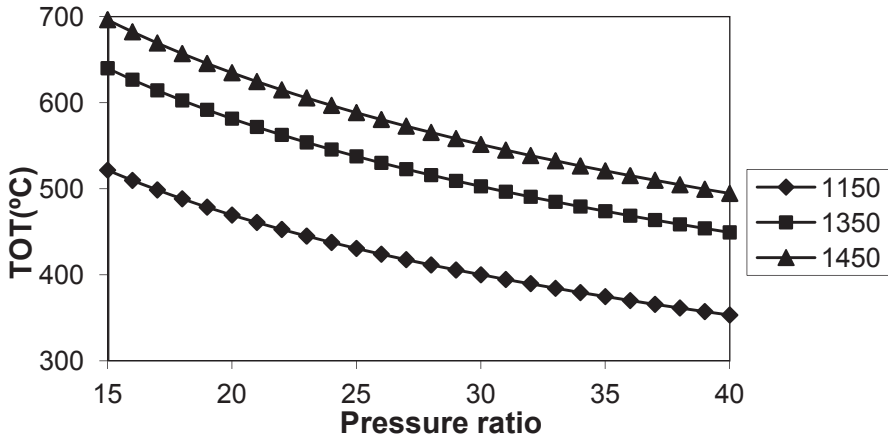


Fig. 11.16 Turbine outlet temperature with the simple cycle (CH_4)

with 129 kg/s exhaust mass flow and $\text{TOT}=436^\circ\text{C}$ (the specific power is 332.6 kJ/kg). The TIT is about 1250°C . So, one can verify that the order of magnitude of the specific power is in accordance with the results in Fig. 11.15. One can also verify the TOT in Fig. 11.16. Again, precise verification is not possible, because the results for TOT strongly depend on the value of TIT and the value of the heat transfer coefficient κ . So, it is quite easy to reproduce the real values of specific power and TOT by adjusting TIT and κ . The fuel-air ratio (Fig. 11.17) is in the order of what we verified earlier. The ratio of the cooling flow rate to the air flow rate aspired by the compressor (Fig. 11.18) is on the order of 4–6%, but the simulations are done with very advanced values of heat transfer coefficient κ and effectiveness ε . Doubling the value of κ means, in principle, doubling the value of the cooling air flow rate.

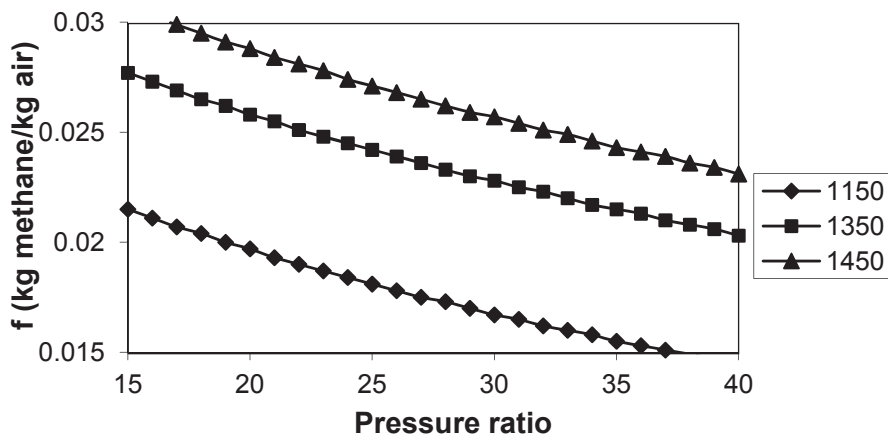


Fig. 11.17 Fuel flow rate to inlet air flow rate with the simple cycle (CH_4)

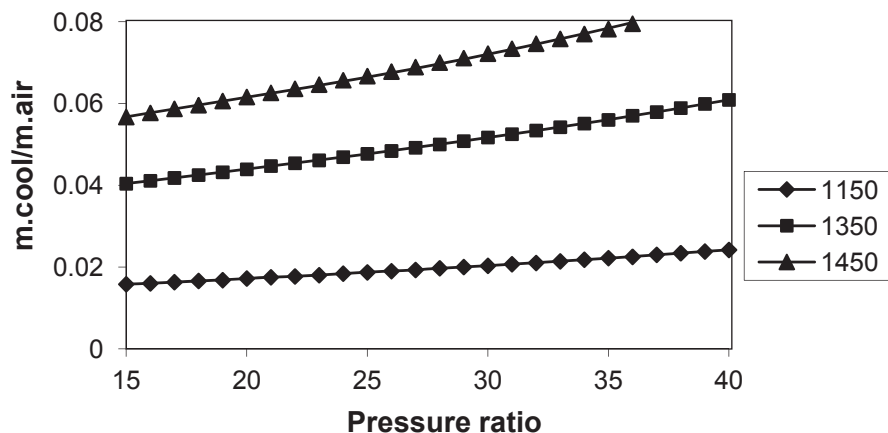


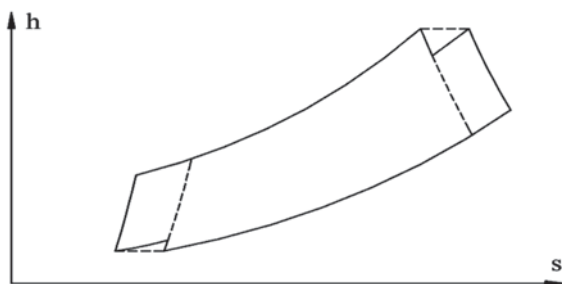
Fig. 11.18 Cooling flow rate to inlet air flow rate with the simple cycle (CH_4)

11.4 Performance of Power Gas Turbines with Enhanced Cycles

11.4.1 Compression with Intercooling

Incorporation of an intercooler into the compressor reduces compressor work. But on the other hand, air led to the combustion chamber needs more heating. An additional effect is reduced cooling flow rate, as the cooling air becomes colder. Intercooling at an early stage in the compression is advantageous for efficiency. The positive effect may be understood by considering a cycle with intercooling as a

Fig. 11.19 Cycle with intercooling in the compressor and reheat in the turbine



superposition of two cycles, as sketched in Fig. 11.19. The same figure also shows a similar interpretation of reheat within the turbine.

Intercooling may be considered as adding a cycle with a lower pressure ratio than with the original cycle, but with better component efficiencies. The compression and the expansion paths run almost parallel, which implies that the additional cycle approximately features the efficiency with ideal components. The exponent of the pressure-temperature relation is $\eta_{\infty} c_{pa} / R$, which is about 3.20. For pressure ratios 20 and 40, the efficiency of the additional cycle is about 0.61 and 0.68, according to formula (11.34) with an adapted exponent. With these high values, intercooling may constitute a significant efficiency gain if the pressure ratio of the additional cycle is not very much lower than that of the main cycle. The above is not exact, as there is an optimum pressure ratio with intercooling. With the simulation methodology used here, the optimum pressure ratio for placing the intercooling comes at about 1.7 for compressor pressure ratio 15 and at about 2.2 for compressor pressure ratio 35 (results not shown in a figure). The optimum intercooling pressure ratio depends somewhat on TIT. The efficiency gain comes at about 1.5% for compressor pressure ratio 15 and at about 5% for pressure ratio 35 (results not shown in a figure). These results are obtained with neglect of pressure losses in the intercooler. So, the performance gain is lower in reality. But that there is a potential for gain is without any doubt. In particular, intercooling is attractive for a gas turbine with high compressor pressure ratio.

There only exists one intercooled gas turbine for power generation, the LMS100 by GE (see website of General Electric). It is an aero-derivative with pressure ratio 42, TIT of about 1380 °C and it attains 46% efficiency. A machine with these features without intercooling would realise an efficiency of about 44% according to Fig. 11.14, but this value is somewhat optimistic. We may compare with the simple-cycle aero-derivative machine LM6000 of GE, with pressure ratio 29.5 and TIT of about 1250 °C. It attains about 41.5% efficiency. The corresponding value in Fig. 11.14 is about 42%. So, Fig. 11.14 overestimates somewhat. Taking this into account, we may conclude that the gain by intercooling with the LMS100 is about 2.5%. This is much lower than the result of the theoretical simulation, but still appreciable. The lower gain in practise is mainly due to pressure losses in collecting the air with a volute after the LP compressor, leading the air to a cooler and bringing the air to the entrance of the HP part of the compressor by a volute. The LMS100

has an LP compressor with 6 stages and a HP compressor with 14 stages. The turbine is split into three parts: two stages HP, two stages IP and five stages LP. There are three shafts. The LP part of the turbine is the power turbine driving the load on the hot end side of the machine. Assuming that the compressor stages all have the same pressure ratio, the pressure ratio of the LP compressor would be about 3, which is a value in accordance with the results of the simulation methodology for optimum intermediate pressure.

11.4.2 *Expansion with Reheat*

Adding reheat to the turbine, which means expanding the combustion gas in one or more turbine stages and reheating it to the original TIT, is principally advantageous for efficiency, if the intermediate heating occurs at an early stage of the expansion. The reason is similar to that with compressor intercooling, as is clear from Fig. 11.19. The exponent of the pressure-temperature relation is $c_{pg} / R\eta_{\infty t}$, which is about 4.80. For pressure ratios 20 and 40, the efficiency of the additional cycle is about 0.464 and 0.536 according to formula (11.34). These values are much less attractive than with intercooling, but are still higher than for the basic cycle. Reheat causes, of course, a higher need for cooling flow, which degrades somewhat the resulting efficiency. Further, there are pressure losses in the second combustion chamber. Whether or not efficiency gain is possible in reality is a matter of debate in the literature [9]. With the simulation methodology used here and ignoring the pressure drop in the second combustion chamber, a small efficiency gain is obtained for larger pressure ratios. There is no gain for compressor pressure ratios lower than about 20 and the gain is about 2.5% for compressor pressure ratio 35 (results not shown in a figure). Moreover, the gain increases somewhat with lower TIT. From these simulation results, we conclude that reheat is feasible with high pressure ratio and preferably with lower TIT. Turbine reheat may be combined with compressor intercooling. The effects approximately add. But there are no gas turbines with combined intercooling and reheat.

At present, there is only one machine with reheat: Alstom GT24/GT26 (see website of Alstom). GT26 is the 3000 rpm version, with pressure ratio 35 and TIT about 1250°C. The efficiency is 40%. According to Fig. 11.14, the efficiency would be about 42% without reheat. This last value is probably somewhat optimistic, but nevertheless shows that there is no efficiency gain by the reheat. For completeness, we have to mention that the objective of Alstom is to reach good efficiency in combined-cycle mode, which requires that the turbine outlet temperature is high enough (see Sect. 11.4.4). With reheat, the TOT of the GT24/GT26 comes at about 605°C, which is much higher than would be the case without reheat (probably around 425°C according to Fig. 11.16). Reheat forms, of course, a technical complication. In the GT24/GT26, the second combustion chamber is placed after the first turbine stage and the turbine has five stages in total. The combustion gas is led through 24 rectangular orifices with triangular vortex generators placed in these. The fuel is in-

jected by lances and surrounded by injected air. Fuel and air mix through the vortex motion and combustion takes places in the second annular combustion chamber.

11.4.3 Recuperator

Incorporation of a recuperator, i.e. a heat exchanger where the turbine exhaust gas heats the air delivered by the compressor, is advantageous for efficiency with lower pressure ratios. For efficiency gain, the outlet temperature of the compressor must be lower than the turbine outlet temperature. With a recuperator, it is always advantageous to provide intercooling on the compressor as well. By this, compressor work is reduced and turbine cooling is more efficient. That there is always a gain in efficiency may be understood from the observation that lowering of the temperature at compressor outlet due to the intercooling is compensated by heating by the recuperator, with no need for an increase of the fuel flow rate. By this we also understand that the most efficient intercooling is reached by the minimum of the compressor work, which means equal pressure ratios before and after the intercooling. Figure 11.20 shows the efficiency by combined recuperator and intercooling. The air is cooled halfway the compression until the inlet temperature (minimum compressor work). The recuperator has effectiveness 0.7. Pressure loss is set to 0.02 bar at the air side of the intercooler and the same value is used at the air side and combustion gas side of the recuperator. The efficiency comes to about 47% for TIT above 1300 °C, almost independent of the pressure ratio.

Reheat, enhancing the efficiency, could be added to a cycle with recuperator. Intermediate cooling in the compressor combined with intermediate heating in the turbine is advantageous, in principle. The reason is that an infinite number of intermediate coolers and intermediate heaters results in a Carnot cycle. But, reheat causes TOT to increase and the recuperator must be able to withstand the higher

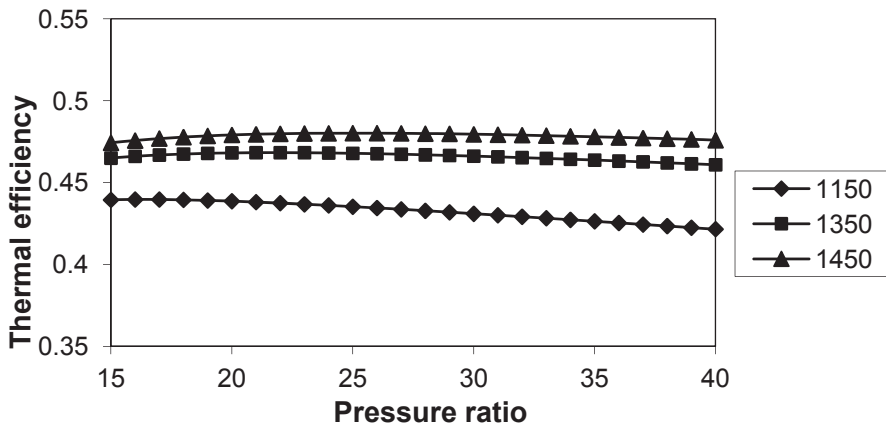


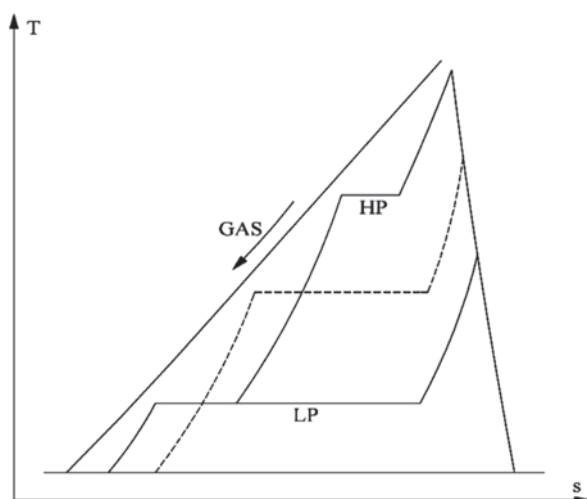
Fig. 11.20 Efficiency of a cycle with intercooling and recuperator (fuel CH_4)

combustion gas temperature. This is a technical problem. There are no gas turbines with recuperator and reheat. The cycle with recuperator and intercooling frequently occurs in marine applications. Implementation of intercooling is easily realised due to the availability of cooling water. Good efficiency is already attained with a lower TIT and low pressure ratio. For completeness, we have to mention that many marine gas turbines are aero-derivatives and that these have a large pressure ratio. The smaller gain in efficiency with intercooling for large pressure ratio is less attractive and the intercooler requires space. Military ships are therefore often equipped with simple-cycle gas turbines.

11.4.4 Combined Gas and Steam Cycles

In a combined-cycle system, the exhaust gas of a gas turbine is used for steam generation in a recovery boiler and led to a steam turbine. For good efficiency of the steam cycle, the inlet temperature of the steam turbine must be sufficiently high. Figure 11.21 sketches the cooling of the combustion gas and the heating of the steam in the T-s diagram of the gas, with rescaled entropy for steam such that gas and steam temperatures correspond to each other, as on the surfaces of the steam generator. The dashed line is the steam path for a single-pressure steam generator. A so-called pinch point forms, which is the smallest temperature difference at the beginning of the evaporation of the water. Due to the pinch point, the temperature difference is quite high between the steam leaving the steam generator and the gas entering it. A similar phenomenon occurs at the outlet side of the gas. These differences may be reduced by using two pressure levels in the steam generator, as shown by the full lines. In practice, even three pressure levels with reheat between the high pressure part and the intermediate pressure part are used. With a triple-pressure

Fig. 11.21 Single pressure level (*dashed line*) and dual pressure level (*full line*) steam generation in a recovery boiler



reheat cycle, the steam cycle efficiency is about 38.5% at gas inlet temperature of 527°C [5]. The corresponding pressure levels are about 120, 15 and 4 bar. The efficiency values are 40% at 577°C and 40.8% at 647°C. The efficiency drops to 34% at 477°C and 31.5% at 427°C. These efficiencies are based on the heat available in the gas by cooling it down to 20°C. The importance of a high inlet temperature at the gas side is obvious. This effect is similar as with a steam cycle with combustion. The efficiency does not attain the 43–44% level as with a fossil fuel plant, due to impossibility of incorporating regenerative feed water preheating and combustion air preheating with combined cycles. Feed water preheating by extraction steam could, in principle, be applied, but would result in a higher outlet temperature at the gas side. Since there is no combustion, the remaining heat cannot be used for preheating combustion air. This makes feed water preheating useless. The cited efficiencies can be improved somewhat by optimisation of the pressure levels [5], but the highest level then becomes much higher (the optimum levels are about 220, 28, 2.2 bar), which means a higher cost of the steam generator and the steam turbine.

Figure 11.22 shows the efficiency obtained with simulation of the combined cycles, with the efficiencies of the steam part as given above. A 96% efficiency of the recovery boiler is assumed. The obtained efficiency is in the order of 57% for pressure ratio above 20 and TIT around 1350°C. This efficiency value is typical for current gas turbines of the F-class (see explanation hereafter). The figure shows that the efficiency is almost not dependent on pressure ratio. So, a high pressure ratio is not useful, but it is not harmful either. The efficiency improves by a higher turbine inlet temperature. This is different from the simple cycle (Fig. 11.14), where the efficiency does not benefit from higher TIT. This observation demonstrates the effect of the better efficiency of the steam cycle with higher inlet temperature. With this observation, we also understand the benefit from the reheat as with the GT24/26 machine of Alstom. The combined-cycle efficiency may be further improved by closed loop steam cooling. The heat removed from the gas turbine by cooling is then

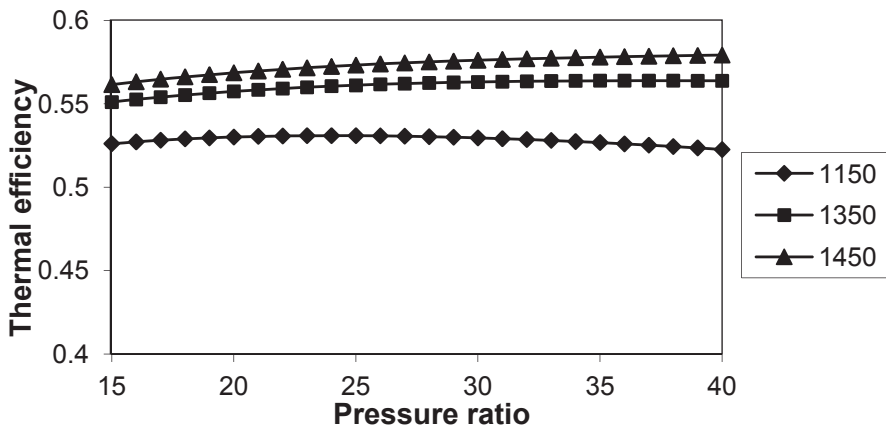


Fig. 11.22 Efficiency of combined gas and steam cycles (CH_4)

used for a superheating part in the steam cycle. With current machines (2014) with steam cooling, the combined-cycle efficiency is above 61 %.

Steam cooling has for a long time been considered as an essential way to reach 60% efficiency of combined steam and gas turbines. With respect to technology steps, it has become customary to denote gas turbine types with subsequent letters of the alphabet. Current classes are E, F, G and H (A, B and C are older types, but some still exist). Class E refers to machines with convection and impingement cooling, originally with a turbine inlet temperature (TIT) around 1100 °C and reaching about 50% combined-cycle efficiency. Modern versions of these machines reach a TIT of 1250 °C due to use of thermal barrier coatings (TBC) and directionally solidified blades. Class E machines are very robust and are typically used with crude fuels, which cause deposits in the turbine, making film cooling impossible. Class F means machines with film cooling, TBC and directionally solidified blades. These allow TIT in the order of 1350 °C and reach above 55% combined-cycle efficiency, typically around 57–58%. Class H meant up to some years ago machines with closed loop steam cooling both in stationary and rotating parts, advanced TBC and single-crystal blades in the first stage of the turbine part. These machines allow TIT in the order of 1450 °C, even 1500 °C, and reach combined-cycle efficiency above 60%. The most recent turbine with closed-loop steam cooling is the GE 9HA from General Electric. The version 02 reaches 470 MW and 41.5% efficiency in simple-cycle mode and 710 MW and 61.4% efficiency in combined-cycle operation. Class G machines have closed-loop steam cooling only in stationary parts, which means steam cooling of the liners with can-annular combustion chambers, the transition pieces and the vanes of the first stages of the turbine part. These machines have a TIT up to 1500 °C, similarly to class H machines, and reach 58–59% combined-cycle efficiency. Steam cooling is still used by the manufacturers General Electric and Mitsubishi, but has been abandoned by Siemens. The reason is that the role of combined gas and steam turbine power plants has moved somewhat from base-load plants to mid-load plants. By mid load we mean plants which follow the variation of the electricity consumption on the time scale of the day. The need for more mid load comes from the growing fraction of electricity produced by wind turbines and solar cells. Combined steam and gas turbines with steam cooling of the gas turbine have a large thermal inertia. This is avoided with pure air cooling. In the past years, much effort has been made by manufacturers to decrease the start-up time of gas turbines. With current F-class machines, the time needed for reaching full power of the gas turbine (not including the steam turbine) starting from standstill has been reduced to about 10 min, which was about 30 min up to 10 years ago. This is not possible with big thermal inertia. It is possible to obtain above 60% combined-cycle efficiency with air-cooled machines. This is proved by the SGT5-8000H machine by Siemens. Siemens describes the machine as H-class, although there is no steam cooling, to express the advanced technology level. The improvement with respect to the F-class comes from improved component design. Compressor efficiency is better due to improved blade design. Turbine efficiency is better, mainly due to a clearance control system (displacement of the shaft in axial direction). This improves the simple-cycle efficiency from 39.5% of the SGT5-4000F to 40% with

the SGT5-8000H. The combined-cycle efficiency is raised by the higher TIT (about 1500 °C) obtained with better TBC and improved cooling and optimisation of the triple-pressure reheat steam cycle (170 bar/600 °C; 35 bar/600 °C; 5 bar/300 °C). The power is 400 MW in simple-cycle mode. In combined-cycle mode, currently (2014), the power is 600 MW and the efficiency is 60.75 %. The most recent gas turbine by Mitsubishi (2014) is the M701J, called of J-class, with power 470 MW and efficiency 41.0% in simple-cycle operation and 680 MW and 61.7% in combined-cycle operation. It has a steam-cooled combustor, but air cooling in the turbine part. The TIT is 1600 °C.

11.4.5 Steam Injection

In a combined-cycle system, steam is generated in the recovery boiler and applied in a steam turbine. But steam injection into the gas turbine is possible as well. Injection of steam into the combustion chamber is the most efficient way, as the mixture of combustion gas and steam then enters the turbine at the original TIT. This requires an increase of the fuel flow rate in order to heat the steam until the TIT. Efficiency with steam injection is lower than with combined cycles, as the steam cycle is less favourable, being identical to the gas cycle. The highest pressure in the cycle is far too low for the steam (30 bar compared to 250 bar), the lowest pressure is far too high (1 bar compared to almost vacuum). The much higher temperature does not compensate for this. Figure 11.23 renders the efficiency attained with the same assumed characteristics of the recovery boiler as with combined cycles, with the application of one pressure level within the recovery boiler at a pressure 3 bar above the gas pressure in the combustion chamber and assuming 10 °C temperature difference at the pinch point. The gain in efficiency with respect

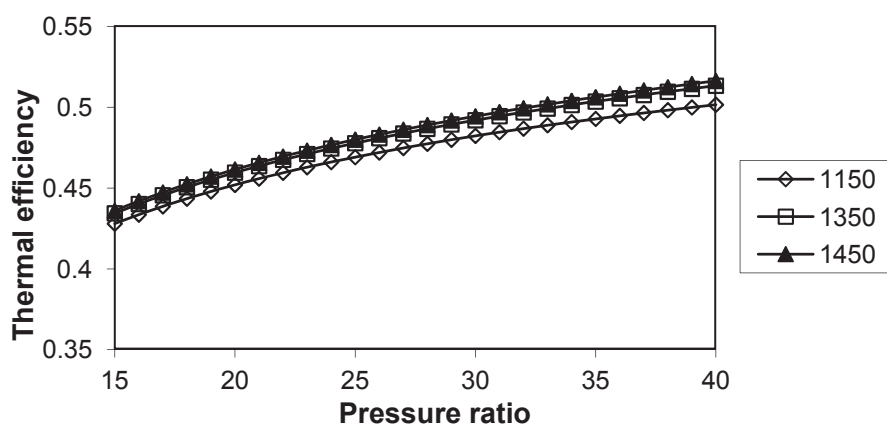


Fig. 11.23 Efficiency of a steam-injected gas turbine (CH₄)

to the simple cycle (Fig. 11.14) is about 8% points, independent of pressure ratio and TIT. For a pressure ratio above 35, the efficiency is above 50%. Difficulties with steam injection are that the steam flow rate is rather high (of the order of 15% of the air flow rate at pressure ratio 30 and TIT=1350°C) and that the required cooling air flow also becomes rather big (also of the order of 15% for pressure ratio 30 and TIT=1350°C). Providing a simple-cycle gas turbine for steam injection with these steam and cooling air flow rates is just impossible. State-of-the-art gas turbines allowing steam injection are limited to steam injection flow rates in the 12% order (e.g. GE LM6000 with steam injection). Adaption to higher steam flow rates is technically possible, but requires a turbine adaption to a higher flow rate, and as a consequence, efficiency loss when running without steam injection.

Steam-injected gas turbines are typically used with cogeneration plants (CHP: combined heat and power). The gas turbine is used then to generate mechanical power for driving an electric generator. Exhaust gases are used for the generation of steam applied in process heating. Steam is only injected into the gas turbine when heat is not required. The steam injection is rather exceptional and for this reason the machine is not optimised for steam injection operation. The steam-loaded exhaust gas is discharged into the atmosphere for the same reason. This means that there is no gas cooler for recovery of the water corresponding to the injected steam, although complete recovery is possible with natural gas (CH_4) as fuel as the combustion then generates much water. With a steam-injected gas turbine continuously running in steam-injected mode, steam cooling would be a profitable option. The cooling air extraction from the compressor would be unnecessary and the steam flow rate to be injected in the combustion chamber would be strongly reduced. Steam required for cooling might also be mixed into the gas flow. Contrary to closed-loop steam cooling, there is no technical implementation problem, the cooling circuit being the same as with air cooling.

References

1. Baehr HD (1966) *Thermodynamik*, 2nd edn. Springer, Heidelberg
2. Chiesa P, Macchi E (2004) A thermodynamic analysis of different options to break 60% electrical efficiency in combined cycle power plants. *J Eng Gas Turbines Power Trans ASME* 126:770–785
3. Cohen H, Rogers GFC, Saravanamuttoo HHH (1996) *Gas turbine theory*, 4th edn. Longman Group, London. ISBN 0-582-23632-0
4. El-Masri MA (1986) On thermodynamics of gas turbine cycles: part 2—A model for expansion in cooled turbines. *J Eng Gas Turbines Power trans ASME* 108:151–159
5. Franco A, Casarosa C (2002) On some perspectives for increasing the efficiency of combined cycle power plants. *Appl Therm Eng* 22:1501–1518
6. Fu WL, Wright LM, Han JC (2005) Heat transfer in two-pass rotating rectangular channels (AR=1.2 and AR=1.4) with smooth walls. *J Heat Transfer ASME* 127:265–277
7. Razak AMY (2007) *Industrial gas turbines; performance and operability*. CRC Press, Florida. ISBN 978-1-84569-205-6

8. Sanjay Y, Singh O, Prasad BN (2008) Influence of different means of turbine blade cooling on the thermodynamic performance of combined cycle. *Appl Therm Eng* 28:2315–2326
9. Sheikhbeigi B, Ghofrani MB (2007) Thermodynamic and environmental considerations of advanced gas turbine cycles with reheat and recuperator. *Int J Environ Sci Technol* 4:253–262
10. Wilcock RC, Young JB, Horlock JH (2005) The effect of turbine blade cooling on the cycle efficiency of gas turbine power cycles. *J Eng Gas Turbines Power Trans ASME* 127:109–120

Chapter 12

Thrust Gas Turbines

Abstract Due to the high power compared to weight and volume, gas turbines are very suitable components of aircraft propulsion systems. Almost all modern aircraft propulsion is gas turbine based. Only with low power (<300 kW), as for very light aircraft, are reciprocating engines used. Aircraft propulsion systems exist in a wide variety of types. The basic principle is always that the propulsive force (thrust) is reaction onto the acceleration of an air flow. In this chapter, we discuss the different systems and we analyse the performance of the core part, which is a gas turbine, and the performance of double-flow engines with mixed and unmixed jets, which are the most commonly used types. The chapter is concluded by a discussion of some technological aspects.

12.1 Thrust Generation

There are three basic propulsion systems: propeller, reactor and rocket. The first two systems are applied in conventional aircraft.

12.1.1 Screw or Propeller

A propeller is a rotor with blades, similar to aircraft wings, but twisted. The blades provide acceleration to a part of the air around the aircraft. A force is generated as reaction to this acceleration. With an aeroplane, the propeller generates the propulsive force, called *thrust*, while lift force is produced by the wings. Helicopter rotors generate both thrust and lift force. Helicopters therefore are sometimes called rotary wing aircraft, to distinguish them from fixed wing aircraft. The acceleration of the surrounding air is generated by forces exerted onto the blades by the relative air flow. Thrust may thus also be considered as a result of the blade forces. Figure 12.1 represents a blade section and the forces on this section.

As an absolute coordinate system, we take a frame bound to the aircraft (moving relative to the surrounding air) and as a relative system, a frame rotating with the propeller. The inflow velocity in the absolute frame is v_o , the flight velocity. Flow accelerates due to propeller action. Within the plane of the propeller, the velocity in

the absolute frame v_l exceeds v_0 . Blade speed is denoted with u , relative velocity with w_l . The relative velocity forms an angle of attack α to the blade. The blade reference line is e.g. the zero-lift line. The stagger angle of the blade is θ (in Fig. 12.1, with respect to the tangential direction). A typical flight velocity is 150 m/s. The blade speed at the tip is typically around 250 m/s. The lift force is perpendicular to the relative velocity (dL). The drag force is along this velocity. Lift may be resolved into an axial component dT , contributing to the thrust and a tangential component dN . The latter causes the power taken from the shaft: $dP = u dN$. The drag force dD has an axial component diminishing the thrust and a tangential component enlarging the power consumed.

Figure 12.1 renders the velocity in the absolute frame on the position of the blade into the axial direction. This is a simplification. In reality, there is also a tangential component as a reaction to the blade forces. This component has two principal consequences. First, the power transferred by the lift increases for the same thrust (dT). The power exchanged is

$$-\overline{dL} \cdot \vec{u} = -\overline{dL} \cdot \vec{v}_1 \quad (\overline{dL} \cdot \vec{w}_1 = 0) \quad \text{and} \quad -\overline{dL} \cdot \vec{v}_1 = -\overline{dL} \cdot \vec{v}_{1a} - \overline{dL} \cdot \vec{v}_{1t}.$$

The first expression demonstrates that lift is a pure active force, as the power taken from the shaft is completely transferred to the flow as mechanical energy (see Chap. 2). The tangential component of v_l increases the power exchanged for given thrust dT , thus given axial velocity rise, as the tangential velocity component is in the sense of blade speed. The second consequence of the tangential component is a change of the active and dissipative parts of the power exchanged by the drag force:

$$-\overline{dD} \cdot \vec{u} = -\overline{dD} \cdot \vec{v}_1 + \overline{dD} \cdot \vec{w}_1.$$

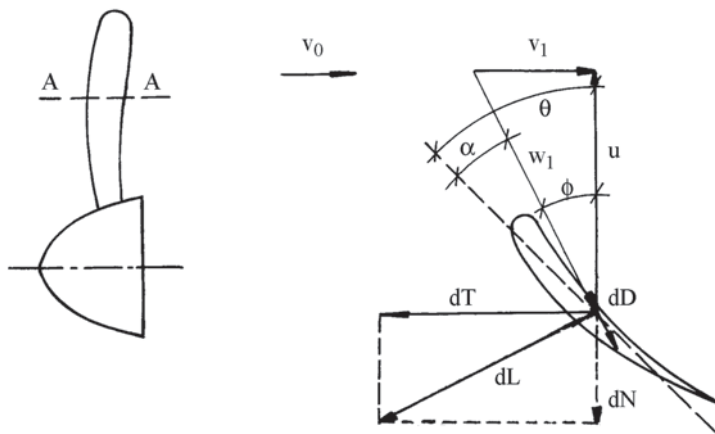


Fig. 12.1 Force generation onto a propeller blade segment

The $\overline{dD \cdot w_1}$ part is the dissipated part of the power exchanged (see Chap. 2). This part reaches the flow as heat. The $-\overline{dD \cdot v_1}$ part causes exchange of mechanical energy. This part is negative with the velocity triangle drawn in Fig. 12.1. In other words, mechanical energy is taken from the flow by the drag force. The tangential component of the velocity v_1 changes somewhat both components of the power exchanged by the drag force.

We further analyse the flow through the propeller with the simplified velocity triangle in Fig. 12.1, so with velocity v_1 in axial direction. The through-flow in one-dimensional representation is sketched in Fig. 12.2. The propeller is represented by a plane perpendicular to the flow. Based on continuity of the mass flow, the axial velocity in the flow through the propeller ($v_1 = v_2$) remains constant. Sections (0) and (3) lay so far upstream and downstream that there is atmospheric pressure in these sections. A control volume is formed with the envelope of a streamtube through the rotor and the inlet and outlet sections (0) and (3). The thrust generated by the rotor is denoted by T . The force denoted by T in Fig 12.2 represents the force onto the flow, so in the sense opposite to the thrust.

From the assumptions follows that thrust is (see Chap. 1, Exercise 1.9.4):

$$T = \dot{m}(v_3 - v_0), \quad (12.1)$$

where \dot{m} is the mass flow rate through the propeller. This result requires the assumption that the resulting force by the pressure and the shear stress on the control volume surface equals zero. In case of absence of losses (see also Sect. 12.1.2), this result is achieved by considering a second streamtube, concentric around the streamtube drawn in Fig. 12.2, with an envelope so far from the propeller that the pressure on it equals atmospheric pressure. As there is no work within the second streamtube, the inflow and outflow velocities thus equal v_0 . The consequence is that

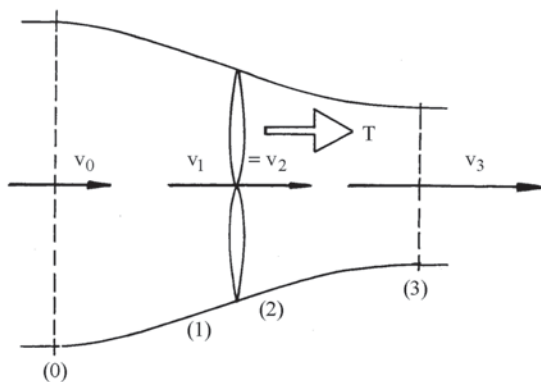


Fig. 12.2 Through-flow of a propeller in one-dimensional representation

there is no change of momentum flux in this streamtube. The resulting force on the entire surface of the second streamtube thus must equal zero. This demonstrates that the resulting force on the envelope of the streamtube through the propeller in Fig. 12.2, in the absence of losses, equals zero.

In absence of losses and ignoring the tangential component of v_i , the power transferred to the flow is

$$T v_1 = \dot{m}(v_3 - v_0) v_1. \quad (12.2)$$

The power corresponding to the mechanical energy rise within the flow, termed *dynamic power* (because there is no pressure rise), is

$$P_{dyn} = \dot{m}(\frac{1}{2}v_3^2 - \frac{1}{2}v_0^2). \quad (12.3)$$

Equating (12.2) and (12.3) gives

$$v_1 = \frac{v_0 + v_3}{2}.$$

The dynamic power (12.3) is the theoretical power required to generate thrust (12.1). In reality, the power extracted from the propeller shaft is larger due to the generation of a tangential flow component, non-uniform axial velocity over the propeller and presence of loss mechanisms. These effects may be studied by means of a multiple streamtube analysis, analogous to the analysis in Chap. 10 on wind turbines (see also Chap. 2, Exercise 2.5.8). For the study of the gas turbine, a detailed analysis of the propeller is not needed, however. Expression (12.1) renders the theoretical value of the velocity increase to be provided by the propeller to the through-flowing air for the generation of the thrust T . Expression (12.3) renders the corresponding theoretical power to be supplied to the shaft by a motor. The real power is larger and the *propeller efficiency* is the ratio of the dynamic power to the shaft power. With analysis of the gas turbine, we assume a certain value of the propeller efficiency. This efficiency reaches about 0.90 with optimally designed propellers.

In propeller theory, the velocity rise locally across the propeller $\Delta v = v_1 - v_0 = v_i$ is called the induced velocity at the propeller and similarly, $\Delta v = v_3 - v_0 = v_{i\infty}$ the induced velocity far downstream ($v_{i\infty} = 2v_i$). The dynamic power (12.3) in propulsion theory is mostly called induced power in propeller theory. The propeller is driven by a motor, which is normally a gas turbine, because of the high ratio of power to weight and power to volume, as already mentioned. The gas ejected by the gas turbine contributes to the thrust. So, strictly spoken, a propeller driven by a gas turbine is a double-jet propulsion system (propeller + reactor, see next section). This explains the name *turbo-propeller* or simply *turboprop*. Double-jet thrust generation is discussed later in this chapter.

12.1.2 Reactor or Jet Engine

Figure 12.3 sketches the through-flow of a reactor. The term reactor refers to an air-breathing system that ingests air and ejects it as a jet with a higher velocity and possibly a pressure exceeding the atmospheric pressure. *Jet engine* is an equivalent term. Henceforth we often just use the term *engine*. The internal part of the reactor in Fig. 12.3 represents a gas turbine without any net shaft power. Its turbine part just drives a compressor. Due to the heating in the combustion chamber, the pressure drop within the turbine is lower than the pressure rise within the compressor. The remaining pressure difference to the atmosphere at the turbine outlet is applied in a nozzle to generate a thrust jet. In present systems, the air delivered by the compressor only partially flows through the combustion chamber and the turbine. Part of the compressor air bypasses the combustion chamber. In many systems, this air flows through a second concentric nozzle. There is then a hot jet and a cold jet. Both jets do not attain the same velocity. Further, we will see that for optimum efficiency, the cold jet velocity has to be somewhat lower than the hot jet velocity. In other systems, the bypass flow is mixed with the outlet flow of the turbine part and the mixed flow feeds a single nozzle. There is then only one thrust jet. So, we distinguish single-jet and double-jet engines. Figure 12.3 suggests a single-jet engine. We first analyse the single-jet engine.

The mass flow passing through the reactor in Fig. 12.3 is denoted with \dot{m} . We ignore the mass flow increase by fuel injection. We consider a control volume with an inlet section far upstream of the reactor and an outlet section at the exit plane of the nozzle. The nozzle outlet pressure is denoted with p_j and outlet velocity with v_j (the subscript j refers to the jet at the nozzle outlet). As the pressure distribution on the envelope of the reactor is not known a priori, we consider besides the streamtube through the reactor, a second concentric streamtube with an envelope so far from the reactor that the pressure on it equals atmospheric pressure. The control volume is formed by the envelope of the outer streamtube. We assume that pressure equals

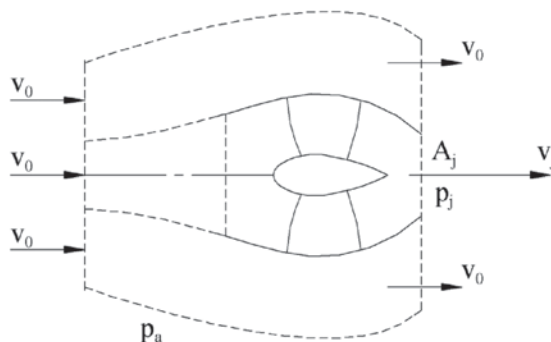


Fig. 12.3 Through-flow of a reactor (single-jet engine variant)

atmospheric pressure in the inlet and outlet planes of the outer streamtube. No energy is added to the flow that does not pass through the reactor. In the outlet plane of the outer streamtube, pressure is atmospheric and velocity thus equals inflow velocity (v_0).

The momentum balance is:

$$\dot{m}(v_j - v_0) = T - A_j(p_j - p_a),$$

or
$$T = \dot{m}(v_j - v_0) + A_j(p_j - p_a) = \dot{m} \Delta v + A_j \Delta p. \quad (12.4)$$

Thrust T thus consists of a momentum part and a pressure part. We notice that the thrust of a propeller (12.1) follows from expression (12.4) for $\Delta p = 0$. In order to absorb the pressure thrust into the momentum thrust, an *effective jet velocity* is defined by

$$v_{je} = v_j + A_j \Delta p / \dot{m},$$

resulting in

$$T = \dot{m}(v_{je} - v_0). \quad (12.5)$$

The nozzle outlet pressure can only exceed atmospheric pressure when choking occurs. In practice, this implies a convergent nozzle with a supercritical pressure ratio. The nozzle outlet is then almost sonic (sonic speed is not fully attained because of losses). Free expansion after the nozzle occurs with losses by oblique shocks. Controlled expansion in a divergent nozzle part may be more efficient. As thrust also may be calculated by a momentum balance on a control volume enlarged to encompass the free expansion, application of a loss-free divergent nozzle implies a thrust increase.

Determination of the possible benefit is rather simple. Isentropic expansion from temperature T_j and pressure p_j to atmospheric pressure results in the end temperature

$$T_e = T_j \left(\frac{p_a}{p_j} \right)^{\frac{\gamma-1}{\gamma}} = T_j \left(\frac{p_j - \Delta p}{p_j} \right)^{\frac{\gamma-1}{\gamma}}.$$

The attainable end velocity is

$$v_e^2 = v_j^2 + 2 C_p (T_j - T_e) = v_j^2 + 2 C_p T_j [1 - (1 - \epsilon)^{\frac{\gamma-1}{\gamma}}],$$

with $\varepsilon = \Delta p / p_j$.

$$\text{Thus: } v_e = v_j \sqrt{1 + \frac{2}{\gamma - 1} \frac{1}{M_j^2} [1 - (1 - \varepsilon)^{\frac{\gamma - 1}{\gamma}}]}.$$

With a choked nozzle, the effective outlet velocity is

$$v_{je} = v_j + \frac{p_j}{\rho_j v_j} \varepsilon = v_j \left(1 + \frac{1}{\gamma} \frac{1}{M_j^2} \varepsilon\right).$$

The gain is $\Delta v_j = v_e - v_{je}$. For $\gamma = 1.33$ and $M_j = 1$, this leads to

$$\varepsilon = 0.2 \quad : \quad \frac{\Delta v_j}{v_j} = 0.0013 \quad ; \quad \varepsilon = 0.5 \quad : \quad \frac{\Delta v_j}{v_j} = 0.0232.$$

The results above render the gain in absence of nozzle losses. Since the gain is small, the conclusion is that, unless the pressure ratio significantly exceeds the critical value, designing the nozzle with a divergent part is inefficient. Henceforth we will calculate with the effective jet velocity and consider the pressure at the outlet of the reactor as atmospheric pressure. This is not an approximation for the majority of turbojets with subcritical nozzles. As with a propeller, the theoretical power required to generate thrust equals the dynamic power. The power released by the fuel is much greater due to a number of loss mechanisms. These will be discussed later in this chapter.

Expression (12.5) is a theoretical thrust value. The thrust transferred to the aircraft is lower because of the drag on the nacelle (the envelope of the engine). Thrust according to (12.5) is called *uninstalled thrust*. Net thrust exerted by the engine on the aircraft is called *installed thrust*. The difference is the *installation drag*. Uninstalled engine thrust may be measured on a stationary test bench, as sketched in Fig. 12.4. The figure sketches the arrangement for measurement of the thrust at sea level. The inlet nozzle guiding the aspirated air into the engine is not connected to the engine. It is used for mass flow measurement based on inlet and outlet pressures. Momentum exchange of the jet lowers the pressure in the closed cabin around the engine. So, for maintaining atmospheric pressure, air has to be fed into the cabin (not shown). Comparison of the control volumes in Figs. 12.3 and 12.4 demonstrates that uninstalled thrust is measured. With uninstalled thrust, no losses between the inlet plane of the control volume in Fig. 12.3 and the engine inlet are assumed. The arrangement is similar for thrust measurement at altitude flight conditions. Then, the inlet air has to be cooled and lowered in pressure. The outlet gas has to be removed with a fan and the pressure in the cabin has to be controlled by adjustment of the air fed to the cabin. In practise, a correction to the measured

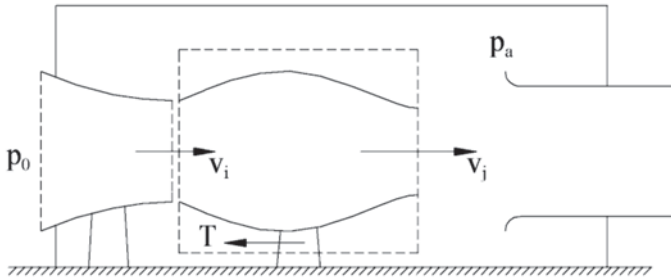


Fig. 12.4 Measuring uninstalled thrust of a jet engine

thrust is necessary because it is almost impossible to realise the correct inflow of the engine. The correction is deduced from the momentum flux determined from measured quantities at the inlet and the momentum flux from an accurate model of the flow approaching the inlet. Installation drag depends on flight conditions. This drag is normally calculated (measurement requires a very big wind tunnel). For calculation, the engine nacelle is divided into a front part (inlet) and a rear part (nozzle). Inlet drag results from ram effect (pressure build-up due to the obstruction by the engine) and friction on the front engine part. Nozzle drag results from friction and from non-uniformity of velocity and pressure due to curvature of streamlines in the flow around the nozzle.

12.1.3 Rocket

With a rocket, no air is aspirated. The ejected gas is generated in a combustion chamber by means of a fuel and an oxidiser. This makes the rocket engine suitable for use outside the atmosphere. The fuel and the oxidiser are the source of the thrust gas and are therefore called propellants. Propellants may be liquid or solid. With fluid propellants, the fuel and the oxidiser are separate liquids. A solid propellant is generally a mixture of a fuel and an oxidiser. A solid fuel may also be combined with a liquid oxidiser.

The thrust formula follows from the reactor formula with $v_0 = 0$:

$$T = \dot{m} v_{je} \text{ with } v_{je} = v_j + \frac{A_j \Delta p}{\dot{m}}.$$

The nozzle pressure ratio is always strongly supercritical with a rocket. The nozzle is thus converging-diverging. As ambient pressure mostly equals zero, the pressure thrust nevertheless is an important component of the overall thrust.

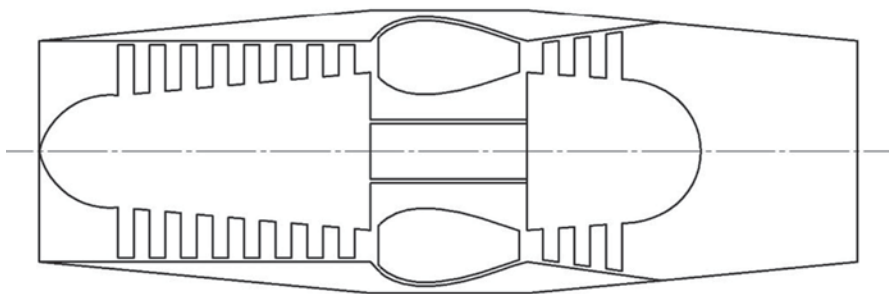


Fig. 12.5 Turbojet

12.2 Overview of Aircraft Gas Turbine Engines

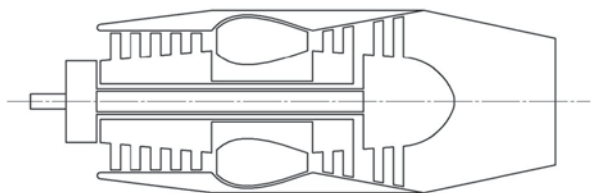
12.2.1 Turbojet

Figure 12.5 represents the simplest form of a jet engine, called *turbojet*. There is one internal flow successively passing through a compressor, a combustion chamber, a turbine and a nozzle. There is a single propulsive jet. This type, historically the first one, is not used anymore, as it is only efficient with flight Mach numbers above 2.5, as we will derive later. There are no such aircraft at present.

12.2.2 Turboprop and Turbo-Shaft

Figure 12.6 is a sketch of the gas turbine part of a turbo-propeller, called shortly a *turboprop*. At the front side of the engine, there is an outgoing shaft that drives the propeller through a gearbox. The figure suggests an epicyclic gearbox, but parallel axis gearboxes are used as well. The gas turbine has a nozzle contributing to the thrust. In the example, the compressor and turbine components are axial and there are two shafts. With smaller engines, the compressor may be composed of axial stages followed by a radial one. There are also single shaft engines. With two-shaft engines, it is typical that no compressor part is mounted onto the outgoing shaft (as in the figure). The turbine that drives the outgoing shaft is then a power turbine run-

Fig. 12.6 Turboprop and turbo-shaft



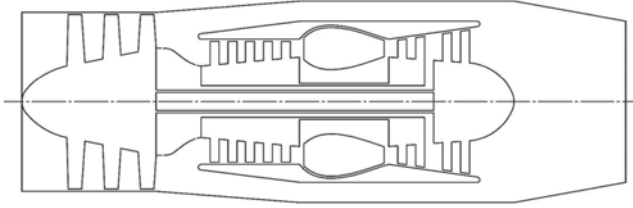


Fig. 12.7 Bypass turbojet

ning at a much lower rotational speed than the core part, i.e. the part on the external hollow shaft. A *turbo-shaft* is similar, but, in principle, no thrust is generated by a nozzle. So, basically, a turbo-shaft does not differ from a power gas turbine, except that a gearbox is integrated. A typical turbo-shaft application is helicopter rotor drive (but some thrust may be generated with an outlet nozzle). Such gas turbines are also applied to drive heavy vehicles as off-road trucks.

12.2.3 Bypass Turbojet

In a bypass turbojet, as sketched in Fig. 12.7, a part of the compressor air is diverted before the final compressor pressure is attained. This air does not pass through the combustion chamber and the turbine parts. It is mixed with the combustion gas that leaves the turbine parts. There are two internal air flows within the engine: a cold flow and a hot one. The mixed flows both feed the nozzle, generating a single jet. This engine is called *bypass turbojet* or bypass jet engine or just *bypass engine*. The bypass ratio, i.e. the ratio of the mass flow rates of the cold and hot flows, is typically between 0.5 and 1. The reason for organising the engine with two internal flows will be discussed in Sect. 12.5.

12.2.4 Turbofan

Figure 12.8 represents a *turbofan*. There are two jets generated by separate nozzles. The compressor part feeding the cold nozzle is called a fan, as its pressure ratio is quite moderate (1.5–1.7). The central part of the fan delivers air passing through the combustion chamber. In current turbofans the ratio of the mass flow rates of the cold flow to the hot flow is 5–7. As with the bypass engine, this ratio is called the bypass ratio. The practical optimum is however about 10–15 for a typical airliner. So there is a reason to increase the bypass ratio. The newest turbofan types (2014) feature a bypass ratio of 10–12. In some turbofan engines, the cold and hot jets partially mix in a common nozzle. The term turbofan is still applied for these types. Further, there is a tendency nowadays to use the term fan also for the low-pressure compressor part in a bypass engine. This makes the distinction between a bypass engine and a

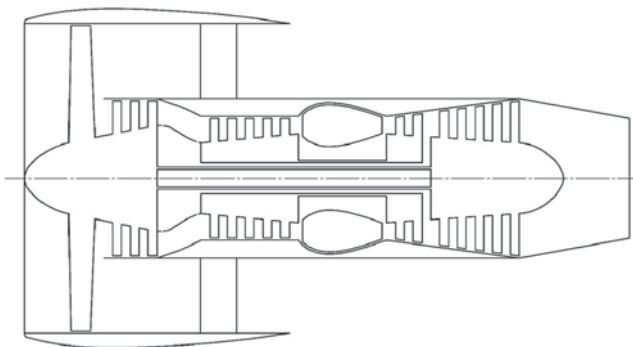


Fig. 12.8 Turbofan

turbofan rather vague. Fundamentally, there is indeed not much difference. Both are jet engines with two internal flows. The variants are that the flows feed separate nozzles or that the flows partially or fully mix at the entrance of a common nozzle. We will analyse in Sect. 12.5 that mixing of the flows principally is beneficial for efficiency, but efficient mixing is only possible for lower values of the bypass ratio.

Figure 12.9 renders a modern turbofan engine: a Trent800 from Rolls-Royce. It is a three-shaft engine. The internal shaft bears the fan and the low-pressure turbine (5 stages). The fan diameter is 2.80 m. There are eight stages in the intermediate-pressure compressor and six stages in the high-pressure compressor. The inlet guide vanes and the vanes of the first two stages of the IP compressor are adjustable. The HP turbine and IP turbine have one stage. Sea level thrust is 330–420 kN, depending on the version. The bypass ratio is 5.7–6.2. Similar engines exist with two shafts. In these engines, there is a small IP compressor part, called a *booster*, running together with the fan, as in Fig. 12.8.

12.2.5 *Prop-fan and Unducted Fan*

A turboprop may be considered as an extreme form of turbofan, namely with a very great bypass ratio. This amounts to about 50. There are propulsive systems that are classified in between the turboprop and the turbofan. They are denominated *prop-fan* or *unducted fan* (UDF). The thrust comes from two *contra-rotating propellers* (two propellers with the same axis of rotation, but rotating in opposite senses). The reason for their existence is that the optimum bypass ratio for flight Mach number 0.85 is between 10 and 15 and that this optimum ratio increases with lowering of the flight Mach number (see Sect. 12.5). Turbofan engines with high bypass ratio have a large fan diameter. The largest turbofans currently (2014) in use on large airliners have a diameter near to 3 m: e.g. Rolls-Royce Trent800 series, General Electric GE90 series, Pratt and Whitney PW4000 series (see websites of these manufacturers) with thrust at sea level of the 400 kN order. The bypass ratios are 6–8. A large

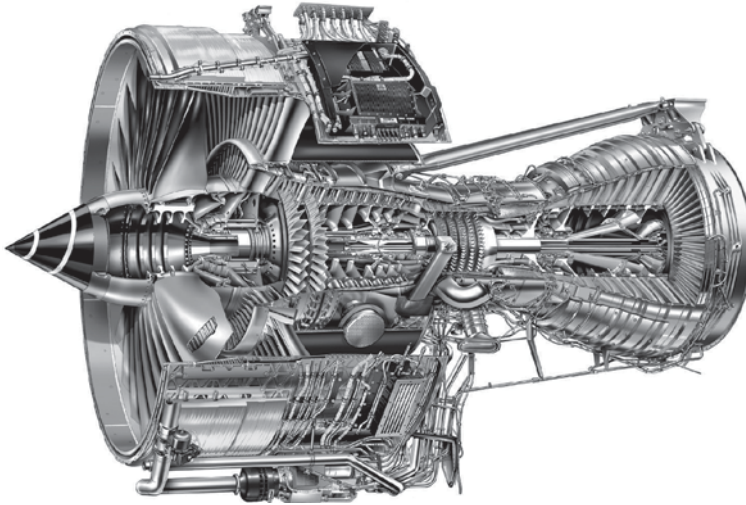
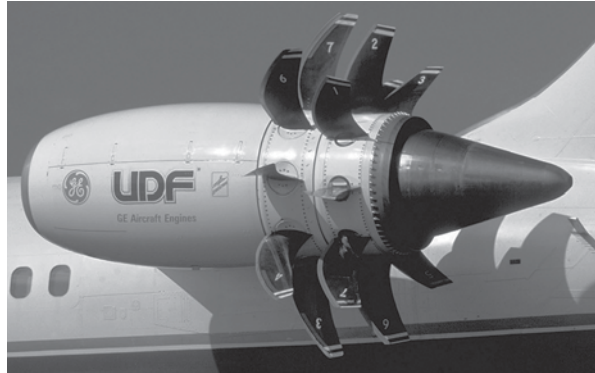


Fig. 12.9 Modern turbofan engine: Trent800. (Courtesy Rolls-Royce)

turbofan engine is mounted under the wings, which requires sufficient distance between the wings and the ground. So, further increase of the bypass ratio and thus the fan diameter becomes problematic. Manufacturers develop now turbofan engines with bypass ratios above 10 (Rolls Royce Trent1000 series, General Electric GENx series), with fan diameter around 3.25 m and sea level thrust around 500 kN. A cruise flight Mach number 0.85 is typical for airliners, as with this flight Mach number shocks in the flow over the suction side of the wings remain rather weak. The flight speed is around 900 km/h at speed of sound about 300 m/s ($T=225$ K at 10 km height). But fuel saving might be realised with a somewhat lower flight Mach number (0.70–0.75). Then, shock losses disappear and a larger part of the wings can be operated with laminar boundary layers (shocks create the risk of separation of a laminar boundary layer). The optimum bypass ratio then increases and the diameter of a turbofan for a large airliner may become impractically large. On the other hand, conventional turbo-propellers are limited in flight speed to about 550–600 km/h. The reason is the necessary limitation of the Mach number of the relative flow attacking the propeller tip. For example, with flight speed 150 m/s (540 km/h) and tip speed 250 m/s, the oncoming flow speed at the propeller tip is, based on the velocity triangle with these speeds, about 290 m/s (the actual speed is somewhat larger due to acceleration of the flow). The corresponding Mach number at sea level (velocity of sound 340 m/s) is about 0.85. So, a larger flight speed requires a lower tip speed of the propeller. For the same velocity increase through the propeller, the solidity then has to be larger. This means a higher number of blades. Further, the optimum bypass ratio at flight speed around 750 km/h may be around 25. The corresponding velocity increase in the flow through the propeller is then larger than in a conventional propeller, but smaller than in a conventional turbofan. Contra-rotating propellers might be a solution. The tip speed is lower than with a conventional propeller and the work done per propeller is larger. The solidity is larger and so is the number

Fig. 12.10 High-bypass unducted fan. (Courtesy GE Aviation)



of blades. The flow turning per propeller is much larger, but the contra-rotation concept allows avoiding post-swirl. Figure 12.10 shows an engine, generally called an *unducted fan*, studied already for a long time by GE Aviation. The propeller blades are mounted on contra-rotating turbines in the rear part of the engine. The blades are swept back at the tips, in order to lower the Mach number of the velocity component perpendicular to the leading edge, as with backswept wings of an aeroplane. The blades have a compensating forward sweep at the hub. The diameter of the forward propeller is larger in order to avoid interference of the tip vortices with the rearward rotor. The pitch angle of the blades can be varied for adjustment of the thrust. The engine in Fig. 12.10 is a pusher, meant for mounting on the rear part of the aircraft fuselage, at a position much higher than the wings. The tip speed of the propellers is to be limited to about 200 m/s at flight velocity 200 m/s (720 km/h). This causes the tip speed of the turbine carrying the propeller blades to be very low. So, the stage work is low and many stages are required. For instance, the GE36 UDF has 14 stages in the LP-turbine driving the propellers (a stage is one blade row; there are no stationary parts). The LP-turbine of a turbofan is much smaller, albeit much bigger than the other turbine parts. The tip speed of the fan is around 400–450 m/s, which brings the tip speed of the driving turbine around 200 m/s. Typically, 5–7 stages are required for bypass ratios from 6 to 10.

An alternative for the low speed power turbine in an unducted fan is a fast running power turbine with a low number of stages, driving the propellers over a reduction gearbox, as with a conventional propeller. The gearbox is then epicyclic with two concentric contra-rotating outgoing shafts. A pusher type (propeller downstream of the gas turbine) and a tractor type (propeller upstream of the gas turbine) are both possible. The concept is called a *prop-fan*. Both variants have been studied for some time by Rolls Royce (RB3011). The tractor type is meant for mounting on the upside of the wings, as with many conventional propellers. A tractor type prop-fan, developed in Ukraine (the D27 by Ivchenko-Progress) is used since the 1980s on the Antonov An-70, which is a medium size transport aircraft. The front propeller with diameter 4.5 m has eight blades and provides the largest part of the thrust. The rear propeller has six blades. The shaft power is about 10 MW and the thrust is about 100 kN at sea level.

The main problem with the unducted fan and the prop-fan is the intense noise emission, much higher than with a conventional propeller. This problem impedes airliner use of these concepts. Further, the prop-fan is limited to medium size aircraft, requiring a thrust per engine of about 100 kN. The reason is the power limitation on the gearbox, currently to about 10 MW. The benefit of reduced fuel consumption would be more interesting with the larger class of engines with thrust of the 400 kN order for large airliners. The problem of noise emission has been under intense study for some time, but significant improvement is certainly still far away. The problem of noise emission can be weakened by shrouding the propellers. This has been studied in the past, but the concept is then not essentially different from a turbofan.

12.2.6 *Geared Turbofan*

A high bypass ratio implies a large fan diameter and a low tip speed of the blades of the driving LP-turbine. The bypass ratio of the turbofan engines under development nowadays (2014) is about 10, as already mentioned. The LP turbine driving the fan is large. The LP-turbine may be compacted by letting it run faster and driving the fan over a reduction gearbox, as with a propeller. The concept is called a *geared turbofan*. Currently (2014), a series of such engines is under development by Pratt and Whitney: the PW1000G series. The engine under test has an epicyclic gearbox with a speed ratio 3:1. The LP turbine has three stages. The bypass ratio is 12 and the thrust at sea level is 100–150 kN. The power passing through the gearbox is about 13.5 MW. Further development aims at increasing the speed ratio of the gearbox (larger bypass ratio) and the power passing through it (larger engine). The technological challenges are development of light, high-strength materials and reduction of the friction heat.

12.3 Performance Parameters of Aircraft Propulsion Systems

We first define some concepts of power and efficiency for single-flow turbojets. Afterwards, these concepts are extended to double-flow systems. With double-flow systems, we treat turbo-propellers, bypass jet engines, turbofan engines, prop-fan engines and unducted fan engines all with the same form of analysis.

12.3.1 *Specific Thrust*

For a single-jet, thrust is given by

$$T = \dot{m} \Delta v,$$

with Δv the effective velocity increase. In the formula, the mass flow increase due to fuel injection is neglected. *Specific thrust* is thrust divided by the mass flow rate aspirated by the propulsion system. With the simplified formula for thrust, this is

$$T_s = T / \dot{m} = \Delta v.$$

The unit thus is m/s. The extension to double-jet propulsion systems is immediate. It is then the total thrust divided by the sum of the aspirated mass flows. With turbofan engines, the order of magnitude is 300 m/s at take-off and 150 m/s at cruise. With propellers, the value varies from 30 to 50 m/s in cruise flight.

12.3.2 Dynamic Power

Dynamic power is the power corresponding to the kinetic energy increase in the flow through the propulsion system:

$$P_{dyn} = \dot{m} \frac{1}{2} (v_j^2 - v_0^2). \quad (12.6)$$

Again, extension of the notion to double-jet systems is immediate.

12.3.3 Gas Power and Dynamic Efficiency

In a single-jet engine, the dynamic power originates from the flow acceleration in the nozzle. The gas entering the nozzle is delivered by a gas turbine, which thus functions as a *gas generator*. The nozzle may then be defined as the *jet generator*. *Gas power* denominates the power that would be delivered to the propulsive jet formed in the nozzle in absence of losses, thus by an isentropic expansion. The gas power is thus the ideal value of the dynamic power. It may be interpreted as the net output of the gas generator and the net input to the jet generator. The efficiency of the jet generator, or the *dynamic efficiency* (η_d), is then defined as the ratio of dynamic power to gas power.

12.3.4 Thermal Power, Thermodynamic Efficiency and Thermal Efficiency

Thermal power is the power released by combustion. *Thermodynamic efficiency* (η_{td}) is the ratio of gas power to thermal power. Thermodynamic efficiency thus characterises the efficiency of the gas generator. *Thermal efficiency* (η_t) of the propulsion system is defined as the ratio of dynamic power to thermal power.

12.3.5 Propulsive Power and Propulsive Efficiency

Propulsive power or *thrust power* is the power consumed by the aircraft for its propulsion:

$$P_{prop} = T v_0.$$

The propulsive power differs from the dynamic power by

$$P_{dyn} - P_{prop} = \frac{1}{2} \dot{m}(v_j^2 - v_0^2) - \dot{m}(v_j - v_0)v_0 = \frac{1}{2} \dot{m}(v_j - v_0)^2.$$

The difference is the flux of kinetic energy in the propulsive jet remaining in the atmosphere behind the aircraft. The power difference is called *residual power* and the kinetic energy is called the *residual kinetic energy*. The residual power is the part of the dynamic power used for generation of the propulsive jet, but not useful for propulsion of the aircraft. *Propulsive efficiency* therefore is defined as the ratio of the propulsive power to the dynamic power:

$$\eta_p = \frac{\dot{m}(v_j - v_0)v_0}{\frac{1}{2}\dot{m}(v_j^2 - v_0^2)} = \frac{2 v_0}{v_j + v_0} = \frac{2}{1 + (v_j/v_0)} = \frac{1}{1 + \frac{1}{2}\frac{\Delta v}{v_0}}. \quad (12.7)$$

The propulsive efficiency can never be near to unity, as it is essential for propulsion that the effective jet velocity exceeds the flight speed. At this stage, we may use the formula for propulsive efficiency in a loose sense also for double-jet systems, in order to obtain an order of magnitude. With a turbofan engine $\Delta v = 150$ m/s and $v_0 = 250$ m/s are typical, and thus $\eta_p \approx 0.77$. With a propeller with a low specific thrust $\Delta v = 30$ m/s and $v_0 = 150$ m/s are typical and thus $\eta_p \approx 0.90$. With $\Delta v = 50$ m/s and $v_0 = 150$ m/s is $\eta_p \approx 0.85$.

12.3.6 Overall Efficiency

The ratio of propulsive power to thermal power is the overall efficiency:

$$\eta = \frac{P_{prop}}{P_{therm}} = \frac{P_{dyn}}{P_{therm}} \frac{P_{prop}}{P_{dyn}} = \eta_t \eta_p. \quad (12.8)$$

It is obvious that the overall efficiency has to be optimised for a propulsive system. This is discussed in one of the following sections.

12.3.7 *Rocket*

Some adaptations of the foregoing concepts are needed with rocket propulsion. Dynamic power is defined as $P_{dyn} = \dot{m} \frac{1}{2} v_j^2$ (v_j stands for effective jet velocity) and a new concept in between dynamic power and propulsive power is needed. With a rocket, dynamic power is not the only power available for propulsion. As the jet is generated exclusively by the carried propellants, their kinetic energy must not be disregarded, as with the reactor (we neglect even the fuel flow with the simplified formulae above). The power available for propulsion with a rocket is $\dot{m}(\frac{1}{2} v_0^2 + \frac{1}{2} v_j^2)$. The difference between this available power and the propulsive power is

$$\dot{m}(\frac{1}{2} v_0^2 + \frac{1}{2} v_j^2) - \dot{m} v_j v_0 = \frac{1}{2} \dot{m} (v_j - v_0)^2.$$

This is the residual power. Propulsive efficiency is then defined by

$$\eta_p = \frac{\dot{m} v_j v_0}{\dot{m}(\frac{1}{2} v_0^2 + \frac{1}{2} v_j^2)} = \frac{2(v_j/v_0)}{1 + (v_j/v_0)^2}.$$

Contrary to the reactor, the propulsive efficiency may become unity. Thrust is not lost with $v_j = v_0$. Further, an instantaneous overall efficiency cannot be defined, as a rocket does not constitute a quasi-steady system. The kinetic energy of the propellants is energy accumulated during foregoing propulsion.

12.3.8 *Generalisation for Double-Flow Engines*

In order to understand the way of generalisation, we consider the transformation of a turbojet into a turboprop. This is achieved by mounting a power turbine at the outlet of the gas generator of the turbojet. The propeller is driven by the power turbine, normally over a reduction gearbox. It is obvious that the conversion is of no use regarding the thermal efficiency of the propulsive system. The gas power, available with a turbojet, can optimally be converted into dynamic power through a nozzle. The efficiency of a nozzle (ratio of dynamic power to gas power) is very high, about 0.98. Dynamic power generation through the propeller involves the power turbine efficiency ($\eta \sim 0.92$), the transmission efficiency ($\eta \sim 0.95$ with a reduction gearbox) and the propeller efficiency (propeller efficiency is the ratio of the dynamic power to the mechanical power: $\eta \sim 0.9$). The efficiency of the conversion only amounts to about 0.80. The difference between both systems is that the jet velocity is high (~ 1125 m/s; we derive the value later) with a turbojet, whereas the jet velocity can be made very low with a propeller. This mainly has significance for the propulsive efficiency.

Examples:

- $T_0 = 225 \text{ K}$ (10 km height), $M_0 = 0.85 \rightarrow v_0 \approx 250 \text{ m/s}$ (900 km/h), for $v_j = 1125 \text{ m/s} \rightarrow \eta_p = 0.364$.
- $T_0 = 225 \text{ K}$, $M_0 = 2.5 \rightarrow v_0 \approx 750 \text{ m/s}$ (2700 km/h), for $v_j = 1125 \text{ m/s} \rightarrow \eta_p = 0.800$.

Achieving good propulsive efficiency with a single-jet engine requires a flight Mach number of about 2.5 or above. The purpose of the second jet is thus obvious. The gas power supplied to the hot nozzle is decreased by converting part of it into mechanical power and by generating a second jet through a compressor, a fan or a propeller so that dynamic power becomes available at a lower jet velocity and with a larger mass flow rate. The higher the bypass ratio, the better the engine is adapted to low flight speed. Of course, the higher the bypass ratio, the lower the final thermal efficiency is. But clearly, the product of thermal efficiency and propulsive efficiency (12.8) must be optimised.

Precise performance analysis requires splitting of a gas turbine based propulsion system into two parts. We discern a *gas generator* and a *jet generator*. First, we discern a hot flow and a cold flow. The hot flow is the flow that passes through the combustion chamber. The gas generator is the part of the engine that processes the hot flow until a section in the turbine such that the part upstream of it drives the hot-flow compressor parts. The compressor and the turbine parts of the gas generator are not always easily discernible. The high-pressure compressor and the high-pressure turbine are part of it in a double-shaft engine. In a triple-shaft engine, it encompasses the high-pressure and intermediate-pressure compressor and turbine parts. In a bypass engine and a turbofan, the low-pressure turbine drives the low-pressure compressor or the fan. These contribute both to the cold and the hot flows. In practice, the term *core engine* denotes the engine part exclusively processing the hot flow (normally the HP and IP parts). So, the term core engine is more restrictive than the term gas generator. For the gas generator, we have to think of the fan in a turbofan and the LP compressor in a bypass engine as split into a hot flow (interior part) and a cold flow (exterior part) part. The hot flow part belongs to the gas generator and the cold flow part belongs to the jet generator. Further, we have to think of the LP turbine as split into a front part belonging to the gas generator and a rear part belonging to the jet generator.

The gas generator is characterised by the thermodynamic efficiency. This is the ratio of gas power to thermal power. The jet generator is characterised by the dynamic efficiency. This is the ratio of the dynamic power (sum of the two jets) to the gas power. The thermal efficiency of a propulsive system is the product of the thermodynamic efficiency and the dynamic efficiency ($\eta_t = \eta_{td}\eta_d$). The overall efficiency is the product of three efficiencies:

$$\eta = \eta_{td}\eta_d\eta_p. \quad (12.9)$$

Optimisation of the propulsive system may be defined as follows: the gas generator is designed for maximum thermodynamic efficiency and the jet generator is designed for maximum product of dynamic efficiency and propulsive efficiency. The

lower the flight speed, the higher the bypass ratio shall be in order to enhance the propulsive efficiency. This inevitably decreases the dynamic efficiency, so that the product of both goes through a maximum. This description is a simplification, as it overlooks that an increase of the bypass ratio causes increased engine dimensions, resulting in additional drag on the aircraft and added weight. An overall evaluation must take engine drag and engine weight into account.

The efficiency terminology with propulsion systems is inevitably more complicated than with power gas turbines. With power generation, thermal efficiency is defined as the ratio of the shaft power to the thermal power. Thermodynamic efficiency may also be introduced, but is not strictly necessary. With power gas turbines, a gas generator may be distinguished from a power turbine. The thermodynamic efficiency is then the gas generator efficiency in the sense discussed. The thermal efficiency is the product of the thermodynamic efficiency and the isentropic efficiency of the power turbine.

12.3.9 *Specific Fuel Consumption*

Thrust specific fuel consumption (TSFC) denominates the fuel consumption per thrust unit. In technical literature, it is mostly expressed in pound mass per hour per pound force (1 lbm=0.4536 kg, 1 lbf=4.448 N). Thrust specific fuel consumption by modern airliner turbofans in imperial units is of the 0.55–0.60 order at cruise. The value at take-off is about 0.30. In international units, thrust specific consumption may be expressed in g/s/kN. Departing from imperial units, multiplication by $10^6/(9.8065 \times 3600)=28.325$ is required, leading to the order 16–17 g/s/kN at cruise conditions.

For an engine driving a propeller, specific fuel consumption is commonly expressed as fuel mass flow rate per unit of power. Technical literature uses pound mass per hour per horsepower (1 HP=745.7 W). In these imperial units, the specific fuel consumption of a turbo-shaft engine is about 0.60 at cruise conditions, so similar to the value of the TSFC of a turbofan. Conversion into kg/kWh requires multiplication by 0.608. So, the order of magnitude is 0.3 kg/kWh in cruise conditions. For a turboprop, the residual thrust, which is the thrust of the nozzle, is converted into mechanical power according to the convention that 1 HP of power is equivalent to 2.5 lbf of thrust (1 kW is about 15 N). The precise value of the conversion factor is not very important as residual thrust is at maximum about 5% of the total thrust. The entire mechanical power achieved is called equivalent or effective shaft horsepower = ESHP.

The concept of thrust specific fuel consumption with jet engines is rather peculiar. It does not strictly express efficiency. The efficiency is given by

$$\eta = \frac{T v_0}{\dot{m}_f H_L}, \quad \text{thus} \quad f_s = \frac{\dot{m}_f}{T} = \frac{v_0}{H_L \eta}.$$

Thrust specific fuel consumption thus depends on the flight speed. Values must be compared with the same flight Mach number. This is not a problem in practice. With airliners, the flight Mach number is always about 0.85. With fighter aircraft, the design flight Mach number is typically around 2. But, there are also applications with other flight Mach numbers. An example is paratrooper transport aircraft with a typical flight Mach number around 0.5. Note that thrust specific fuel consumption has meaning in static conditions (start of take-off at sea level) where efficiency has no meaning.

12.4 Performance of the Gas Generator and the Single-Jet Engine

The gas generator in an aero gas turbine is analogous with a simple-cycle power gas turbine. Good performance therefore requires a high pressure ratio and a high temperature ratio. High pressure ratio is important for thermodynamic efficiency. The temperature ratio mainly determines the specific power. Compared to power gas turbines, aero gas turbines show an important advantage concerning pressure ratio and temperature ratio. Compression is partially obtained aerodynamically by the ram effect of the incoming air within the engine inlet. The ram effect is the spontaneous deceleration due to the obstruction formed by the engine. With an airliner, the aerodynamic compression achieves a very high efficiency. Further, it does not require any corresponding turbine work. Of course, the ram effect causes drag for the engine and for the aircraft. The through-flow Mach number (Mach number of the average meridional velocity component) in an aero-engine compressor is typically around 0.5. In a fan, it is typically higher, around 0.6. The flight Mach number of an airliner is 0.8–0.85. So, the deceleration at the engine entrance is very modest. Hence, the isentropic efficiency of the inlet is very high, of the order of 0.997. For analysis purposes, we will assume it equal to unity. For a supersonic fighter aircraft, the efficiency of the inlet is much lower due to formation of shock waves. The atmosphere temperature is low at cruising altitude: 225 K at 10 km height. At a given combustion temperature, the temperature ratio is thus better than with a power gas turbine. Moreover, the final temperature after compression is lower due to the lower atmospheric temperature, resulting in a more efficient turbine cooling. A turbojet engine consists of a gas generator with a directly joined nozzle. Nozzle efficiency amounts to about 0.98, being very close to 1. The gas generator may be described as a single-jet engine with an ideal nozzle. Gas power and dynamic power are then identical. Henceforth we analyse the single-jet engine with an ideal nozzle. The results strictly apply to the gas generator. Thermal efficiency and specific power values are about 2 % lower with a real turbojet engine. As with a power gas turbine, the major loss in a turbojet engine is thermal, in the sense of remaining heat in the combustion gas after expansion in the nozzle. In second order, there are thermodynamic losses due to irreversibility in the compressor and the turbine and due to cooling of turbine parts. As with the power gas turbine it is therefore relevant to accomplish a first analysis with neglect of thermodynamic losses.

12.4.1 Analysis with Loss-Free Components

The cycle without component losses is sketched in Fig. 12.11. The parts are

0–01:	Inlet
01–02:	Compressor
02–03:	Combustion chamber
03–04:	Turbine
04–4e:	Nozzle (the symbol e denotes the end of an ideal expansion)

States 0 and 4e are static. The other states are total (stagnation with respect to the engine frame).

The total parameters of the oncoming air are

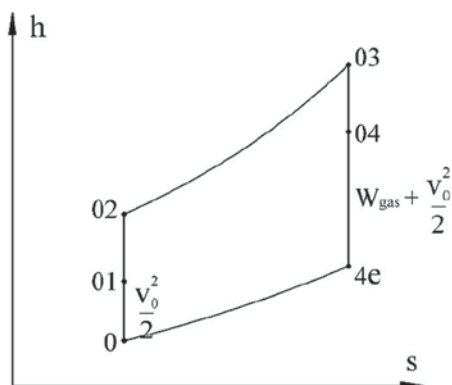
$$h_{00} = h_0 + \frac{v_0^2}{2}, \quad T_{00} = T_0 + \frac{v_0^2}{2C_p}, \quad \frac{p_{00}}{p_0} = \left(\frac{T_{00}}{T_0}\right)^{\frac{\gamma}{\gamma-1}}.$$

a. Inlet

$$p_{01} = p_{00}, \quad T_{01} = T_{00},$$

$$T_{01} = T_0 \left(1 + \frac{\gamma-1}{2} M_0^2\right), \quad \frac{p_{01}}{p_0} = \left(1 + \frac{\gamma-1}{2} M_0^2\right)^{\frac{\gamma}{\gamma-1}} = r_a.$$

Fig. 12.11 Cycle of a single-jet engine without component losses



The p_{01}/p_0 ratio is denominated aerodynamic compression ratio.

b. Compressor

$$r_c = p_{02} / p_{01},$$

$$W_c = C_p (T_{02} - T_{01}) = C_p T_{01} \left(\frac{T_{02}}{T_{01}} - 1 \right) = C_p T_{01} (r_c^{\frac{\gamma-1}{\gamma}} - 1).$$

c. Combustion chamber

$$\Delta Q = C_p (T_{03} - T_{02}).$$

Here, we simplify by the assumption of constant mass flow rate and constant specific heat.

d. Turbine

$$W_t = C_p (T_{03} - T_{04}) = W_c.$$

e. Jet generator

$$\frac{p_{03}}{p_0} = r_a r_c, \quad \frac{T_{03}}{T_{4e}} = (r_a r_c)^{\frac{\gamma-1}{\gamma}},$$

$$W_{gas} = C_p (T_{03} - T_{4e}) - W_c - \frac{v_0^2}{2} = C_p (T_{03} - T_{4e}) - C_p (T_{02} - T_0).$$

$$W_{gas} = C_p T_{03} \left(1 - (r_a r_c)^{-\frac{\gamma-1}{\gamma}} \right) - C_p T_{02} \left(1 - (r_a r_c)^{-\frac{\gamma-1}{\gamma}} \right).$$

Thermodynamic efficiency is: $\eta_{td} = 1 - r^{-\frac{\gamma-1}{\gamma}}$, with $r = r_a r_c$.

We obtain the same expression as with a stationary gas turbine, when the overall pressure ratio is applied, being the product of aerodynamic (r_a) and mechanical (r_c) pressure ratios.

Due to the aerodynamic pressure ratio, the efficiency potential is very high. The mechanical pressure ratio of a modern turbofan engine is around 40 [1, 3]. With this pressure ratio, we obtain:

$$\begin{aligned}
M_0 &= 0.85 : r_a = 1.60 \ (\gamma = 1.40), r = r_a r_c = 64; \eta_{td} = 0.695 \ (\gamma = 1.40); \\
\eta_{td} &= 0.644 \ (\gamma = 1.33); \\
M_0 &= 3 : r_a = 36.7 : \text{with } r_c = 1 : \eta_{td} = 0.643 \ (\gamma = 1.40), \eta_{td} = 0.591 \ (\gamma = 1.33).
\end{aligned}$$

The last result demonstrates that an efficient propulsion system is reached at a sufficiently high flight Mach number, without any compressor and turbine parts. This is called a ramjet (see Exercise 12.7.7).

12.4.2 Analysis with Component Losses

The foregoing analysis with hand calculations may easily be adapted for adiabatic compressor and turbine efficiencies and change of the heat capacity of the working fluid in the combustion chamber (but with constant values for air and for combustion gas). Taking into account cooling of the turbine and variable gas properties requires a numerical simulation technique. With the analysis of power gas turbines (Chap. 11), we observed that the results of hand calculations are quite near to the results of numerical simulations. The main difference is that the effect of the cooling brings the efficiency results for different turbine inlet temperatures near to each other, while these are more distinct with an adiabatic hand analysis. But this is a minor effect. Therefore, we consider here only analysis by hand calculations. We set the polytropic efficiencies of the compressor and the turbine parts at 0.9. We set the heat capacity ratios for air and combustion gas at 1.40 and 1.33, combined with the gas constant 287 J/kgK (these are the typical values in the literature; air is dry in cruise conditions). Further, we consider flight at Mach number 0.85, so that $r_a = 1.60$. We still treat the inlet and the nozzle with efficiency equal to 1.

In the design of an aircraft engine, optimum efficiency is aimed for cruise conditions, but the engine also has to function at take-off and during climb. With the current (2014) typical specifications of cruise conditions: Mach 0.8–0.85 at altitude 10,500 m and lift/drag ratio of the airplane around 18–21, take-off thrust: 0.275–0.3 times the take-off weight and rate of climb at top of climb: 2.5 m/s, the three operating points of the fan, which provides the largest part of the thrust in a turbofan engine (the thrust ratio of the two flows is about the bypass ratio), are close to each other in the non-dimensional performance chart. For concise discussions on the topic, we refer to Crichton et al. [2] and Cumpsty [3]. By the non-dimensional performance chart is meant pressure ratio as a function of the non-dimensional mass flow function $(\dot{m}/A)\sqrt{RT_0}/p_0$ at constant values of the non-dimensional rotational speed $\Omega D/\sqrt{RT_0}$, where A and D are representative values of through-flow area and diameter of the fan (see Chap. 15, Sect. 15.3). Mostly, such a chart is represented in corrected mass flow rate and corrected rotational speed, which means that these quantities are recalculated to reference conditions for p_0 and T_0 according to the non-dimensional expressions. The necessity for having the operating points

at take-off and during climb near to the operating point for cruising comes from the requirement of stable operation of the fan in the other conditions than cruise (sufficient margin to choking and stall; see Chap. 13). In reality, there are more conditions, as all compressor and turbine components should be able to function in all flight conditions of the aircraft. But compressors parts typically have first stages with adjustable stator vane angles, so that their performance parameters may be adjusted. The fan of a turbofan engine has no adjustable parts. The analysis of the equilibrium between the components of an aero gas turbine for different flight conditions and the determination of optimal characteristics of these components is very complicated. We refer to specialist books on aircraft gas turbines [4]. For basic understanding, as intended here, such detailed analyses are not necessary, as will become clear hereafter. Current values of maximum turbine inlet temperature (TIT) and maximum pressure ratio (PR) at take-off are around 1650 °C for TIT and 40 for PR [1, 3]. The limitations come from maintaining sufficient strength of the turbine blades in the HP section and sufficient strength of the outer confinement of the combustion chamber at take-off. At sea level ($T_0 = 288$ K), the temperature ratio is about 6.67. The ratio at cruise cannot be much higher, which means that the TIT at cruise must be much lower than the TIT at take-off. Manufacturers do not reveal values of TIT in cruise conditions and only specify values of maximum TIT. Cumpsty [3] estimates the turbine entry temperature (TET) of the most recent turbofan engines at about 1475 K in cruise conditions. But with TET is meant the temperature at the entrance of the first rotor of the HP turbine. The choking pressure ratio with the combustion gas properties is around 1.82 (see Chap. 4). Typically, stator parts of the HP turbine are just choked (see Chap. 15). The corresponding temperature ratio is about 1.137. With this ratio, the TIT becomes about 1675 K, so about 1400 °C. This TIT is then determined without taking into account the supplementary temperature drop due to cooling and mixing of the combustion gas and the cooling air. So, the temperature drop in the first stage stator vanes, estimated here at 200 K, might even be somewhat higher in reality. With TIT equal to 1675 K and $T_0 = 225$ K, the temperature ratio is about 7.44. So, it seems unlikely that it can be higher. We will use this value of TIT in the following analysis. It will become clear during the analysis that the turbine inlet temperature is a parameter that can be optimised, so that we may obtain it from the analysis itself. It is difficult however to start an analysis without an initial guess of TIT. The analysis will reveal that TIT = 1675 K goes with a very large value of the bypass ratio, of the order of 10–12, as with the most recent turbofan engines. So, in principle, a full analysis should encompass a study of the influence of the TIT on the global performance. But we will not do this, as the only aim here is basic understanding (see however Exercise 12.7.5).

The relations of the previous section are adapted.

a. *Compressor*

$$W_c = C_{pa}(T_{02} - T_{01}) = C_{pa}T_0 \frac{T_{01}}{T_0} \left(\frac{T_{02}}{T_{01}} - 1 \right) = C_{pa}T_0 r_a^{\frac{R}{C_{pa}}} (r_c^{\eta_{sc} \frac{R}{C_{pa}}} - 1).$$

b. *Turbine*

$$W_t = C_{pg}(T_{03} - T_{04}) = C_{pg}T_0 \frac{T_{03}}{T_0} \left(1 - \frac{T_{04}}{T_{03}}\right) = C_{pg}T_0 \frac{T_{03}}{T_0} \left(1 - r_t^{-\frac{\eta_{\infty t} R}{C_{pg}}}\right).$$

Equating compressor and turbine work determines the pressure ratio of the turbine for a chosen pressure ratio of the compressor.

c. *Combustion chamber*

$$\Delta Q = C_{pg}(T_{03} - T_0) - C_{pa}(T_{02} - T_0) = C_{pg}T_0 \left(\frac{T_{03}}{T_0} - 1\right) - C_{pa}T_0 \left(\frac{T_{02}}{T_{01}} \frac{T_{01}}{T_0} - 1\right),$$

$$\frac{\Delta Q}{C_{pa}T_0} = \frac{C_{pg}}{C_{pa}} \left(\frac{T_{03}}{T_0} - 1\right) - \left(r_c^{\frac{R}{\eta_{\infty c} C_{pa}}} r_a^{-\frac{R}{C_{pa}}} - 1 \right).$$

Here, we still simplify by the assumption of constant mass flow rate, but the change of specific heat is taken into account. Further, we take the reference temperature of the lower heating value of the fuel equal to T_0 .

d. *Jet generator*

$$W_{gas} = C_{pg}(T_{04} - T_{4e}) - \frac{v_0^2}{2} = C_{pg}T_{04} \left(1 - \left(\frac{r_a r_c}{r_t}\right)^{-\frac{R}{C_{pg}}}\right) - C_{pa}(T_{01} - T_0).$$

$$\frac{W_{gas}}{C_{pa}T_0} = \frac{C_{pg}}{C_{pa}} \frac{T_{03}}{T_0} (r_t)^{-\frac{\eta_{\infty t} R}{C_{pg}}} \left(1 - \left(\frac{r_a r_c}{r_t}\right)^{-\frac{R}{C_{pg}}}\right) - \left((r_a)^{\frac{R}{C_{pa}}} - 1\right).$$

Results for three values of pressure ratio are listed in Table 12.1.

The obtained values of thermodynamic efficiency are very high. The real values are a few percent lower, but still far above 50%. As expected, the thermodynamic efficiency increases with increasing pressure ratio. So, in principle, it is useful to enlarge the pressure ratio above the current values of around 40. On the other hand, the specific power lowers somewhat with increasing pressure ratio. But this is not always a drawback, as will become clear hereafter. The non-dimensional specific power is about 2.70. The corresponding gas power is about 600 kJ/kg. With flight velocity 250 m/s, the corresponding jet velocity of a single-jet engine is about 1125 m/s. We have used this value in Sect. 12.3.8 and we will use it also in the next section.

Table 12.1 Performance parameters of the gas generator for TIT=1675 K

r_c	r_t	$\frac{W_{gas}}{C_{pa}T_0}$	$\frac{\Delta Q}{C_{pa}T_0}$	η_{td}
30	3.8362	2.8135	5.0540	0.5567
40	4.8431	2.7068	4.7319	0.5720
50	5.9502	2.5917	4.4611	0.5810

12.5 Performance of Double-Flow Engines

A double-flow engine consists of a gas generator with an added turbine that drives the cold air flow compressor, fan or propeller. As already discussed, it is often impossible to distinguish physically the gas generator and jet generator parts in a double-flow engine. The distinction is made here thermodynamically, enabling us to study the effect of the second flow. Additional parameters are the bypass ratio b and the pressure ratio of the cold air flow. Furthermore, there is a difference between engines with both air flows mixed before a common nozzle (bypass engine) and engines with separate nozzles (turbofan).

We assume a given gas generator and a given flight velocity. Engine optimisation implies then obtaining the highest possible thrust per unit of mass flow rate in the hot flow. In the following derivations, the small mass flow increase by adding fuel is not taken into account.

12.5.1 Unmixed Flows (Double-Jet Engine: Turbofan, Turboprop)

A single jet engine has dynamic power

$$P_{dyn} = \frac{1}{2} \dot{m} (v_{j1}^2 - v_0^2).$$

Neglecting nozzle loss, this power also equals the gas power:

$$P_{gas} = \frac{1}{2} \dot{m} v_0^2 (s_1^2 - 1) \quad , \quad s_1 = \frac{v_{j1}}{v_0},$$

where the symbol s denotes a speed ratio.

$$\text{Thrust is } T_1 = \dot{m}(v_{j1} - v_0) = \dot{m} v_0 (s_1 - 1).$$

Fig. 12.12 Cycle of a double-flow engine with component losses

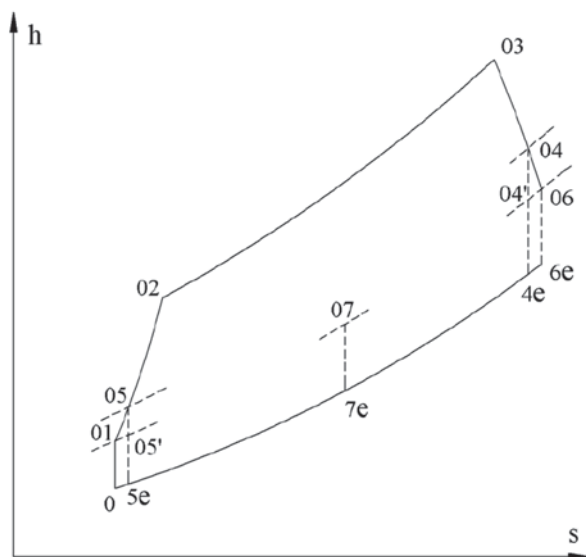


Figure 12.12 sketches the cycle of a double-flow engine in the h - s diagram. Some parts are:

01–02:	Hot flow compressor
01–05:	Cold flow compressor
03–04:	Hot flow turbine
04–06:	Cold flow turbine

The state point 07 is not relevant for the analysis of an engine with separate cold and hot jets, as we perform now (we will use it in the next section).

The cold flow work balance is

$$bC_{pa}(T_{05} - T_{01}) = \eta_{trans} C_{pg}(T_{04} - T_{06}), \quad (12.10)$$

where b is the bypass ratio and η_{trans} is the efficiency of the mechanical transmission between turbine and compressor. The work extracted from the flow by the turbine may be written as

$$C_{pg}(T_{04} - T_{06}) = \eta_t \frac{1}{2}(v_{j1}^2 - v_{j2hot}^2), \quad (12.11)$$

where η_t is the isentropic turbine efficiency, v_{j2hot} is the hot jet velocity of the double-jet engine and where we neglect the isentropic enthalpy difference between the expansions 04'–4e and 06–6e. The work done on the flow by the compressor may be written as

$$C_{pa}(T_{05} - T_{01}) = \frac{1}{\eta_c} \frac{1}{2} (v_{j2cold}^2 - v_0^2), \quad (12.12)$$

where η_c is the isentropic re-expansion efficiency of the compressor, v_{j2cold} is the cold jet velocity of the double-jet engine and where we neglect the isentropic enthalpy difference between the expansions 05'-5e and 01-0.

Combination of (12.10), (12.11) and (12.12) results in

$$b \frac{1}{2} (v_{j2cold}^2 - v_0^2) = \eta_c \eta_{trans} \eta_t \frac{1}{2} (v_{j1}^2 - v_{j2hot}^2), \quad (12.13)$$

which may be written as a balance of dynamic power as

$$\frac{1}{2} (v_{j1}^2 - v_0^2) = \frac{1}{2} (v_{j2hot}^2 - v_0^2) + \frac{1}{2} \frac{b}{\eta_b} (v_{j2cold}^2 - v_0^2), \quad (12.14)$$

where η_b is the product of the efficiencies involved, which we may call the *bypass efficiency*. Henceforth we take as approximate value $\eta_b \approx 0.85$, which is appropriate for a turbofan engine. For a turboprop the value is lower due to the reduction gearbox. Remark that the balance of dynamic power may be written directly in the form (12.14), but the role of the intervening efficiencies is clearer with the derivation in parts.

With velocity ratios, (12.13) is

$$s_{2hot} = \sqrt{s_1^2 - \frac{b}{\eta_b} (s_{2cold}^2 - 1)}. \quad (12.15)$$

The ratio of thrust of the double-jet engine to the single-jet engine is

$$\frac{T_2}{T_1} = \frac{\dot{m}(v_{j2hot} - v_0) + \dot{m} b (v_{j2cold} - v_0)}{\dot{m}(v_{j1} - v_0)} = \frac{(s_{2hot} - 1) + b(s_{2cold} - 1)}{s_1 - 1}.$$

With an assumed bypass ratio b , the hot jet velocity may be chosen as a function of the cold jet velocity, so that the thrust attains a maximum with the double-jet engine. This requires

$$\frac{d s_{2hot}}{d s_{2cold}} + b = 0.$$

Furthermore from (12.15):

$$\frac{d s_{2hot}}{d s_{2cold}} = \frac{1}{2\sqrt{(-)}} \left(-2 \frac{b}{\eta_b} s_{2cold} \right) = -\frac{b}{\eta_b} \frac{s_{2cold}}{s_{2hot}}.$$

Maximum thrust is attained for

$$s_{2cold} = \eta_b s_{2hot}. \quad (12.16)$$

$$\text{Then } s_{2hot}^2 = s_1^2 - b\eta_b s_{2hot}^2 + \frac{b}{\eta_b} \text{ or } s_{2hot}^2 = \frac{s_1^2 + \frac{b}{\eta_b}}{1 + b\eta_b}.$$

The resulting overall efficiency is

$$\eta = \eta_{td} \frac{T_2 v_0}{P_{gas}} = \eta_{td} \left(\frac{T_2}{T_1} \right) \eta_{p1}, \quad \text{and} \quad \eta_d \eta_p = \left(\frac{T_2}{T_1} \right) \eta_{p1}.$$

The cold flow pressure ratio may be calculated from the h-s diagram in Fig. 12.12. Again, we neglect losses in the engine inlet and in the cold flow nozzle.

$$\frac{T_{01}}{T_0} = r_a^{\frac{R}{C_{pa}}}, \quad \frac{T_{05}}{T_{01}} = (r_{cold})^{\frac{R}{\eta_{\infty} C_{pa}}}. \quad (12.17)$$

$$\frac{v_{j2cold}^2}{2} = C_{pa}(T_{05} - T_{5e}) = C_{pa}T_{05} \left(1 - (r_a r_{cold})^{\frac{R}{C_{pa}}} \right),$$

$$\frac{v_{j2cold}^2}{2} = C_{pa}T_0(r_a)^{\frac{R}{C_{pa}}}(r_{cold})^{\frac{R}{\eta_{\infty} C_{pa}}} \left(1 - (r_a r_{cold})^{\frac{R}{C_{pa}}} \right). \quad (12.18)$$

Determination of r_{cold} from (12.18) for given v_{j2cold} requires iteration.

We take as an example the flight velocity 250 m/s, which corresponds approximately to a flight Mach number 0.85 at $T_0 = 225$ K, and the jet velocity of the single-jet engine 1125 m/s. The velocity ratio of the single-jet engine is $s_j = 4.50$. The corresponding propulsive efficiency is $\eta_{p1} = 2/(1 + s_j) = 0.3636$. The results for the double-jet engine for varying bypass ratio are listed in Table 12.2. Taking the drag and the weight of the engine into account, the practical optimum is reached between the bypass ratios 10 and 15. For pressure ratio 40 and bypass ratio 10, the overall efficiency becomes $0.572 \times 0.669 = 0.383$. This is almost exactly the value of 38% cited by Ballal and Zelina [1] for modern turbofan engines. For $b = 10$, the mass averaged speed ratio v_j / v_0 is 1.585. With $v_0 = 250$ m/s, the specific thrust becomes 0.585×250 m/s = 146.3 m/s. The dynamic efficiency is 0.868 and the propulsive efficiency is 0.771 (formula 12.7, which forms an approximation for a double-jet engine gives 0.774). For $b = 5$, the mass averaged velocity ratio is 1.952. With $v_0 = 250$ m/s, the specific thrust becomes 238.0 m/s. For $b = 5$, the specific thrust is

Table 12.2 Performance of a double-jet engine (turbofan) for $s_f=4.50$ and $\eta_b=0.85$

b	s_{2hot}	s_{2cold}	r_{cold}	T_2/T_1	$\eta_d \eta_p$
5	2.231	1.896	2.483	1.632	0.594
10	1.836	1.560	1.700	1.840	0.669
20	1.560	1.326	1.330	2.021	0.735
50	1.348	1.146	1.119	2.185	0.795
100	1.266	1.076	1.050	2.257	0.821

then much too high for reaching a good propulsive efficiency. The specific thrust may be lowered by lowering the TIT. This lowers somewhat the thermodynamic efficiency, but not very much. So, obviously, there is an optimum TIT for each bypass ratio and TIT=1675 K, as used here, is certainly too high for $b=5$. We do not attempt here to determine the optimum TIT, but, of course, results may be recalculated for different values of TIT (see Exercise 12.7.5). Remark that specific thrust may also be lowered by increasing the pressure ratio.

The pressure ratio attainable within a stage of an axial compressor is at maximum about 1.75, when flow velocity and blade speed are set to the maximally attainable values (see Chap. 13). This demonstrates that a single-stage fan becomes optimal for bypass ratio 10 or above it. For bypass ratio 5, the pressure ratio of a single-stage fan is too low for optimum (but the necessary value lowers with lower TIT). With pressure ratio 1.75, the efficiency may be calculated with the above formulae. The results are:

$$b = 5; \quad r_{cold} = 1.75; \quad s_{2cold} = 1.587; \quad s_{2hot} = 3.365; \quad \frac{T_2}{T_1} = 1.514.$$

The value $T_2 / T_1 = 1.514$ is lower than the optimal value $T_2 / T_1 = 1.632$ in Table 12.2. We further note that the cold flow requires several compressor stages for low bypass ratio.

12.5.2 Mixed Flows (Bypass Engine)

Pressures and velocities of two flows to be mixed have to be equal for zero mixing loss. This implies comparable total pressures before mixing. Therefore, for the purpose of the analysis, we take equal total pressures. The h-s diagram is as sketched in Fig. 12.12, but now with the condition that the total pressure at the outlet of the cold flow compressor p_{05} is equal to the total pressure p_{06} at the outlet of the turbine that drives the cold flow compressor. This condition implies a relation between the bypass ratio and the common pressure level $p_{05}=p_{06}$. The state point 07 is the mixed flow entering the common nozzle.

To illustrate the effect of mixing, we take once more: $r_a = 1.60$, $r_c = 40$, $T_0 = 225$ K. We combine it with $T_{03} = 1675$ K and we choose $b = 10$. First, we consider separate hot and cold jets. The compression in the hot flow is determined by

$$\frac{T_{01}}{T_0} = (r_a)^{\frac{R}{C_{pa}}} \quad , \quad \frac{T_{02}}{T_{01}} = (r_c)^{\frac{R}{\eta_{sc} C_{pa}}}.$$

This results in $T_{01} = 257.3$ K and $T_{02} = 830.0$ K. With a chosen cold flow compression ratio r_{cold} , T_{05} follows similarly from (12.17).

The power balance of the hot flow, with transmission efficiency equal to unity, is

$$C_{pg}(T_{03} - T_{04}) = C_{pa}(T_{02} - T_{01}).$$

With $T_{03} = 1675$ K follows $T_{04} = 1177.7$ K.

The power balance of the cold flow, with transmission efficiency equal to unity, is

$$C_{pg}(T_{04} - T_{06}) = b C_{pa}(T_{05} - T_{01}).$$

For a given bypass ratio, this balance determines T_{06} .

From the temperature ratio T_{04} / T_{06} follows the pressure ratio p_{04} / p_{06} . The jet velocities v_{j1} , v_{j2hot} and v_{j2cold} can then be determined. The results are shown in Table 12.3. The bypass efficiency is calculated from (12.13).

In Table 12.3, the maximum of the product $\eta_d \eta_p$ is obtained for $r_{cold} = 1.75$. This value does not correspond completely with the value in Table 12.2, which is 1.70. Also the value of the maximum of $\eta_d \eta_p$ differs somewhat. The reason is that the value of s_1 is not exactly the same (it is 4.541 in Table 12.3) and that the bypass efficiency is much larger in Table 12.3. The larger value of the bypass efficiency comes from the beneficial influence of the reheat effect: increase of the isentropic efficiency of the turbine and the isentropic re-expansion efficiency of the compressor; increase of the cold and hot jet velocities v_{j2cold} and v_{j2hot} (Fig. 12.12). From Table 12.3 follows that equal outlet total pressure of the cold flow compressor and the cold flow turbine is approximately reached for $r_{cold} = 1.60$. With the values for this pressure ratio, we may calculate the performance by mixing the hot and cold flows before entry of a common nozzle. The power balance for the nozzles, ignoring mixing loss, is

$$\frac{1}{2} \dot{m}(b+1)v_{j2}^2 = \frac{1}{2} \dot{m} v_{j2hot}^2 + \frac{1}{2} \dot{m} b v_{j2cold}^2.$$

With the values obtained, the results are $s_2 = 1.623$ and $T_2 / T_1 = 1.935$. The thrust ratio is larger than the values for $r_{cold} = 1.60$ and for $r_{cold} = 1.75$ in Table 12.3. The

Table 12.3 Performance of a double-jet engine (turbofan) for $T_{03} = 1675$ K and $b = 10$

r_{cold}	P_{06}/P_{05}	s_{2hot}	s_{2cold}	T_2/T_1	η_b	$\eta_d\eta_p$
1.50	1.424	2.910	1.443	1.791	0.891	0.646
1.55	1.199	2.721	1.474	1.825	0.888	0.659
1.60	1.010	2.521	1.504	1.853	0.885	0.669
1.65	0.850	2.309	1.533	1.874	0.882	0.676
1.70	0.715	2.079	1.560	1.887	0.880	0.681
1.75	0.601	1.825	1.587	1.890	0.878	0.682
1.80	0.504	1.534	1.612	1.881	0.876	0.679

better result, compared to separate flows, even with optimised velocity ratio, may easily be explained. The efficiency of the mechanical energy transfer (turbine, transmission, fan) is the bypass efficiency, which is significantly lower than unity (about 0.88 in Table 12.3). The thermal energy transfer by the mixing is, in principle, lossless. So, it is clearly advantageous to mix, even if there is some loss during mixing. Not too high bypass ratios, as in military engines ($b = 0.5\text{--}1$), enable a complete mixing of the hot and the cold flow. A lobed mixer surface is sometimes applied to enhance mixing (see further: Fig. 12.17). Application of mixed flows is then always favourable. Complete mixing cannot be realised at higher bypass ratios, because of the limited length of the mixing zone in practise. Some engines with moderate bypass ratio have two versions. An example is the V2500 (IEA). In this engine the bypass ratio is about five. It exists with separate nozzles, but there is also a version with the cold flow brought to the rear of the engine through a long duct. This is favourable for noise reduction, as the engine is then encapsulated. The cold flow is partially mixed with the hot flow without mixer surface.

12.5.3 Intercooling and Recuperation

Figure 12.13 is a sketch of a turbofan engine with intercooling between the IP compressor (booster) and the HP compressor. The cooling air comes from part of the outlet flow of the fan. There is recuperation of outlet heat by a series of heat exchangers preheating the compressor air before entry to the combustion chamber. The thermodynamic benefits of the system are similar as with power gas turbines, but it is, of course, crucial that pressure losses in the heat exchangers be low. Such engines are studied nowadays (2014), but these are not used in practise yet.

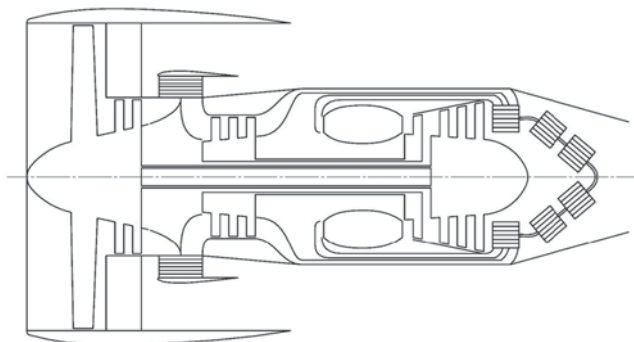


Fig. 12.13 Intercooled recuperated turbofan engine

12.6 Technological Aspects of the Turbofan Engine

12.6.1 *Discs and Shafts*

In Fig. 12.9 it is visible that rotor drums of compressor and turbine parts are made from connected discs (welded or bolted together) with a large hole at the centre. Figure 12.14 is a section of the turbine part of the Trent800. The rotor discs are clearly visible. One of the discs in the LP turbine and the single discs of the HP and IP turbines are connected to concentric hollow shafts. Discs in the LP and IP compressors and in the LP turbine are typically forged from a titanium alloy (alloy with aluminium as most important second component), due to the low weight of titanium. Discs of the HP compressor and the HP and IP turbines are made from nickel-base super-alloys, because titanium alloys cannot withstand a temperature higher than about 540 °C. Shafts are mostly made from steel.

12.6.2 *Vanes and Blades*

Fan blades are typically hollow structures produced from two titanium alloy sheets, shaped by plastic deformation, and a corrugated plate or a honeycomb structure of the same metal in between them. All parts are connected by diffusion bonding. A very modern technology is fan blades in composite materials: graphite fibres and epoxy resin. Vanes and blades in cold parts of the engine (LP and IP compressor, LP turbine) are made from titanium alloys, while nickel-base alloys are used for the hot parts (HP compressor, HP and IP turbines). HP turbine blades are normally cast as a single crystal and IP blades are cast directionally solidified. Vanes and blades in HP and IP turbines have a thermal barrier coating (TBC). Cooling of vanes and blades is based on the same principles as with stationary gas turbines, but inserts are

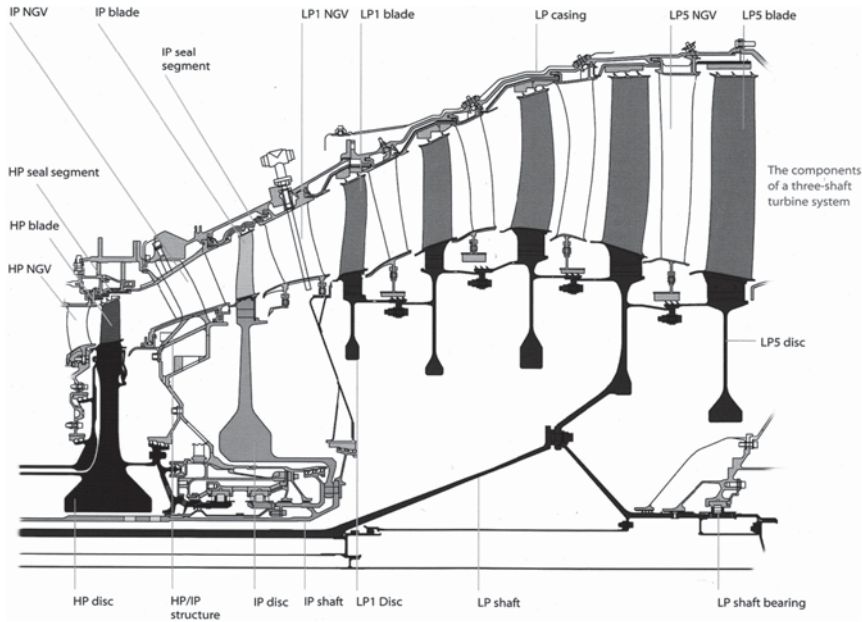


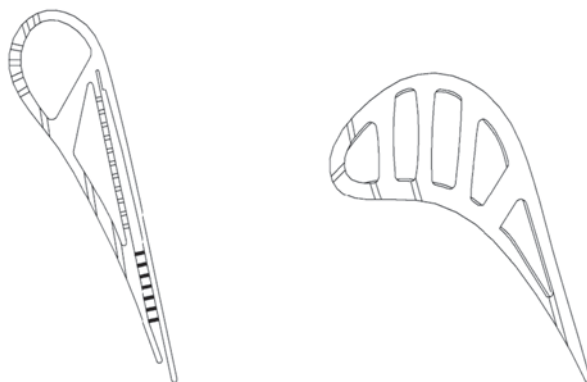
Fig. 12.14 Turbine part of the Trent 800 turbofan engine. (From [6]; permission by Rolls-Royce)

not used in stator vanes. Convection cooling, impingement cooling and film cooling are combined. Figure 12.15 sketches examples of cooling schemes of nozzle vanes and blades. In the vane example, cooling air is fed to two internal channels (convection cooling), which both deliver air for film cooling on the pressure surface. The second channel delivers air through holes in an internal wall, forming impinging jets on the inner side of the suction surface. This air leaves through a trailing edge slot passing over so-called pedestals, which are staggered cylinders creating a high level of turbulence. The rotor blade has three cooling channels. In the middle one, air passes three times.

12.6.3 Combustion Chamber

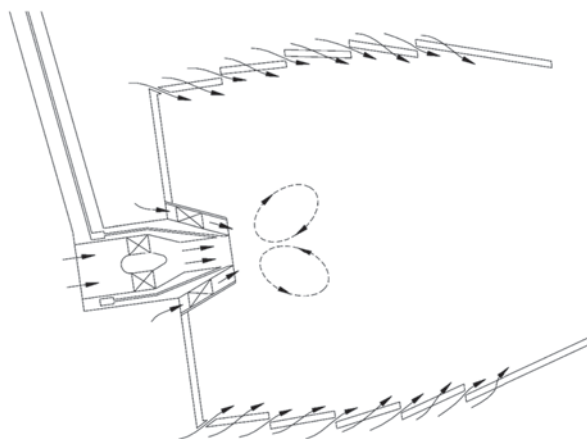
Common modern combustion chambers are of annular type with several injectors. Compared to the can-annular type frequently used earlier, the main advantages are a smaller length and a smaller frontal area, which are vital properties for an aero-engine. The smaller wall area results in lower pressure drop and lower cooling air flow rate. The disadvantage of the annular type is that it is more difficult to manufacture and that it is more difficult to reach perfectly stable combustion resulting in a homogeneous exit temperature. Figure 12.16 is a sketch of a longitudinal section through the liner of a combustion chamber (the inner part that confines the flame) and a fuel injector. The axial Mach num-

Fig. 12.15 Examples of cooling schemes for vanes (*left*) and blades (*right*)



ber range in a compressor of an aero-engine is 0.55–0.65 in front stages, but towards the exit this level is reduced to about 0.3 (velocity about 150 m/s). This velocity level is still much too high for a stable combustion. The air is slowed down by diffuser blades and by dump diffusion. A part of the air is supplied centrally into the combustion chamber through the injectors (primary air). This flow is split into two parts. Flow through the centre of the injector is forced into swirl. The outside flow is forced into swirl as well, but in the opposite sense. Fuel is injected as a liquid sheet between both contra-rotating air flows. The high shear on the liquid flow atomises it into small drops. This disintegrating mechanism enables variation of the fuel-air ratio over a large range, maintaining stable combustion. The swirl of the inner air flow causes a low pressure zone such that hot combustion products are sucked from downstream and transferred to the injector by the recirculation flow pattern. This means that swirl stabilisation is used (see Chap. 11). Part of the air is added around the injector and serves as secondary air (combustion of the CO). This air also cools the liner. Down-

Fig. 12.16 Liner of a combustion chamber and injector (schematic)



stream of the combustion zone, more air is added as dilution air. The liner of Fig. 12.16 is a schematic representation of a thin-wall shell of a nickel-base alloy, covered with a thermal barrier coating (TBC) and cooled by injection of air through arrays of a large number of small holes, either at about 30° in the wall (called effusion cooling) or perpendicular in rings (called diffusion cooling). Heat shielding and cooling are realised by the films formed at the inner side of the liner, but the liner is also cooled by heat removal within the holes. Such liners are nowadays still in development phase for larger engines. More common is a double-wall liner being a metal shell covered at the inside with ceramic tiles cooled by a combination of convection, impingement and film cooling.

The traditional principle for keeping emissions of NO_x and CO low is a sequence of rich burning, quick quenching of the flame and lean burning. The mixture in the primary zone is very rich (about 12 % of the air) so that the combustion temperature is rather low (the combustion temperature is the highest for stoichiometric combustion). This ensures that not much NO_x is formed, but, of course, production of CO and soot (carbon) is high. With addition of the secondary air, the mixture passes quickly from rich to lean (about 50 % of the air in the primary and secondary zones together). This process is called quenching. The mixture passes through a stoichiometric zone with high production of NO_x but this zone is kept very short. In the lean zone, CO and soot are burnt. With this combustion principle, emissions of CO and NO_x are higher than with the Dry Low Emission (DLE) systems of power gas turbines. Staged combustion systems with pilots ensuring stable combustion (diffusion flame) combined with main burners optimised for low NO_x production (lean mixture) are developed by all manufacturers nowadays. These systems are similar to the ones used in DLE systems of power gas turbines: either rows of pilot burners next to rows of lean burners or rows of burners with a pilot core and a lean part around it. These systems are still not fully mature so that it is not meaningful to discuss them in a basic book.

12.6.4 Mixer and Thrust Reverser

Figure 12.17 (left) renders a lobed surface for mixing the hot and the cold flows, typical for low bypass rate engines. Figure 12.17 (right) demonstrates how, by pushing back the cold flow nozzle, the cold flow is deflected to generate reverse thrust for braking immediately after landing.

12.7 Exercises

12.7.1 Single-Flow Jet Engine

With this engine, a single thrust flow is generated by a thermodynamic cycle of compression, heating and expansion. Calculate the thrust per unit of mass flow

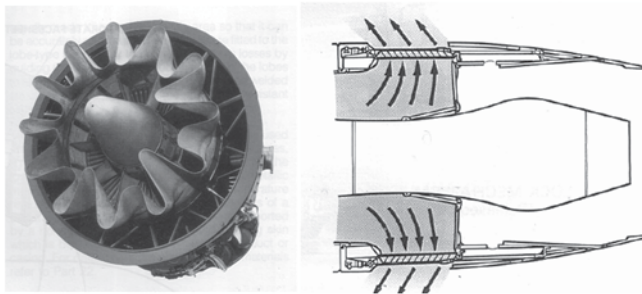


Fig. 12.17 *Left: lobed mixer for mixing cold and hot flows; right: reverse thrust nozzle position.* (From [5]; permission by Rolls-Royce)

rate for $T_0 = 225$ K (10 km height), $M_0 = 0.85$ (flight Mach number), pressure ratio of the compressor: $p_{02}/p_{01} = 40$ and combustion gas temperature at turbine inlet $T_{03} = 1675$ K. Properties of atmospheric air: $C_p = 1005$ J/kgK, $R = 287$ J/kgK. Combustion gas properties $C_p = 1150$ J/kgK, $R = 287$ J/kgK. Assume $\eta_{\infty c} = \eta_{\infty t} = 0.90$ for compressor and turbine and assume $\eta_{\infty} = 0.97$ for the nozzle. Ignore the pressure drop in the combustion chamber (in practice about 4%) and heat losses to the surroundings (in practice about 1%). Ignore the mass flow increase within the turbine and nozzle by adding fuel (in practice about 2%). Ignore losses at the engine inlet.

Determine the energy rise within the generated thrust flow. The corresponding power is the dynamic power. Compare this power with the thermal power, which is the power released by the fuel (take T_0 as reference temperature for the heating value). The ratio of dynamic power and thermal power is the thermal efficiency of the aero-engine. Determine this efficiency. Compare with the results in Table 12.1 (results should be approximately the same).

Determine the propulsive power, which is the power useful for propulsion. Compare propulsive power to dynamic power. The ratio is the propulsive efficiency. Determine this efficiency and establish that it is very low for the aero-engine studied. The reason is the big difference between the jet flow speed and the flight speed so that the kinetic energy dissipated into the atmosphere is high. Determine the overall efficiency. This is the ratio of propulsive power to thermal power.

12.7.2 Single-Flow Jet Engine with Post-Combustion

Consider the engine from the foregoing exercise with added post-combustion before the nozzle, raising the temperature to 1450 K. Determine the specific thrust with post-combustion. Determine the thermal efficiency and the overall efficiency. Compare with the results from Exercise 12.7.1. Establish that thrust increases significantly with a great overall efficiency drop. In military engines (bypass engines with small bypass ratio) post-combustion is switched on at take-off. Due to the strongly increased thrust, the aircraft may reach flight height at a much shorter distance. Post-combustion is also switched on during combat to increase thrust and thus manoeuvrability.

12.7.3 Turbofan with Separate Flows

Consider the engine from Exercise 12.7.1 transformed into a turbofan engine. This is achieved by mounting upstream of the hot nozzle an additional turbine, driving the fan. Take the bypass ratio equal to 5 and the pressure ratio of the fan equal to 1.7. As infinitesimal fan efficiency choose 0.90. First, determine the power required to drive the cold flow part of the fan. Then, determine the pressure ratio of the additional turbine, assuming that the mechanical efficiency of the transmission between the turbine and the fan equals 1. Determine the flow velocities of the cold and the hot flow and the resulting specific thrust. Determine thermal efficiency, propulsive efficiency and overall efficiency. Compare with the results of Exercise 12.7.1. Compare also with the results in Table 12.2. Repeat the calculation for a pressure ratio of the fan 2.5 (attainable in two stages). Evaluate the improvement compared to pressure ratio 1.7.

12.7.4 Turbofan with Mixed Flows

Consider the turbofan engine with pressure ratio of the fan 1.7 from the foregoing exercise and transform it into an engine with mixed flows. The available flows are not perfectly suitable for this, as they do not have the same pressure and the same velocity. Therefore assume a 3% loss when mixing, compared to the overall pressure attained from the mass-averaged value. As total enthalpy after mixing assume the mass-averaged value. Evaluate if flow mixing generates any advantage.

12.7.5 Optimisation of Turbine Inlet Temperature with a Turbofan Engine

Repeat the calculations of Exercises 12.7.1 and 12.7.3 with turbine inlet temperature $T_{03} = 1500$ K and fan pressure ratio 1.7. Observe that the thermodynamic efficiency lowers somewhat, but the propulsive efficiency increases considerably, so that the overall efficiency improves. This observation shows that turbine inlet temperature may be optimised.

12.7.6 Helicopter Rotor

The BK117 helicopter (Eurocopter) has a maximum take-off weight of 3100 kg. The rotor diameter is 11 m. Calculate the rotor shaft power required to take off with maximum weight, ignoring ground effect, in other words, assuming that the helicopter is free in the air, and ignoring the downward force exerted to the fuselage by the rotor flow. Take into account that the incoming velocity of the air is zero with

hovering flight. This means that the through-flow velocity of the rotor is the induced velocity. First, calculate the theoretically required induced power. Then, determine the shaft power, assuming that the rotor efficiency is 0.70. This rotor efficiency is very disadvantageous compared to that of a propeller, where it may be around 0.90, as rotor through-flow with a helicopter in hovering flight is very inhomogeneous. Due to ground proximity the required induced power is somewhat lower (the flow partially thrusts on the ground). On the other hand there is a downward drag on the fuselage due to rotor through-flow. Both effects approximately counterbalance each other.

12.7.7 *Ramjet*

For supersonic flight at very high Mach numbers, e.g. flight Mach number around 5, engines that can be switched from turbojet configuration to ramjet configuration have been studied for some time. With these, the gas turbine is switched off at a sufficiently high Mach number. Aerodynamically compressed air runs from the inlet through a combustion chamber to the nozzle. Calculate the overall efficiency at flight Mach number 5 and nozzle inlet temperature 1675 K. Assume that the efficiency of the aerodynamic compression is 0.90 (losses due to shockwaves during supersonic flight) and take 0.97 nozzle efficiency. Conclude that the overall efficiency is quite high.

References

1. Ballal DR, Zelina J (2004) Progress in aeroengine technology (1939–2003). *J Aircr* 41:43–50
2. Crichton D, Xu L, Hall CA (2007) Preliminary fan design for a silent aircraft. *J Turbomach* 127:184–191
3. Cumpsty NA (2010) Preparing for the future: reducing gas turbine environmental impact—IGTI scholar lecture. *J Turbomach* 132:041017, 1–17
4. Mattingly JD, Heiser WH, Pratt DJ (2002) Aircraft engine design. AIAA education series, ISBN 1-56347-583-3
5. The Jet Engine. (1986) Rolls-Royce, ISBN 0-902121-04-9
6. The Jet Engine. (2005) Rolls-Royce, ISBN 0-902121-2-35

Chapter 13

Axial Compressors

Abstract The chapter starts with an analysis of the circumferentially averaged flow on the mean radius of an axial compressor. Loss representation is discussed together with the diffusion factor concept for estimating the loading capacity of blade rows. A further step is an analysis of the radial variation of flow parameters, but without taking into account the effect of boundary layer flows on the hub and casing. This flow is called the primary flow. A next aspect is the difference between the complete flow and the primary flow, the so-called secondary flow. The different vortex patterns in the secondary flow are described. All considerations together allow a conclusion on the optimal radial distribution of the flow parameters in an axial compressor. Some aspects of three-dimensional blade shaping conclude the flow study. Next, blade profile shapes for subsonic, supercritical, transonic and supersonic cascades are studied. The chapter concludes with a discussion on the performance characteristics and the operating limits due to surge and choke.

13.1 Mean Line Analysis

The term *mean line analysis* refers to an analysis on the average radius. Assumed is that the flow on the average radius is representative for the flow along the entire span. The simplifications are: steady flow; no radial velocity components; no circumferential variations; constant axial velocity through the stage. The analysis is one-dimensional in the sense that changes of parameters only occur with the axial coordinate: tangential velocity component, pressure and density. In a real compressor, the axial velocity component may decrease somewhat within a stage. There is also a decrease of the radial height of the stage, causing small radial velocity components. Periodic variations occur in the circumferential direction due to the influence of the blades. We here consider flow parameters averaged in the circumferential direction. These averaged parameters are steady for constant rotational speed.

13.1.1 Velocity Triangles

Figure 13.1 sketches the velocity triangles for a repeating stage. A stage is composed of a rotor followed by a stator. The conventions are followed as we used for axial turbines in Chap. 6. The vertical direction is the axial direction (x) with the through-flow from top to bottom. The running direction (y) is horizontal, positive from left to right (the symbol u represents the blade speed) and the radial direction (z) is perpendicular to the drawing, positive in upward sense. The xyz coordinate system is right-handed, but the machine is left-running (real machines can be right-running as well). Velocities are denoted by v in the absolute frame (angles are α) and denoted by w in the relative frame (angles are β). The inlet velocity mostly deviates from the axial direction ($\alpha_1 \approx 15^\circ$; see Sect. 13.3). So, a compressor normally starts with a stator vane ring, with *inlet guide vanes*. The flow decelerates in both the rotor and stator parts. The velocity reduction ratio that can be withstood in subsonic flow is about 0.7. With an intended stronger velocity reduction ratio, normally, boundary layer separation occurs (see Sect. 13.1.6). As a consequence hereof, the possible flow turning is limited, typically to about 40° in subsonic flow. This turning limit is not an absolute limit, as the deceleration ratio is the crucial factor. The possible flow turning is further limited by the Mach number level and becomes smaller when this level is higher. $\Delta\alpha = \alpha_2 - \alpha_1$ and $\Delta\beta = \beta_2 - \beta_1$ ($\alpha > 0$, $\beta < 0$) may amount to about 40° with subsonic cascades (all velocities lower than sonic) and supercritical cascades (both inlet and outlet subsonic, but with a supersonic zone within the interior). With transonic cascades (inlet supersonic, outlet subsonic and a strong shock) and supersonic cascades (inlet supersonic, outlet supersonic and weak shocks) small losses are only attainable if the flow turning is limited to about 20° (see Sect. 13.4).

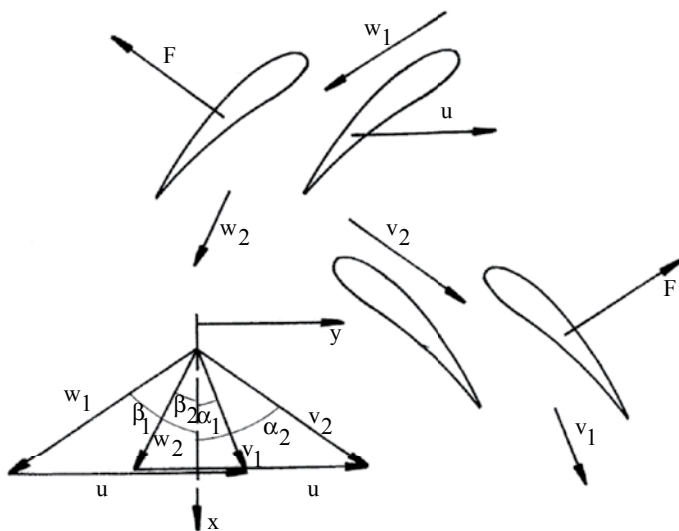


Fig. 13.1 Velocity triangles for an axial compressor stage

13.1.2 Fundamental Equations

We make the analysis for the rotor (it is similar for the stator). Figure 13.2 sketches a control volume for determination of momentum balances.

Axial Momentum

$$\dot{m}(w_{2a} - w_{1a}) \approx A_m(p_1 - p_2) - F_a.$$

F_a is the axial component of the force exerted on the blades and A_m is the area of the average orthogonal section. $-F_a$ is the axial force exerted on the flow. The approximation implies a linear representation of the pressure distribution on the envelope of the control volume.

$$w_a = cst \rightarrow F_a = A_m(p_1 - p_2) = -A_m \Delta p. \quad (13.1)$$

Since $p_2 > p_1$, so $F_a < 0$ (see Fig. 13.1).

Tangential Momentum As we reason with $r = \text{constant}$, the equation of moment of momentum around the shaft equals the equation of tangential momentum:

$$\begin{aligned} \dot{m}(w_{2u} - w_{1u}) &= -F_u, \\ \Delta w_u &= w_{2u} - w_{1u} = v_{2u} - v_{1u} > 0. \text{ Thus: } F_u < 0 \text{ (see Fig. 13.1),} \\ F_u &= -\dot{m} \Delta w_u. \end{aligned} \quad (13.2)$$

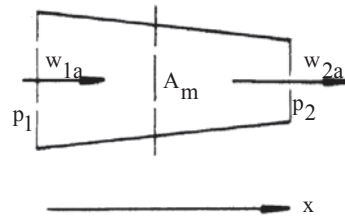
Rotor Work The work done on the flow by the blades, per mass unit (or the power per mass flow rate unit) is given by Euler's formula:

$$\Delta W = \frac{-u F_u}{\dot{m}} = u \Delta w_u. \quad (13.3)$$

Energy In the absolute frame, the total enthalpy rise equals the work done (for adiabatic flow):

$$\Delta W = H_2 - H_1,$$

Fig. 13.2 Control volume for momentum



with

$$H = e + \frac{p}{\rho} + 1/2 v^2 + U.$$

We ignore the effect of gravitational potential energy, resulting in:

$$\Delta W = h_{02} - h_{01},$$

where h_0 is the *stagnation enthalpy*. Further, we apply the term *total enthalpy* to indicate h_0 , by which is meant the sum of static enthalpy and kinetic energy. From the velocity triangles (Fig. 13.1) it follows:

$$\begin{aligned} w_1^2 &= v_1^2 + u^2 - 2u v_{1u} \\ w_2^2 &= v_2^2 + u^2 - 2u v_{2u} \\ \frac{w_1^2 - w_2^2}{w_1^2 - w_2^2} &= \frac{v_1^2 - v_2^2 + 2u \Delta v_u}{v_1^2 - v_2^2 + 2u \Delta v_u} \\ &= v_1^2 - v_2^2 + 2 \Delta W \end{aligned}$$

So:

$$\frac{w_1^2}{2} - \frac{w_2^2}{2} = h_2 - h_1,$$

or

$$h + 1/2 w^2 = h_{0r} = \text{constant}. \quad (13.4)$$

The *total relative enthalpy* h_{0r} is constant. This result stays valid for $v_a \neq \text{cst}$, but $u = \text{cst}$ is a requirement. We express the above result by stating that no work is done in the relative frame. Remark that total enthalpy (but in the absolute frame) is constant in the stator part of a compressor stage as no work is done in a stator.

13.1.3 Loss Representation

Figure 13.3 represents the h-s diagram of a compressor stage.

Loss is conventionally determined by comparing the real process with an isentropic process. For the rotor, the conventional loss is

$$\Delta h_{\text{loss}} = (h_2 - h_1) - (h_{2s} - h_1) = h_2 - h_{2s}.$$

Fundamentally, loss follows from

- Work equation in the rotor: $dW = 0 = d(1/2 w^2) + \frac{1}{\rho} dp + dq_{\text{irr}},$
- Energy equation in the rotor: $dW = 0 = d(1/2 w^2) + dh.$

The difference of these equations is

$$0 = dh - \frac{1}{\rho} dp - dq_{irr} \quad \text{or} \quad dq_{irr} = dh - \frac{1}{\rho} dp.$$

For $\rho = \text{constant}$: $dh_s = \frac{1}{\rho} dp$, or $\Delta h_s = \frac{1}{\rho} \Delta p$.

So : $q_{irr} = \Delta h - \frac{1}{\rho} \Delta p = \Delta h - \Delta h_s$.

So, the conventional loss is the loss the flow would be subjected to, if density were constant.

In order to express the conventional loss with a compressible fluid, a *process average density* may be defined by

$$\Delta h_s = \frac{\Delta p}{\rho_m} \quad \text{or} \quad \rho_m = \frac{\Delta p}{\Delta h_s}.$$

In a compression process, this average density only slightly deviates from the arithmetic average density.

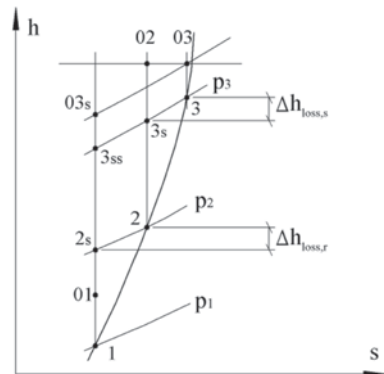
As $p \sim \rho^n \rightarrow \frac{\rho_2}{\rho_1} = \left(\frac{p_2}{p_1} \right)^{1/n}$,

it follows $\rho_r = 1/2 (\rho_1 + \rho_2) = 1/2 \rho_1 (1 + r^{1/n})$, with $r = p_2/p_1$.

From $h_{2s} - h_1 = h_1 \left(\frac{h_{2s}}{h_1} - 1 \right) = h_1 (r^{(\gamma-1)/\gamma} - 1)$,

it follows $\rho_m = \frac{p_1 (r-1)}{C_p T_1 (r^{(\gamma-1)/\gamma} - 1)} = \rho_1 \frac{\gamma-1}{\gamma} \frac{r-1}{r^{(\gamma-1)/\gamma} - 1}$.

Fig. 13.3 h-s diagram of a compressor stage



Further
$$\eta_\infty = \frac{n / (n-1)}{\gamma / (\gamma-1)}.$$

Example: for $r=2$ (so very big), $\eta_\infty=0.9$, $\gamma=1.4 \rightarrow n=1.465$,

$$\rho_r = \rho_1 1.302, \quad \rho_m = \rho_1 1.305.$$

We so may consider ρ_m as the arithmetic average density. With a good approximation, the conventional loss may be written as

$$\Delta h_{loss} = \Delta h - \Delta h_s = \Delta h - \frac{\Delta p}{\rho_m}. \quad (13.5)$$

The conventional loss differs from the real energy dissipation. From the general discussion on polytropic efficiency (Chap. 11, Sect. 11.2.3) we recall:

$$\Delta h_r = \int_1^2 \frac{dp}{\rho} \text{ (reversible work),}$$

$$q_{irr} = \Delta h - \Delta h_r = \Delta h \left(1 - \frac{\Delta h_r}{\Delta h} \right) = \Delta h (1 - \eta_\infty).$$

So:
$$\frac{\Delta h_{loss}}{q_{irr}} = \frac{\Delta h (1 - \eta_s)}{\Delta h (1 - \eta_\infty)}.$$

For $r=2$, $\eta_\infty=0.90$, $\gamma=1.4 \rightarrow \eta_s=0.890$.

So:
$$\frac{\Delta h_{loss}}{q_{irr}} = \frac{0.110}{0.100} = 1.100.$$

The reason for the difference is the reheat effect. Because of the irreversibility during compression, the gas is heated additionally, causing a next compression in a sequence of infinitesimal parts to require more work. In the conventional representation of losses, this additional work is considered as loss as well.

It is remarkable that the term $\Delta p / \rho_m$ constitutes a good approximation of the isentropic enthalpy rise. It may be verified that this applies for a wide range of pressure ratio values and infinitesimal efficiency values (see Exercise 13.6.1). The term sometimes is a slight underestimation and sometimes a slight overestimation. For a compression follows

$$\frac{\Delta p}{\rho_m} \approx \Delta h_s < \Delta h_r < \Delta h.$$

With the average density, the analysis of a compressor cascade may be performed analogously to the analysis of a constant density fluid cascade, as done in Chap. 2 (Sect. 2.2).

13.1.4 Loss Coefficients

With the conventional loss, an *enthalpy loss coefficient* for the rotor is

$$\xi_1 = \frac{\Delta h_{loss}}{1/2 w_1^2}. \quad (13.6)$$

Inlet kinetic energy is chosen as a reference value, as the process in compressor parts is deceleration (Fig. 13.3). We recall that outlet kinetic energy is chosen for turbine cascades (Chap. 6, Sect. 6.4.5).

A *pressure loss coefficient* may also be applied, defined by

$$\omega_1 = \frac{p_{01r} - p_{02r}}{p_{01r} - p_1}. \quad (13.7)$$

The pressure values necessary for (13.7) can accurately be measured, while the enthalpy values for the enthalpy loss coefficient (13.6) typically have large errors due to influence of heat transfer. For a constant density fluid, the expressions (13.6) and (13.7) are identical. For a compressible fluid, there is a difference that increases with increasing inlet Mach number (see Exercise 13.6.3). In practice, the pressure loss coefficient is determined from measurements, but the enthalpy loss coefficient is used in analysis.

13.1.5 Force Components

Introduction of the conventional loss implies

$$\Delta p = \rho_m (\Delta h - \Delta h_{loss}),$$

and so

$$\begin{aligned} F_a &= -A_m \Delta p = -\rho_m A_m (h_2 - h_1 - \Delta h_{loss}), \\ F_a &= -\rho_m A_m (1/2 w_1^2 - 1/2 w_2^2) + \rho_m A_m \Delta h_{loss} \quad (h_{or} = cst) \\ &= \rho_m A_m (1/2 w_{2u}^2 - 1/2 w_{1u}^2) + \rho_m A_m \Delta h_{loss} \quad (w_a = cst) \\ &= \rho_m A_m w_{mu} \Delta w_u + \rho_m A_m \Delta h_{loss}, \\ F_u &= -\dot{m} \Delta w_u = -\rho_m A_m w_a \Delta w_u. \end{aligned}$$

Without losses follows

$$w_a F_a + w_{mu} F_u = 0.$$

This implies that the resulting force is perpendicular to the average velocity. In presence of losses we may define lift as the component of the force perpendicular to the average velocity and drag the component in the direction of the average velocity.

This result is identical with the one attained in Chap. 2 with the analysis of constant density fluid flow through blade cascades. For a compressible fluid, lift coefficient and drag coefficient may be defined in exactly the same way. The only difference is the need to apply the average density.

Drag follows from

$$D = (w_a F_a + w_{mu} F_u) / w_m = \rho_m A_m \Delta h_{loss} \frac{w_a}{w_m} \quad \text{or} \quad D w_m = \dot{m} \Delta h_{loss}.$$

A drag coefficient related to inlet kinetic energy thus is:

$$C_{D1} = \frac{D}{1/2 \rho_m w_1^2 A_b},$$

where $A_b = c \ell$ is an approximation for the blade surface, with c the chord on the average radius and ℓ the average blade height. Further $A_m = s \ell$, with s being the spacing (or pitch). Solidity is defined by $\sigma = c/s$.

It follows that:

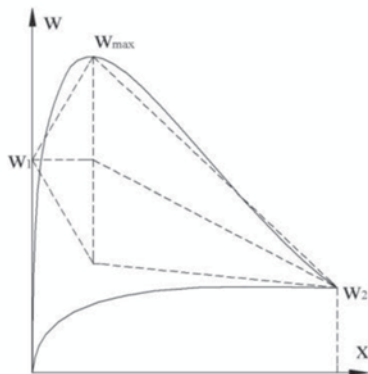
$$C_{D1} = \frac{\Delta h_{loss}}{1/2 w_1^2} \frac{s}{c} \frac{w_a}{w_m} = \frac{\xi_1}{\sigma} \cos \beta_m \quad \text{or} \quad \sigma C_{D1} = \xi_1 \cos \beta_m. \quad (13.8)$$

A lift coefficient may be defined analogously. This is formally possible, but not very useful with compressors. The solidity is mostly so high ($\sigma \approx 1.5$ to 2.0) that it is impossible to relate the lift coefficient of a cascade to the one of an isolated aerofoil and to apply corrections for cascade effect, since these corrections are unreliable for $\sigma > 1.3$ (Chap. 2, Sect. 2.1.7). The lift coefficients for optimum operation and for stall do not have approximate universal values with compressor cascades. A lift coefficient thus cannot be applied reliably for expressing the loading of a cascade and for selecting a cascade that realises a desired flow. In practice, semi-empirical correlations are applied (classic correlations are by Howell and by Lieblein) for determining, with given velocity triangles ($w_1, w_2, \beta_1, \beta_2$), the cascade that realises the desired flow turning $\Delta\beta = \beta_2 - \beta_1$. The discussion of these correlations exceeds the framework of this book however (see [10, 13]). The notion of diffusion factor is applied to determine the solidity required to realise a target flow turning, as discussed hereafter.

13.1.6 Diffusion Factor and Loss Correlations

The loss coefficient ξ_1 is proportional to the drag coefficient (13.8). The loss coefficient is correlated to a factor called *diffusion factor* DF , expressing the cascade loading. The diffusion factor so replaces the lift coefficient and the relation $\xi_1 = f(DF)$ or $\omega_1 = f(DF)$ is equivalent to the polar $C_D = f(C_L)$ of an aerofoil.

Fig. 13.4 Velocity distribution on a compressor blade (rotor)



There are variants of the diffusion factor definition. In Chap. 3 we applied the local diffusion factor D_{loc} . An expression better related to external parameters is the diffusion factor DF (name without any further specification).

$$D_{loc} = \frac{w_{max} - w_2}{w_{max}}, \quad DF = \frac{w_{max} - w_2}{w_1}. \quad (13.9)$$

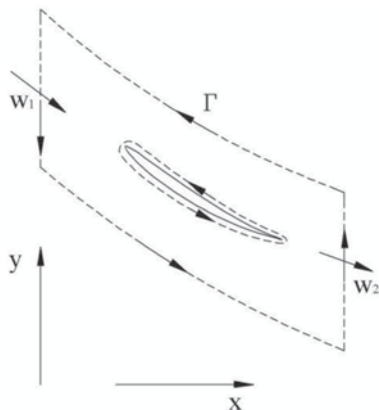
In these expressions, w_{max} is the maximum velocity at the suction side of the blade. Figure 13.4 sketches the velocity distribution on a compressor blade (velocity at the boundary layer edges). The flow at the pressure side is represented as uniformly accelerating, but in reality a zone with slightly decelerating flow may occur (see Sect. 13.4). The strongly decelerating part in the flow on the suction side corresponds to an adverse pressure gradient. For a too large adverse pressure gradient, the boundary layer separates. The diffusion factors are measures for the pressure gradient in the decelerating part of the boundary layer on the suction side. They determine the maximum velocity at the suction side and so the minimum pressure and thus the obtainable tangential force on a compressor cascade. We reason upon this relation intuitively here. A more rigid justification is given by Lieblein et al. [11, 12], based on boundary layer theory.

The diffusion factor can be related to the velocity triangles. This can be understood from expressing the circulation around a blade in two ways as sketched in Fig. 13.5. A first way is along a contour composed by periodic lines in between two neighbouring blades and tangential parts upstream and downstream of the cascade. The second way is along a contour following the edges of the boundary layers and cutting through the wake of the profile. With this second way, the circulation is equal to the surface integral of the velocity plot of Fig. 13.4, but with a curved abscissa following the profile surface. The two expressions of the circulation are equal for lossless flow.

The two expressions of the circulation result in

$$\Gamma = \oint w \, d\ell = s(w_{2u} - w_{1u}) = f_1 f_2 \frac{c}{2} (w_{max} - w_1).$$

Fig. 13.5 Calculation of the circulation around a profile in two ways



The factor f_1 takes into account that the integration path length is larger than the chord and the factor f_2 that the surface is larger than the sum of the triangles drawn in Fig. 13.4.

The relation thus implies $w_{max} - w_1 = f \frac{\Delta w_u}{\sigma}$,

where factor f is the inverse of $f_1 f_2$. The quantity $\Delta w_u / \sigma$ was called the circulation parameter by Lieblein et al. [11, 12] and they proved that the acceleration from the inlet velocity w_1 to the maximum velocity w_{max} can be very well correlated, for a large set of compressor cascade data for attached flow, by

$$w_{max} - w_1 = 0.5 \frac{\Delta w_u}{\sigma} + 0.1 w_1.$$

This allows, by dropping the constant factor 0.1, writing the diffusion factor as

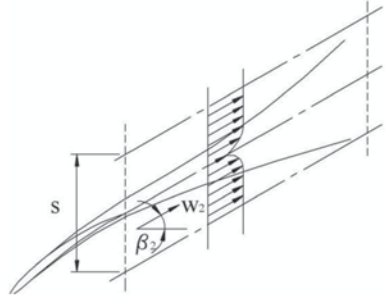
$$DF = 1 - \frac{w_2}{w_1} + \frac{\Delta w_u}{2\sigma w_1}. \quad (13.10)$$

The diffusion factor can be seen as the sum of two terms, one indicating the deceleration in the suction side boundary layer due to the general deceleration in the cascade and one as the supplementary deceleration due to the loading, i.e. the pressure difference between pressure and suction sides. Expressed as a function of the angles (see Fig. 13.1), the diffusion factor is

$$DF = 1 - \frac{\cos \beta_1}{\cos \beta_2} + \frac{\cos \beta_1}{2\sigma} (tg \beta_2 - tg \beta_1). \quad (13.11)$$

Figure 13.6 sketches the boundary layers and the wake of a blade, together with a velocity profile across the wake. The loss effect is noticeable within the wake. The

Fig. 13.6 Boundary layer zones and wake



momentum loss flow rate (defect of momentum flux due to presence of boundary layers) at the trailing edge of a blade may be expressed according to

$$\rho_2 w_2 w_2 (\delta_{2s} + \delta_{2p}).$$

The thickness measure δ_2 is called the momentum loss thickness and subscripts s and p refer to the suction and pressure sides, with w_2 being the average velocity in the core flow (the zone outside the boundary layers) immediately downstream of the cascade. The mixing loss in the wake follows from a momentum balance between a section just downstream of the cascade and a section far downstream with an assumed uniform flow.

The momentum balance, with the subscript m indicating the mixed flow, is

$$\rho_m A w_m w_m - (\rho_2 A w_2 w_2 - \rho_2 w_2 w_2 \delta_2) = (p_2 - p_m) A,$$

with $A = s \cos \beta_2$ and $\delta_2 = \delta_{2s} + \delta_{2p}$ the total momentum loss thickness. This thickness is small with respect to the blade spacing. So, we might ignore the difference between w_2 and w_m (w_2 is somewhat larger than w_m) and ignore the difference between ρ_2 and ρ_m (ρ_2 is somewhat smaller than ρ_m). A consistent approximation of the total pressure loss due to mixing is then

$$\Delta p_0 s \cos \beta_2 = \rho_2 w_2^2 \delta_2,$$

$$\text{so that} \quad \frac{\Delta p_0}{1/2 \rho_2 w_2^2} = \frac{2}{\cos \beta_2} \frac{\delta_2}{s} = \frac{2\sigma}{\cos \beta_2} \frac{\delta_2}{c}. \quad (13.12)$$

The boundary layer momentum thickness at the trailing edge, relative to the chord, δ_2/c , is strongly related to the cascade loading, in other words, the diffusion factor. Further, since the mixing loss is the dominant part of the total loss (the other part is the friction loss on the surfaces), on the basis of the shape of (13.12) we expect a strong correlation between

$$\xi'_I = \xi_I \frac{w_1^2}{w_2^2} \frac{\cos \beta_2}{2\sigma} = \xi_I \frac{\cos \beta_2}{2\sigma} \left(\frac{\cos \beta_2}{\cos \beta_I} \right)^2 \quad (13.13)$$

and the diffusion factor. The strong correlation was proven by Lieblein [11]. Figure 13.7 renders the result. The line shown is an average of very many experimental results, with a small spreading around the line. The loss coefficient rises sharply from $DF=0.6$. This value may be considered as the value above which stall occurs. $DF \approx 0.45$ is mostly accepted as the optimum. It corresponds to the best ratio of the loss coefficient according to (13.13) to the diffusion factor. Henceforth we apply this value to determine the optimum solidity. At present, many compressor cascades have a larger design diffusion factor, namely $DF=0.50$ in stator cascades and up to $DF=0.60$ in rotor cascades. Rotor cascades allow a greater diffusion factor as the boundary layers are reinforced by the centrifugal force (the data of Lieblein are for stationary cascades). The values $DF=0.50$ and $DF=0.60$ refer to cascades with a very high load. The very good correlation shown in Fig. 13.7, together with the sharp rise of the diffusion factor, proves the robustness of the diffusion factor as a measure for the cascade loading. To conclude, we remark that the loss coefficient has a rather good correlation with D_{loc} as well, with a value for strong loss increase around 0.50 [10, 11].

13.1.7 Kinematic Parameters

The degree of reaction is the ratio of static enthalpy rise and total enthalpy rise in the rotor (Fig. 13.3):

$$R = \frac{h_2 - h_1}{h_{02} - h_{01}}.$$

With $h_{or} = cst = h_1 + 1/2 w_1^2 = h_2 + 1/2 w_2^2$,

it follows
$$R = \frac{1/2 w_1^2 - 1/2 w_2^2}{u(w_{2u} - w_{1u})} = \frac{1/2 w_{1u}^2 - 1/2 w_{2u}^2}{u(w_{2u} - w_{1u})} = -\frac{w_{mu}}{u}.$$

Further:

- work coefficient $\psi = \frac{\Delta W}{u^2} = \frac{w_{2u} - w_{1u}}{u},$
- flow coefficient $\phi = \frac{w_a}{u}.$

So:

$$\left. \begin{aligned} \frac{w_{2u}}{u} - \frac{w_{1u}}{u} &= \psi \\ -\frac{w_{2u}}{u} - \frac{w_{1u}}{u} &= 2R \end{aligned} \right\} \quad \begin{aligned} -\frac{w_{1u}}{u} &= R + \frac{\psi}{2}, & -\frac{w_{2u}}{u} &= R - \frac{\psi}{2}. \end{aligned}$$

Fig. 13.7 Loss coefficient as a function of the diffusion factor with compressor cascades, according to Lieblein [11]

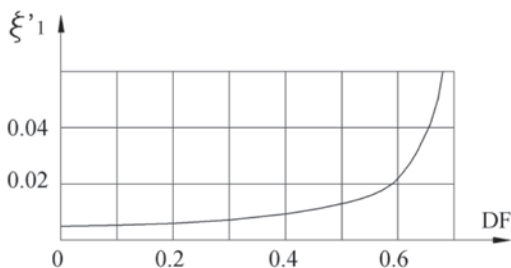
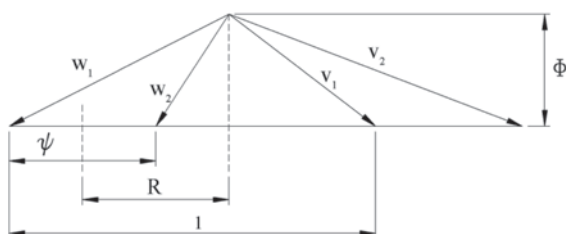


Fig. 13.8 Dimensionless velocity triangles



The parameters R , ϕ and ψ unambiguously determine the shape of the velocity triangles. Therefore, they are denominated *kinematic parameters*. Figure 13.8 represents the velocity triangles with velocity components made dimensionless by dividing them by the blade speed.

The triangles for $R=0.8$, $\psi=0.3$, $\phi=0.4$; $R=0.7$, $\psi=0.4$, $\phi=0.5$; $R=0.5$, $\psi=0.7$, $\phi=0.65$ are sketched in Fig. 13.9. These combinations are representative for the flow near the casing, at mean radius and near the hub of a compressor with radius ratio 1.20/0.75 (see Sect. 13.3). For $R=0.50$, there is symmetry between the rotor and the stator (inlet and outlet velocities are equal). For $R>0.5$, rotor velocities are larger than stator velocities and the turning angle within the stator exceeds that within the rotor. The stage inlet and outlet velocity (v_1) is nearer to the axial direction than with $R=0.5$.

13.1.8 Secondary Flow: Principle

The flow within a turbomachine is generally subdivided into the sum of two flows. The idea is to discern between the losses on the blades and the losses caused by the hub and the casing. The flow that would be generated in absence of viscous effects on the hub and the casing and in absence of clearances between the rotor blades and the casing and between the stator vanes and the hub is called the *primary flow*. So, it is the flow over the blades, confined without clearances by the hub and the casing, the so-called *end walls*, assuming that slip occurs at these surfaces. The difference between the full flow and the primary flow is called the *secondary flow*. The secondary flow thus describes the influence of the end wall boundary layers and the

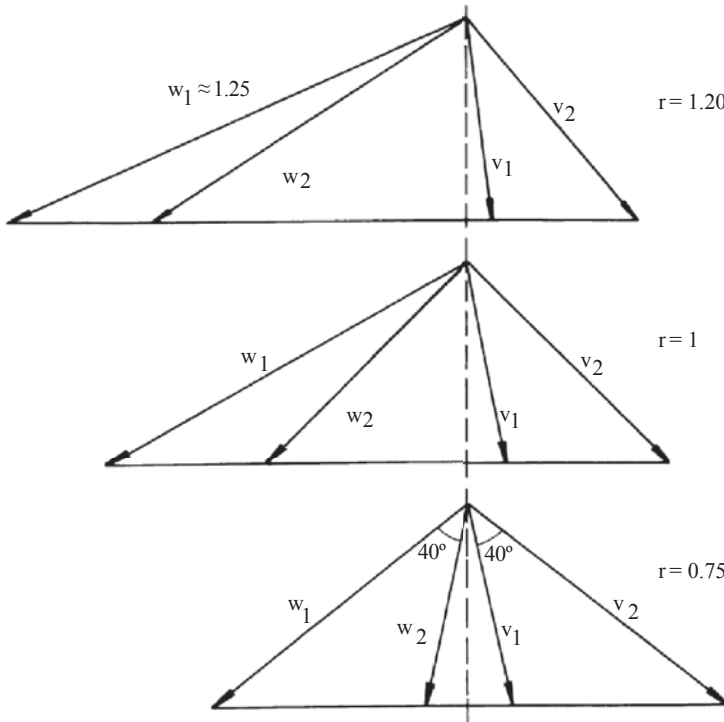


Fig. 13.9 Velocity triangles for $R = 0.8$, $\psi = 0.3$, $\phi = 0.4$ (top); $R = 0.7$, $\psi = 0.4$, $\phi = 0.5$ (middle); $R = 0.5$, $\psi = 0.7$, $\phi = 0.65$ (bottom), representative for the flow near the casing, at mean radius and near the hub of a compressor with radius ratio 1.20/0.75

clearances. The primary flow is sometimes defined more restrictively as the flow on the average radius, which means that the radial variation of the primary flow is then ignored. The latter simplification is not necessary for a good understanding, as will emerge from the discussion in Sect. 13.1.10 about flow optimisation. Some basics of secondary flow and of radial flow variation are required to understand this optimisation. A detailed discussion of these subjects follows later. Here, we briefly discuss secondary flow. The next section deals with a brief discussion of radial variation.

The end wall boundary layers react with the core flow or primary flow. This generates a series of flow patterns, all of them with a vortex character. We therefore refer to these as *secondary vortices*. The dominant vortex is the passage vortex, which is the result of the turning within the primary flow. A centrifugal force that is balanced by the pressure difference between the pressure and the suction sides of the blades corresponds with this turning. But the velocity is lower in the end wall boundary layers than in the core flow. For the same turning, the centrifugal force and the pressure difference are weaker there. The consequence is the generation of

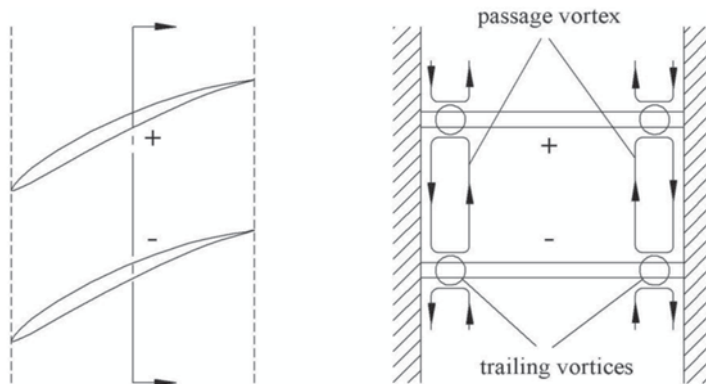


Fig. 13.10 Passage vortex and trailing vortices in wake zones

two vortex motions, as sketched in Fig. 13.10, similar to the vortices in a bend of a pipe (Chap. 2, Sect. 2.3). These are together referred to by the term *passage vortex*. The figure also shows that passage vortices from neighbouring channels may trigger vortex motions in the wake zones of the blades. These vortices are called *trailing vortices*. This is the same name as given to vortices starting from the trailing edge of a blade due to circulation variation along the span (Chap. 3, Fig. 3.30).

A passage vortex changes the direction of the flow near an end wall. With Fig. 13.10, one verifies that the turning increases in the end wall boundary layers and decreases some distance away from the end walls (so-called overturning at the end wall itself). Another consequence is a supplementary loss, caused by the kinetic energy associated to the vortices. This energy is taken from the primary flow and almost completely dissipated downstream of the blade row. The sum of losses due to the secondary flow (sum over several vortices) may be very important. For smaller aspect ratio (say around two), the total secondary flow loss may be comparable to the total loss within the primary boundary layers (the boundary layers on the blades) for optimal incidence (minimum primary loss). The loss in the end wall boundary layers itself is typically half as big as the primary loss with optimum incidence. In other words, end wall effects, i.e. viscous effects, clearances and secondary vortices, may increase the sum of losses with a factor of about 2.5 compared to the losses within the primary flow.

13.1.9 Radial Variation of Flow: Principle

At the inlet and the outlet of a compressor stage, the flow in the absolute system is close to the axial direction (small tangential velocity component; see Fig. 13.1). So, there is only little centrifugal force in the direction from hub to casing within the inlet and the outlet flows. As a consequence, the flow is almost homogenous. The flow has a significant tangential velocity component in the space between the

rotor and the stator. The associated centrifugal force causes a higher pressure at the casing and a lower one at the hub. A stage is normally designed with the same work on all radii. Because of the greater pressure rise within the rotor at the casing and the lower pressure rise at the hub, the degree of reaction increases from the hub to the casing. For example, with $R=0.7$ on the average radius, $R\approx 0.8$ at the casing and $R\approx 0.5$ at the hub may be expected at ratios for outer and inner radii $r_o/r_m = 1.2$ and $r_i/r_m = 0.75$ (a detailed analysis follows in Sect. 13.3). With $\psi \sim 1/u^2$, the velocity triangles are as sketched in Fig. 13.9. We note that the rotor blades have a strong twist and that the flow turnings in rotor and stator are the largest at the hub.

13.1.10 Optimisation of a Stage

From the h-s diagram (Fig. 13.3) it follows

$$\eta_{tt} = \frac{h_{03s} - h_{01}}{h_{03} - h_{01}}.$$

With

$$\begin{aligned} h_{03s} - h_{01} &\approx h_{3ss} - h_1 \approx (h_{3s} - h_2) + (h_{2s} - h_1) \\ &= (h_3 - h_2) - \Delta h_{loss,s} + (h_2 - h_1) - \Delta h_{loss,r}, \end{aligned}$$

it follows that

$$\eta_{tt} \approx 1 - \frac{\Delta h_{loss,s} + \Delta h_{loss,r}}{\Delta W}.$$

Not only primary losses, but also losses within the end wall boundary layers and secondary losses intervene. Primary losses, even, are not dominant. With $R=0.5$, the velocity levels within rotor and stator are the same and flow turnings are the same. So, primary losses in rotor and stator are equal. Thus, with regard to primary losses, $R=0.5$ on the average radius is optimal: minimum sum of losses when both terms are equal. With increasing R , the absolute flow is closer to the axial direction, especially at the casing. Figure 13.11 (left) sketches the entry part of the low-pressure compressor of a bypass aero-engine [2]. The figure is also representative for the first part of a compressor of an industrial gas turbine or a turbofan engine. The hub is built with connected discs. The rotor blades have a clearance at the casing. The boundary layer flow on the casing occurs within the absolute frame, but, of course, the boundary layer gets distorted by the passing of rotor tips. It is obvious that a better axial direction of the boundary layer aligns the momentum better with the adverse pressure gradient. This attenuates the growth of the end wall boundary layer at the casing, causing a decrease of losses in this boundary layer and a decrease of the intensity of the secondary flows generated. A high degree of reaction at the casing is therefore favourable for reduction of secondary losses and boundary layer losses at the casing. Figure 13.11 (right) shows that stator vanes have cover bands with labyrinth seals at the hub [16]. The end wall boundary layer at the hub alternately flows in the absolute frame and the relative frame. Therefore, with regard to minimisation of the whole of losses, 50% degree of reaction at the hub is optimum (symmetry between rotor and stator).

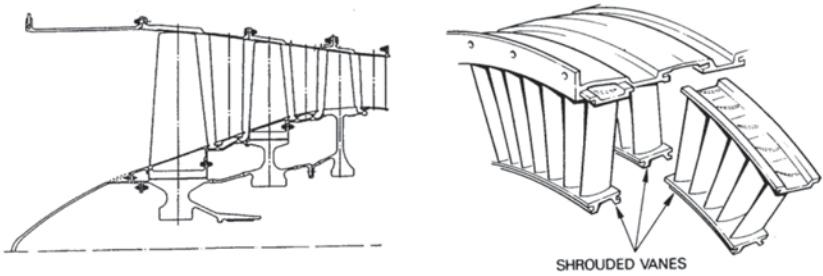


Fig. 13.11 Compressor hub and casing. (*Left* from [2]; permission by SAGE Publications; *right* from [16]; permission by Rolls-Royce)

Because of both effects, a degree of reaction on the average radius above $R=0.5$ is better. Typical values at optimum are (see Sect. 13.3):

Average radius	$R=0.7, \psi=0.4, \phi=0.5$
Casing	$R=0.8, \psi=0.3, \phi=0.4$
Hub	$R=0.5, \psi=0.7, \phi=0.65$

Figure 13.9 sketches the corresponding dimensionless velocity triangles for constant axial velocity (see the later Table 13.2). Due to the deceleration ratio limitation of $w_2 / w_1 \approx 0.70$ and $v_1 / v_2 \approx 0.70$ at the hub, limiting the possible flow turning, ψ on the average radius cannot be higher than about 0.4. The value of ϕ should be chosen as large as possible in order to allow the greatest possible flow rate through the compressor. But $\dot{V} \sim \phi u$ and $\Delta W = \psi u^2$. With regard to stage work it is more advantageous to choose the blade speed u as high as possible and to choose ϕ rather low, taking into account that the Mach number of w_l should be limited at the casing. With an aero-engine compressor, the average radius blade speed typically amounts to about 360 m/s, being about the speed of sound, so that the Mach number corresponding to w_l at the casing is about 1.25 (Fig. 13.9). This can hardly be increased without generating great losses by shock waves. These considerations explain the typical values of degree of reaction, work coefficient and flow coefficient, given above. These values are not universal however. The exact optimum depends very much on the boundary layer status on the end walls, determined strongly by losses in previous stages, and the relative importance of secondary losses and end wall boundary losses, determined strongly by the aspect ratio of the blades (height to chord ratio). The cited values are typical for stages with important secondary losses (aspect ratio around two and not front stages), but still high ratio of casing radius to hub radius, as the second and third stages of the low-pressure compressor of an aero-engine, as shown in Fig. 13.11.

A first stage typically has a somewhat lower degree of reaction at the mean radius (50–60%) and later stages a somewhat higher degree of reaction (80%). A particular case is the fan stage of a turbofan engine. It is the first stage of the engine and the aspect ratio is extremely high. Secondary losses do not have a big role. So,

aiming at a degree of reaction 50% at the hub has no meaning. Further, the variation of the degree of reaction from hub to casing is extreme, which means that the degree of reaction at the hub must be small. The Mach number limitation at the rotor entrance at the tip of the rotor blade is crucial. This means that the velocity triangles at the tip are still close to the triangles shown on top of Fig. 13.9, but with a somewhat larger degree of reaction such that the entrance velocity v_l is in the axial direction (also a somewhat larger Mach number of the relative flow at rotor inlet). The hub has a low degree of reaction. So, rotor flow turning becomes big near the hub and in order to limit it, the work must be lowered near the hub (see Exercise 13.6.5). Thus, the work cannot be constant along the radius.

13.1.11 Blade Shape

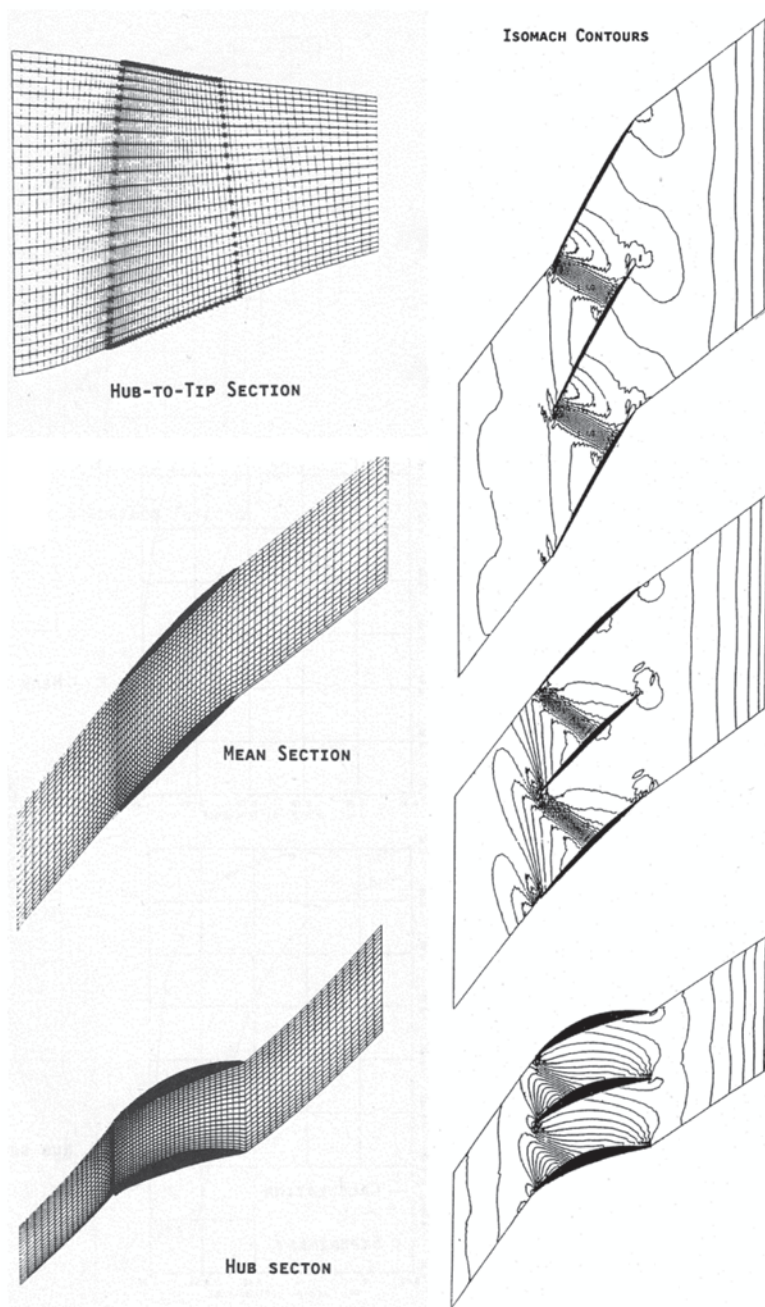
The velocity triangles for the average radius are rendered in Fig. 13.9. Diffusion factors for rotor and stator are

$$DF_r = 1 - \frac{w_2}{w_1} + \frac{\Delta w_u}{2\sigma_r w_1} = 1 - 0.7 + \frac{0.4}{2\sigma_r} = 0.3 + \frac{0.2}{\sigma_r},$$

$$DF_s = 1 - \frac{v_1}{v_2} + \frac{\Delta v_u}{2\sigma_s v_2} = 1 - \frac{0.5}{0.7} + \frac{0.4}{1.4\sigma_s} = 0.286 + \frac{0.286}{\sigma_s}.$$

For $DF=0.45$ it follows $\sigma_r=1.33$ and $\sigma_s=1.75$. These are rather high solidities. Note also that $w_2/w_l=0.69$ and $v_l/v_2=0.72$. So, rather strong velocity reductions are required. About 50% of the kinetic energy at the inlet has to be converted into static enthalpy increase. This is about the possible maximum. We note that the velocity reductions at the hub in Fig. 13.9 amount to about 0.63. Such reductions are actually unrealisable. A solution is discussed in Sect. 13.3.6.

Figure 13.12 shows a rotor example and the computed flow [9]. Grid lines of the computational grid are shown on the left and Mach contour lines are shown on the right. The solidity is about 1.33 on the average radius, 1.70 at the hub and 1.20 at the casing. At the hub, the flow is supercritical, i.e. inlet and outlet flows are subsonic, but a supersonic zone occurs with generation of a normal shock. This shock is rather weak with a Mach number just upstream of the shock about 1.1. On the average radius, the flow is transonic, i.e. the inlet flow is supersonic (the inlet Mach number is just above one) and the outlet flow is subsonic with velocity reduction through a normal shock. The flow is transonic as well at the casing with inlet Mach number about 1.2 and outlet Mach number about 0.9. A compressor stage is called transonic when the relative flow entering the rotor is supersonic in the tip region and subsonic in the hub region. With a subsonic or a supersonic stage, the relative flow at rotor inlet is subsonic or supersonic over the whole span.



13.1.12 Attainable Pressure Ratio

For $u=360$ m/s and $\psi=0.45$ (which is a high value), the stage work is $\Delta W=58.3$ kJ/kg. The temperature rise is then about 57 K. From this follows

$$\frac{p_{02}}{p_{01}} = \left(\frac{T_{02}}{T_{01}} \right)^{\frac{\gamma}{\gamma-1}\eta_{\infty}} \approx \left(1 + \frac{57}{288} \right)^{3.15} \approx 1.75.$$

This level of pressure ratio is attained in the outer part of the fan of a turbofan engine (see Exercises 13.6.5 and 13.6.6). At $u=360$ m/s, the flow at the rotor inlet is supersonic ($w_1 \approx u$; Mach number is about 1.20 for velocity of sound about 300 m/s at 215 K). The cascade is then transonic with subsonic outflow and the pressure rise is mainly by the normal shock in the blade passage (see Sect. 13.4). The drawback of a high Mach number level is the small operating range of the stage (small possible flow rate variation between stall and choke; see Sect. 13.5). For larger operating range, the Mach number level must be lower. With supercritical flow, the inlet Mach number may be about 0.8 so that $w_1 \approx 0.8 \times 300$ m/s ≈ 240 m/s. With $w_1 \approx u$ follows $\Delta W \approx 26$ kJ/kg and $p_{02}/p_{01} \approx 1.28$. In present-day airliner aero-engines, the pressure ratio per stage is about this value, e.g. Trent800 (Rolls-Royce): $r=40$ in 15 stages. A much higher pressure ratio is used in military engines (bypass), e.g. EJ200 (Eurojet): $r=26$ in eight stages, thus 1.50 per stage, resulting in a small operating range. With industrial compressors or compressors of power gas turbines, a large operating range is required and the flow must be completely subsonic (at most supercritical), e.g. the compressor of the power gas turbine SGT6-5000F (Chap. 11): $r=17$ in 16 stages, thus about 1.19 per stage.

The conclusion is that the attainable pressure ratio per stage may be strongly different in different applications and that it is largely determined by the allowable Mach number at the rotor inlet. The allowable Mach number depends strongly on the necessary operating range of the compressor (see Sects. 13.4 and 13.5).

13.2 Secondary Flow

13.2.1 Definition of Secondary Flow

Secondary flow was defined in Sect. 13.1.8. Secondary flow is the difference between the complete flow and the primary flow. The primary flow is the flow that would be obtained in absence of boundary layers and clearances on the end walls. The interaction between end wall boundary layer flows and clearance flows with the primary flow generates a series of vortices called *secondary vortices*.



Fig. 13.13 Horseshoe vortex generation; *left* side view; *right* back view

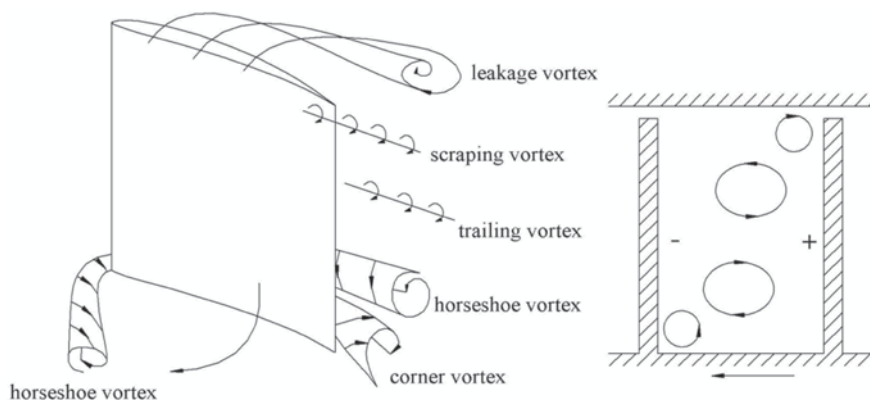


Fig. 13.14 Horseshoe vortex, scraping vortex, leakage vortex, trailing vortex, corner vortex; rotor blade passage with clearance at the casing

13.2.2 Passage Vortex and Trailing Vortices

The passage vortex was already discussed in Sect. 13.1.8. It results from the turning of the primary flow and the centrifugal force associated with it, being stronger in the flow core than in the end boundary layers. Figure 13.10 represents the passage vortex within a linear cascade with added end walls. In a real compressor, the passage vortex is distorted compared to the sketch, because the blade spacing increases with the radius. A significant effect of the passage vortex is a change in the outlet direction of the flow. The flow turning by the blades is increased in the boundary layers at the hub and the casing and reduced some distance away from the end walls. Another passage vortex effect is trailing vortex generation within the wake flow of the blades, as sketched in Fig. 13.10. The trailing vortices may be weak since the passage vortices typically do not come as close to each other as suggested in Fig. 13.10 (see Fig. 13.14).

13.2.3 Corner Vortices

In principle, corner vortices may form, driven by the passage vortex, in the corners between the hub and a blade and between the casing and a blade. According to Fig. 13.10, four corner vortices might be expected in each blade passage. These corner vortices interact however with other vortices, as discussed below.

13.2.4 Horseshoe Vortex

Figure 13.13 demonstrates that the stagnation pressure at the blade leading edge is higher within the core flow than in the end wall boundary layer (the static pressure is constant on a line perpendicular to parallel streamlines). As a consequence thereof, a vortex is generated that wraps around the leading edge, with forming of a pressure side leg and a suction side leg. This vortex is denominated *horseshoe vortex*, because of its shape.

Figure 13.14, left, demonstrates how the passage vortex drives the horseshoe vortex leg at the pressure side to the suction side of the neighbouring blade (a rotor hub zone is shown). The rotation sense of this horseshoe vortex leg is the same as that of the passage vortex. Both vortices merge, making the difference between both of them mostly invisible in the outlet plane of the cascade. The horseshoe vortex leg at the suction side of the blade is driven by the passage vortex into the corner between the blade and the end wall. The rotation sense of this horseshoe vortex leg is opposite to the rotation sense of the passage vortex. The two vortices do not merge, but reinforce each other. The horseshoe vortex leg may be directly in the corner, but a corner vortex may also form underneath the horseshoe vortex, as suggested in Fig. 13.14. In particular, this may happen with separated flow in the corner between the suction side of the blade and the end wall. Typically, no corner vortex forms in the corner at the pressure side, as no stall occurs. Analogous horseshoe vortex legs and corner vortices are generated at the stator vanes near the casing. The same occurs when there is no clearance at the hub (typically: cover bands; see Fig. 13.11). In case of a clearance, a leakage vortex and a scraping vortex are generated, as discussed next.

13.2.5 Leakage Vortex and Scraping Vortex

With rotor blades, there is a clearance at the casing. The leakage flow from the pressure side to the suction side forms a *leakage vortex* and the motion of the blade with respect to the casing causes a *scraping vortex* at the pressure side (Fig. 13.14, left). The leakage vortex and the scraping vortex have the same sense of rotation, opposite to the rotation sense of the passage vortex. Downstream of the blade passage, the leakage and scraping vortices have the tendency to merge. The result is

that downstream of a rotor blade passage, four vortex structures are typically visible (Fig. 13.14, right): a hub passage vortex together with a counter-rotating vortex in the corner between the suction side of the blade and the hub (leg of the horseshoe vortex); a casing passage vortex together with a counter-rotating vortex in the corner between the pressure side of the blade and the casing (the leakage vortex). The other vortices are typically much weaker.

13.2.6 Loss Assessment

The secondary flow generates a loss that may be expressed by an additional drag coefficient. According to Howell's measurements on slender rotor blades (high aspect ratio), approximately applies

$$C_{D,\text{sec}} = 0.018 C_L^2.$$

With a low aspect ratio, secondary flows are higher. Vavra finds (c is chord, h is height):

$$C_{D,\text{sec}} = 0.04 C_L^2 \frac{c}{h}.$$

Both formulae give the same result for $c/h=0.45$, which means that Vavra's formula must be applied with aspect ratio h/c lower than 2.22. The end boundary layers themselves generate a loss as well. The associated drag coefficient is approximately $0.02 s/h$, with s the blade spacing. The typical magnitude of the loss coefficients ($c/s \approx 1.33$, $h/c \approx 2$) is

$$C_{D,\text{prim}} = 0.02, C_{D,\text{end}} = 0.01, C_{D,\text{sec}} = 0.02.$$

This means that the primary loss mostly is not dominant within the total loss.

13.3 Radial Flow Variation

13.3.1 S_1 - S_2 Decomposition

Analytical study of the real three-dimensional flow in a turbomachine is impossible and only numerical solution of the flow equations is achievable. An often used simplification is a *quasi-three-dimensional representation of the flow*. It is assumed then that flow within blade passages occurs on circumferential streamsurfaces (surfaces of revolution). The flow is represented two-dimensionally on such surfaces, denominated S_1 -surfaces or *blade-to-blade surfaces*. The shape of these S_1 -surfaces follows from the streamlines within a meridional section, where the

flow is averaged in the circumferential direction. This again gives a two-dimensional flow denominated flow on the S_2 -surface or the *hub-to-shroud surface*. An S_2 -surface is typically a meridional plane, but it may also be a streamsurface. The equations describing the flow on the S_2 -surface contain terms expressing the average effect of the blade forces. The S_1 - S_2 decomposition technique requires iteration between calculations on the S_2 -surface (through-flow) and calculations on a series of S_1 -surfaces (blade-to-blade flows). No analytical solution is possible for either of these two-dimensional flow types. So the technique has to be a numerical one. A Cartesian-type grid for three-dimensional calculation is represented in Fig. 13.12. The projection of the quasi-radial grid lines and the quasi-axial grid lines on a meridional plane is shown. This hub-to-shroud surface could be an S_2 -surface and the surfaces of revolution obtained with the quasi-axial grid lines could be S_1 -surfaces. The S_1 - S_2 decomposition technique was proposed by C.H. Wu in 1952 as an exact decomposition of a three-dimensional flow into two-dimensional flows. But, S_1 -surfaces are then not surfaces of revolution, but are twisted. The S_2 -surface is twisted too. The exact decomposition leads to a time-consuming iterative calculation with, nowadays, no advantage compared to an entirely three-dimensional flow calculation. Nowadays, the quasi-three-dimensional flow representation is used, typically followed by a fully three-dimensional simulation.

13.3.2 Radial Equilibrium

In the space in between rotor blade rows and stator blade rows, there is no blade force in the circumferentially averaged S_2 -flow. Therefore, the circumferential S_1 -streamsurfaces may be determined approximately on purely geometrical grounds, for instance by equal distances in between them. The momentum equation in the direction perpendicular to the streamsurfaces is then reduced to equilibrium between the centrifugal force associated to the tangential velocity component and a pressure gradient in the normal direction. A further simplification comes with the assumption of cylindrical streamsurfaces. Both forces are in the radial direction then and the equilibrium is called *radial equilibrium*. From the radial equilibrium follows an equation allowing the analysis of the variation in the radial direction of the velocity components. This allows acquiring a qualitative image of the real three-dimensional flow.

The equation of radial equilibrium is

$$\frac{1}{\rho} \frac{dp}{dr} = \frac{v_u^2}{r}.$$

Total enthalpy is

$$h_0 = h + \frac{1}{2}v_a^2 + \frac{1}{2}v_u^2.$$

From derivatives in the radial direction follows

$$\frac{dh_0}{dr} = \frac{dh}{dr} + v_a \frac{dv_a}{dr} + v_u \frac{dv_u}{dr}.$$

With the definition of entropy follows

$$T \frac{ds}{dr} = \frac{dh}{dr} - \frac{1}{\rho} \frac{dp}{dr}.$$

Combination of the three differential equations results in

$$\frac{dh_0}{dr} - T \frac{ds}{dr} = v_a \frac{dv_a}{dr} + \frac{v_u^2}{r} + v_u \frac{dv_u}{dr}. \quad (13.14)$$

A stage is normally designed for constant work over the radius. This implies constant total enthalpy over the radius. Further, it is reasonable to assume constant losses over the radius, which then implies constant entropy over the radius. This approximation is adequate in the core part of the flow, but losses obviously are greater within the end wall boundary layers. With these simplifications, (13.14) becomes

$$v_a \frac{dv_a}{dr} + \frac{v_u^2}{r} + v_u \frac{dv_u}{dr} = 0,$$

or

$$1/2 \frac{dv_a^2}{dr} + \frac{v_u}{r} \frac{d}{dr}(rv_u) = 0. \quad (13.15)$$

Equation (13.14) is denominated the non-isentropic simple radial equilibrium equation (NISRE). Equation (13.15), where the term dh_0/dr might be kept, is denominated the isentropic simple radial equilibrium equation (ISRE). The term simple expresses the assumed absence of a radial velocity component.

13.3.3 Free Vortex Blades

Equation (13.15) is met for constant values of rv_u and v_a . The corresponding blade shape is denominated *free vortex blade*. The term means that the angular momentum within the flow is constant. No twisting is then exerted on circumferential stream-surfaces. The variation of the velocity triangles over the radius is then determined when velocity triangles on the average radius are chosen.

As a first example of kinematic parameters on the average radius we assume

$$\psi = 0.4, \quad \phi = 0.5, \quad R = 0.5.$$

Table 13.1 Flow parameter variation with free vortex blades; $R=0.50$ on the average radius

u	v_a	v_{u1}	v_{u2}	v_l/v_2	w_{u1}	w_{u2}	w_2/w_1
0.75	0.5	0.40	0.933	0.605	-0.350	0.183	0.872
1	0.5	0.30	0.7	0.678	-0.7	-0.3	0.678
1.20	0.5	0.25	0.583	0.728	-0.950	-0.617	0.740
R	α_l	α_m	$\Delta\alpha$	v_2	β_m	$\Delta\beta$	w_l
0.11	38.66	50.24	23.15	1.058	-7.45	55.09	0.610
0.50	30.96	42.71	23.50	0.860	-42.71	23.50	0.860
0.65	26.57	37.98	22.81	0.768	-56.61	11.26	1.074

Table 13.2 Flow parameter variation with free vortex blades; $R=0.70$ on the average radius

u	v_a	v_{u1}	v_{u2}	v_l/v_2	w_{u1}	w_{u2}	w_2/w_1
0.75	0.5	0.133	0.667	0.621	-0.617	0.083	0.638
1	0.5	0.1	0.5	0.721	-0.9	-0.5	0.687
1.20	0.5	0.083	0.417	0.779	-1.117	-0.783	0.759
R	α_l	α_m	$\Delta\alpha$	v_2	β_m	$\Delta\beta$	w_l
0.47	14.57	33.92	38.70	0.84	-30.10	42.02	0.80
0.70	11.31	28.16	33.69	0.71	-52.98	15.95	1.03
0.79	9.09	24.56	30.94	0.65	-61.64	8.60	1.23

We calculate the velocity triangles on the radii $r_o/r_m=1.20$ (outer radius of the flow annulus) and $r_i/r_m=0.75$ (inner radius of the flow annulus). With this choice, the through-flow areas above and under the average radius are equal. The radius variation is rather great, typical for first stages in a real compressor. With a fan stage, the radius ratio is much greater, however. The results are listed in Table 13.1. The velocity components on the average radius follow from the chosen kinematic parameters. The axial velocity is constant over the radius. The tangential velocity components in the absolute frame on the outer and inner radii follow from the free vortex law. The blade speed on the average radius is represented as a unit.

Observations are:

- rotor blade twist is very high: β_m varies from -7.5° to -56.5° : twist $\approx 50^\circ$;
- flow turning at the rotor hub is very high: $\Delta\beta \approx 55^\circ$;
- deceleration at the stator hub is strong: velocity ratio ≈ 0.60 ;
- all inlet Mach numbers are moderate; as the blade speed on the average radius is around the speed of sound, dimensionless velocities are approximately Mach numbers.

A higher degree of reaction on the average radius reduces the observed disadvantages. With $\psi=0.4$, $\phi=0.5$ and $R=0.7$ on the average radius, the results are listed in Table 13.2.

Favourable findings are:

Table 13.3 Flow parameter variation with free vortex blades; $R=0.80$ on the mean radius

u	v_a	v_{u1}	v_{u2}	v_1/v_2	w_{u1}	w_{u2}	w_2/w_1
0.75	0.5	0	0.533	0.684	-0.75	-0.217	0.605
1	0.5	0	0.4	0.781	-1	-0.6	0.698
1.20	0.5	0	0.333	0.832	-1.20	-0.867	0.770
R	α_l	α_m	$\Delta\alpha$	v_2	β_m	$\Delta\beta$	w_l
0.65	0	23.42	46.83	0.73	-39.89	32.85	0.90
0.80	0	19.33	38.66	0.64	-56.81	13.24	1.12
0.86	0	16.84	33.67	0.60	-63.71	7.35	1.30

- rotor blade twist is acceptable: $\approx 31.5^\circ$;
- flow turning at the rotor hub is acceptable: 42° at Mach number 0.80;
- deceleration at the stator hub is less strong: velocity ratio ≈ 0.62 .

Unfavourable findings are that the deceleration at the rotor hub becomes strong and that the Mach number at the rotor inlet at the tip becomes high. Further raising the degree of reaction on the average radius causes further decrease of the deceleration ratio at the rotor hub and further increase of the inlet Mach number at the rotor tip, as demonstrated by the results in Table 13.3 for $\psi=0.4$, $\phi=0.5$ and $R=0.8$ on the mean radius.

Free vortex blades do not result in an entirely advantageous variation of the flow parameters, unless work is decreased (ψ under 0.40 on the mean radius) or the choice for a repeating stage is abandoned. The best flow for the radius ratio 1.20/0.75 is obtained with $R=0.70$ on the mean radius (Table 13.2). The corresponding velocity triangles are shown in Fig. 13.9. Remark that the flow at inlet and outlet of the stage deviates from the meridional plane ($\alpha_l \approx 15^\circ$ at the hub). This deviation from the meridional plane mainly has as benefit that the Mach number of the relative flow at the rotor inlet lowers somewhat with respect to the value without pre-swirl. Further improvement at the rotor tip is possible by forcing the vortex distribution somewhat, as discussed in the next section.

13.3.4 Forcing of the Vortex Distribution

A more favourable variation of flow parameters may be achieved by forcing the swirl distribution somewhat away from the free vortex. The following relations apply:

$$v_{u1} = v_{um} - \frac{\Delta v_u}{2} = v_{um} - \frac{\Delta W}{2u},$$

$$v_{u2} = v_{um} + \frac{\Delta v_u}{2} = v_{um} + \frac{\Delta W}{2u}.$$

ΔW is kept constant over the radius. The variation of v_{um} with free vortex blades is inversely proportional to the radius. This variation may be chosen however. In order to establish the influence of this variation, we assume $v_{um} \sim r^n$. With the exponent $n=-1$, free vortex blades are recovered. Hereafter, we calculate the variation of the flow parameters for $n=0$. Velocities are written in dimensionless form by dividing them by the blade speed on the mean radius. The Eq. (13.15) stays valid with dimensionless quantities. The variation of tangential velocity components follows from

$$\bar{v}_{u1} = \frac{v_{u1}}{u_m} = \frac{v_{um}}{u_m} - 1/2 \frac{\Delta W}{u_m^2} \frac{u_m}{r},$$

$$\text{or} \quad \bar{v}_{u1} = (1 - R_m) \bar{r}^n - 1/2 \psi_m / \bar{r}. \quad (13.16)$$

Analogously it applies that

$$\bar{v}_{u2} = (1 - R_m) \bar{r}^n + 1/2 \psi_m / \bar{r}. \quad (13.17)$$

The parameters R_m and ψ_m are chosen on the mean radius, assuming that the axial velocity on the mean radius is constant, with $R_m = (-w_{mu} / u)_m$. On the mean radius we further choose $\psi=0.4$, $\phi=0.5$ and $R=0.7$. We omit the overbars indicating dimensionless values.

For $n=0$, (13.16) becomes

$$v_{u1} = 0.3 - 0.2 / r \quad \text{or} \quad r v_{u1} = 0.3r - 0.2.$$

Equation (13.15) becomes

$$\frac{d}{dr} v_{a1}^2 = - \left(\frac{0.6}{r} - \frac{0.4}{r^2} \right) 0.3 \quad \text{or} \quad v_{a1}^2 = c - 0.18 \ln r - 0.12 / r.$$

The constant c follows from the value of v_{a1} on the mean radius: $c=0.37$.

Analogously we obtain $v_{a2}^2 = 0.13 - 0.18 \ln r + 0.12 / r$.

The results are shown in Table 13.4.

The flow variation has become more favourable. The blade twist is moderate: 7° on the stator and 26° on the rotor. Maximal flow turnings are acceptable: 40° on the stator hub with Mach number 0.8 and 37° on the rotor hub with Mach number 0.88. The Mach number at the rotor blade tip is certainly acceptable: 1.18. It may even be somewhat higher. We further note that values of the velocity reductions at the stator and rotor hub are 0.62 and 0.64 with a free vortex blade. Actually, such strong reductions are not realisable. Vortex forcing with $n=0$ improves these reductions. The reduction values are 0.63 for the stator and 0.70 for the rotor. Only at the stator hub, the velocity reduction stays too strong.

Table 13.4 Swirl forcing with $n=0$; $R=0.70$ on the mean radius

u	v_{a1}	v_{a2}	v_{u1}	v_{u2}	v_l/v_2	w_{u1}	w_{u2}	w_2/w_l
0.75	0.512	0.585	0.033	0.567	0.63	-0.717	-0.183	0.70
1	0.5	0.5	0.1	0.5	0.72	-0.9	-0.5	0.69
1.20	0.487	0.444	0.133	0.467	0.78	-1.067	-0.733	0.73
R	α_l	α_m	$\Delta\alpha$	v_2	β_m	$\Delta\beta$	w_l	
0.50	3.69	23.90	40.41	0.82	-35.92	37.10	0.88	
0.70	11.31	28.16	33.69	0.71	-52.98	15.95	1.03	
0.80	15.28	30.87	31.17	0.64	-62.14	6.67	1.18	

Vortex forcing aims essentially at two improvements: increasing v_{um} at the casing, which decreases the Mach number level at the rotor inlet and decreasing v_{um} at the hub, which decreases the flow turning within the rotor (turning within the stator increases somewhat). This softens the velocity reduction within the rotor at the hub to an acceptable value. There is still a problem for the stator, but it has not turned worse compared to the free vortex blades. With a blade design according to the above data, stall occurs in the corner of the suction side and the hub of the stator. In the past, many compressors were designed with this stall present. A solution is achieved by choosing a smaller radius ratio or by reducing work. But there is still another solution, discussed in Sect. 13.3.6.

The observed tendencies continue when increasing the exponent n above zero. But there is no benefit in doing this (results not shown). The major disadvantage is that the Mach number increases at the rotor hub. A vortex distribution corresponding with n between -1 and 0 is optimum. The real optimisation, however, is more complex than studied here. Flow within the space outside the blade passages need not be on cylindrical streamsurfaces. Further, the loss distribution should be taken into account. An increase of work at the casing and the hub is desirable in order to homogenise the pressure build-up (see next section). With some compressors, the first stage has an axial inlet (no inlet guide vanes) but no axial outlet. The last stage sometimes has an axial outlet. The axial velocity decreases from the compressor inlet to the outlet.

13.3.5 Effect of End Wall Boundary Layers

Figure 13.15 sketches the velocity triangles at the casing and at the hub with results for $n=0$. The dotted lines render the velocity triangles when the axial velocity is reduced to 75% and when blade outlet angles are kept unchanged. The triangles for reduced flow render what occurs in the end wall boundary layers. There is incidence increase, both on the rotor and the stator, leading to strong increase of flow turning. Further, the velocity reduction factors become stronger. Based on these observations, one would fear strong separation, both at the hub and at the casing.

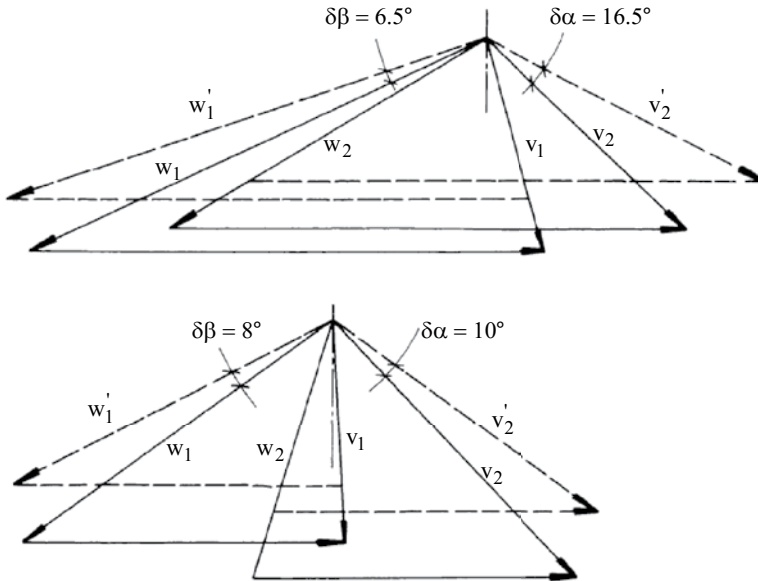


Fig. 13.15 Effect of end wall boundary layers

In order to restore the flow turnings to the original values, the stator stagger angle may be modified until the direction of w'_1 corresponds again to that of w_1 . The flow turnings then approximate the original values, both in stator and rotor parts. The stagger angle adjustment is similar to closing of adjustable stator vanes for adapting a compressor to a reduced flow rate. The stator vane then gets a bended look at the end parts. Such geometry modifications were used in the past, but did not prove to be effective. Their justification is just too two-dimensional and ignores the intense secondary flow phenomena in the end wall regions. In the next section, we discuss how end wall regions are modified with modern blades.

13.3.6 Three-dimensional Blade Design

The quasi-three-dimensional flow representation enables the determination of the required profiles of the different S_1 -sections of a blade. The blade is obtained by stacking these S_1 -sections. However, the quasi-three-dimensional flow representation does not provide a stacking strategy. One could be led by considerations about strength and stack the sections with their centres of gravity on a radial line, but shifting the profiles in the axial and tangential directions generates additional degrees of freedom. The shifts are termed *sweep* and *lean*. The shifts generate radial forces on the flow due the pressure difference on a profile between pressure side and suction side. In reality, the three-dimensional blade design is realised by means of three-

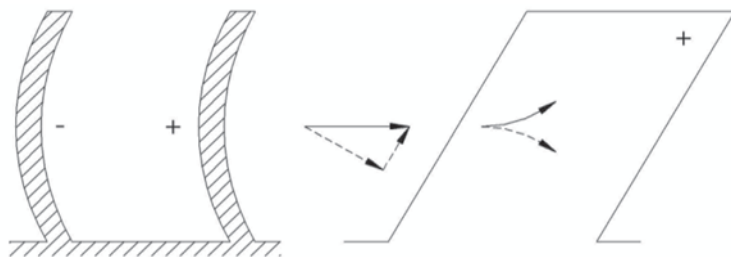


Fig. 13.16 Bowing of a blade (*left: front view*); sweep of a blade (*right: side view*)

dimensional flow simulations, and optimisation of the stacking is quite complex. The main objectives of the shifts can be understood from fundamental arguments, however, as discussed hereafter.

Sweep is displacement of the profile in the chord direction and lean is displacement perpendicular to the chord direction. Both displacements allow exerting radial forces onto the flow, thus influencing the flow rate distribution and the blade load distribution in the radial direction. The effects are similar to those discussed with steam turbines in Sect. 6.9 of Chap. 9, but the terms sweep and lean were used there for inclinations in meridional and orthogonal planes.

A favourable result requires positive lean in the end wall parts, which means shifting the profiles at the end walls in the sense of the lift. A blade then gets a bowed appearance, as sketched in Fig. 13.16 (left). A streamline in the end wall boundary layer near the suction side of a blade is pushed towards the centre of the blade passage at the entrance of the passage. In principle, it returns to the end wall in the outlet part of the passage, but this movement is hindered by the passage vortex. It may also be hindered by boundary layer stall in the corner of the suction side and the end wall (the adverse pressure gradient zone at the suction side). The result of the streamline shift is that the pressure minimum at the suction side is deepened towards the centre of the blade passage and weakened at the end wall. A displacement of a streamline in the end wall boundary layer, in principle, occurs in the other sense near the pressure side, but the possibility for displacement is restricted by the sharp angle and changes in pressure are limited as the pressure at the leading edge is close to the stagnation pressure. A first net result is increased blade loading away from the end wall and reduced loading in the end wall zone [5]. So the strongest boundary layers are loaded more and the weakest boundary layers are loaded less. A second net result is shift of some mass flow from the end wall regions towards the centre of the blade passage. This shift spreads the passage vortex over a somewhat larger radial distance, which reduces the secondary loss (mixing loss). For unchanged blade profiles, as in many experiments, losses decrease at the end walls, but increase away from the end walls and the average losses stay about the same. In order to benefit, blade profiles must be adapted. Typically, a somewhat larger chord is necessary in the zone somewhat away from the end wall.

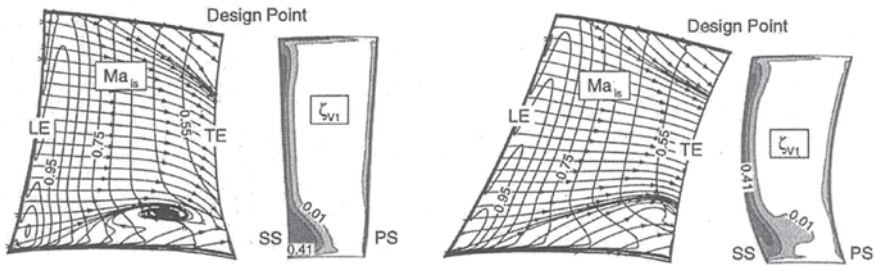


Fig. 13.17 Distribution of loss immediately downstream of a compressor stator cascade: straight stacking line (*left*); bowed and swept stacking line (*right*). (From [7]; permission by ASME)

The effect of sweep is illustrated in Fig. 13.16 (right). Sweep is called positive when the leading edge is moved parallel with the chord towards the oncoming flow. The figure demonstrates positive sweep at the hub and negative sweep at the casing. A first effect of sweep is exerting torsion on the streamsurfaces. The flow velocity at the leading edge may be split in a component parallel to the leading edge and a component perpendicular to it. The parallel component stays nearly unmodified in the flow over the profile. The perpendicular component increases at the suction side and decreases at the pressure side. With positive sweep, the streamline at the suction side moves towards the end wall and the streamline at the pressure side moves away from the end wall. The torsion on the streamsurface results in a vortex motion counteracting the passage vortex (Fig. 13.10). So, secondary flow reduction requires combined sweep, positive at the hub and positive at the casing. But reduction of the secondary flow is not necessarily beneficial, as the secondary vortices move core flow fluid to boundary layer regions and vice versa. A particular beneficial effect of the secondary flow is redistribution of energy between core flow and end wall layers. We note that the vortex induced by positive sweep supplies mass flow from the central part of a blade to the corner of the suction side and the hub. This supply decreases the corner stall. This is certainly favourable for loss reduction in the hub region of a stator. Another favourable effect of sweep is, as with aircraft wings, Mach number lowering of the flow perpendicular to the leading edge, causing reduction of shock loss with supercritical and transonic profiles. This is favourable for rotor tip sections.

Figure 13.17 shows the loss coefficient measured on a stator vane with straight stacking and on a vane with the same profiles, but with a curved stacking line [7]. Contours of isentropic Mach number and limiting streamlines on the suction surface are shown. Bowing is applied, i.e. positive lean both at the hub and at the casing. Positive sweep is applied at the hub and negative sweep at the casing. The reduction of the corner stall at the hub due to the positive sweep is obvious. Herewith we also understand that positive sweep is not necessarily beneficial at the tip, because there is no corner stall there. The effect of the bowing is redistribution of the loss with lower values at the end walls and higher values in the central part of the vane (but profiles are not adapted here).

The same considerations as with stator vanes apply to rotor blades. Applying positive lean and positive sweep at the hub is favourable. Sweep at the casing is favourable to reduce the Mach number of the flow perpendicular to the blade. But this can be obtained both with backward and forward sweep. Further, realisation of a three-dimensional form is more difficult from a structural point of view. At present, rotor blades have typically a slight general sweep (positive at the hub and negative at the casing), as in Fig. 13.17, and a slight positive lean at the hub. The sweep reduces corner stall at the hub. Note that corner stall is less intense with a rotor than with a stator (Table 13.4). Back-sweep at the casing reduces the effective Mach number. At present there are fan blades in turbofan engines with backward sweep at the casing and with forward sweep at the casing. The sweep is applied to reduce the Mach number of the flow attacking the leading edge. It is not fully clear if sweep has to be positive or negative for optimal efficiency (and stall margin). The same applies to the tip of transonic compressor rotors. Probably, forward sweep is the most advantageous, since then the radial outward migration of boundary layer fluid caused by centrifugal effect influences less the blade boundary layer at the tip [8, 18].

13.4 Compressor Blade Profiles

13.4.1 *Subsonic and Supercritical Cascades*

The optimum Mach number distribution (boundary layer edge velocity) and the corresponding profile shape for a stator application are shown in Fig. 13.18. Also shown is the comparison between the optimum profile and a classical profile obtained by a NACA-65 thickness distribution on a circular camber line. The parameters of the stator cascade are:

- inlet Mach number: 0.773 (supercritical)
- flow turning: 39.6°
- pitch-cord ratio: 0.465
- axial velocity-density ratio (AVDR): 1.1.

The features of the optimal Mach number distribution are:

- The acceleration at the leading edge of the suction side runs over about 30% of the chord. The objective of the acceleration is to lower the pressure in order to create pressure difference over the profile. The strength of the acceleration is tuned such that the boundary layer stays laminar within this zone. The boundary layer is kept in laminar state in order to minimise the friction and thus the contribution to the resulting drag.
- The deceleration at the suction side is optimised such that the boundary layer is near to separation at the trailing edge. The boundary layer evolution is such that the maximum possible tangential force is obtained, but in proportion to the drag

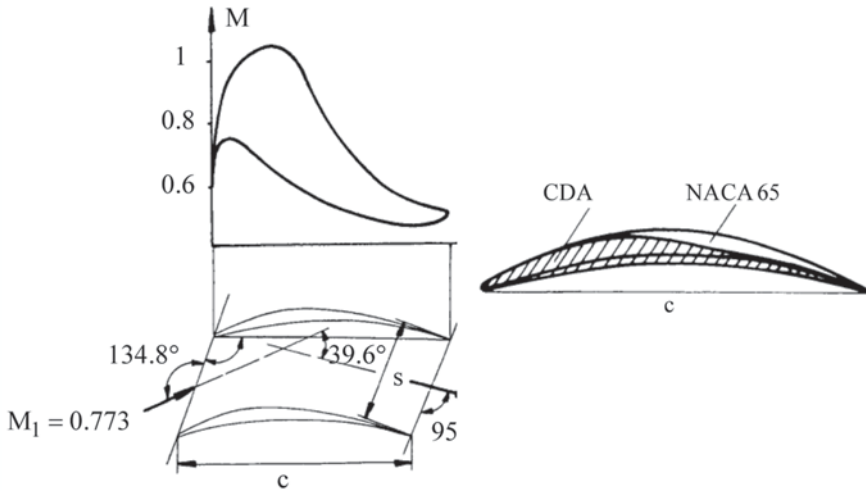


Fig. 13.18 Optimum Mach number distribution for a supercritical compressor cascade; comparison between a controlled diffusion profile and a profile obtained by a NACA-65 thickness distribution on a circular camber line. (Adapted to Rechter et al. [14])

contribution of this part of the profile. In order to withstand the adverse pressure gradient, the boundary layer must turn from laminar state to turbulent state at the maximum in the Mach number distribution.

- The Mach number just upstream of the shock wave on the suction side slightly exceeds one ($M \approx 1.05$) and the boundary layer is turbulent at the shock impact position. With the low upstream Mach number, shock loss is low.
- There is a slight acceleration in the front part of the pressure side caused by the rounding of the leading edge. The acceleration is followed by a deceleration that maximises the pressure difference over the profile, but, as for the suction side, in proportion to the drag contribution of this part of the profile. The optimised evolution ends with a weak acceleration zone at the trailing edge of the pressure side.

The phenomena that strongly determine the profile design are transition from laminar to turbulent flow in the boundary layers and possibility for boundary layer separation in the adverse pressure gradient zones. Since the general flow in a compressor cascade is decelerating, the adverse pressure gradient zones on both the suction side and the pressure side are large and these zones dominate the optimisation. Therefore, an optimised profile is called a *controlled diffusion aerofoil* (CDA).

The turbulence level in the core flow of a compressor is mostly very high. The degree of turbulence is the ratio of the magnitude of the fluctuating velocity to the average velocity. It is typically around 5%, except for the first stage of a turbofan engine. The high free stream turbulence comes from turbulence generated by the wakes of upstream blade rows. Boundary layer transition is then directly induced

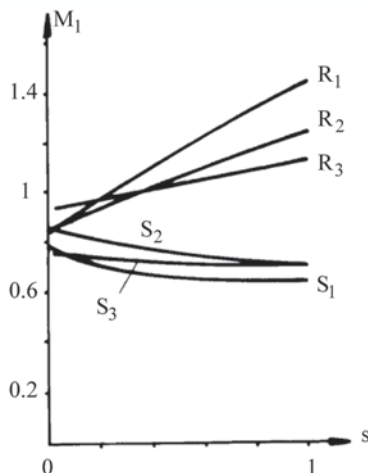
by the fluctuations in the main flow. This means that the transition is not caused by instability of the boundary layer flow with forming of Tollmien-Schlichting waves (see fluid mechanics). Transition caused by instability, called *natural transition*, is typical for aircraft wings in a very low turbulence level flow (typically about 0.01 % turbulence level in cruise conditions). The directly induced transition is called *bypass transition*, meaning that the instability mechanism is bypassed. A consequence for practice is that the boundary layer thickness for transition, normally expressed with a Reynolds number based on momentum thickness, lowers considerably with increasing free stream turbulence level. Further, this critical Reynolds number becomes independent of the pressure gradient for high free stream turbulence. This is in contrast with natural transition where the critical Reynolds number increases in accelerating flow. So, it becomes harder to keep a boundary layer in laminar state in the presence of a high free stream turbulence level. So, the acceleration of the boundary layer in the leading edge zone has to be sufficiently strong in order to keep the momentum thickness Reynolds number below the critical value. Clearly, the optimisation of the accelerated zone strongly depends on the turbulence level of the incoming flow.

A major difference between a laminar boundary layer and a turbulent one is that a turbulent boundary layer can withstand a much higher adverse pressure gradient before entering into separated state. The reason is turbulent exchange of momentum from the outer region of the boundary layer to the near-wall region. So, to avoid separation, it is advantageous to let the boundary layer transition from laminar state into turbulent state at the position where the boundary layer edge flow changes from accelerating flow to decelerating flow. At the other hand, by the turbulent momentum exchange, the shear stress in a turbulent boundary layer is higher for the same edge velocity. So, optimisation includes making a balance between the extent of the laminar part of the boundary layers, with lower shear stress level, and the turbulent part with higher resistance to separation. The optimum strongly depends on the free stream turbulence level, but also on the chord Reynolds number. The lower is the chord Reynolds number, the weaker is a laminar boundary layer against separation under an adverse pressure gradient.

A compressor cascade is called subsonic when the Mach number of the oncoming flow is low enough such that the entire flow over the profile is subsonic. For higher Mach number of the oncoming flow, a supersonic zone may form at the suction side, ending with a normal shock. The flow is then called supercritical (subsonic upstream flow, subsonic downstream flow, but a supersonic zone on the profile). The shock at the suction side creates a sudden pressure rise which may lead to boundary layer separation. In order to avoid shock-induced separation, the Mach number just upstream of the shock should not be too high (a typical limit is 1.25) and the boundary layer state should be turbulent at the shock position (better resistance against separation). The consequence is that the optimum profile shape becomes dependent on the Mach number of the oncoming flow.

The optimisation strategy for supercritical rotor cascades remains as with stator vanes, but with rotor cascades the Mach number is higher and the flow turning is lower (typically under 20° compared to 40°). The resulting blade shape depends

Fig. 13.19 Variation of the Mach number of the oncoming flow (rotor: R ; stator: S) as function of the radius (normalised span) with a three-stage axial compressor. (Adapted to Fottner [6])



on Mach number and turning. Modern optimisation techniques allow supercritical cascades with a loss coefficient ω_l as low as 0.015 [15].

Figure 13.19 is a sketch of the radial distribution of the Mach number in the oncoming flow of rotors and stators within a three-stage transonic axial compressor (LP-compressor of a bypass aero-engine; [6]). Stator cascades are supercritical near the hub and subsonic near the casing. Rotor cascades are supercritical near the hub and transonic near the casing. In compressor terminology, a cascade is transonic when the inlet flow is supersonic and the outlet flow subsonic.

The design strategy of subsonic stator cascades near the casing is the same as with supercritical cascades. A supercritical rotor cascade only differs from a supercritical stator by the higher Mach number level. With regard to shock strength, the maximum Mach number at the suction side should not exceed about 1.25. This limitation is meant to prevent boundary layer separation due to the shock pressure rise. For design conditions, blade shapes may be optimised with deceleration upstream of the shock so that the Mach number just before the shock is close to one. But away from the design operating point, the Mach number in front of the shock may be much higher. The main effect of limiting the maximum Mach number is that the optimum loading of a blade decreases with higher Mach number in the oncoming flow and that solidity thus must increase.

13.4.2 Transonic Cascades

Figure 13.20 shows the shock pattern within a transonic cascade with low or medium high Mach number of the oncoming flow (up to Mach number about 1.2). Each blade has a shock just upstream of the leading edge with an oblique part upstream of the cascade, called the *bow shock* and a part normal to the adjacent blade surface,

Fig. 13.20 Shocks within a transonic compressor cascade for low or medium high inflow Mach number



Fig. 13.21 Transonic compressor cascades with a single normal blade passage shock. **a** Low transonic ($M_1 \sim 1.1$), convex leading suction side. **b** Medium transonic ($M_1 \sim 1.2$), slightly concave leading suction side



the *blade passage shock*. The oblique shock is very weak, with negligible losses. The normal shock provides the main part of the compression. This shock is also the main loss source, not only because of its intrinsic dissipation, but also because of interaction between the shock and the boundary layer. For preventing separation, the boundary layer should be turbulent at the impact zone. Optimisation of a transonic cascade is strongly determined by minimising shock losses. Depending on the Mach number of the oncoming flow, at the suction side in front of the normal shock, either a slight acceleration is tolerable (convex shape), or no acceleration can be allowed (plane shape) or even a deceleration must be realised (concave shape). Downstream of the shock, the flow is subsonic. Within this part of the blade passage, further deceleration combined with flow turning occurs.

Figure 13.21 shows two transonic compressor cascade shapes typical for the middle section and the tip section of a transonic compressor rotor (a rotor is transonic when the inflow Mach number is subsonic at the hub and supersonic at the tip). For the lower inflow Mach number ($M_1 \leq 1.1$), the blade shape is similar to that of a supercritical cascade with higher inflow Mach number ($M_1 \geq 0.80$). The suction side is convex with a small acceleration upstream of the shock. For the higher inflow Mach number, there is a slight supersonic deceleration upstream of the shock (see next section for a further discussion), requiring a slightly concave form of the suction side.

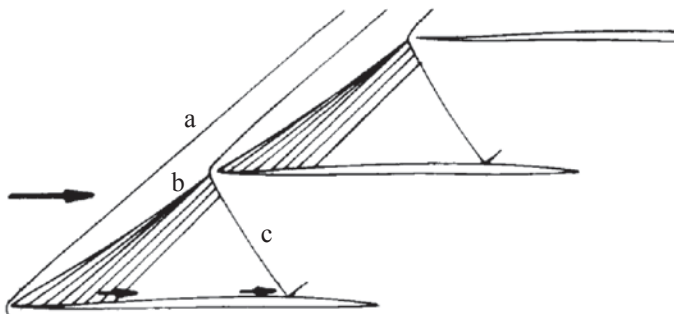


Fig. 13.22 Ideal flow pattern in a supersonic cascade. **a** Bow wave. **b** Pre-compression shock. **c** Oblique shock within the blade passage. (Adapted to Tweedt et al. [17])

13.4.3 *Supersonic Cascades and Transonic Cascades with High Inlet Mach Number*

In compressor terminology a cascade is supersonic when both inlet and outlet Mach numbers are above unity. Figure 13.22 sketches the ideal flow pattern. The suction side is concave at the leading edge. As a consequence, converging compression Mach lines are generated. A so-called pre-compression shock forms. The main compression shock stands within the blade passage, but contrary to the transonic cascades in Fig. 13.21, the blade passage shock is oblique. The suction side shape downstream of the pre-compression and the pressure side shape are such that the flow within the blade passage is so-called started. This means that the shock penetrates into the blade passage. This presumes a sufficiently opened throat. It also presumes acceleration downstream of the pre-compression. Started flow is the principal difference with the flow in the transonic cascades discussed up to now. In these transonic cascades, the flow is not started, which means that the throat is sufficiently narrow so that the blade passage shock stands upstream of the throat and is strong. The cascade starting phenomenon is analogous with starting a supersonic wind tunnel or a supersonic engine inlet (so-called swallowing of the shock wave).

The most striking characteristic of the optimum blade shape of a supersonic compressor cascade is the concave zone at the suction side, responsible for the pre-compression. Blade shapes are therefore denominated *pre-compression profiles*. The leading edge zone has a characteristic S-shape. The ideal flow within a supersonic cascade has an oblique passage shock without reflection. Downstream of it, flow is almost uniform. So, possible flow turning is small with supersonic cascades. In practise, the flow pattern is strongly determined by the boundary layer state on the suction side. Mostly, the boundary layer upstream of the shock impact zone is laminar and the oblique shock then causes boundary layer separation with forming of a lambda shock structure and further strong shock patterns, but finally acceleration into a supersonic outlet flow [17]. Losses of the separated flow are very high,

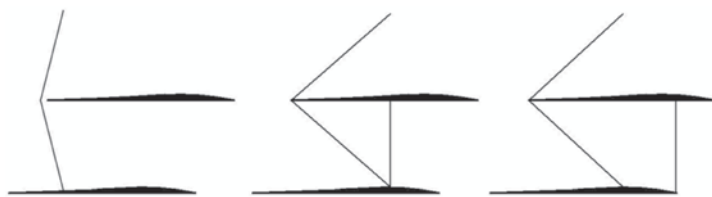


Fig. 13.23 Flow patterns within a transonic cascade with high inlet Mach number ($M_1 \sim 1.4$); *middle*: design flow; *left*: stall; *right*: choking. (Adapted to Boyer and O'Brien [1])

with a loss coefficient in the order of 0.15. The high losses are the reason that, up to now, supersonic cascades cannot be used in practise.

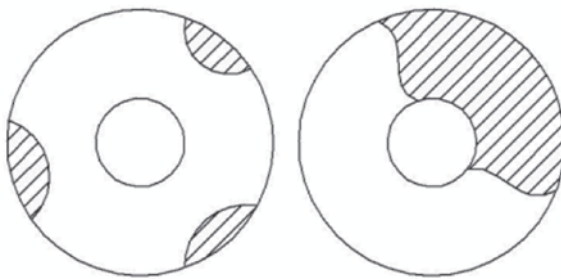
Pre-compression profiles, yet, may be applied efficiently to transonic cascades with high inflow Mach number. From Fig. 13.21 it is clear that the principle of a single normal blade passage shock becomes impractical for a high inflow Mach number ($M_1 \sim 1.3$ to 1.4). The front part of the profile then becomes extremely thin due to the concave shape at the suction side. Figure 13.23 sketches shock patterns in design flow, near stall and near choking (stall and choke are discussed in Sect. 13.5) for pre-compression profiles in a transonic cascade. In the design flow, there is a normal shock immediately following the oblique blade passage shock. With increasing backpressure, the normal shock is pushed forward and merges with the oblique shock, making the merged shock strong (pattern of Fig. 13.20). The *stall limit* is attained when the shock causes boundary layer separation. This happens when the shock gets expelled somewhat from the blade passage. Decreasing the backpressure moves the normal shock downstream. The *choking limit* (blocked mass flow rate) is attained when the normal shock reaches the trailing edge of the suction side profile. With this example, we understand that the stall and choking limit flows are similar with the transonic cascades of Fig. 13.21. In particular, with reduced backpressure, the normal shock is swallowed into the blade passage (started flow) and becomes weak.

13.5 Performance Characteristics and Operating Range

13.5.1 General Shape of a Characteristic Curve

Figure 13.15 demonstrates that the rotor work of an axial compressor stage increases with decreasing flow rate. So, the general shape of the characteristic curve for pressure ratio as a function of mass flow rate at constant rotational speed is a descending line. Figure 13.15 is drawn assuming that the rotor outlet direction (w_2) and the stator outlet direction (v_1) stay unchanged with changing flow rate. On this assumption, which is only approximately satisfied in reality, work increases linearly with decreasing flow rate. But, incidences increase with decreasing flow rate. So,

Fig. 13.24 Cell patterns with rotating stall; part-span and full-span stall



boundary layer separation occurs below a certain flow rate. The flow is then said to be *stalled*, meaning that the compressor does not function properly anymore. In stalled flow, the tangential force of the blade drops. This causes a maximum in the characteristic curve for pressure ratio as a function of flow rate. This maximum may be very sharp.

13.5.2 Rotating Stall

Stall never occurs in a compressor simultaneously on all blades over their full span. First, the incidence margin with respect to stall changes from stage to stage within a multistage compressor, with bigger incidence margin with the first stages (see below). Second, in order to decrease blade torsion, rotor blades are given greater incidence at the tip than at the hub (see Fig. 13.9). So, the incidence margin at the tip is smaller than at the hub. With decreasing flow rate, the flow thus first goes into stall at the tip of a rotor blade. With longer blades, as in the first stages of a compressor, stall zones therefore form at the casing, unless the flow rate reduction with respect to non-stalled flow is extreme. In the last stages of a compressor, where blade height is smaller, full span stall is reached faster. Whether stall is part-span or full-span, it is always organised in cells, rotating in the rotation sense of the compressor. Figure 13.24 sketches possible cell patterns. Low axial velocity zones caused by stall are hatched. The typical speed of part-span cells is about 50% of the rotor speed and with part-span stall, several cells always occur. With full-span stall, there is typically only one cell with speed 20–40% of the rotor speed. There is no simple explanation for the number of cells and their speed [3].

The cell propagation mechanism may be understood with Fig. 13.25. Assume that stall occurs on a specific blade. The flow near the blade channel with stall must then deviate somewhat. Incidence increases on the blade at the suction side of the blade with stall, forcing the flow into stall on the neighbouring blade. Incidence decreases on the blade at the pressure side of the blade with stall. So, tendency to stall is suppressed on this neighbouring blade. It is typical with flow reduction that stall only occurs at a number of blades within a blade row, as there are small geometric differences between the blades. Cells are generated that way. According

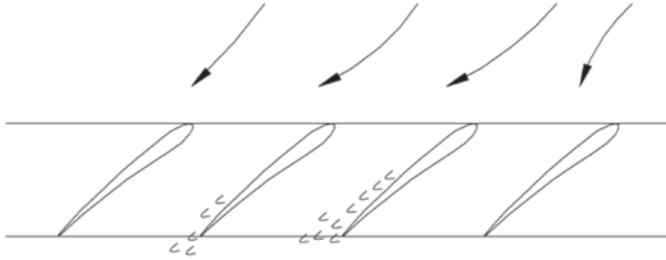


Fig. 13.25 Rotating stall propagation mechanism

to Fig. 13.25, the sense of propagation within the relative frame for a rotor blade row is opposite to the running sense. The propagation speed is lower than the blade speed, causing the stall cells to move in the rotation sense within the absolute frame. With the same figure one sees that the propagation sense of cells in stator vanes is in the running sense of the rotor. Typically, rotating stall cells form in a number of consecutive stator vane rows and rotor blade rows.

13.5.3 Choking

By reduction of the backpressure of a subsonic flow compressor, the flow rate increases and all velocities increase until sonic speed is attained in some through-flow section. With further reduction of the backpressure, the flow rate then stays blocked. This phenomenon is called *choking*. The choking flow rate depends on the rotational speed, both for choking within the rotor blade passages as for choking in the stator vane passages. This may be understood by the following, simplified, derivation.

Within the relative system it applies that

$$I = h + 1/2w^2 - 1/2u^2 = \text{constant.}$$

At the inlet of the rotor, without pre-swirl,

$$w_1^2 = u_1^2 + v_1^2, \quad \text{so that} \quad I = I_1 = h_1 + 1/2v_1^2 = h_{01}.$$

$M = 1$ is attained for $w^2 = c^2 = \gamma RT = (\gamma - 1)h$, so that then

$$h_{01} = h + 1/2(\gamma - 1)h - 1/2u^2 = 1/2(\gamma + 1)h - 1/2u^2,$$

$$\frac{h}{h_{01}} = \frac{2}{\gamma + 1} \frac{h_{01} + 1/2u^2}{h_{01}} = \frac{2}{\gamma + 1} \left(1 + \frac{\gamma - 1}{2} \frac{u^2}{c_{01}^2} \right). \quad (13.18)$$

Sonic flow, if any, will occur near the rotor inlet, since the further the flow enters the rotor, the lower is the velocity w and the higher is the enthalpy h . Thus, the inlet flow is the most critical. The mass flow rate with choking is

$$\dot{m}_c = A_I \rho c = A_I \rho_{0I} c_{0I} \left(\frac{\rho}{\rho_{0I}} \right) \left(\frac{c}{c_{0I}} \right) = A_I \rho_{0I} c_{0I} \left(\frac{h}{h_{0I}} \right)^{\frac{1}{n-1} + \frac{1}{2}}. \quad (13.19)$$

A_I is the through-flow area and n is the polytropic exponent. With an average value of the blade speed at the inlet, an approximation of the choking mass flow rate is obtained. The Mach number is higher at the tip than at the hub at the inlet. Thus, attaining $M=1$ within the entire inlet section is impossible. So, sonic flow can only occur somewhat more inside the rotor. This makes the estimation of the choking mass flow rate with (13.18) and (13.19) approximate. Nevertheless, a clear conclusion is that mass flow rate at choking depends on the rotational speed.

At the inlet of the stator it applies that

$$h_{02} = h_2 + 1/2 v_2^2 = h_2 \left(1 + \frac{\gamma-1}{2} M_2^2 \right).$$

For $M_2 = 1$,

$$\frac{h_2}{h_{02}} = \frac{2}{\gamma+1}.$$

Further :

$$h_{02} = h_{01} + \psi \frac{u_2^2}{c_{01}^2} = h_{01} \left[1 + (\gamma-1) \psi \frac{u_2^2}{c_{01}^2} \right]. \quad (13.20)$$

In (13.20), we write the blade speed as u_2 , which is not necessary for an axial compressor, since $u_1 = u_2$. We do this to reuse the result in the next chapter for centrifugal compressors. The corresponding mass flow rate is

$$\dot{m}_c = A_2 \rho_2 c_2 = A_2 \rho_{02} c_{02} \left(\frac{2}{\gamma+1} \right)^{\frac{1}{n-1} + \frac{1}{2}},$$

with

$$\frac{\rho_{02}}{\rho_{01}} = \left(\frac{h_{02}}{h_{01}} \right)^{\frac{1}{n-1}} \quad \text{and} \quad \frac{c_{02}}{c_{01}} = \left(\frac{h_{02}}{h_{01}} \right)^{\frac{1}{2}}.$$

Thus :

$$\dot{m}_c = A_2 \rho_{0I} c_{0I} \left(\frac{2}{\gamma+1} \right)^{\frac{1}{n-1} + \frac{1}{2}} \left[1 + (\gamma-1) \psi \frac{u_2^2}{c_{0I}^2} \right]^{\frac{1}{n-1} + \frac{1}{2}}. \quad (13.21)$$

This flow rate depends on the rotational speed as well.

The expressions (13.19) and (13.21) are almost identical so that discerning which is most critical for mass flow rate is difficult, at first sight. At the design flow rate, ψ is smaller than 0.5 and this value lowers when the flow rate increases towards

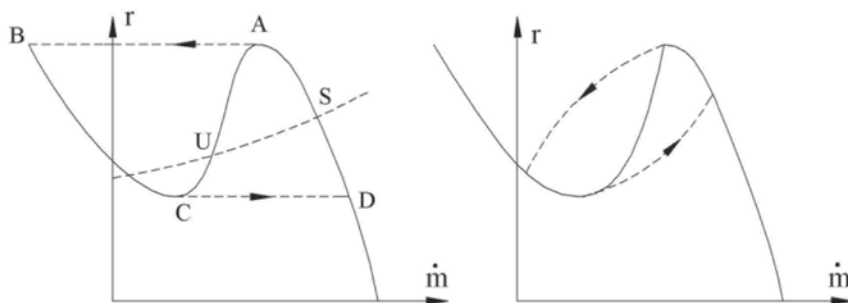


Fig. 13.26 Surge: flow cycle with very large reservoir (*left*) and with smaller reservoir (*right*); soft maximum (*left*) and sharp maximum (*right*) in the compressor characteristic

choking. Moreover, the through-flow area in the rotor is smaller than in the stator, as the rotor velocity is more tangential than the stator velocity. This means that the rotor is typically the most critical with respect to choking. One may also derive this from the observation that for the design flow rate, the Mach number level is the largest in the rotor.

The above derivation is intended to illustrate that the choking mass flow rate depends on the rotational speed. The obtained expressions are approximate, as one-dimensional flow is assumed. Another approximation is that the stage inlet is assumed in the axial direction. The above reasoning for subsonic cascades applies, in principle, to supercritical cascades as well. The choking condition for transonic cascades is different, as explained before.

13.5.4 Surge

The term *surge* refers to flow varying in time between attached flow and separated flow. This periodic type of stall is caused by a dynamically unstable interaction between the compressor and its load. Figure 13.26 (left) renders a possible characteristic of a compressor together with a possible load characteristic.

Just as with pumps (Chap. 8, Sect. 8.3), the intersection U of the load and compressor characteristics is an unstable operating point and intersection S a stable operating point. This may be verified by applying a small perturbation. We take as an example a short duration decrease of the flow delivered by the compressor to the downstream reservoir (e.g. by opening a bypass valve). The pressure in the reservoir then decreases somewhat. The reaction of the compressor for operating point S is flow increase, which is a restoring reaction. The reaction of the compressor for operating point U is flow rate decrease, which is an aggravating reaction. If the backpressure of the compressor is enlarged, the load characteristic shifts upwards until there is only one tangent point with the compressor characteristic in the vicinity of the maximum. With further increase of the backpressure, there is no intersec-

tion anymore for positive mass flow rate and the operating point jumps to the point B on the negative branch. Point B is a stable operating point (this may be verified by a perturbation analysis) and a cycle ABCD is run through, as sketched in Fig. 13.26, left. The cycle is sketched assuming that pressure does not change during the transition from the operating point at the maximum of the characteristic A to the operating point at the negative branch B, and similarly for the transition from C to D. This can only be attained with a very large reservoir. In reality, pressure decreases during the transition from A to B. Similarly, pressure increases during the transition from C to D. So, a real surge cycle rather looks as sketched in the right-hand part of Fig. 13.26. The extension of the cycle depends on the buffer capacity of the reservoir. Negative flow rates may occur with very large reservoir capacity. When the flow rate stays positive, the surge is called mild. When negative flow rates occur, the surge is called deep. From the above description is clear that surge means that the flow as a whole is pulsating and running through states with attached boundary layer flow and states with massively separated boundary layer flow. So, we might also describe the phenomenon as *pulsating stall*. The periodic forces on the blades typically are so high that blades cannot withstand them and surge causes destruction. So, surge is much more destructive than rotating stall and, therefore, surge is considered as not allowable. Appearance of surge is only possible when there is a maximum in the compressor characteristic. As discussed before, this maximum comes from rotating stall. This means that both phenomena go together, which makes flow patterns quite complex. In the right-hand part of Fig. 13.26 a sharp maximum is supposed. This occurs with full-span rotating stall, which is produced at high rotational speed (see next section). When the maximum is smooth, caused by part-span rotating stall at low rotational speed, the precise location of the start of the surge cycle depends on the shape of the load characteristic and the level of kinetic energy at the outflow of the compressor. Often, with a very large reservoir, surge is assumed to start at the maximum of the difference between total pressure at compressor inlet and static pressure at compressor outlet [3]. For a smooth maximum in the characteristic for total pressure ratio, this means a starting point left of the maximum.

13.5.5 Operating Range

Figure 13.27 sketches a field of characteristics for pressure ratio as a function of mass flow rate and efficiency as a function of mass flow rate for an axial compressor. *Choking* is attained at higher rotational speeds. Characteristics are limited at the low flow rate side by a line called the *surge line* (line with short dashes in Fig. 13.27). But surge typically only occurs at higher rotational speed. The characteristic then has a sharp maximum and this maximum is the starting point of a possible surge cycle, independently from the capacity of the downstream reservoir and the capacity of the compressor casing. At low rotational speed, the maximum typically is smooth and surge can only start at an operating point with lower flow rate than at the maximum. The limiting phenomenon is then rotating stall if it becomes

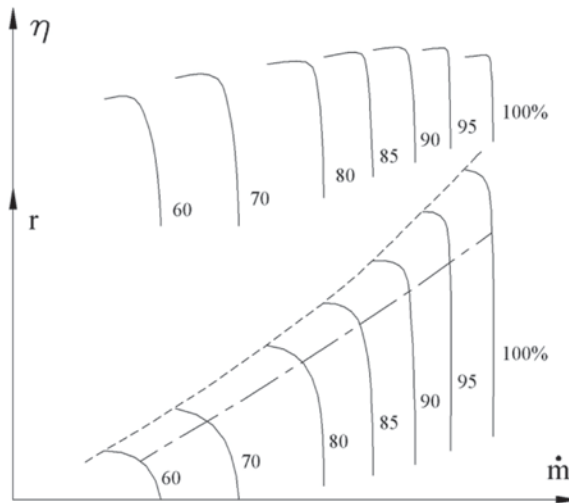


Fig. 13.27 Chart of characteristics of an axial compressor

so intense that there is risk for damage. Conventionally, start of rotating stall is considered as a limiting instability phenomenon. Also conventionally, the limiting instability line in the performance chart is called the surge line, although in practice surge only occurs for the higher rotational speeds.

A possible operating line, imposed by the load, is drawn with short and long dashes in Fig. 13.27. An example of a unique operating line is with steady state operation of the compressor of an aero-engine. The compressor load is generated by the downstream turbine and the downstream nozzle. For a given rotational speed, there is an operating margin against instability and choking. Often, operating range is expressed by the difference between the choking and surge mass flow rates divided by the choking mass flow rate at the design pressure ratio (horizontal line in the chart). But it is rather difficult to determine where exactly choking begins. Therefore, mostly the notion of surge margin is used. Also, avoidance of surge is much more critical than avoidance of choking. Surge margin may mean the difference in pressure ratio between the instability and optimum efficiency values for the design mass flow rate as a fraction of the optimum efficiency value (vertical line in the chart). Expressed this way, the surge margin is typically around 25% for a compressor in an aero-engine [3]. A similar expression is based on the mass flow rates at instability and optimum efficiency at the design pressure ratio (horizontal line in the chart). The operating line is not unique because of load transients. For instance, when an aero-engine is accelerated from lower speed to higher speed by fuel flow increase, the transient operating line comes closer to the surge line than the line of steady operating points. Actually, the maximum acceleration is limited by the margin between the line of steady operating points and the surge line.

A particular problem arises with connecting stages in series. If, for design rotational speed, stages are matched to each other in the sense that the operating point of each stage has a sufficient margin against instability and against choking, it is not guaranteed that a similar margin is kept at lower rotational speed. At a reduced rotational speed, the pressure build-up is lower and the density in the rear stages is below the design value. For a constant density fluid, the shape of the velocity triangles of the stages does not change when the stages maintain their flow coefficient and their work coefficient. So, stage matching is maintained for an operating point that obeys kinematic similitude. The reduced density rise with a compressor causes a deviation to the kinematic similitude with increased through-flow velocity in the rear stages and decreased through-flow velocity in the front stages. So, the tendency is that rear stages are pushed towards choking and front stages towards stall (we discussed this phenomenon already in Sect. 11.1.4 of Chap. 11 for explaining the need of adjustable stator vanes). In order to maintain stage matching, incidences may be set to smaller values than those for optimum efficiency in the first stages and to larger values in the last stages. These settings diminish the efficiency at the design operating point somewhat. It is also obvious that a large choking margin of the last stages is favourable. The Mach number level in the last stages is therefore lower than in the first ones (see Fig. 13.19). The consequence is that the stall margin of rear stages is the smallest at design rotational speed, but that the stall margin of the front stages becomes the smallest at low rotational speed. With increased backpressure, the following effects result: surge in the rear stages at design rotational speed or a somewhat enlarged or reduced speed, full-span rotating stall with one cell in the middle stages at reduced speed and rotating stall with several cells at the casing within the front stages at low rotational speed [4].

High pressure ratio compressors (say $r=20$ and above) cannot maintain stage matching at reduced speed without variable geometry, which means the possibility for stator vane angle adjustment. The dashed lines in Fig. 13.15 may also be seen as obtained with global mass flow rate reduction. The figure demonstrates that angle adjustment of stator vanes at reduced flow rate allows both the readjustment of inlet rotor velocity (w_1) and of inlet stator velocity (v_2) into the original direction. The adjustment is attained by a more tangential position of the stator vanes. This means *closing of the compressor*. Closing results in a comparable work, and thereby pressure ratio, but with a smaller flow rate than originally. The compressor characteristics are thus shifted towards lower flow rate this way.

With compressors operating with a largely changing load, many stages in the front part may be provided with variable geometry. This may be done with industrial compressors or compressors of stationary gas turbines for power generation. Aero-engines operate most of the time in cruise conditions. Actually, compressors of these gas turbines only have a problem at start-up. Often, only one or two stages in the front are provided with variable geometry. Installation of bleeds onto the first stages is an alternative for variable geometry. Sufficient segmentation of the gas turbine is another method. E.g., some Rolls Royce Trent engine types have three shafts and no variable geometry (but the Trent800 taken as example in Chap. 12 has variable geometry in the front stages of the IP-compressor).

13.6 Exercises

13.6.1 Average Density with Compression Verify that the average density is well-suited to approximate the isentropic enthalpy change with a compression process. Calculate for air as an ideal gas ($\gamma=1.40$) for pressure ratio values 1.2, 1.4, 1.7, 2 and infinitesimal efficiency values 1, 0.95, 0.90: Δh_s , Δh_r , $\Delta p/\rho_m$. Establish that $\Delta p/\rho_m$ is a very good approximation of Δh_s (sometimes overestimation, sometimes underestimation) and a somewhat inferior approximation of Δh_r (always underestimation).

13.6.2 Average Density with Expansion The average density concept is applicable with expansion processes as well. The term $\Delta p/\rho_m$ constitutes an approximation of the isentropic enthalpy change, but is much less accurate than with a compression. For an expansion the following applies:

$$\Delta h < \frac{\Delta p}{\rho_m} \approx \Delta h_s < \Delta h_r.$$

Calculate for air as an ideal gas ($\gamma=1.40$) for pressure ratio values 1.2, 1.4, 1.7, 2 and infinitesimal efficiency values 1, 0.95, 0.90: Δh_s , Δh_r , $\Delta p/\rho_m$. Establish that $\Delta p/\rho_m$ results in a slight underestimation of Δh_s , and a somewhat stronger underestimation of Δh_r .

13.6.3 Loss Coefficient Verify numerically that the enthalpy loss coefficient ζ_l (13.6) and the pressure loss coefficient ω_l (13.7) are nearly equal for low inlet Mach number. Assume a compressor cascade with air and infinitesimal efficiency 0.9. Consider inlet Mach numbers 0.3, 0.7 and 1.2. Assume, by way of simplification, zero outlet velocity. Observe that the energy loss coefficient increases weakly with increasing inlet Mach number and that the pressure loss coefficient increases quite strongly. Observe that ω_l is always larger than ζ_l . Remark that the Mach number influence on ω_l may be neutralised by taking the logarithm of pressure instead of pressure. Such a loss coefficient is 1 minus the infinitesimal efficiency (similarly as with expansions; see Exercise 6.10.1).

13.6.4 Lift Coefficient and Diffusion Factor Formulate the relationship between the lift coefficient and the diffusion factor. Establish that, for a given diffusion factor value, e.g., $DF=0.60$, a great variation of the lift coefficient is possible, strongly dependent on the general deceleration value w_2/w_1 . This demonstrates that lift coefficient is an unworkable concept with compressor cascades.

13.6.5 Radial Variation with a Fan Stage The radius ratio chosen in Sect. 13.3 is 1.60 (1.20/0.75). This ratio is smaller with many compressor stages, but it is much greater with a fan stage, where it may be up to four. Study a fan stage with free vortex flow (same work on all radii) and radius ratio 4. Take as an example the fan of the Tent800 (Fig. 12.9). Tip and hub radii are 1.40 m and 0.35 m. Take radius 1 m as approximation of the equal area average radius. Consider the fan on the ground with $T_{00}=288$ K and $p_{00}=100$ kPa. Take tip blade speed 420 m/s and inflow velocity (absolute system) in axial direction, constant over the radius, equal to 200 m/s (Mach

number approximately 0.6). Determine the velocity triangles on the mean radius taking into account that the deceleration ratios in the rotor (w_2/w_1) and the post-connected stator (v_2/v_3) cannot be lower than 0.7. Consider constant axial velocity across the stage. Determine the work coefficient and the total pressure ratio, assuming a polytropic efficiency of 0.9 (A: $\psi \approx 0.49$, $p_{03}/p_{01} \approx 1.56$). Observe that it is not possible to realise the same work at the hub with the same limits on the deceleration ratios. Determine the velocity triangles at the hub for constant axial velocity in the stage and the strongest deceleration ratio at 0.7. Observe that this leads to a degree of reaction approximately zero and a symmetric rotor blade profile (verify the realism on Fig. 12.9). Observe that at the casing, the free vortex flow condition leads to a rather low work coefficient (A: $\psi \approx 0.25$). So, larger work is possible (see next exercise). Remark the somewhat larger values of work coefficient and flow coefficient on the mean radius of a fan, compared to a typical compressor (Sect. 13.3) and the very large work coefficient at the hub (A: $\psi \approx 2$).

13.6.6 Obtainable Pressure Ratio at the Tip of a Transonic Fan Stage Calculate the total pressure ratio over the fan rotor at the tip with the data of the previous exercise, assuming that the flow in the relative system is straight and that all compression comes from a normal shock. Derive the flow parameters downstream of the shock from balances of mass, momentum and energy. Observe that a quadratic equation in velocity is formed from the energy equation by substitution of density as a function of velocity from the mass balance and substitution of pressure as a function of velocity from the momentum balance (so, specific shock formulae from fluid mechanics are not needed). Determine the Mach number at rotor inlet, the work coefficient and the isentropic re-expansion efficiency of the rotor (A: $M_{w1} \approx 1.42$, $p_{02}/p_{01} \approx 2.11$; $\psi \approx 0.42$, $\eta_{sre} \approx 0.95$). Remark the large work coefficient, the large pressure ratio and the high efficiency, but boundary layer losses in the rotor are not taken into account and neither are the losses in the post-connected stator.

References

1. Boyer KM, O'Brien WF (2003) An improved streamline curvature approach for off-design analysis of transonic axial compression systems. *J Turbomach* 125:475–481
2. Calvert WJ, Ginder RB (1999) Transonic fan and compressor design. *IMEchE J Mech Eng Sci* 213:419–436
3. Cumpsty NF (1989) Compressor aerodynamics. Longman Scientific & Technical, New York, ISBN 0-582-01364-X
4. Day IJ, Freeman C (1994) The unstable behavior of low and high-speed compressors. *J Turbomach* 116:194–201
5. Fischer A, Riess W, Seume JR (2004) Performance of strongly bowed stators in a four-stage high-speed compressor. *J Turbomach* 126:333–338
6. Fottner L (1989) Review of turbomachinery blading design problems. Chapter 1 in AGARD LS 167. Blading design of axial turbomachines. AGARD, ISBN 92-835-0512-3
7. Gümmer V, Wenger U, Kau H-P (2001) Using sweep and dihedral to control three-dimensional flow in transonic stators of axial compressors. *J Turbomach* 123:40–48

8. Hah C, Shin H-W (2012) Study of near-stall flow behaviour in modern transonic fan with compound sweep. *J Fluids Eng* 134:071101
9. Happel H-W, Stubert B (1988) Application of a 3D time-marching Euler code to transonic turbomachinery flow. Proceedings 7th GAMM-conference on numerical methods in fluid dynamics. Vieweg Verlag, ISBN 3-528-08094-9, pp 120–129
10. Lewis RI (1996) Turbomachinery performance analysis. Wiley, New York, ISBN 0-470-23596-9
11. Lieblein S (1965) Experimental flow in two-dimensional cascades. Chapter 6 of aerodynamic design of axial-flow compressors. NASA SP-36
12. Lieblein S, Schwenk FC, Broderick RL (1953) Diffusion factor for estimating losses and limit blade loadings in axial-flow compressor blade elements. NACA RM E53D01
13. NASA-SP-36 (1965) several authors, aerodynamic design of axial-flow compressors. No ISBN
14. Rechter H, Steinert W, Lehmann K (1985) Comparison of controlled diffusion airfoils with conventional NACA 65 airfoils developed for stator blade application in a multistage axial compressor. *J Eng Gas Turbines Power* 107:494–498
15. Sieverding F, Ribi B, Casey M, Meyer M (2004) Design of industrial axial compressor blade sections for optimal range and performance. *J Turbomach* 126:323–331
16. The Jet Engine (1986) Rolls-Royce, ISBN 0-902121-04-9
17. Tweedt DL, Schreiber HA, Starken H (1988) Experimental investigation of the performance of a supersonic compressor cascade. *J Turbomach* 110:456–466
18. Wadia AR, Szucs PN, Crall DW (1998) Inner workings of aerodynamic sweep. *J Turbomach* 120:671–682

Chapter 14

Radial Compressors

Abstract Radial compressors (or centrifugal compressors) resemble radial fans and radial pumps for basic operation aspects. So, based on the study of fans and pumps, which we have done in previous chapters, we can understand the basic operation of centrifugal compressors. In this chapter, we repeat the analysis of the working principles of centrifugal machines, but applied to centrifugal compressors. We discuss applications and the aspects that are particular for centrifugal compressors. These are the inducer part at the inlet of a rotor for large work and the diffuser downstream of the rotor. We also analyse the operating characteristics with the limits caused by stall and choking.

14.1 Construction Forms and Applications

14.1.1 Rotor Types

Figure 14.1 shows a radial or centrifugal compressor for use in chemical plants and refineries and for transport of natural gas. The terms radial and centrifugal are equivalent with compressors. The successive rotors have increasingly smaller through-flow areas due to increasing density. A rotor is mostly called an *impeller*, which means the element that actuates the fluid. The rotors of Fig. 14.1 have a shroud, so are closed, and the blades are moderately swept backward at the outlet. There is no strong difference with rotors of a centrifugal pump. At the rotor inlet, blades begin downstream of the orthogonal inlet plane. At the leading edge of the rotor blades, the velocity has both an axial and a radial component. Blades with a leading edge positioned so far downstream of the inlet plane of the rotor such that there is no axial velocity component are very rare. This means, with centrifugal pump terminology, that blades mostly are extended into the suction eye. The blades feature double bending, which means that the bending in different orthogonal sections differs, but the axial variation of the bending is very moderate. Compared to pumps, the ratio of the inlet diameter to the outlet diameter of the rotors is mostly higher (this ratio lowers in the successive rotors), and the backward sweep of the blades at rotor outlet is less. This means that flow factors and work factors are

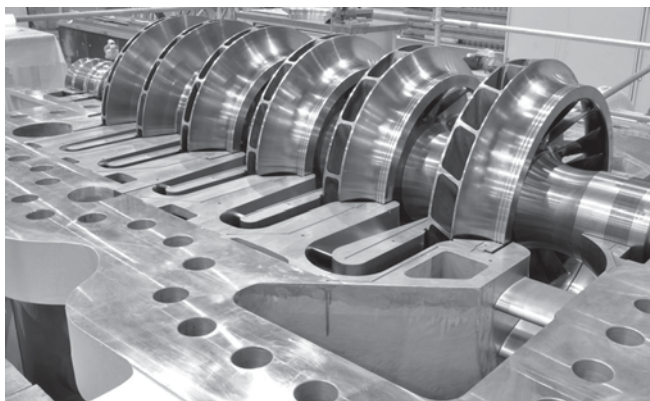
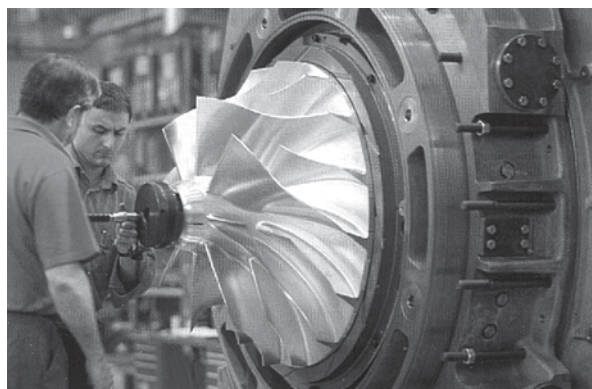


Fig. 14.1 Multistage centrifugal compressor for chemical plants, refineries and gas transport (courtesy MAN Diesel & Turbo)

typically higher. The tendency to higher values comes from the lower density of the fluid. Most applications require pressure ratios far above 10. The compressor must then have multiple stages, which creates the tendency towards rather large work per stage. The tendency towards large flow factors comes from better efficiency of screw compressors and reciprocating compressors for low flow rates.

Figure 14.2 shows the compressor rotor of a turbocharger for a large diesel engine. The rotor is open with an axial inlet part (the leading edges of the longest blades are in the orthogonal inlet plane of the rotor) and slightly backward swept blades at the outlet (typical is about $20\text{--}30^\circ$ backward sweep). Rotors of this shape are intended to realise a large pressure ratio and a large flow rate. A high peripheral speed, typically $400\text{--}450\text{ m/s}$, is used therefore. With a high peripheral speed, a shroud on the rotor would cause too high stress on the blades due to the centrifugal force. Also, for limiting bending stresses, a blade should not deviate too strongly from the radial direction at the rotor outlet. Rotors with pure radial end blades occur as well. For the same reason, the inlet part of the blades is composed of radial

Fig. 14.2 Open radial compressor rotor with inducer part (axial part) and splitter blades; blades have slight backward sweep at the rotor outlet; compressor part of a diesel engine turbocharger (courtesy ABB Turbo Systems)



filaments. The rotor inlet part resembles an axial compressor. This part is termed an *inducer*. Half of the blades are extended into the inducer part, the other half are not. In other words, there are *primary blades* and *splitter blades*. Splitter blades divide the channel that is formed by primary blades into two parts, from a certain distance beyond the rotor inlet plane. The reason for the presence of splitter blades will be discussed later. The figure is also intended to demonstrate that even the primary blades do not have a very complex shape.

14.1.2 General Shape of a Radial Compressor

Figure 14.3 sketches a single-stage radial compressor with an open rotor. The incoming flow is in the axial direction. Some machines feature a stationary blade row at the inlet. The inlet guide vanes are intended to give swirl to the rotor inlet flow, so to deviate it from the axial direction. The role of pre-swirl vanes is to change the operating characteristic (see Exercise 14.7.2). The inlet velocity triangle is drawn at the inducer tip. The rotor has blades with a radial end. Slip has been taken into account with the velocity triangle at the rotor outlet, so that the relative outlet flow is inclined somewhat backward. With radial end blades, the tangential outlet velocity component (v_{2u}) is somewhat lower than the peripheral speed (u_2). The rotor work is

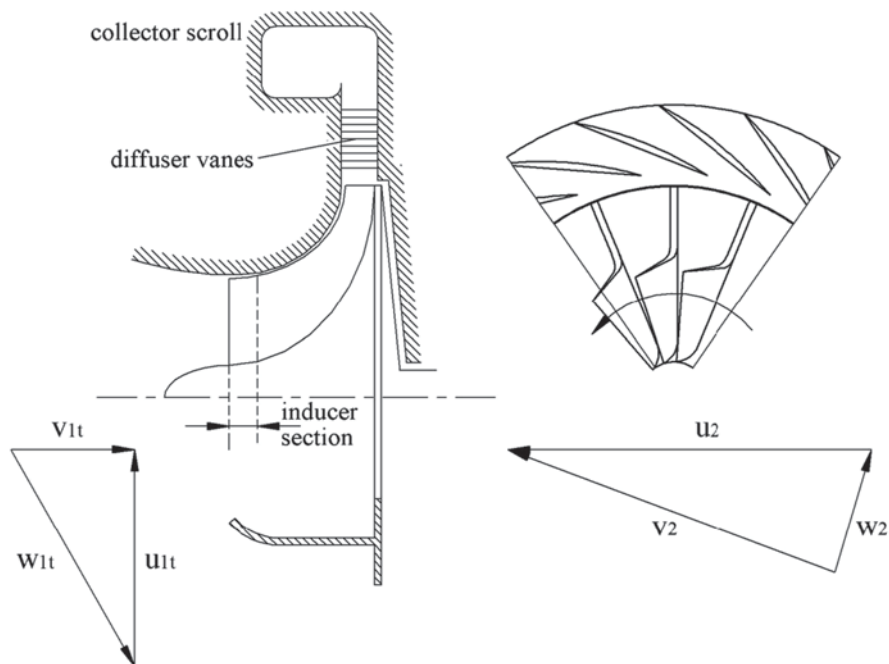


Fig. 14.3 Radial compressor: parts and velocity triangles

$$\Delta W = u_2 v_{2u}$$

When the blades are inclined more backward, the rotor work decreases. Weak backward sweep is thus favourable with regard to the realisable pressure ratio, but leads to a high outlet velocity of the impeller. So, a diffuser becomes necessary. A diffuser with vanes is sketched. Other diffuser shapes are possible and will be discussed in a later section. A scroll-shaped collector comes around the diffuser. Diffusers inherently feature great losses (see later discussion). Compressors with slightly backward swept blades thus have a lower efficiency than compressors with more inclined ones. Rotors with forward inclined blades are never used.

14.1.3 Comparison Between Radial and Axial Compressors

The fundamental difference between both types is that radial compressors, for equal external diameters, handle a lower flow rate, but realise a larger stage work. With an axial compressor, 75 % of the frontal area may be available for through-flow (at a 0.5 radius ratio) with an axial velocity up to about 50 % of the blade speed on the average radius (about 40 % of the tip speed). A flow coefficient defined with the frontal area and the peripheral speed thus may reach about 0.30. The flow area with a radial compressor maximally covers about 45 % of the frontal area with a through-flow velocity maximally about 50 % of the blade speed at the inlet tip (about 35 % of the peripheral speed of the rotor). The flow coefficient, according to the above definition, is maximally about 0.15. Shrouded rotors (Fig. 14.1) often feature a much lower flow coefficient. The flow factor varies between about 0.02 to 0.15, with the largest values obtained by open rotors.

With an axial compressor, the work coefficient on the average radius is at maximum about 0.4 ($\psi = \Delta W / u^2$). Related to tip speed it is maximally about 0.3. With a radial compressor, the work coefficient may reach until about 0.9 when applying radial end blades.

The peripheral speed is comparable for both machines; maximally until about 400–450 m/s with open rotors. Strength does not strictly limit this speed. With titanium alloys in axial compressors and high-quality aluminium alloys in open rotor centrifugal compressors, 550 m/s is achievable with both types (with steel, it is about 400–450 m/s). A speed limitation normally follows from choking prevention. At 400 m/s peripheral speed, the relative velocity on the average radius at the rotor inlet of an axial compressor is slightly supersonic and the absolute velocity at the rotor outlet of a radial compressor is slightly supersonic too. With shrouded rotors made of steel, the maximum peripheral speed is limited by strength to about 350 m/s.

The efficiency of an axial compressor is significantly better than that of a radial one: the isentropic total-to-total efficiency is about 0.92 at the maximum compared to maximally about 0.84 for a centrifugal compressor with open rotor and slightly backswept blades. The efficiency improves with more backward sweep and closed

rotors to maximally about 0.87. The main reason is the very inhomogeneous flow at the rotor outlet of a radial compressor, caused by turbulence segregation by the Coriolis force, as with radial pumps and fans (Sect. 3.3.4 in Chap. 3). The Coriolis force drives high-energy cores within the turbulent motion from the suction side to the pressure side. This leads to a lowered velocity level near the suction side (see Sect. 14.5.1). The inhomogeneity of the rotor outlet flow causes a significant mixing loss downstream of the rotor. Further, rotors with radial end blades or with slight backward sweep, i.e. with machines intended for high work, require a significant velocity reduction in a diffuser downstream of the rotor. A strong deceleration inevitably creates large loss. A third reason is rather important leakage loss with an open impeller.

14.1.4 Examples of Radial Compressors

Some industrial centrifugal compressors resemble centrifugal pumps. Figure 14.1 is an example. Rotors have backward swept blades, as pumps do. After each rotor, there is a ring-shaped vaneless chamber, functioning as a diffuser, followed by a chamber with return channels leading the flow to the next stage. After the last stage, the gas is collected with a scroll. Work per rotor is not very high in compressors as in Fig. 14.1. The stage work coefficient is maximally about 0.5. So, the rotor outlet velocity is maximally about 50 % of the peripheral speed. Therefore, a vaneless annular chamber is sufficient as diffuser (see Sect. 14.5). A compressor as in Fig. 14.1 is intended to allow significant flow rate variation. The flow range is limited by rotating stall or surge at low flow rate and choking at high flow rate (similar as with axial compressors). The operating range will be discussed in Sect. 14.6. With moderate backward sweep of the blades and vaneless diffusers, the design flow rate has a large margin against the limiting phenomena.

The air compressor shown in Fig. 14.4 features a first open rotor stage (but there are no splitter blades), followed by three shrouded ones. With this type, the first stage has an open rotor because the volume flow rate is the largest in the first stage. The compressor shown in Fig. 14.4 is intended for a relatively high flow rate. Similar machines exist with only shrouded rotors, intended for lower flow rates. The air is cooled after each stage (called an isothermal compressor). Coolers are integrated into the machine. The supply to the coolers requires a rather special vaned chamber, functioning as diffuser. A simpler vaned chamber guides the flow from the outlet of a heat exchanger to the inlet of a rotor. Figure 14.5 shows cross sections of the chambers. The successive radial stages feature increasingly smaller through-flow areas. The rotors have moderately backswept blades, resulting in a higher work coefficient than typical for pump rotors. This implies the need for more blades. Typically, rotors have 16–20 blades (see also Fig. 14.1). Construction mostly encompasses milling of the back disc together with the blades from a massive block, lathing of the shroud and welding of the shroud onto the blades. As compressor rotors run much faster than pump rotors, finishing must be far more accurate. These

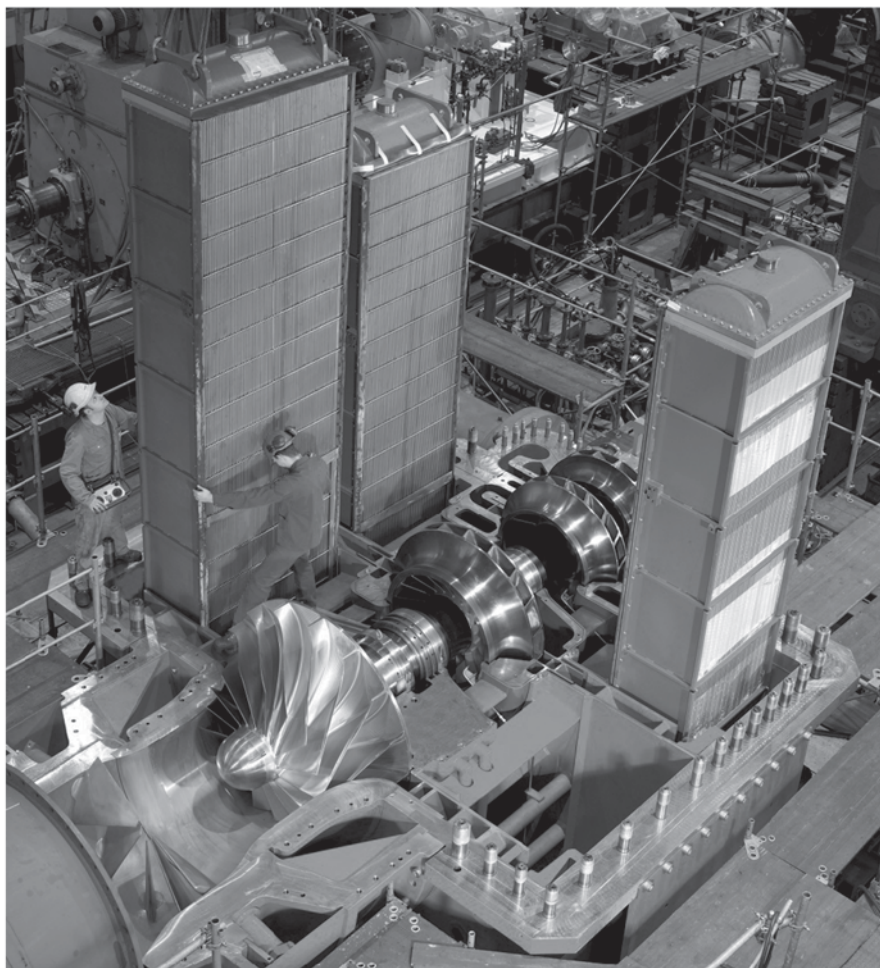


Fig. 14.4 Radial air compressor with integrated coolers (courtesy MAN Diesel & Turbo)

rotors must be stronger as well. Rotor casting, as typical for pumps, is not feasible. Welding of the shroud is normally possible, as the rotor channels are rather open.

Fig. 14.6 renders a radial compressor with ten stages and an *integrated gearbox* (integrally geared compressor). This arrangement is an alternative to an inline construction. The objective is to obtain a sufficiently high and approximately equal peripheral speed of the successive stages with decreasing diameter for compressors with rather small rotor dimensions. Figure 14.7 shows a diesel engine turbocharger with a radial compressor for high work and an axial turbine. Further, radial compressors are often used as the last stage of the compressor of a small gas turbine for helicopter rotor drive. The general appearance is then somewhat similar to the

Fig. 14.5 Cross sections of the vaned chambers for inlet to (*left*) and outlet from (*right*) the radial rotors of Fig. 14.4

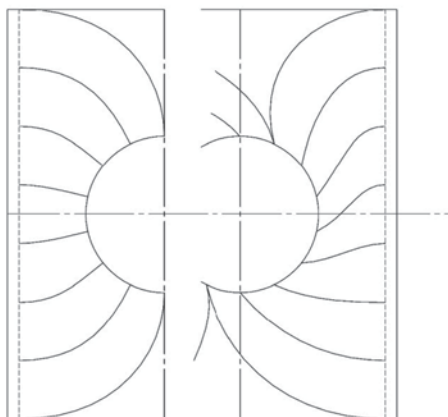
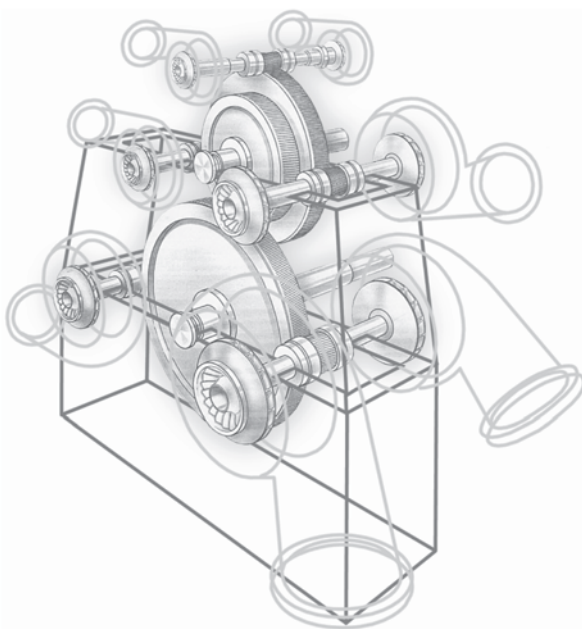


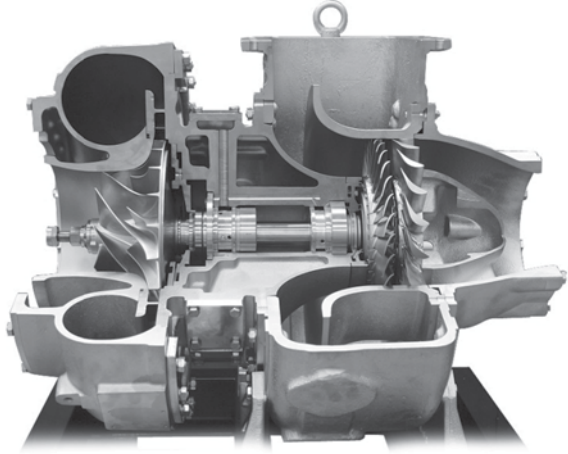
Fig. 14.6 High-pressure 10-stage centrifugal compressor for CO₂ with integrated gearbox (courtesy MAN Diesel & Turbo)



turbocharger of Fig. 14.7, but with one or two axial stages upstream of the radial compressor and addition of a power turbine stage.

The operating range of a compressor is small with small backward sweep and high peripheral speed. Flow rate decrease compared to the design flow rate rather quickly brings the operating point to the maximum of the characteristic curve and so to surge. Flow rate increase rather quickly leads to choking. The application therefore should allow a narrow operating range. Mostly, there is no problem with a narrow operating range for an air compressor and for compressors in small gas turbines.

Fig. 14.7 Diesel engine turbocharger with a radial compressor and an axial turbine (courtesy KBB GmbH)



14.2 Kinematic Parameters

We take a machine with radial end blades, as sketched in Fig. 14.3, as an example. Departing from the results with this rotor shape, we determine the influence of the backward sweep.

The work coefficient is
$$\psi = \frac{\Delta W}{u_2^2} = \frac{u_2 v_{2u}}{u_2^2} = \frac{v_{2u}}{u_2}. \quad (14.1)$$

The degree of reaction is
$$R = \frac{h_2 - h_1}{h_{02} - h_{01}},$$

with $h_{02} - h_{01} = u_2 v_{2u}$ and $h_2 - h_1 = u_2 v_{2u} - (1/2 v_2^2 - 1/2 v_1^2).$

We use here that the absolute inlet velocity lies in the meridional plane. We further assume a constant meridional velocity component (v_m) within the rotor, so that

$$v_2^2 = v_{2u}^2 + v_{2m}^2 \quad \text{with} \quad v_{2m} = v_1.$$

Thus

$$\begin{aligned} h_2 - h_1 &= u_2 v_{2u} - 1/2 v_{2u}^2, \\ R &= 1 - 1/2 \frac{v_{2u}}{u_2} = 1 - 1/2 \psi. \end{aligned} \quad (14.2)$$

This relation is the same as the one derived for radial fans in Chap. 3. For radial end blades: $\psi \approx 0.9$, thus $R \approx 0.55$. Backward sweep of the blades decreases the work coefficient and increases the degree of reaction.

Fig. 14.8 h-s diagram of a centrifugal compressor with radial end blades ($R=0.55$)

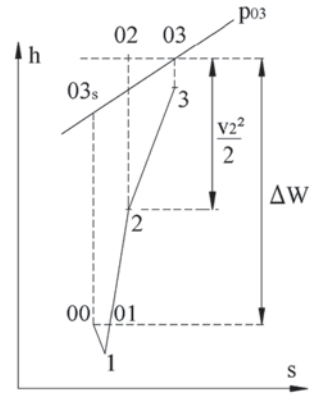


Figure 14.8 sketches the h-s diagram of the compression process for $R=0.55$. The kinetic energy at the rotor outlet amounts to about half the rotor work. So the diffuser has a very crucial role. Blade backward sweep increases the degree of reaction and decreases the kinetic energy to be transformed by the diffuser. Losses within the rotor are quite small, due to the lossless contribution to the static enthalpy rise by the centrifugal force. The enthalpy rise is

$$h_2 - h_1 = \frac{1}{2}(u_2^2 - u_1^2) + \frac{1}{2}(w_1^2 - w_2^2).$$

With the velocity triangles in Fig. 14.3, the centrifugal force contributes to the enthalpy rise for about 90% (taking an average w_1 at the rotor inlet). As usual, station 2 is the outlet of the rotor. Losses downstream of this station are accounted to the subsequent stator part, encompassing a mixing space, a vaned or vaneless diffuser and a volute. The biggest loss is the mixing loss immediately downstream of the rotor (see discussion in the later Sect. 14.5.2). With a low degree of reaction ($R=0.55$), mainly the stator loss determines the overall efficiency. Compressor efficiency is generally defined between the total state at the machine inlet, which is the rotor eye inlet (state 00), and the total state at the machine outlet, which is the volute outlet (state 03). The total state at the machine inlet is generally taken as the reference state for determination of dimensionless quantities. We further adhere to this convention. This way, the classic definition of isentropic internal efficiency is (see Fig. 14.8):

$$\eta_{it} = \frac{h_{03s} - h_{00}}{h_{03} - h_{00}} = \frac{\Delta h_{0s}}{\Delta h_0} = \frac{\Delta h_{0s}}{\Delta W}.$$

The third kinematic parameter, the flow coefficient, follows from efficiency optimisation. It is commonly assumed, as a first approximation, that maximum efficiency is obtained by minimising the Mach number of the relative velocity at the inducer inlet, at the casing position (tip): w_{1t} [3, 4]. The main objective of this minimum is

to obtain the lowest possible relative velocity at the impeller outlet, so that the mixing loss at the impeller outlet is minimal. Further, the rotor outlet velocity in the absolute frame is then as tangential as possible. This minimises the radial dimensions of the diffuser and the volute, which reduces the losses within these elements. Minimising the Mach number at the inlet also realises the greatest possible margin against choking, if the rotor inflow is the most critical for choking (see discussion in Sect. 14.6).

$$w_{lt}^2 = u_{lt}^2 + v_l^2 \quad \text{with} \quad u_{lt} = \frac{\Omega d_{lt}}{2},$$

$$\dot{m} = \rho_l v_l A_l \quad \text{with} \quad A_l = \frac{\pi}{4}(d_{lt}^2 - d_{lh}^2) = \frac{\pi}{4} k d_{lt}^2 \quad (k \approx 0.85),$$

$$h_l = h_{0l} - 1/2 v_l^2 \quad \text{and} \quad \frac{\rho_l}{\rho_{0l}} = \left(\frac{h_l}{h_{0l}} \right)^{\frac{1}{\gamma-1}},$$

$$w_{lt}^2 = \frac{\Omega^2}{4} d_{lt}^2 + \left(\frac{\dot{m}}{\rho_l \frac{\pi}{4} k} \right)^2 (d_{lt}^2)^{-2}.$$

We take here as diameter ratio at inlet $d_{lh}/d_{lt} = 0.4$, so that the obstruction factor k is about 0.85. The dependence of ρ_l to v_l is ignored in the following derivations in order to simplify the reasoning. The effect of variable density will be approximately corrected afterwards. With constant density, the Mach number minimum corresponds to the velocity minimum. With a given mass flow rate and rotational speed, the minimum is attained for

$$\frac{\Omega^2}{4} - 2 \left(\frac{\dot{m}}{\rho_l \frac{\pi}{4} k} \right)^2 (d_{lt}^2)^{-3} = 0 \quad \text{or} \quad (d_{lt}^2)^3 = \frac{8}{\Omega^2} \left(\frac{4\dot{m}}{\pi \rho_l k} \right)^2.$$

Thus

$$(d_{lt})_o \approx 1.53 \left(\frac{\dot{m}}{\rho_l k \Omega} \right)^{1/3} \approx 1.62 \left(\frac{\dot{m}}{\rho_l \Omega} \right)^{1/3}, \quad (14.3)$$

and

$$\text{tg}(-\beta_{lt})_o = \left(\frac{u_l}{v_l} \right) = \frac{\Omega (d_{lt})_o}{2} \frac{\rho_l \pi k (d_{lt})_o^2}{4\dot{m}} = \frac{\sqrt{8}}{2} = \sqrt{2},$$

from which $(\beta_{lt})_o \approx -55^\circ$. Due to the variable density, the minimum Mach number is attained for a somewhat smaller value of v_l , so that $(\beta_{lt})_o \approx -60^\circ$. Then $v_l/u_{lt} \approx 0.577$. The coefficient in (14.3) then becomes about 1.73 instead of 1.62. The exact result depends somewhat on the Mach number of v_l [4]. An alternative approach, with about the same result, consists in maximising the mass flow rate for a given Mach number of the relative tip speed [3, 4].

Further, a strong deceleration ratio w_2/w_1 is required to attain the absolute rotor outlet velocity as tangential as possible. Extreme decelerations are applied with radial end blades or slightly backswept blades, until $w_2/w_{1t} \approx 0.60$ (a typical value is 0.65). It is surprising that such strong decelerations can be realised without an extreme form of flow separation. The reason is that very intense secondary flows occur within radial impellers, driving core flow fluid to the boundary layers. Strengthening of the boundary layers within high-deceleration zones may thus be attained by an appropriate rotor channel design, similar to the optimisation of bent diffusers with hydraulic turbines. Strong deceleration generates a high non-homogeneity of the rotor outflow, of course, causing large mixing loss. Backward sweep of the blades reduces the need for strong deceleration. Complete optimisation is thus very delicate and requires accurate numerical simulation tools. So, the foregoing derived optimum inlet diameter (14.3) (with coefficient 1.73) is only very approximate.

With (14.3) a flow coefficient may be formed ($k \approx 0.85$, $\rho_1/\rho_{00} \approx 0.9$) as

$$\phi_1 = \frac{\dot{m}}{\rho_{00} \Omega d_{1t}^3} \approx \frac{1}{(1.73)^3} \frac{\rho_1}{\rho_{00}} \approx 0.173. \quad (14.4)$$

Specific speed follows from $\Omega_s = \frac{\Omega \sqrt{\dot{V}_{00}}}{(\Delta h_{0s})^{3/4}}$,

with $\dot{V}_{00} = \phi_1 \Omega d_{1t}^3$ and $\Delta h_{0s} = \eta_{it} \psi u_2^2$,

so that

$$\Omega_s = \frac{\sqrt{8\phi_1}}{(\eta_{it}\psi)^{3/4}} \left(\frac{r_{1t}}{r_2} \right)^{3/2}. \quad (14.5)$$

With radial end blades, $\psi \approx 0.9$ and $\eta_{it} \approx 0.82$, so that the coefficient in (14.5) is about 1.50. To $r_{1t}/r_2 = 0.75$, which is about the maximum possible diameter ratio, corresponds $\Omega_s \approx 1$. A lower specific speed is attained with a lower diameter ratio and a lower flow coefficient. A higher specific speed is attained with a higher flow coefficient and blade backward sweep at the impeller outlet. The specific speed ranges over about 0.4–1.4. The best efficiency is reached in the 0.7–1.1 range, with closed rotors with backward sweep in the range 25–50° [1, 2]. A still higher specific speed is possible with a mixed flow impeller, but mixed flow machines are rare, as typically the aim of a radial compressor is to obtain a much larger pressure ratio than with axial compressors.

14.3 Pressure Ratio

Again, we take a compressor with radial end blades, as sketched in Fig. 14.3, as an example. The slip velocity at the rotor outlet v_s (difference between the actual tangential velocity component v_{2u} and the geometrical one) may be expressed by

the slip factor σ , with $1 - \sigma = v_s / u_2$. According to Wiesner (Chap. 3, Sect. 3.3.3), it applies that

$$1 - \sigma = \frac{\sqrt{\cos \beta_2^b}}{Z^{0.7}},$$

with β_2^b the outlet blade angle. For radial end blades $\beta_2^b = 0$. With $Z = 20$, it follows that $\sigma \approx 0.9$.

Rotor work is $\Delta W = u_2 v_{2u} = \sigma u_2^2$.

The pressure ratio follows from $\frac{p_{03}}{p_{00}} = \left(\frac{T_{03s}}{T_{00}} \right)^{\frac{\gamma}{\gamma-1}}$.

Total-to-total efficiency is $\eta_{tt} = \frac{T_{03s} - T_{00}}{T_{03} - T_{00}}$.

Thus:

$$T_{03s} = T_{00} + \eta_{tt} (T_{03} - T_{00}) = T_{00} + \eta_{tt} \frac{\Delta W}{C_p} = T_{00} \left(1 + \eta_{tt} \frac{\Delta W}{C_p T_{00}} \right).$$

Further: $C_p T_{00} = \frac{\gamma}{\gamma-1} R T_{00} = \frac{1}{\gamma-1} c_{00}^2$.

For radial end blades:

$$r = \frac{p_{03}}{p_{00}} = \left[1 + \eta_{tt} (\gamma - 1) \frac{\sigma u_2^2}{c_{00}^2} \right]^{\frac{\gamma}{\gamma-1}}.$$

Example: $T_{00} = 300$ K, $c_{00} = 347$ m/s, $u_2 = 450$ m/s, $\gamma = 1.4$, $\eta_{tt} = 0.8$, $\sigma = 0.9$.

This combination gives $r = \frac{p_{03}}{p_{00}} = 4$.

The peripheral rotor speed is commonly expressed by a Mach number, called the *rotor Mach number*, as $M_{u0} = \frac{u_2}{c_{00}}$.

To the given example corresponds $M_{u0} = 1.3$. The outlet Mach number may, with radial end blades, be determined with the approximation $v_2 \approx u_2$ (Fig. 14.3).

So $h_{02} = h_{00} + \Delta W$,

or $h_2 + \frac{1}{2} v_2^2 = h_{00} + \sigma u_2^2$, thus $h_2 \approx h_{00} + (\sigma - \frac{1}{2}) u_2^2$,

or $\frac{1}{\gamma-1} c_2^2 \approx \frac{1}{\gamma-1} c_{00}^2 + (\sigma - \frac{1}{2}) u_2^2$.

$$\text{Thus } M_2^2 = \frac{v_2^2}{c_2^2} \approx \frac{u_2^2}{c_{\theta 0}^2 + (\gamma - 1)(\sigma - 1/2)u_2^2} = \frac{M_{u0}^2}{1 + (\gamma - 1)(\sigma - 1/2)M_{u0}^2}.$$

With $M_{u0} = 1.3$ it follows that $M_2 \approx 1.15$. This means that, with pressure ratio equal to 4, the rotor outlet is slightly supersonic. Some deceleration within a vaneless space may reduce the Mach number to just below 1 ($M \approx 0.9$). This allows leading the flow into a vaned diffuser, just avoiding choking.

The conclusion is that a pressure ratio equal to 4 may be attained with a single-stage radial compressor by applying radial end or slightly backward swept blades at a high peripheral speed. The machine then has a limited operating range. In practice, radial compressors with pressure ratio up to 4 and somewhat above this value are applied. A larger pressure ratio is attainable, in principle, since the peripheral speed can exceed 450 m/s, but at a pressure ratio above 4, supersonic inlet flow to the diffuser becomes unavoidable. Shock waves occur then at the diffuser inlet (vaned diffuser), impairing the efficiency. Moreover, the operating range becomes narrow. Single-stage radial compressors with a pressure ratio 6 or even 8 do exist, but can only be used for a limited number of applications.

14.4 Rotor Shape

14.4.1 Number of Blades

Determination of the minimum required number of blades with radial rotors was already discussed in Chap. 3 (Sect. 3.3.4 and 3.3.5). We repeat some elements of the reasoning, but adapted to centrifugal compressors. In Chap. 3, we analysed fans, which are machines of low solidity and therefore we used an estimate of the velocity difference between the suction and pressure sides of a blade based on Pfleiderer's reasoning for rotors with small overlap of the blades. In compressors, the solidity is high and the reasoning according to Stodola, considering the rotor as composed of blade channels, is more appropriate.

The equation for the velocity difference over a blade at a given radius (Chap. 3, Eq. 3 14) is

$$w_s - w_p = \Delta\theta \cos\beta \left[2\Omega r + \frac{d}{dr}(r w_u) \right], \quad (14.6)$$

with $\Delta\theta = 2\pi/Z$ and Z the number of blades. This equation was derived in Chap. 3 from flow analysis in the rotating frame and considering the circulation of the relative velocity on two different contours. The first term between the square brackets originates from the Coriolis force, while the second term comes from the streamline curvature, i.e. the lift. For radial end blades and blades with backward sweep at the

rotor outlet, the second term is negative at the rotor outlet. The equation may also be derived directly, albeit with the necessity of some approximations, from a moment of momentum balance on a streamtube with infinitesimal radial length, spanning a blade passage (see Exercise 14.7.1). Based on (14.6), we may write at the rotor outlet:

$$(w_s - w_p)_2 = \frac{2\pi}{Z} \cos \beta_2 u_2 f_R,$$

$$\text{and} \quad (w_s - w_2)_2 = (w_2 - w_p)_2 = \frac{2\pi}{Z} \cos \beta_2 u_2 f_R, \quad (14.7)$$

where w_2 is the average relative flow velocity at the rotor outlet and f_R is a factor smaller than unity, expressing the influence of the curvature of the streamlines in backward sense. Figure 14.9 sketches an average streamline, the intervening forces and the resulting flow velocity variation transverse to the streamlines.

From the flow pattern we understand that two criteria for avoiding separation at the rotor outlet should be met. Firstly, there must be a sufficient number of blades, so that the Coriolis force cannot generate flow reversal at the pressure side. Secondly, the blade loading must be limited to avoid separation near the trailing edge at the suction side, as a consequence of the adverse pressure gradient on the boundary layer.

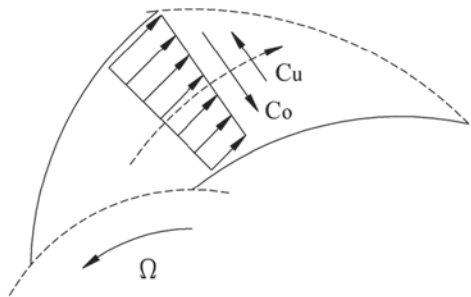
Flow reversal at the pressure side is avoided for

$$w_2 > \frac{2\pi}{Z} \cos \beta_2 u_2 f_R. \quad (14.8)$$

Avoidance of boundary layer separation at the suction side may be expressed by a local diffusion factor criterion as

$$\frac{w_s - w_2}{w_s} = D_{loc} < 0.5 \quad \text{or} \quad w_s - w_2 = \frac{D_{loc}}{1 - D_{loc}} w_2. \quad (14.9)$$

Fig. 14.9 Average streamline within a rotor and transverse velocity variation: Coriolis force Co, Centrifugal force by streamline curvature Cu



For $D_{loc} < 0.5$ this criterion also results in (14.8). This value of D_{loc} is the critical value for separation in axial cascades. Deceleration in the boundary layer at the suction side is more disadvantageous with a centrifugal rotor, due to the turbulence segregation effect by the Coriolis force (Chap. 3, Sect. 3.3.4). The Coriolis force drives high-energy cores within the turbulent motion away from the suction side to the pressure side. This effect weakens the suction side boundary layer. Therefore, the critical value of D_{loc} is rather 0.45. So, in practice, separation at the suction side occurs rather than flow reversal at the pressure side. Therefore, we further apply criterion (14.9) as

$$\frac{2\pi}{Z} \cos \beta_2 u_2 f_R < 0.80 w_2. \quad (14.10)$$

The effect of streamline curvature in the vicinity of the rotor outlet is quite modest with centrifugal compressors. In practice, only rotors with radial end blades ($\beta_2 = -15^\circ$, after slip), with slight backward sweep ($\beta_2 = -20^\circ$ to -30°) and with moderate backward sweep ($\beta_2 = -45^\circ$) are applied. The curvature factor f_R in (14.10) may therefore, by way of simplification, be taken as 0.80, so that approximately holds

$$\frac{2\pi}{Z} \cos \beta_2 u_2 < w_2. \quad (14.11)$$

This simplification spares us then deriving an expression for the curvature effect, as in Chap. 3. Note that the reasoning in Chap. 3 is not applicable to centrifugal compressors for high work due to the presence of the inducer. The effect of the curvature is rather a local rotor outlet phenomenon with a centrifugal compressor, but the reasoning in Chap. 3 deducts the curvature effect from the overall rotor through-flow. This is only justified for centrifugal fans since these have small or modest solidity. For the same reason, the Wiesner formula for slip is better justified for centrifugal compressors than the Pfeleiderer formula.

With the velocity triangles of Fig. 14.3, we may estimate the ratio w_2/u_2 to about 0.35. With $\beta_2 \approx -15^\circ$, it follows from (14.11) that $Z_{min} \approx 17$. For $\beta_2 \approx -45^\circ$ ($\beta_2^b \approx -40^\circ$), w_2/u_2 may be up to 0.45, which results in $Z_{min} \approx 10$. Values used in practice are often 20 and 14 or 16.

14.4.2 Inducer

Rotors with radial end blades or with slightly backward swept blades are intended to realise the maximum attainable work. Therefore, such applications aim at maximum attainable peripheral speed (Figs. 14.2 and 14.7). This requires adaptation of the rotor inlet. Bending stress generated by the centrifugal force at the inlet side of the impeller must be avoided. This may be achieved by adding an axial part, termed

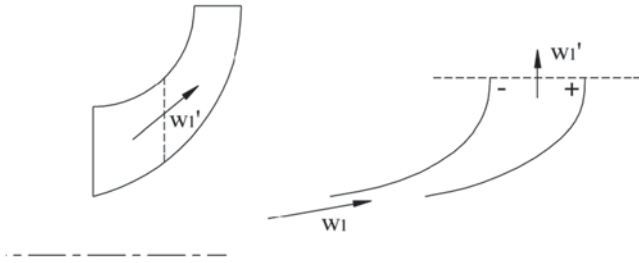


Fig. 14.10 Inducer of a high-speed centrifugal compressor; *left*: meridional view; *right*: mean circumferential streamsurface section

an *inducer*, as sketched in Fig. 14.10. Within the inducer, the relative velocity w_1 is bent toward the meridional plane such that the relative velocity at the inducer outlet no longer has a tangential component. Downstream of the inducer, the blade may be purely radial, eliminating bending stresses by the centrifugal force. The inducer itself may be composed of radial filaments, avoiding bending stresses. In reality, the rotor does not have to be completely free from bending stresses. So, some backward sweep of the blades at the impeller outlet is allowed, as well as some deviation from radial filaments in the inducer part.

An inducer functions as an axial compressor, with the difference that no trailing edge occurs. Figure 14.11 sketches the pressure distribution with an axial compressor and with an inducer. The boundary layer loading at the suction side is much more advantageous with an inducer due to the pressure difference at the outlet between the pressure and the suction sides. Maintaining this pressure difference, when the flow passes to the radial part, is essential. This may be attained by providing a radial component to the velocity w'_1 (Fig. 14.10). The associated Coriolis force then generates a pressure difference within the radial part of the rotor. The inducer part should be matched to the radial part, so that the pressure difference by lift within the inducer smoothly shifts to the pressure difference by Coriolis force within the radial part. We use here the term radial part to denote the second part of the impeller, but it is clear that this part does not have to be fully radial.

The diffusion factor within the inducer part is

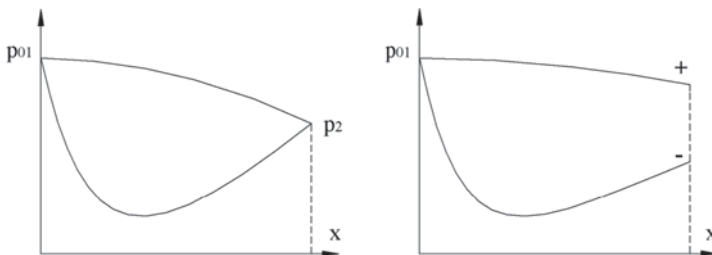


Fig. 14.11 Pressure distribution with an axial compressor (*left*) and an inducer of a radial compressor (*right*)

$$DF = 1 - \frac{w'_l}{w_l} + \frac{\Delta w_u}{2\sigma w_l},$$

with $\Delta w_u = u_l$; $\frac{u_l}{w_l} = |\sin \beta_l| \approx 0.766$; ($\beta_l \approx -50^\circ$).

The contribution of the blade loading in the diffusion factor is $0.383/\sigma$ for $\beta_l = -50^\circ$ as mean value at the inlet. A general deceleration is not required for inducer functioning. So, the magnitudes of w'_l and w_l might even be equal. Further, the diffusion factor may exceed that of an axial compressor due to absence of a trailing edge. For equal velocity magnitudes and $DF=0.6$ follows $\sigma=0.64$, which is a low value. This implies that a general deceleration is possible ($w'_l < w_l$). Even for a rather strong deceleration, e.g. $w'_l = 0.7 w_l$, solidity still does not have to be very high. An inducer may thus be realised with much fewer blades than needed for the radial part. Application of splitter blades therefore is customary. This means that the inducer has half the number of blades of the radial rotor part (Figs. 14.2 and 14.7). With such an inducer, the displacement by the blades within the suction eye is lower, which increases the maximum possible flow rate.

14.5 Diffusers

14.5.1 Flow Non-homogeneity at Rotor Outlet

Within the radial part of a rotor with high work, the flow splits, due to *turbulence segregation*, into a high-velocity zone, called the *jet flow* and a low-velocity zone, called the *wake flow*. Within the turbulent motion, there are fast and slow fluid parts. The fast parts experience a larger Coriolis force than the slow ones and migrate to the pressure side in a blade channel. The slow parts assemble at the suction side. Splitting into high-energy and low-energy flow parts leads to an almost lossless jet flow, while the wake flow systematically accumulates flow losses. A segregated flow thus resembles a separated one. The jet flow is not subjected to diffusion, as the space made available by the widening of a blade channel is filled by the wake. This is once more analogous to a separated flow. The deflection from axial to radial direction within the inducer generates a centrifugal force, which causes segregation as well. The jet flow thus comes into the zone formed by the pressure side of a blade and the rotor disc. The wake flow sits in the corner formed by the suction side and the shroud. Within each zone, a velocity gradient due to Coriolis force, as sketched in Fig. 14.9, occurs. The consequence is that the outflow of the impeller is very inhomogeneous, which leads to a significant downstream mixing loss. The segregation phenomenon is less intense the more the impeller has backward sweep, since flow curvature compensates partly the effect of the Coriolis force. So, backward sweep reduces the irregularity of the flow leaving the impeller. The phenomenon

of migration within the turbulent motion is not fully understood yet. The concept of turbulence segregation, used here, is actually more a description than an explanation. For a more detailed discussion, but again without a full explanation, we refer Cumpsty [2], where a description is given in terms of stabilisation (tendency towards laminar flow) at the suction side and destabilisation (tendency to increased turbulence) at the pressure side.

14.5.2 *Mixing Zone*

Jet and wake flows mix at a short radial distance downstream of the rotor, due to strongly different velocity directions in the absolute frame, as sketched in Fig. 14.12. The collision of the two flow parts leads to a rather large mixing loss. The effect of the Coriolis force is at its strongest with radial end blades. Backward sweep generates a lift force opposing the Coriolis force. So, backward sweep softens the segregation, causing a decrease of the mixing loss. But, backward sweep decreases the rotor work. Thus, the rotor must run somewhat faster to compensate for that. Backward sweep also diminishes the number of blades required, resulting in less friction loss. The velocity magnitude at the diffuser entry decreases as well. Taking all these effects together, regarding efficiency, some backward sweep of the blades is advantageous. Therefore, impellers with radial end blades are used only very exceptionally, only when obtaining the maximum possible work is essential. Examples are compressors of light-weight gases, e.g. helium. Usually, a high work impeller has about $20\text{--}30^\circ$ backward sweep, as in Figs. 14.2 and 14.7. But also with small backward sweep, there is non-homogeneity of the outlet flow of the impeller. This means that some radial space without vanes is necessary for the mixing. Downstream of this space, a vaned diffuser may be mounted.

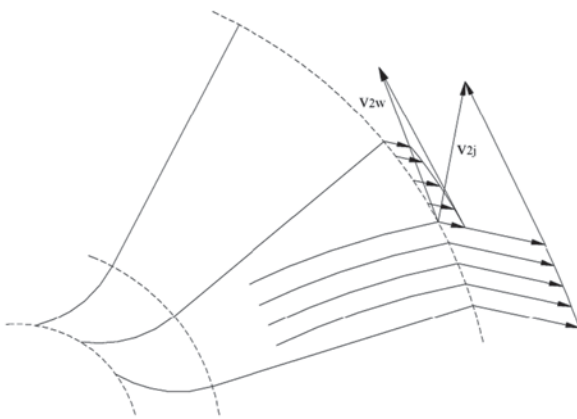


Fig. 14.12 Mixing of jet flow and wake flow downstream of the rotor

14.5.3 Vaneless Diffusers

Vaneless diffusers with parallel walls are applied in compressors with moderate rotor work. The diffuser inlet velocity is then subsonic. They are also applied as an entry part of a vaned diffuser in compressors with large rotor work. The outlet velocity of the impeller may then be supersonic. The vaneless space is then meant to mix the jet and wake flows and to decrease the Mach number level of the flow.

In a vaneless diffuser, streamlines are long due to the small flow angle with respect to the tangential direction. Long streamlines result in large friction loss and thick boundary layers. The streamline length increases when the flow rate decreases. As streamlines run rather tangentially and the pressure gradient is in the radial direction, boundary layers do not have much momentum in the pressure gradient direction. There is thus a strong tendency towards flow reversal in the radial direction within the boundary layers. At low flow rate, radial backflow occurs within the boundary layers. The backflow forms in cells rotating in the rotor running sense, analogous to rotating stall in a vane system. Choking can only occur if the radial velocity attains the speed of sound. This never happens in practice. No shock waves can occur and there is no incidence loss. All these features together cause a vaneless diffuser to be well suited when the velocity reduction downstream of the rotor is moderate. For strong deceleration, the necessary radial dimensions become big, which means big losses and strong risk for flow instability.

14.5.4 Vaned Diffusers

Mounting vanes aims at forcing the streamlines into a more radial direction than attained by a vaneless diffuser. With a large rotor work, the tangential velocity component at the impeller outlet is much bigger than the radial component (see Fig. 14.3). Therefore, reduction of the tangential velocity component becomes increasingly advantageous as the impeller work is larger. Figure 14.13 sketches the two common forms, called *cascade diffusers* and *channel diffusers*. The diffuser is normally followed by a collector scroll. Cascade diffusers are built with curved plates or profiled vanes. Cascade diffusers are not appropriate for very large pressure ratio.

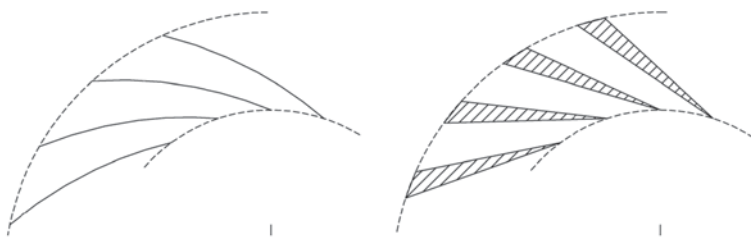


Fig. 14.13 Cascade diffuser (*left*) and channel diffuser (*right*)

The divergence angle of the channels formed by the vanes must be limited to about 10–12° in order to avoid separation. So, strong velocity reduction requires a large radius ratio, which makes channel diffusers more efficient. They mostly start from a square throat section, with an increasing width within the orthogonal plane and constant axial width. The blades are called vane islands or blades with blunt trailing edge. With a given divergence angle and radius ratio, these diffusers attain a higher velocity reduction, as the tangential velocity component decreases more strongly. The sudden widening at the outlet generates a dump diffusion loss. This dump loss is not very significant, as it only affects the radial velocity component. The cascade diffuser is the most efficient one with a weaker velocity reduction within the diffuser. The channel diffuser is better for a stronger velocity reduction. Some designs come in between, being cascade diffusers with blades with finite trailing edge thickness or curved channel diffusers. The pipe diffuser is a variant of the channel diffuser. Pipe diffusers feature a cylindrical throat and a conical divergent. They are seldom used, as their construction is more complicated and they feature no advantages compared to channel diffusers. Separation occurs under off-design conditions with reduced flow rate. The separation may be rotating or pulsating. Flow rate increase generates choking when the sonic speed is attained in the entrance region of a vane channel.

14.6 Performance Characteristics

14.6.1 Flow Instability

Reduced flow rate compared to the design flow rate, at constant rotational speed, may generate rotating stall within the inducer or within a vaned diffuser. Rotating flow reversal may occur within a vaneless diffuser. These phenomena generate losses, causing a decrease of the pressure ratio of the compressor, which generates a maximum in the characteristic for pressure ratio as a function of mass flow rate. There is also a maximum in the characteristic with radial end blades or with small backward sweep, without these phenomena. This implies that surge then may occur without rotating stall or rotating flow reversal (partial separation).

14.6.2 Choking

The choking conditions in rotor and stator are the same as with axial compressors. So, expressions (13.19) and (13.21) describe approximately the choking mass flow rates. The mass flow rate with choking in the rotor is (13.19):

$$\dot{m}_c = A_1 \rho_{01} c_{01} \left(\frac{2}{\gamma + 1} \right)^{\frac{1}{n-1} + \frac{1}{2}} \left(1 + \frac{\gamma - 1}{2} \frac{u_1^2}{c_{01}^2} \right)^{\frac{1}{n-1} + \frac{1}{2}}. \quad (14.12)$$

A_I is the through-flow area and n is the polytropic exponent. The inducer inlet is the most critical since the further the flow enters the impeller, the lower is the velocity w and the higher is the enthalpy h . By introducing an average value of the blade speed at the inlet, we obtain an approximation of the choking mass flow rate. The choking mass flow rate for a vaned diffuser (13.21) is

$$\dot{m}_c = A_2 \rho_{0I} c_{0I} \left(\frac{2}{\gamma + 1} \right)^{\frac{1}{n-1} + \frac{1}{2}} (1 + (\gamma - 1) \psi \frac{u_2^2}{c_{0I}^2})^{\frac{1}{n-1} + \frac{1}{2}}. \quad (14.13)$$

The choking flow rate depends on the rotational speed for both rotor and stator. Attaining $M=1$ occurs with radial end blades or slightly backswept blades rather at the diffuser inlet than at the inducer inlet, as conditions respectively are approximately $u_2 \approx \sqrt{\gamma R T_2}$ and $u_1 \approx \sqrt{\gamma R T_1}$. The velocity ratio is around $u_2/u_1 \approx 2$, but the temperature ratio is much less than 4. Attaining $M=1$ at the diffuser inlet does not necessarily imply choking, however. There is always a vaneless space, so that the Mach number at the inlet of the vaned part is significantly lower. Also, no choking can occur within a vaneless diffuser. If the flow at the impeller outlet is highly supersonic, which occurs with large pressure ratio ($r > 6$; $r = 4$ just being sonic), the flow at the vaned diffuser entry may be supersonic. A normal shock then forms within the semi-vaneless space upstream of the throat section of the diffuser, which makes the flow subsonic in the throat. When the flow rate increases compared to the design flow rate, the velocity within the throat increases and choking may occur. The flow at the inducer inlet is normally subsonic as the blade speed at the tip is typically lower than the velocity of sound and the same applies to w_{I1} . If the Mach number of w_I becomes sufficiently high, flow within the inducer becomes supercritical. A further increase of w_I may generate choking. But from the above analysis follows that the diffuser normally determines the choking in case of a vaned diffuser. It should also be emphasised that expressions (14.12) and (14.13) only render the choking mass flow rates very approximately.

14.6.3 Operating Characteristics and Operating Range

The term characteristic is mostly used without any further specification for the dependence of the pressure ratio on the mass flow rate at constant rotational speed. Figure 14.14 sketches the field of characteristics of a centrifugal compressor with a design pressure ratio 5. The shape of the characteristics is similar to that of an axial compressor, but with a lower efficiency.

The characteristic at a given rotational speed may be changed by adjustable inlet guide vanes or adjustable diffuser vanes (see Exercise 14.7.2). With adaptation to another operating point by adjustable vanes, the efficiency decreases. A change of rotational speed, as typically applied to pumps and fans, is a better procedure.

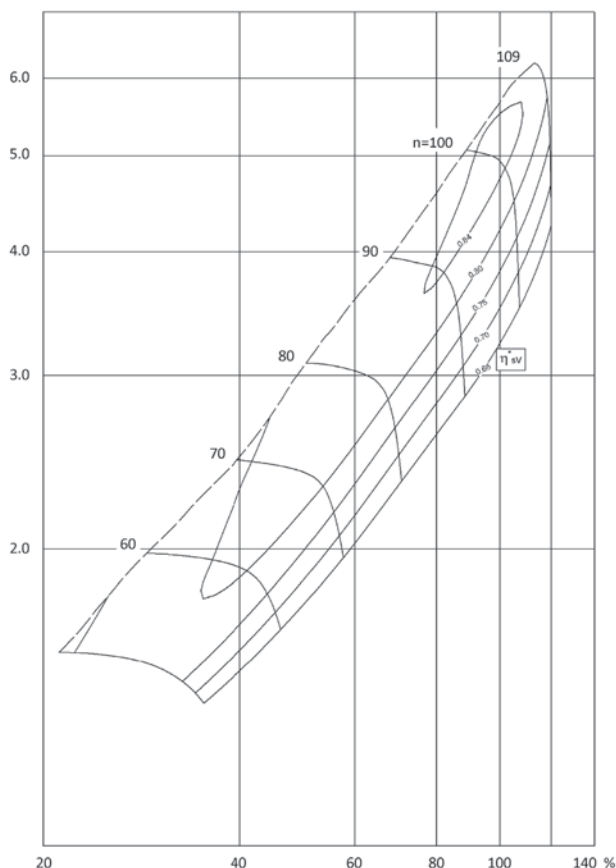
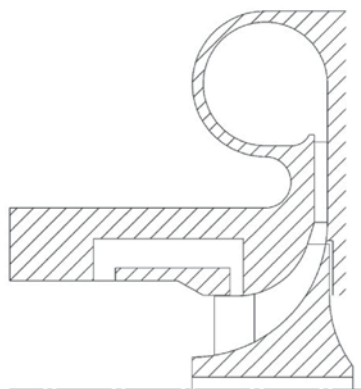


Fig. 14.14 Characteristics of a turbocharger centrifugal compressor with a large design stage pressure ratio (courtesy ABB Turbo Systems)

The operating range of a centrifugal compressor decreases as the pressure ratio in the design point is higher. With a rotor pressure ratio significantly above 4 in air, the design point may even be near to the choke limit (Fig. 14.14). A narrow operating range is practicable for a number of applications, for others it is not. A process compressor (Fig. 14.1) requires a large operating range. The blades are swept moderately backwards (blade angle -40°) and the rotor outlet Mach number is much lower than 1. A wide operating range is generally not necessary with air compressors, small turbo-shaft engines (typical for helicopters) and turbo-expanders. Small turbo-shaft engines may feature axial and radial compressors, but two radial stages as well. The pressure ratio of a radial stage may exceed 4, with a small operating range at the design point. This is acceptable, as the engine is seldom used at its maximum power. A turbo-expander is an expansion turbine combined with a compressor driven by the turbine, similar to a turbocharger. This type of machine is applied in process engineering. The gas cools down by expansion, allowing e.g. the separation of moisture.

Fig. 14.15 Casing treatment for enlarging the surge margin

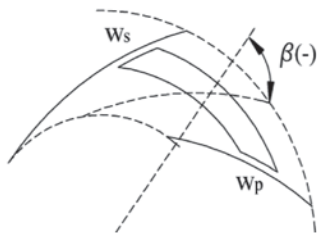


The dried gas gets compressed again. A large operating range is normally not required. The compressor of a diesel engine turbocharger requires a relatively large operating range. Therefore, up to a pressure ratio around 4, vaneless diffusers are used. Cascade diffusers are used with larger pressure ratio. The surge margin is often enlarged by a *casing treatment*, also called a *recirculation device*, as shown in Fig. 14.15. Similar devices are used with axial and mixed-flow compressors. It consists of two circumferential slots in the casing, one at the inducer mid region and one in the suction eye, connected with an annular chamber. The principle is that near stall, when the inducer is highly loaded, pressure difference drives flow from the inducer mid region to the inlet. The local mass flow rate at the leading edge of the inducer tip is enlarged this way, postponing stall in the inducer. When the compressor operates near choke, pressure difference drives flow into the inducer mid region. This increases the choking mass flow rate in case of a vaneless diffuser. With vaned diffusers, stall may also occur in the diffuser. Increase of the stall margin then requires vanes in the annular chamber creating a swirl component in opposite sense to the impeller rotation in the recirculating flow led to the rotor tip near stall. Rotor work is enlarged somewhat this way, causing an increase of the steepness of the characteristic near stall, which means a stabilising effect.

14.7 Exercises

14.7.1 Velocity Variation at Constant Radius in a Rotor

Derive the expression (14.6) for the velocity difference over a blade from a moment of momentum balance on a streamtube with infinitesimal radial length spanning a blade passage as sketched in the figure below.



A: The mass flow rate through the blade channel may be approximated by

$$\dot{m}_b = \rho \frac{2\pi r}{Z} w \cos \beta,$$

where ρ is an average value of the density and w is an average value of the relative velocity at the position of the infinitesimal streamtube and β is the local angle of the mean streamline with respect to the radial direction. The moment of momentum transferred to the mass flow in the infinitesimal streamtube is

$$M = \dot{m}_b \frac{d}{dr} (r v_u) dr,$$

with v_u averaged over the blade passage.

This is equal to the moment of the pressure force on the blades (neglecting a possible moment by friction forces):

$$M = (p_p - p_s) dr r,$$

where the subscripts p and s refer to pressure and suction sides. The Bernoulli equation on a streamline in a rotor is

$$d \frac{1}{2} u^2 = d \frac{1}{2} w^2 + \frac{1}{\rho} dp + dq_{irr}.$$

Therefore, on a constant radius, neglecting losses, and assuming that the integration constant of the Bernoulli equation is the same on all streamlines (which is satisfied for constant enthalpy and free vortex flow upstream of the rotor inlet; see Chap. 3, Sect. 3.3.2):

$$\frac{1}{2} (w_s^2 - w_p^2) = \frac{1}{\rho} (p_p - p_s),$$

where an average value of the density has to be used. From the last equation follows an approximation of the pressure difference over a blade:

$$p_p - p_s = \rho w (w_s - w_p).$$

Combination of the equations above results in

$$\rho w(w_s - w_p) r dr = \rho \Delta\theta r w \cos\beta [d(ru) + d(rw_u)],$$

with $\Delta\theta = \frac{2\pi}{Z}$ and $v_u = u + w_u$. From this follows (14.6).

14.7.2 Variable Geometry

Derive from the velocity triangles in Fig. 14.3 that adjustable inlet guide vanes allow adaptation to a lower flow rate with almost unchanged rotor work. Note that incidence occurs at the inlet of a vaned diffuser at a reduced flow rate, decreasing the efficiency. Observe that a radial compressor may be adapted to a lower flow rate with almost unchanged rotor work by turning diffuser vanes into a more tangential position (through-flow area is reduced). This generates incidence at the impeller inlet.

References

1. Balje OE (1981) Turbomachines: a guide to design, selection and theory. Wiley, New York. ISBN 0-471-06036-4
2. Cumpsty NA (1989) Compressor aerodynamics. Longman Scientific and Technical, London. ISBN 0-582-01364-X
3. Dixon SL, Hall CA (2014) Fluid mechanics and thermodynamics of turbomachinery, 7th edn. Elsevier, Amsterdam. ISBN 978-0-12-415954-9
4. Whitfield A, Baines NC (1990) Design of radial turbomachines. Longman Scientific and Technical, London. ISBN 0-582-49501-6

Chapter 15

Axial and Radial Turbines for Gases

Abstract Fundamentals of axial turbines were discussed in the chapter on steam turbines (Chap. 6). Design of turbine parts in gas turbines follows the same principles. When analysing the performance of axial turbines, we assumed, by way of a simplification, a given stator outlet angle ($\alpha_1 = 72^\circ$ and 75°). The analysis is generalised here and completed with a discussion of blade design and operating characteristics. The fundamental theory of radial turbines was treated in the chapter on hydraulic turbines (Chap. 9). The specific aspects for a compressible fluid are discussed in the present chapter. In particular, the rotor has an exducer part. Operating characteristics of radial turbines are derived. The chapter concludes with the non-dimensional form of the operating characteristics of turbomachines with a compressible fluid.

15.1 Axial Turbines

15.1.1 Kinematic Parameters

Figure 15.1 sketches the flow through a repeating stage of an axial turbine. As with the analysis of axial compressors, flow angles are measured with respect to the axial direction, positive in the rotation sense (α for stator, β for rotor). Constant axial velocity through the cascade is assumed. The fundamental relations are similar to these with compressors.

Work coefficient (or stage loading coefficient), flow coefficient and degree of reaction are

$$\psi = \frac{\Delta W}{u^2} = \frac{v_{1u} - v_{2u}}{u}, \quad \phi = \frac{v_a}{u}, \quad R = \frac{h_1 - h_2}{h_{01} - h_{02}} = -\frac{w_{mu}}{u}.$$

Thus:
$$\frac{w_{1u}}{u} - \frac{w_{2u}}{u} = \psi \quad \text{and} \quad -\frac{w_{1u}}{u} - \frac{w_{2u}}{u} = 2R.$$

From this follows

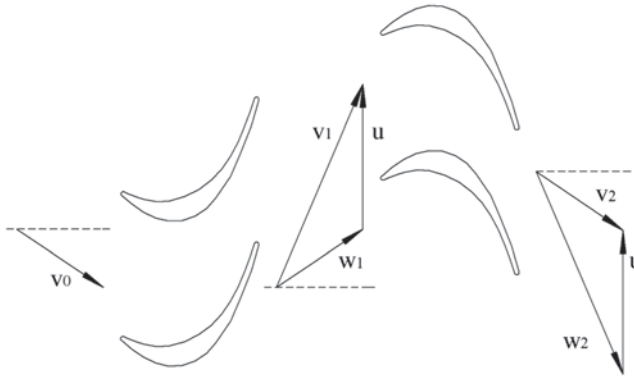


Fig. 15.1 Flow through a repeating axial turbine stage ($\psi = 1.8$, $\phi = 0.6$, $R = 0.5$)

$$\frac{w_{1u}}{u} = -R + \frac{\psi}{2}, \quad \frac{w_{2u}}{u} = -R - \frac{\psi}{2}, \quad \frac{v_{1u}}{u} = 1 - R + \frac{\psi}{2}, \quad \frac{v_{2u}}{u} = 1 - R - \frac{\psi}{2}. \quad (15.1)$$

Figure 15.2 sketches some examples of velocity triangles for $\phi = 2/3$. The conventions are as for axial turbines in Chap. 6. The vertical direction is the axial direction (x) with the through-flow from top to bottom. The running direction (y) is horizontal with the running sense from left to right and the radial direction (z) is perpendicular to the drawing, upward. The xyz frame is right-handed, but the machine is left-running. There is symmetry in the relations: replacing R by $1 - R$ causes a change of w_1 by $-v_2$ and w_2 by $-v_1$. For $\psi = 2(1 - R)$, the cascade inlet and outlet velocities lie in the meridional plane. For a larger value of ψ , there is outlet swirl in the contra-rotation sense ($v_{2u} < 0$). With a higher degree of reaction this already occurs with a moderately high work coefficient.

Figure 15.3 sketches an h - s diagram.

Using stage repetition, the total-to-total isentropic efficiency is

$$\eta_{tt} = \frac{\Delta W}{h_{00} - h_{02s}} = \frac{h_0 - h_2}{h_0 - h_{2ss}}. \quad (15.2)$$

Ignoring the divergence of the isobars, it follows

$$h_0 - h_{2ss} = h_0 - h_2 + (h_1 - h_{1s}) + (h_2 - h_{2s}) = \Delta W + \xi_s \frac{v_1^2}{2} + \xi_r \frac{w_2^2}{2},$$

so that
$$\eta_{tt} = \frac{\Delta W}{\Delta W + \xi_s \frac{v_1^2}{2} + \xi_r \frac{w_2^2}{2}}. \quad (15.3)$$

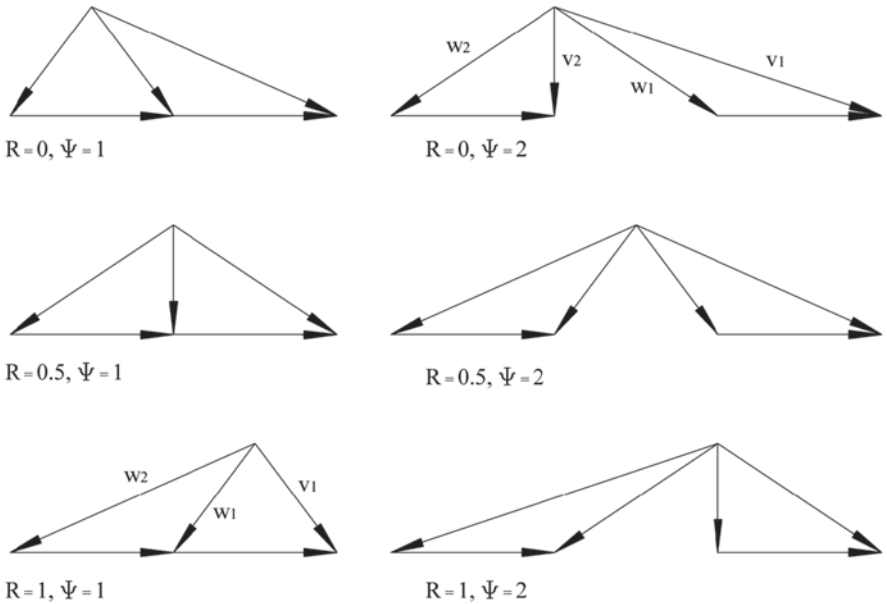
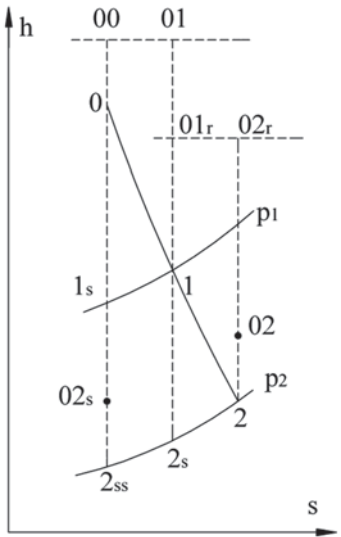


Fig. 15.2 Axial turbine velocity triangles with varying degree of reaction and work coefficient

Fig. 15.3 h-s diagram for an axial turbine



The coefficients ξ_s and ξ_r are the enthalpy loss coefficients of stator and rotor.

With (15.1), (15.3) results in

$$\eta_u = \frac{\psi}{\psi + 1/2\xi_s \left[\phi^2 + \left(1 - R + \frac{\psi}{2} \right)^2 \right] + 1/2\xi_r \left[\phi^2 + \left(R + \frac{\psi}{2} \right)^2 \right]}.$$

The optimum solidity of a blade row (ratio of chord c to spacing s) may be derived from Zweifel's tangential force coefficient (Chap. 2, Sect. 2.2.8), written here for a rotor:

$$C_{Fu} = \frac{|F_u|}{1/2\rho_2 w_2^2 c_a} = \frac{\rho_2 w_{2a} s |w_{lu} - w_{2u}|}{1/2\rho_2 w_2^2 c_a} = \frac{2|\Delta w_u| w_{2a}}{\sigma_a w_2^2}. \quad (15.4)$$

We recall that the tangential force coefficient of a turbine cascade is the equivalent of the lift coefficient of a wing profile and that the optimum value of the coefficient is quite universally around unity. $|F_u|$ is the magnitude of the blade force in the tangential direction per unit of span. The term $\frac{1}{2}\rho_2 w_2^2$ is the incompressible lossless value of $p_{0Ir} - p_2$, which is the difference between the total pressure at inlet and the static pressure at outlet. c_a is the axial chord and σ_a the axial solidity. The Zweifel coefficient is almost universally used in its incompressible lossless form. The reason is the observation that optimum solidity does not depend greatly on the Mach number of the outlet flow.

Loss coefficients may be determined by Soderberg's correlation (Chap. 6, Sect. 6.4.5), representing the losses in an accelerating cascade with optimal solidity (Zweifel tangential force coefficient near to unity) as a fraction of the outlet kinetic energy, with

$$\xi = \xi_1 + \xi_2 \quad \text{with} \quad \xi_1 = 0.025 \left(1 + \left(\frac{\delta^0}{90} \right)^2 \right) \quad \text{and} \quad \xi_2 = 3.2 \left(\frac{c_a}{h} \right) \xi_1. \quad (15.5)$$

Here, δ^0 represents the flow turning within the cascade in degrees. The coefficient ξ_1 determines friction losses on the blades, with factor 0.025 for a Reynolds number based upon the hydraulic diameter and the outlet velocity equal to 10^5 . With a lower Reynolds number, the factor is somewhat higher. Coefficient ξ_2 determines the losses in the end wall boundary layers and the losses by secondary flows. Henceforth we will take aspect ratio, which is the ratio of the blade height h to the axial chord c_a , equal to 4 as an example. Soderberg's loss formulae are intended for subsonic flow. If need be, losses for shock waves have to be added. The loss formulae do not encompass clearance losses and losses by film cooling either. At the other hand, the formulae overestimate somewhat the blade friction losses and secondary losses for modern blade rows. So, we write

$$\xi = 0.045 \left(1 + \left(\frac{\delta^\circ}{90} \right)^2 \right) \text{ with } \delta = \Delta\alpha = \alpha_1 - \alpha_2 \text{ or } \delta = \Delta\beta = \beta_1 - \beta_2.$$

Angles follow from (15.1) with

$$\operatorname{tg} \alpha_1 = \frac{v_{1u}}{v_a}, \quad \operatorname{tg} \alpha_2 = \frac{v_{2u}}{v_a}, \quad \operatorname{tg} \beta_1 = \frac{w_{1u}}{v_a}, \quad \operatorname{tg} \beta_2 = \frac{w_{2u}}{v_a}.$$

Figure 15.4 renders efficiency contour lines for $R=0, 0.25, 0.5$ and 0.75 . The strongly rising dashed straight lines represent $\alpha_1 = 70^\circ$ and $\alpha_1 = 60^\circ$. The other dashed straight lines represent $\alpha_2 = 0$ and $\alpha_2 = \pm 30^\circ$. The efficiency contours for $R=0.25$ and $R=0.75$ are identical. We find, in accordance with the results in Chap. 6, that the efficiency is maximum for $R=0.50$. The corresponding work and

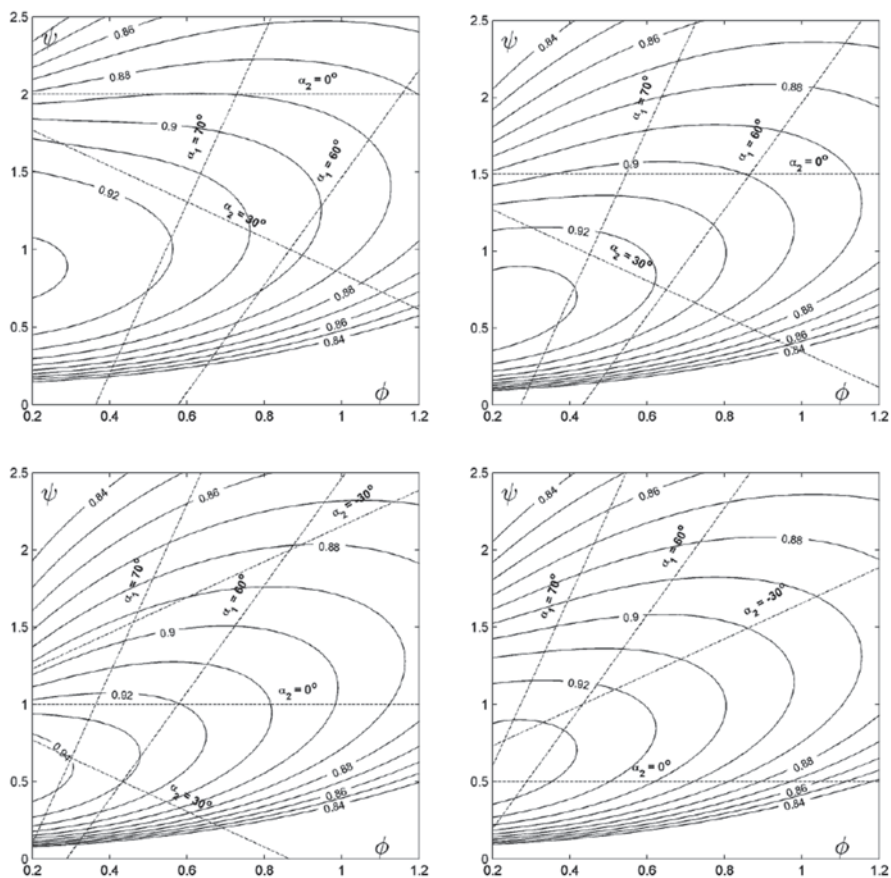


Fig. 15.4 Efficiency dependent on work coefficient and flow coefficient: *top left:* $R=0$; *top right:* $R=0.25$; *bottom left:* $R=0.50$; *bottom right:* $R=0.75$

Table 15.1 Maximum total-to-total efficiency as a function of degree of reaction R for chosen values of work coefficient ψ

	$R=0$	$R=0.25$	$R=0.50$	$R=0.75$
$\psi=1.0$	0.921	0.923	0.922	0.923
$\psi=1.5$	0.909	0.903	0.900	0.903
$\psi=2.0$	0.890	0.883	0.882	0.883
$\psi=2.5$	0.869	0.865	0.864	0.865

flow coefficients are small however: $\psi \approx 0.60$, $\phi \approx 0.30$. For larger values of ψ and ϕ , efficiency is almost independent of the degree of reaction. This insensitivity is illustrated in Table 15.1, with the maximum efficiencies derived from Fig. 15.4 for chosen values of the stage loading ψ , but where α_t is not allowed to exceed 70° . The results in Table 15.1 show that efficiency is almost independent of the degree of reaction and that it decreases with increasing stage loading.

With gas turbines, a high work coefficient in the turbine part is always aimed at. This certainly applies to aero-engines, where limitation of weight is crucial. But it applies to power gas turbines as well. The number of stages in the turbine part is always taken as low as possible, limiting in this way the total blade surface and thus the necessary amount of cooling air. The low sensitivity of the efficiency to the degree of reaction for higher values of ψ and ϕ allows the representation of efficiency as a function of ψ and ϕ only. Manufacturers use such a diagram composed from turbine data that are publically available and from their own data. This type of diagram is mostly called a Smith chart, after S.F. Smith, who composed this type of diagram for the first time in 1965 [4, 5, 6]. The optimum value of ϕ as a function of ψ for degrees of reaction between 25 and 75 %, according to Fig. 15.4, is approximately given by a straight line through the couples ($\phi=0.3$; $\psi=1$) and ($\phi=1$; $\psi=2.4$). In reality, the larger values of ϕ are taken somewhat lower due to Mach number effects.

It is not possible to derive practical values of ψ and ϕ from efficiency considerations alone. With gas turbines, values of ψ and ϕ are much higher than for optimum efficiency. The most extreme values, which are $\psi \approx 2.20$ together with $\phi \approx 0.9$ on the mean radius, are applied in the LP turbine part of aero-engines. The objective is then weight limitation. In HP and IP turbine parts of an aero-engine and in power gas turbines, $\psi \approx 1.5$ – 2.0 together with $\phi \approx 0.5$ – 0.6 . In aero-engines, HP and IP blades are rather short and the mean blade speed is very high, up to 450 m/s. Blades may be shrouded or unshrouded (Rolls-Royce practise is shrouded blades; e.g. Trent 800, Fig. 12.14). With $\psi=1.80$ and $u=450$ m/s on the mean radius, the stage work is about 350 kJ/kg. In power gas turbines, the blade height is much larger and the mean blade speed is lower, typically around 350 m/s. Blades are not shrouded in cooled stages and shrouded in non-cooled stages (e.g. SGT6-5000F, Fig. 11.6). With $\psi=1.80$ and $u=350$ m/s on the mean radius, the stage work is about 220 kJ/kg.

The degree of reaction follows from efficiency optimisation for chosen values of ψ and ϕ . The optimum is strongly influenced by clearance losses, not taken into account in Soderberg's correlation. With a degree of reaction lower than 50%,

the pressure drop over the stator is larger than over the rotor. There is only little leakage over a stator. At the hub side, vanes are shrouded and there is a sealing (typically a labyrinth sealing) between the vane shroud and the hub. Leakage loss encompasses two parts. The first is overflow from the pressure to the suction side of a blade or vane. This component depends on the pressure difference between the pressure and the suction sides, which does not specifically depend on the degree of reaction. This component does not exist when a shroud is applied. It is often reduced with an unshrouded blade by a *tip treatment* (a partial form of shroud). The second component originates from the through-flow, so from the pressure drop in the axial direction. The axial component is strongly reduced, but does not disappear completely, with shrouded blades. This component decreases considerably with unshrouded blades by lowering the degree of reaction. Note that also with shrouded blades, leakage losses decrease somewhat with a degree of reaction lower than 50 %, because the radius at which leakage occurs is lower with a stator than with a rotor [8]. With shrouded blades, the optimal degree of reaction on the mean radius is close to 50 %, but somewhat smaller, typically 0.40–0.45. For a stage with long unshrouded rotor blades, a degree of reaction much lower than 50 % on the mean radius is optimal.

Combining all considerations, the conclusion is that there is no universal optimum of the kinematic parameters at the mean radius of a turbine stage in a gas turbine. Turbine optimisation is delicate, with a big role of three-dimensional effects. The topic is far above the possibilities of the present book. The above analysis only allows demonstration of tendencies, but not derivation of precise results. It should also be noticed that stages in a real turbine are not always repeating stages. At the outlet of a first stage, negative post-swirl may be given, enlarging the stage work (an example is Fig. 11.5; even more post-swirl may be chosen). We keep in mind that the work coefficient is always very large. Referring to Figs. 15.2 and 15.4, this means that there is typically strong negative post-swirl at the outlet of a stage (Fig. 15.1). At the outlet of a turbine part, sometimes outlet guide vanes are required for turning the flow into the meridional direction. For a recent design example of the LP part of an aero-engine, we refer to [2].

15.1.2 Radial Variation of Flow Parameters

The equation for simple radial equilibrium (Eq. 13.15) reads:

$$\frac{v_u^2}{r} + \frac{d}{dr} \left(\frac{1}{2} v_a^2 + \frac{1}{2} v_u^2 \right) = 0 \quad \text{or} \quad \frac{v_u}{r} \frac{d}{dr} (r v_u) + \frac{d}{dr} \left(\frac{1}{2} v_a^2 \right) = 0. \quad (15.6)$$

The equation is satisfied for $r v_u = cst$ together with $v_a = cst$. For axial outlet flow is $v_{2u} = 0$. Then follows $v_{2a} = \text{constant}$. For constant work distribution over the radius, $\Delta W = u v_{1u}$, the equation is also satisfied for $r v_{1u} = cst$ together with $v_{1a} = cst$. The blade form is then called a free vortex blade. The disadvantage with a great radius change is a rather strong variation of the stator outlet angle α_l from a higher

value at the hub to a lower value at the casing. This rather strong variation cannot be matched with the weak variation on the maximum efficiency line in the Smith chart: Fig. 15.4. In using this figure, one has to take into account that high values of ψ and ϕ occur at the hub, so where the degree of reaction is the lowest, and low values at the casing, so where the degree of reaction is the highest. Examples are $\psi=2.4$ and $\phi=1$ at $R=0.25$ and $\psi=1$ and $\phi=0.3$ at $R=0.75$. These sets do not go together with free vortex blades. But the radial equilibrium equation can be satisfied in other ways, e.g. for constant stator outlet angle.

With $tg\alpha_I = v_{Iu} / v_{Ia} = \text{constant}$, (15.6) becomes for the stator outlet:

$$\frac{v_{Ia}^2}{r} tg^2 \alpha_I = -\frac{d}{dr} \left(\frac{1}{2} v_{Ia}^2 (1 + tg^2 \alpha_I) \right) \quad \text{or} \quad \frac{v_{Ia}}{r} \sin^2 \alpha_I = -\frac{d}{dr} v_{Ia}.$$

The equation is satisfied for $v_{Ia} = Cr^{-\sin^2 \alpha_I}$.

The axial velocity v_{Ia} is then higher at the hub and lower at the casing.

With a very high radius ratio, as with the final stage of the LP part of a steam turbine, the stator outlet velocity variation is in between the results for free vortex flow and constant stator angle, but close to this last one (Exercise 6.10.5 in Chap. 6 shows that the efficiency is close to optimum on every radius for $\alpha_I = \text{ct.}$). With gas turbine stages with high radius ratio, a similar distribution is chosen.

15.1.3 Blade Profiles

The general flow in turbines is accelerating. This facilitates the blade profile design compared to that of a compressor. Compressor blade profiles are strongly determined by the limitation of the loading due to the strong adverse pressure gradient in the rear part of the suction side. Turbines allow, due to the generally accelerating flow, much higher loading (work coefficient around 1.80 compared to 0.4 for compressors). This results in much higher flow turnings with turbines.

Subsonic and Supercritical Cascades

Subsonic and supersonic rotor cascades occur within the low pressure turbine (LP) part of a high bypass ratio turbofan engine, as direct fan drive results in low running speed in the LP turbine. Within the high pressure (HP) part, blade speed is higher and rather determined by strength limitations, resulting in transonic cascades as a rule. Subsonic or supersonic rotor cascades mostly also occur in the high-pressure and the intermediate-pressure parts of steam turbines. Steam turbine blades are manufactured of cheaper materials (steel alloys), which results in lower blade speeds.

Figure 15.5, left, sketches the optimum Mach number distribution on a subsonic rotor cascade. The right-hand part of the figure sketches the corresponding momentum loss thickness distribution [1].

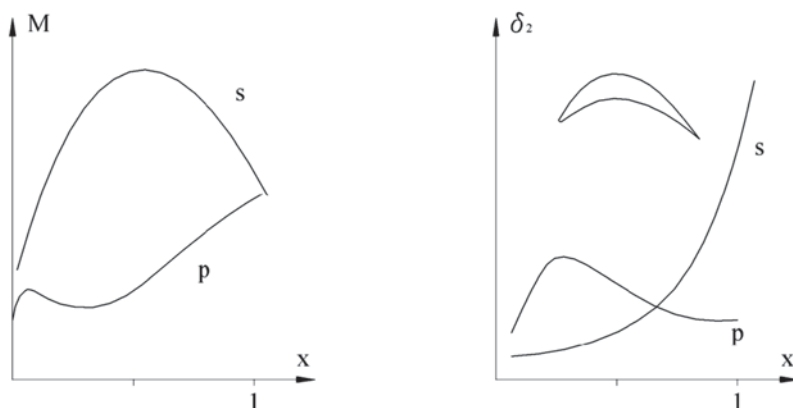


Fig. 15.5 Mach number and momentum loss thickness distribution with a subsonic turbine rotor cascade

Optimisation, in principle, means minimisation of the sum of the momentum loss thicknesses, relative to the blade distance perpendicular to the outlet flow. This implies that the spacing should be as great as possible, just avoiding separation at the suction side. For the basic aspects concerning separation and transition, we refer to Sect. 13.4.1. The pressure side features a strong acceleration immediately downstream the stagnation point. This reduces the loading capacity of the profile, but is unavoidable if the profile should have a certain thickness. After the initial acceleration, a weak deceleration is built in, in order to increase the loading capacity. This may continue onto nearly laminar separation. Then, acceleration follows towards the trailing edge, sufficiently strong for keeping the boundary layer laminar. The objective is to keep the boundary layer laminar on the whole pressure side. Friction is then minimal. The boundary layer thickness at the pressure side decreases during the last phase. Strong acceleration first occurs at the suction side. This acceleration continues over a long distance, becomes then weaker and is followed by a deceleration. The objective of the strong acceleration phase is keeping the boundary layer laminar over the longest possible distance. Friction is then minimal. The boundary layer becomes transitional when acceleration decreases. In order to withstand the following deceleration, the weak acceleration phase must be such that the boundary layer becomes turbulent before the velocity maximum. If not, the deceleration could generate laminar separation. The turbulent boundary layer grows strongly in the deceleration phase.

Optimisation of the turbine blade is strongly determined by the suction side laminar-turbulent transition position. Control of this position is difficult in the LP turbine part of an aero-engine, due to the low Reynolds number. Gas temperature is high, generating a high dynamic viscosity. Moreover, the pressure within an LP turbine is low in cruise conditions, generating a low density. Both effects result in a high kinematic viscosity. Dependent on the engine dimension, Reynolds numbers may be as low as 250 000–50 000 [1]. For the lower Reynolds numbers, laminar separation at the suction side is unavoidable. Care has to be taken then that transition occurs

within the separated boundary layer with turbulent reattachment and formation of a separation bubble. Driving the laminar separated boundary layer into turbulence is often realised by appropriate impact of passing wake zones of an upstream blade row (relative motion between stator and rotor). Tuning the impact is difficult. So, optimising a turbine cascade is mainly a matter of boundary layer control. Optimum profiles are therefore termed *controlled boundary layer* (CBL) profiles.

Within a turbine, the turbulence level in the core flow is very high. The degree of turbulence, i.e. the magnitude of the fluctuating velocity compared to the average velocity, typically exceeds 5%. Transition in an attached boundary layer is then directly induced by fluctuations of the main flow, without necessity for instability of the boundary layer flow, as with a very quiet main flow (natural transition by Tollmien-Schlichting waves). Transition is then termed *bypass transition*, meaning that the instability is bypassed (see discussion in Sect. 13.4.1). With impact of a wake zone of a preceding blade, transition is very quick in an attached boundary layer due to the kinematic impact together with a high turbulence level within the wake. The boundary layer may become laminar again after the wake has passed. With wake impact onto a separated boundary layer, the separated shear layer quickly becomes turbulent due to instability (Kelvin-Helmholtz instability), strongly increasing the potential for reattachment. With a low Reynolds number, the momentum loss thickness at the end of the suction side is mainly determined by the size of the separation bubble. It is then favourable to choose a profile shape with the velocity peak rather far forward and a high wake impact frequency. The separation bubble decreases by that. The turbulent part of the boundary layer increases, causing friction loss increase in that part, but this increase does not counterbalance the strong decrease of the mixing loss behind the separation bubble. With a higher Reynolds number the bubble size is already small spontaneously. It is then favourable that the velocity peak lies rather far backward and that the frequency of the wake impact is lower. So the optimum profile shape depends strongly on the Reynolds number [3].

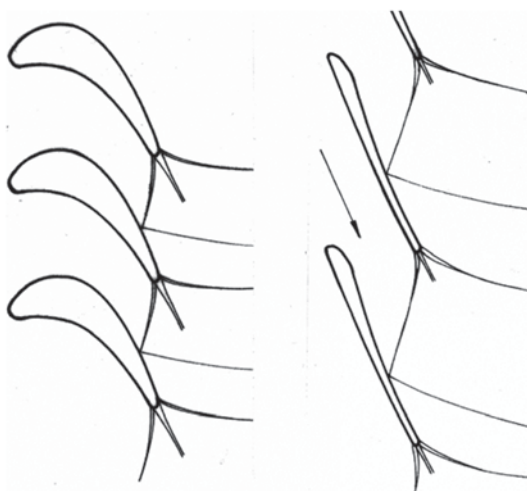
Adaptation to supersonic conditions is done the same way as with an aerofoil. The Mach number distribution of Fig. 15.5 does not change essentially. The flow becomes locally supersonic at the suction side and the supersonic zone ends with a normal shock. The suction side shape must be such that the Mach number just upstream of the normal shock is as low as possible.

Optimisation of a stator cascade does not principally differ from that of a rotor cascade, but the general acceleration with a stator cascade is larger for a low degree of reaction of the stage. With a limitation on the maximum Mach number at the suction side, the decelerating zone in Fig. 15.5, left, becomes weaker. This is beneficial for the loss coefficient, but the level of outlet kinetic energy is higher.

Transonic Cascades

A transonic cascade means subsonic inlet and supersonic outlet. These cascades occur in both rotors and stators. Figure 15.6, left, sketches the shock waves within a

Fig. 15.6 Shock patterns with transonic rotor turbine cascades; *left*: high flow turning; *right*: rotor tip section of the last stage of a steam turbine



rotor cascade with high flow turning. Such cascades feature oblique shock patterns starting from the trailing edge. One of the shocks impacts on the suction side of the adjacent blade. The boundary layer should not separate under the impact. Therefore, the suction side is designed such that the boundary layer is turbulent at the impact zone. Figure 15.6, right, sketches the shock waves at the tip section of a rotor blade of the last stage of an LP part of a steam turbine.

Supersonic Cascades

Supersonic cascades only occur in impulse turbines. These cascades are designed with a free vortex flow in the blade passage. Transition segments at inlet edge and outlet edge generate appropriate accelerations and decelerations (see Sect. 6.4.4 in Chap. 6).

15.1.4 Three-dimensional Blade Design

High flow turnings with turbines have as consequence that secondary flows may be significant for low aspect ratio vanes and blades, although the boundary layers with turbines are thinner than with compressors. Lowering the losses in end wall regions of low aspect ratio stages is mainly achieved by bowing the stator vanes. The effect of bowing is the same as discussed for compressors in Sect. 13.3.6. The possible benefit from bowing is in the order of two percentage points in adiabatic efficiency. Combined sweep and lean of high aspect ratio stator vanes is typically used to generate radial forces for limiting the variation of the degree of reaction in the LP turbine part of an aero-gas turbine, similarly as in the LP part of steam

turbines (Chap. 6, Sect. 6.9.2). Observe the combined sweep and lean of some stator vanes at the casing in the LP turbine part in Fig. 12.9 (Trent 800). Sweep is also visible in Fig. 12.14.

15.1.5 Vane and Blade Clocking

Clocking is setting the relative position of two subsequent stators (or rotors) with an equal number of blades. Maximum efficiency is obtained when wake segments of the upstream row impinge the leading edge of the downstream row. The efficiency is lowest when the wake segments follow a path midway the downstream blades as then wake mixing is the strongest and so is the mixing loss. The principle is also used with axial compressors. A subtle difference is that with turbines it is mostly advantageous to shift the impacting wake somewhat to the suction side. This helps in promoting transition in the suction side boundary layer. The possible adiabatic efficiency improvement with clocking is in the order of 0.5 percentage points, similarly with turbines and compressors.

15.1.6 Operating Characteristic of Axial Turbines

In order to express that the outlet angles of the vanes and the blades α_1 and β_2 are approximately constant with varying flow rate, we note

$$\psi = \frac{v_{1u} - v_{2u}}{u} = \frac{v_{1u} - u - w_{2u}}{u},$$

with
$$tg\alpha_1 = \frac{v_{1u}}{v_a} \quad \text{and} \quad tg\beta_2 = \frac{w_{2u}}{v_a}.$$

Thus :
$$\psi = \phi(tg\alpha_1 - tg\beta_2) - 1. \quad (15.7)$$

The angle α_1 is about 60° to 70° and the angle β_2 about -60° to -70° . So, the term $tg\alpha_1 - tg\beta_2$ is always strongly positive with an order of magnitude 5. Increasing flow rate increases the stage work. In practice, this implies that the flow rate increases with increasing pressure ratio over the turbine (p_{01}/p_{02}), with a zero flow rate for pressure ratio 1. The relation (15.7) further implies that with increased rotational speed, the pressure ratio increases more than the flow rate (work $\sim u^2$, flow rate $\sim u$). Thus, for a higher rotational speed, the characteristic curve of mass flow rate as a function of pressure ratio lies under that for a lower rotational speed (see Fig. 15.7, below).

Choking may occur with increasing pressure ratio.

Within the stator: $h_{01} = h_1 + 1/2 v_1^2$. $v_1 = c_1$ is reached for $v_1^2 = c_1^2 = (\gamma - 1)h_1$.

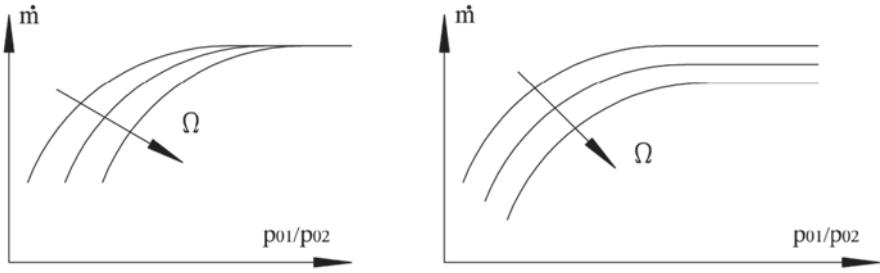


Fig. 15.7 Mass flow rate of an axial turbine as a function of pressure ratio; *left*: choking in stator; *right*: choking in rotor

Thus is then

$$h_{0l} = \frac{\gamma + 1}{2} h_l.$$

The corresponding pressure ratio and mass flow rate are

$$\frac{p_l}{p_{0l}} = \left(\frac{h_l}{h_{0l}} \right)^{\frac{n}{n-1}} = \left(\frac{2}{\gamma + 1} \right)^{\frac{n}{n-1}}, \quad (15.8)$$

$$\dot{m}_c = A_l \rho c = A_l \rho_{0l} c_{0l} \left(\frac{h_l}{h_{0l}} \right)^{\frac{1}{n-1} + \frac{1}{2}}, \quad (15.9)$$

where n is the polytropic exponent and A_l the stator blade passage area. With $\gamma = 1.33$ and $n = 1.30$ it follows that $p_l / p_{0l} \approx 0.5$. The corresponding choking pressure ratio p_{0l} / p_{02} over the entire turbine is slightly above 2 with a low degree of reaction. At 50 % degree of reaction, it is about $(1 / 0.5)^2 = 4$.

Within the rotor :

$$h_{0l} - h_{02} = u_l v_{lu} - u_2 v_{2u},$$

or

$$h_{0l} - u_l v_{lu} = h_2 + 1/2 v_2^2 - u_2 v_{2u}.$$

For the outlet velocity triangle:

$$w_2^2 = u_2^2 + v_2^2 - 2u_2 v_{2u}.$$

Thus :

$$h_{0l} - u_l v_{lu} = h_2 + 1/2 w_2^2 - 1/2 u_2^2.$$

This expression is noted more generally ($u_l \neq u_2$) than needed for an axial turbine, as we further perform a similar analysis for a radial turbine with use of the result found here.

A sonic state is achieved for $w_2^2 = (\gamma - 1)h_2$.

So
$$h_{01} - u_1 v_{1u} = \frac{\gamma + 1}{2} h_2 - \frac{1}{2} u_2^2,$$

and
$$\frac{h_2}{h_{01}} = \frac{2}{\gamma + 1} \left(1 - \frac{u_1 v_{1u} - \frac{1}{2} u_2^2}{h_{01}} \right).$$

The term $u_1 v_{1u} - \frac{1}{2} u_2^2$ is positive for sufficiently large ψ . Pressure ratio and mass flow rate with choking are

$$\left(\frac{p_2}{p_{01}} \right) = \left(\frac{h_2}{h_{01}} \right)^{\frac{n}{n-1}} = \left(\frac{2}{\gamma + 1} \right)^{\frac{n}{n-1}} \left(1 - \frac{u_1 v_{1u} - \frac{1}{2} u_2^2}{h_{01}} \right)^{\frac{n}{n-1}}, \quad (15.10)$$

$$\dot{m}_c = A_2 \rho c = A_2 \rho_{01} c_{01} \left(\frac{h_2}{h_{01}} \right)^{\frac{1}{n-1} + \frac{1}{2}}. \quad (15.11)$$

With choking in the rotor, pressure ratio and mass flow rate thus depend on rotational speed.

With a low degree of reaction, the overall pressure ratio over the turbine corresponding to (15.10) exceeds the one corresponding to (15.8). The stator then determines choking. This is also clear from the higher amplitude of v_1 with respect to w_2 for a low degree of reaction in Fig. 15.2. The choking mass flow rate is then independent of rotational speed and the choking pressure ratio is slightly above 2. With a high degree of reaction, choking in the rotor is more critical than in the stator (see also Fig. 15.2). The corresponding pressure ratio p_{01}/p_{02} may then exceed 2, but not very much, as the term $u_1 v_{1u} - \frac{1}{2} u_2^2$ is rather small compared to h_{01} . So, the choking total pressure ratio is again slightly above 2 (say 2.5). The rotational speed dependence following from (15.10) and (15.11) implies that with a higher rotational speed, the choking pressure ratio increases somewhat, with a decrease of the corresponding mass flow rate. Characteristics thus look as sketched in Fig. 15.7. In reality, curves may lie very close together, since the term $u_1 v_{1u} - \frac{1}{2} u_2^2$ is typically small compared to h_{01} .

We note that a total pressure ratio of 2 is not very high for an axial turbine.

$$\left(\frac{p_{01}}{p_{02}} \right) = \left(\frac{T_{01}}{T_{02}} \right)^{\frac{n}{n-1}}.$$

E.g. with $\Delta W = 220$ kJ/kg is $\Delta T = T_{01} - T_{02} \approx 200$ K. With $n = 1.30$, $T_{01} = 1500$ K, follows $p_{01}/p_{02} = 1.86$. With $T_{01} = 1000$ K, follows $p_{01}/p_{02} = 2.63$. Thus, turbines with a high stage work often operate with choking. Normally, this is no drawback. The flow rate is then proportional to the inlet density, and thus, at a given inlet temperature, proportional to the inlet pressure. Usually, this is a perfectly practicable characteristic.

15.2 Radial Turbines

15.2.1 Shape and Functioning

Figure 15.8 shows the rotor of a small gas turbine with a centrifugal compressor (at the right side) mounted back to back with a radial turbine (at the left side). The compressor rotor has splitter blades and the blades are about 30° swept back at the periphery. The turbine rotor has a lower number of blades (12 in the example) and the blades are purely radial at the inflow. Figure 15.9 sketches the meridional section and an orthogonal view of a radial or centripetal turbine for gas expansion. The gas is typically supplied from a volute followed by a stator vane ring. As with an axial turbine, the flow leaves the stator vanes quite near to the tangential direction. The curvature of the vanes is very low. The flow leaving the volute is already near

Fig. 15.8 Rotor of a small gas turbine with radial compressor (*right*) and radial turbine (*left*). (courtesy Dresser-Rand)

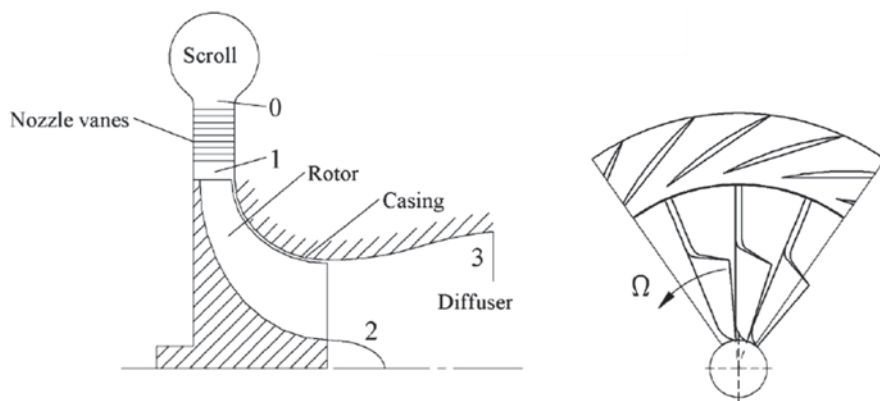
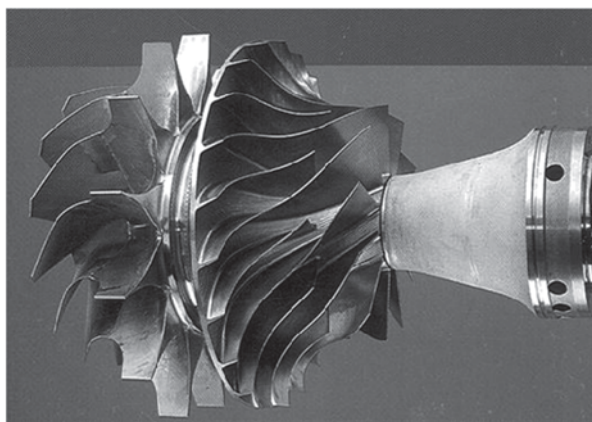


Fig. 15.9 Radial turbine components

to the tangential direction. As the figure demonstrates, stator vanes normally direct the flow somewhat more into the radial direction. From this also emerges that radial turbines may be built without a stator vane ring. The rotor blades are purely radial at the inlet. The gas is deflected into the axial direction in the meridional plane. At the outlet, the gas has a significant tangential component in the relative frame. The diffuser downstream of the rotor recovers pressure from the kinetic energy at outlet and so decreases the pressure at the rotor outlet.

The principal functioning of a centripetal turbine for gas expansion does not differ much from a hydraulic turbine of Francis type. Some parameters differ, however. The biggest difference is the rotor shape. The rotor is open and its outlet lies in an orthogonal plane. There is an *exducer* part, analogous to the inducer part of a radial compressor. An expansion turbine is normally designed for maximum rotor work. This is commonly achieved by a high blade speed, typically around 400 m/s at the rotor periphery. This requires an open rotor with purely radial blade form at the rotor entry and an exducer part formed by radial filaments. As a consequence of the expansion, the outlet area must be larger than the inlet area. A centripetal gas expansion turbine features thus a rather high ratio of outlet diameter to inlet diameter, typically around 0.7 (see below). Figure 15.10 shows the velocity triangle at the rotor inlet and rotor outlet (tip of the blades) and a sketch of the inlet flow. The relative vortex in the blade channels deflects the relative velocity w_1 from the radial direction, generating a phenomenon analogous to the slip at the outlet of a centrifugal rotor. The tangential component of the absolute inlet velocity may be expressed with a slip factor as $v_{1u} = \sigma u_1$. The slip factor can be determined by the same formulae as with compressors.

In order to prevent separation, the number of blades of a centripetal rotor has to be similar to that of a centrifugal rotor. As Fig. 15.10 demonstrates, the pressure difference over the blades is mainly generated by Coriolis force. The flow curvature generates a centrifugal force or lift, opposite to the Coriolis force, but this force is weak. With an exactly radial inlet, about 20 blades are required to avoid separation. This may be determined in the same way as with centrifugal rotors. Adapting (14.11) to turbine inflow, the condition for prevention of flow reversal is

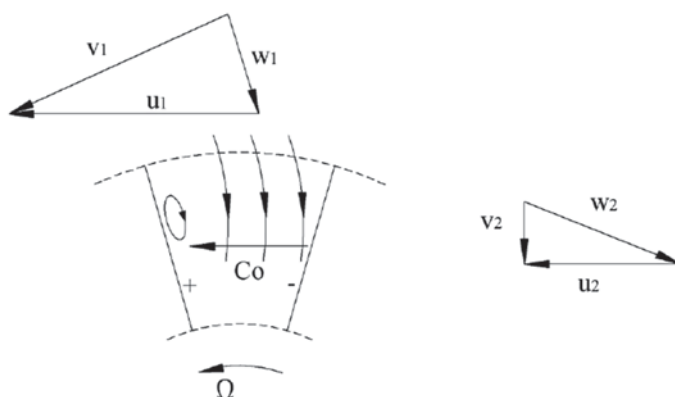


Fig. 15.10 Flow at rotor inlet and rotor outlet of a radial turbine

$$w_I > \frac{2\pi}{Z} u_I.$$

Approximately,

$$\operatorname{tg} \alpha_I = \frac{\sigma u_I}{w_I}, \quad \text{so that} \quad \frac{\sigma u_I}{\operatorname{tg} \alpha_I} > \frac{2\pi}{Z} u_I \quad \text{or} \quad Z > \frac{2\pi \operatorname{tg} \alpha_I}{\sigma}.$$

With $\alpha_I \approx 70^\circ$ and $\sigma \approx 0.8$ – 0.9 it follows that $Z \approx 20$.

The difference with a centrifugal rotor is that a separation bubble at the inlet of a centripetal rotor is acceptable, because the flow reattaches deeper in the rotor, as is clear from Fig. 15.10. Typically, far fewer blades are mounted than needed to prevent separation: $Z \approx 12$. This results in smaller blade surface and, as a consequence, less friction. The axial rotor part, the exducer, thus may have the same number of blades as the radial part. In other words, splitter blades are not necessary. The consequence of a lower number of blades is a slip factor lower than typical with a centrifugal rotor: $\sigma \approx 0.8$.

Figure 15.10 shows a velocity triangle at the rotor outlet. Kinetic energy supplied to the diffuser can only be recovered partially, i.e. to about 50%. The outlet thus should be exactly axial and the value of the outlet velocity v_2 as low as possible. So the outlet angle β_2 has to be large, typically around -60 to -70° at the tip.

15.2.2 Kinematic Parameters

Total enthalpy is constant in the volute and the nozzles:

$$h_{00} = h_I + \frac{1}{2} v_I^2.$$

Rothalpy is constant within the rotor:

$$I = h + \frac{1}{2} w^2 - \frac{1}{2} u^2 = \text{cst.}$$

The velocity triangle at inlet, Fig. 15.10, is approximately rectangular, as $\alpha \approx 70^\circ$:

$$w_I^2 + v_I^2 \approx u_I^2.$$

So to the inlet applies $I \approx h_I - \frac{1}{2} v_I^2$.

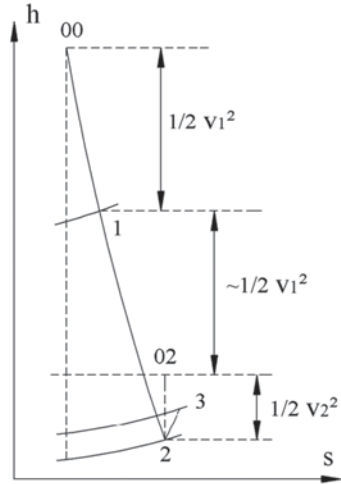
To the outlet applies, with exact axial v_2 :

$$I = h_2 + \frac{1}{2} w_2^2 - \frac{1}{2} u_2^2 = h_2 + \frac{1}{2} v_2^2 = h_{02}.$$

Rotor work is $\Delta W = \sigma u_I^2$. With $\sigma \approx 0.8$, it follows that ΔW is about v_I^2 .

An h-s diagram rendering the previous relations is shown in Fig. 15.11.

Fig. 15.11 h-s diagram for expansion in a centripetal turbine



The degree of reaction follows from

$$1 - R = \frac{\frac{1}{2}v_1^2 - \frac{1}{2}v_2^2}{u_1 v_{lu}}$$

With $v_2 \approx v_{lr}$: $R \approx 1 - \frac{1}{2} \frac{v_{lu}^2}{u_1 v_{lu}} = 1 - \frac{1}{2} \frac{v_{lu}}{u_1} = 1 - \frac{\sigma}{2} \approx 0.6$.

The work coefficient is $\psi = \frac{u_1 v_{lu}}{u_1^2} = \sigma \approx 0.8$.

Regarding work, a radial turbine is not very advantageous, as the work coefficient is lower than with a typical axial turbine, for which it may even reach values above 2. The peripheral speeds are comparable, namely about 400 m/s. The observation that there is no strict limitation to the flow turning of an accelerating flow implies that the work coefficient is not better. Within an axial turbine, the flow turning in the rotor may amount to about 140°. There is a limitation to about 70° with a radial turbine.

It is typical for a radial turbine that backpressure is given. This implies that the total-to-static efficiency has to be maximised. When defining speed ratio, the total-to-static enthalpy drop should be used. The rotor work is

$$\Delta W = \sigma u_l^2 = \eta_{ts} \Delta h_s.$$

With the total-to-static efficiency of about 0.8, it follows that

$$u_l^2 \approx \Delta h_s = v_s^2 / 2 \quad \text{thus} \quad \lambda = \frac{u_l}{v_s} = \frac{1}{\sqrt{2}} \approx 0.7.$$

Two kinematic parameters are thus determined: R and ψ (or λ). The third parameter, the flow coefficient ϕ , follows from efficiency optimisation.

Losses are very low within the volute and the vane ring. Losses within the rotor are significantly higher, due to the separation bubble and the segregation as a consequence of the Coriolis force and the centrifugal force associated to the flow turning in the meridional plane. A significant loss further occurs due to the clearance between the open rotor and the casing and to the high friction velocity on the casing (absolute velocity). A closed rotor would be more advantageous regarding these aspects. The losses within the diffuser are also very high. Optimisation thus means, in principle, minimising the sum of rotor and diffuser losses. This optimisation cannot be achieved with simple means, as the result depends strongly on the loss coefficient values, which cannot be expressed by simple correlations. The result is similar to that with Francis turbines. The optimum outlet angle approximately corresponds to [4, 7]:

$$\phi = \frac{v_{2m}}{u_l} \approx 0.25.$$

Specific speed is $\Omega_s = \frac{\Omega \sqrt{\dot{V}}}{\Delta h_s^{3/4}},$

with $\dot{V} = k \pi r_{2t}^2 v_{2m}$ being the volume flow rate at the rotor outlet and k being an obstruction factor. Thus

$$\Omega_s \approx \frac{\Omega r_{2t} \sqrt{k \pi 0.25} \sqrt{u_l}}{(u_l)^{3/2}} \approx 0.8 \frac{r_{2t}}{r_l}.$$

This result demonstrates that the attainable specific speed at a good efficiency is 0.5–0.7. The optimum efficiency is about 0.85. With a flow coefficient somewhat deviating from the optimal value and some reduction of the efficiency (efficiency ~ 0.80), the realisable range is $\Omega_s \approx 0.3$ –0.9.

15.2.3 Operating Characteristic of Radial Turbines

The analysis is entirely analogous to that of axial turbines. The operating characteristic follows from

$$\psi = \frac{u_l v_{lu} - u_2 v_{2u}}{u_l^2} = \frac{u_l v_{lu} - u_2 (u_2 + w_{2u})}{u_l^2} = \frac{v_{lu}}{u_l} - \frac{u_2^2}{u_l^2} - \frac{u_2}{u_l} \frac{w_{2u}}{u_l},$$

with $\operatorname{tg} \alpha_l = \frac{v_{lu}}{v_{lm}}$ and $\operatorname{tg} \beta_2 = \frac{w_{2u}}{v_{2m}}.$

With $v_{2m} = v_{1m} :$
$$\psi = \phi \left(\operatorname{tg} \alpha_1 - \frac{u_2}{u_1} \operatorname{tg} \beta_2 \right) - \frac{u_2^2}{u_1^2}.$$

Characteristics are thus similar as rendered in Fig. 15.7.

Conditions for choking within the stator are given by (15.8) and (15.9), those within the rotor by (15.10) and (15.11). The difference with an axial turbine is that u_2 is smaller than u_1 . The consequence is that the pressure ratio p_{01}/p_{02} for choking within the rotor is higher. Which of the two conditions is the most stringent strongly depends on the value of h_{01} . In case of a high h_{01} value, the rotor determines the choking and the corresponding pressure ratio $p_{01}/p_{02} \approx 2$, and this value slightly depends on the rotational speed. For a low h_{01} value, the stator may determine the choking and $p_{01}/p_{02} \approx 4$, independent of the rotational speed. The rotor determines the choking in absence of stator vanes. The pressure ratio for choking then depends on the rotational speed and may be rather high in case of a low h_{01} . No universal value can be attributed to this pressure ratio. E.g. with $T_{01} = 500$ K, $u_1 = 400$ m/s, $u_2 = 200$ m/s, it corresponds to (15.10):

$$\frac{p_{02}}{p_{01}} \approx \left(\frac{2}{\gamma + 1} \right)^{\frac{n}{n-1}} \left(1 - \frac{0.8 \times 400^2 - 0.5 \times 200^2}{1150 \times 500} \right)^{\frac{n}{n-1}} \approx 0.20 = 1/5.$$

15.2.4 Radial Turbine Applications

The work coefficient with radial turbines is lower than with axial turbines. The efficiency is lower as well. As a consequence hereof a radial turbine is only applied if an axial type is impossible, this means with small dimensions. Efficiency then becomes disadvantageous with axial turbines, due to relatively high clearances and relatively high blade thickness at the trailing edge compared to the spacing. A typical application is the turbine in turbochargers, except for the big ones. Radial turbines are also used with very small gas turbines. Due to their ability to cope with high pressure ratios before choking, they also are applied in expansion processes in chemical plants. Efficiency is not very crucial with these applications.

15.3 Dimensional Analysis with Compressible Fluids

15.3.1 Independent and Dependent Π -groups

A flow within a turbomachine with a compressible fluid features eight independent parameters: $R, C_p, \mu, p_{00}, T_{00}, \dot{m}, \Omega, D$. The gas is determined by the gas constant R , specific heat C_p and viscosity μ . Gas properties C_p and μ are temperature-dependent and thus should be given at a reference temperature (e.g. at T_{00}). Dynamic viscosity μ may be substituted by kinematic viscosity ν . The initial state is determined by p_{00}

and T_{00} . Mass flow rate \dot{m} and rotational speed Ω determine the operating point. D is a characteristic diameter allowing identification of the machine within a family of similar machines. Note that the operating point may also be determined by the pressure ratio and the rotational speed. It is sometimes a matter of point of view to consider mass flow rate as independent and pressure ratio as dependent (the standard choice with compressors), or vice versa (the standard choice with turbines). We opt for mass flow rate here, as this option is the most complex one for a dimensional analysis, the pressure ratio spontaneously being a dimensionless group.

The intervening dimensions are length, mass, time and temperature. There are thus four independent Π -groups of general form

$$\Pi = R^a C_p^b \mu^c p_{00}^d T_{00}^e \dot{m}^f \Omega^g D^h.$$

The choice of independent dimensionless groups is not unambiguous. It is customary to form dimensionless groups that characterize, as well as possible, the fluid (R , C_p and μ) and the operating point (\dot{m} and Ω).

R and C_p feature the same dimension. Their ratio thus is a Π -group, resulting in the specific heat ratio:

$$\Pi_1 = \gamma = C_p / C_v, \quad R = C_p - C_v.$$

A dimensionless expression of viscosity is the Reynolds number:

$$\Pi_2 = Re = \frac{\Omega D^2}{\nu}.$$

The two remaining groups may be formed by dimensionless expressions of the mass flow rate and the blade speed based on the density and the speed of sound at the machine inlet.

$$\Pi_3 = \frac{\dot{m}}{\rho_{00} \sqrt{\gamma R T_{00}} D^2} = \frac{\dot{m} R T_{00}}{p_{00} \sqrt{\gamma R T_{00}} D^2} \quad \text{and} \quad \Pi_4 = \frac{\Omega D}{\sqrt{\gamma R T_{00}}}.$$

Usually $\sqrt{\gamma}$ is left out, resulting in

$$\Pi_3 = \frac{\dot{m} \sqrt{R T_{00}}}{p_{00} D^2} \quad \text{and} \quad \Pi_4 = \frac{\Omega D}{\sqrt{R T_{00}}}.$$

Sometimes, R is replaced by C_p .

The dimensionless representation of the mass flow rate, as derived here and applied typically, is different from that with incompressible fluids. The flow coefficient customary with incompressible fluids is found by dividing Π_3 by Π_4 .

Dimensionless dependent groups are e.g. pressure ratio p_{03}/p_{00} , temperature ratio T_{03}/T_{00} (for a compressor) and efficiency η . In order to obtain a dimensionless expression for power, it must be divided by reference values of mass flow rate and energy. This group thus gets the form obtained by $\Pi_3 \Pi_4^2$:

$$\frac{P}{p_{00} D^2 \sqrt{RT_{00}}}.$$

Dependent dimensionless groups are expressed as functions of independent dimensionless groups according to

$$\frac{p_{03}}{p_{00}} = f \left[\frac{\dot{m} \sqrt{RT_{00}}}{p_{00} D^2}, \frac{\Omega D}{\sqrt{RT_{00}}}, Re, \gamma \right],$$

with γ being a constant for a given gas. If the Reynolds number is sufficiently large, it does not constitute a strong condition for similarity. The preceding relation thus mostly may be simplified to

$$\frac{p_{03}}{p_{00}} = f \left[\frac{\dot{m} \sqrt{RT_{00}}}{p_{00} D^2}, \frac{\Omega D}{\sqrt{RT_{00}}} \right].$$

15.3.2 Dimensionless Compressor and Turbine Characteristics

Performances characteristics do not change in general appearance when drawn in dimensionless form. For compressors, charts may be as in Fig. 13.27 with pressure ratio and efficiency as functions of dimensionless mass flow rate for constant values of the dimensionless rotational speed. An alternative representation is with efficiency by contour lines, as in Fig. 14.14. For turbines, the chart is dimensionless mass flow rate as a function of pressure ratio for constant values of dimensionless rotational speed (see Fig. 15.7). The chart may be completed with efficiency as a function of pressure ratio. In practice, flow rate curves for various rotational speeds are so close together that rendering the efficiency by contour lines is not possible.

15.3.3 Corrected Quantities

Testing a compressor or a gas turbine (D constant) generates characteristics depending on ambient pressure and temperature. This complicates the comparison of test results performed under different atmospheric conditions. It is therefore advisable to reduce characteristics to a standard temperature (e.g., 288.2 K) and a standard pressure (e.g., 101.33 kPa). The real flow is then substituted by a dynamically similar flow, occurring under standard atmospheric conditions. According to the above formulae, the following expressions should remain constant:

$$\frac{\Omega}{\sqrt{RT_{00}}}, \frac{\dot{m} \sqrt{RT_{00}}}{p_{00}}, \frac{p_{03}}{p_{00}}, \frac{T_{03}}{T_{00}}, \frac{P}{p_{00} \sqrt{RT_{00}}}, \eta.$$

The expressions for corrected rotational speed and mass flow rate are

$$\Omega^* = \Omega \sqrt{\frac{288.2 \text{ K}}{T_{00}}}, \quad \dot{m}^* = \dot{m} \sqrt{\frac{T_{00}}{288.2 \text{ K}}} \left(\frac{101.33 \text{ kPa}}{p_{00}} \right).$$

Fan testing requires a similar adaptation. The above formulae may be applied, but a simpler method is possible. With an incompressible fluid, meaning that density changes very little within the machine and that the Mach number influence is negligible, flow rate is proportional to density and rotational speed. Rotational speed may be kept constant and mass flow rate adapted according to

$$\dot{m}^* = \dot{m} \frac{\rho_{00}^*}{\rho_{00}} = \dot{m} \left(\frac{T_{00}}{288.2 \text{ K}} \right) \left(\frac{101.33 \text{ kPa}}{p_{00}} \right).$$

15.4 Exercises

15.4.1 Consider an axial turbine composed of a stator ring of nozzle vanes with a flow entering in axial direction, turned over a large angle (approximately 70°), followed by two contra-rotating rotors with large flow turning (blade shapes as on Fig. 15.1). In case of post-swirl at the outflow of the second rotor, the rotors may be followed by a stator ring of outlet guide vanes bringing the flow into the axial direction. Take as fluid a combustion gas, considered as an ideal gas, with properties $R=288 \text{ J/kgK}$ and $\gamma=1.30$ at 1600 K at the turbine inlet. Take on the mean radius as blade speeds $u_1=300 \text{ m/s}$ and $u_2=-300 \text{ m/s}$ (thus equal magnitude $u=300 \text{ m/s}$; but opposite running senses) and constant axial velocity through the turbine with value 400 m/s .

- Sketch the velocity triangles. Take as notation 1–2 for the first rotor and 3–4 for the second rotor. Take arbitrary kinematic parameters at this stage, but large flow turning in the nozzle ring and the rotors.
- Determine the velocity triangles for impulse blades on both rotors, meant as $|w_1|=|w_2|$ and $|w_3|=|w_4|$, thus kinematic degree of reaction equal to zero, such that the outlet of the second rotor is in the axial direction. Remark that such a turbine is equivalent with a Curtis turbine, resulting in $\psi_1=6$ and $\psi_2=2$ (work coefficient: $\psi = \Delta W/u^2$).
- Determine the relative inflow Mach numbers of both rotors (A: $M_{w1}=1.644$, $M_{w3}=0.834$).
- Determine the velocity triangles for degree of reaction on the first rotor equal to 50% and work coefficients $\psi_1=5$ and $\psi_2=3$ (so same total work as with the impulse blades). Remark that there is post-swirl at outlet of the second rotor (A: $\alpha_4=36.87^\circ$). Determine the degree of reaction of the second rotor (A: 50%).

- Determine the relative inflow Mach numbers of both rotors (**A**: $M_{w1}=1.071$, $M_{w3}=0.805$). Remark that the inlet Mach number of the first rotor is much lower than with impulse blades. This is a big advantage for the 50 % degree of reaction turbine.
- Determine the deceleration ratio in the outlet guide vanes (**A**: 0.80). The necessity for a deceleration in the outlet guide vane ring is a small disadvantage of the reaction turbine (but see next exercise).

15.4.2 Consider once more the axial turbine of the previous exercise, composed of a stator ring of nozzle vanes, followed by two contra-rotating rotors with large flow turning and a stator ring of outlet guide vanes. Take the same values for blade speed, axial through-flow velocity and gas properties. We will adapt the machine in three steps into a turbine with only rotating components.

- Determine the velocity triangles for $\psi_1=4$ and $\psi_2=4$, such that the couple of the two contra-rotating rotors forms a repeating system. Remark that these conditions do not determine the system uniquely. Take as particular choice identical blade shapes, symmetrically positioned, in both rotors (**A**: obtained for $v_{2u}=2u$).
- Determine the degree of reaction of both rotors (**A**: 100 %). Remark that the turbine is equivalent with a Ljungström turbine (see Chap. 6, Sect. 6.2).
- Determine the relative inflow Mach numbers of both rotors (**A**: $M_{w1}=0.693$, $M_{w3}=0.778$). Remark that these are lower than the values of the 50 % degree of reaction turbine of the previous exercise.
- Determine the deceleration ratio in the outlet guide vanes (**A**: 0.555). Remark that the deceleration ratio is much too strong for practical realisation of the vanes.
- Replace the nozzle vane ring with a rotor rotating together with the second rotor of the repeating couple (same speed and same sense) such that the inflow and outflow velocities remain unchanged (**A**: this requires $\psi=2$). Determine the degree of reaction of this rotor (**A**: 200 %: this rotor generates an increase of kinetic energy in the absolute frame equal to the work done).
- Replace the outlet guide vane ring with a rotor rotating together with the first rotor of the repeating couple (same speed and same sense) such that the inflow and outflow velocities remain unchanged (**A**: this requires $\psi=2$ and $R=0$).
- The resulting turbine is solely composed of rotors. The inner repeating couple may be repeated a number of times. A turbine of this type may be used in a prop-fan or unducted fan aero-engine for driving the contra-rotating propellers.

References

1. AGARD-LS-167 (1989) Blading design for axial turbomachines. AGARD, Paris. ISBN 92-835-0512-3
2. Bertini F, Credi M, Marconcini M, Giovannini M (2013) A path toward the aerodynamic robust design of low pressure turbines. J Turbomach 135:021018

3. Coull JD, Thomas RL, Hodson HP (2010) Velocity distributions for low pressure turbines. *J Turbomach* 132:041006
4. Dixon SL, Hall CA (2014) *Fluid mechanics and thermodynamics of turbomachinery*, 7th edn. Elsevier, London. ISBN 978-0-12-415954-9
5. Lewis RI (1996) *Turbomachinery performance analysis*. Arnold, London. ISBN 0-340-63191-0
6. Moustapha H, Zelesky M, Baines C, Japikse D (2003) *Axial and radial turbines*. Concepts NREC. ISBN 0-0933283-12-0
7. Whitfield A, Baines NC (1990) *Design of radial turbomachines*. Longman, London. ISBN 0-582-49501-6
8. Yoon S (2013) The effect of the degree of reaction on the leakage loss in steam turbines. *J Eng Gas Turbines Power* 135:022602

Index

A

Abott, I.H., 49
Active force, 8
Adachi, T., 128, 129
Adams, T., 269
Aero-derivative gas turbine, 376
Angle of attack, 49
Angle of incidence, 61
Aungier, R.H., 125, 126, 129
Axial chord, 72

B

Baehr, H.D., 393, 396
Balje, O.E., 240, 260, 519
Bernoulli's work equation, 8
Blade
 backward curved blades, 34, 35, 104
 forward curved blades, 35, 104
 radial end blades, 104
 splitter blades, 511
Blade passage shock, 495
Blade speed, 3, 15
Blade-to-blade surfaces, 481
Bleier, F.P., 145
Blower, 97
Booster, 429
Boundary layer
 boundary layer separation, 52–55
 controlled boundary layer, 544
Bowing, 232
Bow shock, 494
Brennen, C.E., 285
Bypass turbojet, 428

C

Casarosa, C., 414
Casey, M.V., 269
Casing treatment, 531
Cavitation, 283
 attached cavitation, 285
 implosion, 283
Chiesa, P., 396
Choking, 162, 497, 499, 502
Chord, 49
Coandă-effect, 125
Cohen, H., 377
Contra-rotating propellers, 429
Controlled diffusion aerofoil, 492
Cooling
 convection cooling, 379
 film cooling, 379
 impingement cooling, 379
 steam cooling, 407
Cordier line, 259
Core engine, 436
Critical pressure, 161
Critical state, 161
Cross-flow fans, 100
Cumpsty, N.A., 519, 526

D

Degree of reaction
 action part, 23, 28
 isentropic degree of reaction, 218
 kinematic degree of reaction, 103, 218
 pressure degree of reaction, 103
 reaction part, 23, 28
 thermodynamic degree of reaction, 218

- Denton, J.D., 233
 Diameter number, 256
 Diaphragms, 212
 Dietzel, F., 261, 267, 332, 334
 Diffuser, 5, 24, 525–528
 cascade diffuser, 527
 channel diffuser, 527
 vaned diffuser, 527, 528
 vaneless diffuser, 527
 Diffusion factor, 466
 Lieblein diffusion factor, 74, 75
 local diffusion factor, 74
 Dimensionless group of parameters, 248
 Directionally solidified, 379
 Discharge, 33
 Dixon, S.L., 75, 209, 335, 517, 518
 Drag, 48
 Draught tube, 4
- E**
 Eck, B., 113, 125, 129, 276
 Effective jet velocity, 424
 Efficiency of components
 propeller efficiency, 422
 infinitesimal efficiency, 165, 168, 389
 internal efficiency, 26, 199
 isentropic efficiency, 167
 isentropic re-expansion efficiency, 386
 mechanical efficiency, 25, 134
 polytropic efficiency, 165, 168, 390
 small stage efficiency, 389
 total-to-static efficiency, 205, 386
 total-to-total efficiency, 205, 386
 volumetric efficiency, 135
 Efficiency of systems
 bypass efficiency, 446
 dynamic efficiency, 433
 propulsive efficiency, 434
 thermal efficiency, 199, 403, 433
 thermodynamic efficiency, 433
 El-Masri, M.A., 396, 397, 401
 End walls, 17, 471
 Energy
 residual kinetic energy, 434
 energy dissipation, 55–57
 energy equation, 13
 mechanical energy, 12, 388
 pressure potential energy, 11
 Enthalpy, 10
 Euler's work equation, 20
 Exducer, 550
- F**
 Forcing of the swirl distribution, 485
 Franc, J.-P., 284, 285
 Franco, A., 414
 Free vortex blade, 483
 Free vortex flow, 61
 Freris, L.L., 365
 Friction
 disc friction moment, 17
 wheel friction moment, 17
 Friction drag, 51
 Fuchslocher-Schulz, H., 258
- G**
 Gas generator, 371, 433, 436
 Gauge pressure, 175
 Geared turbofan, 432
 Ghofrani, M.B., 411
 Girdhar, P., 311
 Greim, R., 226
 Guide ring, 2
 Gülich, J.F., 129, 286
- H**
 Hall, C.A., 75, 209, 335, 517, 540, 553
 Havakechian, S., 226
 Head, 12, 386
 head coefficient, 211
 head loss, 13, 264
 isentropic head, 211, 386, 390, 391
 isentropic re-expansion head, 390
 manometric head, 30, 32
 polytropic head, 390, 392
 Heavy duty gas turbine, 373, 377
 Hirt, L., 233, 235
 Horseshoe vortex, 480
 Hub, 16
 Hub-to-shroud surface, 482
 Hunt, V.D., 363, 365
- I**
 Impeller, 4, 509
 Impulse turbine, 222
 Incidence angle, 120
 Inducer, 292, 511, 523
 Industrial gas turbine, 369
 Infinite number of blades, 101
 Inlet guide vanes, 460
 Interference factors, 90
 Irrotational flow, 67

J

Japikse, D., 75, 125, 126, 129, 291
 Jet flow, 525
 Jet generator, 433, 436

K

Karassik, I.J., 311
 Kim, K.-Y., 129
 Kim, S., 129
 Kinematic parameter, 28, 332, 517
 Knill, T.J., 58

L

Laminar profile, 58
 Lampart, P., 233, 235
 Leading edge, 49
 Leakage vortex, 480
 Lean, 235, 488
 Lean premixing, 382
 Lewis, R.I., 209
 Lift, 48
 Liner, 381
 Load characteristic, 264
 Loss
 energy loss coefficient, 208
 enthalpy loss coefficient, 208, 465
 friction loss, 57
 head loss, 264
 internal loss, 26
 loss coefficient, 68
 mechanical loss, 26
 mixing loss, 57
 pressure loss coefficient, 208, 465
 rotor velocity coefficient, 204
 thermodynamic loss, 26
 total pressure loss coefficient, 208

M

Mach number, 159
 Mean circumferential stream surface, 6
 Mean line analysis, 6, 459
 Meridional component, 16
 Meridional section, 16
 Michel, J.M., 284, 285
 Miller, D.S., 77, 82–85
 Model laws, 272
 Moment solidity, 117
 Moniz, O., 311
 Moustapha, H., 209

N

Net positive suction head, 287, 291, 292

O

Obstruction factor, 122
 Operating point
 stable operating point, 297, 501, 502
 unstable operating point, 297, 298, 501

P

Partial admission, 198
 Passage vortex, 232, 473
 Performance characteristic, 36
 Performance parameters, 104
 Pfleiderer, C., 60, 113, 144, 261, 271, 276
 Pfleiderer moment coefficient, 115–118
 Pilot burner, 382
 Pitch, 61
 Pitch control, 352
 Power
 dynamic power, 422, 433
 gas power, 433
 propulsive power, 434
 residual power, 434
 thermal power, 433
 internal power, 134
 rotor power, 134
 shaft power, 134
 Power gas turbine, 369
 Power specific speed, 263
 Power turbine, 371
 Pre-compression profiles, 496
 Pressure drag, 50
 Pressure recovery, 79
 Pressure side, 48
 Primary flow, 471
 Priming, 293
 self-priming, 293
 Prop-fan, 429

Q

Qiu, X., 115
 Quasi-three-dimensional flow, 482, 488

R

Radial equilibrium, 482
 Razak, A.M.Y., 377
 Reaction turbine, 222
 Recuperator, 370
 Regenerator, 371
 Reheat effect, 165, 170, 387
 Repeating stage, 205
 Rosic, B., 233
 Rothalpy, 16
 Rotor(s), 1
 rotor disc, 17
 rotor Mach number, 520

shrouded rotor, 16
 unshrouded rotor, 16
 Runner, 3

S

Sanjay, Y., 396
 Scraping vortex, 480
 Secondary flow, 232, 473
 Secondary vortices, 478, 490
 Seo, S.-J., 129
 Sheikhbeigi, B., 411
 Simple cycle, 371
 Single crystal, 379
 Slip, 112
 Slip factor, 112
 Solidity, 59, 61
 Spacing, 59, 61
 Specific diameter, 255
 Specific fuel consumption, 437
 Specific speed, 255
 Specific thrust, 434
 Speed number, 256
 Speed of sound, 156
 Speed ratio, 90, 210, 257
 Spontaneous pre-swirl, 34
 Spouting velocity, 210
 Staged combustion, 384
 Stage loading coefficient, 211
 Stagnation enthalpy, 16, 462
 Stagnation pressure, 16, 51
 Stagnation state, 155, 385
 Stall, 499, 500
 pulsating stall, 502
 steady stall, 81
 transitory stall, 81
 Stall control, 353
 Static enthalpy, 16
 Static pressure, 16
 Strub, L.A., 269
 Suction, 33
 Suction eye, 34
 Suction side, 48
 Suction specific speed, 290
 Surge, 503
 surge line, 502
 Sweep, 235, 490
 Swirl stabilisation, 383

T

Thermal barrier coating, 381
 Thrust, 421
 Tip treatment, 543
 Total enthalpy, 10, 16, 154, 464

Total pressure, 16, 51
 Total pressure drop, 68
 Total relative enthalpy, 462
 Total state, 155, 385
 Trailing edge, 49
 Trailing vortices, 479
 Transition
 bypass transition, 493, 544
 natural transition, 493
 Turbofan, 430
 Turbojet, 428
 Turboprop, 427, 428
 Turbo-shaft, 430, 437
 Turbulence migration, 77
 Turbulence segregation, 77
 Turbulent profile, 58
 Tuzson, J., 291

U

Unducted fan, 431

V

Vivier, L., 327, 332, 334
 Volute, 35
 Von Doenhoff, A.E., 49

W

Wake flow, 527
 Whitfield, A., 517, 518
 Wilcock, R.C., 396
 Work
 deformation work, 12, 56
 displacement work, 10, 12, 56, 71, 72
 rotor work, 19, 21, 24
 rotor work equation, 20–23
 work coefficient, 211, 214, 216
 work equation, 13, 20
 Work reduction factor, 114, 115, 281

X

Xu, L., 233

Z

Zero-lift line, 49, 59, 60, 420
 Zweifel tangential force coefficient, 72